

THEORY OF PARTICULATE PROCESSES

ANALYSIS AND TECHNIQUES OF CONTINUOUS CRYSTALLIZATION

SECOND EDITION

Alan D. Randolph

*Department of Chemical Engineering
University of Arizona
Tucson, Arizona*

Maurice A. Larson

*Department of Chemical Engineering
Iowa State University of Science and Technology
Ames, Iowa*



ACADEMIC PRESS, INC.

Harcourt Brace Jovanovich, Publishers

San Diego New York Berkeley Boston
London Sydney Tokyo Toronto

COPYRIGHT © 1988 BY ACADEMIC PRESS, INC.

ALL RIGHTS RESERVED.

NO PART OF THIS PUBLICATION MAY BE REPRODUCED OR
TRANSMITTED IN ANY FORM OR BY ANY MEANS, ELECTRONIC
OR MECHANICAL, INCLUDING PHOTOCOPY, RECORDING, OR
ANY INFORMATION STORAGE AND RETRIEVAL SYSTEM, WITHOUT
PERMISSION IN WRITING FROM THE PUBLISHER.

ACADEMIC PRESS, INC.

1250 Sixth Avenue

San Diego, California 92101

United Kingdom Edition published by

ACADEMIC PRESS INC. (LONDON) LTD.

24-28 Oval Road, London NW1 7DX

Library of Congress Cataloging-in-Publication Data

Randolph, Alan D., Date

Theory of particulate processes.

Includes index.

I. Crystallization. I. Larson, Maurice A.,

Date. II. Title.

TP156.C7.R3 1988 660.2'84298 87-14968

ISBN 0-12-579652-8 (alk. paper)

PRINTED IN THE UNITED STATES OF AMERICA

88 89 90 91 9 8 7 6 5 4 3 2 1

To Peggy and Ruth

PREFACE TO THE SECOND EDITION

The second edition of *Theory of Particulate Processes* seemed necessary because of the large volume of population balance–based particulate studies that have appeared since the first edition. Some of these latter studies were motivated, or at least influenced in some way, by population balance ideas set forth in the first edition. Therefore, we have included a more extensive bibliography in Appendix D, which should make this book more valuable as a research reference volume. It was impossible to cite all pertinent references at the end of each chapter. We hope we have been fair in giving credit for key ideas that have advanced this field so extensively.

This second edition, in outline, reflects in many ways the notes for an industrial short course on crystallization that we have frequently given. The book is, and should remain, useful as a text in such an industrial short course. The additional problems that have been added in Appendix C should also make the second edition a useful text for a senior elective or special-topics graduate course. We frequently offer such a graduate course at the University of Arizona and Iowa State University, respectively.

While this book is intended mainly for those concerned with crystallization processes, it should also be useful for those interested in other fields in which it is necessary to model particulate processes. Chapters 1, 2, and 3 are general in nature and lay out the methods for representation of particle distributions and a systematic approach to the predictive modeling of processes where there is a need to characterize distributions in time and space and by some identifying property. Chapter 4 provides a specific and more elementary approach to modeling crystal size distributions. The reader new to the field might find it beneficial to begin study with Chapter 4 and then return to Chapters 2 and 3. Chapter 5 lays the groundwork for

modeling the kinetics of crystal nucleation and growth rates. Such kinetics are necessary for modeling crystallization processes. Chapters 6, 7, and 8 address a wide range of system analysis and design considerations specific to crystallization for both the steady state and unsteady state. The general reader should find in these chapters several topics that would be adaptable to other systems. Chapter 9 addresses the collection of experimental data and in particular illustrates the use of a population balance analysis to interpret data from both laboratory and process equipment. Finally, Chapter 10 briefly discusses a wide variety of particulate processes and systems for which the population balance analysis is useful. Readers concerned with dispersed phase mass transfer, comminution, aerosols, agglomeration, biological processing, and polymerization will find examples of how the population balance has been effective in process analysis.

In summary, those not concerned with crystallization should find the material in Chapters 1, 2, 3 and 10 particularly useful. The discussion of crystallization in the remaining chapters should provide concepts or techniques that may be useful in other fields.

PREFACE TO THE FIRST EDITION

The need for this book has arisen from the burst of research activity over the last ten years in the area of industrial crystallization from solution. This work began with the first attempts to rationalize, model, and predict crystal-size distributions (CSD) from realistic mixed-magma crystallizers and was based on the concept of a population balance of crystal particles along the particle-size axis. The scope of this general attack on the CSD problem was quickly enlarged to include three main areas of research which have seen much attention during the last decade. These areas, introduced, motivated, and sometimes necessitated by the original CSD studies, are listed below:

Use of the population balance to predict CSD in various crystallizer process configurations with assumed crystal kinetics. This work included studies of fines removal, staging, product classification, and CSD instability as well as the inherent CDS effects to be expected of various crystallization kinetics, e.g., size-dependent growth rates and magma influenced (secondary) nucleation.

Use of the idealized mixed-suspension, mixed-product-removal (MSMPR) crystallizer at the bench-scale, pilot plant, and industrial levels to assemble nucleation and growth rate kinetics correlations in realistic mixed-magma suspensions. This work, performed in both industrial and university laboratories, led to the realization of the importance of secondary nucleation mechanisms in continuous mixed-magma crystallizers and the assembly of large amounts of nucleation-growth rate data which could be adequately correlated with simple exponential (power-law) kinetic expressions.

Extension of the simple size-axis population balance to a generalized continuity equation in particle phase space which can serve as the analytical

framework for studies of population dynamics in other particle processes, e.g., comminution, microbial distributions, and dispersed phase extraction systems, constitutes a formalized theory of multivariate distributions in particulate systems. This is not to say that population balances were not used, in fact were not the framework, in such studies; however, the CSD problem yielded perhaps the most fruitful applications of this population balance theory (undoubtedly because of the simple, but useful, closed-form solutions, e.g., MSMPR model) and thus it was in this context that the full formalism of the population balance in particle phase space was developed.

The fortuitous circumstance of their initial collaboration in 1960 enabled the authors to be a part of this rapid burst of activity from its beginnings. This book is a natural summary of the work over the past decade on CSD in which the authors have participated or are intimately aware.

The main purposes of this book are to present the work on CSD as a more or less complete topic, introduce the reader to the complex subject of secondary nucleation and growth mechanisms which are only now being unfolded, and to present the generalization from CSD studies as a unified predictive theory of particulate systems. No attempt is made at a comprehensive treatment of work other than CSD studies, yet it is hoped that details in the treatment of crystallization processes will be of value to researchers in other areas.

The material in this book has been used as lecture notes for a graduate level special topics course in particulate systems. The material for this graduate course was presented in approximately the same order and level of comprehension as in the book and was supplemented by individual studies from the current literature. Representative particle distribution problems from the appropriate chapters are presented in Appendix C. These problems plus the broad, but elementary, attention given to systems other than crystallization should make this book a worthwhile text for use in such graduate level special topics courses as well as to reinforce the researchers' understanding of the material.

It is hoped that the student and researcher alike will not be overwhelmed by the attention paid to crystallization systems but will use this theory as a helpful and logical organization in the understanding of particulate processes.

ACKNOWLEDGMENTS

We wish to acknowledge the influences of our colleagues in process crystallization and in particular the efforts of all our graduate students who have contributed so much to this work. The creativity and initiative of our graduate students were the factors that provided the fuel for the completion of much of this work.

We also wish to acknowledge Dr. David R. Boylan, the Director of the Iowa State University Engineering Research Institute, who provided the opportunity for our initial collaboration.

PARTICULATE PROCESSES

1.1 Particulate Processes and Particle-Size Distribution

The particulate nature of solids is characterized by form and size, as opposed to liquids or gases, which assume the shape of the volume within which they are contained. Some examples of processes that yield a product that is particulate in nature are crystallization, comminution, aerosol, and emulsion processes. If a solid material is produced, the particles are characterized by both a size and a representative shape. If liquid droplets are produced, the shape is usually spherical and the particles are characterized by their diameter (or volume). As no two particles will be exactly the same size, the material must be characterized by the distribution of sizes or particle-size distribution (PSD). Examples are the crystal-size distribution (CSD) produced in a precipitation or crystallization process or the powder from crystals or raw minerals produced by comminution of the original crystals or ore. The shape of particles from grinding or crystallization processes is often uniform enough that a characteristic shape factor can be defined and the particles can be described using a one-dimensional distribution function. A single-variable distribution function is sufficient to describe liquid drop-size distribution unless a second independent variable is required to describe the chemical composition or age distribution of the droplets. Additional properties, such as composition, can be associated with the particles, thus yielding a multivariable distribution. The additional

complication is seldom worth the effort, however. A multidimensional generalization of particle “size” is developed in Chapter 3.

The CSD or PSD can be the major determining factor in the ultimate use of a particulate material. It is often important to be able to quantitatively describe the CSD as well as to model it from *a priori* principles. This book attempts to summarize the equations and properties of some well-known distribution functions that are useful to describe the CSD (PSD) in a quantitative way, as well as to develop a complete population balance theory of particulate processes that can be used in the *a priori* modeling of such systems.

Most of the examples in this book refer to crystallization applications of the theory of particulate systems, because of the particular background of the authors; however, this theory can be broadly applied to many other systems. Certainly crystallization is a very ordered, if complex, process, and much effort has been devoted to attacking the CSD problem in its many aspects. This book draws generously on these earlier efforts. The generalization of CSD theory to that of a unified theory of multidimensional distributions in particulate processes is valid, however, and it is hoped that the reader who is interested in other particulate processes will not be overwhelmed by the attention devoted to crystallization.

1.2 Properties Relating to PSD and CSD

The PSD of a solid material often is important, even critical, in the end-use applications of the material. (No one would tolerate brushing their teeth with a toothpowder that had the same PSD and “feel” as beach sand!) On the other hand, the CSD from a crystallization process can have dramatic process interactions in addition to the same end-use properties as given for any particulate matter. Table 1.2-1 lists some of the common end-use properties of PSD or CSD together with some of the crystallizer process interactions unique to CSD.

Some of the more important problems in the operation of industrial crystallizers involve (a) crystal-size distribution, (b) crystal habit and purity, (c) salting (fouling), (d) capacity and scale-up, and (e) crystallizer stability. All of these problems interact strongly with the CSD being produced and, in fact, most of these problems could be listed as subheadings under the CSD problem.

The crystallizer interactions of CSD with crystallizer operation, as listed in Table 1.2-1, are brought about by the effects of different supersaturation levels on the factors listed. In turn, the differing levels of supersaturation are strongly influenced by the prevailing CSD, especially in continuous

1.2 PROPERTIES RELATING TO PSD AND CSD / 3

Table 1.2-1

Some End-Use Properties of PSD and Crystallizer Interactions with CSD

End use (PSD or CSD)	Crystallizer interactions (CSD)
Filtration rate	Vessel fouling rate
Entrainment of liquid after dewatering	Changes in crystal habit
Dissolution rate	Changes in crystal morphology
Caking properties in storage	Mother-liquor inclusions
Fluidization properties	CSD instability
Pneumatic handling properties	
Bulk density	
Esthetic appearance	

crystallizers. Crystallization is a crystal surface-dependent mass-transfer operation, and the surface (or perhaps active sites) can vary widely as the CSD varies. This complex interaction of the CSD with the same factors that form the CSD is illustrated in the information diagram of Fig. 1.2-1. This diagram shows how each of the crystallization kinetic factors is related, such as nucleation rate, growth rate, and particle residence time (as described by the population balance). The principal feedback interactions are shown in Fig. 1.2-1, but research continues to expand on this detail. Note the strong feedback relationship between the level of supersaturation driving force and some measure of crystal surface area (and hence CSD). It is precisely this feedback of information that causes the crystallizer/CSD interactions listed in Table 1.2-1. Such crystallizer/CSD interactions can

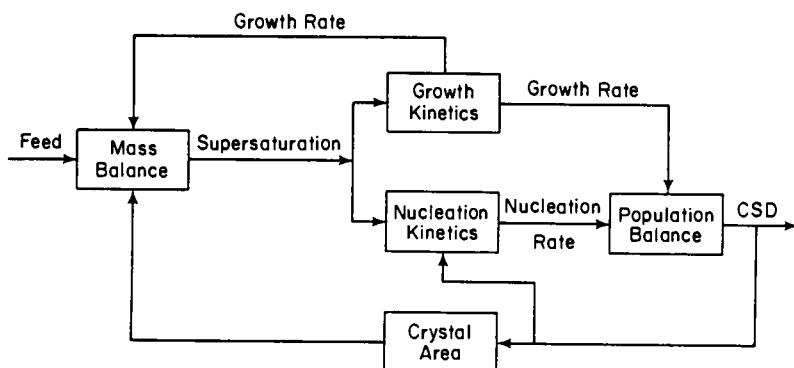


Fig. 1.2-1 Information diagram showing feedback interaction of crystallization factors.

profoundly influence the operation of steady-state continuous crystallizers but are of course operative in transient and/or batch operation. We will refer many times to this flow of information in crystallization processes, particularly in Chapter 8.

1.3 Crystallizer/CSD Interaction

Specific examples of crystallizer/CSD interaction are numerous. We cite the following from operation of a 20-l bench-scale KCl crystallizer.

In operation mode 1 a run is commenced by filling the clean vessel with slightly undersaturated hot feed liquor ($\sim 150^{\circ}\text{F}$). The cooling water in the vessel is turned on, and within 20 min the contents have dropped to the steady operating temperature of 100°F and an initial CSD has formed. The run is continued at constant temperature and with constant feed and discharge rates. Inevitably the run must be shut down after a few hours and before a steady-state CSD is obtained due to extreme vessel fouling, particularly on the cooling coils submerged in the agitated magma. The decision to shut down the run is made because temperature control can no longer be maintained in the vessel. Admittedly, if temperature drop was obtained by flash cooling the incoming hot brine, then a much longer run time could be achieved, but initial fouling would still have started on the walls of the vessel. This fouling would eventually require premature shut-down.

In operation mode 2 the crystallizer is filled with a saturated mother liquor and crystal magma, which roughly approximates the eventual steady-state magma to be expected. (This starting crystallizer magma is often obtained from the previous run.) When the starting magma has been charged, the run is started by admitting hot concentrated feed and initiating temperature and product discharge controls. In start-up mode 2, it is observed that the crystallizer can operate for up to 48 h without extensive cooler fouling and a steady state CSD is obtained.

Potassium chloride is a difficult system to operate on a small scale because of its fouling tendencies, yet the above illustration is representative of the extreme operating difficulties that can be encountered because of the feedback of information between the current CSD (as given by the active crystal surface area) and the supersaturation driving force.

A subtle and perhaps more industrially relevant illustration of the feedback relationship shown in Fig. 1.2-1 is the trade-off between making larger (and perhaps more desirable) crystals using the technique of fines dissolving versus the more frequent washout cycles that might result from the higher supersaturation created. Larger crystals have less surface area per

unit weight, and therefore to make the same production rate on a smaller total crystal surface area the crystal growth rate (and hence supersaturation) must necessarily increase. The probability of increased fouling rate and lost time due to crystallizer washouts should be considered when contemplating changes that would make a larger-sized crystal product.

The CSD interactions illustrated in Fig. 1.2-1 can be quantified and simply stated as a constraint on the crystal growth rate for the case of high-yield crystal systems. For such systems, typically most inorganics, the operating level of supersaturation in the mother liquor is small compared to the slurry density that has precipitated from solution (both expressed on the same basis, say mass per volume of liquor). For such systems a constraint on the average growth rate (this will be shown in Chapter 4 to derive directly from a solute mass balance) becomes

$$\bar{G} = k \delta C / \tau A \quad (1.3-1)$$

In words, Eq. (1.3-1) says that the average crystal growth rate is proportional to the drop in concentration between feed and discharge liquors and inversely proportional to the time available for growth and the area over which growth can be deposited. Equation 1.3-1 (for a high-yield system) succinctly states the feedback interactions implicit in Fig. 1.2-1.

Scale-up of crystallization processes from bench scale to pilot size to industrial size is a difficult problem and again relates to the CSD problem. In general, if the intensive properties of an element of mixed crystal magma remain invariant upon scale-up, CSD will remain invariant or at least can be predicted from the size-dependent residence-time distribution of the particles. However, supersaturation generation, flow patterns, degree of mixedness, and factors affecting secondary nucleation do not remain invariant with a change in scale of the process. For example, supersaturation is produced in a two-dimensional manner through vaporization at a boiling surface or cooling across a surface exchanger, while the volume of a crystallizer scales in a three-dimensional manner. Thus, as the size of a crystallizer increases, assuming constant magma circulation velocities, an element of fluid at the zone of supersaturation creation must circulate a longer time before reaching the extremities of the crystallizer. Therefore, constant properties in this element of magma cannot be maintained and changes of CSD with scale-up occur. The art of CSD scale-up involves understanding the factors resulting in a given CSD at each level of operation and then predicting the magnitude of these factors and the resulting CSD in the desired full-scale operation.

Stability of operation is directly related to CSD. The transients of CSD are characterized by long lag times. Typical upsets consist of idling the discharge, water addition, temperature excursions during washouts, tempor-

arily stopping feeds, and recycling or accelerated removal of crystal magma. Hydraulically speaking, the crystallizer, having a large retention time, is quite stable to such process interruptions; however, CSD may be profoundly influenced by such upsets. During the long recovery time of CSD (hydraulic and temperature upsets may have long since stabilized) there is a great temptation to make further operating changes which again affect CSD. Excursions in dilution and/or temperature of a crystallizer can have a pronounced effect on CSD because of changes in the nucleation rate. Such upsets require a maximum recovery time to return to a stable CSD.

The distribution of crystal sizes as well as the magnitude of particle size can also be an important factor in the use of a material as well as an important factor contributing to process interactions. In general, uniformly

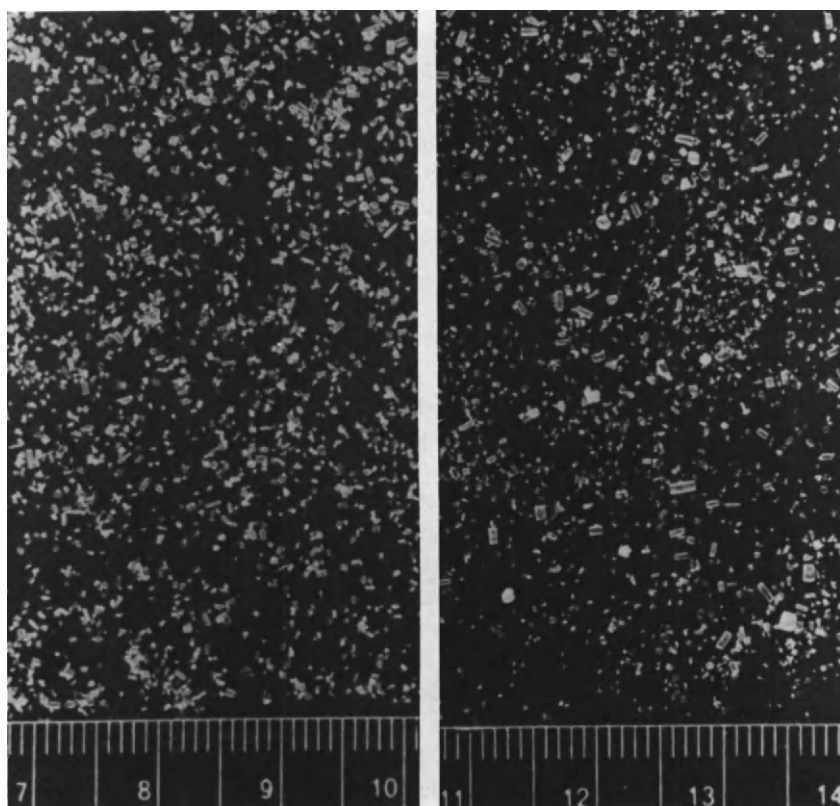


Fig. 1.3-1 Photomicrographs of $(\text{NH}_4)_2\text{SO}_4$ crystals having mean size of $300\ \mu\text{m}$ with a coefficient of variation (a) 0.25 and (b) 0.6.

sized particles are easier to handle, filter, and dewater, and hence are more desirable. An example is the emphasis on production of a narrow CSD in the raw sugar industry. The purification step becomes significantly easier if a large ($\sim 800 \mu\text{m}$) and narrow CSD can be produced. Desirable CSDs are reflected in the value of the product.

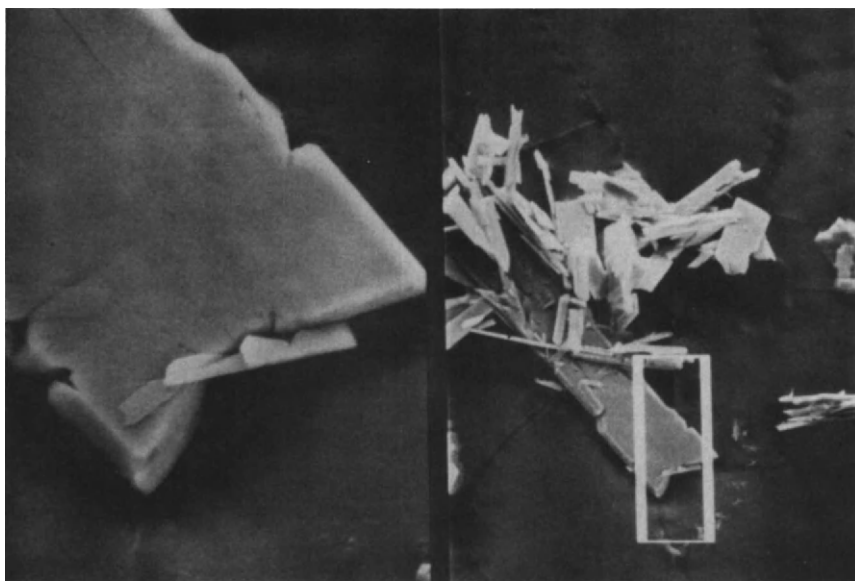
On the other hand, narrow CSDs can exacerbate transient upsets and even result in unstable crystallizer operation. Crystallizer instability is discussed at length in Chapter 8.

The appearance of a granular material is also affected by its size distribution. Ordinary table sugar and salt are two commodities whose acceptance by the homemaker is largely related to their appearance of uniformity and hence their size and size distribution. A narrow particle-size distribution, indicated by a low coefficient of variation (variance of particle size divided by mean particle size), appears much more homogeneous than distributions with a large coefficient of variation. This is illustrated by Fig. 1.3-1, which shows photomicrographs of $(\text{NH}_4)_2\text{SO}_4$ crystals with approximately the same mean but with coefficient of variation (weight basis) of (a) 0.25 and (b) 0.60. The appearance of uniformity (visual) is a function of absolute sizes as well as of the width of the distribution, and a few very large particles can give an otherwise uniform distribution a heterogeneous appearance. If esthetic visual appeal is an important market factor, this fact often necessitates scalping of the oversize from the product crystals.

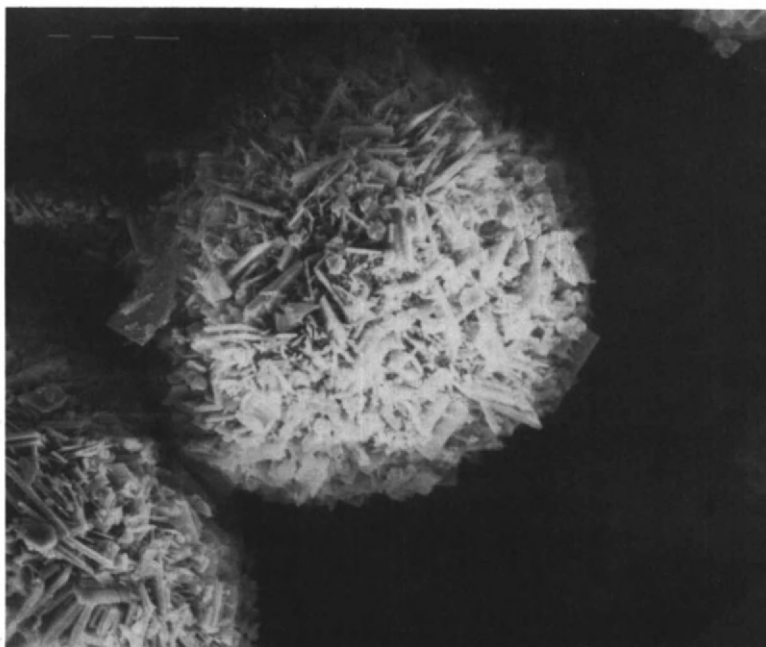
1.4 Particle Shape and Appearance

Particle morphology (as opposed to the more specific terms crystal morphology and habit) is a term that is used to describe the overall external shape and appearance of particulate solids. For example, crystals can have a conglomerate or rosette appearance (particle morphology) due to multiple twinning or surface nucleation and resulting polycrystalline growth. Such polycrystalline growth is contrasted to faceted or continuous-domain single crystals wherein the molecular crystal lattice structure is continuous and repeating throughout the crystal, extending to the clearly defined crystal faces. These two types of different outwardly appearing crystals are often loosely referred to as multicrystals versus single crystals. High levels of supersaturation often result in multicrystals having a rosette particle morphology. Figures 1.4-1(a) and 1.4-1(b) illustrate calcium sulfite crystals, produced under different conditions, that have different particle morphology.

The process of comminution typically results in particles with a rough morphology. The strength of mineral bonds along the major crystal axes



(a)



(b)

Fig. 1.4-1 Crystals of $\text{CaSO}_3 \cdot \frac{1}{2}\text{H}_2\text{O}$ showing different particle morphology: (a) faceted, (b) rosette.

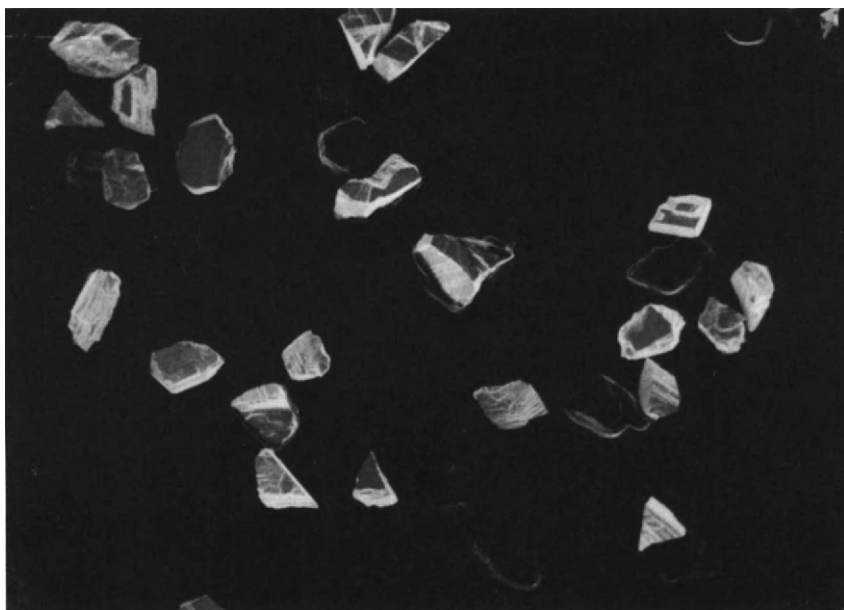


Fig. 1.4-2 Typical morphology of ground particles (lead-zinc ore). (Courtesy of the Material Science Department, University of Arizona.)

and dispersion of discrete mineral phases within the overlying rock matrix in combination with the particular fracture mechanisms of a crushing mill determine the morphology of ground particles. Figure 1.4-2 illustrates the typical morphology of ground lead-zinc ore. Notice that the surfaces created are predominantly along planes of cleavage of the particles. It is possible to produce a needle-like or platelet-like particle in grinding processes if large differences of molecular bonding energies occur along the different mineral crystal axes.

A conglomerate particle morphology is also evidenced by ground or crystallized particles that have undergone agglomeration and/or aggregation subsequent to their production in grinding mills or crystallizers. It is difficult and often impossible to tell from just photographic evidence whether a conglomerate particle morphology in a crystalline product is due to polycrystalline growth or agglomeration/aggregation. Both mechanisms can produce conglomerate particle morphologies indistinguishable in photomicrographs.

Crystal morphology and crystal habit are well-defined terms that respectively describe the appearance of faceted crystals due to the specific

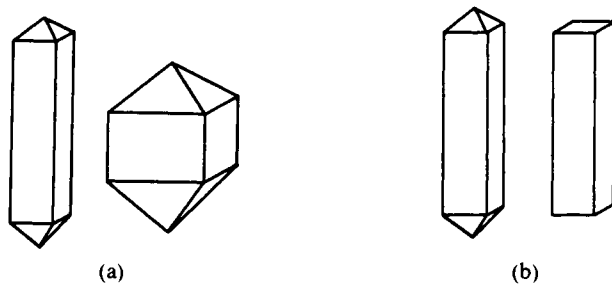


Fig. 1.4-3 Schematic of crystals with different habits and morphologies. (After Toschev [2].) (a) Same morphology but different habit. (b) Same habit but different morphology.

crystallographic faces showing versus the crystal shape given by the relative length to width of the crystal faces. The Miller indices of the different crystal faces showing give the crystal morphology. Terms like equant, acicular (needle-like), plate-like, columnar (rod-like), cube, etc. are used to qualitatively describe crystal habit. Only certain morphologies (crystal faces showing) are possible for any given crystal system (molecular lattice struc-

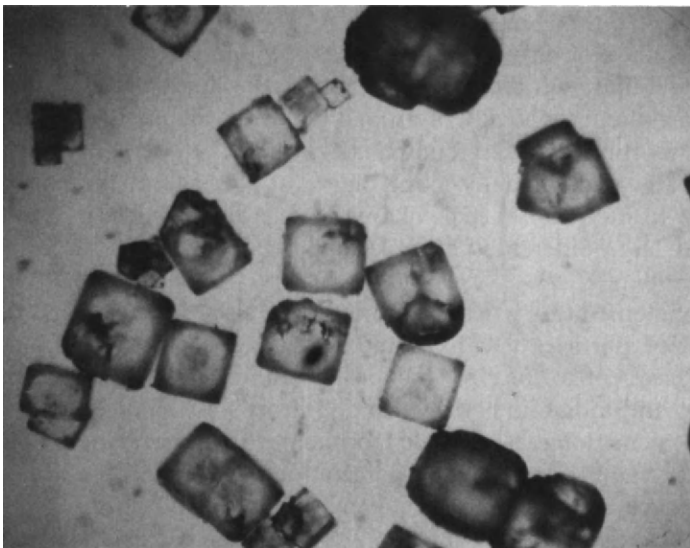


Fig. 1.4-4 Crystals with same crystal morphology but different particle morphology: single crystals and multicrystals of KCl.

ture), but both morphology and habit depend on growth conditions and can vary with the level of supersaturation.

An excellent description and illustration of crystal morphology and habit is given by Touche and Hartman (1973). Figures 1.4-3(a) and 1.4-3(b) (after Hartman) respectively illustrate crystals of the same morphology but different habit and of different habits with the same crystal morphology. Figure 1.4-4 illustrates multicrystals and single crystals with the same crystal morphology but different particle morphology.

1.5 Particle Size

Particles and particle size in this book follow the definitions of Irani and Callis [1]; that is, a particle may be thought of as the element of matter that best describes the state of subdivision of the material and has a shape characteristic of the processes and forces producing the particles. With this definition of a particle, then particle size must be the linear dimension that best characterizes the state of subdivision of the material within the context of the typical shape of the particles. A characteristic dimension of a particle can be thought of as a line passing through the center of mass of the particle and intersecting two opposing surfaces. Figure 1.5-1 sketches an irregular particle with three such characteristic sizes drawn through its center of mass. For highly irregular particles, such characteristic sizes are infinite in number and themselves can be represented by a one-dimensional frequency distribution as also shown in Fig. 1.5-1. Fortunately, this variation in characterization of individual sizes is averaged when a size distribution is obtained on a sample containing a large number of particles. The actual size that is measured in a particle-size distribution analysis lies between the minimum and maximum characteristic sizes shown in Fig. 1.5-1 and depends on the method of measurement. A comprehensive discussion of the definitions and techniques of particle-size measurement is outside the scope of this book [1]. However, it is essential to note that no definition of particle size is complete without specifying the technique of size measurement. A simple illustration involving *a priori* calculation of particle shape factor illustrates this point. The volumetric shape factor k_v is a dimensionless constant relating particle volume v to the cube of particle size L :

$$k_v = v/L^3 \quad (1.5-1)$$

Assume elongated parallelepipeds of dimension $L' \times W \times W$ having an aspect ratio of five, that is, $L'/W = 5$. Such particles would lie on a microscope slide with the L' dimension horizontal, the easiest to measure,

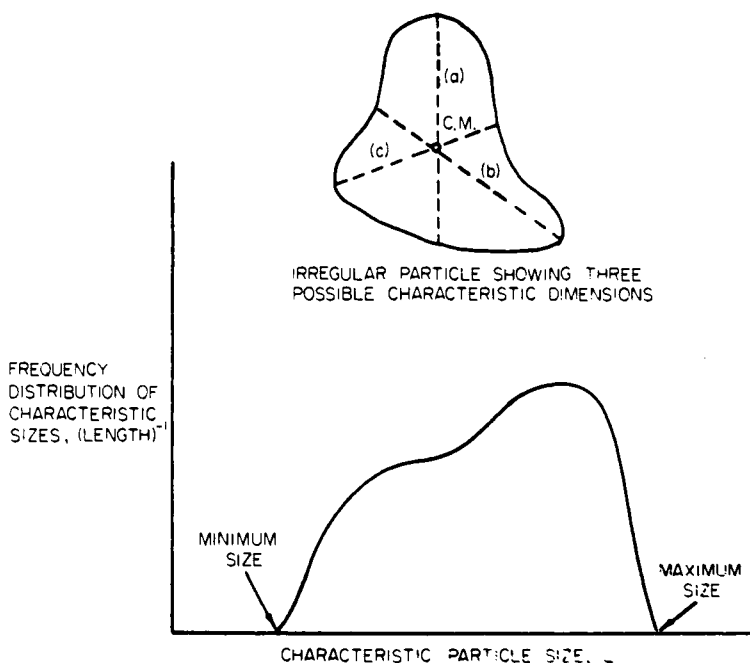


Fig. 1.5-1 Variation in characteristic particle size for an irregular particle.

and typically used as the measure of particle size. For these particles, k_v would be computed as $k_v = \frac{1}{25}$. If the particles were sieved, a completely different size would be reported. Sieves typically segregate particles into size fractions with $L = [L_{\min} L_{\max}]^{1/2}$; that is, size L is the geometric mean of the largest and smallest dimension of the particle. Thus sieving this sample¹ might indicate a size as

$$L = (L' \times W)^{1/2} \quad (1.5-2)$$

For this case the volumetric shape factor would be

$$k_v = (W/L')^{1/2} = 0.45.$$

In fact, sieving of irregular but geometrically similar particles typically gives volumetric shape factors of 0.5 to 0.7. These shape factors are remarkably constant for the given particles, even over large size ranges. The actual sieve-determined shape factor can easily be determined by counting and weighing a few crystals from a narrow (e.g., $\sqrt[4]{2}$) sieve size cut. If \bar{L} is the

¹ The particle dimension obtained by sieving also depends on other factors, such as sieving time, sample loading, and levitation on the sieve.

average of the sieve aperture, N is the number of particles counted, and W is their weight, then volumetric shape factor is calculated simply as

$$k_v = W/\rho N\bar{L}^3 \quad (1.5-3)$$

where ρ is particle density.

A third commonly used method of particle size measurement is by electronic zone sensing instruments, for example, the Coulter Counter® or PDI Elzone® counters. These instruments operate on the principle of passing electrical current between two electrodes in a conductive fluid. The electrodes are on the inside and outside of a small quartz finger electrically connected by a small orifice having a diameter of a few tens to hundreds of micrometers. This orifice provides the only electrical passage between the inner and outer electrodes. As particles flow through the orifice (by applying a controlled vacuum to the quartz tube), they interrupt the current, thus producing a series of electrical pulses shown to be proportional to the volume of the particle. These pulses are counted and scaled in an electrical pulse-height analyzer circuit, thus yielding a PSD.

Zone sensing instruments have a constant and predictable volumetric shape factor of $k_v = \pi/6$, that is, the shape factor of a sphere. This is because calibration is performed using narrow distributions of spherical particles. The size reported by such zone-sensing instruments is then the diameter of a sphere having the same volume as the (perhaps) irregularly shaped particles passing through the orifice. There would be merit in reporting all PSDs in terms of equivalent spherical diameter, regardless of the sizing instrument. Unfortunately, this is not a universal practice.

1.6 Particle-Size Distributions

Many analytical formulations are available to present the CSD. In principle, such analytical formulations are equivalent and can be transformed one to the other through straightforward equations. This section sets forth several common systems that are frequently seen in the literature, with illustrations showing plots and conversions of typical CSD data between systems. CSD data can be presented as cumulative totals (or cumulative fractions) of a measured quantity (number, mass, area, etc.) versus specific levels of some particle characteristic that can be measured for each member of the distribution (most likely, in our case, particle size). Here we might think concretely of a cumulative mass fraction versus particle size distribution.

Alternately, the distribution may be formulated as a density distribution, that is, as the approximate derivative of the cumulative distribution. Similar

to the density function is the histogram, which merely plots the amount of measured quantity (say, mass) that appears over each increment of the measured characteristic (say, particle size). Typically, both histograms and density functions are plotted at the midpoint of the increment measured. If we let ΔM_j be the measured quantity at each of the increments of measured characteristic L_j , then cumulative, density and histogram presentations can be summarized as follows:

$$\text{Cumulative} \quad \sum_{j=1}^{j=J} \Delta M_j \quad \text{versus} \quad \sum_{j=1}^{j=J} \Delta L_j \quad (1.6-1)$$

$$\text{Density} \quad \Delta M_j / \Delta L_j \quad \text{versus} \quad \sum_{j=1}^{j=J-1} \Delta L_j + \frac{\Delta L_J}{2} \quad (1.6-2)$$

$$\text{Histogram} \quad \Delta M_j \quad \text{versus} \quad \sum_{j=1}^{j=J-1} \Delta L_j + \frac{\Delta L_J}{2} \quad (1.6-3)$$

Four density-distribution functions that often appear in the literature are particle number or mass density versus particle size (linear) or particle volume. Thus by definition of the density function, particle number or mass is described as follows. The lower-case letter represents the density function and the upper-case letter represents the quantity that is distributed:

$$dN(L) = n(L) dL \quad (1.6-4)$$

which is the number of particles appearing in particle size range (linear) L to $L + dL$;

$$dM(L) = m(L) dL \quad (1.6-5)$$

which is the mass of particles appearing in particle size range L to $L + dL$;

$$dN(v) = n(v) dv \quad (1.6-6)$$

which is the number of particles appearing in particle volume range v to $v + dv$; and

$$dM(v) = m(v) dv \quad (1.6-7)$$

which is the mass of particles appearing in particle volume range v to $v + dv$.

As particle-size measurement usually involves taking discrete samples from a larger volume (e.g., samples from the crystallizer magma), then cumulative or density distributions are expressed per unit of sample volume or per unit of filtered sample volume.

The population density versus size function of Eq. (1.6-4) is typically used to model CSDs. Population is used as the distributed variable (rather than mass) because of the importance of nucleation to the crystallization process. Linear size is used as the independent variable (rather than particle volume) because the rate of change of size, $G = dL/dt$, is often observed to

depend only on supersaturation rather than size. (This observation is stated as McCabe's ΔL law of crystal growth.)

The population versus particle volume function of Eq. (1.6-6) is typically used to model aerosols or CSD when breakage or agglomeration is more important than crystal growth in shaping the CSD. Volume v rather than size L is used because the volume (or mass) is conserved in breakage or agglomeration events but linear size is not conserved. For example, if a particle breaks into two pieces, the sum of the new masses equals the original mass but the sum of the new linear sizes does not equal the original size.

The mass versus particle volume function of Eq. (1.6-7) is useful for grinding simulations because mass is conserved in breakage events and because the PSD is not driven by population events at small sizes (nucleation).

It should be emphasized that *any* of the above density formulations could be used to model any particulate process. For example, agglomeration and/or breakage events can be formulated or transformed to conserve mass when using any of the above density functions.

Usage has naturally evolved into variables that are the most convenient for the system being studied.

EXAMPLE 1.6-1 CALCULATION OF CRYSTAL POPULATION DENSITY

Crystals from a crystal magma are sampled. The crystals are filtered quickly, dried and weighed. The slurry density M_T is found to be 0.1 g/cm³ of filtrate. The crystals are then sieved, and it is found that 0.1 mass fraction of the sample is in the size range 100–120 μm . The crystal density is $\rho = 2.0$ g/cm³ and the volumetric-shape factor is estimated to be $k_v = 0.6$. Calculate the population density at 110 μm . Express as number/cm³ μm and in SI units.

- i. Using the definition of population density from Eq. (1.6-4),

$$n_i = \Delta N_i / \Delta L_i$$

- ii. The number of crystals in the size range is calculated from the mass and shape factor using Eq. (1.5-3) as

$$\Delta N_i = \frac{\Delta M_i}{\rho k_v L_i^3} = \frac{(\Delta W_i) M_T}{\rho k_v L_i^3}$$

- iii. Thus population density is computed as

$$n_i = \frac{M_T (\Delta W_i / \Delta L_i)}{\rho k_v (\bar{L}_i)^3}$$

where \bar{L}_i is the average crystal size in the given size range.

iv. Substituting the previous numbers, we calculate population density as

$$n = \frac{(0.1 \text{ g/cm}^3)(0.1/20 \text{ } \mu\text{m})}{(0.6)(2.0 \text{ g/cm}^3)[(100 + 120)/2 \text{ } \mu\text{m}]^3} \times 10^{12} \text{ } \mu\text{m}^3/\text{cm}^3$$

or

$$n = 313 \text{ number/cm}^3 + \mu\text{m}$$

In SI units, the population density is

$$n = 3.13 \times 10^{14} \text{ number/m}^4 \quad \blacklozenge$$

Figure 1.6-1 illustrates the characteristic appearance of CSD plots presented as cumulative and density functions for number and mass versus particle size. The transformation from one presentation to the next (in the direction of the arrows) is also shown in this figure.

We have shown that particle distributions can be given by one of several analytical presentations. At this point, modeling of particulate processes can take one of two courses, namely, descriptive or predictive. That is, the CSD can be *described* using suitable analytic, but empirical, distribution functions with one or more adjustable parameters, or the CSD can be *predicted* from the solution of differential equations representing a balance of particles in the particle size domain. In this case the parameters of the

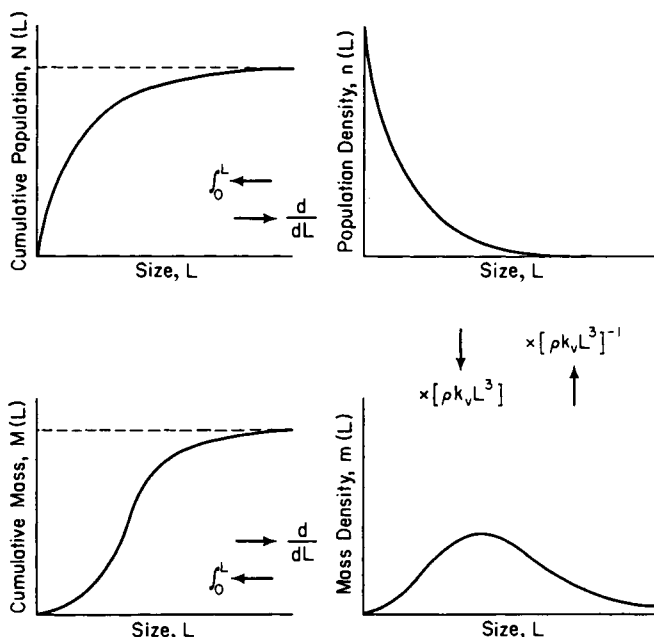


Fig. 1.6-1 A typical CSD presented in various forms: cumulative and density distributions of mass and number.

distribution are nested in the solution of the differential equation and often can be associated with a physical meaning, such as growth or nucleation rate.

The emphasis in this book will be almost entirely on the latter approach. However, Chapter 2 sets forth several common two-parameter empirical distribution functions. These empirical distribution functions can be quite useful to compress the CSD data into the numerical values of only two distribution parameters. Commercial materials can be bought and sold based on size specifications represented by these empirical distribution parameters.

1.7 Glossary of Particle Terms

It is recognized that many terms describing particle systems are used in a colloquial sense. For example, the terms agglomerate and aggregate are often used interchangeably in the engineering literature with little regard to prior definitions. Nevertheless, we set forth definitions of terms that are used consistently in this book, many of which have prior accepted definitions and usages.

*Agglomerate*²: A collection of two or more particles held together with strong interparticle forces, such as crystal bonds. Agglomerates cannot be broken up short of the stresses which would result in particle fracture.

*Aggregate*²: A collection of two or more particles held together with weak cohesive forces, such as Van der Waals forces. Aggregates can be dispersed with shear and/or solvents. Also called a flocculate.

Conglomerate: A particle morphology with a polycrystalline or aggregated appearance. Can be caused by aggregation of several particles, surface nucleation, and/or extensive twinning with growth of the newly formed surfaces. Generally used industrial term describing crystals that are *not* faceted.

*Crystal habit*³: The general shape of a crystal as given by the relative length of the various major axes. Words such as equant, columnar, acicular, tabular, and platelet are sometimes used to describe habit.

*Crystal morphology*³: The general appearance of crystals described by the Miller indices of the faces that show and give the crystals their characteristic shape.

Multicrystals (polycrystals): Highly twinned crystals or crystals with extensive surface nucleation, which grow randomly oriented crystal faces

²We follow here definitions different from those presented by Irani and Callis [1]. These definitions are consistent with, but not identical to, ASTM definitions [3].

³We follow here definitions and descriptions used in Toschev [2].

having a conglomerate appearance. Not faceted. Often have rosette appearance.

Particle: The smallest state of subdivision of solid matter that maintains the physical properties of the material and has a shape characteristic of the process that formed the material.

Particle morphology: The overall appearance and shape of particles, whether crystals or not.

Faceted (single crystals): Single-domain crystals with well-developed planar faces, usually with a specific crystal habit.

Twinned crystal: Faceted crystals that grow opposing faces at a reproducible angle relative to a line of symmetry passing through the crystal.

This list of terms is not exhaustive but illustrates many of the particle terms that will be used in this book. These are working definitions and do not ascribe any particular mechanism to the formation of such particles.

1.8 Summary

In this chapter we have motivated the study and prediction of PSD or CSD by illustrating the importance of particle size in the use and/or production of particulate materials. In particular, we describe some of the significant and unique interactions of CSD with the crystallization process. Some of the basic terms describing particle size, shape and appearance are defined, illustrated, and then summarized in a glossary of terms.

Presentation of data is illustrated using density and cumulative distribution functions, which are then defined in text. The alternatives of a descriptive vis-à-vis a predictive approach in formulating a theory of particulate processes are discussed, and the stage is set for the predictive theory that is developed throughout most of this book.

References

1. Irani, R. R., and Callis, C. F. (1963). "Particle Size: Measurement, Integration, and Application." Wiley, New York.
2. Toshev, S. (1973). In "Crystal Growth: An Introduction" (P. Hartman, ed.). North Holland/Ames Elsevier Press, Amsterdam.
3. American Society for Testing and Materials (1985). ASTM Designation E-20-85, Vol. 14.02, p. 19.

PARTICLE DISTRIBUTIONS

2.1 Introduction

Particulate dispersed-phase systems are inherently more difficult to describe than systems comprised of one or more bulk phases. Whereas temperature and composition, together with rate or equilibrium relationships, are often sufficient to characterize the latter systems, additional information is often needed and in fact is vital in characterizing particulate systems. Such additional information arises from the fact that one or more independent properties can be given values for each individual particle entity in the dispersed system. For example, consider droplets of one phase dispersed in a second, immiscible, phase, with mass transfer of a third, dilute, component occurring across the droplet interface. For each droplet, we can assign a value for its size and a value for the average concentration of the component being transferred. Thus, particle size and particle concentration are two independent property coordinates that can be given values at any time for each member in the system. A droplet can change in size by molecular additions or subtractions due to equilibrium changes in the amounts of the two immiscible phases or disappear as an entity by coalescence or redispersion, while particle concentration in a drop changes as mass transfer occurs. It is precisely these changes in the internal coordinate properties of the droplets that we wish to describe.

However, not all droplets are of the same size nor of the same concentration. Thus, there is a distribution of sizes and a distribution of concentra-

tions in the liquid droplets. In practice, it is usually not the coordinate property values of any one droplet that are of interest, but the entire distribution of values. Thus, the discrete particles in the system, with their individual coordinate values, are thought of as a continuous distribution. This continuous distribution may be represented analytically or empirically by a variety of graphical plots. This continuum approach to an inherently discrete system is quite justified when a large number of members are contained in any discrete sampling range of the particular property of interest.

Once a distribution function for a particulate system is obtained, all the properties of interest regarding the particulate phase are, in principle, known. Often, all that is required in an engineering problem is that some average property of the particulate phase be known. The distribution function can be readily integrated to obtain such averages.

The above two points regarding the continuum assumption and averages over the entire distribution point up some very practical considerations regarding sample size when experimental sampling of a distribution is to be done. The sample size (finite increment of the coordinate property) must be small enough so that, in fact, a point on the distribution curve is obtained, rather than the average, but large enough so that the number of members in the increment is significant. As an example of this point, consider the screening of a granular product that has been formulated by mixing 5 g of $(-100 + 120)$ -mesh material with 5 g of $(-140 + 170)$ -mesh material. Assume that a deck of 60-, 100-, and 170-mesh screens is used for analysis. All of the product reports to the 170-mesh screen, and all that can be said is that the material ranges from 88 to 149 μm in size. If the full $2^{1/4}$ range of screens is used, the material is seen to lie in the two size ranges, $-100 + 120$ and $-140 + 170$ mesh. If, on the other hand, the particles are divided into smaller and smaller size ranges, say by individual measurement under the microscope, there will eventually be a size range small enough so that either one or no particles are in that size range. At this point, indeed before this point, the continuum assumption breaks down and the discrete nature of the distribution becomes evident.

So far, two examples of property coordinates associated with individual members of a distribution have been mentioned. These examples were size and concentration distribution of droplets in a two-phase liquid suspension and size distribution of a granular material. These are, respectively, two- and one-dimensional distributions. It is evident that one may generalize the concept of size and say that a "size" distribution of a particulate system is a multidimensional distribution of the members of the system about their respective independent coordinate property axes. Complete information is known about the system when all of the coordinate proper-

ties necessary to characterize the system are included as independent variables in the distribution function.

It should be noted that the coordinate properties must be independent in order to completely specify the system with a minimum number of variables. In the previous example, the weight of the individual droplets could be specified as a third coordinate property. However, the weight of each droplet is a unique function of its size and concentration, and thus, droplet weight is a dependent variable and could not be used together with size and concentration to specify the distribution. Any two of the three variables—weight, size, and concentration—could be used as independent coordinate properties, and a two-dimensional distribution about these axes would uniquely specify the system.

One of the two examples chosen illustrates another property that sometimes is associated with a distribution, namely, its spatial concentration. In the case of the two-phase suspension, the droplets were distributed, uniformly in this case, in the continuous phase. In a poorly mixed system, we need to consider the distribution in space of the droplets in order to completely characterize such a system. In the case of the granular solid, spatial concentration has no meaning, and the material can be characterized by a single dimension, namely, particle size.

It is convenient to refer separately to the two types of coordinate axes as discussed above. Thus, we define:

1. Internal coordinate properties: properties associated with the internal state of the particle, such as size, concentration, chemical activity, or temperature.
2. External coordinates: x , y , z spatial coordinates giving the location of the particle.

The combined internal and external region is referred to as the particle phase space. In general, given m independent internal coordinates, particle phase space is an $(m + 3)$ -dimensional space, and an $(m + 3)$ -dimensional distribution is required to completely characterize the particulate phase.

2.2 Representation of Distributions

A variety of empirical forms exists to express a one-dimensional distribution about a coordinate axis. Such functions may represent the distribution of members of a population having the respective values of the independent property coordinate, that is, a population distribution, or the distribution function may represent the occurrence of some other dependent property of the population as it is distributed about the independent coordinate axis,

such as mass. These two distribution functions are, of course, closely related to each other, and can, in general, be transformed one to the other. An example is the particle-size distribution of a granular material. Such a size distribution can be expressed as population versus size or weight versus size. For geometrically similar particles, particle weight is proportional to particle size cubed, and thus, the weight distribution can be obtained from the population distribution by multiplying by size cubed.

Several one-dimensional two-parameter unimodal distribution functions are known¹ that can be used to empirically represent the PSD or CSD. Any number of parameters might be used in the distribution function, but a minimum of two is necessary to describe both the mean and variance of the distribution. If the function has more than two parameters, they are difficult to uniquely estimate from experiential data. Thus we choose five two-parameter unimodal distribution functions as illustrations and display various PSD properties of interest as a function of the two distribution parameters. The form of the distribution functions is flexible enough that most unimodal experimental distributions, such as number or mass, can be represented by one of the functions with an appropriate choice of parameters.

In the following discussion of empirical distribution functions, we use the terms described below.

$f(L)$, Density function of independent size variable L . The function $f(L)$ is normalized such that $\int_{L_{\min}}^{L_{\max}} f(L) dL = 1$.

$dF = f(L) dL$, Fraction of the distribution found in the size range L to $L + dL$.

$F(L)$, Cumulative function defined as $F = \int_{L_{\min}}^L f(L) dL$.

\bar{L} , Mean of distribution, defined as

$$\bar{L} = \int_{L_{\min}}^{L_{\max}} L f(L) dL$$

σ^2 , Variance of distribution, defined as

$$\sigma^2 = \int_{L_{\min}}^{L_{\max}} (L - \bar{L})^2 f(L) dL$$

(L_{\min}, L_{\max}) , Range of independent variable over which the distribution is defined and normalized.

¹See Kelly, Spottiswood [2] for an excellent discussion of empirical distribution functions commonly used to represent PSD from comminution processes.

2.3 Empirical Representation of Distributions

2.3.1 The Normal Distribution

The most widely known one-dimensional distribution function is the normal distribution, given as

$$f(L) = [1/\sigma(2\pi)^{1/2}] \exp[-(L - \bar{L})^2/2\sigma^2] \quad (2.3-1a)$$

Several properties of this distribution deserve mention. This distribution has two adjustable parameters, σ^2 and \bar{L} , which are, respectively, the variance and the mean, and are a measure of the uniformity and absolute size of the members of the population. It is obvious from the squared argument in the exponent that this function is symmetric about the mean, $L = \bar{L}$. Further, the distribution is normalized on the interval L in $(-\infty, \infty)$. The distribution is reduced by the dimensionless substitution

$$p = (L - \bar{L})/2^{1/2}\sigma \quad (2.3-1b)$$

Thus normalization is proved by substituting Eq. (2.3-1b) into Eq. (2.3-1a) and integrating over the entire distribution. Thus

$$\frac{1}{\pi^{1/2}} \int_{-\infty}^{\infty} e^{-p^2} dp = 1 \quad (2.3-1c)$$

Using the substitution of Eq. (2.3-1b), it is easily shown that the parameters σ^2 and \bar{L} in Eq. (2.3-1a) satisfy the definitions of variance and mean.

The normal distribution is widely used in the engineering sciences, but is of little or no use in describing particle-size distributions either population or weight basis simply because these distributions are typically very asymmetric and are poorly represented by the normal distribution. A further objection to use of the normal distribution in describing particle-size distributions is that finite populations are predicted for negative values of the size coordinate L . However, for large ratios of \bar{L}/σ , vanishingly small populations are predicted for negative values of L , and this fact in no way limits the use of this distribution function under such circumstances. The only valid objection is simply that this distribution function does not often fit the data.

The cumulative distribution F is given by substituting Eq. (2.3-1b) into Eq. (2.3-1a) and integrating over $(-\infty, p)$. Making use of symmetry and the fact that Eq. (2.3-1a) is an even function gives the cumulative function as

$$F(p) = 0.5[1 + \text{erf}(p)] \quad (2.3-1d)$$

where $\text{erf}(p) = (2/\pi^{1/2}) \int_0^p e^{-x^2} dx$. The value of p can be computed for any given values of L , mean \bar{L} , and variance σ^2 , as per Eq. (2.3-1b). Note that

$p < 0$ for all $L < \bar{L}$ and that $\text{erf}(-p) = -\text{erf}(p)$. The cumulative fraction $F(p)$ is then readily calculated from the error function. Note that at $L = 0$, $p = 0$ and $F(0) = 0.5$. Thus the mean is also the median for the normal distribution. Differentiation of the density distribution of Eq. (2.3-1a) and setting the deviative to zero gives $L_{\max} = \bar{L}$ (the mode). For the normal distribution, the mean, median, and mode are thus equal to the parameter \bar{L} .

2.3.2 Log-Normal Distribution

The log-normal (L-N) distribution is simply a normal distribution in terms of $\log L$. Thus the L-N distribution expressed as a density function is distributed about values of $\log L$ and is given as

$$f(\log L) = \left(1 / \left[(2\pi)^{1/2} \log \sigma'\right]\right) \times \exp\left[-(\log^2 L / \bar{L}') / (2 \log^2 \sigma')\right] \quad (2.3-2a)$$

with

$$dF = f(\log L) d(\log L)$$

The parameters \bar{L}' and σ' are respectively the geometric mean and geometric standard deviation. The fact that the mean is a geometric rather than arithmetic mean can be illustrated simply by considering the average (mean) with just two numbers in the distribution, L_1 and L_2 . Thus the mean \bar{L}' is seen to be

$$\log \bar{L}' = (\log L_1 + \log L_2) / 2 = \log(L_1 \times L_2)^{1/2}$$

or $\bar{L}' = (L_1 \times L_2)^{1/2}$, the geometric mean. The parameter σ' is similarly seen to be the standard deviation of the ratio L/\bar{L}' . The L-N distribution is normalized over the range $\log L$ in $(-\infty, \infty)$ or L in $(0, \infty)$. The dimensionless substitution that reduces the L-N is given as

$$p' = (\log L - \log \bar{L}') / 2^{1/2} \log \sigma' \quad (2.3-2b)$$

Normalization is demonstrated by bringing Eq. (2.3-2b) to Equation 2.3-2a and integrating over $\log L$ in $(-\infty, \infty)$ [or L in $(0, \infty)$]. Thus

$$\frac{1}{\pi^{1/2}} \int_{-\infty}^{\infty} e^{-p'^2} dp' = 1 \quad (2.3-2c)$$

The cumulative distribution is then calculated by bringing Eq. (2.3-2b) to Eq. (2.3-2a) and integrating over p' in $(-\infty, p')$ for $\log L$ in $(-\infty, \log L)$. Thus the cumulative distribution is given as

$$F(p') = 0.5[1 + \text{erf}(p')] \quad (2.3-2d)$$

It is thus seen that the cumulative F functions for the normal and

log-normal distributions are exactly the same; only the normalizing variables p and p' are different as calculated by Eq. (2.3-1b) and Eq. (2.3-2b).

Differentiation of the L-N density function and setting the derivative to zero shows that $\log L_{\max} = \log \bar{L}'$ and hence \bar{L}' is the mode size. The dimensionless variable $p' = 0$ at $\bar{L} = L'$ and hence $F(p' = 0) = 0.5$. Thus, as with the parameter \bar{L} in the normal distribution, the parameter \bar{L}' in the L-N distribution is the mode and the median. However, \bar{L}' is not the arithmetic mean of the L-N distribution.

2.3.3 Gamma Distribution

The density function for the gamma distribution is given in terms of the two parameters a and b as

$$f(L) = [\Gamma(a+1)(b/a)^{a+1}]^{-1} L^a \exp(-aL/b) \quad (2.3-3a)$$

The dimensionless substitution that reduces the gamma distribution is given as

$$z = aL/b \quad (2.3-3b)$$

Normalization is demonstrated by bringing Eq. (2.3-3b) to Eq. (2.3-3a) and integrating over the range L in $(0, \infty)$. Thus

$$\Gamma^{-1}(a+1) \int_0^\infty z^a e^{-z} dz = 1 \quad (2.3-3c)$$

The parameter b can be shown to be the mode size, while the parameter a determines whether the distribution is wide or narrow; large values of a give narrow distributions. The cumulative distribution is calculated by integrating the density distribution over the range $(0, L)$ and making the dimensionless substitution shown in Eq. (2.3-3b). Thus

$$F(z) = \Gamma^{-1}(a+1) \int_0^z z^a e^{-z} dz \quad (2.3-3d)$$

This cumulative gamma function for integer values of a can be integrated by parts and expressed as the finite series

$$F(z) = 1 - e^{-z}(1 + z + z^2/2! + z^3/3! + \cdots + z^a/a!) \quad (2.3-3d')$$

The gamma distribution is the predicted form of the number, area, and mass distributions for the mixed-suspension, mixed-product-removal (MSMPR) crystallizer discussed in Chapter 4. The mass distribution for the MSMPR crystallizer is given by the parameter $a = 3$ in the gamma distribution and is tabulated in Appendix A.

2.3.4 Rosin–Rammmler Distribution

The Rosin–Rammmler (R–R) distribution is a modified gamma function with a variable power of L in the exponential argument. Thus the R–R density function is given as

$$f(L) = nb'L^{(n-1)} \exp(-b'L^n) \quad (2.3-4a)$$

where n and b' are the two adjustable parameters in the distribution. A dimensionless substitution that reduces the R–R distribution is

$$x = b'L^n \quad (2.3-4b)$$

Normalization is demonstrated by bringing Eq. (2.3-4b) to Eq. (2.3-4a) [which reduces $f dL$ to $\exp(-x) dx$] and integrating over the limits L in $(0, \infty)$. Thus

$$\int_0^\infty \exp(-x) dx = 1 \quad (2.3-4c)$$

The cumulative distribution is then calculated simply as a zero-order gamma function of the argument $x = b'L^n$. Thus

$$F(x) = 1 - \exp(-x) \quad (2.3-4d)$$

The L–N, gamma, and R–R distributions are all useful for fitting experimental PSDs on a weight-size basis that are typically unimodal but skewed to the right (skewed toward the larger-sized particles).

2.3.5 Gaudin–Melloy Distribution

The Gaudin–Melloy (G–M) distribution is a modified power-law distribution that is commonly used to fit cumulative weight-size PSDs obtained from comminution processes. The density function for the G–M distribution is given as

$$f(L) = (m/L_m)[1 - (L/L_m)]^{m-1} \quad (2.3-5a)$$

where m and L_m are the two adjustable parameters. The distribution is normalized over the range L in $(0, L_m)$ and L_m has the meaning of the largest size of the particle distribution. The G–M distribution is reduced by the substitution

$$p = L/L_m \quad (2.3-5b)$$

Normalization is demonstrated by substitution of Eq. (2.3-5b) into Eq. (2.3-5a) and integrating on L in $(0, L_m)$. Thus

$$\int_0^1 m(1-p)^{m-1} dp = 1 \quad (2.3-5c)$$

The cumulative function is calculated as the integral of the density function. Thus

$$F(p) = 1 - (1 - p)^m \quad (2.3-5d)$$

The G-M density distribution is a monotonic function on the interval L in $(0, L_m)$.

2.4 Plotting and Parameter Estimation

Data are typically plotted on a cumulative basis, both to test the goodness of fit to a given distribution form and for estimation of the distribution parameters. If a linear plot of some function of $F(L)$ versus L can be found, a discrimination of the degree of data fit can easily be made, for example with a linear least-squares calculation. The normal (N), L-N, and R-R distributions all have characteristic linear plots that can be made from raw size data expressed on a cumulative basis, that is, the $F(L)$ function. The G-M distribution can also be plotted directly on a log plot, provided the maximum size parameter L_m is known or estimated. Specific model parameters can be obtained from these linear plots, as well as a judgment as to the appropriateness of the distribution function. Density plots are seldom used for parameter estimation but are often the best way to present data to exhibit specific characteristics, such as bimodal form. Figure 2.4-1 plots density functions from the N, L-N, and gamma distributions having the same mode and coefficient of variation. Note that these curves are not all normalized on the linear size axis L used in this common plot. It would be difficult to distinguish which empirical function gave the best fit to an experimental distribution based on such density plots.

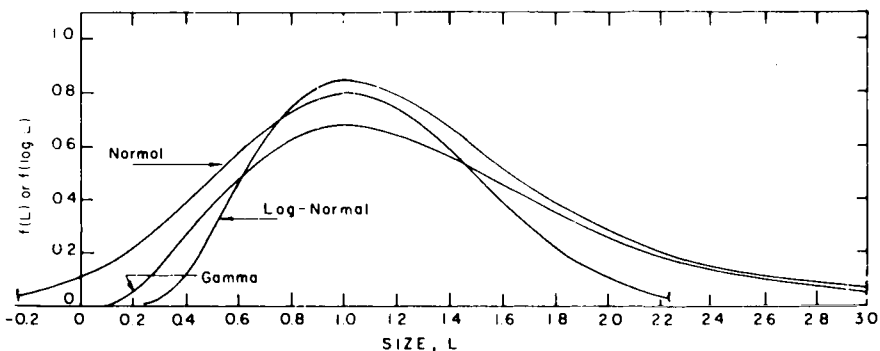


Fig. 2.4-1 Plot of three distribution functions having identical modes and coefficients of variation.

2.4.1 Plotting the Normal Distribution

The normal distribution is linear when cumulative fraction is plotted on normal probability paper. The parameters \bar{L} and σ are readily found from the $F(p)$ function. Thus at $L = \bar{L}$, $p = (\bar{L} - \bar{L})/2^{1/2}\sigma = 0$. From Eq. (2.3-1d), $F(0) = 0.5$. Thus the parameter \bar{L} is merely the size on the normal probability plot at which $F = 0.5$, that is, the median size. The parameter σ can be found by evaluating the $F(p)$ distribution at $L = \bar{L} + \sigma$, that is, one standard deviation above the median. Thus

$$p = (\bar{L} + \sigma - \bar{L})/2^{1/2}\sigma = \frac{1}{2}^{1/2}$$

Thus $F(0.707)$ from Eq. (2.3-1d) is found to be 0.84 and the parameter σ is

$$\sigma = L[F(\bar{L} + \sigma)] - L[F(\bar{L})]$$

or

$$\sigma = L_{84} - L_{50}$$

Advantage can be taken of the symmetry of the N distribution. Thus perhaps a more accurate estimation would be

$$\sigma = (L_{84} - L_{16})/2$$

2.4.2 Plotting the Log-Normal Distribution

The L-N distribution is merely an N distribution in terms of $\log L$. The cumulative function F plots linearly on log-probability paper. The parameters are obtained as above with the N-distribution except that $\log L$ instead of L is used. Thus

$$p'(\bar{L}') = (\log \bar{L}' - \log \bar{L}')/(2^{1/2} \log \sigma') = 0$$

Thus \bar{L}' (or $\log \bar{L}'$) is again the median size and would be found as L_{50} on the log-probability plot. The parameter $\log \sigma'$ is found by evaluating $F(p')$ at

$$\begin{aligned} p' &= (\log \bar{L}' + \log \sigma' - \log \bar{L}')/2^{1/2} \log \sigma' \\ &= \frac{1}{2}^{1/2} \end{aligned}$$

which again gives $F(0.707) = 0.84$. Similarly, $\log \sigma'$ is found as

$$\log \sigma' = \log L[F(\log \bar{L}' + \log \sigma')] - \log L[F(\log \bar{L}')]]$$

which gives

$$\log \sigma' = \log L_{84} - \log L_{50}$$

or

$$\sigma' = L_{84}/L_{50}$$

2.4.3 Gamma Distribution

No variable grouping exists that reduces the $F(z)$ function for the gamma distribution to a single unique plot. This conclusion can readily be deduced from Eq. (2.3-3d'), which shows a variable number of terms as a function of the wideness parameter a . Thus it is impossible to *a priori* test the gamma function for goodness of fit or obtain parameter estimates from a simple linear plot. However, the mode size is represented by the parameter b , and this parameter could be crudely estimated as the maximum in a density function plot. For the particular gamma function of the MSMPR crystallizer (see Chapter 4), the wideness parameter is $a = 3$ and the median size occurs at $z = 3.67$. This observation can sometimes be used in conjunction with the MSMPR crystallizer meaning of the parameters a and b to rapidly estimate crystal growth and nucleation rate.

EXAMPLE 2.4.1

In Chapter 4 it is shown that the parameter ratio b/a for the MSMPR distribution is equal to $G\tau$, the product of crystal growth rate with retention time. Estimate the crystal growth rate if the retention time is 1 h and the median size is $L_{50} = 400 \mu\text{m}$. Thus

$$z_{\text{median}} = 3.67 = L_{50}/G\tau$$

or

$$G = 400 \mu\text{m} / (3.67 \times 60 \text{ min})$$

$$G = 1.8 \mu\text{m}/\text{min} \quad \blacklozenge$$

2.4.4 Plotting the Rosin–Rammler Distribution

The F function for the R–R distribution is given by Eq. (2.4-4d) as $F(z) = 1 - \exp(-x)$ where $x = b'L^n$. Rearranging gives $1 - F = \exp(-x)$. Taking logs of both sides gives $\log[1 - F]^{-1} = b'L^n$. Again, taking the log of both sides gives

$$\log[\log(1 - F)^{-1}] = \log b' + n \log L$$

where it is recognized that $\log(1 - F)^{-1}$ is a positive quantity. Thus a plot of $\log[-\log(1 - F)]$ versus $\log L$ should be a straight line with a slope of n and intercept $\log b$. This R–R plot is commonly used to represent unimodal weight–size distributions. The R–R parameters n and b' are readily obtained from such plots.

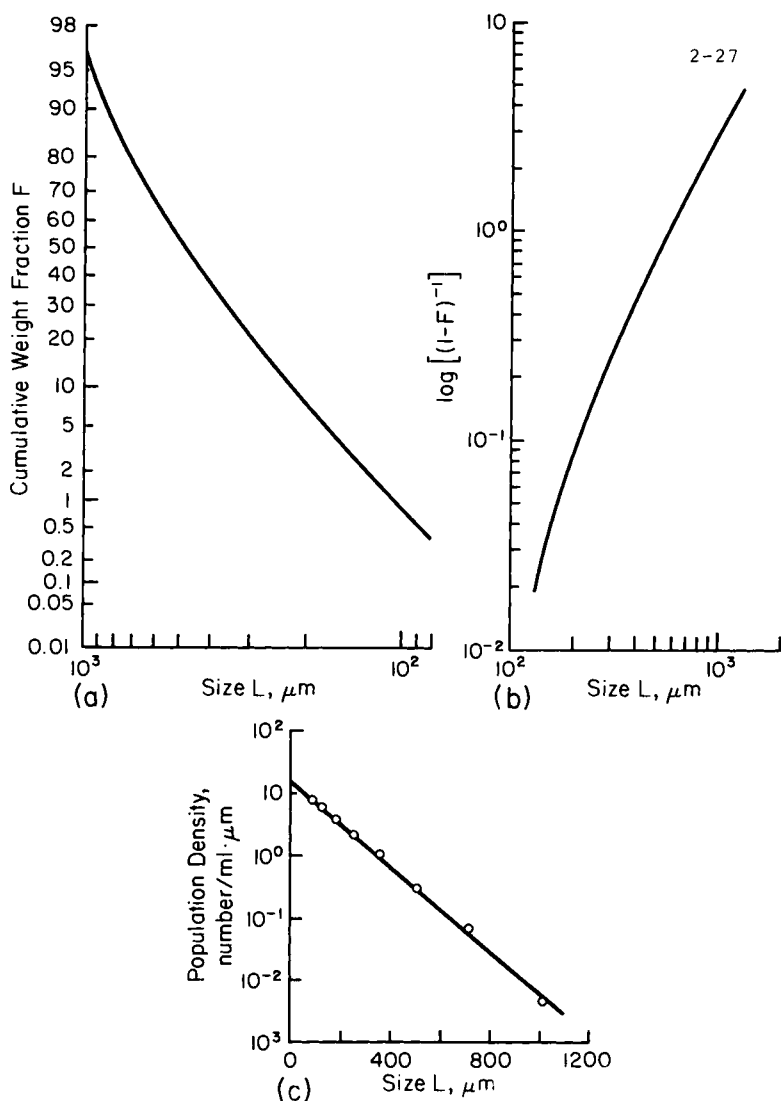


Fig. 2.4-2 Cumulative weight fraction and population density plots for KCl produced in an MSMPR crystallizer. (a) Weight fraction as log-normal plot, (b) weight fraction as Rosin-Rammler plot, and (c) population density on semilog plot.

2.4.5 Plotting the Gaudin-Melloy Distribution

The cumulative function for the G-M distribution was given as

$$F(p) = 1 - (1 - p)^m \quad (2.3-5d)$$

This form suggests plotting $\log[1 - F]$ versus $\log(1 - p)$. Such a plot should be linear and have a slope of m .

Figure 2.4-2 plots KCl population data from an MSMR crystallizer as (a) converted to weight fraction and plotted on log-probability plot, (b) the same on R-R plot, and (c) a log population density n versus L plot as indicated for the MSMR distribution (see Chapter 4). These data fit the theoretical MSMR distribution tabulated in Appendix A, represented by the parameters $a = 3$ and $b = 130 \mu\text{m}$ (of the gamma weight distribution). Note that neither Fig. 2.4-2a nor Fig. 2.4-2b yields straight lines when plotting third-order gamma distributions.² However, the L-N and R-R distributions would probably be more appropriate than either the normal or G-M distributions. No linear way is known to plot these data as a gamma distribution except on a population basis, that is, as per Fig. 2.4-2c. Later chapters will show that $\log n$ versus L is the characteristic plot for CSD from continuous crystallizers, and such plots reveal much information about the mode of operation.

2.5 Average Properties from Density-Distribution Functions

If the size-distribution information contained in a two-parameter distribution function were to be compressed into two terms that best described the distribution in a qualitative sense, these terms would undoubtedly be the mean and the coefficient of variation, that is, how large the particles are and how much size variation they have relative to the mean size. The arithmetic mean and coefficient of variation are respectively defined in terms of a normalized density function as

$$\bar{L} = \int_0^\infty L f(L) dL \quad (2.5-1)$$

and

$$\text{c.v.} = \sigma / \bar{L} \quad (2.5-2)$$

where the variance is given as

$$\sigma^2 = \int_0^\infty (L - \bar{L})^2 f(L) dL \quad (2.5-3)$$

² If we *a priori* assume $a = 3$, the gamma distribution is reduced to one parameter b , and a unique $F(L)$ versus L plot can be made. Appendix A shows gamma-3 paper, which can be used for plotting cumulative weight distributions from continuous MSMR crystallizers.

Equations (2.5-1) and (2.5-3) show that the mean size is given by the first moment of the distribution (the moment about size zero), while σ^2 can be expanded in terms of the first three moments. Thus a desirable property of any empirical distribution function is that the moments are easily determined in terms of the distribution parameters.

2.5.1 Moments of Normal Distribution

The moments of the normal distribution are found in terms of the distribution parameters, \bar{L} and σ . Thus the j th moment of the distribution is defined as

$$m_j \equiv \int_{L_{\min}}^{L_{\max}} L^j f(L) dL \quad (2.5-4)$$

For the normal distribution this becomes

$$m_j \equiv \frac{1}{\sigma(2\pi)^{1/2}} \int_{-\infty}^{\infty} L^j \exp\left[-\frac{(L - \bar{L})^2}{2\sigma^2}\right] dL \quad (2.5-5)$$

Again define $z = (L - \bar{L})/2^{1/2}\sigma$. Thus

$$m_j = \pi^{-1/2} \int_{-\infty}^{\infty} L^j \exp(-z^2) dz \quad (2.5-6)$$

But

$$L^j = (\bar{L} + 2^{1/2}\sigma z)^j$$

which can be expanded using the binomial expansion as

$$L^j = \sum_{r=0}^j c_r^j (2^{1/2}\sigma z)^{j-r} (\bar{L})^r$$

where

$$c_r^j = j! / (j-r)! r!$$

Substituting gives

$$m_j = \frac{1}{\pi^{1/2}} \int_{-\infty}^{\infty} \sum_{r=0}^j \left[\frac{j!}{(j-r)! r!} \right] (2^{1/2}\sigma z)^{j-r} (\bar{L})^r \exp(-z^2) dz \quad (2.5-7)$$

Recognizing that the odd terms in z will integrate to zero over the interval $(-\infty, \infty)$ and interchanging integration and summation gives

$$m_j = \int_r \frac{(2^{1/2}\sigma)^{j-r} (\bar{L})^r j!}{(j-r)! r!} \left(\frac{1}{\pi^{1/2}} \right) \int_{-\infty}^{\infty} z^{j-r} \exp(-z^2) dz \quad (2.5-8)$$

where

$$\begin{aligned} r &= 0, 2, 4, \dots, j && \text{for } j \text{ even} \\ r &= 1, 3, 5, \dots, j && \text{for } j \text{ odd} \end{aligned}$$

However, the expression under the integral can be integrated to

$$\int_{-\infty}^{\infty} z^{2n} \exp(-z^2) dz = [1 \cdot 3 \cdot 5 \cdots (2n-1)/2^n] \pi^{1/2}, \quad n = 0, 1, 2, \dots \quad (2.5-9)$$

Thus, the j th moment of the normal distribution function is given as

$$m_j = \sum_r \left[(2^{1/2} \sigma)^{j-r} (\bar{L})^r j! \cdot \frac{1 \cdot 3 \cdots (j-r-1)}{(j-r)! r! 2^{(j-r)/2}} \right] \quad (2.5-10)$$

where again

$$\begin{aligned} r &= 0, 2, 4, \dots, j && \text{for } j \text{ even} \\ r &= 1, 3, 5, \dots, j && \text{for } j \text{ odd} \end{aligned}$$

Writing this expression out for the first few moments, in terms of the mean and coefficient of variation, \bar{L} and σ/\bar{L} , the following equations result:

$$\begin{aligned} m_0 &= 1, & m_1/\bar{L} &= 1 \\ m_2/(\bar{L})^2 &= 1 + (\sigma/\bar{L})^2, & m_3/(\bar{L})^3 &= 1 + 3(\sigma/\bar{L})^2 \\ m_4/(\bar{L})^4 &= 1 + 6(\sigma/\bar{L})^2 + 3(\sigma/\bar{L})^4 \end{aligned} \quad (2.5-11)$$

Note that for a single-size distribution, $\sigma/\bar{L} = 0$, and the j th moment is equal to the j th power of the (uniform) size. The normal distribution clearly does not satisfy the desirable property of being easy to integrate.

2.5.2 Moments of the Log-Normal Distribution

For the log-normal distribution, the j th moment is defined as

$$m_j \equiv \frac{1}{(2\pi)^{1/2} \log \sigma'} \int_{-\infty}^{\infty} L^j \exp \left[-\frac{(\log L - \log \bar{L}')^2}{2 \log^2 \sigma'} \right] d(\log L) \quad (2.5-12)$$

Letting $z = (\log L - \log \bar{L}')/(2^{1/2} \log \sigma')$ gives

$$m_j = (\bar{L}')^j \pi^{-1/2} \int_{-\infty}^{\infty} \left(\frac{L}{\bar{L}'} \right)^j \exp(-z^2) dz \quad (2.5-13)$$

But

$$L/\bar{L}' = \exp(2^{1/2} \log \sigma' z)$$

Thus

$$m_j = (\bar{L}')^j \pi^{-1/2} \int_{-\infty}^{\infty} \exp\{-[(-j2^{1/2} \log \sigma' z) + z^2]\} dz \quad (2.5-14)$$

Completing the square gives

$$m_j = (\bar{L}')^j \pi^{-1/2} \exp\left(\frac{1}{2} j^2 \log^2 \sigma'\right) \int_{-\infty}^{\infty} \exp(-p^2) dp \quad (2.2-15)$$

where

$$p = z - j(2^{1/2}/2) \log \sigma'$$

Finally, recognizing the value of the above integral as $\pi^{1/2}$ gives

$$m_j = (\bar{L}')^j \exp\left(\frac{1}{2} j^2 \log^2 \sigma'\right) \quad (2.5-16)$$

or, in terms of log functions,

$$\log m_j = j \log \bar{L}' + \frac{1}{2} j^2 \log^2 \sigma' \quad (2.5-17)$$

Writing this out for the first few moments gives

$$\begin{array}{ll} \log m_0 = 0 & \text{or} \quad m_0 = 1 \\ \log m_1 = \log \bar{L}' + \frac{1}{2} \log^2 \sigma' & \text{or} \quad m_1/\bar{L}' = \exp\left(\frac{1}{2} \log^2 \sigma'\right) \\ \log m_2 = 2 \log \bar{L}' + 2 \log^2 \sigma' & \text{or} \quad m_2/(\bar{L}')^2 = \exp(2 \log^2 \sigma') \\ \log m_3 = 3 \log \bar{L}' + 4.5 \log^2 \sigma' & \text{or} \quad m_3/(\bar{L}')^3 = \exp(4.5 \log^2 \sigma') \end{array} \quad (2.5-18)$$

Again, for a single-size distribution, $\log \sigma' = 0$, and the j th moment is equal to the j th power of the size.

2.5.3 Moments of the Gamma Distribution

Compute the j th moments of the normalized gamma distribution given by Eq. (2.2-3a). By definition,

$$m_j \equiv \left(\int_0^{\infty} L^j L^a e^{-aL/b} dL \right) / \Gamma(a+1) \left(\frac{b}{a} \right)^{a+1} \quad (2.5-19)$$

Canceling $(b/a)^{a+1}$ terms and recognizing the integral as a gamma function gives

$$m_j = b^j \Gamma(j+a+1) / a^j \Gamma(a+1) \quad (2.5-20)$$

from which it is apparent that $m_0 = 1$, a necessary check on the normalization of the original distribution function. The first few moments can be

written out in terms of the two parameters a and b as

$$\begin{aligned} m_1/b &= \Gamma(a+2)/a\Gamma(a+1) = (a+1)/a \\ m_2/b^2 &= \Gamma(a+3)/a^2\Gamma(a+1) = (a+2)(a+1)/a^2 \\ m_3/b^3 &= \Gamma(a+4)/a^3\Gamma(a+1) = (a+3)(a+2)(a+1)/a^3 \end{aligned} \quad (2.5-21)$$

Note that the parameter b in the distribution function is an equivalent size, and in fact is the mode of the distribution. Differentiating the gamma distribution, Eq. (2.2-3a), with respect to L and setting the derivation to zero indicates that the mode of the distribution occurs at $L = b$, independent of the parameter a . As the parameter a increases, the distribution narrows and approaches the single uniform mode size b . Thus for $a \rightarrow \infty$, $[\Gamma(a+j+1)/a^j\Gamma(a+1)] \rightarrow 1$, and the j th moment equals the mode size raised to the j th power.

2.5.4 Moments of the Rosin–Rammler Distribution

The j th moment of the R–R distribution can be written using the R–R density distribution [Eq. (2.3-4a)],

$$m_j = nb' \int_0^\infty L^{n+j-1} \exp(-b'L^n) dL \quad (2.5-22)$$

Again this integral is reduced by the substitution $z = b'L^n$. With this substitution the j th moment becomes

$$m_j = [(b')^{-j/n}] \int_0^\infty z^{j/n} \exp(-z) dz \quad (2.5-23)$$

or

$$m_j = (1/b')^{j/n} \Gamma(j/n + 1) = (1/b')^{j/n} \Gamma(j + n)/n \quad (2.5-24)$$

where $\Gamma(x+1)$ is the gamma function equal to $x!$ for x an integer and is a widely tabulated function for noninteger arguments. Writing out the first few moments of the R–R distribution gives

$$m_0 = 0! = 1$$

(which demonstrates normalization)

$$\begin{aligned} m_1 &= [1/(b')^{1/n}] \Gamma[(n+1)/n] \\ m_2 &= [1/(b')^{2/n}] \Gamma[(n+2)/n] \\ m_3 &= [1/(b')^{3/n}] \Gamma[(n+3)/n] \\ &\vdots \end{aligned} \quad (2.5-25)$$

Note that for $n = 1$ these moments reduce to the moments of the zero-order gamma distribution. [For this case $\lim(a/b)_{\Gamma \text{ dist}} = 1/b'_{\text{R-R dist}}$].

2.5.6 Moments of the Gaudin–Melloy Distribution

The j th moment of the G–M distribution can be written in terms of the density distribution as

$$m_j = \frac{m}{L_m} \int_0^{L_m} L^j \left[1 - \left(\frac{L}{L_m} \right) \right]^{m-1} dL \quad (2.5-26)$$

Reducing Eq. (2.5-2b) with the transformation $p = L/L_m$ gives the moments as

$$\frac{m_j}{L_m^j} = m \int_0^1 p^j (1-p)^{m-1} dp \quad (2.5-27)$$

Equation (2.5/27) can be integrated by parts repeatedly to give the j th moment as

$$m_j/L_m^j = j! / [(m+1)(m+2) \cdots (m+j)] \quad (2.5-28)$$

For the parameter $m \rightarrow 0$ the G–M distribution approaches a monosize distribution at $L \rightarrow L_m$ and $m_j \rightarrow L_m^j$.

2.6 Mean Size and Coefficient of Variation

As discussed in Section 2.5, the two most representative terms describing a particle distribution are the mean and the coefficient of variation (c.v.) (wideness of the distribution). We indicated that these terms were derivable directly in terms of the leading moments of the distribution, and having found the moments we are now in a position to state the mean and c.v. in terms of the two parameters of the distribution function.

The calculated moments of a distribution function might not be normalized, and thus we develop formulas that will apply to functions that may or may not be normalized. The mean is given as

$$\bar{L}_{1,0} = \int_0^\infty L f(L) dL / \int_0^\infty f(L) dL \quad (2.6-1)$$

or

$$\bar{L}_{1,0} = m_1/m_0$$

Thus the mean is seen to be the ratio of the first to zeroth moments of a given distribution function, whether normalized or not.

The coefficient of variation is given as

$$\text{c.v.} = \sigma / \bar{L}_{1,0} \quad (2.6-2)$$

where

$$\sigma^2 = \frac{1}{m_0} \int_0^\infty (L - \bar{L}_{1,0})^2 f(L) dL$$

This equation can be expanded in terms of the moments of the distribution as

$$\sigma^2 = m_2/m_0 - m_1^2/m_0 \quad (2.6-3)$$

Thus c.v. is given in terms of the moments as

$$\text{c.v.} = (m_0 m_2 / m_1^2 - 1)^{1/2} \quad (2.6-4)$$

or, for a normalized distribution, the familiar formula

$$\text{c.v.} = (m_2 / m_1^2 - 1)^{1/2} \quad (2.6-4')$$

is given.

Nothing has been implied thus far in this chapter as to the physical representation given by the various distribution functions described, that is, whether they represent weight-size, number-size, number-volume, etc. Thus all statistical terms reported are for the distribution itself. If in fact the distribution were a population-size distribution, then properties expressed in terms of moments could be found for the weight-size distribution by simply incrementing 3 in the order of the moments. As a specific example, if the leading moments were obtained from integration of a numerically defined population density function, then³

$$\bar{L}_{\text{pop}} = m_1/m_0 = \bar{L}_{1,0} \quad (2.6-5)$$

and

$$\bar{L}_{\text{wt}} = m_4/m_3 = \bar{L}_{4,3}$$

Similarly,

$$(\text{c.v.})_{\text{pop}} = (m_0 m_2 / m_1^2 - 1)^{1/2} \quad (2.6-6)$$

and

$$(\text{c.v.})_{\text{wt}} = (m_3 m_5 / m_4^2 - 1)^{1/2}$$

If analytical empirical distribution functions are given, it is then simple to express all calculated terms as functions of the two distribution parameters.

2.6.1 Mean and Coefficient of Variation for the Normal Distribution

The parameter \bar{L} in the normal distribution satisfies the definition of mean, while the parameter σ^2 satisfies the definition of variance. Thus

$$\bar{L}_{1,0} = \frac{1}{(2\pi)^{1/2}\sigma} \int_{-\infty}^{\infty} L \exp\left[-\frac{(L-\bar{L})^2}{2\sigma^2}\right] dL \quad (2.6-7)$$

and

$$\sigma^2 = \frac{1}{(2\pi)^{1/2} \log \sigma} \int_{-\infty}^{\infty} (L-\bar{L})^2 \exp\left[-\frac{(L-\bar{L})^2}{2\sigma^2}\right] dL \quad (2.6-8)$$

³We use the convention throughout this book that $\bar{L}_{i,j}$ is the ratio of moments m_i/m_j .

However, we can use the previously calculated moments with Eq. (2.6-1) and (2.6-4) to directly solve for the mean and coefficient of variation in terms of the distribution parameters. Thus

$$\bar{L}_{1,0} = m_1/m_0 = \bar{L}/1.0 = \bar{L} \quad (2.6-9)$$

and

$$\text{c.v.} = (m_0 m_2 / m_1^2 - 1)^{1/2} = \left(\frac{\bar{L}^2 + \sigma^2}{\bar{L}^2} - 1 \right)^{1/2} = \frac{\sigma}{\bar{L}} \quad (2.6-10)$$

2.6.2 Mean and Coefficient of Variation for the Log-Normal Distribution

Again we use the calculated moments of the L-N distribution together with Eq. (2.6-1) and (2.6-4). Thus

$$\bar{L}_{1,0} = L' \exp[1/(2 \log^2 a')]/1 \quad (2.6-11)$$

and

$$\text{c.v.} = \left\{ \frac{(\bar{L}')^2 \exp(2 \log^2 \sigma')}{[\bar{L}' \exp(\frac{1}{2} \log^2 \sigma')]^2} - 1 \right\}^{1/2} \quad (2.6-12)$$

$$\text{c.v.} = [\exp(2 \log^2 \sigma' - \log^2 \sigma') - 1]^{1/2}$$

$$\text{c.v.} = [\exp(\log^2 \sigma') - 1]^{1/2}$$

2.6.3 Mean and Coefficient of Variation for Gamma Distribution

Again, we calculate

$$\bar{L}_{1,0} = m_1/m_0 = (b/a)(a+1) \quad (2.6-13)$$

and

$$\text{c.v.} = [(m_2/m_1^2) - 1]^{1/2}$$

$$\text{c.v.} = \{[\Gamma(a+3)\Gamma(a+1)/\Gamma^2(a+2)] - 1\}^{1/2}$$

Using the recursive relationship

$$\Gamma(a+1) = a\Gamma(a)$$

then

$$\text{c.v.} = \{[(a+2)/(a+1)] - 1\}^{1/2}$$

or finally,

$$\text{c.v.} = 1/(a+1)^{1/2} \quad (2.6-14)$$

2.6.4 Mean and Coefficient of Variation for Rosin-Rammler Distribution

$$\bar{L}_{1,0} = m_1/m_0 = (1/b')^{1/n} \Gamma[(n+1)/n] \quad (2.6-15)$$

Table 2.6-1

Properties of Some Empirical Distribution Functions^a

	Normal	Log-normal	Gamma	Rosin-Rammler	Gaudin-Melloy
Density distribution	$f(L) = [(2\pi)^{1/2} \sigma]^{-1} \times \exp\left[-\left(\frac{L - \bar{L}}{\sqrt{2} \sigma}\right)^2\right]$	$f(\log L) = [(2\pi)^{1/2} \log \sigma']^{-1} \times \exp\left[-\left(\frac{\log L/\bar{L}'}{\sqrt{2} \log \sigma'}\right)^2\right]$	$f(L) = [\Gamma(a+1)(b/a)^{a+1}]^{-1} L^a \exp(-aL/b)$	$f(L) = nb' L^{n-1} \exp(-b' L^n)$	$f(L) = (m/L_m)[1 - L/L_m]^{m-1}$
Parameter range	L in $(-\infty, \infty)$	L in $(0, \infty)$	L in $(0, \infty)$	L in $(0, \infty)$	L in $(0, L_m)$
Dimensionless size	$p = (L - \bar{L})/2^{1/2} \sigma$	$p' = \log(L/\bar{L}')/2^{1/2} \log \sigma'$	$z = aL/b$	$x = b' L^n$	$p = L/L_m$
Cumulative distribution	$F(p) = 0.5[1 + \operatorname{erf}(p)]$	$F(p') = 0.5[1 + \operatorname{erf}(p')]$	$F(z) = 1 - \exp(-z)[1 + z + z^2/2! + 2^3/3! + \dots + z^a/a!]$, a an integer	$F(x) = 1 - \exp(-x)$	$F(p) = 1 - (1-p)^m$
Mean size	\bar{L}	$\bar{L}'[\exp(0.5) \log^2 \sigma']$	$b(a+1)/a$	$1/b'$	$L_m/(m+1)$
Mode size	\bar{L}	\bar{L}'	b	$1/(nb')^{1/n}$	—
Median size	\bar{L}	\bar{L}'	Median is a function of parameter a : $L_{50} = 3.67b/a$ for $a = 3$ (MSMPR distribution); $L_{50} \rightarrow b/a$ for $a \rightarrow \infty$	$L_{50} = [(\log 2)/b']^{1/n}$	$L_{50} = L_m[1 - (0.5)^{1/m}]$
Moments about $L = 0$	$m_0 = 1$; $m_1 = \bar{L}$; $m_2 = (\bar{L})^2 + \sigma^2$ $m_3 = (\bar{L})^3 + 3\sigma^2 \bar{L}$ $m_4 = (\bar{L})^4 + 6\sigma^2 \bar{L}^2 + 3\sigma^4$	$m_j = (\bar{L}')^j \exp[0.5 j^2 \log^2 \sigma']$	$m_j = b' \Gamma(a+j+1)/a' \Gamma(a+1)$	$m_j = b^{-j/n} \Gamma[(n+j)/n]$	$m_j = L_m j! / [(m+1)(m+2) \dots (m+j)]$
Coefficient of variation	σ/\bar{L}	$[\exp(\log^2 \sigma') - 1]^{1/2}$	$1/(a+1)^{1/2}$	$\{\Gamma[(n+2)/n]/\Gamma^2[(n+1)/n] - 1\}^{1/2}$	$[m/(m+2)]^{1/2}$

^aSeveral properties of the PSD might be modeled by these distributions. These average properties will be different for a given PSD depending on what is represented by the distribution, such as population, area, or mass. For example, the "mean size" could be a population, area, or mass mean size, depending on the quantity modeled by the distribution function.

and

$$\text{c.v.} = \left\{ \frac{(1/b')^2 \Gamma[(n+2)/n]}{(1/b')^2 \Gamma^2[(n+1)/n]} - 1 \right\}^{1/2} \quad (2.6-16)$$

or

$$\text{c.v.} = \{ \Gamma[(n+2)/n] / \Gamma^2[(n+1)/n] - 1 \}^{1/2} \quad (2.6-17)$$

2.6.5 Mean and Coefficient of Variation for Gaudin-Melloy Distribution

$$\bar{L}_{1,0} = m_1/m_0 = L_m/(m+1) \quad (2.6-18)$$

$$\text{c.v.} = \left[\frac{2L_m^2/(m+1)(m+2)}{L_m^2/(m+1)^2} - 1 \right]^{1/2} \quad (2.6-19)$$

or

$$\text{c.v.} = [m/(m+2)]^{1/2} \quad (2.6-20)$$

Table 2.6-1 displays properties of the five empirical distributions discussed in this chapter.

2.7 Truncated Distributions, Skewness, and Kurtosis

2.7.1 Truncation

In many cases, classification and growth processes truncate a distribution of particles below a minimum size L_1 and/or above a maximum size L_2 . A four-parameter distribution useful for the characterization of such particle distributions is

$$f(\log L) = \frac{1}{(2\pi)^{1/2} \log \sigma'} \exp \left\{ - \left[\log \frac{(L-L_1)(L_2-L_1)/(L_2-L)\bar{L}'}{2^{1/2} \log \sigma'} \right]^2 \right\} \quad (2.7-1)$$

where L_1 , L_2 , \bar{L}' , and σ' are the four adjustable parameters. As $L_1 \rightarrow 0$ and $L_2 \rightarrow \infty$, Eq. (2.7-1) reduces to Eq. (2.3-2a), the log-normal distribution. This equation is also normalized over the particle range of interest such that

$$\int_{L=L_1}^{L=L_2} f(\log L) d \left\{ \log \left[\frac{(L-L_1)}{(L_2-L)} \right] \right\} = 1 \quad (2.7-2)$$

The parameters \bar{L}' and σ' have equivalent definitions in terms of the

argument $d\{\log[(L - L_1)/(L_2 - L)]\}$. Thus,

$$\begin{aligned} \log \bar{L}' &\equiv \int_{L=L_1}^{L=L_2} \log \left[\frac{(L - L_1)(L_2 - L_1)}{(L_2 - L)} \right] \\ &\quad \times f(\log L) d \left\{ \log \left[\frac{(L - L_1)}{(L_2 - L)} \right] \right\} \end{aligned} \quad (2.7-3)$$

and

$$\begin{aligned} \log^2 \sigma' &\equiv \int_{L=L_1}^{L=L_2} \left\{ \log \left[\frac{(L - L_1)(L_2 - L_1)}{(L_2 - L)} \right] - \log \bar{L}' \right\}^2 \\ &\quad \times f(\log L) d \left\{ \log \left[\frac{(L - L_1)}{(L_2 - L)} \right] \right\} \end{aligned} \quad (2.7-4)$$

Again \bar{L}' and σ' as defined in Eqs. (2.7-3) and (2.7-4) are the same as the parameters in Eq. (2.7-1).

Equation (2.7-1) has been used for the representation of abnormal particle-size distributions created by classification, sieving, and/or mixing particle samples [1].

Although the log-normal distribution is purely empirical, and there is no direct relation between the parameters \bar{L}' and σ' and processes governing the formation of a particle distribution, nevertheless this distribution form is widely used in the analysis and characterization of particulate materials. Ranges of the parameters \bar{L}' and σ' are often stated as part of the specifications in the purchase of granular material.

2.7.2 Skewness and Kurtosis

Thus far, two measures have been developed to describe the absolute size and the relative size uniformity of the members of a distribution. These measures are the mean \bar{L} and the relative size spread or coefficient of variation σ/\bar{L} . In addition to these measures, two other numbers are often used to qualitatively indicate the shape of a distribution. These latter measures are the skewness and kurtosis of the distribution, both measured relative to a normal distribution. Skewness is a measure of the symmetry about the mean and is zero for symmetric distributions. Define the j th moment about the mean as

$$\mu_j \equiv \int_{-\infty}^{\infty} (L - \bar{L})^j f(L) dL \quad (2.7-5)$$

By definition, $\mu_1 = 0$ for a symmetric distribution. Recall that $\mu_j = 0$ for j odd, if $f(L)$ is an even function of $L - \bar{L}$. The skewness is defined in terms of the lowest nonvanishing odd moment μ_3 , which will be nonzero if $f(L)$

is not symmetric about $L = \bar{L}$. Thus, we define skewness in a normalized form as

$$\text{Skewness} = \gamma_1 \equiv \mu_3 / \sigma^3 \quad (2.7-6)$$

In terms of the m_j moments about $L = 0$,

$$\gamma_1 = (m_3 - 3m_1m_2 + 2m_1^3) / (m_2 - m_1^2)^{3/2} \quad (2.7-7)$$

For a normal distribution, $m_3 = \bar{L}^3 + 3\sigma^2\bar{L}$, $m_2 = \bar{L}^2 + \sigma^2$, and $m_1 = \bar{L}$. Thus, for a normal distribution,

$$\gamma_1 = [(\bar{L}^3 + 3\sigma^2\bar{L}) - 3\bar{L}(\bar{L}^2 + \sigma^2) + 2\bar{L}^3] / \sigma^3 = 0 \quad (2.7-8)$$

Qualitatively, $\gamma_1 > 0$ indicates a distribution skewed to the right and $\gamma_1 < 0$ indicates a distribution skewed to the left of the mean. Characteristically, particle-size distributions have positive skewness, as do the log-normal and gamma distributions.

Kurtosis is a measure of the shape of a distribution curve at the extreme ends, relative to a normal distribution. A distribution with positive kurtosis will have a sharper peak but broader tails than a normal distribution. Kurtosis is defined for a distribution as

$$\text{Kurtosis} = \gamma_2 \equiv (\mu_4 / \mu_2^2) - 3 \quad (2.7-9)$$

or, in terms of the moments about zero,

$$\gamma_2 = \frac{(m_4 - 4m_1m_3 + 6m_1^2m_2 - 3m_1^4)}{(m_2^2 - 2m_1^2m_2 + m_1^4)} - 3 \quad (2.7-10)$$

Recognizing that for a normal distribution $m_4 = \bar{L}^4 + 6\sigma^2\bar{L}^2 + 3\sigma^4$, it can easily be shown that $\gamma_2 = 0$ for a normal distribution.

The four measures \bar{L} , c.v., γ_1 , and γ_2 qualitatively indicate the character of a given distribution and are especially useful in describing the qualitative character of abnormal distributions. These four parameters are uniquely defined by specifying a distribution function $f(L)$. The converse is not true, and these four measures are not sufficient to uniquely specify the distribution function $f(L)$.

2.8 Suspension Properties from the Population-Density Distribution

In principle, a distribution function $f(L)$ completely characterizes a particle distribution, and all properties of interest can be uniquely calculated, such as cumulative distributions (weight or population basis), mass or number in a finite size interval, and specific surface area.

Let $n(L)$ be a distribution function representing the distribution of population about a particle-size coordinate L for values of L in $(0, \infty)$. Further, let the distribution function represent the number of particles as a

function of L per unit volume of solids-free liquid in a liquid-solid particulate system. The function $n(L)$ is then defined as the *population density* of particles in the system. By definition of the distribution function, the number of particles of size L to $L + dL$ found in a volume of liquid V (solids-free basis) is given as

$$dN = Vn(L) dL \quad (2.8-1)$$

The units of population density are thus seen to be $(\text{m}^{-3})(\text{m}^{-1})$, or m^{-4} . The number of particles per unit volume of liquid in some finite size range L_1 to L_2 is found by integrating. Thus,

$$N(L_1, L_2) = \int_{L_1}^{L_2} n(L) dL \quad \text{particles in } (L_1, L_2)/\text{m}^3 \quad (2.8-2)$$

while the total concentration of particles is given as

$$N_T = \int_0^{\infty} n(L) dL \quad \text{total particles}/\text{m}^3 \quad (2.8-3)$$

Note that we do not require $n(L)$ to be normalized over the entire size range $(0, \infty)$, and thus this latter integral does not have the value of unity. Of course, we can define a normalized distribution function $f(L) = n(L)/N_T$ having this property. The fraction of particles in size range L_1 to L_2 is thus

$$F(L_1, L_2) = \left[\int_{L_1}^{L_2} n(L) dL \right] / N_T \quad (2.8-4)$$

The cumulative number fraction of particles having size less than L is given as

$$F(L) = \left[\int_0^L n(p) dp \right] / N_T \quad (2.8-5)$$

The function $F(L)$ increases monotonically from 0 to 1 as L goes from 0 to ∞ .

Let the particles in the above distribution be geometrically similar. The weight of each particle can then be related to the cube of its size. Thus

$$m_p = \rho k_v L^3 \quad (2.8-6)$$

where k_v is a volumetric shape factor relating particle volume to size cubed. The shape factor is independent of size for geometrically similar particles. The mass of particles per unit volume of liquid which are in size range L to $L + dL$ is thus the mass per particle times the number of particles:

$$dM = \rho k_v L^3 n(L) dL \quad (2.8-7)$$

The mass concentration in a finite size range L_1 to L_2 is obtained by

integration:

$$M(L_1, L_2) = \rho k_v \int_{L_1}^{L_2} L^3 n(L) dL \quad (2.8-8)$$

Total solids concentration in the fluid-solid system, expressed as kilograms per cubic meter of solids-free liquid, is then given as

$$M_T = \rho k_v \int_0^\infty L^3 n(L) dL \quad (2.8-9)$$

The weight fraction in any size range and the cumulative weight fraction distribution are then readily given as

$$W(L_1, L_2) = \left[\rho k_v \int_{L_1}^{L_2} L^3 n(L) dL \right] / M_T \quad (2.8-10)$$

and

$$W(L) = \left[\rho k_v \int_0^L p^3 n(p) dp \right] / M_T \quad (2.8-11)$$

The primary distribution can of course be a weight distribution rather than a population distribution. The weight density distribution function can be obtained from differentiation of the cumulative distribution (see Chapter 1),

$$w(L) \equiv dW/dL \quad (2.8-12)$$

and the weight density distribution function is thus given in terms of the population density as

$$w(L) = \rho k_v L^3 n(L) / M_T \quad (2.8-13)$$

It is obvious from Eqs. (2.8-11) and (2.8-12) that $w(L)$ is normalized over the range $(0, \infty)$ such that $\int_0^\infty w(L) dL = 1$.

A development similar to Eqs. (2.8-6)–(2.8-9) can be made for the surface area of particles in a fluid-solid system. Thus, the area of a particle is given as

$$a_p = k_a L^2 \quad (2.8-14)$$

where k_a is a shape factor relating area to size squared. The surface area per unit volume of solids-free liquid is given as

$$dA = k_a L^2 n(L) dL \quad (2.8-15)$$

while the surface area in some size range (L_1, L_2) is given as

$$A(L_1, L_2) = k_a \int_{L_1}^{L_2} L^2 n(L) dL \quad (2.8-16)$$

and the total surface area per unit volume in the suspension (m^2/m^3) is

$$A_T = k_a \int_0^\infty L^2 n(L) dL \quad (2.8-17)$$

EXAMPLE 2.8-1

It can be shown that for geometrically similar particles having a more or less continuous distribution of particle diameters from a minimum to a maximum, an intermediate diameter can always be chosen as the characteristic dimension L such that $k_a = 6k_v$. The volumetric shape factor k_v must of course be in reference to this characteristic size. For cubes and spheres, it is readily demonstrated that $k_a = 6k_v$. Thus, for a sphere, $v = \frac{1}{6}\pi D^3$ and $a = \pi D^2$. Choosing the characteristic dimension $L = D$ immediately gives $k_a = 6k_v$. For cubes, $v = L^3$ and $a = 6L^2$, giving directly $k_a = 6k_v$. This relationship is true for any *equidimensioned* regular object where geometric similarity requires equal growth rates along every particle axis. This can be easily demonstrated for particles having such a constant growth rate G . Thus, equating change of volume (for a growing particle) to the rate of advance of the particle's surface gives

$$dv_p/dt = \frac{1}{2}Ga_p$$

but $v_p = k_v L^3$ and $a_p = k_a L^2$; thus,

$$3k_v L^2 dL/dt = (1/2)Gk_a L^2$$

but $dL/dt = G$; canceling GL^2 terms gives $k_a = 6k_v$.

For particles having a separate growth rate G_j for each crystal face a_j , the above relationship is only true for the characteristic size L chosen as some suitable intermediate size. Repeating the previous derivation for this case gives

$$\frac{dv_p}{dt} = \sum_j \frac{1}{2}G_j a_j$$

Let the growth rate along the j th axis be related to the growth rate G along the characteristic axis L_c by a constant factor $G_j = c_j G = (L_j/L_c)G$. Thus, using the definition of shape factor gives

$$\frac{d}{dt}(k_v L_c^3) = \frac{1}{2} \sum_j c_j a_j$$

or $6k_v L_c^2 = \sum_j c_j a_j$. But as $a_p = \sum_j a_j = k_a L_c^2$, then it is obvious that the relation $k_a = 6k_v$ can be preserved by choosing L_c such that $\sum_j c_j a_j = \sum_j a_j = a_p$. In practice, particle measurement techniques, such as screening, measure an average particle size such that $k_a \approx 6k_v$ even for highly irregular particles. ♦

Similar integral equations can be written in terms of the integrand $Ln(L)$ to determine the length functions in suspension (length of the crystals per

unit volume laid end-to-end along their characteristic axes), but these functions are seldom calculated because of lack of physical motivation, except as they are used in calculating average particle size.

Finally, the population density function can be used to calculate average particle size, weighted in some sense, in the particle suspension. The mean particle size in the suspension, weighted on a population basis, is given as

$$\bar{L}_{1,0} = \left[\int_0^\infty L n(L) dL \right] / N_T = m_1 / m_0 \quad (2.8-18)$$

The length-weighted mean particle size is given as

$$\begin{aligned} \bar{L}_{2,1} &= \int_0^\infty L [L n(L)] dL / \int_0^\infty L n(L) dL \\ &= m_2 / m_1 \end{aligned} \quad (2.8-19)$$

The area-weighted mean particle size is given as

$$\begin{aligned} \bar{L}_{3,2} &= \left\{ \int_0^\infty L [L^2 n(L)] dL \right\} / \left[\int_0^\infty L^2 n(L) dL \right] \\ &= m_3 / m_2 \end{aligned} \quad (2.8-20)$$

It is obvious that a family of possible mean particle sizes is generated by the ratio of the $(i+1)$ 'th to the i 'th moment of the distribution about $L=0$. Thus, if the i 'th moment is defined as $m_i = \int_0^\infty L^i n(L) dL$, then a suitable mean particle size is given as the ratio of any two succeeding moments. Thus,

$$\bar{L}_{i+1,i} = m_{i+1} / m_i \quad (2.8-21)$$

Another closely related set of mean particle sizes can be defined in terms of the population density distribution function. These are respectively the length-, area-, and mass-average sizes. The total length, area, and mass of a suspension, all on a unit volume basis, are defined in terms of the first, second, and third powers of these average sizes. Thus, the total particle length is given as

$$\bar{L}_T = L_L N_T \quad (2.8-22)$$

or

$$\bar{L}_L = \int_0^\infty L n(L) dL / \int_0^\infty n(L) dL = m_1 / m_0 = \bar{L}_{1,0} \quad (2.8-23)$$

which is the population-weighted size as defined in Eq. (2.8-18). Total suspension area (m^2/m^3) is given in terms of the area-average size as

$$A_T = k_a (\bar{L}_a)^2 N_T \quad (2.8-24)$$

or

$$\bar{L}_a = \left[\int_0^\infty L^2 n(L) dL / \int_0^\infty n(L) dL \right]^{1/2} = (m_2/m_0)^{1/2} \quad (2.8-25)$$

Finally, the total mass concentration (kg/m³) is given in terms of the mass-average size as

$$M_T = \rho k_v (\bar{L}_m)^3 N_T \quad (2.8-26)$$

or

$$\bar{L}_m = \left[\int_0^\infty L^3 n(L) dL / \int_0^\infty n(L) dL \right]^{1/3} = (m_3/m_0)^{1/3} \quad (2.8-27)$$

It is obvious from the preceding discussion that a desirable property of an empirical distribution function is that it can be easily integrated so that cumulative properties can be evaluated and so that averages can be determined in terms of moments of the distribution. These moments will then simply be functions of the parameters of the distribution. All of the mean sizes discussed previously can be represented by the generalized equation

$$\bar{L}_{j,k} = (m_j/m_k)^{1/(j-k)}$$

EXAMPLE 2.8-2

What is the cumulative number-fraction distribution of particles for a population distribution represented by a normal distribution with mean size \bar{L} and variance σ^2 ? Estimate the fraction of particles which this empirical form of distribution predicts to be less than size zero, assuming $\sigma/\bar{L} = 2^{1/2}$. From Eq. (2.3-1d) we find the cumulative number fraction of particles as

$$F(p) = 0.5[1 + \text{erf}(p)] \quad (2.3-1d)$$

where $p = (L - \bar{L})/2^{1/2}\sigma$. For the case $L = 0$ and $\bar{L}/\sigma = (2)^{1/2}$, the value of p is calculated as $p = (0 - \bar{L})/\sigma 2^{1/2}$ or $p = -2^{1/2}/2^{1/2} = -1$. From a table of the error function we find $\text{erf}(-1.0) = -\text{erf}(1.0) = 0.843$ and $F(-1.0) = 0.0785$. Thus the number of particles less than size zero is calculated to be approximately 8%! Such obvious inconsistencies still would not invalidate use of the normal distribution; the main problem would be lack of fit over the entire size range. ♦

2.9 Summary

In this chapter, we have indicated that more information is needed to completely specify dispersed-phase particulate systems than is needed to

describe one-phase homogeneous systems. This additional information consists of a multidimensional distribution function for the particulate entities distributed about the least number of independent coordinate axes necessary to describe the state of the particles. Such independent coordinates comprise the particle phase space over which the particles are distributed. It is convenient to think of this phase space to be composed of two subregions consisting of external and internal coordinates. External coordinates give the spatial distribution of the particles, while internal coordinates refer to properties attached to each particle, such as size, concentration (chemical), activity, or age.

Often a single internal coordinate is sufficient to specify a particle distribution, for example, particle-size distribution in a granular material. Such experimental distributions can often be represented empirically by analytical distribution functions. We present five distribution functions that are used for such purposes: the normal, log-normal, gamma, Rosin-Rammler, and Gaudin-Melloy distributions. The normal distribution is widely used in the engineering and life sciences, especially for theoretical studies, but the latter distributions are of more utility in characterizing particle-size distributions, mainly because of the typical skewness of such experimental distributions, which can be accounted for with the log-normal, gamma, Rosin-Rammler, and Gaudin-Melloy forms. Properties of the distributions, such as mean and coefficient of variation, are presented as a function of the two parameters for these empirical distribution functions. Finally, suspension properties such as slurry density, crystal area, and mean sizes are shown as integrals of the population density distributions.

Nomenclature

a	Width parameter in gamma distribution.	k_v	Volumetric shape factor.
a_j	Area of j th crystal face.	L	Independent variable of distribution function, size.
a_p	Total surface area of an individual particle of size L .	\bar{L}	Arithmetic mean size in normal distribution.
$A(L)$	Specific surface area of particles up to size L .	L_m	Size parameter in Gaudin-Melloy distribution.
b	Size parameter in gamma distribution, equal to mode.	L'	Geometric mean size in log-normal distribution.
b'	Reciprocal size parameter in Rosin-Rammler distribution.	m	Exponent in Gaudin-Melloy distribution.
$f(L)$	Normalized one-dimensional distribution function.	m_j	j th moment about zero.
$F(L)$	Cumulative fraction of a distribution up to size L .	m_p	Total mass of individual particle.
G	Linear particle growth rate.	$M(L)$	Specific mass of particles up to size L .
k_a	Area shape factor.	n	Exponent in Rosin-Rammler distribution.

$n(L)$	Population density distribution function.	σ'	Width parameter in log-normal distribution, equal to geometric standard deviation.
$N(L)$	Cumulative members of a population distribution.	τ	Mean retention time.
$m(L)$	Mass density distribution function.	μ_j	j th moment about the mean \bar{L} .
x	Dimensionless crystal size equal to particle size divided by product of growth rate and residence time.		

GREEK SYMBOLS

ρ	Particle density.
σ	Width parameter in normal distribution, equal to standard deviation.

SUBSCRIPTS

T	Total specific quantity in particle suspension, per unit volume of suspension.
---	--

References

1. Irani, R. R., and Callis, C. F. (1963). "Particle Size: Measurement, Interpretation, and Application." Wiley, New York.
2. Kelly, E. G., and Spottiswood, D. J. (1982). "Introduction to Mineral Processing." Wiley, New York.

THE POPULATION BALANCE

3.1 Introduction

Chapter 2 discussed the concept of multidimensional particle population distributions in particle phase space. Certain one-dimensional distribution functions were discussed. These distribution functions are useful in the *empirical* characterization of particle distributions. An obvious limitation of such empirical characterization is the difficulty of relating the parameters in the distribution function to the factors in the process environment that produced the given distribution. In this chapter, we shall develop a *predictive* multidimensional particle distribution theory, which, in the case of certain well-defined regular processes of particle formation, is useful in the *a priori* prediction of the *form* and often the *magnitude* of the particle distribution. The distribution function is defined by the solution of a differential equation, rather than given by a specific algebraic form. The physical parameters affecting the formation of the distribution are nested in the differential equation, thus allowing the theory to be useful in a predictive as well as a descriptive sense. In addition, the transient response of particle processes can be quantitatively described by this theory.

3.2 Particle Phase Space

Particle phase space consists of the least number of independent coordinates attached to a particle distribution that allow a complete description of the properties of the distribution. Particle phase space may conveniently (and arbitrarily) be divided into two subregions given by internal and external particle coordinates. External coordinates refer simply to the spatial distribution of the particles. Such external coordinates are of course unnecessary, for example, in the description of a well-mixed particulate process, although it may be quite convenient to report the distribution on a unit-volume basis. Internal coordinate properties refer to those properties attached to each individual particle and that quantitatively measure its state, independent of its position. The prime example of an internal coordinate property is particle size; other examples would be chemical activity (e.g., of a catalyst particle), particle age (since birth or since entering a particular environment), chemical composition (as for a particle or droplet undergoing mass transfer), and particle energy content.

In the following treatment, we will consider an $(m + 3)$ -dimensional particle distribution function $n(R, t)$ defined over a region R consisting of the three spatial dimensions plus m independent internal property coordinates. From the definitions in Chapter 1, the number of particles existing at time t in an incremental region of particle phase space dR is given as

$$dN = n dR \quad (3.2-1)$$

while the total number of particles in some finite subregion of particle phase space R_1 is

$$N(R_1) = \int_{R_1} n dR \quad (3.2-2)$$

We shall presently make use of these definitions to formulate a population balance of particles in the particle phase space.

3.3 Population Fluxes: Convection, Birth, and Death

In any particulate process giving rise to the formation of a particle distribution, individual particles are continually changing their position in the particle phase space; that is, each particle moves along the various internal and external coordinate axes. If these changes are gradual and continuous, we refer to this movement as a convection along the respective particle coordinates and refer to the rate of change of the coordinate property of a particle as the convective particle velocity along that coordi-

nate axis. Thus, we define the vector particle phase-space velocity as

$$\mathbf{v} = v_x \delta_x + v_y \delta_y + v_z \delta_z + v_1 \delta_1 + v_2 \delta_2 + \cdots + v_m \delta_m \quad (3.3-1)$$

or

$$\mathbf{v} = \mathbf{v}_e + \mathbf{v}_i$$

where the v terms are the particle velocity components and the δ terms are the unit vectors along the external and internal coordinate axes. It should be noted that the external velocity v_e is not necessarily the same as the fluid velocity u in a particle suspension. In general, particle velocity must be computed from the fluid velocity u and a suitable momentum exchange (friction factor) relationship in an auxiliary force balance for each particle. In a well-mixed suspension, motions u and v_e are both quite random and no attempt would be made to follow particle motion in the external particle phase-space coordinates.

The internal particle velocities v_i are assumed to be a unique function of the state of the particle. An example of internal convection velocity is that of the linear rate of growth of a crystal in a supersaturated solution, determined mainly by the level of surrounding supersaturation. As discussed in Chapter 1, the definition of the linear size of a particle is often a difficult choice and certainly depends on how particle size is measured. However, given the definition of particle size L , the linear growth rate is just the rate of change of L . Thus, $G = dL/dt$, where G is the convective velocity of a particle along the L axis. An important restriction that will be made in developing this particle-size distribution theory is that *each* particle behaves identically at a given point in particle phase space. Thus, for the case of linear growth rate, G may vary with particle size and/or position in the suspension, but each particle of the same size and in the same environment (i.e., at the same state in phase space) would grow at the same linear growth rate.¹

¹In the case of crystal growth, recent evidence conclusively shows that crystals of identical size and environment do not necessarily grow at the same rate, but there is an inherent dispersion of particle growth rates under identical conditions. If a given particle has a repeatable growth rate under identical conditions, then it behaves properly in its particle phase space and one can view the growth dispersion phenomenon as the result of having a distribution of particle phase planes in the suspension, with each particle being a member of one of the phase planes. Alternatively, one can say that the distribution was not adequately represented by a single coordinate axis, particle size, but should be represented by a two-dimensional distribution—say, particle size plus inherent growth activity. The latter internal property is perhaps given by dislocation density on the crystal surface, which would be an exceedingly difficult property to relate to the state of the crystal. Thus, an inherently two-dimensional distribution might reasonably be described, in an engineering sense, using one-dimensional distribution theory, with the result that the unaccounted-for growth-dispersion phenomenon would produce a “smearing” of the distribution not predicted by the one-dimensional theory. Fortunately, in the case of crystallization, residence-time distribution factors override growth-dispersion effects in determining the particle-size distribution, especially for the larger sizes, which dominate the distribution on a weight basis. Much emphasis

Finally, we recognize the possibility of particles suddenly appearing or disappearing at a point in the internal particle phase space, which can be represented by birth and death functions of the particle distribution. Again, we restrict our attention to regular processes where these birth and death events can be related (at least statistically) to the state of the total system and/or to the position of a particle in the particle phase space. An example of birth and death events is particle breakage in a suspension. Breakage of a given particle results in a death event at the original particle size and birth events at the sizes of the resulting pieces. Such death events might reasonably be statistically correlated with the position of the particle in particle phase space (say, particle size), while birth events at a given particle size would depend on the entire distribution of particles (state of the total system) above that size. Such a description usually involves integrals of the distribution function, with the result that the particle distribution is described by solution of a set of integro-differential equations.

Let B and D represent such empirical birth and death density functions at a point in phase space. The net appearance of particles at a given point is then given as $(B - D) dR$. It should be emphasized that this formulation is only symbolic and is of little value unless reasonable theoretical or empirical forms for these birth and death terms can be stated in terms of the distribution function and point in particle phase space as discussed above. Specific formulations of the B and D functions will be presented in subsequent sections.

3.4 Particle-Number Continuity Equation

A population balance for particles in some fixed subregion of particle phase space can be stated as

$$\begin{aligned} \text{Accumulation} = & \text{Input} - \text{Output} \\ & + \text{Net generation} \end{aligned} \quad (3.4-1)$$

If we consider the subregion, say R_1 , to move convectively with the particle phase-space velocity v (i.e., take the Lagrangian viewpoint), then the population balance for particles in subregion R_1 may be stated simply as

$$\frac{d}{dt} \int_{R_1} n dR = \int_{R_1} (B - D) dR \quad (3.4-2)$$

has recently been focused on the phenomenon of growth-rate dispersion, especially as this complicates the problem of extrapolating to obtain the nucleation rate. The phenomenon of growth-rate dispersion is discussed in detail in Chapter 4.

The former term may be expanded to

$$\frac{d}{dt} \int_{R_1} n dR = \int_{R_1} \frac{\partial n}{\partial t} dR + \left(n \frac{d\mathbf{x}}{dt} \right) \Big|_{R_1} = \int_{R_1} \left[\frac{\partial n}{\partial t} + \nabla \cdot \left(\frac{d\mathbf{x}}{dt} n \right) \right] dR \quad (3.4-3)$$

where \mathbf{x} is the set of internal and external coordinates comprising the phase space R . Recognizing that

$$d\mathbf{x}/dt = \mathbf{v} = \mathbf{v}_e + \mathbf{v}_i \quad (3.4-4)$$

then the population balance can be written for the Lagrangian region R_1 as

$$\int_{R_1} \left[\frac{\partial n}{\partial t} + \nabla \cdot (\mathbf{v}_e n) + \nabla \cdot (\mathbf{v}_i n) + D - B \right] dR = 0 \quad (3.4-5)$$

As the region R_1 was arbitrary, the integrand must vanish identically. Thus, the population balance is given as

$$\frac{\partial n}{\partial t} + \nabla \cdot (\mathbf{v} n) - B + D = 0 \quad (3.4-6)$$

or, in terms of the $m + 3$ coordinates,

$$\frac{\partial n}{\partial t} + \frac{\partial}{\partial x} (v_x n) + \frac{\partial}{\partial y} (v_y n) + \frac{\partial}{\partial z} (v_z n) + \sum_{j=1}^m \frac{\partial}{(\partial x_i)_j} [(v_i)_j n] - B + D = 0 \quad (3.4-6')$$

Equation (3.4-6) is a number continuity equation in particle phase space. This equation, together with mass and energy balances (which constrain the values of the internal coordinate velocities \mathbf{v}_i), particle-number formation kinetics² (nucleation kinetics), and side conditions representing entry or exit of particle suspension from the region of interest, completely determine the formation and dynamics of multidimensional particle distributions formed in processes obeying the very general restraints discussed in this chapter. Equation (3.4-6) is completely general and is used when the particles are distributed along both external and internal coordinate space. More convenient, but more restricted, forms of the population balance will subsequently be developed.

EXAMPLE 3.4-1

Reduce Eq. (3.4-6') to obtain the differential equation governing formation of the particle-size distribution of crystals produced in an isothermal

²Note that $B(L)$ is *not* the nucleation rate, as nuclei are assumed to be of vanishingly small size. However, the birth function $B(L)$ has been used to represent the nucleation rate when nuclei spontaneously formed as a distribution over a finite size range. CSD calculations using a $B(L)$ function to input the experimentally determined range of secondary nuclei sizes show little or no difference in product CSD. There appears to be no loss in generality if nuclei are introduced as a side condition at $L = 0$ in CSD calculations.

plugflow crystallizer with negligible breakage operating at steady state. Indicate a method of solution from the form of the population balance equation, and outline the auxiliary equations needed to complete the solution of the problem.

At steady state, with negligible breakage, the population balance reduces to

$$\nabla \cdot \mathbf{v}_c n + \sum_{j=1}^m \frac{\partial}{(\partial x_i)_j} [(v_i)_j n] = 0 \quad (3.4-7)$$

The external coordinate system may be represented by the single crystallizer length dimension x , while the internal coordinate may be taken as particle size L . Thus, the population balance becomes

$$\frac{\partial}{\partial x} (v_x n) = - \frac{\partial}{\partial L} (Gn) \quad (3.4-8)$$

where $G = dL/dt$ is the linear crystal growth rate.³ For small particles and high velocities, the particle velocity v_x may be taken as the plugflow velocity u_x . Assuming that growth rate remains independent of size, an empirical observation known as McCabe's ΔL law, which often holds true, then Eq. (3.4-8) reduces to

$$\partial n / \partial x = - (G/u_x) \partial n / \partial L \quad (3.4-9)$$

This equation is a one-dimensional wave equation and thus suggests the method of characteristics for solution. The particle distribution defined by the partial differential equation of Eq. (3.4-8) can be reduced to two ordinary differential equations of the particle characteristic and of the particle distribution along the characteristic. The characteristic solution is constructed as follows:

$$n = n(L, x) \quad (3.4-10)$$

or taking the differential along a characteristic s gives

$$\frac{dn}{ds} = \left(\frac{\partial n}{\partial L} \right) \frac{dL}{ds} + \left(\frac{\partial n}{\partial x} \right) \frac{dx}{ds} \quad (3.4-11)$$

But from Eq. (3.4-8),

$$0 = \left(\frac{\partial n}{\partial L} \right) G + \left(\frac{\partial n}{\partial x} \right) u_x \quad (3.4-8)$$

Equating coefficients on the bracketed terms in Eqs. (3.4-11) and (3.4-8)

³In this chapter the problem of growth-rate dispersion is ignored; G may be thought of as an average phase plane velocity of the faster-growing crystals that survive to populate the product CSD.

gives the equation for the characteristic curve. Thus

$$\text{and} \quad \left. \begin{aligned} dL/ds &= G \\ dx/ds &= u_x \end{aligned} \right\} \quad \text{or} \quad dL/dx = G/u_x \quad (3.4-12)$$

which defines the characteristic in the L - x plane. Along the characteristic curve the population density is then given as $dn/ds = 0$, that is, the population distribution along a characteristic remains constant (in this example). The method of characteristics is a natural technique for solution of hyperbolic wave equations of the form of Eq. (3.4-8), and useful numerical solutions can be obtained. Calculation of characteristic curves in the x - L plane thus allows calculation of the particle-size distribution at any point x in the crystallizer.

Side conditions and auxiliary equations necessary for solution of the population balance are growth rate

$$G = G(C) \quad (3.4-13)$$

density of nuclei

$$n(0, x) = B^0(C)/G(C) \quad (3.4-14)$$

and a mass balance

$$\frac{u_x dC}{dx} = -\frac{1}{2} \rho k_a G \int_0^\infty n(L, x) L^2 dL \quad (3.4-15)$$

with boundary conditions

$$C(0) = C^0, \quad n(L, 0) = f(L) \quad \blacklozenge \quad (3.4-16)$$

Solution of the above set of integrodifferential equations would, in principle, uniquely define the particle-size distribution at each point in the isothermal plugflow crystallizer. Note that in the above equations, the two dependent variables C and n are respectively one- and two-dimensional distributions. This incompatibility of dimension results in the difficult-to-solve integro-partial differential form of the equations, which was circumvented by solution of an ordinary differential equation (ODE) along the particle characteristic. This difficulty of simultaneous solution of ODEs with the partial differential equation (PDE) of the population balance will also be eliminated with the moment transformation. This useful transformation is presented in Section 3.6.

3.5 Population Balance over a Macroscopic External Coordinate Region

In practice, many engineering problems involving dispersed-phase particulate systems are carried out in one or more regions that can each be considered to be well mixed. In such cases, the chief concern is not the

spatial distribution of particles, but rather, the system can be described knowing only the distribution of particles in the internal phase space. Equation (3.4-6), which is distributed in both external and internal phase space, can be transformed by averaging in the external phase space to yield a much more useful equation for such backmixed systems. Thus, we choose a suitable volume $V(t)$ of external phase space having an arbitrary number of inputs and outputs of flow rate Q_k and population density n_k and integrate the population balance over this region. We need consider only one region, as any complex multistage recycle process can always be decomposed into separate regions with only input and output streams. Multiplying Eq. (3.4-6) by dV and integrating over $V(t)$ gives

$$\int_V \left(\frac{\partial n}{\partial t} + \nabla \cdot \mathbf{v}_e n + \nabla \cdot \mathbf{v}_i n + D - B \right) dV = 0 \quad (3.5-1)$$

As the suspension is mixed, n , D , and B are functions only of time and the internal coordinates and can be taken out of the integration. The second term, an integral over the volume of the spatial divergence of the population flux, can be converted into a surface integral of the population flux flowing through the moving surfaces of the system. Thus,

$$\int_V \nabla \cdot \mathbf{v}_e n dV = \int_{S_m} v_N n dS_m \quad (3.5-2)$$

where v_N is the average particle velocity normal to the surface and S_m is the sum of all moving surfaces of the system. The term S_m may be considered to be composed of three components:

a. The k input and output streams to the volume V . The integral of $v_N n dS_m$ over these streams represents the inflow and outflow of slurry to the system. These terms can be represented as

$$\int_{S_k} v_N n dS = \sum_k Q_k n_k \quad (3.5-3)$$

where Q_k is taken as positive for flow out of V and negative for flow into V (sign convention assuming outward-directed normal to surface is positive).

b. Changes in system volume due to accumulation at a free interface. The contribution of this term, assuming n is independent of position, is

$$\int_{S_s} v_N n dS = n \int_{S_s} v dS = n \frac{dV_s}{dt} \quad (3.5-4)$$

where V_s is the change at the free surface of the solids-free volume of liquid in the system and S_s is the free surface of liquid in the vessel.

c. Change in void fraction of solids in the system. The contribution of this term for a mixed suspension is

$$n \int_{S_e} v_N dS = -n \frac{dV_e}{dt} \quad (3.5-5)$$

where V_e is the volume occupied by the solids and S_e is the total particle-fluid interface.

The total rate of change of solids-free volume⁴ is due to changes at a free surface and to changes of void fraction. Thus,

$$dV/dt = (dV_s/dt) - (dV_e/dt) \quad (3.5-6)$$

and the total contribution of the last two terms can be written as

$$\int_{S_e} v_N n dS + \int_{S_s} v_N n dS = n dV/dt \quad (3.5-7)$$

Thus, the total contribution of the spatial flux divergence term is given as

$$\int_V \nabla \cdot \mathbf{v}_e n dV = \sum_k Q_k n_k + n \frac{dV}{dt} \quad (3.5-8)$$

and the spatial-averaged balance may be written as

$$V \left(\frac{\partial n}{\partial t} + \nabla \cdot \mathbf{v}_i n + D - B \right) + n \frac{dV}{dt} = - \sum_k Q_k n_k \quad (3.5-9)$$

Or, dividing by V and rearranging,

$$\frac{\partial n}{\partial t} + \nabla \cdot \mathbf{v}_i n + n \frac{d(\log V)}{dt} = B - D - \sum_k \frac{Q_k n_k}{V} \quad (3.5-10)$$

Equation (3.5-10), the macroscopic population balance, is averaged in external phase space and distributed in internal phase space. It is the most useful form of the population balance and is used to describe transient and steady-state particle-size distributions in well-mixed vessels.

⁴Population density can be based either on solids-free or total volume. In the latter case, the term dV_e/dt would vanish and the only change in volume would be due to changes in total system volume at a free interface. In any case, the term dV_e/dt is negligible for "thin" suspensions. The two viewpoints, n based on solids-free or total volume, are completely equivalent. Recent work that explores secondary nucleation mechanisms indicates that secondary nuclei originate at or adjacent to a solid crystal surface. Thus there is no reason per se to base population density on a solids-free basis in order to be able to calculate the nucleation from solution. A solids-free basis is convenient, however, as filtrate volume is easy to measure and to incorporate into a solute mass balance.

EXAMPLE 3.5-1

Simplify the macroscopic population balance to describe the transient particle-size distribution in a continuous, constant-volume, isothermal, well-mixed crystallizer with mixed product removal. Assume the crystallizer feed streams are free of suspended solids and that the crystallizer operates with negligible breakage. Writing the macroscopic population balance, Eq. (3.5-10), gives

$$\frac{\partial n}{\partial t} + \frac{\partial(Gn)}{\partial L} + D - B + n \frac{d(\log V)}{dt} = - \sum_k \frac{n_k Q_k}{V} \quad (3.5-11)$$

The breakage and volume accumulation⁵ terms can be set equal to zero as indicated above. The right-hand side of Eq. (3.5-11) represents only the mixed suspension discharge. Again assuming McCabe's ΔL law, Eq. (3.5-11) reduces to

$$\frac{\partial n}{\partial t} + G \frac{\partial n}{\partial L} + \frac{n}{\tau} = 0 \quad (3.5-12)$$

where $\tau = V/Q_0$ is the drawdown time of the vessel. Additional constraints and side conditions necessary to solve Eq. (3.5-12) are initial distribution, density of nuclei, and growth rate:

$$n(0, L) = f(L) \quad (3.5-13)$$

$$n^0 = B^0(C)/G(C) \quad (3.5-14)$$

$$G = G(C) \quad (3.5-15)$$

and a dynamic mass balance on solute being crystallized,

$$\frac{dC}{dt} = \frac{Q_i C_i}{V} - \frac{Q_0 C}{V} - \frac{\rho k_a G}{2} \int_0^\infty n L^2 dL \quad (3.5-16)$$

Many inorganic systems operate with negligible supersaturation, that is, operate very near the solubility diagram even in transient operation. In such systems, the per-pass yield is essentially constant at 100%, independent of the particle-size distribution. For such high-yield systems supersaturation is immeasurable and may be eliminated as a parameter, with density of nuclei correlated to crystal growth rate. For such systems, side and auxiliary Eqs. (3.5-14) and (3.5-16) can be simplified to

$$n^0 = n^0(G) \quad (3.5-17)$$

and

$$G = \frac{1}{3} \tau \int_0^\infty n L^3 dL \bigg/ \int_0^\infty n L^2 dL \quad (3.5-18)$$

⁵Assuming a "thin" suspension with negligible change in solids-free volume.

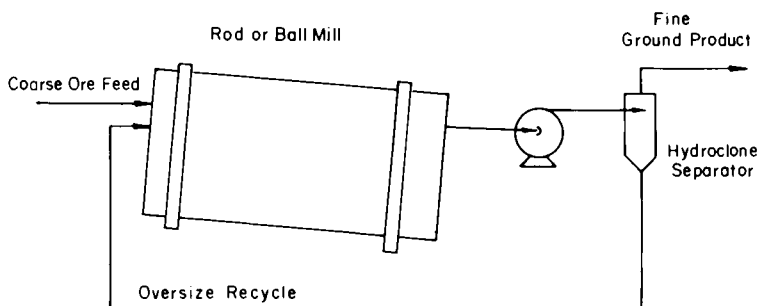


Fig. 3.5-1 Schematic diagram of closed-circuit grinding mill. (Preprint 71-B-78 presented at AIME Meeting, New York, March 3, 1971.)

the latter resulting from equating the rate of make to the production rate. However, invariance of yield implies that solids concentration is constant and hence the third moment of the particle distribution is invariant. Thus, Eq. (3.5-18) may be written as

$$G = M_T / \left(3\rho k_v \tau \int_0^\infty n L^2 dL \right) \quad (3.5-19)$$

and growth rate is seen to be inversely proportional to crystal area at a constant rate of make. ♦

These equations for transient particle-size distribution in a well-stirred, isothermal, mixed-product removal crystallizer have been extensively studied and will be discussed in detail in a subsequent chapter.

EXAMPLE 3.5-2 TRANSIENTS IN A CLOSED GRINDING CIRCUIT

Utilize the macroscopic population balance, Eq. (3.5-10), to describe transient particle-size distribution in a closed-circuit grinding mill, as shown in Fig. 3.5-1. Indicate the empiricisms necessary to describe this system.

Assuming that all size reduction occurs via the birth and death functions, rather than in a continuous manner, $v_i = G = 0$, and we need not consider convection along an internal coordinate. Further, we recognize that there would be some size-distribution gradients in the axial direction, but the typical ball mill, being nearly as large in diameter as in length, more nearly approaches the backmixed than the plugflow condition. Thus, Eq. (3.5-10), using the nomenclature from Fig. 3.5-1, reduces to

$$\frac{\partial n}{\partial t} = B(L, n) - D(L) + \frac{Q_F n_F}{V} + \frac{Q_R n_R}{V} - \frac{Q_T n}{V} \quad (3.5-20)$$

where the Q terms and V are solids-free water flow rates and ball-mill

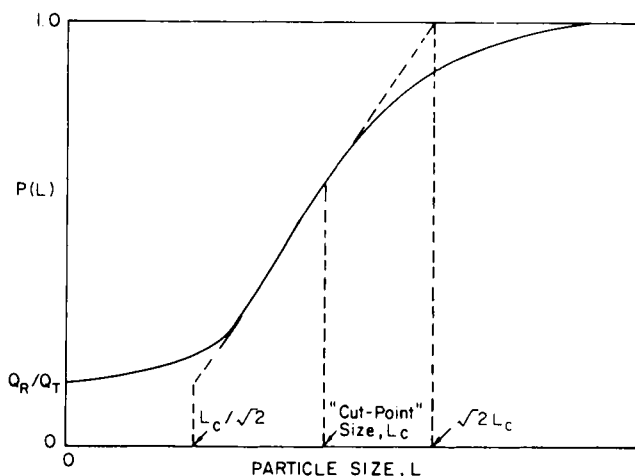


Fig. 3.5-2 Typical size-classification curve for hydroclone classifier. (Preprint 71-B-78 presented at the AIIME Meeting, New York, March 3, 1971.)

holdup, respectively, and where the birth function $B(L, n)$ is indicated to depend on size L as well as the distribution n above L that could conceivably break down to size L . The death function $D(L, n) dL$ is merely the rate of breakage at a given size (number/ m^3 s), and for constant mill configuration and operation would depend only on particle size and the population at that size. The birth function B must of course be consistent with D , as birth events result from death events. Specific forms for the birth and death functions⁶ are considered in Chapter 10.

To complete a description of the system, n_R must be related to n through a size-separation description of the classifier. Hydroclones operate by excluding oversize from the overflow rather than concentrating the under-size. Thus, if the fraction of feed material at a given size reporting to the underflow is plotted versus size, the separation curve, for zero size, asymptotically approaches the underflow-to-feed ratio Q_R/Q_T , and asymptotically approaches unity as size increases. The size at which 50% of the particles are removed from the overflow is termed the size separation or "cut point" of the classifier under those conditions of operation. A typical classification curve for hydroclone separation is shown as Fig. 3.5-2, where it is seen that the classification function $P(L)$ can be closely represented by a straight line joining the two asymptotes Q_R/Q_T and 1.0 over one sieve

⁶A convenient coordinate system in which to formulate mass-conserving B and D functions is the population-particle volume system. If B and D are density functions in particle volume space then $\int_0^\infty [B(v) - D(v)]v dv = 0$, that is, mass is conserved as breakage occurs.

size above and below the cut point, that is, $L_c/2^{1/2}$ to $L_c 2^{1/2}$. The separating curve for a particular cyclone under a particular set of operating conditions can of course be determined by direct measurement of feed and underflow particle-size distributions.

Assuming the classification curve is known, the recycle stream can be related to the grind distribution and flow as

$$Q_R n_R = P(L) Q_T n \quad (3.5-21)$$

Thus, the transient particle-size distribution in a closed-circuit grinding mill can be represented as

$$\frac{dn}{dt} = B(L, n) - D(L, n) + \frac{Q_F n_F}{V} + \frac{P(L) - 1}{V} Q_T n \quad (3.5-22)$$

where the empirical functions B , D , and P must be ascertained from the particular geometric and operating conditions of the mill. ♦

It should be emphasized that Eq. (3.5-22) represents the open-loop (i.e., uncontrolled) dynamics of the closed-circuit grinding mill described, under the restriction of constant slurry density, and that additional equations would have to be added to describe a closed-loop system wherein manipulation of flows and/or slurry density were implemented in response to changing mill conditions.

3.6 Moment Transformation of Population Balance

In many systems of engineering interest, a knowledge of the complete particle distribution is unnecessary. Rather, some average or total quantities are sufficient to represent the particle distribution. In Chapter 2 we discussed how these average or total properties, such as average size or surface area or mass concentration, could be obtained in terms of integrals of the distribution function — in particular, moments of the distribution.

Further, Example 3.4-1 alluded to a basic incompatibility of the population balance equation vis à vis the transport equations for mass, momentum, and energy: namely, that these equations are respectively of $m + 3$ and 3 dimensions. This difference in dimensionality leads to difficulty in simultaneous solution of the transport equations together with the population balance equation, usually resulting in integrodifferential equations, as illustrated in Examples 3.4-1 and 3.5-1.

Thus, we seek a transformation of the population balance equation that will average the distribution with regard to the internal coordinate properties and that will reduce the dimensionality to that of the transport equations. This closed set, with appropriate side conditions, can be thought

of as a complete mathematical representation of particulate systems, a general theory of particulate systems holding under the stated restrictions.

Assume a spatially distributed particulate process that can be described adequately with one internal coordinate⁷ in particle phase space. The population balance can be written for this system as

$$\frac{\partial n}{\partial t} + \nabla \cdot \mathbf{v}_e n + \frac{\partial}{\partial L}(Gn) + B - D \quad (3.6-1)$$

where the single internal coordinate L can be thought of as particle size. Assume that the particle growth rate $G = dL/dt$ varies no more than linearly with particle size. Thus,

$$G = G_0(1 + aL) \quad (3.6-2)$$

Define the j th moment of the distribution as

$$m_j(\mathbf{x}_e, t) + \int_0^\infty n L^j dL \quad (3.6-3)$$

The population balance can now be averaged in the L dimension by multiplying by $L^j dL$ and integrating from zero to infinity. Thus,

$$\int_0^\infty L^j \left[\frac{\partial n}{\partial t} + \nabla \cdot \mathbf{v}_e n + \frac{\partial}{\partial L}(Gn) - B + D \right] dL = 0 \quad (3.6-4)$$

Reversing order of integration and differentiation gives the first two terms as

$$\int_0^\infty L^j \left(\frac{\partial n}{\partial t} + \nabla \cdot \mathbf{v}_e n \right) dL = \frac{\partial m_j}{\partial t} + \nabla \cdot \mathbf{v}_e m_j \quad (3.6-5)$$

which assumes that $\mathbf{v}_e \neq \mathbf{v}_e(L)$.

In general, the birth and death terms, B and D , will be given in terms of the distribution function n as well as the independent coordinates \mathbf{x}_e and L . Assume that the averaging (moment integration) of these functions can be expanded in terms of the first k moments of the distribution,⁸

⁷The following moment transformation can be applied to a multidimensional internal distribution, obtaining mixed moments along the internal coordinates x_1 and x_2 of the form $m_{j,k} = \int_0^\infty \int_0^\infty x_1 x_2 n dx_1 dx_2$. Further, these moments form a closed set under the conditions, for each axis, of Eq. (3.6-8). However, the mathematical difficulty of recovering a multivariate distribution from the set of mixed moments limits utility of the moment transformation to a single internal coordinate (see Hulburt and Katz [1]).

⁸Because of the diverse nature of physical phenomena represented by the B and D functions (e.g., coalescence, agglomeration, disruption, fracture), it is not at all certain that the B and D functions could be expanded analytically in terms of the leading moments. However, numerical integration of the $B - D$ terms with moment inversion to approximate n can always be accomplished, thus leading to iterative semianalytical solutions of the moment equations.

m_0, m_1, \dots, m_k . Thus, we write

$$\int_0^\infty [B(\mathbf{x}_e, L, n, t) - D(\mathbf{x}_e, L, n, t)] L^j dL = \bar{B}(\mathbf{x}_e, t, m_k) - \bar{D}(\mathbf{x}_e, t, m_k) \\ j = 0, 1, 2, \dots \geq k \quad (3.6-6)$$

Finally, the third terms in the population balance can be integrated by parts to give

$$\int_0^\infty L^j \frac{\partial}{\partial L} (Gn) dL = -0^j \cdot B^0 - jG_0(m_{j-1} + am_j) \quad (3.6-7)$$

where B^0 is the number flux entering the internal coordinate region at $L = 0$ (the nucleation rate in the case of crystallization). The moment transformation of the population balance for one internal coordinate can thus be written as

$$\partial m_j / \partial t + \nabla \cdot \mathbf{v}_e m_j = 0^j \cdot B^0 + jG_0(m_{j-1} + am_j) + \bar{B} - \bar{D} \\ j = 0, 1, 2, \dots \geq k \quad (3.6-8)$$

For any maximum integer $j = J$, Eq. (3.6-8) forms a closed set in terms of the moments m_j . Notice that it was necessary to limit the dependency of the growth rate to the first power of L as well as the expansion of the birth and death functions to the k th-order moment ($k \leq J$) in order to close the set at the J th moment. Equation (3.6-8) is observed to be of the same dimensionality as the transport equations and can be solved side by side with the equations of mass, momentum, and energy transport to yield a complete mathematical description of the particulate process. Further, average and/or total properties of the distribution can be obtained directly from these time- and position-dependent moments. Such information is often sufficient to describe the particulate phase. In effect, this moment transformation has resulted in a tradeoff in which the dimensionality of the system has been reduced by one at the price of obtaining average, rather than distributed, information concerning the particle-size distribution. Alternatively, one can view this transformation as a tradeoff between a single four-dimensional equation, to an infinite set of three-dimensional equations, which can fortunately be truncated to a finite set, usually three or four equations, the third moment (fourth equation) entering in the mass balance and closing the set. Computationally, this transformation is often of great utility.

Finally, the question of dynamic stability of a particulate process can be answered by solving the truncated set of moment equations. Certainly, instability of the averaged quantities (moments) indicates instability of the distributed system. This technique will be illustrated in a later chapter.

EXAMPLE 3.6-1

Write the moment equations for the isothermal, plugflow crystallizer described previously in Example 3.4-1.

Assuming steady state, negligible breakage, and a particle velocity equal to the plugflow velocity u_x , the moment equation reduces to

$$u_x \frac{dm_j}{dx} - 0^j \cdot B^0 = jGm_{j-1}, \quad j = 0, 1, 2, \dots \quad (3.6-9)$$

which assumes $G \neq G(L)$. The question now arises, "How many moment equations should be retained in the simulation?" Assuming that the entire distribution as a function of size is not required, but rather the amount of yield to solid material and/or average properties are desired, then this question is answered by writing the equations to the highest moment interacting with side conditions and auxiliary equations. Thus, we write the mass-balance and boundary conditions. The mass balance is given as

$$u_x \frac{dC}{dx} = - \frac{\rho G k_a m_2}{2} \quad (3.6-10)$$

which is seen to involve the second moment of the particle distribution. Finally, growth rate and nucleation rate are given by their respective kinetic equations as

$$B^0 = B^0(C) \quad (3.6-11)$$

$$G = G(C) \quad (3.6-12)$$

Assuming an unseeded pregnant feed liquor, an additional set of side conditions that must be met is

$$m_j(0) = 0 \quad (3.6-13)$$

$$C(0) = C^0 \quad (3.6-14)$$

The moment equations are thus closed at the second moment, and the moment equations and mass balance can be solved simultaneously to obtain yield and average properties of the distribution, all as a function of position in the reactor. ♦

3.6.1 Macro-Moment Equations

The moment transformation can also be applied to the spatially averaged, or macroscopic, form of the population balance. Thus, multiplying the macroscopic balance by $L^j dL$ and integrating on $(0, \infty)$ gives

$$\int_0^\infty L^j \left[\frac{\partial n}{\partial t} + \frac{\partial}{\partial L}(Gn) + n \frac{d(\log V)}{dt} + \sum_k \frac{Q_k n_k}{V} + D - B \right] dL = 0 \quad (3.6.1-1)$$

where again the single internal particle coordinate L can be thought of as particle size.

The first, third, and fourth terms can be integrated directly to give

$$\begin{aligned} \int_0^\infty L^j \left[\frac{\partial n}{\partial t} + n \frac{d(\log V)}{dt} + \sum_k \frac{Q_k n_k}{V} \right] dL \\ = \frac{dm_j}{dt} + m_j \frac{d(\log V)}{dt} + \sum_k \frac{Q_k m_{j,k}}{V} \end{aligned} \quad (3.6.1-2)$$

Again, assuming the growth rate varies with no more than the first power of size L , the second term can be integrated by parts to give

$$\int_0^\infty L^j \frac{\partial}{\partial L} (Gn) dL = -0^j \cdot B^0 - jG_0(m_{j-1} + am_j) \quad (3.6-7)$$

Assuming the birth and death terms can be expanded in terms of the first k moments, these terms can be written symbolically as in Eq. 3.6-6. Thus, the macro-moment form of the population balance is given as

$$\begin{aligned} \frac{dm_j}{dt} + m_j \frac{d(\log V)}{dt} = jG_0(m_{j-1} + am_j) + 0^j \cdot B^0 - \sum_k \frac{Q_k m_{j,k}}{V} + \bar{B} - \bar{D} \\ j = 0, 1, 2, \dots \end{aligned} \quad (3.6.1-3)$$

Note that the only derivative remaining is the ordinary derivative with respect to time. At steady state, these equations reduce to a set of nonlinear, algebraic equations.

EXAMPLE 3.6.1-1

Write the macro-moment equations for the transient, well-mixed isothermal crystallizer described in Example 3.5-1. Using the limiting approximation of a high-yield, constant-slurry-density crystal system, then solids-free volume is also constant in a constant-total-volume system. Thus, the term $d(\log V)/dt$ vanishes. Assuming liquid feeds and a single mixed discharge, the summation and subscript k can be dropped from the slurry input-output terms. Again, assume $G \neq G(L)$. Equation (3.3-1) can thus be written for the well-stirred, constant-yield, constant-volume, isothermal, dynamic crystallizer as

$$\frac{dm_j}{dt} + \frac{m_j}{\tau} - 0^j \cdot B^0 = jGm_{j-1}, \quad j = 0, 1, 2, \dots \quad (3.6.1-4)$$

Again, the question of how many moments to include in the simulation must be answered from the goals of the study. Assuming that the transient particle-size distribution is not to be recovered from the moments, the set

may be closed after the second moment. This may be seen by writing the side conditions and auxiliary constraints

$$G = k/m_2 \quad (3.6.1-5)$$

$$B^0 = B^0(G) \quad (3.6.1-6)$$

with initial conditions

$$m_j(0) = m_j^0 \quad (3.6.1-7)$$

These auxiliary equations involve no moments higher than m_2 , and the set can be closed after the second moment. These equations will be examined in a later chapter to investigate the problem of stability of particle-size distribution in a mixed suspension crystallizer. ♦

3.6.2 Recovery of the Particle-Size Distribution Function from the Moments

In the previous section, we transformed the population balance equation, distributed along one internal coordinate axis, into a set of J equations in terms of the first J moments of the particle distribution defined as

$$m_j(\mathbf{x}_e, t) \equiv \int_0^\infty n(\mathbf{x}_e, L, t) L^j dL, \quad j = 0, 1, 2, \dots, J \quad (3.6-3)$$

We now ask the question, “Given a set of the first J moments of a distribution function, can we reconstruct the original function in some approximate sense?” Obviously, a continuous distribution function, containing an infinite amount of information, cannot be exactly specified with the finite information contained in a finite set of numbers $\{m_j\}$. Yet, we might hope to recover n from a limited set $\{m_j\}$ to an accuracy adequate for, and an amount of effort consistent with, the aims of an engineering simulation of a particulate process. A simple matrix inversion technique has been used by the authors to recover the CSD from the moments in a plugflow precipitator [2]. Another proposed method of recovering the distribution from the leading moments involves expansion of the distribution in terms of gamma functions. This gamma distribution has correction terms involving Laguerre polynomials with moment-dependent coefficients [3].

In this section we take the simpler and more direct approach of moment formulation as a matrix and inversion to recover n . Thus

$$m_j \doteq \sum_{k=1}^N n_k L_k^j \Delta L_k \quad (3.6.2-1)$$

where n_k is the value of n at the midpoint L_k of a size range ΔL_k . Rewriting Eq. (3.6.2-1) as a linear combination of the N ordinate values of

the distribution $\{n_k\}$ gives

$$m_j = \sum_{k=1}^N a_k^{(j)} n_k \quad (3.6.2-2)$$

where

$$a_k^{(j)} = L_k^j \Delta L_k = a_{jk} \quad (3.6.2-3)$$

The set of moments can then be written in matrix notation as

$$\mathbf{m} = \mathbf{A} \mathbf{n} \quad (3.6.2-4)$$

where the matrix \mathbf{A} is the $N \times N$ matrix of coefficients $a_k^{(j)}$. Thus, we write the approximate solution as

$$\mathbf{n}(L) \doteq \mathbf{A}^{-1} \mathbf{m} \quad (3.6.2-5)$$

Equation (3.6.2-4) represents a set of N linear algebraic equations in terms of N values of population density and can be inverted by standard techniques to obtain an approximate distribution function given at N values of L . This technique has proven quite satisfactory in practical engineering simulations.

The question of how many moments should be included in the inversion must be determined by numerical experimentation. Higher moments unduly weight the distribution toward the larger sizes, where perhaps the distribution is not well-defined and where it is possible for the continuum assumption in the particle continuity equation to fail. Preliminary calculations with Eq. (3.6.2-5) indicate that four to five moments satisfactorily reproduce an original empirical distribution $n(L)$.

After recovering the population density, the mass density can then be calculated simply as $m(L) = \rho k_v n L^3$. The above matrix inversion technique is simple to implement and is usually accurate enough for engineering purposes. The main advantage of the moment transformation/inversion is that it allows solution of algebraic relationships or ODEs (the moment equations) while recovering a one- or two-dimensional distribution function, $n(L)$ or $n(t, L)$, respectively.

3.7 The Population Balance in Other Coordinate Systems

It is possible, and often quite useful, to phrase the population balance in other variable coordinate systems, such as those discussed in Section 1.5, either by transforming the population balance or by rederivation in the new coordinates. In this section we consider two such alternate forms and comment on specific uses of such formulations.

3.7.1 Population Density-Particle Volume Formulation

Consider the population per unit volume of suspension dN of particles that reside in the particle volume range v to $v + dv$. Thus $dN = n(v) dv$, and we use this term to represent numbers in the population balance. Creation and disappearance of particles at a size (coalescence, agglomeration, breakage, etc.) is similarly represented with B and D density functions. The convection, birth, death, and input-output terms are thus defined as

$[B(v) - D(v)] dv$, Net creation of particles at size v , number/m³ s
 $G_v n$, Convection of particles down the volume axis by growth, number/m³ s.

$G_v = dv/dt$, Growth rate expressed as the rate of change of particle volume, (μm)³/s

$\sum_k Q_k n_k dv$, Summation of the k input-output streams (Q_k has the same meaning as in Section 3.5), number/m³ s

If we consider particles in an arbitrary suspension of volume V and size range Δv , a balance of particles over time Δt gives

$$\begin{aligned} \text{Accumulation} &= [\text{Input} - \text{Output}]_{\text{growth}} \\ &\quad + [\text{Input} - \text{Output}]_{\text{flow}} \\ &\quad + \text{Generation} \end{aligned} \quad (3.7.1-1)$$

In terms of the above variables, the population balance becomes

$$\begin{aligned} \Delta[Vn \Delta v] &= \{G_v n|_v - G_v n|_{v+\Delta v}\} V \Delta t - \sum_k Q_k n_k \Delta V \Delta t \\ &\quad + V[B - D] \Delta t \Delta v \end{aligned} \quad (3.7.1-2)$$

Dividing by $\Delta v \Delta t$ and taking the limit as $\Delta t, \Delta v \rightarrow 0$ gives the population balance in the $n(v)$ system. Thus

$$\frac{\partial(nV)}{\partial t} + \frac{\partial}{\partial v}[(G_v n)]V + \sum_k Q_k n_k = [B - D]V \quad (3.7.1-3)$$

EXAMPLE 3.7.1-1

Use Eq. (3.7.1-3) to model aerosol PSD in a fixed volume V and illustrate the form of the B and D functions appropriate to model aerosol coalescence. We start with an initial aerosol PSD $n(t_0, v)$ and wish to model the effect of particle coalescence to determine the distribution $n(t, v)$ at time t . Assume that the particles are in vapor equilibrium with the surrounding vapor and furthermore that the aerosol droplets are large enough that size-dependent changes in vapor pressure can be neglected. Thus we assume

that changes in particle size due to growth can be neglected ($G_v = 0$) and that only coalescence events change the PSD. There are no flows coming into or out of V . Therefore both the second and third terms of Eq. (3.7.1-3) can be neglected and the population balance becomes

$$V \frac{dn}{dt} = B - D \quad (3.7.1-4)$$

where the $B - D$ terms represent particle coalescence. These terms are conventionally represented by collision integrals taken over the entire PSD (e.g., Swift and Friedlander [4], Drake [5]). Thus

$$B(v) = \frac{1}{2} \int_0^v C(u, v-u) n(u) n(v-u) du \quad (3.7.1-5)$$

Equation (3.7.1-5) represents the rate at which a particle of volume u coalesces with a particle of volume $v - u$ to make a new particle of volume v . Note that the rate of coalescence is proportional to the product of the population densities at the respective sizes. Thus coalescence events tend to increase as the square of the number concentration of particles in a system.

Any given particle of volume v has a possibility of coalescing with any other particle in the distribution. Thus a death term consistent with Eq. (3.7.1-5) is given as

$$D(v) = n(v) \int_0^\infty C(v, v') n(v') dv' \quad (3.7.1-6)$$

where the variable v' is merely a dummy variable of integration. The function $C(x, y)$ is the coagulation kernel that describes the rate at which particles of volumes x and y collide and coalesce. Much of the science and engineering modeling of aerosols involves prediction and/or selection of the coagulation kernel $C(x, y)$. Both the magnitude and the functionality of this kernel are strong functions of the flow field containing the particles. Some proposed coagulation kernels in various flow fields are illustrated below [5].

1. Brownian motion

$$C(x, y) = K_a [x^{1/3} + y^{1/3}] [x^{-1/3} + y^{-1/3}] \quad (3.7.1-7)$$

2. Shear flow

$$C(x, y) = K_a [x^{1/3} + y^{1/3}]^3 \quad (3.7.1-8)$$

3. Turbulent flow, inertial mechanism [6]

$$C(x, y) = K_a [x^{1/3} + y^{1/3}] |x^{2/3} - y^{2/3}| \quad (3.7.1-9)$$

Note that the constant K_a in the above equations has the meaning of a

coalescence rate constant and itself can be predicted or correlated with conditions in the flow field, such as temperature (in gases), shear rate, and viscosity. ♦

Formulation of the population balance in the number–volume coordinate system is also a fruitful way of modeling crystal growth, agglomeration, and aggregation in continuous or batch crystallizers. An advantage of using particle volume v rather than linear size L as the independent variable is that mass-conserving $B(v)$ and $D(v)$ functions are easier to formulate than in the $n(L)$ coordinate system. A disadvantage of formulation in the $n(v)$ system is that there is no simple linear plot to express idealized distributions, such as the linear $\log n$ versus L plot for the MSMPR crystallizer distribution with negligible breakage.

EXAMPLE 3.7.1-2

Model the CSD in a continuous shear-flow crystallizer/agglomerator using Eq. (3.7.1-3). Assume that nucleation, growth, and agglomeration events all occur simultaneously in the crystallizer. The following assumptions are made to define the crystallizer configuration and operation.

The crystallizer is continuously seeded with an input distribution $n_i(v)$.

A turbulent shear field is created in the crystallizer vessel by rotation of an inner cylindrical spindle in the outer cylinder. The crystallizer is the annular volume between the two cylinders.

The shear-flow field in the annular crystallizer is dominated by turbulence and can be considered back-mixed.

Both crystal agglomeration and agglomerate rupture occur. These events are not reversible and must be modeled with separate birth and death functions.

Steady state can be assumed. Flow rate in and out of the crystallizer is constant at Q , volume per time.

Equation (3.7.1-3) can be written for this system as

$$\frac{d}{dV}(G_v n) + \frac{Q}{V}(n - n_i) = (B - D)_A + (B - D)_R \quad (3.7.1-10)$$

where the subscripts A and R on the birth and death terms refer to agglomeration and rupture, respectively. The agglomeration term can be formulated analogously to the formulation of coalescence of aerosols. Thus

$$\begin{aligned} (B - D)_A = & \frac{1}{2} \int_0^v C_A(v, v-u) n(u) n(v-u) du \\ & - n(v) \int_0^\infty C_A(v, u) n(u) du \end{aligned} \quad (3.7.1-11)$$

where $C_A(x, y)$ is the agglomeration rate kernel between crystals with respective volumes of x and y . The functionality of $C_A(x, y)$ must be specified using some theoretical or empirical model, but the magnitude of C_A would surely depend on the shear-flow intensity in the crystallizer. The agglomerate rupture kinetics $(B - D)_R$ must be stated independently of agglomeration kinetics. For example, an agglomerate containing 50–100 individual loosely bound crystals might rupture into three or four pieces of roughly equal volume. Such rupture events are modeled below with a simple two-body equal-volume rupture model to complete this illustration. In general, the rupture kinetics D_R must be stated as a function of the state of the system. The distribution-of-pieces function must be contained in the birth kinetics B_R . The formulation of such birth and death kinetics is completely analogous to formulations used to model comminution processes.

We conclude this example with the following two-body power-law rupture kinetics. Thus

$$D_R(v) = K_R v^a n(v) \quad (3.7.1-12)$$

which states that the rupture of agglomerates is proportional to their population and to their volume raised to an exponent a . A two-body equal-volume birth function that is consistent with this rupture function is given as

$$B_R(v) = 2 D_R(2v) \quad (3.7.1-13)$$

or specifically,

$$B_R = 2 K_R (2v)^a n(2v) \quad (3.7.1-13')$$

The model is completed by specifying G_v and nucleation as a function of the supersaturation in the crystallizer.

A specific example of such a shear-flow crystallizer in which nucleation, growth, agglomeration, and rupture are simultaneously occurring will be considered for the calcium oxalate system in Chapter 10. ♦

3.7.2 Mass Density–Particle Size Formulation

The population balance on a number-size basis can be transformed to a mass-size basis simply by multiplying term by term by $\rho k_v L^3$. Thus $m(L) = \rho k_v L^3 n(L)$. We use the macroscopic population balance [Eq. (3.5-10)] for this transformation, and restrict ourselves to one internal coordinate, $x_1 = L$. Thus

$$\rho k_v L^3 \left[\frac{\partial n}{\partial t} + \frac{\partial}{\partial L} (Gn) + n \frac{d(\log V)}{dt} - B + D + \sum_k \frac{Q_k n_k}{V} \right] = 0 \quad (3.7.2-1)$$

All terms in Eq. (3.7.2-1) convert directly to the equivalent term in $m(L)$

except the second term in the square brackets. Thus

$$\frac{\partial m}{\partial t} + m \frac{d(\log V)}{dt} - B_m + D_m + \frac{Q_k m_k}{V} = -G\rho k_v L^3 \frac{\partial n}{\partial L} \quad (3.7.2-2)$$

which for simplicity assumes $G \neq G(L)$. The subscripts on the B_m and D_m functions indicate that these must be expressed as density functions on a mass basis. The term on the right-hand side is recognized as one term in the expansion of $\partial(L^3 n)/\partial L$. Thus

$$L^3 \frac{\partial n}{\partial L} = \frac{\partial(L^3 n)}{\partial L} - 3nL^2 \quad (3.7.2-3)$$

Bringing Eq. (3.7.2-3) to Eq. (3.7.2-2) gives the population balance transformed to mass-size coordinates. Thus

$$\begin{aligned} \frac{\partial m}{\partial t} + m \frac{d(\log V)}{dt} + \sum_k \frac{Q_k m_k}{V} + G\rho k_v \frac{\partial}{\partial L}(L^3 n) - B_m + D_m \\ = G\rho k_v 3nL^2 \end{aligned} \quad (3.7.2-4)$$

Recognizing that the crystal surface area at size L is $A = 6k_v n L^2$ gives the final form of the population balance in mass-size coordinates as

$$\frac{\partial m}{\partial t} + m \frac{d(\log V)}{dt} + \sum_k \frac{Q_k m_k}{V} + \frac{\partial}{\partial L}(Gm) - B_m + D_m = \rho \left(\frac{G}{2} \right) A \quad (3.7.2-5)$$

Comparing Eq. (3.5-10) (population-size) and Eq. (3.7.2-5) (mass-size) shows that they are identical in form except for the term on the right-hand side of Eq. (3.7.2-5). This term, $\rho(G/2)A$, represents a generation term, specifically the growth of crystal mass over the crystal surface area. This term is present in the mass-size form but not the population-size form of the population balance. Generation of crystal mass but not crystal population occurs in the size range L to $L + dL$.

3.8 Random Fluctuations in Growth Rate and/or Slurry Velocity

The population balances presented in Chapter 3 have thus far assumed that crystals moved convectively in the particle phase plane with constant velocities (at a given time and supersaturation). The convective number flux in the particle phase plane has been modeled as

$$\mathbf{N} = \mathbf{v}_i n + \mathbf{v}_e n \quad (3.8-1)$$

Specifically, for particle size and one-dimensional flow in the x direction as

the internal and external coordinates, respectively, the number flux becomes

$$N = Gn + u_x n \quad (3.8-2)$$

Equation (3.8-2) does not take into account any fluctuations in growth velocity or dispersion of particles in the flow field. If the fluctuations (relative to the mean) of growth rate and/or flow rate can be considered random in nature, then the dispersion of CSD caused by such fluctuations can be modeled simply by adding effective diffusivity terms to the number flux equation.

Evidence suggests that such random fluctuations in growth rate [7] and axial flow do exist, and in fact are expected. A good example of a crystallizer design where growth-rate fluctuations would be expected is in a poorly mixed calandria-heated pan where the crystals circulate through different zones of supersaturation because agitation is solely due to thermal convection. Size spreading can also occur due to Taylor diffusion in a plugflow configuration.

We will model the size spreading caused by random fluctuation in growth rate and/or axial flow using effective diffusivities [8] and incorporate these changes in the previously derived population balance equations. Thus we represent population flux along the particle size and spatial axes as

$$N = \left(Gn - D_G \frac{\partial n}{\partial L} \right) + \left(u_x n - D_a \frac{\partial n}{\partial x} \right) \quad (3.8-3)$$

where D_G and D_a are the respective growth and axial flow diffusivities and are assumed constant in the population balance equation. Substitution of Eq. (3.8-3) in the previously derived population balance equations gives:

1. Microdistributed population balance (one internal and external coordinate):

$$\frac{\partial n}{\partial t} + u_x \frac{\partial n}{\partial x} + \frac{\partial (Gn)}{\partial L} = B - D + D_a \frac{\partial^2 n}{\partial x^2} + D_G \frac{\partial^2 n}{\partial L^2} \quad (3.8-4)$$

2. Macrodistributed population balance (one internal coordinate):

$$\begin{aligned} \frac{\partial n}{\partial t} + \frac{\partial (Gn)}{\partial L} + n \frac{\partial (\log V)}{\partial t} + \sum_k \frac{Q_k n_k}{V} \\ = B - D + D_G \frac{\partial^2 n}{\partial L^2} \end{aligned} \quad (3.8-5)$$

This simple approach to modeling of size spread caused by fluctuations in growth and flow velocities is also amenable to the moment transformation, as the second derivatives of n in size and space can also be transformed.

Thus,

3. Macromoment population balance (neglecting B and D terms):

$$\begin{aligned}\frac{dm_0}{dt} + m_0 \frac{d(\log V)}{dt} + \sum_k \frac{Q_k m_{0,k}}{V} &= Gn(0) + D_G n(0) \\ \frac{dm_1}{dt} + m_1 \frac{d(\log V)}{dt} + \sum_k \frac{Q_k m_{1,k}}{V} &= Gm_0 + D_G n(0) \\ &\vdots \\ \frac{dm_j}{dt} + m_j \frac{d(\log V)}{dt} + \sum_k \frac{Q_k m_{j,k}}{V} &= jGm_{j-1} + j(j-1)D_G m_{j-2}\end{aligned}\quad (3.8-6)$$

EXAMPLE 3.8-1

Show that the addition of an effective growth rate diffusivity to the MSMPR equations does not change the exponential form of the population density and, in fact, would be unobservable from experimental data. The population balance for a mixed-suspension, mixed-product removal (MSMPR) crystallizer is obtained by writing out Eq. (3.8-5). Thus assuming no breakage, unseeded feed, size-independent growth, and steady state, Eq. (3.8-5) becomes

$$G \frac{dn}{dL} + \frac{n}{\tau} - D_G \frac{d^2 n}{dL^2} = 0 \quad (3.8-7)$$

where $\tau = V/Q$. A nucleation boundary value for Eq. (3.8-7) is given as

$$B^0 = Gn(0) - D_G \dot{n}(0) \quad (3.8-8)$$

which takes into account the reduction in $n(0)$ due to growth diffusivity. The following dimensionless substitutions are brought to Eqs. (3.8-7) and (3.8-8):

$$x = L/G\tau, \quad y = nG/B^0, \quad \text{Pe} = G(G\tau)/D_G$$

where Pe is a Peclet number for growth diffusivity.

With these substitutions, Eqs. (3.8-7) and (3.8-8) become

$$\ddot{y} - \text{Pe} \dot{y} - \text{Pe} = 0, \quad 1 = y(0) - (1/\text{Pe}) \dot{y}(0) \quad (3.8-9)$$

The characteristic equation of Eq. (3.8-9) has two roots, m^+ and m^- , which are respectively positive and negative. The general solution of Eq. (3.8-9) will be of the form

$$y = C_1 \exp(m^+ x) + C_2 \exp(m^- x) \quad (3.8-10)$$

where $m^{+/-} = (\text{Pe}/2)[1 \pm (1 + 4/\text{Pe})^{1/2}]$. The solution with the positive

root must be rejected to prevent unbounded solutions as $x \rightarrow \infty$. Thus $C_1 = 0$, and the population density is given as

$$y = C_2 \exp \left\{ \frac{\text{Pe}}{2} \left[1 - \left(1 + \frac{4}{\text{Pe}} \right)^{1/2} \right] x \right\} \quad (3.8-11)$$

or in dimensional variables,

$$n(L) = k_1 \exp(-k_2 L) \quad (3.8-11')$$

Experimental data from the MSMRP crystallizer are fitted to the form

$$n(L) = n^0 \exp(-L/G\tau) \quad (3.8-12)$$

where n^0 and G are adjustable parameters. As the forms of Eqs. (3.8-11') and (3.8-12) are identical, and they differ only in the value of their adjustable parameters, it can be concluded that random fluctuations in growth rate do not change the form of the MSMRP distribution and are in fact unobservable. ♦

Chapter 4 will discuss a different model of intrinsic (rather than random) growth-rate dispersion wherein each crystal of the distribution grows at its own constant growth rate, which is different from other crystals in the distribution. This can be thought of as a crystal suspension having a distribution of growth-rate (size versus residence time) phase planes, with each individual crystal born into and remaining in its given phase plane. It will be shown that such an intrinsic distribution of growth rates does change the form of the MSMRP distribution and in fact shows up as apparent size-dependent growth rate, $G = G(L)$.

Both random and intrinsic models of growth-rate dispersion cause widening of a narrow CSD, but the random model preserves the form of the exponential population distribution.

3.9 Summary

In this chapter, we have developed the need for a *predictive* as well as a *descriptive* theory of multivariable particle distributions in particulate processes. The population balance (number-continuity) equation together with associated mass, momentum, and energy transport equations and with appropriate boundary conditions involving mass and number kinetics provides a unified predictive theory for such regular particulate systems obeying the restrictions implicit in the derivation of these equations. This population balance was presented in four forms, each having advantages in the description of certain systems. These four forms of the population

balance, together with restrictions and advantages of that form, are listed below for easy reference. The addition of random growth rate dispersion is omitted from this summary of equations. See Section 3.8 for equations with dispersion added.

3.9.1 Microdistributed Population Balance

From Eq. (3.4-6), we have

$$\partial n / \partial t + \nabla \cdot \mathbf{v}_e n + \mathbf{V} \cdot \mathbf{v}_i n = B - D$$

Uses and characteristics: (a) Most general form of population balance; (b) emphasizes mathematical similarity with mass continuity equation; (c) useful for spatially distributed systems.

Assumptions and limitations: (a) Particles are numerous enough to approximate a continuum; (b) each particle has identical trajectory in particle phase space.

3.9.2 Macrodistributed Population Balance [Eq. (3.5-10)]

$$\frac{\partial n}{\partial t} + \nabla \cdot \mathbf{v}_i n + n \frac{d(\log V)}{dt} = - \sum_k \frac{Q_k n_k}{V} + B - D$$

Uses and characteristics: (a) Useful for back-mixed systems in any configuration; (b) reduces to ordinary differential equation for steady-state distribution along one internal coordinate; (c) birth and death functions may be expressed in any form that can be computed numerically.

Assumptions and limitations: (a) Same as microdistributed equations; (b) suspension is mixed or balance is over all particles in suspension with average B , D , and v_i ; (c) only internal coordinate particle distributions are considered.

3.9.3 Micromoment Population Balance [Eq. (3.6-8)]

$$\frac{\partial m}{\partial t} + \nabla \cdot \mathbf{v}_e m_j = 0^j \cdot B^0 + j G_0(m_{j-1} + a m_j) + \bar{B} - \bar{D}, \quad j = 0, 1, 2, \dots$$

Uses and characteristics: (a) Reduces dimensionality of population balance to transport equations; (b) reduces magnitude of computation for spatially distributed systems; (c) averages internal coordinate in naturally occurring moments.

Assumptions and limitations: (a) Same as microdistributed equation; (b) birth and death terms, if used, must be independent of n or expandable in terms of leading moments; (c) only one internal coordinate considered.

3.9.4 Macromoment Population Balance [Eq. (3.7-3)]

$$\frac{dm_j}{dt} + m_j \frac{d(\log V)}{dt} = jG_0(m_{j-1} + am_j) + 0^j \cdot B^0 - \sum_k \frac{Q_k m_{j,k}}{V} + \bar{B} - \bar{D}$$

$$j=0, 1, 2, \dots$$

Uses and characteristics: (a) Reduces dimensionality of population balance to only time dependence, that is, ordinary differential equation; (b) useful for stability and transient studies of particle distributions; (c) averages internal coordinate in terms that occur in auxiliary equations and constraints.

Assumptions and limitations: Same as microdistributed, macrodistributed, and micromoment equations.

The above four forms of the population balance equations, together with the transport equations and auxiliary side conditions, form a complete mathematical theory of particulate systems. The only restrictions to the use of these equations are those listed above and the individual's adeptness for using mathematical equations to represent physical reality.

This chapter presented a brief outline of techniques that can be used to recover, in some approximate sense, a particle distribution function from the first k moments of the distribution. In some cases, it appears that the most efficient method of solution of these particle equations is to solve the moment equations together with, and with the same dimensionality of, the transport equations and then to recover the particle-size distribution from the moments.

Finally, the population balance was expressed in the number-volume and mass-size coordinate systems. Mass-conserving birth and death functions can be easily formulated in these systems. The former system is extensively used in the aerosol literature, while the latter system is useful for modeling comminution processes.

Nomenclature

$B(L)$	Particle birth function at size L	k_a	Area shape factor
\bar{B}	Transformed birth function in moment equation	k_v	Volumetric shape factor
B^0	Nucleation rate	L	Particle size
C	Solute concentration	m_j	j th moment of population distribution
$C_A(x, y)$	Coagulation kernel for particles of volumes x and y	n	Population density at size L
D	Particle death function at size L	n^0	Population density of nuclei
\bar{D}	Transformed death function in moment equation	$P(L)$	Size separation function of hydroclone classifier
G	Linear particle growth rate	Q	Volumetric flow rate
		R	Region in particle phase space

s	Particle characteristic	SUBSCRIPTS	
S	Surface bounding particle suspension	e	Fluid-particle interface
u	Solution velocity	F	Feed stream
v	Particle velocity in region R or particle volume	i	Inlet stream
v_e	External (spatial) particle velocity	k	k th stream
v_i	Internal particle velocity	m	Moving surface
V	Suspension volume	o	Outlet stream
x	Vector coordinates of region R	R	Recycle stream
		s	Free surface
		T	Total

GREEK SYMBOLS

ρ	Particle density
τ	Mean particle retention time

References

1. Hulburt, H. M., and Katz, S. (1964). *Chem. Eng. Sci.* **19**, 555.
2. Rivera, T., and Randolph, A. D. (1978). *ICH&C Proc. Des. Dev.* **17**, 182.
3. Hulburt, H. M., and Katz, S. (1964). *Chem. Eng. Sci.* **19**, 572-574.
4. Swift, D. L., and Friedlander, S. K. (1964). *J. Colloid Sci.* **19** 621.
5. Drake, R. L. (1972). In "Topics in Current Aerosol Research," Part 2 (G. M. Hidy and J. R. Brock, eds.). Pergamon Press, New York.
6. Levich, V. G. (1962). "Physiochemical Hydrodynamics," Prentice-Hall, Englewood Cliffs, New Jersey.
7. Human, H. J., Enkevort, W. J. P., and Bennema, P. (1982). In "Industrial Crystallization 81" (S. J. Jancic and E. J. deJong, eds.), p. 387, North Holland, Amsterdam.
8. Randolph, A. D., and White, E. T. (1977). *Chem. Eng. Sci.* **32**: 1067.

MODELING CONTINUOUS AND BATCH CRYSTALLIZERS

The previous chapters have dealt with the ideas inherent in the mathematical description of the particle-size distributions in dispersed systems. It was pointed out that the preferred distribution representations are those that derive directly from the physics and chemistry of the process by which they are produced. This means that the adjustable parameters and the form should arise directly from the process. In the case of crystallization, the crystal-size distribution depends on the kinetics of nucleation and growth as well as the constraints and the geometry of the system. The influence of these factors should be evidenced in the distribution function. We will now show how the size distribution of the product of a continuous mixed-suspension, mixed-product-removal (MSMPR) crystallizer is obtained.

4.1 Continuous Systems: Definition and Constraints

We now consider a continuously fed crystallizer of volume V , containing crystals dispersed in mother liquor as shown in Fig. 4.1-1. In the general case, it can be assumed that seed crystals are present in the volume V because of supersaturation. The supersaturation can be generated by chemical reaction, evaporation, or cooling. The following detailed treatment is specifically for a cooling system, although the result is applicable to other types.

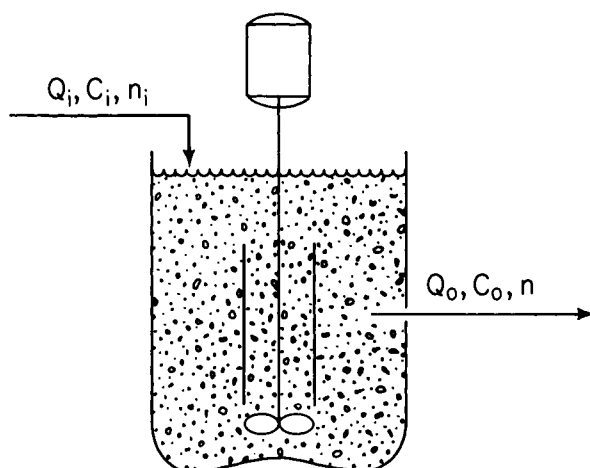


Fig. 4.1-1 Schematic representation of MSMPR crystallizer.

Crystallizers of the continuous mixed-suspension, mixed-product-removal type are widely used in industry and the laboratory. The constraints and conditions permitting this type of operation are relatively easy to attain. Figure 4.1-2 illustrates an industrial crystallizer of the draft-tube baffle (DTB) type, which normally approximates these constraints everywhere except in the annular space between the baffle and wall. Such crystallizers behave as though they are perfectly mixed. That is, in any arbitrary small element of the volume, regardless of its location in the mixed section of the crystallizer, a full and uniform particle-size continuum can be assumed to exist. Further, such a crystallizer has unclassified withdrawal. This means the particle-size distribution of the product crystals is the same as the distribution in the volume V of the crystallizer.

In many systems, crystal breakage or fracture is negligible except for attrition, which results in minute particles of near-nucleus size with no measurable reduction in the size of the parent crystal.

It is also quite common for crystals of different sizes to have the same crystal habit or shape. If this is the case, the crystal size may be represented by one characteristic linear dimension, usually the second-longest axis. In practice, the size is usually the size of a standard screen through which it just passes. If the habits of different sizes are the same, the volume, mass, or area of a crystal can be determined by use of an appropriate shape factor.

The above characterizing dimension will be given the symbol L and will be the screen size of the particle. The rate at which this dimension grows will be termed the growth rate G .

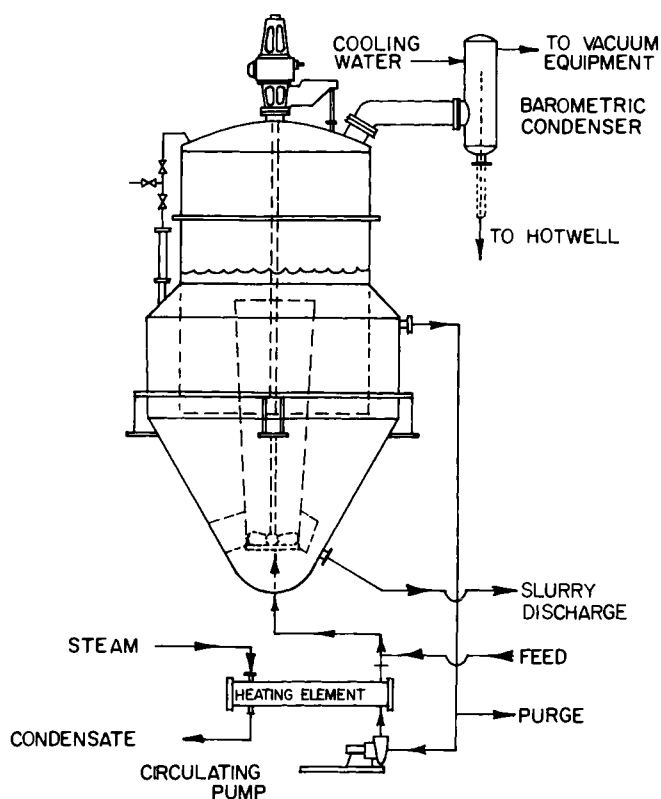


Fig. 4.1-2 Schematic diagram of industrial draft-tube baffle (DTB) crystallizer. (After Bennett and Van Buren [7].)

In conformance with previous developments, we will represent the distribution of sizes in terms of a population density n , defined such that

$$\Delta N = \int_{L_1}^{L_2} n dL \quad (4.1-1)$$

where N is the number of crystals in size range L_1 to L_2 per unit volume of suspension, with n being some function of L yet to be determined. The population density n has dimensions¹ of numbers per length per volume. If L_1 and L_2 represent the sizes of two adjacent screens in a stack of testing

¹In the following development, we choose suspension volume, rather than mother-liquor volume, as the basis. The two bases, suspension volume and clear liquid volume, are essentially the same when suspension density is less than 15%.

sieves, N is the *number* of crystals on the sieve in size range L_1 to L_2 in a unit volume of suspension.

In conformity with the discussion above, the constraints and assumptions used in the subsequent analysis may be summarized as follows: (a) perfect mixing; (b) no classification at withdrawal; (c) breakage assumed negligible; and (d) uniform shape factor.

Steady state operation requires that the feed rate, composition, and temperature remain constant, and that the crystallizer volume and temperature remain constant.

4.2 Steady-State Population Balance

The number of crystals in a given size range must be conserved with no accumulation if the system described in Section 4.1 is to operate at steady state. That is, the number rate of crystals entering a size range must equal the number rate leaving. We now use this requirement to derive the form of the size distribution.

Consider an arbitrary size range L_1 to L_2 in the volume V in Fig. 4.1-1, having population density n_1 and n_2 , respectively, at sizes L_1 and L_2 . The growth rate of crystals of size L_1 is G_1 and that of size L_2 is G_2 . For an increment of time t , the number of crystals entering this range because of growth is given by

$$Vn_1G_1\Delta t \quad (4.2-1)$$

Similarly, the number of crystals leaving by growth is

$$Vn_2G_2\Delta t \quad (4.2-2)$$

If the feed stream contains seed crystals in this range, then the input to the distribution in the volume V is

$$Q_i\bar{n}_i\Delta L\Delta t \quad (4.2-3)$$

where Q_i is the volumetric flow rate, \bar{n}_i is the average population density in the range L_1 to L_2 in the feed, and $L = L_2 - L_1$. Similarly, the number removed by bulk flow of crystals in this range is given by

$$Q\bar{n}L\Delta t \quad (4.2-4)$$

The output subscripts in the above term have been dropped because of the assumption of mixed removal. Combining Eqs. (4.2-1), (4.2-2), (4.2-3), and (4.2-4) in a number balance gives input to size range ΔL = output from size range ΔL , or

$$Q_i\bar{n}_i\Delta L\Delta t + Vn_1G_1\Delta t = Q\bar{n}\Delta L\Delta t + Vn_2G_2\Delta t \quad (4.2-5)$$

Dropping the Δt terms and rearranging gives

$$V(G_2 n_2 - G_1 n_1) = (Q_i \bar{n}_i - Q \bar{n}) \Delta L \quad (4.2-6)$$

Clearly, as ΔL approaches zero, the average values of n become point values and the equation takes the form

$$V d(Gn)/dL = Q_i n_i - Qn \quad (4.2-7)$$

For an unseeded system or at least for a system that has no crystals in the input large enough to be in the size range under consideration, $n_i = 0$ and

$$(V/Q) d(Gn)/dL + n = 0 \quad (4.2-8)$$

This is the useful form for the population balance obtained from a MSMPR crystallizer. Under most industrial conditions, McCabe's ΔL law may be assumed to hold. This requires that G not be a function of L . Using this assumption and defining τ , the drawdown time, equal to V/Q gives

$$G\tau(dn/dL) + n = 0 \quad (4.2-9)$$

This result can also be obtained from the macrobalance, Eq. (3.5-12), $(\partial n/\partial t) + d(\partial n/\partial L) + (n/\tau) = 0$, which reduces to Eq. (4.2-9), $G\tau(dn/dL) + n = 0$ for steady state.

We now define n^0 as the population density of the embryo-size crystals and we let the size of these crystals be vanishingly close to zero. Using this boundary condition, Eq. (4.2-9) can be integrated:

$$\int_{n^0}^n \frac{dn}{n} = - \int_0^L \frac{dL}{G\tau} \quad (4.2-10)$$

which gives

$$n = n^0 \exp(-L/G\tau) \quad (4.2-11)$$

Equation (4.2-11) represents the expected number distribution of the crystal product obtained from a crystallizer satisfying the assumptions and constraints discussed in Section 4.1. We note that it was derived for a cooling crystallizer but that it is not restricted to systems with that particular method of producing supersaturation. Equations (4.2-9)–(4.2-11) are applicable to MSMPR crystallizers so long as the holding time is the mean residence time of the *crystals* in suspension. In the case of mixed product removal, this is true if $\tau = V/Q_0$, where V is the crystallizer volume and Q_0 is the slurry withdrawal rate. In later chapters we will discuss other configurations.

The MSMPR concept has been used widely in the laboratory as well as in practice. Figure 4.2-1 shows a typical precipitation-type laboratory crystal-

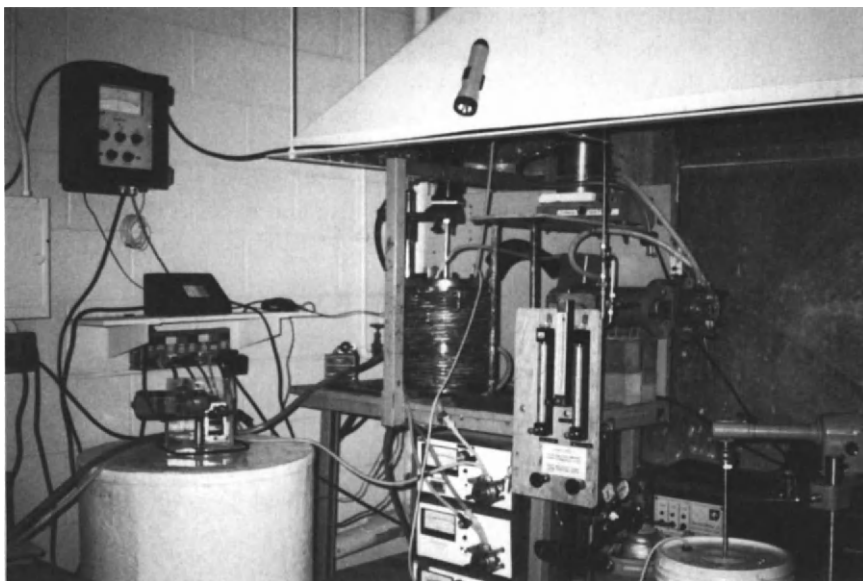


Fig. 4.2-1 Bench-scale MSMPR crystallizer used to obtain nucleation-growth kinetics. Supersaturation may be generated by cooling or by salting out with miscible third component. (Apparatus used in the Chemical Engineering Department, University of Arizona.)

lizer used at the University of Arizona. Industrial systems of this kind are also used. Typical of these are the draft-tube baffle (Fig. 4.1-2) and forced-circulation (FC) systems used widely in evaporative crystallization. These systems are designed to circulate the magma so that the solids in suspension will be well mixed and so that solids are present at the boiling surface. The result is a more uniform level of supersaturation throughout the crystallizer, which results in lower nucleation rates. Even large crystallizers approximate the well-mixed conditions and produce size distributions represented by Eq. (4.2-11).

4.3 Significance of the Model

The distribution represented by Eq. (4.2-11) has many advantages over an empirically formed distribution representation. Although it is a two-parameter model, each parameter can be related to the kinetics of the system and the imposed system constraints.

The parameter $G\tau$ is the product of the crystal growth rate and the mean retention time of the crystals in suspension. The growth rate G is directly determined by the kinetics of growth and τ is the drawdown time, which is known in any operating system. In practice, one cannot, in general, fix these two quantities independently. As we shall see later, one fixes the mass and energy flows, and the kinetics of nucleation and growth peculiar to the crystal-solvent system determine the growth rate that exists. The adjustable controls include the feed concentration, rate of energy input or removal, and feed rate.

The parameter n^0 , the population density of the nucleus-size crystals, is related to the kinetics of nucleation in the following way.

Let the nucleation rate B^0 be represented by

$$B^0 = (dN/dt)|_{L \rightarrow 0} = dN^0/dt \quad (4.3-1)$$

Note that the dimensions of Eq. (4.3-1) are number per time per volume. The growth rate G may be thought of as the differential dL/dt . Thus,

$$(dN/dt)_{L \rightarrow 0} = [(dL/dt)(dN/dL)]_{L \rightarrow 0} \quad (4.3-2)$$

Remembering that

$$dN^0/dL = (dN/dL)_{L \rightarrow 0} = n^0 \quad (4.3-3)$$

gives

$$B^0 = n^0 G \quad (4.3-4)$$

The parameter n^0 therefore is a representation of the nucleation kinetics, by Eq. (4.3-4). Thus the parameters are related to the crystallization rates operative in the system. These rates derive from the fundamental kinetic laws for nucleation and growth and the constraints imposed on the system, that is, system parameters such as flow rate, vessel size, concentrations, and energy input or removal rate.

EXAMPLE 4.3-1

Suppose that the crystal product from a system such as that described in Section 4.1 is sized and the population density function determined. If the data are plotted on semilog paper, they should form a straight line as shown in Fig. 4.3-1. The slope of the line is $-1/2.303G\tau$. With the holding time or drawdown time equal to 15 min, the growth rate from Fig. 4.3-1 is 2.7 $\mu\text{m}/\text{min}$.

The intercept n^0 is 4×10^6 number/ μm l. Multiplying n^0 and G gives the nucleation rate

$$B^0 = (4 \times 10^6)(2.7) = 10.8 \times 10^6 \text{ number/l min} \quad \blacklozenge$$

This example shows how the growth and nucleation rates can be determined simultaneously and shows how these rates affect the distribution.

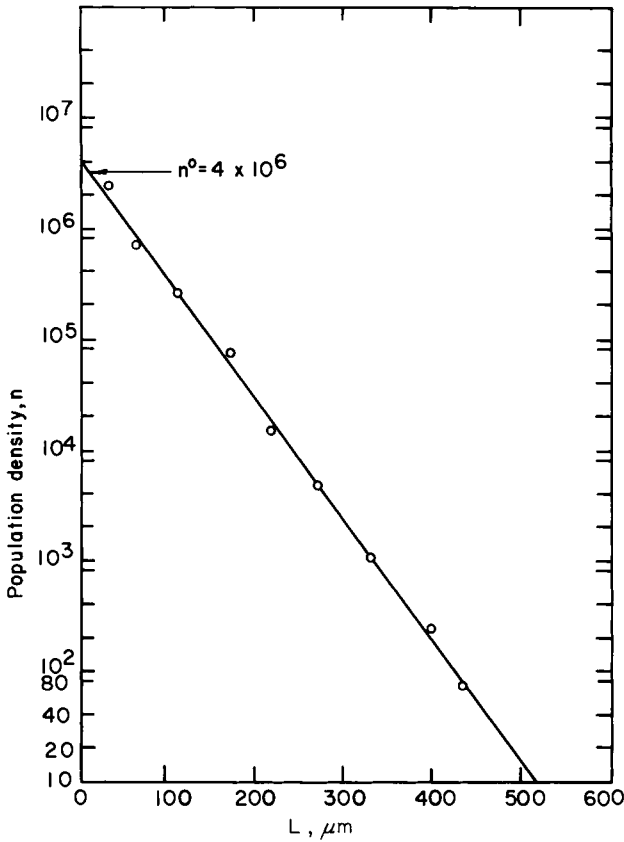


Fig. 4.3-1 Semilog population density plot from MSMPR crystallizer.

In Chapter 9, the experimental procedure and data obtained by exploiting this relationship will be discussed.

Note that the form of the distribution remains the same regardless of the fundamental kinetic laws of nucleation and growth as long as growth rate G is not a function of crystal size L . This being the case, the properties of this distribution can be generalized by using a dimensionless form. Let $y = n/n^0$ and $x = L/G\tau$. Substituting these quantities into Eq. (4.2-11) gives

$$y = \exp(-x) \quad (4.3-5)$$

The above equation describes the dimensionless distribution function for the MSMPR crystallizer. In the next section, it will be demonstrated how this equation can be used to develop information about crystallizing systems.

4.4 The Exponential Distribution

For practical purposes, one is not usually interested in the number distribution, but in the mass or weight distribution. In fact, frequently the distribution is represented only by the mass-averaged size and a coefficient of variation. We now show how these other distributions for the MSMR crystallizer can be obtained from the fundamental number distribution function n .

From the definition of the population density, the total number of crystals in a unit volume of a system was given in Section 2.3 by Eq. (2.3-3):

$$N_T = \int_0^{\infty} n(L) dL$$

We assume of course that the function $n(L)$ is such that the integral converges. For the exponential distribution, this is the case, and therefore

$$N_T = \int_0^{\infty} n^0 \exp\left(-\frac{L}{G\tau}\right) dL \quad (4.4-1)$$

or

$$N_T = m_0 = n^0 G\tau \quad (4.4-2)$$

The above is termed the zeroth moment of the distribution and represents the number of crystals in the volume under consideration.

Similarly, the higher moments represent other physical quantities pertaining to the crystals in a crystallizer. The first moment is termed the specific length L_T and is the sum of the characteristic lengths of all the crystals in the distribution. The second moment multiplied by an area shape factor is the specific surface area of the distribution. The third moment multiplied by a volume shape factor represents the specific volume of the crystals in the distribution. If the third moment is also multiplied by the crystal mass density, the product is the specific mass of crystals in the distribution. These moments are summarized as follows.

$$\begin{aligned} L_T = m_1 &= \int_0^{\infty} L n^0 \exp\left(-\frac{L}{G\tau}\right) dL \\ &= n^0 (G\tau)^2 \end{aligned} \quad (4.4-3)$$

$$\begin{aligned} A_T = k_a m_2 &= k_a \int_0^{\infty} L^2 n^0 \exp\left(-\frac{L}{G\tau}\right) dL \\ &= 2k_a n^0 (G\tau)^3 \end{aligned} \quad (4.4-4)$$

$$\begin{aligned} M_T = k_v m_3 \rho &= k_v \rho \int_0^{\infty} L^3 n^0 \exp\left(-\frac{L}{G\tau}\right) dL \\ &= 6k_v \rho n^0 (G\tau)^4 \end{aligned} \quad (4.4-5)$$

Equation (4.4-5) is an application of Eq. (2.8-8).

It is convenient to discuss these moments in dimensionless form and define the dimensionless number, length, area, and mass cumulative fractions as F , \mathcal{L} , \mathcal{A} , and W , respectively, as previously discussed in Section 2.8. Using Eq. (4.3-5) gives

$$\begin{aligned} F &= \frac{N}{N_T} = \int_0^x \exp(-x) dx \bigg/ \int_0^\infty \exp(-x) dx \\ &= 1 - \exp(-x) \end{aligned} \quad (4.4-6)$$

$$\begin{aligned} \mathcal{L} &= \frac{L}{L_T} = \int_0^x x \exp(-x) dx \bigg/ \int_0^\infty x \exp(-x) dx \\ &= 1 - \exp(-x)(1 + x) \end{aligned} \quad (4.4-7)$$

$$\begin{aligned} \mathcal{A} &= \frac{A}{A_T} = \int_0^x x^2 \exp(-x) dx \bigg/ \int_0^\infty x^2 \exp(-x) dx \\ &= 1 - \exp(-x)\left(1 + x + \frac{1}{2}x^2\right) \end{aligned} \quad (4.4-8)$$

$$\begin{aligned} W &= \frac{M}{M_T} = \int_0^x x^3 \exp(-x) dx \bigg/ \int_0^\infty x^3 \exp(-x) dx \\ &= 1 - \exp\left(1 + x + \frac{1}{2}x^2 + \frac{1}{6}x^3\right) \end{aligned} \quad (4.4-9)$$

At the outset of this discussion, we were concerned with the number density or the distribution function representing the distribution of numbers. We now generalize the define the dimensionless distribution functions for length, area, and mass as well. Let y , l , a , and w be the distribution functions for number, length, area, and mass, respectively. Differentiating Eqs. (4.4-6)–(4.4-9) gives

$$y(x) = \frac{d}{dx}[1 - \exp(-x)] = \exp(-x) \quad (4.4-10)$$

$$l(x) = \frac{d}{dx}[1 - \exp(-x)(1 + x)] = x \exp(-x) \quad (4.4-11)$$

$$a(x) = \frac{d}{dx}\left[1 - \exp(-x)\left(1 + x + \frac{x^2}{2}\right)\right] = \frac{x^2 \exp(-x)}{2} \quad (4.4-12)$$

$$w(x) = \frac{d}{dx}\left[1 - \exp(-x)\left(1 + x + \frac{x^2}{2} + \frac{x^3}{6}\right)\right] = \frac{x^3 \exp(-x)}{6} \quad (4.4-13)$$

These functions are plotted in Fig. 4.4-1. The function $w(x)$ is the distribution function used in Example 2.2-1 to calculate the coefficient of variation. Similar coefficients of variation can be determined for the functions of Eqs. (4.4-11) and (4.4-12).

Two parameters are required to specify the above distribution of the MSMPR crystallizer. In addition to the coefficient of variation, a convenient second parameter is the average size. A number of averages was defined as in Section 2.8. For the exponential distribution, these averages are the maxima (modes) on the curves shown in Fig. 4.4-1. Note that the values of these maxima are 1, 2, and 3, respectively. The definitions of these averages on a population basis, a length-weighted basis, and an area-weighted basis are:

$$\begin{aligned}\bar{x}_{1,0} &= \int_0^\infty xy \, dx \bigg/ \int_0^\infty y \, dx \\ &= \int_0^\infty x \exp(-x) \, dx \bigg/ \int_0^\infty \exp(-x) \, dx = 1\end{aligned}\quad (4.4-14)$$

$$\begin{aligned}\bar{x}_{2,1} &= \int_0^\infty x^2 y \, dx \bigg/ \int_0^\infty xy \, dx \\ &= \int_0^\infty x^2 \exp(-x) \, dx \bigg/ \int_0^\infty x \exp(-x) \, dx = 2\end{aligned}\quad (4.4-15)$$

$$\begin{aligned}\bar{x}_{3,2} &= \int_0^\infty x^3 y \, dx \bigg/ \int_0^\infty x^2 y \, dx \\ &= \int_0^\infty x^3 \exp(-x) \, dx \bigg/ \int_0^\infty x^2 \exp(-x) \, dx = 3\end{aligned}\quad (4.4-16)$$

In dimensional form, letting $x = L/G\tau$, then

$$\bar{L}_{1,0} = G\tau \quad (4.4-17)$$

$$\bar{L}_{2,1} = 2G\tau \quad (4.4-18)$$

$$\bar{L}_{3,2} = 3G\tau \quad (4.4-19)$$

From these equations, it would seem that the average size depends only on growth rate and residence time. However, as will be seen later, under the constraints of the system, growth rate is intimately connected to the nucleation rate; therefore, the dominant size obtainable is determined by the kinetic rates of both phenomena.

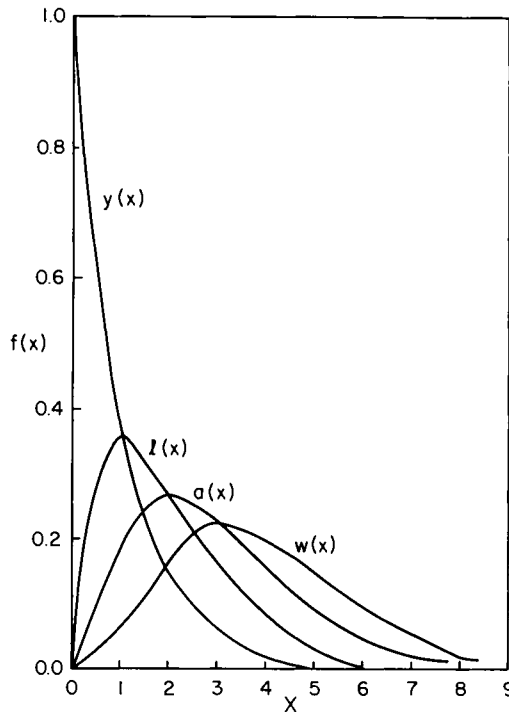


Fig. 4.4-1 Number, length, area, and mass distribution functions in an MSMPR crystallizer.

EXAMPLE 4.4-1

From Eq. (4.4-5), the solids concentration of crystals per unit volume is $M_T = 6k_v \rho n^0 (G\tau)^4$. Following the development in Section 2.8, the mass concentration in a given size range is given by

$$dm = d\left(k_v \rho \int_0^L L^3 n dL\right) = \rho k_v L^3 n dL \quad (4.4-20)$$

The weight fraction is then dm/M_T , and thus

$$\begin{aligned} w(L) &= dW/dL = L^3 n / 6n^0 (G\tau)^4 \\ &= L^3 n^0 \exp(-L/G\tau) / 6n^0 (G\tau)^4 \end{aligned} \quad (4.4-21)$$

Where dW/dL is the weight-fraction distribution of crystals in suspension and is the dimensionless version of Eq. (4.4-13). The maximum of the curve represented by Eq. (4.4-21) is the dominant size of the mass distribution.

Thus, at this dominant size,

$$dW/dL = 3L^2 \exp(-L/G\tau) - (L^3/G\tau) \exp(-L/G\tau) = 0 \quad (4.4-22)$$

Canceling $L \exp(-L/G\tau)$ gives

$$\bar{L}_{3,2} = L_d = 3G\tau \quad (4.4-23)$$

Thus, the mode $\bar{L}_{3,2}$ may be thought of as the dominant particle size. ♦

In many cases the mean size used is the mass-weighted mean size, namely, $\bar{L}_{4,3} = 4G\tau$.

4.5 The Steady-State Mass Balance

In Example 2.2-1, it was shown that for the distribution function of Eq. (4.4-13) (which is the mass distribution function for crystal product from an MSMPR crystallizer), the coefficient of variation is always 50. Consequently, the location of this distribution on the size axis can be characterized by one parameter, namely, the product of the growth rate and mean residence time. Three times this parameter is the domain particle size, which, along with the coefficient of variation, completely characterizes the distribution.

As mentioned before, the value of this parameter is related to the kinetic rates of nucleation and growth and the constraints on the system. A relationship will now be developed to show how these various factors determine the magnitude of this size parameter.

Up to this point, only the population balance has been considered. It is now necessary to incorporate a mass balance to fully define the system. The assumptions and constraints previously mentioned still apply.

The rate at which solute is lost from the mother liquor must equal the rate at which mass is gained by the solid phase. Thus,

$$Q_i C_i - Q_o C_o = Q_o M_T \quad (4.5-1)$$

Because the mass rate of phase change due to nucleation is negligibly small, the rate of make, $Q_o M_T$, can be set equal to the rate of growth on the surface of the suspended particles. Therefore,

$$\frac{1}{2} G A_T \rho V = Q_i C_i - Q_o C_o = Q_o \delta C \quad (4.5-2)$$

where $\delta C = Q_i / Q_o C_i - C_o$. The $\frac{1}{2}$ arises because G is the growth rate of crystal diameter and Eq. (4.5-2) requires facial growth rate.

$$G = 2(\delta C) / \left(\rho k_a \tau \int_0^\infty n L^2 dL \right) \quad (4.5-3)$$

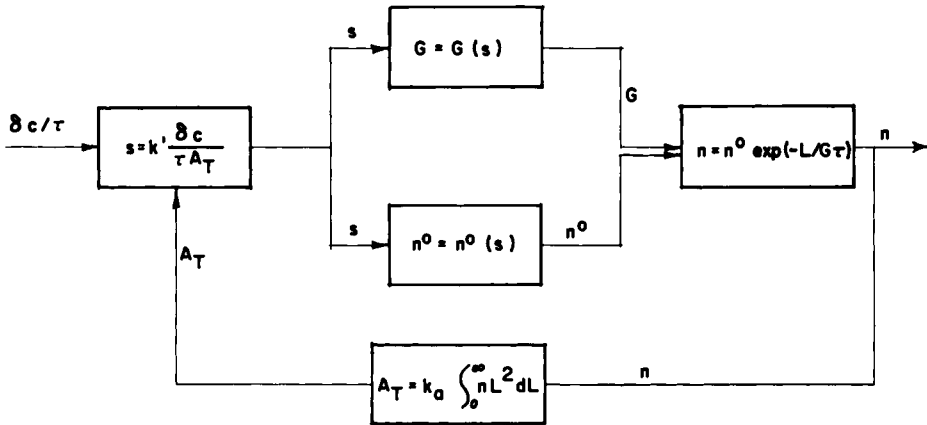


Fig. 4.5-1 Information flow diagram illustrating the interrelationship of crystal growth rate, nucleation rate, and crystal-size distribution.

We note that the solute concentration drop across the crystallizer depends on the retention time τ , as well as on energy inputs, for systems that operate with measurable unrelieved supersaturation. Such systems, whose yield depends on throughput, are referred to as class I systems. In class II systems, the exit concentration approaches C_{eq} and the per pass yield is independent of throughput. Equation (4.5-3) is valid at steady state for both class I and class II systems. This equation shows that the growth rate is inversely proportional to the surface area of crystals in suspension. This area is related to the size distribution by Eq. (4.4-4). The size distribution in turn is determined by the growth rate and nucleation rate. These rates appear in the distribution function as G and n^0 . This interrelationship forms a feedback loop, which is described by Fig. 4.5-1.

We recognize that growth is a function of supersaturation, often a linear function, and therefore Eq. (4.5-3) can be written

$$s = k' \delta C / \left(\tau \int_0^\infty n L^2 dL \right) \quad (4.5-4)$$

where $s = C - C_{eq}$. Nucleation rate B^0 is also a function of s ; consequently n^0 can be expressed as a function of s . For a class II system, $\delta C / \tau$ is a design choice and can be thought of as an input to the feedback loop shown in Fig. 4.5-1.

In general, nucleation rate is more sensitive to supersaturation changes than is growth rate. When this is the case, the diagram shows that for longer holding times, larger and consequently fewer crystals would be expected. The net result is that G decreases less than the increase in holding time τ ,

with a consequent increase in dominant particle size L_d , where again, from Eq. (4.4-19), $L_d = 3G\tau$. In many applications, however, substantial increases in size cannot be obtained using longer retention times.

Higher input concentrations with an equivalent change in energy input (or removal) to produce the same final mother liquor concentration should give a larger particle size. In most cases, this does not occur. This will be considered in later chapters when homogeneous and secondary nucleation mechanisms are discussed.

4.6 Batch Systems Definition and Constraints

The modeling of crystal size distribution obtained from batch crystallization systems is much more complex than the modeling of CSD from continuous systems. The assumption of steady state cannot be made; thus, a partial differential equation results from the population balance. The CSD is therefore time-dependent as well as size-dependent. Moreover, the initial conditions become more important because the initial shower of nuclei or the seeds used become part of the final crystal product and affect the CSD. In some instances the initial crystal size distribution dominates the character of the final crystal size distribution. The CSD models obtained therefore will be highly dependent on the process conditions at the start of the batch and the degree to which conditions *change* as the batch crystallization proceeds. The models developed here will be for specific and defined conditions and are thus to be regarded as illustrations. It should be recognized that greatly different models for CSD will be obtained for other possible system conditions and constraints.

It is more convenient to start with Eq. (3.5-11), developed in Chapter 3 for the basic batch equation, then to use the development used in Section 4-2 for the continuous system. A batch system, or unseeded semibatch system, has no net inflow or outflow of crystals. Therefore the population balance of Eq. (3.5-11) reduces to

$$\frac{\partial(nV)}{\partial t} + \frac{\partial(nGV)}{\partial L} = 0 \quad (4.6-1)$$

Because the working volume of a batch or semibatch² system may be time-varying, it is convenient to redefine the number density on the basis of the total operating volume of the crystallizer; thus,

$$\tilde{n} = nV \quad (4.6-2)$$

²A semibatch system is one that has a continuous feed but withdrawal only at the end of the batch run.

With this substitution, Eq. (4.6-1) becomes

$$\frac{\partial \tilde{n}}{\partial t} + \frac{\partial (G\tilde{n})}{\partial L} = 0 \quad (4.6-3)$$

A boundary condition with respect to size can be provided by defining a time-dependent nucleation rate B^0 , where B^0 is the number of nuclei produced per unit volume per unit time at zero size. Thus, from Eq. (4.3-4),

$$\tilde{n}^0 = B^0 V / G \quad (4.6-4)$$

Equations (4.6-3) and (4.6-4), along with an initial crystal size distribution, define the final batch CSD at $t = t_f$. This set cannot be solved explicitly until the batch operating conditions are defined and an appropriate mass or energy balance is made. The appropriate mass balance is

$$\frac{d(CV)}{dt} + \frac{d\tilde{W}}{dt} = 0 \quad (4.6-5)$$

where \tilde{W} is the mass of solids in suspension and C is the concentration of solute in solution. The mass balance for a semibatch system would contain an additional term for solute input. For a class II evaporative system, the first term in Eq. (4.6-5) becomes $C dV/dt$ and for a cooling batch system the first term becomes $V dC/dt$. For linear solubility dC/dt becomes $k dT/dt$ where T is the temperature of the crystallizing suspension. In order to relate \tilde{W} to the crystal size distribution and thus the rate of nucleation and growth, the moment equations must be used. In this instance, however, the moments are time-dependent; thus,

$$\begin{aligned} d\tilde{N}/dt &= B^0 V \\ \frac{d\tilde{\mathcal{L}}}{dt} &= \tilde{N} G \\ \frac{d\tilde{A}}{dt} &= 2k_a \tilde{\mathcal{L}} G \\ \frac{d\tilde{W}}{dt} &= 3\rho \frac{k_v}{k_a} \tilde{A} G \end{aligned} \quad (4.6-6)$$

If an initial condition for the size distribution [$\tilde{n} = \tilde{n}(0, L)$] is known or can be assumed, and if appropriate kinetic models for nucleation and growth are known, Eqs. (4.6-3)–(4.6-6) can be solved to give the CSD for a batch or semibatch system as a function of time. The equations can also be used to give a batch evaporation or cooling program necessary to achieve a desired CSD. In general the model must be solved numerically.

Baliga [1] solved the set for the very limited case of an evaporative system required to operate at a constant growth rate and an assumed constant B^0 (B^0 taken as nuclei per unit time per unit volume). The moment equations [Eq. (4.6-6)] reduce to

$$\frac{dV^4}{dt^4} + 4a^2V = 0 \quad (4.6-7)$$

where

$$4a^2 = \frac{6k_v B^0 G^3}{C}$$

The solution of Eq. (4.6-7) is

$$V(t) = V_0 (\cos at)(\cosh at) \quad (4.6-8)$$

and gives the rate at which solvent must be evaporated to maintain a constant growth rate, and thus a constant supersaturation. Baliga also

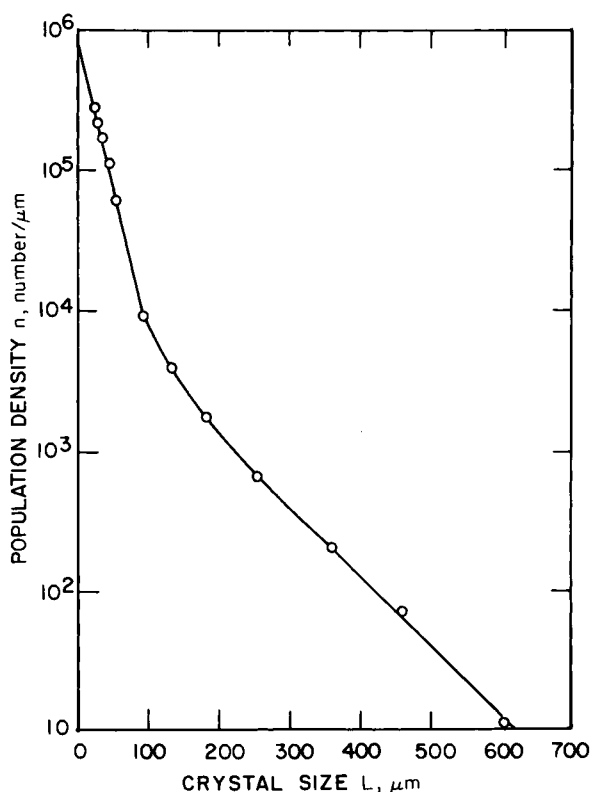


Fig. 4.6-1 Initial CSD for batch crystallization of K_2SO_4 . (After Baliga [1].)

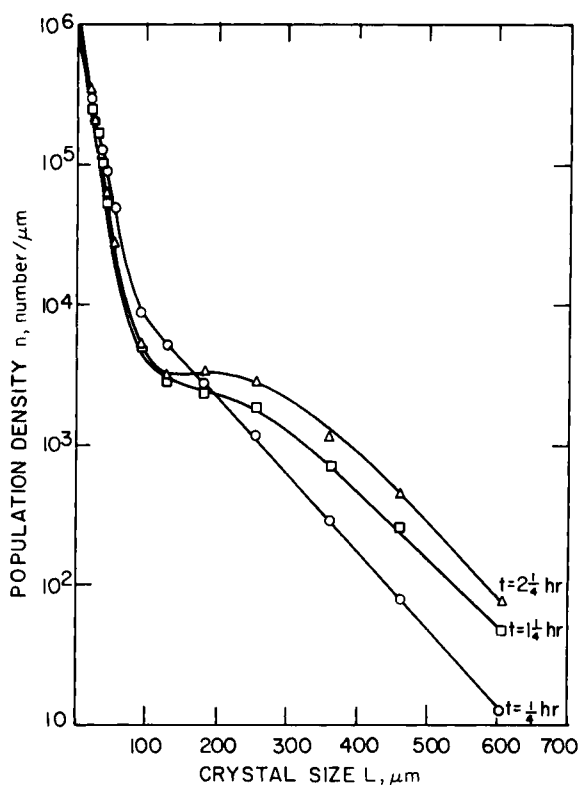


Fig. 4.6-2 CSD after various time for batch crystallization [1].

solved the set for the CSD expected, which is given as

$$\tilde{n} = \tilde{n}^0 \{ [\cos a/G](Gt - L) \} \{ [\cosh(a/G)](Gt - L) \} [1 - U(L - Gt)] \quad (4.6-9)$$

where \tilde{n}^0 is the initial population density of nuclei. This solution does not represent a realistic case on two counts. It is not possible to achieve the initial conditions as used, nor is it likely even at constant supersaturation that nucleation per unit volume could be expected to be constant.

In any real unseeded crystallizer, initial nucleation can occur by several mechanisms and usually occurs as an initial shower followed by a reduced nucleation rate. This being the case, one cannot realistically use the zero initial condition for the size distribution. In reality, an initial distribution exists and subsequent nucleation is of the secondary³ type.

³ This will be discussed in Chapter 5.

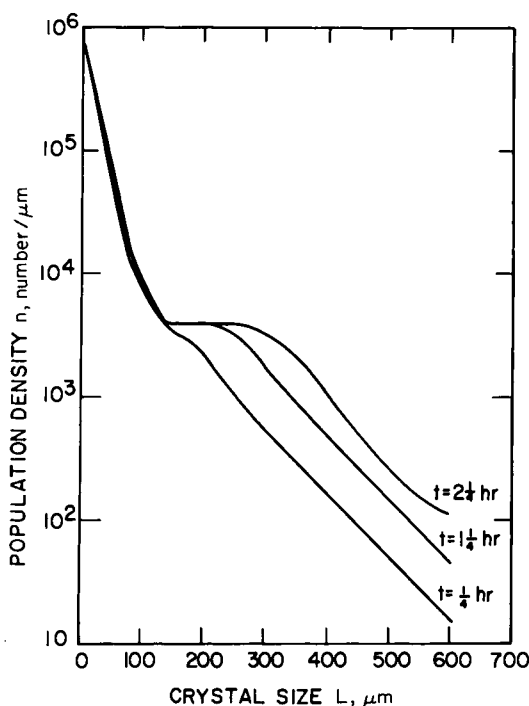


Fig. 4.6-3 Computed CSD using initial condition from Fig. 4.6-1 [1].

Baliga [1] obtained the initial CSD shown in Fig. 4.6-1 in the batch evaporative crystallization of K_2SO_4 . This distribution was determined within 10 min of the observed onset of nucleation. The distribution obtained after batch times of $\frac{1}{4}$, $1\frac{1}{4}$, and $2\frac{1}{4}$ h are shown in Fig. 4.6-2. These distributions are typical of those from seeded as well as unseeded batch crystallizers. Baliga [1] was able to model these distributions numerically using Eqs. (4.6-3)–(4.6-6) along with the initial CSD shown in Fig. 4.6-1. The results are shown in Fig. 4.6-3. It was necessary to use a size-dependent growth model, however, a growth model that will be discussed in subsequent paragraphs.

A more easily modeled example is a system where growth rate (and thus supersaturation) is to be maintained at a level just below the level where nucleation occurs. Under such conditions a seeded system can be modeled to determine the evaporation or evaporation rate that will give a predetermined growth rate. In this case the rate of change of the zeroth moment, $d\tilde{N}/dt$, is zero and the set of equations result in a third-degree polynomial rather than a fourth-degree polynomial as indicated by Eq. (4.6-8). The

solution for this model is shown in Chapter 6 and gives the optimum evaporation rate for an evaporative batch crystallizer.

4.7 Modeling CSD When Growth is Size-Dependent

In deriving the basic model for CSD from a continuous crystallizer, we assumed for the sake of simplicity that all crystals grow at the same rate. There is some evidence that, due to a variety of reasons, crystals of different sizes may grow at different rates even though they exist in the same supersaturated solution. The reasons will be discussed in Chapter 5. Here the expected CSD will be modeled for a particular size-dependent growth model that has been shown to fit experimental data quite well. The evidence for size-dependent growth has almost always shown that when size-dependent growth is observed, large crystals grow more rapidly than small crystals.

When size-dependent growth is accounted for, the differential equation resulting from the population balance must, for a continuous crystallizer, be written

$$d(Gn)/dL + n/\tau = 0 \quad (4.7-1)$$

A size-dependent growth function can now be inserted in place of G and the indicated differential equation integrated as before. Abegg *et al.* [2] have shown that the form

$$G = G_0(1 + \gamma L)^b, \quad b < 1 \quad (4.7-2)$$

can be used to fit most data. Here G_0 , b , and γ are experimentally determined constants, G_0 being the supersaturation-dependent growth rate of a “zero” size crystal. Insertion of Eqs. (4.7-2) and (4.7-1) and integration from 0 to L gives

$$n(L) = Kn^0(1 + \gamma L)^{-b} \exp\left[-(1 + \gamma L)^{1-b}/G_0\tau\gamma(1 - b)\right] \quad (4.7-3)$$

where $K = \exp[1/G_0\tau\gamma(1 - b)]$ and b is < 1 .

Equation (4.7-3) satisfies all the moment equations previously developed and therefore is quite useful in analyzing systems that exhibit size-dependent growth. It is convenient to cast Eq. (4.7-3) in dimensionless form for analysis of its characteristics. Let $x = L/G_0\tau$ and $y = n/n_0$ and let $\gamma = 1/G_0\tau$ [reducing Eq. (4.7-3) to a one-parameter size-dependent equation]:

$$y = K(1 + x)^{-b} \exp\left[-(1 + x)^{1-b}/(1 - b)\right], \quad b < 1 \quad (4.7-4)$$

Figure 4.7-1 is a plot of this equation for various values of b . When growth rate increases with size, b is positive and one obtains semilog plots that are

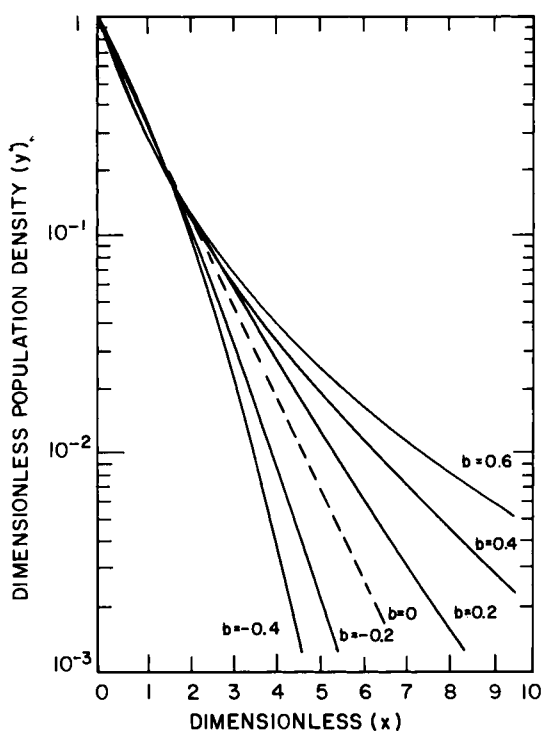


Fig. 4.7-1 Dimensionless CSD from Eq. (4.7-4). (After Abegg *et al.* [2].)

concave upward. That is the most probable occurrence experimentally if size-dependent growth occurs.

One must be extremely careful in interpreting experimental data from MSMPR crystallizers in light of this equation, however. For example, it is known that the removal of slurry at something other than isokinetic velocity will cause classification at the discharge. In this event, the residence-time distribution of the crystals is no longer a constant τ , but a function of size, $\tau(L)$. Incorporating such a functional relationship in Eq. (4.7-1) will give a result qualitatively indistinguishable from Eq. (4.7-3). This phenomenon will be discussed later.

Equally important is the fact that most crystals exhibit growth dispersion. That is, crystals have a distribution of growth rates. Thus fast-growing crystals will be larger because they grow rapidly, and are consequently not growing rapidly because they are large. It is impossible to distinguish between size-dependent growth on the one hand and growth dispersion on the other by analyses of MSMPR size alone. The matter of growth dispersion will be taken up in the next paragraphs.

4.8 Modeling CSD with Growth Dispersion

A far more difficult modeling problem is that of developing a model to predict CSD from batch and continuous crystallizers when the crystallized material exhibits growth dispersion. The factors contributing to growth dispersion are discussed in Chapter 5. Here the problem of predicting CSD when the phenomena exists will be addressed.

The term *growth dispersion* is used to describe the fact that crystals of the same size can and do grow at different rates because they see different environments in the crystallizer or because of inherent structural conditions that differ from crystal to crystal. There seem to be at least two manifestations of this phenomenon, each of which results in a different effect on CSD. First, in some instances it appears that the growth of an individual can change in a random manner so that over the period of time the crystal is in the crystallizer it can have several growth rates. We term this phenomenon *random growth dispersion*. Second, experimental evidence [3] has shown that in some crystal systems each crystal exhibits a characteristic growth rate and maintains that growth rate throughout its residence in the crystallizer. We term the phenomenon *intrinsic growth dispersion*. Random growth dispersion has been shown to affect narrow batch-produced CSD but has no effect on the form of steady-state crystal size distributions from continuous crystallizers. *Intrinsic growth dispersion* affects the CSD in both batch and continuous crystallizers. Models for CSD from batch system will be derived for random growth dispersion (RGD), and models for CSD from continuous systems will be derived from intrinsic growth dispersion (IGD).

4.8.1 Random Growth Dispersion Diffusivity Model

The growth of crystals along a size axis is analogous to molecular velocity in a flow field. If the growth rate fluctuates randomly around a mean growth rate, it can be represented analogously to molecular diffusion flux due to a concentration gradient [4]. Thus from Eq. (3.5-10) (Chapter 3), for a batch system,

$$\frac{\partial n}{\partial t} + G \frac{\partial n}{\partial L} - D_G \frac{\partial^2 n}{\partial L^2} = 0 \quad (4.8-1)$$

where G is the mean growth rate and D_G is empirically defined as *growth diffusivity*. It is convenient to cast Eq. (4.8-1) in moment form to illustrate the effect on mean size and coefficient of variation (c.v.). Let $y = nG/B^0$, $x = L/L_1$, $\theta = Gt/L_1$, $Pe_B = GL_1/D_G$. Here we consider only a seeded batch system where no nucleation takes place and the system is seeded with seeds of mean size L_i and variance s^2 . The quantity Pe_B will be referred to

as the batch Peclet number for size dispersion. The dimensionless batch moment equation for this case can then be written

$$\begin{aligned}\frac{df_0}{d\theta} &= 0, & f_0(0) &= 1 \\ \frac{df_1}{d\theta} &= f_0, & f_1(0) &= 1 \\ \frac{df_2}{d\theta} &= 2f_1 + \frac{2}{\text{Pe}_B}f_0, & f_2(0) &= \frac{s_i^2}{L_i^2} + 1 = (\text{c.v.})_i^2 + 1\end{aligned}\quad (4.8-2)$$

Recall that the dimensionless moments f_0 , f_1 , and f_2 represent the number, length, and area, respectively. Defining as the dimensionless standard deviation s/L_i and σ^2 as the dimensionless variance, the solution to Eq. (4.8-2) is

$$\begin{aligned}f_0 &= 1 & f_1 &= \theta + 1 \\ f_2 &= \sigma_i^2 + 1 + \theta^2 + 2\theta + \frac{2\theta}{\text{Pe}_B}\end{aligned}\quad (4.8-3)$$

The dimensionless variance of the crystal product is given by

$$\sigma^2 = f_2 - f_1 = \sigma_i^2 + 2\theta/\text{Pe}_B \quad (4.8-4)$$

and the increase in population variance due to growth rate fluctuations is given by

$$\Delta\sigma^2 = \sigma^2 - \sigma_i^2 = \frac{2}{\text{Pe}_B}(\theta) \quad (4.8-5)$$

or in terms of the dimensionless variance s ,

$$\Delta s/\Delta t = 2D_G \quad (4.8-5)$$

The coefficient of variation of product crystal is

$$\text{c.v.} = \frac{\sigma}{f_1} = \frac{[(\text{c.v.})_i^2 + 2\theta/\text{Pe}_B]^{1/2}}{1 + \tau} \quad (4.8-6)$$

Note the dimensionless standard deviation $\sigma_i = s_i/L_i = (\text{c.v.})_i$.

This equation is plotted in Fig. 4.8-1 and shows how c.v. varies with batch time and growth diffusivity. For the growth of a batch of crystals with no nucleation and no dispersion ($\text{Pe}_B = \infty$) it can be seen that c.v. decreases as growth proceeds, since mean size increases without any change in the size spread. With growth dispersion, the spread increases; therefore c.v. may increase or decrease.

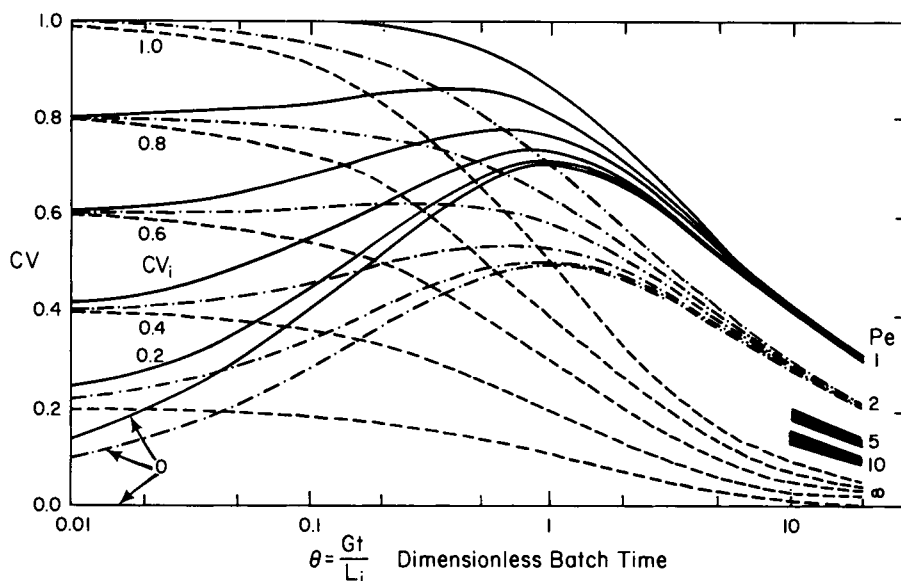


Fig. 4.8-1 Coefficient of variation (c.v.) for batch crystallization showing effect of growth dispersion. (After Randolph and White [4].)

4.8.2 Intrinsic Growth Dispersion

If individual crystals exhibit a characteristic growth rate and maintain that growth rate for their entire crystallizer retention time, a different modeling approach must be used [5]. Consider a suspension of growing crystals, each with an intrinsic growth rate g_i . The distribution of these growth rates in the crystal suspension is given by the function $\eta(g)$ such that the total number of crystals is given by

$$N = \sum_{i=0}^{\infty} \eta(g_i) = \int_0^{\infty} \eta(g) dg \quad (4.8-7)$$

Thus the CSD for all crystals with growth rate g_i produced by an MSMR crystallizer is given by

$$n_i(L) = n_i^0 \exp(-L/g_i\tau) \quad (4.8-8)$$

and the number of crystals greater than size L with growth rate g_i is

$$N_i(L) = \int_L^{\infty} n_i dL = B_i^0 \tau \exp\left(-\frac{L}{g_i\tau}\right) \quad (4.8-9)$$

Since g_i is independent of size L , the CSD of the total product $N(L)$ is merely the sum of the distributions for each group of crystals, with growth

rate g_i ($i = 1, 2, 3, \dots$), and is given by

$$N(L) = \sum_{i=0}^{\infty} B_i^0 \tau \exp\left(-\frac{L}{g_i \tau}\right) \quad (4.8-10)$$

or in terms of population density,

$$n(L) = \sum_{i=0}^{\infty} n_i(L) = \sum_{i=0}^{\infty} n_i^0 \exp\left(-\frac{L}{g_i \tau}\right) \quad (4.8-11)$$

If $\eta(g)$ represents the distribution of growth rates of the crystals, then $\eta(g) dg$ is the fraction of crystals having the growth rate g . Thus for growth rate g_i , Eq. (4.8-9) can be written as

$$N_i(L) = B^0 \tau \exp\left(-\frac{L}{g_i \tau}\right) \eta(g)_i \quad (4.8-12)$$

where $B^0 \tau$ is the total number of crystals in the crystallizer and B^0 is the total nucleation rate. Further, the total number of crystals with size greater than L with all possible growth rates is

$$N(L) = \int_0^{\infty} N_i = \int_0^{\infty} B^0 \tau \exp\left(-\frac{L}{g \tau}\right) \eta(g) dg \quad (4.8-13)$$

The fraction of crystals greater than size L is

$$F(L) = \frac{N(L)}{B^0 \tau} = \int_0^{\infty} \exp\left(-\frac{L}{g \tau}\right) \eta(g) dg \quad (4.8-14)$$

and the dimensionless size distribution function is

$$y_L = \frac{n(L)}{n^0} \int_0^{\infty} \frac{1}{g \tau} \exp\left(-\frac{L}{g \tau}\right) \eta(g) dg \quad (4.8-15)$$

This equation has been solved numerically to give the CSD expected from normal and gamma growth-distribution function by Larson *et al.* [5]. Following the work of Janse and de Jong [6], an analytical solution for a so-called inverse gamma-function distribution is also given by Larson *et al.* [5]. Figure 4.8-2 compares the three growth distributions all with a common mean \bar{g} .

It is equally useful to relate the growth distribution function to the expected CSD by formulating the moment equations for the two distributions. Multiplying both sides of Eq. (4.8-15) by $L^j dL$ and integrating gives

$$\int_0^{\infty} L^j y(L) dL = j! \tau^j \int_0^{\infty} g^j \eta(g) dg \quad (4.8-16)$$

The left-hand side of the equation is simply the j th moment of the CSD, and the right-hand integral is the j th moment of the growth-rate distribu-

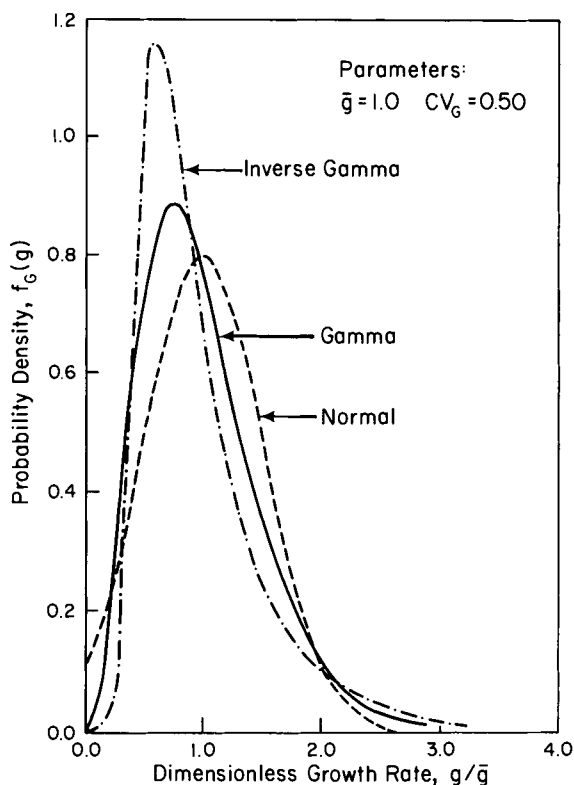


Fig. 4.8-2 Growth rate distribution for $c.v._g = 0.5$ and $\bar{g} = 1.0$. (After Larson *et al.* [5].)

tion. Thus

$$(m_L)_j = j! \tau^j (m_g)_j \quad (4.8-17)$$

For $j = 1$ and 2 ,

$$(m_L)_1 = \tau (m_g)_1 \quad (4.8-18)$$

$$(m_L)_2 = 2\tau^2 (m_g)_2 \quad (4.8-19)$$

From Eqs. (4.8-18) and (4.8-19), it can be shown that the coefficient of variation of the size distribution on a population basis can be related to the coefficient of variation of the growth distribution by

$$(c.v.)_L = \sqrt{2(c.v.)_g^2 + 1} \quad (4.8-20)$$

A relationship between $(c.v.)_g$ and the coefficient of variation on a mass basis can also be obtained. Figure 4.8-3 compares the CSD predictions for

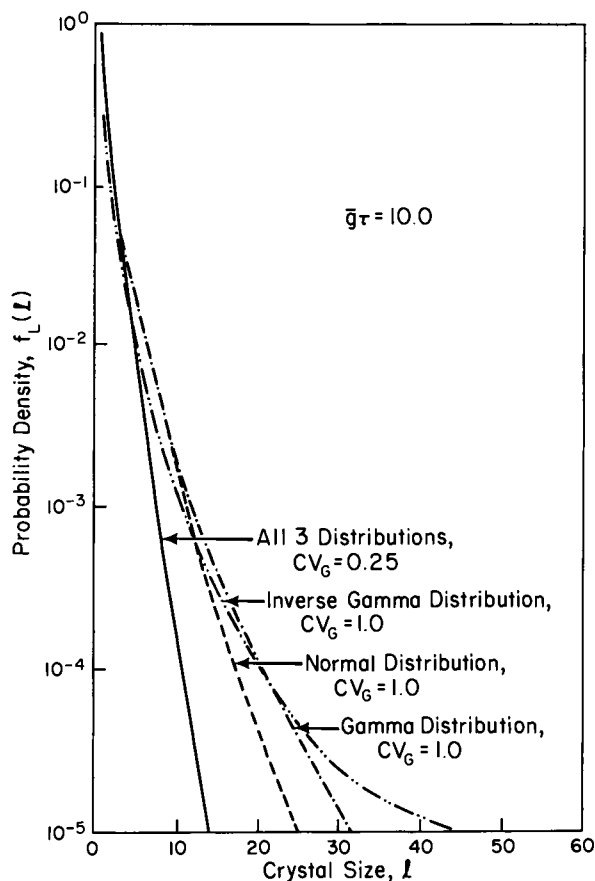


Fig. 4.8-3 Comparison between CSD for three different growth dispersion functions. (After Larson *et al.* [5].)

three growth distribution functions all having the same $(c.v.)_g$. The growth rate distribution must be quite broad before appreciable effects are noted in the CSD.

4.9 Summary

This chapter presented the classical model for crystal size distribution obtained from the population balance for MSMPR crystallizers and batch crystallizers. The models for the various CSD properties that obtain were also presented. In addition, the effects of certain growth phenomena on CSD were delineated.

When the growth rates of all crystals are the same in a given environment, the basic exponential distribution obtains for the MSMR crystallizer operating at steady state. The moments of this distribution can be used to calculate mean size on various bases, but the coefficient of variation of such a distribution is always 50%. For batch systems the size distribution depends heavily on the initial conditions and how conditions vary during the batch run.

When growth is not the same for all crystals, deviations from the exponential distribution occur. These deviations can be attributed to non-uniform environments (poor mixing) or to inherent properties of the crystals themselves. In either case the deviation from the exponential distribution is usually an excessive number of crystals in the small end of the size range. This is usually caused by growth dispersion or size-dependent growth. More detailed discussion of why this occurs will be addressed in subsequent chapters. This chapter has discussed the effect of these crystal phenomenon on CSD. In subsequent chapters we will discuss the effect of process and equipment configuration on CSD.

Nomenclature

a	Constant area distribution	M	Cumulative crystal mass distribution
a	Dimensionless area distribution	n	Population density
A	Cumulative crystal surface area distribution	n^0	Population density of nuclei
\mathcal{A}	Dimensionless cumulative crystal surface area	N	Cumulative number distribution
B^0	Nucleation rate	Pe_B	Batch Peclet number
c.v.	Coefficient of variation	Q	Volumetric feed and discharge rate
C	Solute concentration	s	Variance
D_G	Growth diffusivity	s	Supersaturation
f	Dimensionless moment	t	Time
F	Dimensionless cumulative number of crystals	V	Crystallizer volume
g	Growth rate	w	Dimensionless mass distribution
G	Linear crystal growth rate	W	Dimensionless cumulative mass distribution
G_0	Growth of zero size	x	Dimensionless crystal size
k_a	Area shape factor	y	Dimensionless population density
k_v	Volume shape factor		
K	Constant		
l	Dimensionless length distribution		
L	Crystal size		
\mathcal{L}	Dimensionless cumulative crystal length		
L_i	Seed size		
m_j	j th moment of the distribution		

GREEK SYMBOLS

ρ	Crystal density
γ	Parameter of Eq. (4.7-2)
σ	Standard deviation
τ	Holding time

SUBSCRIPTS

d	Dominant
i	Inlet stream
o	Outlet stream
T	Total quantity

SUPERSCRIPTS

b	Exponent of Eq. (4.7-2)
\sim	Total volume basis

References

1. Baliga, J. B. (1970). Crystal nucleation and growth kinetics in batch evaporative crystallization. Ph.D. Dissertation, Iowa State University, Ames, Iowa, unpublished.
2. Abegg, C. F., Stevens, J. D., and Larson, M. A. (1968). *AIChE J.* **14**, 118.
3. Berglund, K. A., and Larson, M. A. (1984). *AIChE J.* **30**(2), 280.
4. Randolph, A. D., and White, E. T. (1977). *Chem. Eng. Sci.* **32**, 1067.
5. Larson, M. A., White, E. T., Ramanarayanan, K. A., and Berglund, K. A. (1985). *AIChE J.* **31**, 90.
6. Janse, A. H., and de Jong, E. J. (1976). The occurrence of growth dispersion and its consequences. In "Industrial Crystallization" (J. W. Millin, ed.), p. 145. Plenum Press, New York.
7. Bennett, R. C., and Van Buren, M. (1969). *Chem. Eng. Progr. Symp. Ser.* **95**(65), 44.

CRYSTALLIZATION KINETICS

Crystallization from solution occurs when the solute concentration in a solvent exceeds its solubility. Such a solution is said to be supersaturated. Supersaturation can be generated by cooling a solution below its saturation temperature, by evaporating the solvent from solution, or by adding to the solution a third miscible component that changes the solubility of the solute. Supersaturation is also generated when two or more soluble reactants react to produce a product of very low solubility. Such reaction processes are most often termed precipitation processes, even though in many instances substantial crystal growth occurs. Thus for crystallization from solution to take place, supersaturation must exist. However, the supersaturated state alone does not ensure phase change by nucleation, nor does it ensure growth of crystals. The level of supersaturation, the hydrodynamic conditions in the crystallizer, and the presence of other material either in suspension or in solution all affect the degree to which crystals form and grow. Under some conditions crystals will form (nucleate) but not grow; under other conditions crystals will grow but nucleation will not take place.

The literature is replete with discussions addressing the points made above. Those most pertinent to industrial crystallization from solution are listed in Appendix C. In this chapter we discuss the basic concepts and the phenomena, both theoretically developed and experimentally observed, that have important impact on control of crystal quality and crystal size. No

attempt is made to exhaustively review all aspects of the formation and growth of crystals from solution.

5.1 Supersaturation

Supersaturation is usually generated by evaporating solvent from a concentrated solution or by cooling a concentrated solution to a temperature below the solute solubility temperature. Often, as in the case of vacuum crystallizers, both the evaporation and the cooling effect of evaporation combine to generate supersaturation. While much is known about the state of the solute in dilute solutions, the structure of concentrated and supersaturated solutes is not well understood. It is not now known with certainty to what extent clustering of solute occurs prior to nucleation or to addition of solute as growth units to growing crystals. Most nucleation theories assume that clustering must occur, but growth theories are somewhat ambiguous. Most studies that have been made to more clearly characterize concentrated solution structure have considered aqueous solutions of ionizable salts.

It is well known that dilute solutions of inorganic ionizable salts are more or less totally ionized with each ion associated with a primary hydration sphere because of the polar nature of water. It is also presumed that there is a more loosely associated secondary hydration sphere that is constantly interchanging water molecules with the surroundings. As concentration increases, ionization decreases and solvated ion pairs—that is, unionized solute—represent an appreciable portion of the solute solution. As concentration increases it is expected that clusters of solute molecules form with more or less the same structure as the solid state but too small to be regarded as a separate phase. Indeed, it is the formation of such clusters that forms the basis for the homogeneous nucleation theory. What is in question is the life span of the cluster. The life span is presumed to be very short, and it is also presumed that at low supersaturation no cluster achieves a sufficient size to become a nucleus. Evidence of clustering of a more permanent nature was first reported by Mullin and Leci [1] in citric acid solutions and later by Allen *et al.* [2] for sucrose solutions. They observed that supersaturated solutions maintained isothermally in columns in a gravitational field generated concentration gradients but saturated or undersaturated solutions did not. These gradients developed because of the gravitational effect on large clusters of solute still in solution having a density substantially different from that of the solution. Larson and Garside [3] repeated these experiments with a number of solutes and showed that when clusters of sufficient magnitude exist, an “equilibrium” concentration

gradient should exist. In order for the molar free energy of a component of a continuous phase to be uniform throughout the phase, the following relationship must be satisfied:

$$\ln \frac{x_2}{x_1} = \frac{(yM - yvp)}{RT} gH \quad (5.1-1)$$

where M and v are the molecular weight and molecular volume of the solute, respectively, and y is the number of molecules in a cluster. The data taken for various organic and inorganic solutes gave cluster sizes of order 10^3 molecules and equivalent spherical diameters of 50–125 Å. Raman spectroscopic work by Hussman *et al.* [4] and McMahon *et al.* [5] also indicated the presence of species in alkali nitrate solutions with the characteristic solute solid-state spectra not only in supersaturated solutions but in solutions below saturation as well.

Clearly clusters of solute exist in solution and have a reasonably long life and are indeed important in the nucleation process. Ion pairs and clusters are apparently the principal diffusing species in crystal growth. While a great deal is yet to be discovered about the state of solvation of the solute in crystallization systems, the nature of this solvation and clustering is important to the understanding of phase change. The degree to which the presence of other soluble substances affects the solvation and clustering of the crystallizing solute is extremely important in the determination of the kinetic rates of nucleation and growth.

Supersaturated solutions exhibit a metastable region in which growth occurs but nucleation normally does not occur. The width of this region depends on the degree of agitation, the concentration of crystalline solids in suspension, and the degree to which other solutes are present in solution. A complete understanding of this phenomenon rests in a more thorough understanding of the solute clustering phenomenon.

5.2 Primary Nucleation

New crystal formation (nucleation) in both batch and continuous crystallizers can occur by either primary or secondary mechanisms. The various recognized modes of nucleation are shown in Fig. 5.2-1. The term *primary nucleation* is used to describe the nucleation mechanisms which produce nuclei whether or not suspended crystals are present. Nucleation from a single-phase system is an example of primary nucleation. The term *secondary nucleation* is used to describe any nucleation mechanism that requires the presence of suspended solute crystals. The categorization of the different secondary mechanisms in Fig. 5.2-1 is somewhat arbitrary, but all mechanisms involve the surface of a growing crystal.

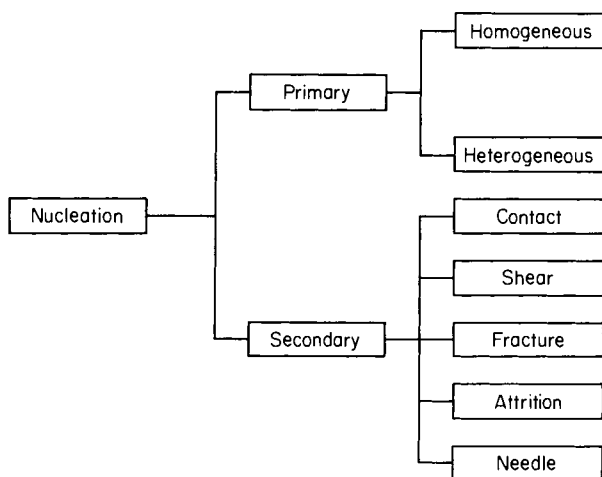


Fig. 5.2-1 Nucleation mechanisms.

Nucleation and crystal growth were described by Gibbs [6] as discontinuous changes of phase that are large in degree but, at least initially, small in extent in space. When a phase changes to a more stable phase, the atoms in one region of the first phase must become arranged in the characteristic configuration of the second, if indeed such a configuration exists. A phase change resulting in *crystal* formation does result in such a characteristic formation. The thermodynamic requirements for such an event involve the energy required for interface formation and the energy change required for change from the liquid state to the solid crystalline state. Thus the free-energy change resulting from a crystal nucleating homogeneously from solution is given by

$$\Delta G = \Delta G_s + \Delta G_v \quad (5.2-1)$$

where G_s is the free-energy change required to form the surface of the nucleus and G_v is the free-energy change resulting when the solute changes from the liquid to the solid state and is a function of the supersaturation level. The former is a positive quantity and the latter is a negative quantity; G_s is proportional to the surface area and thus the square of the nucleus radius, and G_v is proportional to the nucleus volume and thus the cube of the radius. Assuming a spherical nucleus, Eq. (5.2-1) can be written

$$\Delta G = 4\pi r^2 \sigma + (4/3)\pi r^3 \Delta G_v \quad (5.2-2)$$

The nucleus radius is r , σ is the specific surface energy, and ΔG_v is the bulk free-energy change per unit volume; ΔG_s , ΔG_v , and their sum ΔG are plotted in Fig. 5.2-2.

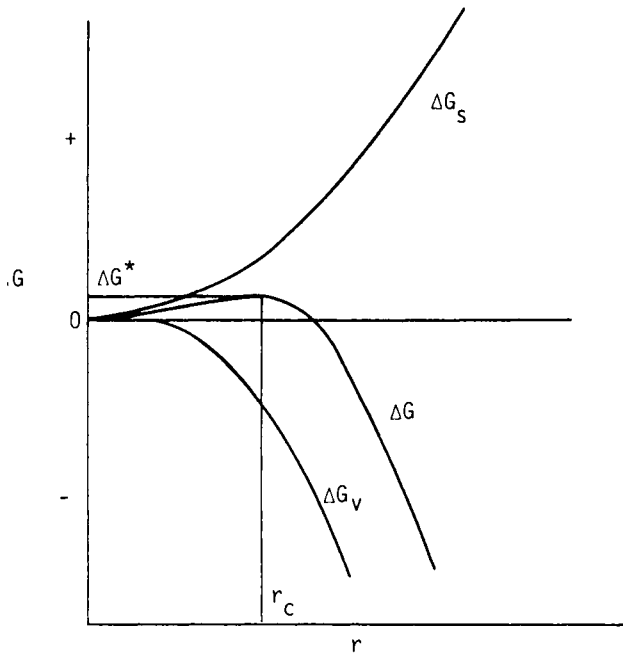


Fig. 5.2-2 Free-energy change for homogeneous nucleation.

From Fig. 5.2-2, it is clear that for clusters of solute with a size smaller than radius r_c to grow requires an increase in free energy, while the growth clusters larger than r_c will result in a decrease in free energy. Thus r_c is termed the critical nucleus size. It is presumed that in supersaturated solutions, solute clusters are constantly forming and dispersing but only those exceeding size r_c result in viable nuclei and thus contribute to the nucleation process. The term ΔG^* is termed the activation energy, and both ΔG^* and r_c decrease as supersaturation increases. The critical size r_c is related to the specific surface energy σ and the bulk free energy change ΔG_v by

$$r_c = -2\sigma/\Delta G_v \quad (5.2-3)$$

How a cluster reaches critical size can only be explained by local energy fluctuations in the solution.

It has been observed that the solubility of small crystals varies with solution concentration. The resulting equation that represents this behavior, known as the Gibbs–Thompson equation, is

$$\ln(C/C^*) = \ln S = 2\sigma v/kTr_c \quad (5.2-4)$$

where C^* is the saturation concentration, k is Boltzmann's constant, v is the molecular volume, and r_c is the size of a critical nucleus.

In the above developments it was assumed that the specific surface energy was constant and equal to the interfacial energy for an infinite interface. Gibbs [6] has shown for very small entities suspended in a different phase that the thickness of the interfacial region is of importance. When the particle radius is of the same order of magnitude as the interfacial thickness, the interfacial energy is reduced. Following the work of Tolman [7], and taking this factor into consideration, Larson and Garside [8] derived the following equation for the energy change for particle formation:

$$\Delta G = 4\pi r^2 \sigma_\infty e^{-2\delta/r} + (4/3)\pi r^3 \Delta G_v \quad (5.2-5)$$

which is plotted in Fig. 5.2-3. Here σ_∞ is the interfacial energy for an infinite surface and 2δ is the thickness of an interface. The plot shows a minimum at a very small size, about 100 Å, predicting that a supersaturated solution will contain a population of clusters of solute which have a maximum size r_{c1} . It is probably these clusters that coalesce when coming in contact with each other, producing homogeneous nuclei. As supersaturation increases, r_{c1} increases and the critical nucleus size decreases, increasing the probability that a nucleus will be formed.

So far we have discussed only the thermodynamic conditions necessary for homogeneous nucleation to occur. The nucleation rate B_0 , the number of nuclei produced per unit volume per unit time, can be expressed as an Arrhenius-type equation similar to those representing the rate of chemical reaction. Thus

$$B^0 = C \exp(-\Delta G^*/kT) \quad (5.2-6)$$

where ΔG^* is the critical free-energy change to form a critical nucleus r_c . Combining with Eqs. (5.2-2), (5.2-3), and (5.2-4) gives

$$B^0 = C \exp \left[- \frac{16\pi\sigma^3 v^2}{3k^3 T^3 (\ln S)^2} \right] \quad (5.2-7)$$

When B^0 is expressed in nuclei per second per cubic centimeter, the constant C has been reported to have value of 10^{25} to 10^{30} for sparingly soluble salts such as BaSO_4 .

The difficulty with the above expression is that it predicts nucleation only at extremely high supersaturations, far in excess of supersaturation levels observed in most inorganic crystallization schemes. For some reaction precipitation systems, it does quite well, however.

On the other hand, it has been observed in clean systems, where dust and extraneous material have been meticulously removed, that nucleation does

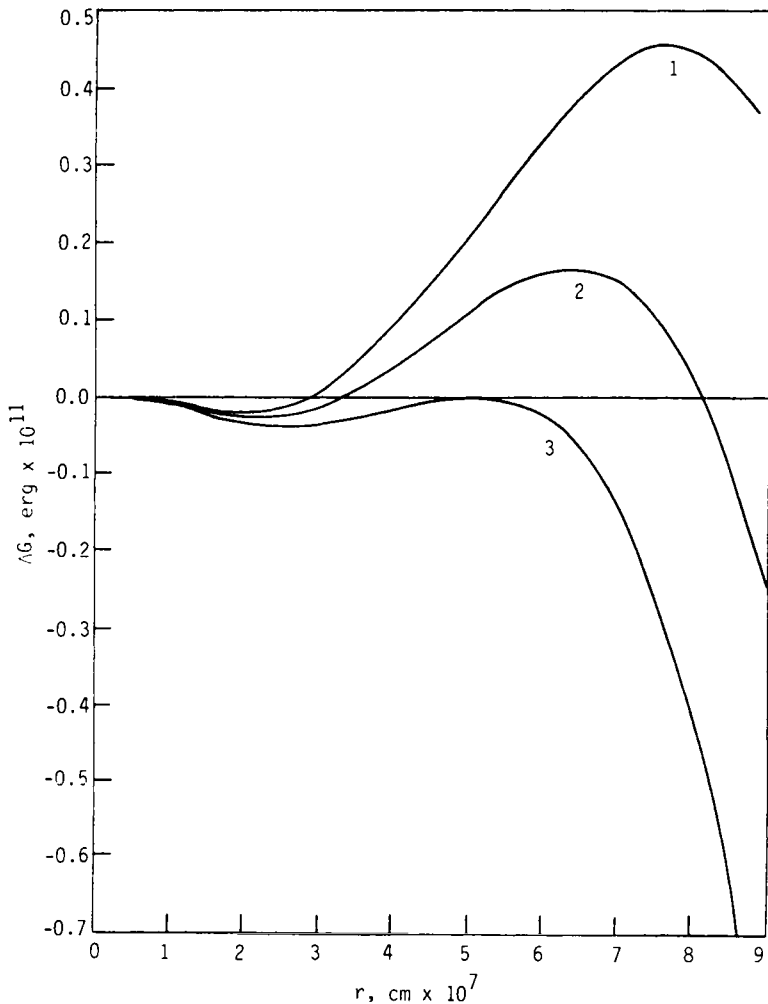


Fig. 5.2-3 Free-energy change when surface energy varies. (1) $\Delta G_v = 0.90 \Delta G_{v1}$, (2) $\Delta G_v = \Delta G_{v1}$, (3) $\Delta G_v = 1.10 \Delta G_{v1}$.

not take place even at very high supersaturations. In addition to the fact that the equation does not predict rates in a practical sense, it also contains quantities such as surface energy σ , the values of which are known only approximately or cannot be determined with any degree of confidence.

It is evident that homogeneous nucleation is not ordinarily an important phenomenon in industrial crystallizers; thus heterogeneous nucleation and secondary nucleation are generally the most important contributors to new

particle formation. The crystallization of solute on suspended dust particles or apparatus surfaces is termed heterogeneous nucleation. Its rate depends not only on supersaturation but the availability of active sites for nucleation to occur. A model for heterogeneous nucleation has been proposed that accounts for these effects [9], namely,

$$B = B_n \exp \left[- \frac{16\pi\sigma^3\nu^2b}{3k^3T^3(\ln S)^2} \right] \quad (5.2-8)$$

Here b is a factor less than 1 that accounts for the fact that crystallization on a substrate requires less interfacial area to be formed, and B_n is related to the number of sites available for nucleation and hence the surface area of the nucleating substrate. If this equation were to be adapted to secondary nucleation, B_n would depend on the surface area of solute in suspension. Even with such a modification, little success has been achieved in modeling experimental behavior using the homogeneous nucleation theoretical equation as the basis for modeling.

Neilsen [10] noted that Eq. (5.2-7) can be approximated by a power law function of supersaturation. However, such approximations require very large power-law exponents. A proposed equation of power-law form, but that accounts for the observed fact that nucleation of any kind does not occur at very low supersaturations, is based on the concept of the metastable limit [11] and is given as

$$B^0 = k(c - c_m)^i \quad c_m > c_s \quad (5.2-9)$$

where c is the solute concentration and c_m is the concentration at the metastable limit. It is referred to as the Meirs model. Unfortunately, the metastable limit is often a function of agitation and other physical conditions, although Chang and Myerson [12] have shown that it can be interpreted as occurring at the solubility spinodal. In most inorganic systems c_m is close to c_s and the equation can be written

$$B^0 = k(c - c_s)^i = ks \quad (5.2-10)$$

While this empirical model has been used with success, it is more useful in modeling secondary nucleation rather than primary nucleation.

It is interesting to note that the Meirs model is more nearly analogous to those used in reaction kinetics than is Eq. (5.2-7), if it is recognized that the rate constant k is usually a function of temperature. Thus the Meirs model can be represented as

$$B^0 = k_0 e^{-(\Delta E/kT)} (c - c_s)^i \quad (5.2-11)$$

where ΔE is the activation energy of the reaction. Some work has been

done using the model, but often positive activation energies have been obtained. This apparent inconsistency results from the fact that secondary nucleation is being measured.

Because secondary nucleation is related to the growth rate of existing crystals, a detailed discussion is deferred until growth mechanisms are addressed.

5.3 Crystal Growth Mechanisms

The mechanism of crystal growth from solution requires that solute be transported to the crystal surface and then oriented into the crystal lattice. Two successive steps are required, a diffusional step followed by a surface reaction step. This latter step is sometimes referred to as the particle integration step, and the rate at which the crystal grows because of this mechanism is called the particle integration rate.

The exact species that diffuse to the surface and ultimately form a part of the crystal are now known. The solute must desolvate as it proceeds to the crystal surface, and the solvent must counterdiffuse away from the surface. Most treatments assume molecular diffusion, but in light of the confirmed presence of solute clusters of considerable size (100 Å) in some systems, it is clear that the diffusion of both molecules and clusters plays an important role in the growth process. It is also clear, however, that when both sparingly soluble material and highly soluble material are considered, it is to be expected that there is a wide variation among systems in the manner in which the diffusion and integration takes place. But in every case solvated solute must diffuse toward the surface and solvent must diffuse away from the surface. At some point near the surface, surface reaction mechanisms predominate over diffusion mechanisms. Generally the proposed growth models are independent of the species involved in the growth process, with the species affecting only the magnitude of the diffusion coefficient or of the surface reaction rate constant.

If growth rate is limited by the rate of diffusion through a laminar layer of solution the growth, is said to be diffusion-controlled. In many non-agitated systems this is indeed the controlling mechanism, and the growth rate can be represented by the simple mass transfer equation

$$\frac{dM}{dt} = \frac{D}{x} A (c - c_s) \quad (5.3-1)$$

where D is a diffusion coefficient, x is a film thickness, A is the surface area of the crystal, and $c - c_s$ is the difference between the actual concentration and the saturation concentration. As in most mass transfer situations the

thickness of the "film" is not known; thus a mass-transfer coefficient is used.

$$\frac{dM}{dt} = KA(c - c_s) \quad (5.3-2)$$

Because crystals are usually sized on the basis of diameter rather than mass, it is more useful to cast Eq. (5.3-2) in a form giving the growth rate of characteristic dimension L . If L is a characteristic diameter and k_v is a volume shape factor, then $m = \rho k_v L^3$ and crystal surface area is equal to $k_a L^2$ where k_a is an area shape factor. Using these expressions in Eq. (5.3-2) gives

$$\begin{aligned} k_v \rho \frac{d(L)^3}{dt} &= K k_a L^2 (c - c_s) \\ 3k_v L^2 \frac{dL}{dt} &= K k_a L^2 (c - c_s) \\ \frac{dL}{dt} &= \frac{K k_a}{3k_v \rho} (c - c_s) \end{aligned}$$

or

$$G = K_g s \quad (5.3-3)$$

The final form of Eq. (5.3-3) was the form used in Eq. (4.5-4). For very small crystals, crystals of order $0.1 \mu\text{m}$ or less the diffusion coefficient is a function of size, and for such crystals

$$G = ks/L \quad (5.3-4)$$

When diffusion is the controlling mechanism, the crystal growth rate increases as the velocity of supersaturated solution is increased relative to the crystal surface. When a further increase in velocity no longer increases growth rate, we say the growth is surface integration-controlled. The rate of growth under these conditions depends not only on the supersaturation but also on the mechanism of solute integration with the crystal surface. The secondary nucleation work of Clontz and McCabe [13] as well as work by Garside, Rusli, and Larson [14] have demonstrated the existence of an absorbed layer of solute on the surface of a growing crystal. This layer is conceptually shown in Fig. 5.3-1. This "third phase" is composed of partially ordered solute, perhaps in a partially desolvated lattice. Mullin [15] has suggested that it might be 100 \AA in extent. Secondary nucleation experiments, which consisted of subjecting growing crystals to sliding contacts, have, however, indicated that it may be of much greater thickness. It is perhaps a very thick layer and may be a diffuse phase boundary, as suggested by the theories of spinodal decomposition in crystallization from

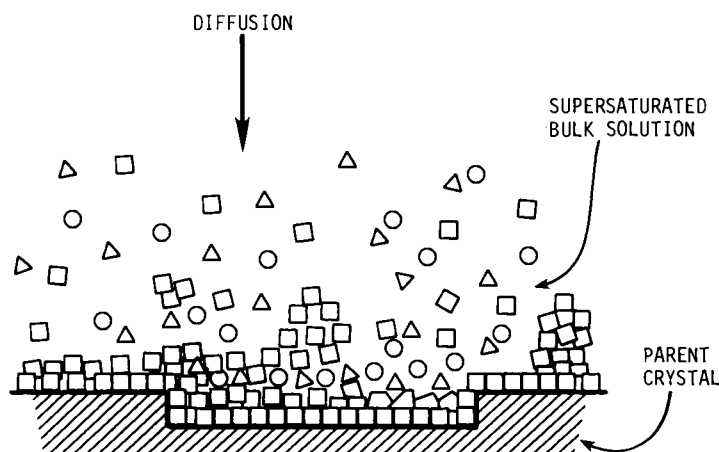


Fig. 5.3-1 Absorbed layer of solute on the surface of a growing crystal. \square , $A_m B_n \cdot pH_2O$; \circ , hydrated A^{+n} ions; \triangle , hydrated B^{+m} ions.

the melt. The thickness of this layer is related to the relative rates of diffusion and surface integration. As the surface reaction increases relative to the diffusion rate, the layer thickness decreases. The exact nature of this layer is yet to be determined, but it appears to consist of solute clusters formed in supersaturated solution diffusing along the surface until oriented for incorporation into the crystal lattice at an appropriate site.

There are many theories describing the actual integration step. Here we will mention three general categories. The details are rather complex, and more detailed treatments are necessary for complete exposition. Garside [16] categorizes growth theories as continuous growth, surface nucleation, and continuous step growth. The *continuous growth model* assumes a rough surface, as shown in Fig. 5.3-2a, where the growth unit will integrate at a site of the lowest energy for its orientation. Site 1 would be such a site. Because of the larger number and random locations of such sites, the growth rate of a face is given directly by

$$R = Cs \quad (5.3-5)$$

where C is a constant that defines the maximum growth rate of a crystal.

Surface nucleation growth is controlled by the frequency of formation of two-dimensional nuclei on the smooth face of a growing crystal. The controlling step is the nucleation, the subsequent spread around the nucleus being much more rapid because of the lower energy requirements. The model is shown in Fig. 5.3-2b, is termed the birth and spread model, and is fully described by O'Hara and Reid [17]. The energy requirement for

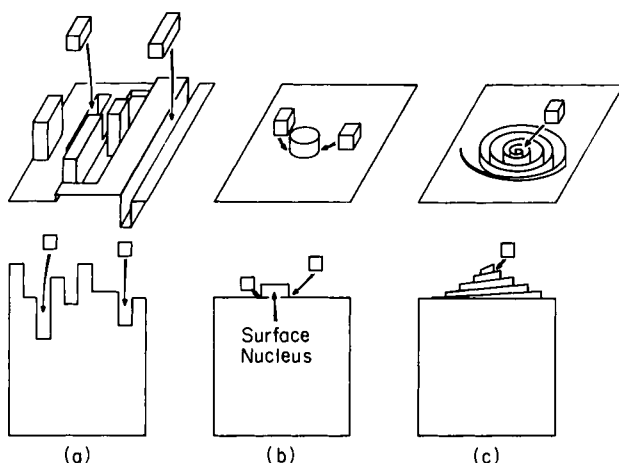


Fig. 5.3-2 Crystal growth model. (a) Continuous growth, (b) birth and spread, (c) screw dislocation (BCF).

surface nucleation is

$$G = 2\pi r h \sigma + \pi r^2 h \Delta G_v \quad (5.3-6)$$

where σ is the surface energy, r is the radius of the nucleus, and h is the height of the nucleus. The facial growth rate is

$$R = A's^p \exp(-B'/s) \quad (5.3-7)$$

where A' , p , and B' are constants, and p is generally taken as between 1 and 2.

The most used model for crystal growth and the one that is most often applicable is a form of the continuous-step model. The form that is preferred is the Burton–Cabrera–Frank model [18] (BCF). This model incorporates the idea of a self-perpetuating kink or ledge and leads to concept of a screw dislocation as shown in Fig. 5.3-2c. The addition of a growth unit not only fills a kink site but creates another which is favorable to growth. Screw dislocations have been found on etched surfaces of crystals and have also been observed on growing surfaces by reflective microscopy. It is quite clear that the growth units must be larger than molecular size or larger even than the unit cell size.

The BCF theory predicts that the facial growth rate is related to the supersaturation by

$$R = As^2 \tanh B/s \quad (5.3-8)$$

At low supersaturations, however, the equation reduces to a parabolic law,

$$R = Cs^2 \quad (5.3-9)$$

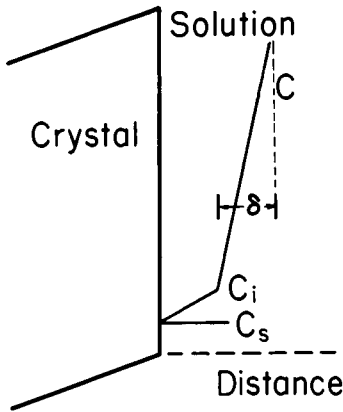


Fig. 5.3-3 Interfacial resistance to growth.

For high supersaturation, Eq. (5.3-9) can be approximated by Eq. (5.3-5), the equation for continuous growth.

If both diffusion resistance and integration rate affect the overall growth rate, then a growth-rate equation must include both. Assuming that the surface reaction is linear, then the resistance to growth can be represented conceptually as shown in Fig. 5.3-3. As shown, δ is the diffusion-layer thickness. In this illustration the diffusion resistance is greater than the surface integration resistance. Then

$$\frac{dM}{dt} = k_d A (c - c_i), \quad \frac{dM}{dt} = k_r A (c_i - c_s) \quad (5.3-10)$$

or

$$\frac{dM}{dt} = K_G A (c - c_s), \quad K_G = \frac{k_d k_r}{k_d + k_r}$$

and as before

$$G = \frac{dL}{dt} = k_G (c - c_s), \quad k_G = \frac{K_a k_a}{3k\nu\rho} \quad (5.3-11)$$

As mentioned in Chapter 4, crystals in mixed suspensions exhibit growth behavior that cannot be totally explained by the models we have presented. In the case of apparent size-dependent growth, it is clear that the growth rate of large crystals could be increased because of an increase in their fluid settling velocity. This does not, however, explain some of the large differences in growth rate observed among crystals of different sizes in the same suspension. As shown by the work of Berglund and Larson [19], large crystals do grow more rapidly than small ones, but this is not because they

are large. They have become large because they *have* an inherent higher growth rate. This is the manifestation of the phenomena of growth dispersion previously discussed. Crystals have a variety of growth rates and the growth rate appears to depend on the origin of the nuclei. Crystals with a greater number of dislocations per unit area should grow faster than those with less. Garside *et al.* [20] have shown that plastically deformed crystals grow very slowly or not at all, and J. N. Sherwood (private communication, Glasgow, 1984) has shown that crystals under tensile stress cease to grow altogether. Clearly if nuclei are produced in solution primarily by secondary contact nucleation, their origin can result from fracture, and from deformation, as well as homogeneously from the absorbed layer on the surface of a growing crystal. Thus each crystal will have a unique set of structural properties contributing to its growth.

5.4 Secondary Nucleation

5.4.1 Sources of Secondary Nuclei

The most likely source of new crystals in continuous stirred crystallizers or seeded batch crystallizers is the crystal suspension itself. The formation of new crystals (nucleation) can occur by any of a number of crystal surface phenomena associated with agitated growing crystals. We describe secondary nucleation by six somewhat arbitrary mechanisms, one of which is by far the major source of nuclei in mixed suspensions.

Initial breeding as described by Strickland-Constable [21] results from crystalline "dust" adhering to larger seeds introduced into batch crystallizers. This would occur only if the seeds were dry and were directly introduced into the crystallizer. Because this occurs only in seeded systems, we will not discuss it further.

Nucleation by some sort of *fracture* process occurs in systems that produce crystals that break easily, where the suspension is very dense, and where the suspension is subjected to violent agitation or high-velocity pumping. The crystalline product usually has a rounded appearance because of the high fracture and usually shows a deficiency of crystals in the large size range. The damage is usually done by impact with the impeller or sharp changes in the flow path. Fracture from crystal-crystal interactions probably does not occur.

Nucleation by *attrition* is merely fracture of a lesser degree and results from crystal-crystal interaction at high suspension densities as well as from crystal-apparatus contact. The crystal product may or may not exhibit obvious damage, but visible damage is usually slight. This and fracture nucleation can only be reduced by reduced agitation or pumping, by

reduced suspension density, or by soft linings and coverings on the crystallizer walls and impeller.

Needle breeding occurs because of dendritic growth on crystals. While reduced agitation and suspension density reduces this phenomenon, it is best controlled by reducing the driving force for growth, that is, supersaturation, or using appropriate additive to change the crystal habit or tendency to form dendrites.

Nucleation by *fluid shear* results when the fluid velocity relative to the crystal velocity is large and some of the "adsorbed layer" is removed. The adsorbed layer, being nearly entirely solute, will nucleate if the clusters are sufficiently large. Sung, Estrin, and Youngquist [22] have shown that shear produced nuclei must ordinarily be exposed to a much higher supersaturation than the one in which they were produced, in order to grow. As a consequence, it would not be expected that nucleation by fluid shear represents an important source of nuclei.

The most important source of nuclei in mixed suspension is the source that is described as *contact nucleation*, and results when crystals contact the agitator, pump, flow lines or other crystals. In every contact there may be some fracture and usually some attrition, but by far the major production of nuclei is from the displacement the adsorbed layer of solute that has not yet become crystalline. Moreover, the attrition or fracture pieces that are formed grow at a lower rate and thus contribute little mass to the crystalline product, as will be discussed in more detail in the next section. Secondary nuclei produced by contact nucleation can be produced by energy levels far below that required for fracture or attrition.

5.4.2 Contact Nucleation

Powers [23] postulated an adsorbed layer as the source of secondary nuclei and Strickland-Constable [21] demonstrated that by sliding a growing crystal along the bottom of a beaker, nucleation was induced and in due course new crystals appeared on the bottom of the beaker. Clontz and McCabe [13] confirmed such a mechanism as a source of nuclei. They showed that low-energy contacts normal to the surface of a growing crystal produced a number of new crystals after a short growth period. In neither experiment was visible crystal damage required to produce nuclei, but the contacted crystal had to be a *growing* crystal in order to produce nuclei. Clontz and McCabe showed that not only did the contact energy affect the number of nuclei produced but the supersaturation also had a marked affect on the number. The supersaturation level affects the number produced in two ways. At high supersaturation the adsorbed layer is thicker, and thus more particles are produced on contact. In addition, at high

supersaturation the critical nucleus size is smaller, and thus a greater fraction of the particles produced survive to become viable crystals.

Youngquist and Randolph [24] conducted experiments using a continuous mixed-suspension crystallizer seeded with relatively large monodisperse crystals. They provided a continuous-withdrawal method by which only crystals smaller than seed crystals would be removed. The effluent was analyzed with a Coulter counter. In transient studies they found that the number of crystals in the effluent was directly related to the degree of agitation and the suspension, increasing as either or both were increased. The seeds exhibited some attrition, but far less than could account for the number of new crystals produced.

Garside, Rusli, and Larson [14] devised a system in which a single crystal would be contacted with a fixed energy. The crystal was fixed in an otherwise well-mixed batch-type crystallizer. The size distribution of the nuclei produced after contacting the growing crystal was measured *in situ* with a Coulter counter. The CSD of these nuclei was a function of supersaturation and was highly reproducible. Their data for potassium alum are shown in Fig. 5.4-1, which gives the size distribution immediately after contact as a function of supersaturation. Larson and Bendig [25], using a continuous version of this apparatus, showed that repeated contacts on the same site resulted in reduced nuclei production, and that there was a critical frequency of contact below which the number of nuclei per contact was reduced. This indicates the presence of an absorption layer which requires time for regeneration. Because energy of contact is important, very small crystals—less than, say, 100 μm —were usually not instrumental in producing secondary nuclei.

None of the above experiments clearly show what happens to individual crystals. Berglund and Larson [19] conducted a number of experiments using sliding contacts in the growth cell shown in Fig. 5.4-2. A growing crystal was pulled across a glass surface and the area was immediately photographed through an optical microscope. The same behavior was observed, and a size distribution of new crystals was immediately produced without observable attrition of the parent crystal. The nuclei size sometimes reached 10 μm .

In summary, it is clear that contact nucleation is the primary source of new crystal formation in mixed-suspension crystallizers and probably many other configurations. Crystals are produced in a very short time at measurable sizes. While some fracture or attrition is apparent, the resulting particles are small in number compared with the true contact nuclei. The number produced depends on supersaturation and can usually be represented by a power law relationship. The work of Bennett, Fiedelman, and Randolph [26] has shown that the nucleation rate can also be correlated

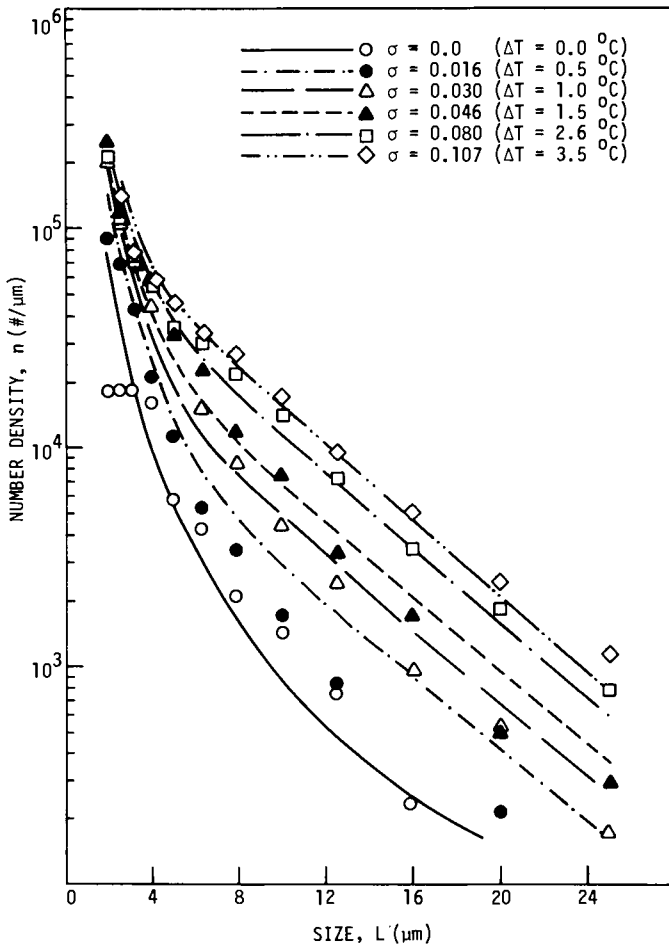


Fig. 5.4-1 Nuclei size distribution from contact nucleation.

with the degree of agitation as expressed by the tip speed of a pump impeller or vessel agitator. Nucleation is also often observed to be an inverse function of the ambient temperature. This can also be explained in terms of an adsorbed layer. Assuming the surface reaction (integration) rate is increased by temperature level, at higher temperatures its rate would increase more, relative to the diffusion rate, resulting in a thinner adsorbed layer and thus fewer nuclei when contacted.

For design and analysis purposes, correlations have been successfully used as follows:

$$B^0 = k(T) \omega^i M^{j_s} \quad (5.4-1)$$

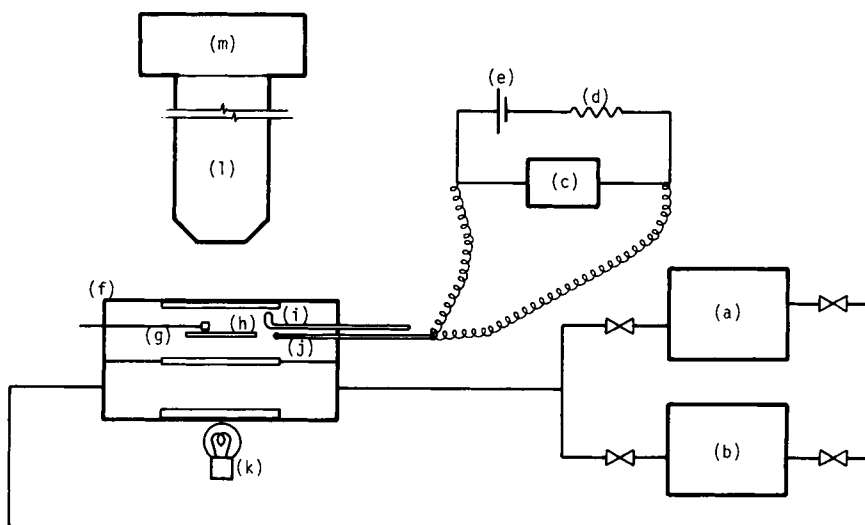


Fig. 5.4-2 Secondary nucleus cell (a), (b) saturation chambers; (c) voltmeter; (d) resistance; (e) battery; (f) cell; (g) crystal holder; (h) contact surface; (i) crystal contactor; (j) thermistor; (l) microscope; (m) camera.

where the rate constant k is a function of temperature, ω is a measure of mechanical agitation, M is the suspension density, and s is the degree of supersaturation. If the size distribution is wide, this must be taken into account also. The exponents must be determined experimentally, but j is usually 1 and i is usually from 1 to 3.

5.4.3 Growth of Secondary Nuclei

The phenomenon of growth dispersion has a pronounced effect on the size distribution of crystals of near-nuclei size. Experimental data show a wide variation in the growth rates of very small crystals. This leads to difficulty in interpreting nucleation data. It has been estimated that it takes perhaps only 10–15% of the number of nuclei formed in the crystallization of a highly soluble material such as sodium nitrate to account for 95% of the mass of the crystalline product. The growth rate of the other 85–90% of the number is too low to produce appreciable mass during their residence time in the crystallizer. Because of this phenomenon, crystal products from continuous crystallizers often show orders of magnitude more crystals in the small size ranges (for NaNO_3 , 4–20 μm) than predicted by the population balance. Larson and Bendig [25] observed the same phenomenon in continuous experiments when the nuclei source was a single contact

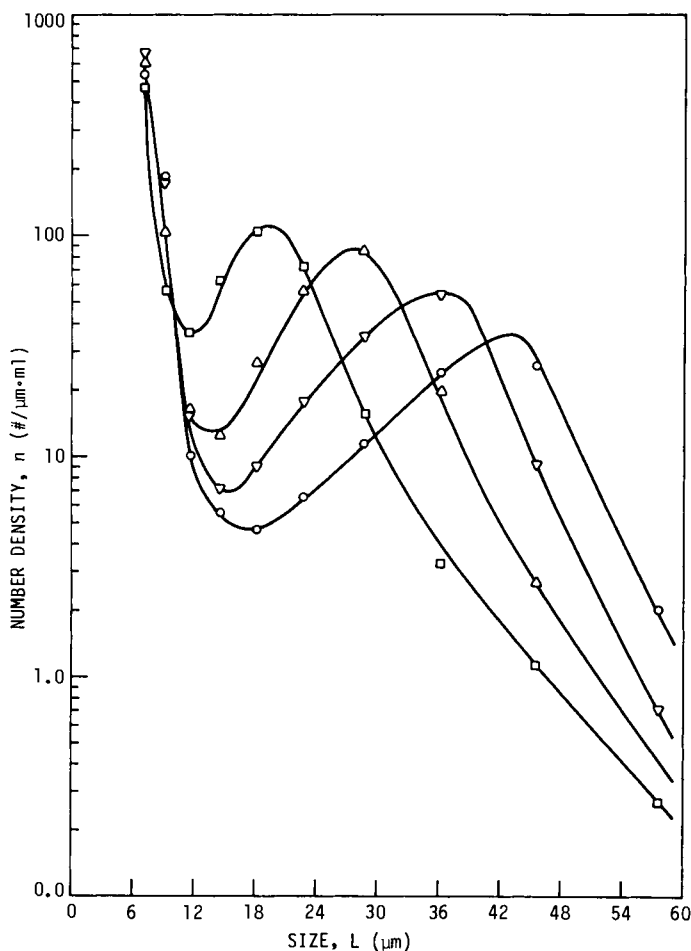


Fig. 5.4-3 Evidence of nuclei growth dispersion in batch crystallization of KNO_3 . $\Delta T = 0.20^\circ\text{C}$. Time after nucleation: \square , 20 sec; \triangle , 40 sec; ∇ , 60 sec; \circ , 80 sec.

point on a large crystal. Garside, Rusli, and Larson [14], using a batch crystallizer with $\text{MgSO}_4 \cdot 7\text{H}_2\text{O}$, showed that crystals in the same environment could have growth rates differing by as much as an order of magnitude. Figure 5.4-3 shows the results of experiments of Purves and Larson [27]. They contacted a single crystal in a batch stirred vessel and monitored the CSD of the nuclei produced over a period of time. The data show a large number of crystals that do not grow and a lesser number that appear to grow at the same rate. Figure 5.4-4 is data of Larson and Berglund for citric acid nuclei produced in a cell previously described. The points

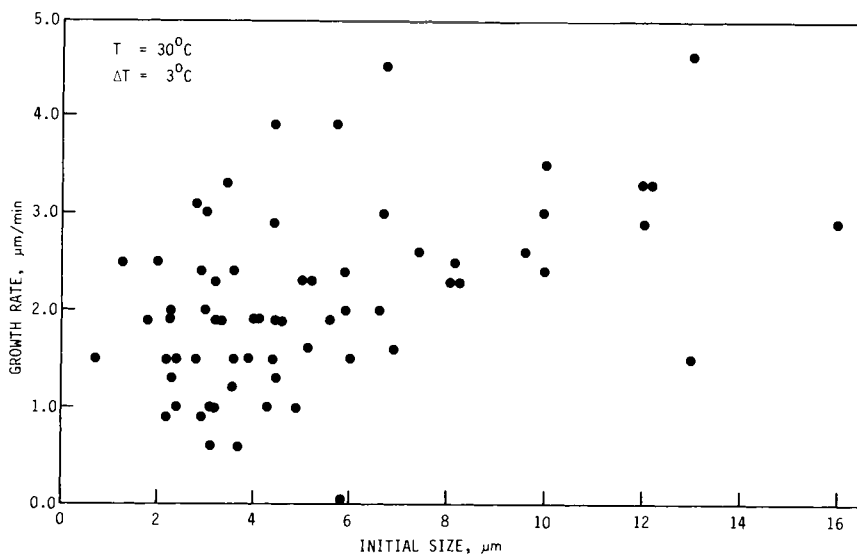


Fig. 5.4-4 Evidence of nuclei growth dispersion in citric acid.

indicate the growth rates of individual crystals related to their initial size. There is a wide range of crystal sizes produced with a wide range of growth rates, but there is no correlation between initial size and growth rate. This work also showed that at least for a short period each crystal has a characteristic growth rate which it maintains. This is the basis for the growth-dispersion model described in Chapter 4. All of the above experiments involved secondary nucleation. Garside and Risitic [28] have shown, however, that growth dispersion occurs in nuclei produced the primary mechanisms as well.

Growth dispersion is not completely understood, but it is extremely important and must be recognized as a factor in analysis of systems, especially when nucleation rates are of concern. Growth dispersion can occur because of many factors. Janse and de Jong [28] found that fracture pieces in NaCl crystals grew very slowly or not at all where other contact nuclei grew at a higher rate. Garside *et al.* [20] have shown that small milled crystals that have undergone plastic deformation have little or no rate of growth when exposed to conditions where other crystals grow rapidly. J. N. Sherwood (private communication, Glasgow, 1984) has shown that crystals subjected to tensile stress cease to grow, but when the stress is relieved they again begin to grow. All growth dispersion cannot be explained, however, on the basis of stress or strain. Growth rate is a function of the number of dislocations on the faces of growing crystals. A greater density of disloca-

tions should result in higher growth rates. While this explanation seems adequate, there are yet many questions to be answered. Growth is very sensitive to dissolved impurities and surface-active impurities in very small quantities, and it is entirely possible that random distribution of surface-active impurities is also a factor in growth dispersion. In the control of CSD it is essential to consider the factors contributing to growth dispersion as well as factors contributing to nucleation.

5.5 Effects of Impurities and Additives on Growth and Nucleation

The presence of chemical species in solution, in addition to the solute and solvent, can have a pronounced effect on the crystallization kinetics even if present in trace amounts. Indeed, the solvent itself can have a marked effect [30]. For example, it would be expected that the relationship between growth and nucleation kinetics would not be the same when crystallizing ammonium sulfate from water as it would be if it were crystallized from an alcohol–water mixture. Because material such as high-valence metallic ions and certain surface-active agents have very marked effects when present in only a few parts per million, extreme care must be exercised in interpreting growth and nucleation data. It is a rare solution that does not have present, at least in parts per million, some known or unknown impurity. This being the case, actual plant liquors should be used at some stage of any experimental program directed toward the design of a plant-sized crystallizer. While often the presence of impurities is detrimental to the desired objectives of a crystallization process, many times the presence of impurities is essential. The classic example is the crystallization of gypsum from phosphoric acid in the wet phosphoric acid process. Here some of the impurities present in the phosphate rocks are essential in order to obtain the desired crystal size and habit.

It has long been known that impurities can have a marked effect on crystal habit, which is concomitant with their effect on bulk growth and nucleation kinetics. This effect results from the differing effect the impurities have on the different crystallographic faces of a crystal. Davey [31, 32] points out that facial growth rates may be increased, decreased, or remain the same in the presence of additives. The effect of impurities or additives on growth rate also translates into an effect on solubility, and solubility may be increased or decreased. The effect of impurities is generally thought to result from adsorption on the surface of the growing crystal. Adsorption has two effects. The adsorption of additives generally decreases the interfacial tension, thus resulting in greater surface nucleation in the birth and spread mode of growth. The same effect narrows the step packing in BCF

growth. In each case growth rate would be increased. On the other hand, impurity adsorption will block growth sites, thus reducing growth rate in both modes of growth. If solubility is affected by additives, increases in solubility will result in a decrease in supersaturation and thus reduce apparent growth rate. It is clear that the effects of impurities are quite complex and not easily predicted.

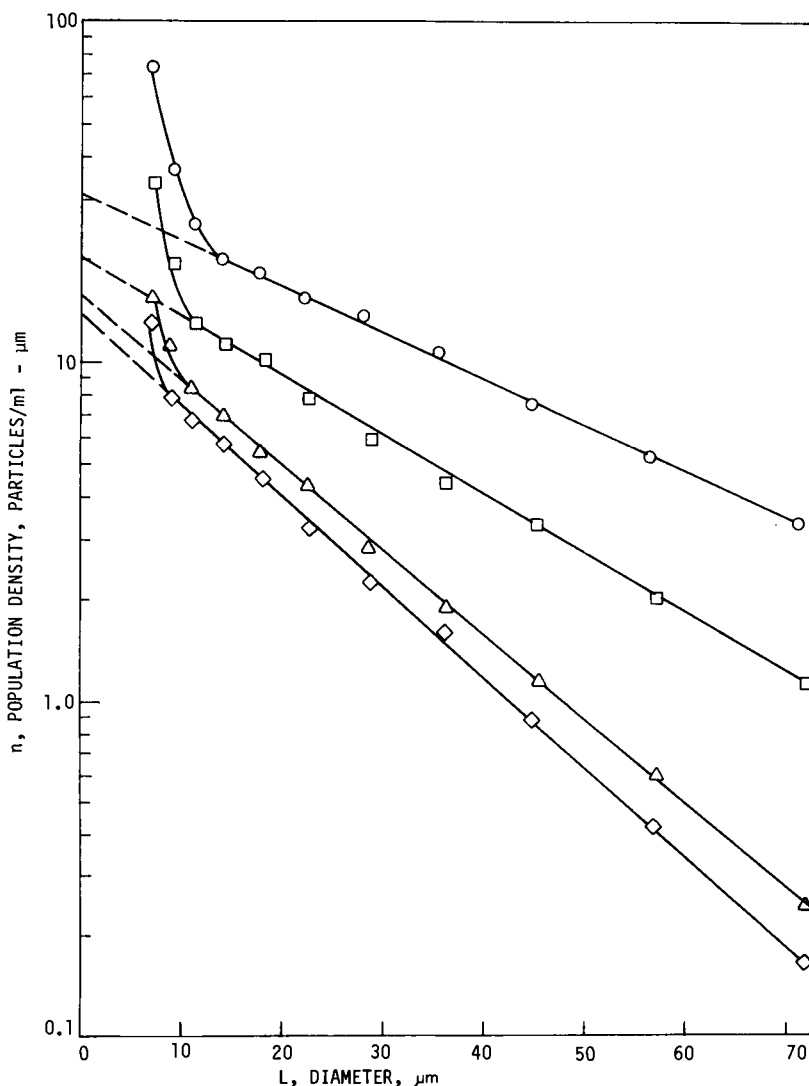


Fig. 5.5-1 Effect of Cr^{3+} on $\text{MgSO}_4 \cdot 7\text{H}_2\text{O}$ crystallization. Chromium ion concentration: \circ , 3 ppm; \square , 8 ppm; \triangle , 15 ppm; \diamond , 30 ppm. (After Khambaty and Larson [33].)

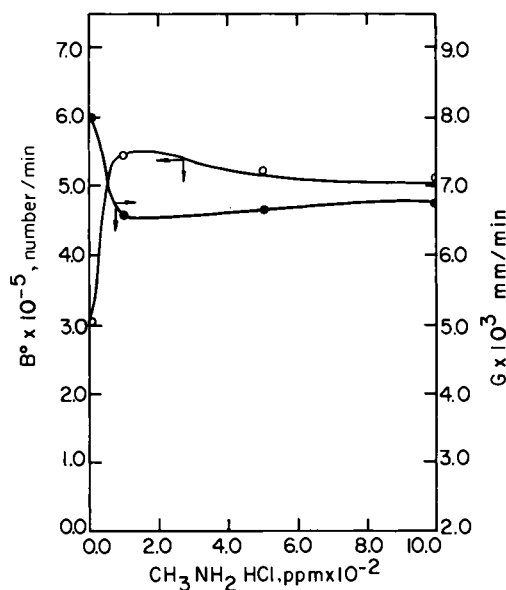


Fig. 5.5-2 Effect of surface-active agents on CSD.

The effect of impurities and additives on nucleation is even less understood. However, inasmuch as secondary nucleation is related to the thickness of the adsorbed layer of solute on a growing crystal surface, the thickness of that layer will affect the rate of contact nucleation. The thicker the layer, the greater the nucleation rate. Thus in instances where growth rate is enhanced by additives, one would expect nucleation rate to decrease. This is not always the case. The data of Khambaty and Larson [33] taken from a continuous MSMPR crystallizer with a point source of contact nuclei, show that Cr^{3+} ion in $\text{MgSO}_4 \cdot 7\text{H}_2\text{O}$ crystallization decreases both nucleation and growth rates. This is shown in Fig. 5.5-1. The change in slope of the CSD curve shows the decreased growth rate, and the decrease in extrapolated intercept indicates the decrease in nucleation rate.

On the other hand, some surface-active agents tend to increase nucleation, as shown by the data of Shor and Larson [34] for KNO_3 (Fig. 5.5-2). These data were obtained from an MSMPR crystallizer.

The effect of additives is often pronounced but is extremely varied and systematic approaches to additive selection are rare. As most applications are proprietary, it is difficult to obtain data for purposes of generalization. It is very important, however, that one be extremely careful in interpreting data. The presence of additives may, for example, decrease growth rate but in a constrained system result in large crystals. This results because the nucleation rate was also reduced and the net result was that the system was

forced to higher supersaturation. One should refer to Chapters 4 and 7 for detailed discussions on how the process constraints interact with kinetics to produce a crystal size distribution.

5.6 Summary

We have discussed, in this chapter, the relationship of solution structure to nucleation and growth and have defined various mechanisms of nucleation and growth. This discussion is not meant to be exhaustive, and there are surely additional theoretical mechanisms that can be used to explain observed phenomena. However, the mechanisms of nucleation and growth presented here are those most accepted as applicable in industrial crystallization from solution. Clearly, secondary contact nucleation is the most important mechanism in stirred suspensions, and in order to control CSD secondary nucleation must be controlled. We have discussed the various factors that are important in the secondary mechanism. Design procedures should address these factors. Additives and impurities play an important role, whether intentionally added or not. There is no systematic way of approaching the use of additives, but it must be remembered that impurities exist in every system and may or may not affect the CSD. In evaluating kinetics and how kinetics are affected by additives, care must be taken to that the less obvious effects of system constraints do not give rise to erroneous interpretations of results.

Nomenclature

a	Constant in surface-energy equation	ΔG^*	Critical free energy
A	Area	ΔG_v	Specific bulk free energy
A'	Constant in growth equation	ΔG_s	Surface free-energy change
b	Constant in heterogeneous nucleation equation	ΔG_v	Total bulk free-energy change
B	Constant in BCF equation	H	Column height
B^0	Nucleation rate	i	Exponent in nucleation equations
B_n	Heterogeneous nucleation rate constant	j	Exponent in nucleation equations
B'	Constant in growth equation	k	Boltzmann constant, and constant
c	Concentration	k_a	Area shape factor
c_s	Saturation concentration	k_d	Diffusion coefficient
c_m	Concentration at metastable limit	k_v	Volume shape factor
C	Constant	k_r	Growth-rate constant
D	Diffusivity	k_G	Growth rate constant
g	Gravitational constant	K_G	Mass-transfer coefficient
G	Crystal growth rate	l	Exponent in nucleation equation
ΔG	Free-energy change	L	Crystal diameter
		m	Mass
		M	Molecular weight
		M_T	Suspension density

P	Exponent in growth equation	x	Diffusion layer
r	Cluster radius	x_1	Cluster concentration, top
r_c	Critical nucleus	x_2	Cluster concentration, bottom
r_{c1}	Critical cluster size	y	Number of molecules in cluster
r_{c2}	Critical nucleus radius	y_i	Dimensionless size distribution
R	Gas constant		
R	Facial growth rate		
s	Supersaturation, $(c - c_s)/c_s$	GREEK LETTERS	
S	Supersaturation, c/c_s	δ	Interfacial thickness
t	Time	ρ	Density
T	Temperature	σ	Surface energy
v	Molecular volume	σ_∞	Surface energy, infinite plane

References

1. Mullin, J. W., and Leci, C. L. (1969). *Phil. Mag.* **19**(161), 1075.
2. Allen, A. T., McDonald, M. P., Nicol, N. W., and Wood, R. M. (1972). *Nature, Phys. Sci.* **235**(54), 360.
3. Larson, M. A., and Garside, J. (1986). Solute clustering in supersaturated solutions. *Chem. Eng. Sci.* **41**, 1285.
4. Hussmann, G. A., Larson, M. A., and Berglund, K. A. (1984). Characterization of solution structure near the surface of a growing crystal by Raman spectroscopy. In "Industrial Crystallization 84" (S. J. Jancic and E. J. de Jong, eds.), p. 21. Elsevier, Amsterdam.
5. McMahon, P., Berglund, K. A., and Larson, M. A. (1984). Raman spectroscopy studies of the structure of supersaturated KNO_3 solutions. In "Industrial Crystallization 84" (S. J. Jancic and E. J. de Jong, eds.), p. 229. Elsevier, Amsterdam.
6. Gibbs, J. W. (1928). "Collected Works," Vol. 1, p. 219. Longmans Green, New York.
7. Tolman, R. C. (1949). *J. Chem. Phys.* **17**(3), 333.
8. Larson, M. A., and Garside, J. (1986). "Solute clustering and interfacial tension." *Journal of Crystal Growth* **76**, 88–92.
9. Turnbull, D., and Fisher, J. C. (1965). *J. Chem. Phys.* **17**, 71.
10. Nielsen, A. E. (1964). "Kinetics of Precipitation," p. 16. Macmillan, New York.
11. Miers, H. A., and Isaac, F. (1906). *J. Chem. Soc. Lond.* **89**, 413.
12. Chang, Y. C., and Myerson, A. S. (1984). Diffusion coefficients in supersaturated solutions. In "Industrial Crystallization 84" (S. J. Jancic and E. J. de Jong, eds.), p. 27. Elsevier, New York.
13. Clontz, N. A., and McCabe, W. L. (1971). *Chem. Eng. Prog. Symp. Ser.* **110**, 67.
14. Garside, J., Rusli, J. T., and Larson, M. A. (1979). *AIChE J.* **25**(1), 57.
15. Mullin, J. W. (1972). "Crystallization," 2nd ed. Butterworth, London.
16. Garside, J. (1984). Advances in crystallization from solution. *AIChE Symp. Ser.* **240**(80), 23.
17. O'Hara, M., and Reid, R. C. (1973). "Modelling Crystal Growth Rates from Solution." Prentice-Hall, Inc., Englewood Cliffs, New Jersey.
18. Burton, W. K., Caberra, N., and Frank, F. C. (1951). *Phil. Trans. R. Soc.* **A243**, 299.
19. Berglund, K. A., and Larson, M. A., (1982). *AIChE Symp. Ser.* **215**(78), 9.
20. Garside, J., Webster, G., Davey, R. J., and Reiddick, A. J. (1984). The relationship between growth rate dispersion and the mechanical properties of crystals. In "Industrial Crystallization 84" (S. J. Jancic and E. J. de Jong, eds.), p. 459. Elsevier, Amsterdam.

21. Strickland-Contable, R. F. (1968). "Kinetics and Mechanisms of Crystallization." Academic Press, London.
22. Sung, C. Y., Estren, J., and Youngquist, G. R. (1973). *AIChE J.* **19**(5), 957.
23. Powers, H. E. C. (1963). *Ind. Chem.* **39**, 31.
24. Youngquist, G. R., and Randolph, A. D. (1972). *AIChE J.* **18**(2), 421.
25. Larson, M. A., and Bendig, L. L. (1976). *AIChE J. Symp. Ser.* **72**(153), 21.
26. Bennett, R. C., Fiedelman, H., and Randolph, A. D. (1973). *Chem. Eng. Progr. Symp. Ser.* **69**, 86.
27. Purves, W. T., and Larson, M. A. (1980). European Federation of Chem. Eng. Publ. Ser. No. 9, p. 7:5/1.
28. Garside, J., and Risitic, R. F. (1983). *J. Cryst. Growth* **61**, 215.
29. Janse, A. H., and de Jong, E. J. (1976). The occurrence of growth dispersion and its consequences. In "Industrial Crystallization" (J. Mullin, ed.), p. 145. Plenum Press, New York.
30. Mullin, J. W. (1979). Crystal growth in pure and impure solutions. In "Industrial Crystallization 78" (E. J. de Jong and S. J. Jancic, eds.), p. 93. North Holland, Amsterdam.
31. Davey, R. J. (1979). The control of crystal habit. In "Industrial Crystallization, 78" (E. J. de Jong and S. J. Jancic, eds.), p. 169. North Holland, Amsterdam.
32. Davey, R. J. (1982). Role of additives in precipitation processes. In "Industrial Crystallization, 81" (S. J. Jancic and E. J. de Jong, eds.), p. 123. North Holland, Amsterdam.
33. Khambaty, S., and Larson, M. A. (1976). *AIChE Symp. Ser.* **72**(1953), 21.
34. Shor, S. M., and Larson, M. A. (1971). *Chem. Eng. Progr. Symp. Ser.* **67**(110), 32.

CRYSTAL SIZE RESPONSES FOR CONTINUOUS AND BATCH CRYSTALLIZERS

The mechanisms of new crystal formation and crystal growth are the dominant factors that determine particle size and to some extent the form of the size distribution. It has been shown by experiments that nucleation is in general a nonlinear function of supersaturation, is sometimes a function of the amount of solids in suspension, and is dependent on many mechanical factors of crystallizer design, especially the system geometry and the energy input due to agitation. Generally, increased agitation causes increased new crystal formation. This particle generation is sometimes due to attrition but is more often a result of a secondary nucleation phenomenon. Particle size is affected less by growth than nucleation kinetics, but where size-dependent growth or growth dispersion occurs, the form of the distribution is dependent on the growth kinetics.

In this chapter, we will show how the various mechanisms are manifest in observed product size distributions from batch and continuous mixed-suspension mixed-product-removal (MSMPR) crystallizers, as well as other crystallizer systems. In later chapters, we will discuss the effects of unusual residence-time distributions resulting from unusual and complex system geometries.

6.1 Effect of Supersaturation on CSD

The level of supersaturation in an MSMPR crystallizer often markedly affects the CSD of the product. To illustrate the effect of supersaturation on CSD, we now consider a crystallizer operating at steady state and operable such that suspension density can be fixed at a given level regardless of the holding time. Normally such a system would be of the class II type, but the relationships that are developed are applicable for either class I or class II systems if the above-mentioned constraint can be applied.

The crystal growth rate is assumed to be a simple function of supersaturation so that the actual magnitude of the supersaturation can be parametrically excluded from the development; thus,

$$G = G(s) \quad (6.1-1)$$

For a nucleation rate that is independent of the effect of suspended solids, we let

$$B^0 = B^0(s) \quad (6.1-2)$$

Eliminating s and assuming a power-law form for the relationship for both Eqs. (6.1-1) and (6.1-2) gives

$$B^0 = B^0(G) = k_N G^i \quad (6.1-3)$$

Because the nucleation rate does not occur explicitly in the expression representing CSD, it is necessary to introduce the relationship

$$B^0 = n^0 G \quad (6.1-4)$$

Combining Eqs. (6.1-3) and (6.1-4) gives

$$n^0 = k_N G^{i-1} \quad (6.1-5)$$

Thus Eq. (6.1-5) relates the population density of nuclei to the crystallization kinetics.

It was shown previously for the MSMPR crystallizer, where crystal growth is not size-dependent, that the size distribution given in terms of population density is

$$n = n^0 \exp(-L/G\tau) \quad (6.1-6)$$

Further, it was shown that the suspension density expressed in terms of the distribution is

$$M_T = k_v \rho \int_0^\infty n L^3 dL = 6k_v \rho n^0 (G\tau)^4 \quad (6.1-7)$$

A mass balance relates growth rate to the rate of phase change. Thus,

$$G = \frac{\delta C}{3k_v \rho \int_0^\infty n L^2 dL} = \frac{\delta C}{6k_v \tau \rho n^0 (G\tau)^3} \quad (6.1-8)$$

For a system that has only one mixed withdrawal point, $\delta C = M_T$ and Eq. (6.1-8) becomes

$$G = M_T / 6k_v \tau \rho n^0 (G\tau)^3 \quad (6.1-9)$$

[Equation (6.1-9) is identical to Eq. (6.1-7).]

In order to compare the effects of supersaturation on CSD, consider two crystallizations carried out at the same temperature but at different supersaturations. A convenient way to assure different supersaturations is to operate a completely well-mixed crystallizer at different holding times τ while maintaining the same suspension density. We see from Eq. (6.1-9) that because of the necessity to conserve mass under such constraints, operation at shorter holding times must produce higher growth rates and hence higher supersaturations.

For crystallizations 1 and 2 operating to produce the same suspension density M_T , we have from Eqs. (6.1-7) or (6.1-9)

$$M_T = 6k_v \rho n_1^0 (G_1 \tau_1)^4 = 6k_v \rho n_2^0 (G_2 \tau_2)^4 \quad (6.1-10)$$

or

$$n_2^0 / n_1^0 = (G_1 \tau_1 / G_2 \tau_2)^4 \quad (6.1-11)$$

Using Eq. (6.1-5) to eliminate G_1 and G_2 gives

$$n_2^0 / n_1^0 = (\tau_1 / \tau_2)^{4(i-1)/(3+i)} \quad (6.1-12)$$

and combining Eqs. (6.1-11) and (6.1-5) to eliminate n^0 gives

$$G_2 / G_1 = (\tau_1 / \tau_2)^{4/(i+3)} \quad (6.1-13)$$

Examination of Eqs. (6.1-6), (6.1-12), and (6.1-13) for $\tau_1 > \tau_2$ gives rise to the following observations:

(a) When the kinetic order i is equal to 1, the size distribution is unaffected by supersaturation level, that is, $n_1^0 = n_2^0$, $G_1 \tau_1 = G_2 \tau_2$, although growth rates increase in proportion with (τ_1 / τ_2) .

(b) When the kinetic order i is greater than 1, say 3, n^0 increases with a decrease in holding time (increase in supersaturation) by a factor $(\tau_1 / \tau_2)^{4/3}$ and G again increases but to a lesser degree than when $i = 1$, namely, by the factor $(\tau_1 / \tau_2)^{2/3}$. The net result is smaller crystal size at shorter holding times (higher supersaturation).

(c) When kinetic order is less than 1, the mean crystal size increases with increases in supersaturation.

In summary, it appears that the higher the supersaturation, the smaller the crystal size for systems that exhibit kinetic orders greater than 1, and further, the higher the order of nucleation, the more difficult it will be to produce crystals of large size.

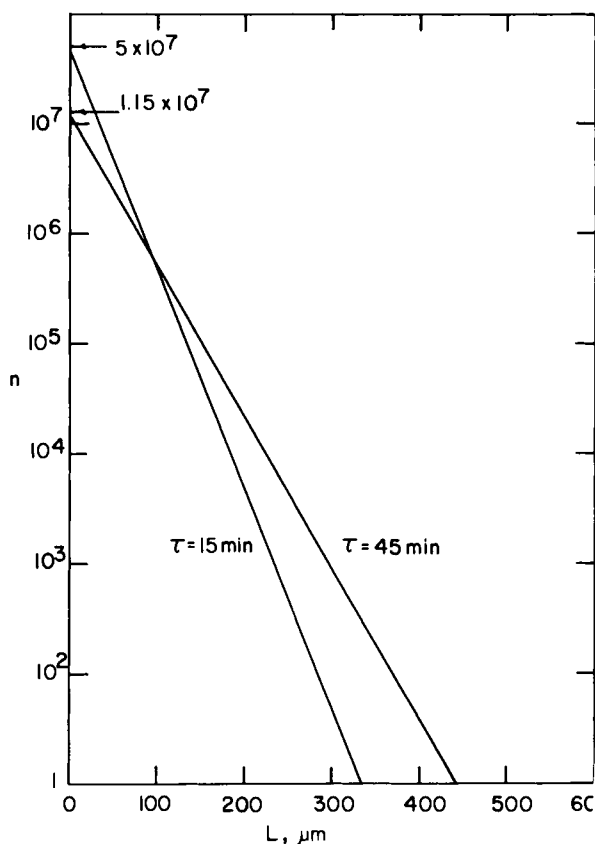


Fig. 6.1-1 Size distribution from crystallization at two different holding times.

EXAMPLE 6.1-1

Two MSMPR crystallizations are carried out at holding times of 15 and 45 min, respectively. The experiments are conducted so that the suspension density M_T is the same for each experiment. The size distributions of the crystalline product are shown in Fig. 6.1-1. Find the order of nucleation for this system.

From Eq. (6.1-12),

$$n_{15}^0/n_{45}^0 = 5 \times 10^7 / 1.15 \times 10^7 = (45/15)^{4(i-1)/(i+3)}$$

and for $i = 3$,

$$4.35 = (3)^{4/3}$$

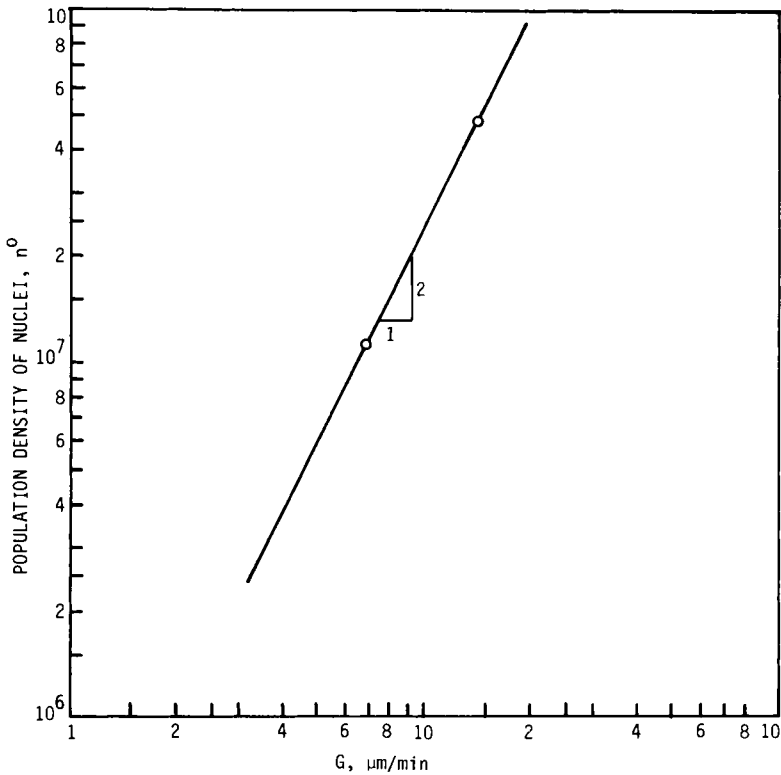


Fig. 6.1-2 Correlation of kinetic order of nucleation i . Slope $i - 1 = 2$.

Also, from Eq. (6.1-3) and the slopes from Fig. (6.1-1),

$$G_{15}/G_{45} = 1.45/0.70 = (45/15)^{4/(i+3)}$$

For $i = 3$,

$$2.07 = (3)^{2/3}$$

and the dominant particle size for the two cases are related by

$$\frac{L_{D,15}}{L_{D,45}} = (15/45)^{(i-1)/(i+3)}$$

Alternately, the intercepts from Fig. 6.1-1 can be plotted on log-log paper versus the growth rate obtained from the slopes as shown in Fig. 6.1-2. From Eq. (6.1-5) the slope of such a plot is $i - 1$. From Fig. 6.1-2 the slope $i - 1 = 2$.

If the growth rate is linear with supersaturation, the above example illustrates a useful method for finding i , the nucleation order with respect to supersaturation. If the growth is not linear then the slope of the plot is $i/h - 1$, where h is the kinetic order of growth. ♦

6.2 Effect of Suspended Solids on CSD

Heavy slurry densities provide more surface area for deposition of solute; thus for a given rate of make, lower supersaturations are necessary. This usually results in larger crystals when suspension density is high. In Chapter 7, we will discuss this effect in the context of a growth-type crystallizer that has a clear mother-liquor withdrawal stream. Here we will examine the effect of suspension density on CSD for an MSMPR crystallizer with only one withdrawal point and for the case where suspended solids are not a source of nuclei. Crystallization systems of this type require an increased rate of make to increase the suspension density.

Consider crystallizations 1 and 2 operated at the same holding time and temperature but with different feed concentration (i.e., $\delta C_1 \neq \delta C_2$). Remembering that $\delta C = M_T$ and $\tau_1 = \tau_2$ from Eq. (6.1-7),

$$\tau^4 = M_{T1}/6k_v\rho n_1^0 G_1^4 = M_{T2}/6k_v\rho n_2^0 G_2^4 \quad (6.2-1)$$

or

$$M_{T1}/n_1^0 G_1^4 = M_{T2}/n_2^0 G_2^4 \quad (6.2-2)$$

Rearranging and using the kinetic relationship of Eq. (6.1-5), Eq. (6.2-2) becomes

$$G_2/G_1 = (M_{T2}/M_{T1})^{1/(i+3)} \quad (6.2-3)$$

or

$$n_2^0/n_1^0 = (M_{T2}/M_{T1})^{(i-1)/(i+3)} \quad (6.2-4)$$

Finally, the dominant particle size previously given as $L_d = 3G\tau$ is related to the suspension density by

$$L_{d2}/L_{d1} = (M_{T2}/M_{T1})^{1/(i+3)} \quad (6.2-5)$$

The plot shown in Fig. 6.2-1 shows the comparative size distributions where the suspension density (and rate of make) differ by a factor of 3. For this example, the kinetic order was 2. The nucleation rate, the growth rate, and the dominant particle size are increased with increased suspension density. The distribution curve for the higher suspension density is always above the

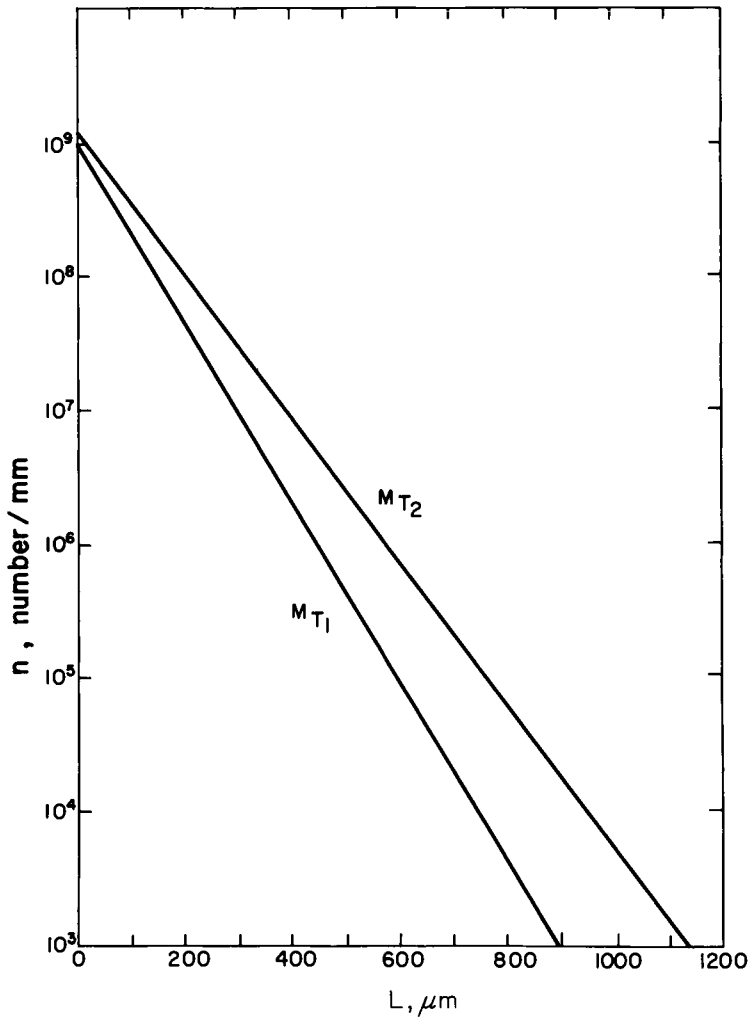


Fig. 6.2-1 Comparison of CSD from crystallization with different suspension densities (nonsecondary nucleation). $M_{T2} = 3M_{T1}$; kinetic order = 2. (After Larson *et al.* [10].)

one for the lower density because the average crystal size is larger and there are more total crystals present. Higher kinetic orders would result in less difference in the observed CSD.

From the above, it is reasonable to expect that for systems where nucleation rate is not of the secondary type, increased suspension density should produce larger crystals. However, any possible difference is small.

6.3 Effects of Secondary Nucleation

Most crystallization systems exhibit secondary nucleation effects. When these effects are present, the analysis in Section 6.2 does not apply; therefore, it is necessary to use a kinetic model that accounts for the nuclei formation directly related to the solids in suspension.

Assume that the secondary nucleation rate is related to solids in suspension and supersaturation by

$$B^0 = kM_T^j s^i \quad (6.3-1)$$

where the quantity M_T^j accounts for the secondary nucleation effects. Eliminating supersaturation using a linear form of Eq. (6.1-1) gives

$$B^0 = k_N M_T^j G^i \quad (6.3-2)$$

and in terms of the population density of nuclei,

$$n^0 = k_N M_T^j G^{i-1} \quad (6.3-3)$$

Consideration of a system under the same constraints as that in Section 6.2 operating at two different suspension densities gives

$$M_{T1}/n_1^0 G_1^4 = M_{T2}/n_2^0 G_2^4 \quad (6.3-4)$$

Combining this with Eq. (7.3-2) gives

$$n_2^0/n_1^0 = (M_{T2}/M_{T1})^{(i+4j-1)/(i+3)} \quad (6.3-5)$$

or

$$G_2/G_1 = (M_{T2}/M_{T1})^{(1-j)/(i+3)} \quad (6.3-6)$$

In many instances, the secondary nucleation is found to be proportional to suspension density, and hence $j = 1$. For this case,

$$G_2/G_1 = (M_{T2}/M_{T1})^{0.0} = 1 \quad (6.3-7)$$

and

$$n_2^0/n_1^0 = (M_{T2}/M_{T1})^{(i+3)/(i+3)} = M_{T2}/M_{T1} \quad (6.3-8)$$

From the above equation, growth rate does not change with suspension density, and the population density of nuclei changes proportionately with the suspension density (rate of make), regardless of the supersaturation kinetic order i . Consequently, no change in size distribution can be achieved by changing the suspension density of a system with a linear secondary nucleation effect. Size distributions for crystallization with a threefold difference in suspension density are shown in Fig. 6.3-1. Suspension-density changes in systems that exhibit secondary nucleation will not affect CSD unless very large increases are made. In this case crystal size may decrease because of increased nucleation.

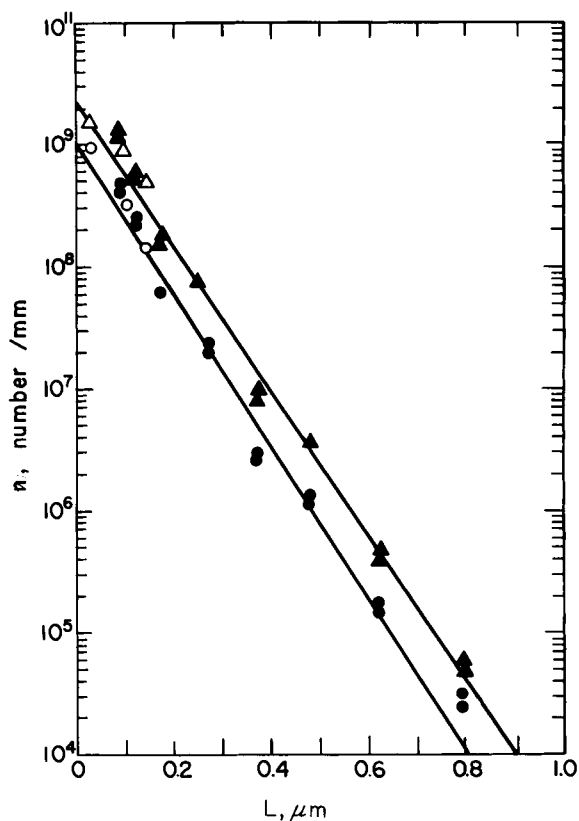


Fig. 6.3-1 Comparison of CSD from crystallization with different suspension densities (secondary nucleation). (After Larson *et al.* [11].)

We note here that the same result would occur if secondary nucleation had been assumed to be dependent on crystal area. This analysis cannot distinguish the mechanism of secondary nucleation.

This illustration and that in Section 6.2 indicate only two of the effects that can be examined using the results of the population balance. It is clear that the rate constant k_N is a function of the hydrodynamic conditions as well as the temperature. In these cases, a more complex analysis and comparison must be made to determine the effect of these conditions and kinetics on size distribution. In subsequent chapters, these factors will be examined in the context of reported experimental data, and the effect of residence time will also be examined in the context of systems exhibiting classification.

6.4 Crystallizer Cascades

Crystal size distribution can be altered by crystallizing in a series of crystallizer bodies such that the entire magma flows from one stage to another [1]. Various strategies can be employed to alter the CSD. Among these are conditions that permit nucleation in the first stage but only growth in the second, and the use of classified product removal from each stage. It is more realistic, however, to recognize that both nucleation and growth will take place in each stage and that classified product removal increases the tendency toward instability.

Relatively simple design measures can be taken to alter CSD, however, by arbitrarily fixing different retention times and production rates in each stage. For cooling systems, the former is accomplished by using different body sizes in the cascade, and the latter is accomplished by imposing different rates of energy removal on each stage.

Our objectives in this section are to show what CSD could result from various operating conditions. We will first give the applicable material and population balance equations for a cascade, then cast these equations in dimensionless form for ease in manipulation. As will be discussed in Chapter 7, the cascaded crystallizer can be described by the general CSD algorithm. Here, however, we examine the special case of equal flows, no fines destruction, and unclassified product removal to illustrate the fundamental behavior of cascaded systems. Two- and three-stage cascade systems will then be used to illustrate the effects of these constraints on CSD.

Consider a cascade of m well-stirred stages operated so that no seeding is required in stage 1 and the entire slurry is carried forward to each

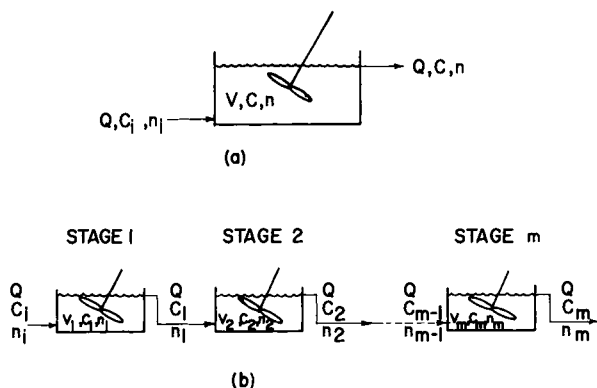


Fig. 6.4-1 Crystallizers: (a) single stage, and (b) cascade system. (After Larson and Wolff [1].)

subsequent stage as shown in Fig. 6.4-1. A steady-state number balance around each stage results in

$$\begin{aligned} V_1 [d(G_1 n_1)/dL] &= -Q_1 n_1 \\ V_2 [d(G_2 n_2)/dL] &= Q_1 n_1 - Q_2 n_2 \\ V_m [d(G_m n_m)/dL] &= Q_{m-1} n_{m-1} - Q_m n_m \end{aligned} \quad (6.4-1)$$

A mass balance on the solute crystallized in each stage gives

$$\begin{aligned} Q_i C_i &= Q_1 C_1 + \rho k_v Q_1 \int_0^\infty n_1 L^3 dL \\ Q_{m-1} C_{m-1} &= Q_m C_m + \rho k_v Q_m \int_0^\infty n_m L^3 dL \end{aligned} \quad (6.4-2)$$

From the previous development in Section 4.5 for a single stage, Eq. (6.4-2) can be rearranged to give the following constraint on growth rate:

$$G_j = [(C_{j-1} Q_{j-1}/Q_j) - C_j] / \left[3k_v \rho (V_j/Q_j) \int_0^\infty n_j L^2 dL \right], \quad j = 1, \dots, m \quad (6.4-3)$$

The nucleation and growth kinetics expressed as before are

$$(n^0)_j = k_N G_j^{i-1} \quad (6.4-4)$$

When Q_j is the same for all j , the set to be solved is

$$V_j [d(G_j n_j)/dL] = Q(n_{j-1} - n_j)$$

and from Equation (6.4-2),

$$G_j = \delta C_j / \left(3k_v \rho \tau_j \int_0^\infty n_j L^2 dL \right) \quad (6.4-5)$$

and from Eq. (6.4-4),

$$(n^0)_j = k_N G_j^{i-1}$$

where $j = 1, 2, \dots, m$.

The effects of staging on CSD can best be illustrated by comparing the CSD with that expected from a single-stage system for the same system retention time and production. To do this, it is necessary to define a set of dimensionless variables and cast Eqs. (6.4-2), (6.4-4), and (6.4-5) in dimensionless form. These variables will be slightly different from those previously used. They are defined in Table 6.4-1.

Table 6.4-1

Dimensionless Variables

Variable	Dimensionless symbol	Single-stage symbol	<i>j</i> th-Stage symbol	Dimensionless definition
Size	x	L	L	LQ/GV
Number density	y_j	n	n_j	n_j/n^0
Density of nuclei	y_j^0	n^0	n_j^0	n_j/n^0
Crystal surface area	α_j	A	A_j	A_j/A
Growth rate	ρ_j	G	G_j	G_j/G
Production	σ_j	δC	δC_j	$\delta C_j/\delta C$
Body volume	γ_j	V	V_j	V_j/V
Flow	q_j	Q	Q_j	Q_j/Q

For the purpose of the subsequent development, it will be assumed that the kinetic parameters for each of the j stages are identical to those in the single-stage reference case. That is, they are independent of temperature. For cooling systems, we assume Q_j is a constant, and therefore q_j is 1 and the parameter characterizing retention time in each stage is γ_j . The definitions of γ_j and σ_j require that

$$\sum_{j=1}^m \gamma_j = 1, \quad 0 < \gamma_j < 1 \quad (6.4-6)$$

$$\sum_{j=1}^m \sigma_j = 1, \quad 0 < \sigma_j < 1$$

Using the substitutions given in Table 6.4-1, Eqs. (6.4-2), (6.4-4), and (6.4-5) become

$$\rho_j \gamma_j (dy_j/dx) = y_{j-1} - y_j, \quad \rho_j = \sigma_j / \gamma_j \alpha_j, \quad y_j^0 = \rho_j^{j-1} \quad (6.4-7)$$

In addition, the dimensionless area α_j is defined by

$$\alpha_j = \int_0^\infty y_j x^2 dx \bigg/ \int_0^\infty y x^2 dy = \frac{1}{2} \int_0^\infty y_j x^2 dx \quad (6.4-8)$$

Equations (6.4-7) and (6.4-8), along with the constraint of Eq. (6.4-6), define the problem. The choice parameters are γ_j and σ_j , representing the stage retention time and the stage production rate, respectively.

Before considering the CSD obtained from staged systems, we now repeat the solution of the single-stage equation for the size distribution. For

$m = 1$, the solutions are

$$y = \exp(-x), \quad \alpha = 1, \quad \rho = 1 \quad (6.4-9)$$

the cumulative mass distribution is Eq. (4.4-9),

$$W = 1 - \exp(-x) \left(1 + x + \frac{1}{2}x^2 + \frac{1}{6}x^3\right)$$

and the differential mass distribution function is Eq. (4.4-13),

$$w = x^3 \exp(-x)/6$$

Equation (4.4-13), previously plotted in Fig. 4.4-1, is plotted in subsequent sections for comparison purposes with distributions obtained from staged systems.

With no attempt to be exhaustive, we now give several examples of the size distribution expected from two- and three-stage systems.

EXAMPLE 6.4-1

Consider a two-stage cascade with nucleation in the first stage only. Assume equal-size bodies and equal production rates. Therefore, $\sigma_1 = \sigma_2 = \frac{1}{2}$ and $\gamma_1 = \gamma_2 = \frac{1}{2}$.

Stage 1:

$$y_1 = y_1^0 \exp(-2x/\rho_1), \quad y_1^0 = \rho_1^{i-1}, \quad \rho_1 = 1/\alpha_1, \quad \alpha_1 = y_1^0 (\rho_1/2)^3 \quad (6.4-10)$$

Stage 2:

$$y_2 = y_1^0 [\rho_1/(\rho_1 - \rho_2)] [\exp(-2x/\rho_1) - \exp(-2x/\rho_2)] \quad y_2^0 = 0$$

$$\alpha_2 = y_1^0 [\rho_1/(\rho_1 - \rho_2)] \{ [\rho_1/2]^3 - [\rho_2/2]^3 \}$$

$$\begin{aligned} W_2 = y_1^0 [\rho_1/(\rho_1 - \rho_2)] \{ & [(\rho_1^4 - \rho_2^4)/2^4] + \exp(-2x/\rho_2) \\ & \times [(\rho_2/2)^4 + (\rho_2/2)^3 x + \frac{1}{2}(\rho_2/2)^2 x^2 + \frac{1}{6}(\rho_2/2) x^3] \\ & - \exp(-2x/\rho_1) [(\rho_1/2)^4 + (\rho_1/2)^3 x + \frac{1}{2}(\rho_1/2)^2 x^2 + \frac{1}{6}(\rho_1/2) x^3] \} \end{aligned} \quad (6.4-11)$$

$$w_2(x) = y_1^0 [\rho_1/(\rho_1 - \rho_2)] (x^3/6) [\exp(-2x/\rho_1) - \exp(-2x/\rho_2)]$$

The distribution $w_2(x)$ for stage 2 is plotted in Fig. 6.4-2, along with the distribution for a single stage.

The normalized growth rate for a single stage is unity, by Eq. (6.4-9). From Eqs. (6.4-10), we get for stage 1 of this two-stage system the

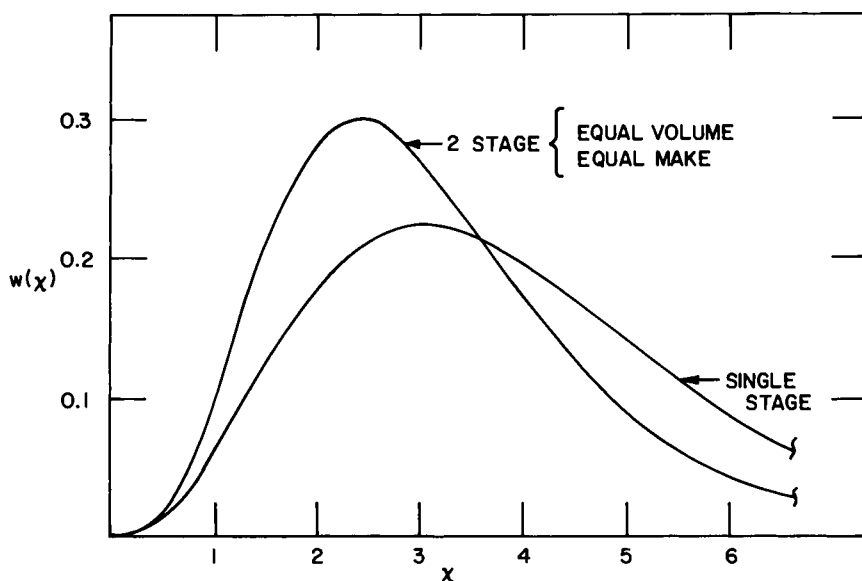


Fig. 6.4-2 Mass distribution for a two-stage system with equal volumes and equal make (no nucleation in stage 2).

dimensionless growth rate

$$\rho_1 = (8)^{1/(3+i)} \quad (6.4-12)$$

Under the assumed conditions, the growth rate must always be greater in stage 1 than in a single-stage system. ♦

EXAMPLE 6.4-2

Consider two stages with conditions such that the growth rates are equal and the retention times are equal.

This necessarily means that the production rate in stage 2 would be greater than in stage 1 because of the greater surface area available for deposition of solute.

The solution for the first stage is identical to that in Example (6.4-1) except for the mass balance relationship. Here,

$$\rho_1 = 2\sigma_1/\alpha_1 \quad (6.4-13)$$

and

$$\rho_1 = \rho_2, \quad \sigma_1 < \sigma_2 \quad (6.4-14)$$

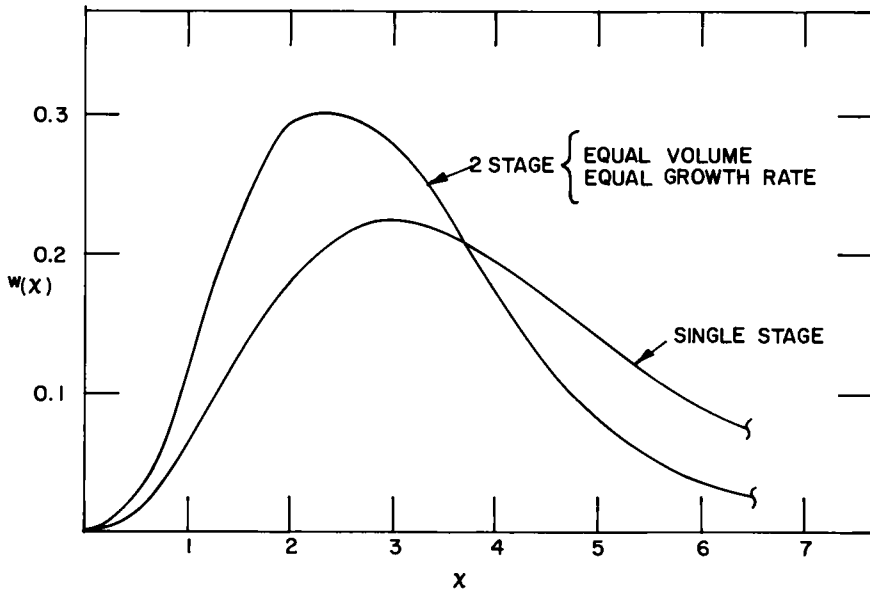


Fig. 6.4-3 Mass distribution for a two-stage system with equal volumes and equal growth rates (nucleation in both stages).

For stage 2:

$$\begin{aligned}
 y_2 &= y_1^0 (2x/\rho) \exp(-2x/\rho) + y_2^0 \exp(-2x/\rho) \\
 \rho_2 &= 2\sigma_2/\alpha_2, \quad \alpha_2 = (3y_1^0 + y_2^0)(\rho/2)^3 \\
 W_2 &= y_2^0 \left\{ (\rho/2)^4 - \exp(-2x/\rho) \left[(\rho/2)^4 + (\rho/2)^3 x \right. \right. \\
 &\quad \left. \left. + \frac{1}{2}(\rho/2)^2 x^2 + \frac{1}{6}(\rho/2) x^3 \right] \right\} \\
 &\quad + 4y_1^0 (2/\rho) \left\{ (\rho/2)^5 - \exp(-2x/\rho) \left[(\rho/2)^5 + (\rho/2)^4 x \right. \right. \\
 &\quad \left. \left. + \frac{1}{2}(\rho/2)^3 x^2 + \frac{1}{6}(\rho/2)^2 x^3 + \frac{1}{24}(\rho/2) x^4 \right] \right\} \quad (6.4-15) \\
 w_2 &= (x^3/6) [y_1^0 (2x/\rho) \exp(-2x/\rho) + y_2^0 \exp(-2x/\rho)]
 \end{aligned}$$

Figure 6.4-3 compares the mass distribution from a single-stage with that for a two-stage system with equal growth rates for a system with nucleation order 2 and with nucleation in both vessels. These plots again show a smaller mean crystal size in a two-stage system but little change in the coefficient of variation.

Note that the fraction of production required in stage 2 to achieve this result is

$$\sigma_2 = \sigma_1 (\alpha_2/\alpha_1) \quad \blacklozenge \quad (6.4-16)$$

EXAMPLE 6.4-3

The following solution is for an arbitrary allocation of production and retention time in a two-stage crystallizer for a class II system. Solutions are given for the number distribution, the area, and the growth rate. The assumed kinetics are continuous over the range of supersaturation, and the nucleation kinetics are assumed independent of solids in suspension. The mass distribution is not given because of its complexity.

For stage 1:

$$\begin{aligned} y_1 &= y_1^0 \exp(-x/\rho_1 \gamma_1), & \alpha_1 &= y_1^0 (\sigma_1/\alpha_1)^3 \\ \rho_1 &= \sigma_1/\alpha_1 \gamma_1, & y_1^0 &= \rho^{i-1} \end{aligned} \quad (6.4-17)$$

For stage 2:

$$\begin{aligned} y_2 &= y_2^0 \exp(-x/\rho_2 \gamma_2) + y_1^0 [\rho_1 \gamma_1 / (\rho_1 \gamma_1 - \rho_2 \gamma_2)] \\ &\quad \times [\exp(-x/\rho_1 \gamma_1) - \exp(-x/\rho_2 \gamma_2)] \\ \alpha_2 &= y_2^0 (\sigma_2/\alpha_2)^3 + (y_1^0 \sigma_1/\alpha_1) \\ &\quad \times [(\sigma_2^2/\alpha_2^2) + (\sigma_1 \sigma_2/\alpha_1 \alpha_2) + (\sigma_1^2/\alpha_1^2)] \\ \rho_2 &= \sigma_2/\alpha_2 \gamma_2, & y_2^0 &= \rho_2^{i-1} \quad \blacklozenge \end{aligned} \quad (6.4-18)$$

We give here, for completeness, the solution for the third stage of a three-stage cascade with arbitrary allocation of total crystal volume and production in each stage:

$$\begin{aligned} y_3 &= y_3^0 \exp\left(-\frac{x}{\rho_3 \gamma_3}\right) + y_2^0 \left(\frac{\rho_2 \gamma_2}{\rho_2 \gamma_2 - \rho_3 \gamma_3}\right) \left[\exp\left(-\frac{x}{\rho_2 \gamma_2}\right) - \exp\left(-\frac{x}{\rho_3 \gamma_3}\right)\right] \\ &\quad + y_1^0 \left\{ \frac{\rho_1^2 \gamma_1^2}{(\rho_1 \gamma_1 - \rho_2 \gamma_2)(\rho_2 \gamma_2 - \rho_3 \gamma_3)} \left[\exp\left(-\frac{x}{\rho_1 \gamma_1}\right) - \exp\left(-\frac{x}{\rho_3 \gamma_3}\right)\right] \right. \\ &\quad \left. - \frac{\rho_1 \rho_2 \gamma_1 \gamma_2}{(\rho_1 \gamma_1 - \rho_2 \gamma_2)(\rho_2 \gamma_2 - \rho_3 \gamma_3)} \left[\exp\left(-\frac{x}{\rho_2 \gamma_2}\right) - \exp\left(-\frac{x}{\rho_3 \gamma_3}\right)\right] \right\} \\ \alpha_3 &= y_1^0 \left(\frac{\rho_1^2 \gamma_1^2}{\rho_1 \gamma_1 - \rho_2 \gamma_2}\right) \left(\frac{\sigma_1^2}{\alpha_1^2} + \frac{\sigma_1 \sigma_3}{\alpha_1 \alpha_3} + \frac{\sigma_3^2}{\alpha_3^2}\right) \\ &\quad - \left[y_1^0 \frac{\rho_1 \rho_2 \gamma_1 \gamma_2}{(\rho_1 \gamma_1 - \rho_2 \gamma_2)} - y_2^0 \rho_2 \gamma_2 \right] \left(\frac{\sigma_2^2}{\alpha_2^2} + \frac{\sigma_2 \sigma_3}{\alpha_2 \alpha_3} + \frac{\sigma_3^2}{\alpha_3^2}\right) + y_3^0 \frac{\sigma_3^3}{\alpha_3^3} \\ \rho_3 &= \frac{\sigma_3}{\alpha_3 \gamma_3} \end{aligned} \quad (6.4-19)$$

The implicit nature of these quantities makes them difficult to evaluate. However, the above equations define the system. The nomenclature listed in Table 6.4-1 applies to all previous examples and the system described by Eqs. (6.4-7) and (6.4-8).

In many instances, secondary nucleation effects must be considered. These may be handled by using the power-law model.

$$n^0 = k_N G^{i-1} M_T^j$$

Here, we assume that the phenomenon of secondary nucleation is related to the solids density. In dimensionless form, this becomes, for the k th stage,

$$y_k^0 = \rho_k^{i-1} \sigma_k^j \quad (6.4-20)$$

All previous solutions still apply except that nuclei population densities are replaced by $\rho^{i-1} \sigma^j$ instead of ρ^{i-1} when calculations are made.

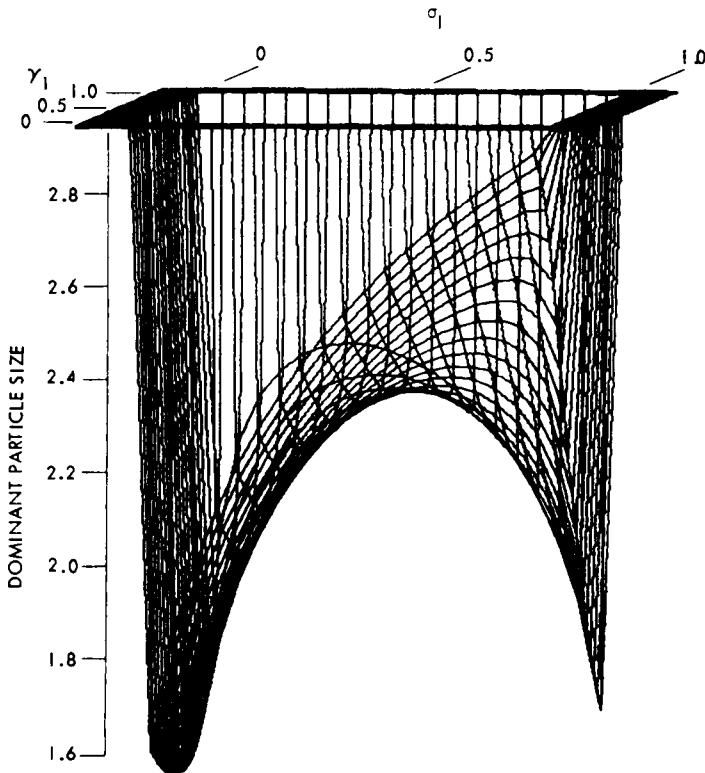


Fig. 6.4-4 Dominant particle size for a two-stage crystallizer of arbitrary productions σ_1 and σ_2 ($\sigma_1 + \sigma_2 = 1$) and arbitrary volumes γ_1 and γ_2 ($\gamma_1 + \gamma_2 = 1$). (After Wolff and Larson [1].)

Figure 6.4-4 is a plot of dimensionless dominant particle size for a two-stage class II cascaded system. In this example a secondary nucleation model was used. The independent variables γ_1 and σ_1 are respectively the fraction of the total residence time and the production allocated to the first stage. Note that the dimensionless dominant particle size x_d has the value of 3 for a one-stage system and that the dominant size produced in this two-stage system is less than in the single-stage case.

In most applications, staged systems are used for different reasons than for CSD control. These will be discussed in Chapter 7. In these applications, classification takes place at each crystallizer, and product is removed and fines are advanced.

6.5 Effects of Simple Fines Destruction

As can be seen from previous sections, one cannot change CSD appreciably by changing retention time or suspension density. While some increase in size can be achieved by such a change, it is at a high cost in production rate for a given crystallizer. In the previous examples, changing retention time by a factor of 3 (one-third the production rate) increased the mean size by only a factor of 2. This is not assured, however, because increased retention time may result in higher secondary nucleation rates per unit mass of product. Moreover, staged systems generally narrow the CSD but also result in a reduction of mean size if total retention time is the same as for a single stage. For a given set of kinetic relationships, the only way the coefficient of variation (c.v.) can be reduced or mean size increased is by using an internal classification system that separates fines and either destroys or removes them while they are at a very small size. Classified product removal may also be used to remove only large crystals, but such a withdrawal system must be accompanied by a fines destruction system to satisfy the population balance. This system will be discussed in detail in Chapter 7; here we will examine a simple fines removal and fines destruction system to illustrate the effect of such a system on overall CSD.

Consider an unseeded draft tube baffle crystallizer such as that shown in Fig. 4.1-2. The upward flow velocity in the annular space is fixed at the settling velocity of the largest crystal to be separated and destroyed. Its size will be denoted as L_F . The remainder of the crystallizer body of volume V will be considered to be perfectly mixed with a perfectly mixed slurry product removal as indicated. It is presumed that no crystal growth takes place in the annular space so that the effective volume for crystallization is the well-mixed volume V . The liquor and fines removed are passed through a heat exchanger, mixed with the feed, and returned to the crystallizer. The

volumetric flow rate through the fines removal system is Q_o and the flow through the slurry discharge system is Q_u . There will only be crystals from 0 to L_F in the overflow and crystals from 0 to L_{\max} in the underflow. Thus crystals of different sizes will have different retention times. To account for this, the number balance must be written in two parts. Following Eq. (4.2-8),

$$GV \frac{dn_F}{dL} + (Q_o + Q_u)n_F = 0 \quad L \leq L_F \quad (6.5-1)$$

and

$$GV \frac{dn}{dL} + Q_u n = 0 \quad L \geq L_F \quad (6.5-2)$$

Because all growth takes place in the well-mixed volume V , the growth rate is the same for each part of the number balance. Letting $V/(Q_o + Q_u) = \tau_F$ and $V/Q_u = \tau_p$,

$$\frac{dn_F}{dL} + \frac{n_F}{G\tau_F} = 0 \quad L \leq L_F \quad (6.5-3)$$

$$\frac{dn}{dL} + \frac{n}{G\tau_p} = 0 \quad L \geq L_F \quad (6.5-4)$$

and integrating Eq. (6.5-3) from 0 to L and Eq. (6.5-4) from L_F gives

$$n_F = n^0 \exp(-L/G\tau_F) \quad L \leq L_F \quad (6.5-5)$$

$$n = n^0 \exp(-L_F/G\tau_F) \exp(-L/G\tau_p) \quad L \geq L_F \quad (6.5-6)$$

Plotting Eqs. (6.5-5) and (6.5-6) gives the CSD shown in Fig. 6.5-1.

Equations (6.5-5) and (6.5-6) together represent the total product distribution. Equation (6.5-5) represents the CSD of the crystals in the fines loop. The two equations may be integrated piece-wise to obtain the moments of the distribution:

$$N_T = \int_0^{L_F} n_F dL + \int_{L_F}^{\infty} n dL \quad (6.5-7)$$

$$A_T = k_A \left[\int_0^{L_F} L^2 n_F dL + \int_{L_F}^{\infty} L^2 n dL \right] \quad (6.5-8)$$

$$M_T = k_v \rho \left[\int_0^{L_F} L^3 n_F dL + \int_{L_F}^{\infty} L^3 n dL \right] \quad (6.5-9)$$

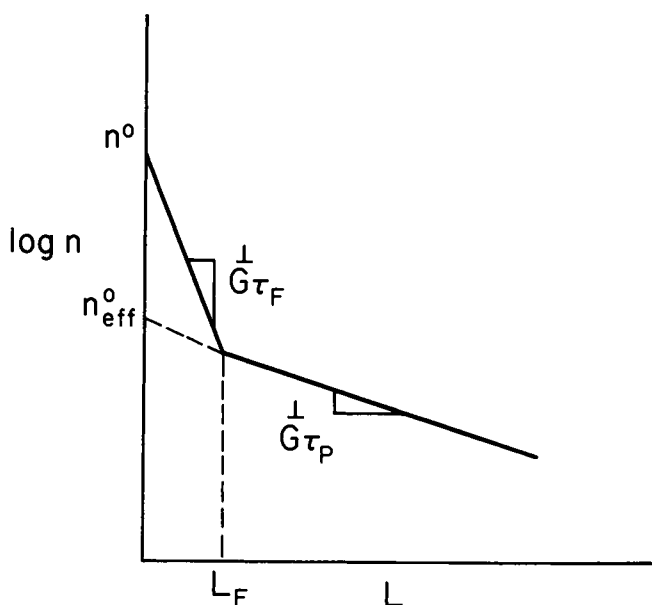


Fig. 6.5-1 CSD with fines dissolving.

and the mean size can be calculated by

$$\bar{L}_{4,3} = \frac{\int_0^{L_F} L^4 n_F dL + \int_{L_F}^{\infty} L^4 n dL}{\int_0^{L_F} L^3 n_F dL + \int_{L_F}^{\infty} L^3 n dL} \quad (6.5-10)$$

All other mean sizes previously discussed can be similarly calculated.

EXAMPLE 6.5-1

Compare the CSD from a MSMPR crystallizer with a suspension retention τ_p of 100 min with a crystallizer with fines dissolving having the same suspension retention time. The fines dissolver returns the overflow to the crystallizer and its flow rate is such that the fines retention time is $\tau_F = 10$ min. The baffle is designed so that $L_F/G_2\tau_1 = 4$, where G_2 is the growth rate required in the crystallizer with fines dissolving. Then G_1 is the growth rate in the MSMPR crystallizer that produces a product with dominant size $L_{D1} = 450 \mu\text{m}$. The crystal nucleation kinetics are $B^0 = kG^2$ or in terms of nuclei population density $n^0 = kG^2$. Each crystallizer will produce at the same mass rate, so that $\tau_{p1} = \tau_{p2}$, $V_1 = V_2$, and $M_{T1} = M_{T2}$.

Find growth rate G_1 :

$$G_1 = \frac{L_{D1}}{3\tau_p} = \frac{450}{300} = 1.5 \text{ } \mu\text{m/min}$$

Find G_2 necessary to achieve the same net production M_{T1} . For the MSMPR crystallizer,

$$n_1 = n_1 \exp(-L/G_1\tau_p) = kG_1 \exp(-L/G_1\tau_p)$$

$$M_{T1} = \int_0^\infty k\rho k_v G_1^2 \exp(-L/G_1\tau_p) dL = 6k_v k\rho G_1^2 (G_1\tau_p)^4$$

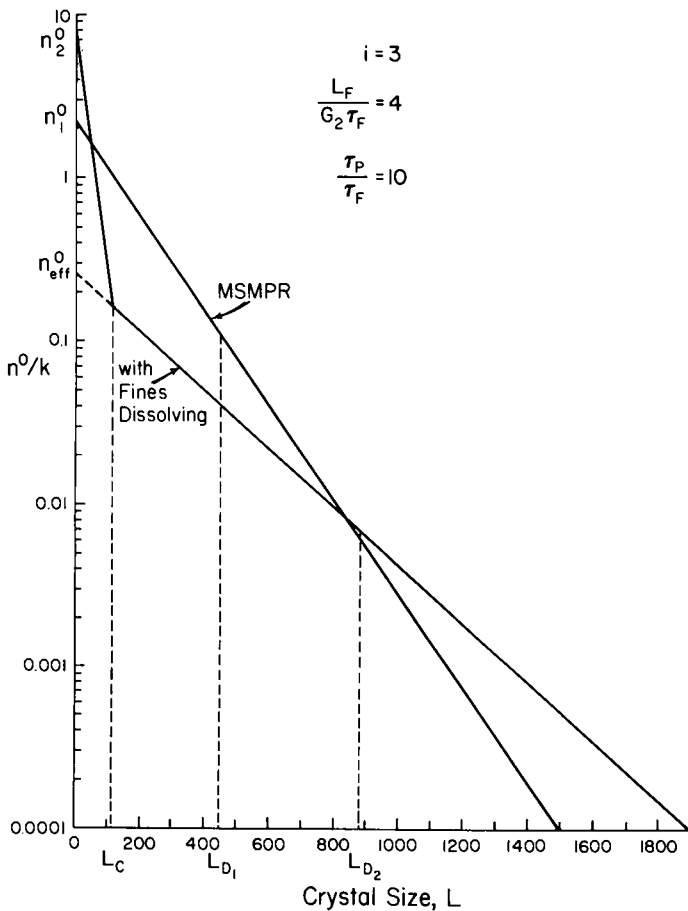


Fig. 6.5-2 CSD of equivalent MSMPR and fines-dissolving crystallizer.

For the fines-dissolving crystallizer,

$$n_{2F} = n_2 \exp(-L/G_2\tau_F) = kG_2^2 \exp(-L/G_2\tau_p) \quad L \leq L_F$$

$$\begin{aligned} n_2 &= n_2 \exp(-L_F/G_2\tau_p) \exp(-L/G_2\tau_p) \\ &= kG_2 \exp(-L_F/G_2\tau_F) \exp(-L/G_2\tau_p) \quad L \geq L_1 \end{aligned}$$

$$\begin{aligned} M_{T_2} &= G_2 k \rho k_v \left[\int_0^{L_F} \exp(-L/G_2\tau_F) dL \right. \\ &\quad \left. + \int_{L_F}^{\infty} \exp(-L_F/G_2\tau_F) \exp(-L/G_2\tau_p) dL \right] \end{aligned}$$

Very little mass is represented by the left-hand integral; therefore,

$$\begin{aligned} M_{T_2} &\cong G^2 k \rho k_v \exp(-L_F/G_2\tau_F) \int_0^{\infty} \exp(-L/G_2\tau_p) dL \\ &\cong 6k_v \rho k \exp(-L_F/G_2\tau_F) G_2 (G_2\tau_p)^4 \end{aligned}$$

But $M_{T_1} = M_{T_2}$ and $L_F/G_2\tau_F = 4$. Thus

$$[\exp(-4)] G_2 (G_2\tau_p)^4 = G_1 (G_1\tau_p)^4$$

and

$$G_2 = G_1 \exp(4/6) = (1.5)(1.95) = 2.92 \quad \mu\text{m}/\text{min}$$

$$L_{D_2} = L_{D_1}(1.95) = 878 \quad \mu\text{m}$$

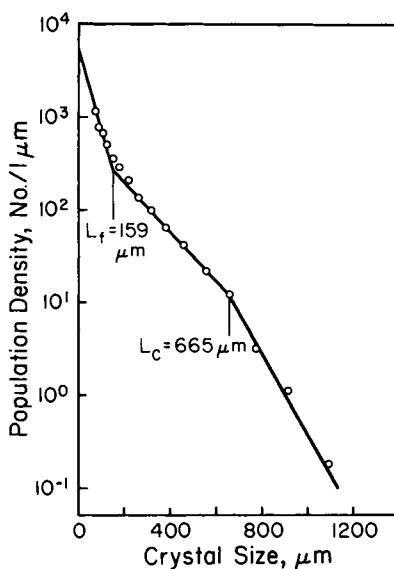


Fig. 6.5-3 Experimental KNO_3 CSD from laboratory crystallizer with fines removal. $\tau = 18$ min, $M_T = 5$ g/l, $G = 9$ $\mu\text{m}/\text{min}$, $Q_o/Q_u = 3.29$, $L_F = 159$ μm . (After Juzaszek and Larson [2].)

The nuclei population densities are

$$n_1^0/k = (G_1)^2 = 2.25 \quad n_2^0/k = (G_2)^2 = 8.53$$

and the nucleation rates compare as

$$B_2^0/B_1^0 = (1.95)^3 = 7.42$$

The two distributions are plotted in Fig. 6.5-2. Figure 6.5-3 shows the CSD obtained by Jazaszek and Larson [2] from a small laboratory crystallizer with fines removal. Their data showed inadvertent classified product removal as well because of the reduced number of larger crystals. ♦

In the example, it was necessary to circulate liquor through the fines distribution system at a rate approximately nine times faster than the throughput and dissolve crystals up to one-eighth the mean size of the product crystals in order to increase the mean size by a factor of 2. Because some crystals are dissolved, crystallization must be carried on at a higher rate in order to achieve net production rate equivalent to the MSMR crystallizer. This forces the supersaturation rate up, thus producing a nuclei population density four times that of the MSMR. However, because the small crystals were dissolved, the effective nuclei population density (n_{eff}^0) was reduced to about one-tenth that of the MSMR. This, coupled with the increased growth rate, resulted in the increased size of the crystals. A price has to be paid for this, however, in the increased energy requirement to dissolve the fines and to recrystallize them.

6.6 Effects of Mixing and Withdrawal Characteristics

So far only perfectly mixed continuous crystallizers with clearly defined withdrawal characteristics have been considered. Deviations from such conditions intentionally or unintentionally can have pronounced effects on the CSD of the product. In large production systems it is often difficult to achieve the desired mixing conditions. Crystallization systems are always two-phase systems and often three-phase. The solid dispersed phase consists of a distribution of sizes. To achieve perfect mixing so that a complete distribution of sizes exists in all parts of the mixed volume is difficult. Moreover, there is no absolute assurance that any withdrawal stream will contain a complete distribution or a predetermined portion of the distribution. It is important to consider how various deviations from the ideal will affect the CSD obtained.

6.6.1 Ineffective Volume

If, in the case of a reaction precipitation crystallizer, the flow pattern is such that all of the reaction takes place in the immediate region near the

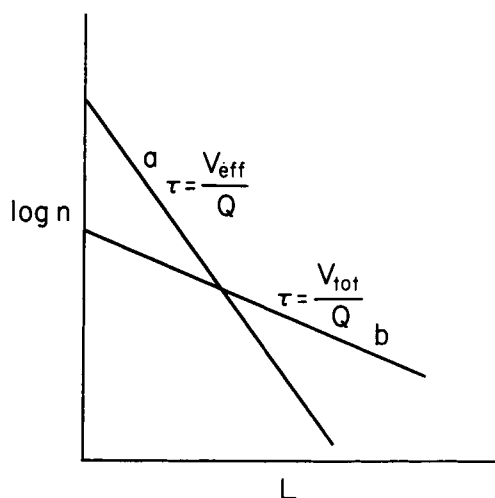


Fig. 6.6-1 Ineffective volume effect on CSD. Line (a), expected CSD if only a small portion of the volume is effective. Line (b), expected CSD if total crystallizer volume is effective.

feedpoint, nearly all of the supersaturation will be relieved in this region and the remainder of the crystallizer volume will act merely as a holding tank. The net result is that the actual mean crystal growth retention time is much less than that intended. The effect will be the same as that illustrated in Chapter 4 for short retention time. Figure 6.6-1 compares qualitatively the CSD obtained in such a case with the CSD obtainable if the whole volume were effectively used.

The term V_{eff} refers to the small volume where the reaction takes place. If the flow pattern is changed to make the whole volume effective for growth, then a reduction in nucleation should be expected with a resulting increase in mean size. This situation could occur in other crystallizers as well. For example, if the vapor release surface is separated from the main body of an evaporative system, all supersaturation may be released near this surface, resulting in the remainder of the vessel acting only as a holding tank.

An extreme example of this situation is one in which the effective reaction volume is so low and thus the supersaturation is so high that crystals will be produced that are too small to exist in the remaining volume because of the Gibbs-Thompson effect. The resulting CSD would then have the character as shown in Fig. 6.6-2.

An example of where this phenomenon could occur is in the precipitation of silver halides for photographic purposes.

If the flow pattern in a crystallizer that shows such behavior cannot be changed, it must be modeled as multistage crystallizer, and the CSD

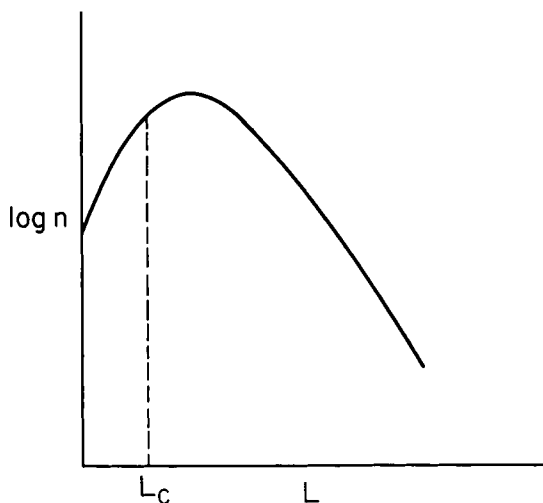


Fig. 6.6-2 CSD when nuclei are not viable in the principal volume of the crystallizer; L_c , critical crystal size in principal volume.

obtained has the same characteristics as the product of the staged crystallizer described in Section 6.4.

6.6.2 Poorly Mixed Dispersed Phase

A different effect occurs if the crystallizer flow pattern is such that the fluid phase is well mixed but there exists internal size classification of the suspended crystals. The actual effect will depend on where the continuous slurry product discharge is located. If internal classification exists and the discharge is in a region that has a deficiency of the large size end of the CSD, then fines will be removed preferentially and the CSD will appear as in Fig. 6.6-3. This is the same result as is achieved for intentional fines removal.

An example of circumstances that give rise to this situation are those where the large crystals are inefficiently circulated to the top of a vessel and discharge is near the surface. If the discharge is near the bottom, under the same mixing conditions, then large crystals are preferentially removed and the CSD appears as shown in Fig. 6.6-4.

6.6.3 Nonisokinetic Withdrawal

Nonisokinetic withdrawal often results in classification even though the crystallizer is well mixed. If the direction of withdrawal is different from or at a velocity different from the internal flow incident to the withdrawal

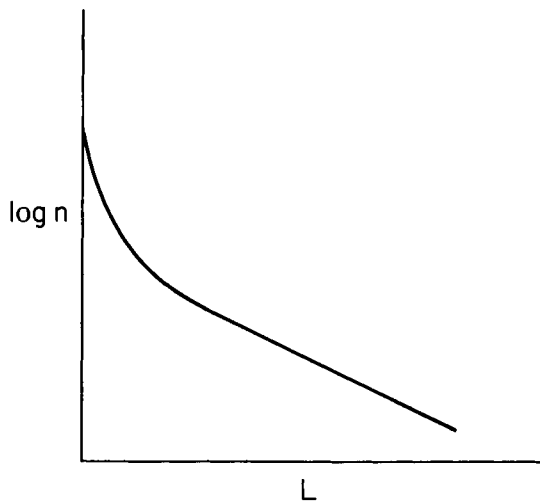


Fig. 6.6-3 Preferential removal of small crystals.

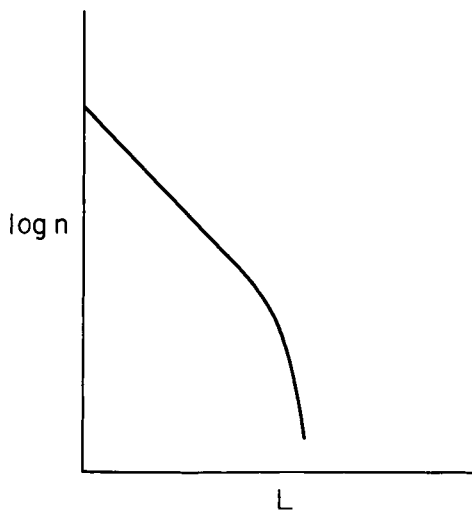


Fig. 6.6-4 Preferential removal of large crystals.

point, classification can also result. Depending on the conditions, small or large crystals can be removed preferentially. Figure 6.6-5 shows the CSD that results when the nonisokinetic nature of withdrawal inhibits the removal of large crystals.

One of the most effective designs to assure uniform distribution of both phases is the draft-tube design shown in Chapter 4. Flow can be in either

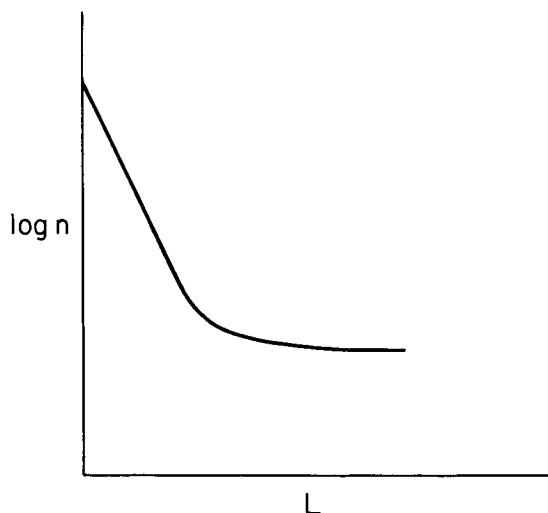


Fig. 6.6-5 CSD when nonisokinetic withdrawal causes retention of large crystals.

up the draft tube or down the draft tube, but for small nonevaporative crystallizers flow down the draft tube minimizes power requirements for total crystal suspension. This design is, however, subject to the possible production of anomalous CSD as well. Experiments conducted by Randolph *et al.* [3] have shown that classification is possible if the discharge is improperly located. They conducted experiments with a small draft tube crystallizer with the discharge positioned as shown in Figs. 6.6-6 and 6.6-7. The discharge could be achieved in the upward or downward position. It was found that both positions produced anomalous CSD.

In this system the large crystals concentrated on the outer wall of the crystallizer because of the circulation velocity, and when the discharge tube took in solution from below (isokinetically) it removed large crystals preferentially, and when it took in solution from above (nonisokinetically) large crystals were retained in the crystallizer. The effects here reflected the effects of both internal classification and nonisokinetic withdrawal.

The effects discussed here refer only to the steady-state behavior. In most of the cases mentioned, the classification product removal that results from these conditions also results in substantial instabilities in both CSD and magma density. These effects will be addressed in Chapter 8.

One more word of caution is in order. The above forms of CSD can be caused by other conditions as well. Size-dependent growth and growth dispersion can result in CSDs similar to those in Figs. 6.6-3 and 6.6-5, while crystal attrition can result in CSDs similar to those in Fig. 6.6-4. Care must be taken in interpreting data in light of these factors.

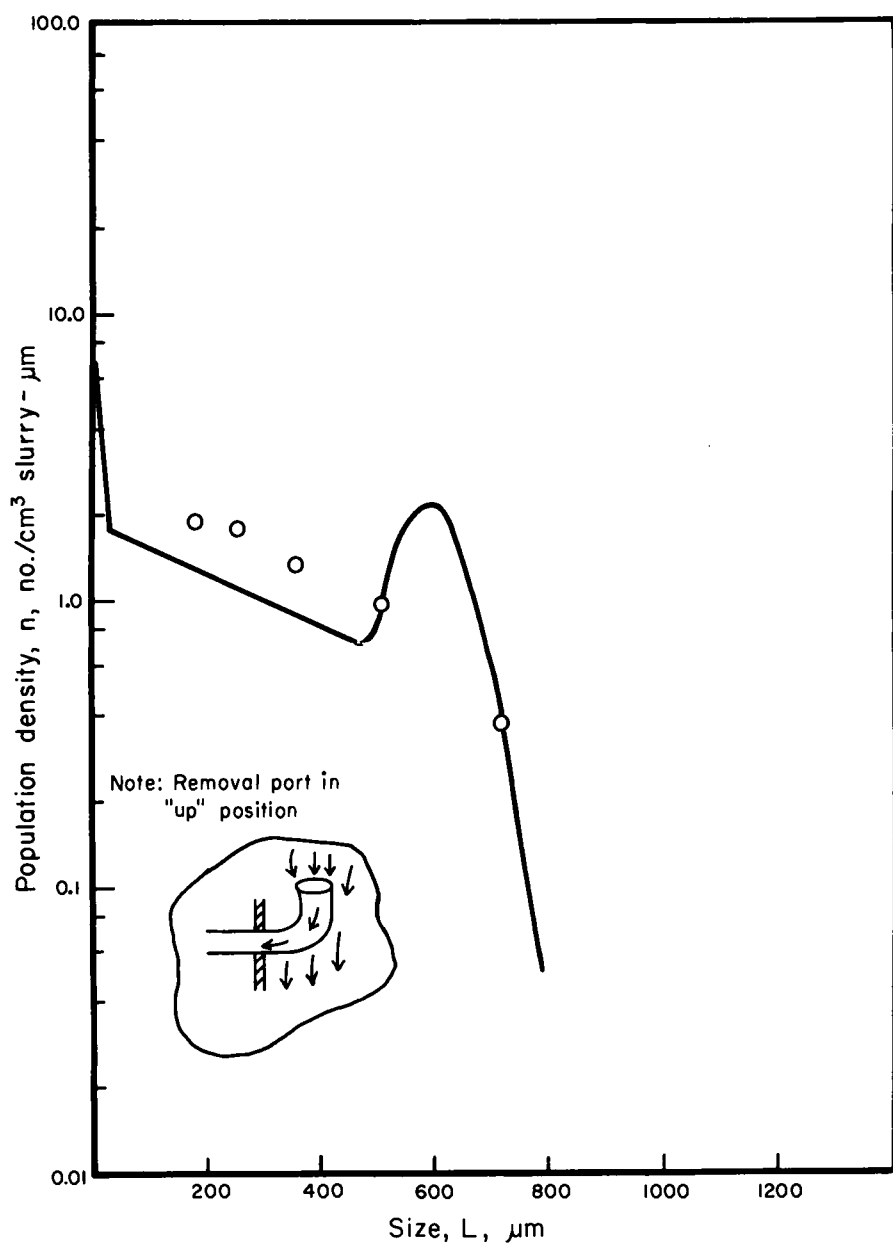


Fig. 6.6-6 CSD from a crystallizer with intake from above. (After Randolph *et al.* [3].)

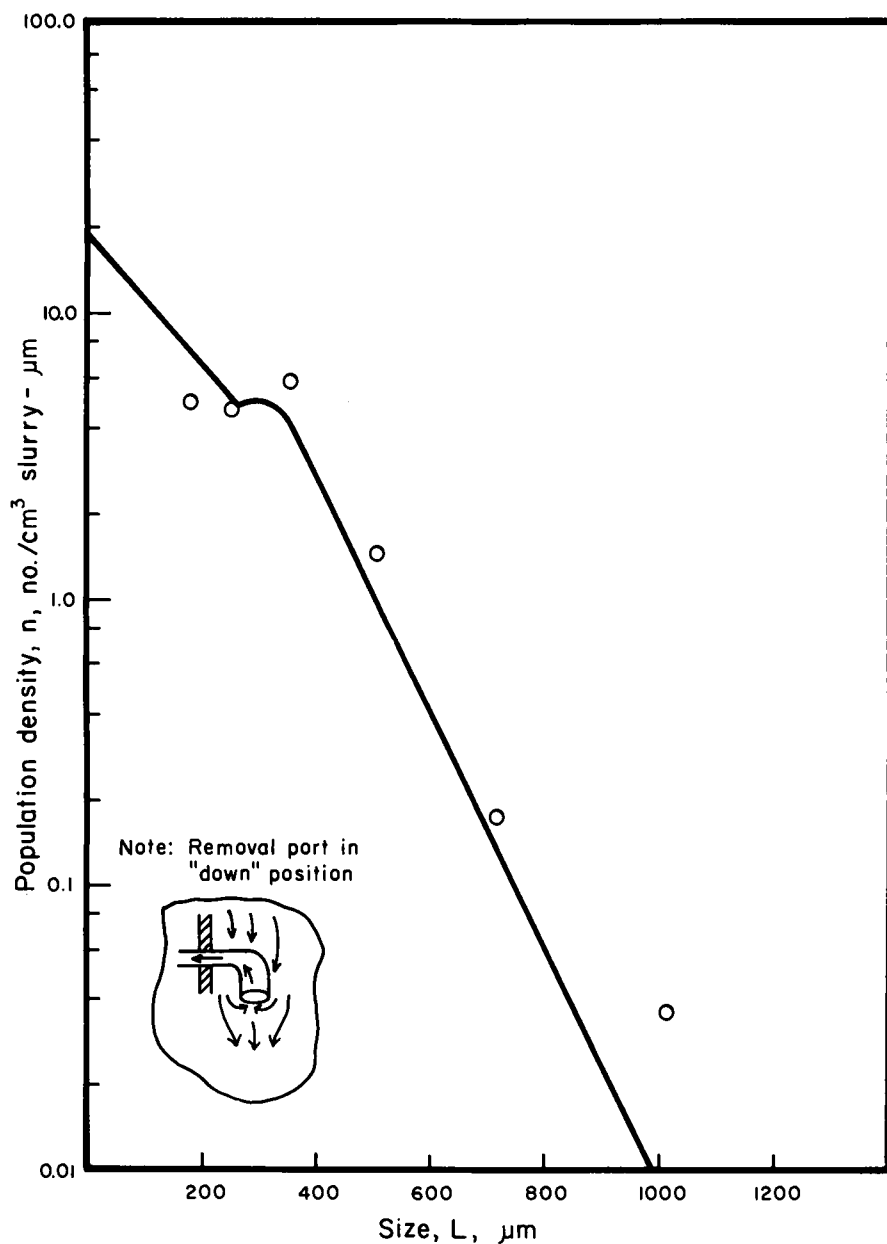


Fig. 6.6-7 CSD from crystallizer with intake from below. (After Randolph *et al.* [3].)

6.7 Growth Dispersion and Size-Dependent Growth

Growth dispersion and size-dependent growth have apparent identical effects on the CSD obtained from continuous crystallizers. The effect usually appears as an excessive population of both fines and large crystals. However, what appears to be size-dependent growth is usually only the consequence of growth dispersion. True size-dependent growth can only be modeled empirically as was shown in Chapter 4. We will limit our discussion here to the consequences of growth dispersion in continuous crystallizers. In the following example we will assume intrinsic growth dispersion (IGD) to demonstrate how growth dispersion affects the various properties of the CSD. The particular mathematical growth dispersion distribution function used is one that can be handled analytically; however, other functions can be used but can be handled only using numerical techniques.

EXAMPLE 6.7-1 (INVERSE GAMMA FUNCTION)

The analyses of Janse and de Jong [4] and Larson *et al.* [5] show how a growth distribution represented by an inverse gamma function will affect the CSD obtained from an MSMR crystallizer.

The requisite distribution function is

$$f_G(g) = (a^{k/1}/\Gamma(k-1))g^{-k}\exp(-a/g) \quad a > 0, \quad k > 3 \quad (6.7-1)$$

$$g_G(g) dg = 1, \quad f_G(0) = 0$$

Letting $k = 10$, the mean growth rate is

$$\bar{g} = \frac{m_{G1}}{m_{G0}} = \frac{\int_0^\infty g f_G dg}{\int_0^\infty f_G dg} = \frac{a}{k-2} = \frac{a}{8}$$

The standard deviation is

$$\begin{aligned} \sigma &= (m_{G2} - m_{G1}^2)^{1/2} = \frac{a}{k-2} \left(\frac{1}{\sqrt{k-3}} \right) \\ &= \frac{\bar{g}}{\sqrt{k-3}} = \frac{\bar{g}}{\sqrt{7}} \end{aligned}$$

and the coefficient of variation of the growth distribution is

$$\text{c.v.}_G = \sqrt{1/(k-3)} = \sqrt{1/7} = 0.38$$

The j th moment of the growth distribution is

$$\begin{aligned} m_{Gj} &= \frac{a^j \Gamma(k-1-j)}{\Gamma(k-1)} \\ &= (8\bar{g})^j \frac{\Gamma(9-j)}{\Gamma(9)} \end{aligned}$$

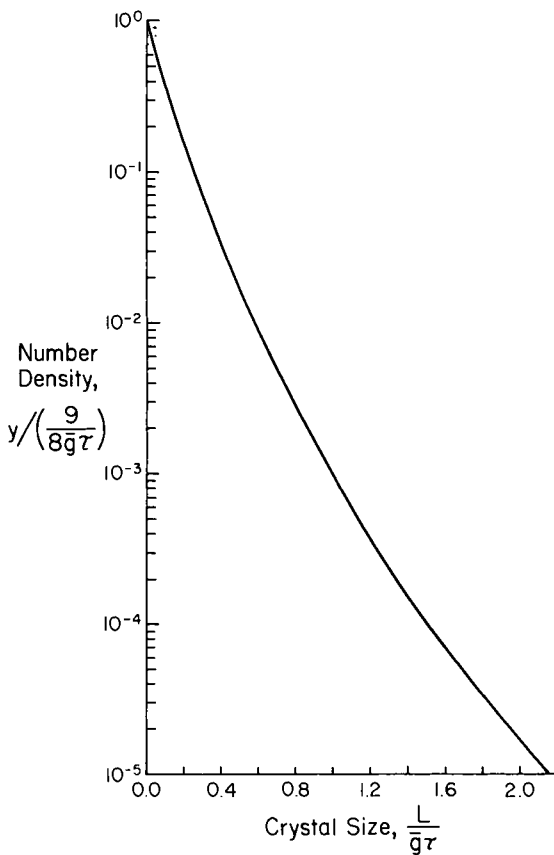


Fig. 6.7-1 CSD from inverse gamma-function growth dispersion.

and the j th moment of the size distribution is

$$\begin{aligned}
 m_{Lj} &= j! \tau^j m_{Gj} \\
 &= j! (8\bar{g})^j [\Gamma(9-j)], \quad j < (k-1)
 \end{aligned}$$

The dimensionless CSD is given by

$$\begin{aligned}
 y_L(L) &= \int_0^\infty \frac{1}{g\tau} \exp\left(-\frac{L}{g\tau}\right) \frac{(8\bar{g})^9}{\Gamma(9)} g^{-10} \exp\left(-\frac{8\bar{g}}{g}\right) dg \\
 &= 9(8g\tau)^9 / (L + 8\bar{g}\tau)^{10}
 \end{aligned}$$

This distribution is plotted in Fig. 6.7-1. The growth distribution function is similar in shape to the corresponding function plot shown in Chapter 4.

This is a normalized function, and its integral is

$$\int_0^\infty \frac{9(8\bar{g}\tau)^4}{(L + 8\bar{g}\tau)} dL = 1$$

$$y_L(0) = \frac{9}{8\bar{g}\tau} \quad \bar{L}_D = 3\bar{g}\tau \frac{k-2}{k-4} = 4\bar{g}\tau$$

$$\text{c.v.}_M = \frac{1}{2}\sqrt{(k-1)/(k-6)} = 0.75 \quad \blacklozenge$$

In the example the mass-based coefficient of variation is greater than that for an MSMR crystallization with no growth dispersion. However, when the growth coefficient of variation c.v._G is 0.25 or less, the CSD from an MSMR crystallization is barely distinguishable from that without growth dispersion. In continuous crystallizations the retention-time parameter is far more important in determining the nature of the CSD than are small growth-dispersion effects. In batch crystallization, however, the effect of growth dispersion is of considerable importance.

6.8 Batch-Crystallization CSD

In Chapter 4 we introduced the basic model from CSD from a batch crystallizer. The formulation is trivial if no nucleation occurs after initial seeding or initial nucleation and if the crystals do not exhibit growth dispersion. However, if nucleation continues throughout the batch run and/or if the system exhibits growth dispersion, the effect on CSD is far more pronounced than on the CSD from a continuous crystallizer. In a batch crystallizer all nuclei remain in the system until the batch run is terminated. The manner and magnitude of the initial nucleation event directly affect the product crystal size distribution. As a consequence, the most useful application of the population balance is in analyses to determine the process conditions and strategies that minimize the effects of nucleation and growth dispersion on crystal size distribution. One of the most important objectives of a batch-crystallization process is to produce a product with a narrow size distribution. This requires the suppression of nucleation after initial seeding or initial nucleation, as well as the reduction of the effects of growth dispersion. Another objective is to minimize fouling on the surfaces of the equipment. Suppression of nucleation and fouling requires that supersaturation be low during the initial period of batch, a situation difficult to achieve.

We first consider the effects of growth dispersion. Consider a batch process that is initially seeded with monodisperse crystals of very small relative size. Let these seeds have a growth dispersion function $f_G = g \exp(-ag)$ where f_G is the dimensionless growth distribution previously

discussed. It can be shown that if no nucleation takes place the final CSD at bath time t is

$$y_L = \frac{1}{t} f_G \left(\frac{L}{t} \right) = \frac{L}{t^2} \exp \left(- \frac{aL}{t} \right) \quad (6.8-1)$$

The size distribution will have the same characteristics as the growth distribution and will continually widen as the batch time increases. The only way the batch CSD can be narrowed is to change f_G . Because growth dispersion is not well understood, it is not always possible to change f_G . However, it might be possible to change the source of seeds. For example, seeds grown homogeneously from solution may have a different growth dispersion characteristic than those produced by milling large crystals. Soluble additives have also been used to affect the growth dispersion characteristics of some systems.

Significant improvement in CSD can however be achieved using strategies designed to control nucleation. Most systems exhibit a metastable supersaturation region where crystal growth continues but the supersaturation is too low for nucleation to take place. Thus if a system can be maintained at a constant supersaturation within the metastable region after initial seeding, then only growth on the seeds will occur. Moreover, under these low supersaturations, fouling is also reduced. The following example shows how the population balance and the mass balance can be used to determine the evaporation strategy necessary to maintain a constant supersaturation (thus a constant growth rate) throughout a batch run. This example follows the analysis of Mullin and Nyvlt [6] and Larson and Garside [7].

EXAMPLE 6.8-1

Determine the evaporation program for an evaporative seeded batch crystallizer operating at a constant temperature and pressure, which will maintain a constant supersaturation and thus a constant growth rate. The growth rate chosen is to be at a level such that nucleation will not occur.

For no nucleation $dN/dt = 0$, and thus the combination of Eqs. (4.6-5) and (4.6-6) gives

$$C \frac{d^3 V}{dt^3} = 6k_v \rho G^3 \tilde{N} = 0 \quad (6.8-2)$$

with initial conditions

$$\begin{aligned} V_{(0)} &= V_0 \\ \dot{V}_{(0)} &= -3k_v G \rho (L_s \tilde{N}) / C \\ \ddot{V}_{(0)} &= -6k_v G^2 \rho (L_s \tilde{N}) / C \end{aligned} \quad (6.8-3)$$

where L_s is the seed size and \tilde{N} is the number of seeds introduced at the start of the run. The solution to Eq. (6.8-2) with initial conditions of Eqs. (6.8-3) is

$$C(V_0 - V) = k_{v\rho}G^3\tilde{N}t^3 + 3k_{v\rho}G^2L_s\tilde{N}_1t^2 + 3k_{v\rho}GL_s^2\tilde{N}_1t \quad (6.8-4)$$

Letting

$$\phi = \frac{VC}{3k_{v\rho}L_s^2\tilde{N}} = \frac{VC}{3\tilde{M}_s} \quad \text{and} \quad Z = \frac{Gt}{L_2}$$

gives

$$\phi_0 - \phi = Z^3/3 + Z^2 + Z \quad (6.8-5)$$

or

$$-d\phi/dZ = Z^2 + 2Z + 1 \quad (6.8-6)$$

Equation (6.8-6) gives the net rate at which solvent must be evaporated to produce the growth rate G without nucleation. Larson and Garside [7] solved the equation for a system producing 1000 kg crystals per batch from 1 kg of 10^{-4} -m seeds having a volume shape factor of 1. The crystal density was 1.5×10^3 kg/m³ and the final desired product size was 10^{-3} m. The saturation concentration was 200 kg solute/m³ solvent. The evaporation rate plotted as a function of time is shown in Fig. 6.8-1. The rate must be low initially because there is very little crystal surface for growth, as the suspension density increases the evaporative rate, and thus the mass production rate increases.

The same equation is obtained for a cooling crystallizer, except that the dimensionless variables are defined differently. Assuming the solubility is linear with temperature $C_s = a + bT$, then $dC_s/dt = b dT/dt$. Using the

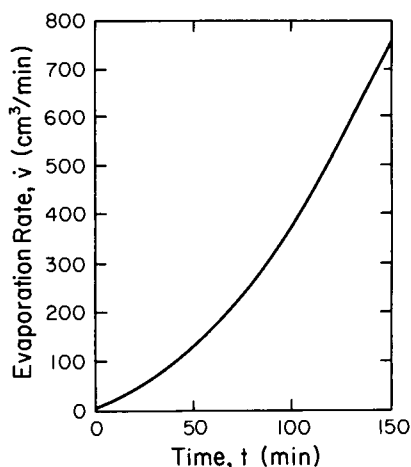


Fig. 6.8-1 Evaporation program to maintain a constant growth rate.

mass balance and solving for ϕ' ,

$$\phi' = bVT/3\tilde{M}_s$$

and $d\phi'/dZ$ is the dimensionless cooling rate,

$$d\phi'/dZ = Z^2 + 2Z + 1 \quad \blacklozenge \quad (6.8-7)$$

Jones and Mullin [8] have shown that cooling programs determined by the above analysis markedly narrow the CSD obtained from batch potassium sulfate crystallization.

In actual operation, nucleation cannot be totally suppressed. Jones *et al.* [9] have shown that the incorporation of fines destruction in a batch system can markedly offset the effects of nucleation on batch CSD. Figure 6.8-2 shows the cumulative mass oversize for batch crystallization of K_2SO_4

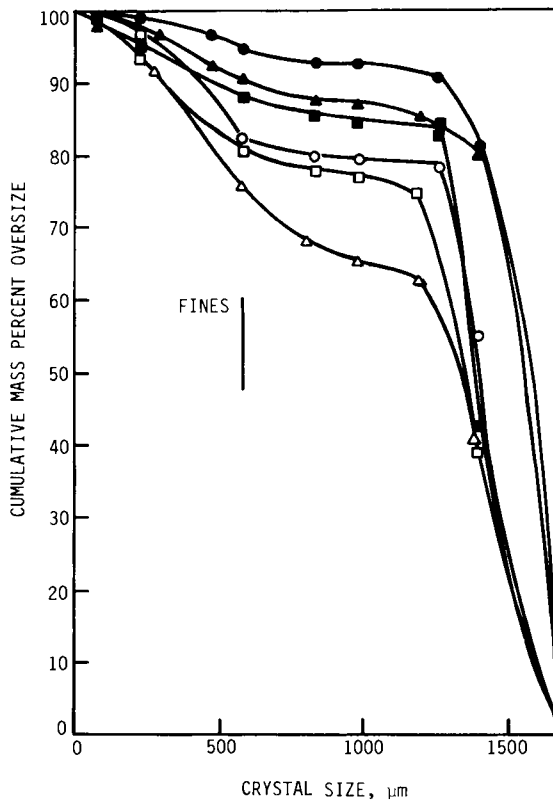


Fig. 6.8-2 Cumulative mass oversize in batch crystallization with and without fines dissolving. (After Jones *et al.* [10].) (a) with fines dissolving ● 500 rpm, ▲ 550 rpm, ■ 600 rpm, (b) without fines dissolving ○ 500 rpm, △ 550 rpm, □ 600 rpm.

with and without fines dissolving. With fines dissolving, 90% of the mass was 500 μm or greater. Without fines dissolving, only 75% of the mass had size greater than 500 μm . In the following examples we show how a particular fines-removal strategy will operate to increase the size and narrow the size distribution of a batch product.

EXAMPLE 6.8-2

Compare the CSD obtained from an evaporative batch system that exhibits nucleation with the CSD from a nucleation batch system that utilizes fines destruction.

If primary nucleation occurs, then assuming linear growth kinetics,

$$B^0 = dN/dt = k_N G^i \quad (6.8-8)$$

Incorporating Eq. (6.8-8) into the set of equations used in Example 6.8-1 gives

$$C \frac{d^4 V}{dt^4} + 6k_v \rho k_N G^{i+3} = 0 \quad (6.8-9)$$

with initial conditions

$$\begin{aligned} V_{(0)} &= V_0, & V_{(0)} &= -3k_v \rho (L_s^2 \tilde{N}) G \\ V_{(0)} &= -6k_v \rho (L_s \tilde{N}) G^2, & V_{(0)} &= -6k_v \rho \tilde{N} G^3 \end{aligned} \quad (6.8-10)$$

Integrating gives

$$\frac{V_0 - V}{k_v \rho} = \frac{k_N G^{i+3} t^4}{4} + \tilde{N} G^3 t^3 + 3L_s \tilde{N} G^2 t^2 + 3L_s^2 \tilde{N} G t \quad (6.8-11)$$

Equation (6.8-11) determines the evaporative program to produce a constant growth and nucleation rate (assuming primary nucleation).¹ To examine the effect of fines dissolving on CSD, it is necessary to formulate the second and third moments of the distribution, the ratio of which is the mean size $L_{3,2}$.

The second moment (the suspension area) is the solution of the set $d\tilde{N}/dt = k_N G^i$, $dL/dt = \tilde{N} G$, and $dA/dt = 2k_a L G$, which gives

$$\frac{\tilde{A}}{k_a} = \frac{k_N G^{i+3} t^3}{3} + \tilde{N} (G^2 t^2 + 2L_s G t = L_s^2) \quad (6.8-12)$$

The third moment (the volume of crystals in suspension) is

$$\frac{\tilde{V}}{k_v} = \frac{k_N G^{i+3} t^4}{4} + \tilde{N} (G^3 t^3 + 3L_s G^2 t^2 + 3L_s^2 G t + L_s^3) \quad (6.8-13)$$

¹ If secondary nucleation is assumed, the solution must be done numerically. It is a more likely situation and would result in increased nucleation as the suspension density increased.

and in dimensionless form

$$m_2 = \frac{\tilde{A}}{k_a(Gt)^2} = \frac{k_N G^i t}{3} + \tilde{N}(1 + 2x + x^2) \quad (6.8-14)$$

$$m_3 = \frac{\tilde{V}}{k_v(Gt)^3} = \frac{k_N G^i t}{4} + \tilde{N}(1 + 3x + 3x^2 + x^3) \quad (6.8-15)$$

where the first term on the right represents the contribution of the nuclei and N represents the number of seed initially introduced. The term x is the dimensionless size L_s/Gt when t is the batch time.

$$m_3/m_2 = \bar{X}_{3,2}$$

The mean size based on area is

$$L_{3,2} = (m_3/m_2)Gt = \bar{X}_{3,2}Gt$$

Let $kG^i t = \tilde{N}_N$, the total number of nuclei produced during a batch run. Then for $N_N \gg \tilde{N}$ (no seeding),

$$\frac{m_3}{m_2} = \frac{1/4}{1/3} = 0.75, \quad \bar{L}_{3,2} = 0.75Gt$$

For $\tilde{N} \gg N_N$ (no nucleation) and $Gt = 10L_s$,

$$\frac{m_3}{m_2} = \frac{1.33}{1.21} = 1.10, \quad \bar{L}_{3,2} = 1.10Gt$$

Compare CSD with and without fines dissolving for $\tilde{N}_N/\tilde{N} = 1000$ with a fines destruction system that dissolves 99% of the nuclei produced.

Without fines dissolving,

$$\frac{m_3}{m_2} = \frac{1000/4 + 1.33}{1000/3 + 1.21} = 0.752, \quad L_{3,2} = 0.752Gt$$

with fines dissolving for $\tilde{N}_N(\text{net})/\tilde{N} = 10$, then

$$\frac{m_3}{m_2} = \frac{10/4 + 1.33}{10/3 + 1.21} = 0.844 \quad L_{3,2} = 0.844Gt$$

Such a fines removal system would require a circulation rate through a fines trap such that the volumetric velocity would be $V(100)/t$ where V is the crystallizer volume.

6.9 Summary

The analyses of crystallization strategies and crystallizer configurations using the population balance demonstrate that some strategies and configurations have very little effect on CSD while others have pronounced effects. While changes in retention time in MSMR crystallizers have an effect on CSD and experiments utilizing this fact can be used to determine nucleation and growth models, changes in retention time are usually not effective enough to markedly change crystal size. Because secondary nucleation is almost always a factor in new crystal formation, increases in suspension density are not especially effective in changing CSD. In some instances increased suspension density may decrease size. Continuous crystallizers without classification produce products with a c.v. of 50%, a quite wide distribution. Growth dispersion and size-dependent growth tend to widen the CSD in continuous systems. Inadequate mixing and nonisokinetic product withdrawal can have a variety of effects on the CSD. One of the most effective ways to alter CSD is with internal fines separation and destruction coupled with classified withdrawal. Strategies and configurations for such systems will be discussed in the following chapter.

Control of nucleation is one of the most important factors in batch crystallization. A population-balance analysis can be used to derive cooling or evaporation programs to minimize initial nucleation as well as nucleation throughout batch runs. Internal fines separation and destruction can also be used to alter CSD from batch systems. Growth dispersion is, however, a continuing problem in batch crystallization, and a great deal more needs to be known about the phenomenon before adequate control of batch-produced CSD.

Nomenclature

a	Constant in growth dispersion function	G	Growth rate
B^0	Nucleation rate	k	Constant
C	Solute concentration	k_a	Area shape factor
$c.v._G$	Coefficient of variation, growth dispersion	k_N	Nucleation rate constant
$c.v._L$	Coefficient of variation, size based on length	k_v	Volume shape factor
$c.v._m$	Coefficient of variation, size based on mass	L	Crystal size
f_G	Growth dispersion function	L_D	Dominant crystal size
g	Dispersion growth rate	L_F	Fines cut size
\bar{g}	Mean growth rate	L_s	Seed size
		m_G	Moment of growth dispersion
		m_L	Moment of size distribution
		M_T	Total mass
		M_s	Mass of seeds

n^0	Nuclei population density
\tilde{N}	Number of crystals in crystallizer
Q_o	Volumetric overflow rate
Q_u	Volumetric underflow rate
s	Supersaturation
t	Time
T	Temperature
V	Crystallizer volume, or solvent volume
V	Crystal suspension volume

GREEK LETTERS

τ	Retention time
τ_F	Fines retention time
τ_p	Product retention time
ω	Stirrer speed

References

1. Larson, M. A., and Wolff, P. R. (1971). *Chem. Eng. Progr. Symp. Ser.* **110**(67), 97.
2. Jazaszek, P., and Larson, M. A. (1977). *AIChE J.* **23**, 460–468.
3. Randolph, A. D., Beckman, J. R., and Kraljevich, Z. I. (1977). *AIChE J.* **23**(4), 500.
4. Janse, A. H., and deJong, E. J. (1976). In “Industrial Crystallization” (J. W. Mullin, ed.), p. 145. Plenum Press, New York.
5. Larson, M. A., White, E. T., Ramanaraganon, K. A., and Berglund, K. A. (1985). *AIChE J.* **31**(1), 90.
6. Mullin, J. W., and Nyvlt, J. (1971). *J. Chem. Eng. Sci.* **26**, 369.
7. Larson, M. A., and Garside, J. (1973). *Chem. Eng.* **June**, 318.
8. Jones, A. G., and Mullin, J. W. (1974). *Chem. Eng. Sci.* **29**, 105.
9. Jones, A. G., Chianese, A., and Mullin, J. W. (1984). In “Industrial Crystallization 84” (S. J. Jancic and J. W. Mullin, eds.), p. 191. Elsevier, Amsterdam.
10. Larson, M. P., Timm, D. C., and Wolff, P. R. (1968). *AIChE J.* **14**, 448.

REACTION ENGINEERING OF CSD

The process reaction engineering of CSD is a widely practiced art and forms a well-developed subset of reaction engineering topics. Process manipulation to alter the CSD can be done for a given crystallizer configuration by changing the external inputs to the system, such as feed rate and composition, temperature, boil-up rate, or agitation. In addition, existing internal zones of classification in the crystallizer magma can be utilized or can be created to effect a size-dependent residence-time distribution (RTD) of the crystal particles. Such size-dependent removal rates of crystals can have a dramatic effect in shaping the CSD, both within the suspension and in the product withdrawn. Both external inputs and size-dependent RTD interact with the system kinetics to determine the level of crystallizer nucleation and growth rates. This interaction of process configuration, inputs, and system kinetics results in the complex flow of information depicted in the information flow diagram of Fig. 1.2-1 in Chapter 1. Often many process inputs are fixed for a given process, while changes in crystallizer configuration (leading to size-dependent RTD) would require changes in process equipment. The art of CSD design, simulation, and manipulation lies in understanding and utilizing the interaction of these factors.

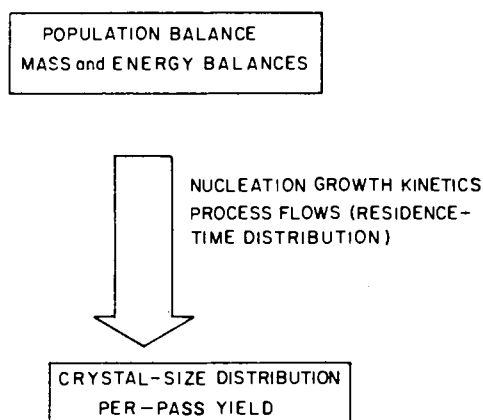


Fig. 7.1-1 General algorithm for calculation of crystal-size distribution.

7.1 Reaction Engineering Models for the CSD

A general CSD algorithm (Fig. 7.1-1) for a backmixed stage of volume V can be developed that can account for completely arbitrary residence-time distributions. Consider the most general case of a back-mixed, steady-state crystal magma (Fig. 7.1-2) having j slurry inputs of flow rate $Q_{i,j}$ with population density $n_{i,j}$ and k slurry outputs with flow $Q_{o,k}$ and population density $n_{o,k}$. The steady-state macroscopic population balance for this case, assuming negligible crystal fracture, reduces to

$$V \frac{d}{dL}(Gn) = \sum_j Q_{i,j} n_{i,j} - \sum_k Q_{o,k} n_{o,k} \quad (7.1-1)$$

Equation (7.1-1) can be reduced to a nonhomogeneous, variable-coefficient equation of fixed form whose solution generates CSD for completely

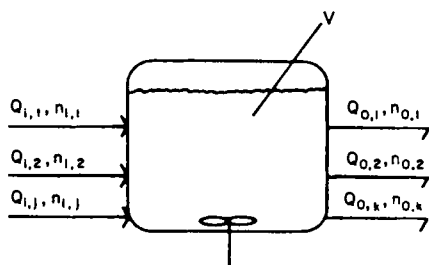


Fig. 7.1-2 Generalized model of a mixed-magma crystallizer with arbitrary process

arbitrary process configurations, depending only upon the form of the nonhomogeneous, non-constant-coefficient terms. These terms are composed after consideration of the particular process configuration to be simulated, and input into the population balance used as a general CSD algorithm. Development of this idea proceeds as follows. Choose a reference flow Q_B . It is normally chosen as net liquor flow. Define a bucket-mixing average for inlet slurries as

$$Q_i n_i = \sum_j Q_{i,j} n_{i,j}, \quad \text{where} \quad Q_i = \sum_j Q_{i,j} \quad (7.1-2)$$

Further, define each outlet stream as being proportional to the distribution n . Thus,

$$\sum_k n_{o,k} Q_{o,k} \equiv \sum_k Q_{o,k}(L) n \quad (7.1-3)$$

where $\sum_k Q_{o,k}(L)$ is the equivalent mixed-suspension removal rate at size L . Equation (7.1-3) is a modeling simplification that has a profound effect in reducing the complexity of the set of equations that satisfactorily describe the system. Physically this modeling simplification says that particle classification occurs as a noncapacitive size split at the point of withdrawal, thus preserving the mixed-suspension (MS) part of the MSMR concept. As internal flows are often high compared to the net withdrawal of crystal product, this modeling simplification is often well justified. The mathematical implication of this assumption is that the process nonlinearities, which might have to be described by a linked set of ODEs for each significant subregion of the magma, can be described (for each overall volume V) by a single linear equation with nonconstant (size-dependent) coefficients.

Define total removal at size L as $\sum_k Q_{o,k}(L) = Q_o(L)$. Further, define a withdrawal function $C_w(L)$ as $C_w(L) = Q_o(L)/Q_B$. Thus, the total output term is given as

$$\sum_k Q_{o,k} n_{o,k} = Q_B C_w n \quad (7.1-4)$$

Substitution in the population balance gives

$$V \frac{d}{dL} (Gn) = Q_i n_i - Q_B C_w n \quad (7.1-5)$$

Assume that growth rate is some function of L . Define $g(L) = G(L)/G_0$, where G_0 is some reference growth rate, usually the average growth rate, in some sense, or the zero-sized particle growth rate. Making the substitution gives

$$G_0 V [d(gn)/dL] = Q_i n_i - Q_B C_w n \quad (7.1-6)$$

as the generalized population balance for the back-mixed volume V . Let $y = gn/n_0^0$, giving $n = yn_0^0/g$. Then

$$n_0^0 G_0 V (dy/dL) = Q_i n_i - (Q_B C_w n_0^0 y/g) \quad (7.1-7)$$

Let a dimensionless x be given as $x = LQ_B/VG_0$. Making this substitution gives

$$dy/dx = (Q_i n_i / n_0^0 Q_B) - [C_w(x)/g(x)]y \quad (7.1-8)$$

Further, let $Q_i/Q_B = \alpha$ and $y_i = g(0)n_i/n_0^0$. Then

$$dy/dx + [C_w(x)/g(x)]y = \alpha y_i(x)/g(0) \quad (7.1-9)$$

If $G_0 = G(0)$, then $g(0) = 1$ and a boundary condition for solution of this equation becomes $y(0) = 1$. Equation (7.1-9) is a dimensionless, variable-coefficient, nonhomogeneous differential equation that is constant in form and serves as a central algorithm for CSD computations; it is dependent in its solution on the form of the size-dependent inputs $g(x)$, $y_i(x)$, and $C_w(x)$.

The crystallizer is assumed to be at steady state and therefore at constant production rate, even if it does not represent 100% yield. This production will also be a function of how much mass is fed into the vessel as seed, if the crystallizer is seeded. Writing the production in terms of exit slurry flows gives

$$P = \sum_k Q_{o,k}^P M_{o,k} \quad (7.1-10)$$

where $Q_{o,k}^P$ is that outlet stream going to product and $M_{o,k}$ is the solids concentration in the stream. (Note: There is an essential difference between the cases of fines dissolution and split underflow/overflow discharge; not all of the withdrawn streams in the former case go to the product stream. Clearly, $\sum_k Q_{o,k}^P M_{o,k} \leq \sum_k Q_{o,k} M_{o,k}$.) Solids concentration is given in terms of population density as

$$M_T = \rho k_v \int_0^\infty n L^3 dL \quad (7.1-11)$$

Production is thus given in terms of population density and withdrawal flow to product as

$$P = \rho k_v \int_0^\infty Q_o^P(L) n L^3 dL \quad (7.1-12)$$

Defining $C_p = Q_o^P(L)/Q_B$, then

$$P = Q_B \rho k_v \int_0^\infty C_p n L^3 dL \quad (7.1-13)$$

where clearly $C_w \geq C_p$. Equations (7.1-9) and (7.1-13) are solved, together

with appropriate nucleation–growth rate kinetics, to define population densities in the system.

Finally, CSDs on a weight basis, in the suspension and product, are calculated from the population distribution as

$$W(L) = \int_0^L nL^3 dL / \int_0^\infty nL^3 dL \quad (7.1-14)$$

and

$$W_p(L) = \int_0^L C_p(L)nL^3 dL / \int_0^\infty C_p(L)nL^3 dL \quad (7.1-15)$$

EXAMPLE 7.1-1 USE OF GENERALIZED BACK-MIXED MODEL

Briefly explain how this generalized CSD algorithm would be used to simulate the cases of staging (or seeding), size-dependent growth rate, classified product removal, and fines dissolving.

A. Staging (Seeding)

Staging is a special case of seeding wherein all but the first vessel are seeded by the discharge from previous stages. This is handled, say for the k th stage, by allowing

$$\alpha y_i = (Q_B C_w n)_{k-1} / (Q_B n_0^0)_k \quad (7.1-16)$$

which can be programmed in a sequence of applications of the central back-mixed algorithm. If seeding is achieved through addition of a truly external source, say from another system, then the function αy_i can be constructed from the cumulative CSD, solids concentration, and source of the external slurry stream from the preceding development and the definition

$$n_i = (M_{Ti})(dW_i/dL)/\rho k_v L^3 \quad (7.1-17)$$

B. Size-Dependent Growth Rate

If the coefficient $g(x)$ in Eq. (7.1-9) varies with x , this simulates size-dependent growth rate. The most convenient normalization of the size-dependent growth rate would be division by the nucleus growth rate $G(0)$, thus preserving the unity boundary condition for Eq. (7.1-9). The function $g(x) = 1$ for all x is tantamount to McCabe's ΔL law. If the function $g(x)$ increases with x , the distribution is wider than the MSMPR case; if $g(x)$ decreases with x , a narrower distribution is produced. Changes in growth rate with size are similar, but not identical, to changes in mean retention probability as a function of size, given as $\tau(x) = V/Q_o(x)$ and represented by the $C_w(x)$ function.

C. Classified Product Removal

In this mode of operation, separations of residence-time probability as a function of size, $C_p(x) = V/Q_o(x)$, is accomplished by size-segregation devices, such as wet screens, hydroclones, and eleutriators. For this case, the classification occurs in the product stream and $Q_o(x) = Q_o^p(x)$. Such classification is handled by the $C_w(x) = C_p(x)$ functions, which physically can be interpreted as the ratio of actual removal at size L to the removal rate expected with mixed withdrawal.

A highly idealized representation of product classification useful for simulation of wet screens and hydroclones is

$$Q_o(L) = Q_o \quad \text{for } L < L_p$$

$$Q_o(L) = zQ_o \quad \text{for } L > L_p$$

or equivalently,

$$C_w = C_p = 1 \quad \text{for } x < x_p$$

$$C_w = C_p = z \quad \text{for } x > x_p$$

where z is the feed-to-product ratio of the classifying device, L_p is the size cut point, and Q_o is the mother-liquor flow rate carried with the product.

D. Fines Removal

The effect of fines removal is simulated by the function $C_w(x)$. In this case, fine particles less than some small size, say L_F , are removed at an accelerated rate. Thus, to simulate this process modification, let

$$C_w > 1 \quad \text{for } x < x_F$$

$$C_w = 1 \quad \text{for } x > x_F$$

For this case, $C_p = 1$ for all sizes as the fines are dissolved, not sent to product. (Note: As far as the distribution that develops in the mixed suspension is concerned, it matters little whether the fines are dissolved and recycled, sent to product, or dumped on the floor, although growth rate will be higher in the former case.) ♦

All of the above four process configurations and any combination of them can be rigorously simulated by empirical specification of the four functions of size, namely, $y_i(x)$, $g(x)$, $C_p(x)$, and $C_w(x)$, together with numerical solution of Eqs. (7.1-9) and (7.1-13) and with an empirical expression for secondary nucleation kinetics. CSD expressed on a weight basis is then calculated, in suspension and product, from Eqs. (7.1-14) and (7.1-15).

7.2 Accelerated Removal of Fine Crystals

7.2.1 Growth-Type Crystallizer

In commercial crystallizer designs, residence times of mother liquor and solids are often separated to provide better yield and size improvement. In such a design, the so-called “growth-type” crystallizer, a clear-liquor advance is provided from a quiescent settling zone (external or internal to the main crystallizer body), allowing removal of a heavier slurry at a lower rate in a mixed-suspension underflow stream. Such operation results in higher yields from class I systems and, depending upon the form of secondary nucleation kinetics, can improve or degenerate particle size.

Such a process configuration can easily be analyzed if the idealization that particles are completely removed from the clarified stream is made, as the MSMPR form of the distribution remains unaltered. If the carryover size of particles in the clarified overflow stream is known, the process can be analyzed by the more rigorous treatment described in Section 7.2-2. In practice, it is difficult or impossible to remove a “clear” liquor overflow without removing fines, typically up to $\sim 100 \mu\text{m}$ in brine-like mother liquors. Thus this configuration becomes essentially a low-capacity fines removal system operating with a high slurry density. Some of the particle-size increases observed with this configuration are undoubtedly due to fines removal. Removal of fines with the clear-liquor overflow also clouds interpretation of CSD data and gives erroneous (low) estimates of nucleation rate when CSD data are interpreted with MSMPR theory. Nevertheless, consider the idealized case where a perfectly clear mother liquor Q_o is assumed to be removed in the settled overflow stream. Mixed discharge occurs in the underflow stream Q_u , and thus CSD is given by the MSMPR relation as

$$n = n^0 \exp(-LQ_u/GV) \quad (7.2-1)$$

Further, assume nucleation–growth rate kinetics are given as

$$n^0 = k_N G^{i-1} \quad (7.2-2)$$

which at this point neglects any explicit CSD dependence of secondary nucleation. This is a very restrictive assumption and will be relaxed later. Assuming a high yield (class II system), production rate is independent of the amount of clear liquor overflow. Thus, comparing crystallizers under the above assumptions with or without clear-liquor overflow, referred to with subscripts 2 and 1, respectively, gives

$$P_1 = P_2$$

or

$$Q_{u1} \rho k_v \int_0^\infty n_1 L^3 dL = Q_{u2} \rho k_v \int_0^\infty n_2 L^3 dL \quad (7.2-3)$$

Performing the indicated integrations and canceling yields

$$Q_{u1}(G_1\tau_1)^4 n_1^0 = Q_{u2}(G_2\tau_2)^4 n_2^0 \quad (7.2-4)$$

Substituting kinetics gives

$$Q_{u1}(G_1\tau_1)^4 G_1^{i-1} = Q_{u2}(G_2\tau_2)^4 G_2^{i-1} \quad (7.2-5)$$

Multiplying and dividing each side by $(V/Q_u)^{i-1}$ and recognizing that $3G\tau = L_d$ is the dominant size in the distribution gives

$$L_{d2}/L_{d1} = (Q_{u1}/Q_{u2})^{i/(i+3)} \quad (7.2-6)$$

Thus, as the flow ratio $Q_{u1}/Q_{u2} = (Q_u + Q_o)/Q_u > 1$, then, as Q_u is reduced due to clear-liquor overflow Q_o , some size improvement is expected in a growth-type crystallizer. However, if nucleation is a sensitive function of slurry density, then a decrease in particle size (sometimes a total degeneration) is observed. The assumption that secondary nucleation did not depend explicitly on CSD was of dubious validity. More reasonable secondary nucleation kinetics include the effects of solids concentration, as in the general power-model form

$$n^0 = k_N G^{i-1} M_T^j \quad (7.2-7)$$

Repeating the previous derivation with the above kinetics gives a more realistic appraisal of expected size improvement. Again, production rate, with or without clear-liquor overflow, is a constant. Thus,

$$Q_{u1} M_{T1} = Q_{u2} M_{T2} \quad (7.2-8)$$

But from the definition of solids concentration and power-law kinetics of the form of Eq. (7.2-7) one obtains

$$M_T^{1-j} = 6\rho k_v k_N (G\tau)^{i+3} Q_u^{i-1} / V^{i-1} \quad (7.2-9)$$

Or, substituting,

$$Q_{u1} [Q_{u1}^{i-1} (G_1\tau_1)^{i+3}]^{1/(1-j)} = Q_{u2} [Q_{u2}^{i-1} (G_2\tau_2)^{i+3}]^{1/(1-j)} \quad (7.2-10)$$

Again, recognizing that the dominant size is proportional to the growth rate times retention time gives

$$L_{d2}/L_{d1} = (Q_{u1}/Q_{u2})^{(i-j)/(i+3)} = \left(\frac{Q_u + Q_o}{Q_u} \right)^{(i-j)/(i+3)} \quad (7.2-11)$$

Note that when $j = 0$, Eq. (7.2-11) reduces to the special case of Eq. (7.2-6). When the nucleation power-law exponents on growth rate and solids concentration are equal, no size improvement occurs. When the exponent on solids concentration exceeds that on growth rate, particle size decreases. As an example, for typical values of the power-law exponents, say $i = 2$ and

$j = 1$, the size improvement ratio would vary with the one-fifth power of the total flow/underflow ratio, indicating relatively small size improvement.

In fact, growth-type crystallizers often improve particle size more effectively than suggested by Eq. (7.2-11). This is undoubtedly due to the significant decay of population that occurs due to the so-called “clear” overflow stream. Thus, in any real classification system, the overflow stream acts as a low-capacity fines-removal system, increasing particle size. Such a process could be rigorously analyzed by the methods of Section 7.1 as detailed in Section 7.2.2. Vessel fouling is nearly always reduced with clear-liquor overflow. Reduced fouling and increased per pass yield, rather than particle-size increases, are often the motivation for using this crystallizer configuration. In crystal systems with a high natural slurry density, the ratio Q_o/Q_u is limited by the increase in slurry density that results from this type of operation.

7.2.2 The Double Draw-Off (DDO) Crystallizer

Section 7.2.1 describes a crystallizer configuration wherein a “clear” liquor is advanced from a suspension, leaving a thickened mixed removal underflow. Application of MSMPR theory to this idealized configuration [Eq. (7.2-11)] indicates that particle size could increase or decrease, depending on the relative values of the nucleation kinetics parameters i and j . In fact, particle size typically increases (even when the measured kinetics indicate that $i < j$). This observation can be explained by considering the fines removal that occurs in the “clear” overflow stream.

The double draw-off (DDO) configuration utilizes this exponential decay of population in the overflow stream, thus operating with larger Q_o/Q_u ratios while removing a fines distribution ($L < L_F$) in the overflow stream. This fines distribution represents a significant fraction of the total production rate, typically 10–30%. The classified overflow and mixed underflow streams are then combined as the final product, resulting in an increase in particle size in the total mixed stream. Figure 7.2-1 shows a schematic flow diagram of this crystallizer configuration. The classified overflow stream is typically removed from a skirted baffle around the perimeter of the crystallizer vessel and/or through classifying hydrocyclones. The DDO configuration is particularly suited for class I systems having weak natural slurry density. It is possible to increase per pass yield, slurry density, and size while reducing vessel fouling. Randolph *et al.* [1] described an experimental study of the DDO configuration applied to the gypsum system. Significant size improvement and reduction in vessel fouling was observed. The DDO configuration can be readily modeled using the equations developed in Section 7.1. The modeling equations are set forth using the nomenclature

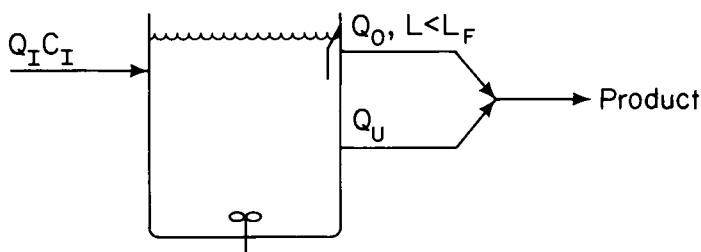


Fig. 7.2-1 Schematic flow diagram of the DDO crystallizer.

developed in the preceding section and as shown in Fig. 7.2-1. Thus:

1. Population balance

$$GV \frac{dn}{dL} + Q_u C_w n = 0 \quad (7.2-12)$$

where

$$C_w \equiv \frac{Q_o R}{Q_u} \begin{cases} (Q_o + Q_u)/Q_u; & L < L_F \\ Q_u/Q_u = 1; & L > L_F \end{cases}$$

2. Mass balance

$$Q_i C_i = (Q_o + Q_u) C + P \quad (7.2-13)$$

where

$$P = Q_u \rho k_v \int_0^\infty C_p n L^3 dL \quad \text{and} \quad C_p = C_w$$

3. Growth-rate kinetics

$$G = k_g (C - C_{\text{sat}})^a \quad (7.2-14)$$

4. Nucleation-rate kinetics

$$B^0 = k_N G^i M_T^j \quad (7.2-15)$$

Figure 7.2-2 shows a semilog population plot from a gypsum DDO crystallizer [1] using representative gypsum kinetic parameters (independently measured) to model the system.

7.2.3 Fines Destruction with Solute Recycle

Relative nucleation-growth rate kinetics of many crystal systems are such that under ordinary process conditions in an MSMPR crystallizer, the particles are of less than desired average size. Increases in the mean retention time, besides increasing capital investment and/or decreasing

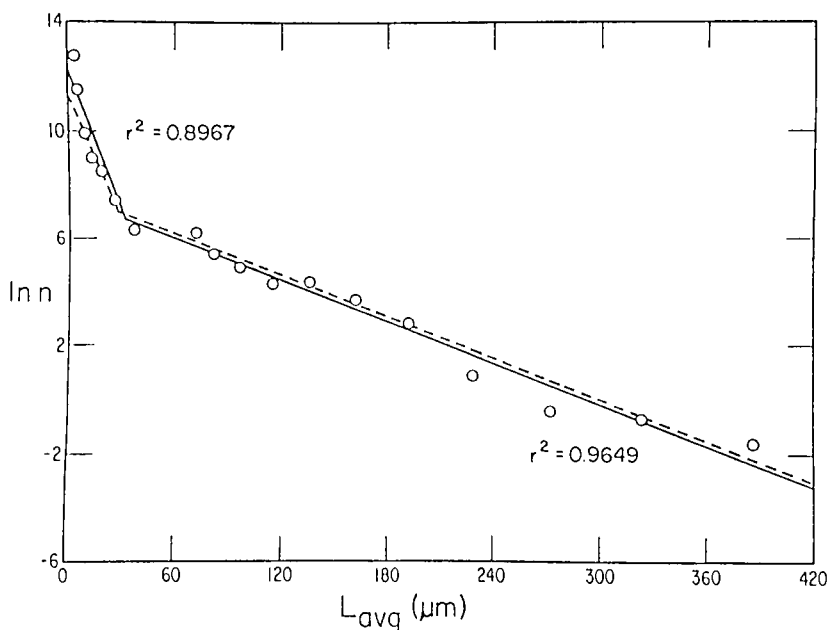


Fig. 7.2-2 Typical semilog plot of population density versus average size using Microtrac and sieve data for DDO configuration (run 27). (After Randolph *et al.* [1].) Open circle: data point, solid line: least square fit, dashed line: computer CSD.

production throughput, are not very effective in bringing about an increase in particle size. The predicted variation in dominant particle size derived analogously to Eq. (7.2-11), using the realistic secondary nucleation kinetics of Eq. (7.2-7), for a class II MSMPR crystallizer, is

$$L_{d2}/L_{d1} = (\tau_2/\tau_1)^{(i-1)/(i+3)} \quad (7.2-16)$$

Note that for a class II system, solids concentration is independent of retention time and the exponent j does not appear in Eq. (7.2-16). As values of i for low-order secondary nucleation kinetics might typically be in the range 0–3, it is obvious that little size improvement, and perhaps even size degeneration, will be brought about by increases in total retention time.

A more practical way of increasing particle size is by preferential removal of the smaller sizes, leaving the remaining crystals to grow to larger average size. If fines can be removed at a small enough size, it is immaterial to size improvement whether they are advanced to product or dissolved and recycled; however, the removal of large flows of liquor associated with the fines dictates that they be dissolved and the liquor recycled. The net effect

of fines destruction is to force the growth rate to higher levels, producing the same production on fewer crystals of larger average size.

7.2.3.A Point Fines Dissolver

The potential and limitations of size improvement with fines destruction can be easily developed using the concept of a point fines trap, that is, fines removal at a size negligibly small compared to product-size crystals. For this case, both solids concentration (for class II system) and the mean retention time of the surviving crystals remain invariant when fines destruction is implemented; thus the growth rates, and hence dominant particle sizes, are inversely proportional to specific crystal surface area. The ratio of size improvement with the destruction of nuclei is then given as

$$L_{d2}/L_{d1} = \int_0^\infty n_1 L^2 dL / \int_0^\infty n_2 L^2 dL = n_1^0 (L_{d1})^3 / \beta n_2^0 (L_{d2})^3 \quad (7.2-17)$$

where β is the fraction of nuclei surviving the fines-destruction system and where the subscripts 2 and 1 refer to the cases with and without fines destruction, respectively. Assuming the power-law form of kinetics of Eq. (7.2-7) gives

$$(L_{d2}/L_{d1})^4 = (G_1/G_2)^{i-1} / \beta \quad (7.2-18)$$

Multiplying top and bottom by τ^{i-1} and solving for the size improvement ratio gives

$$L_{d2}/L_{d1} = (1/\beta)^{1/i+3} \quad (7.2-19)$$

Thus, because of the increased nucleation caused by higher driving forces, the effectiveness of fines destruction in increasing particle size decreases with systems having a high sensitivity of nucleation to growth rate, indicated by large values of the parameter i . From this equation, one could deduce that a fines-removal system would be quite ineffective in increasing particle size beyond a level where the increased driving forces pushed nucleation past a metastable limit. The maximum size improvement occurs with the lowest nucleation-growth rate sensitivity measured by the parameter i . Values of β as small as 10^{-3} , that is, only one nuclei in one thousand surviving the fines-destruction system, can occur in commercial units, and thus fines destruction within the metastable range of operation is an effective means of size improvement.

7.2.3.B Fines Destruction at Larger Sizes

The effect of fines destruction when the fines are not negligibly small compared to product-size crystals and represent an appreciable solute recycle stream, thus increasing the internal rate of make and altering the form of CSD, can be rigorously analyzed by the techniques in Section 7.1. In terms of the general algorithm, fines destruction is simulated by allowing

the removal function $C_w(L)$ to be much greater than unity for sizes less than the maximum fines size L_F , and equal to unity for sizes larger than L_F . Assuming the fines are dissolved and recycled, the product removal function $C_p(L)$ is unity for all sizes. If fines are advanced to product rather than dissolved, $C_p(L) = C_w(L)$ for all L . Physically, the $C_w(L)$ function represents the ratio of the combined fines and mixed-product flow rates to the mixed-product rate.

Accelerated removal of fines often produces a bimodal weight distribution in the product crystals: a small peak within the size range $(0, L_F)$ and the normal mode at the dominant crystal size. Such a bimodal mass distribution will occur any time smaller crystals have an appreciably shorter mean retention probability than larger crystals, such as in a growth-type crystallizer with a partially clarified overflow stream. The condition for producing a mass peak in a small size range $(0, L_F)$, and hence a bimodal distribution, is

$$3GV/(Q_F + Q_m) < L_F \quad (7.2-20)$$

where Q_F is the fines-removal rate (or overflow rate for growth-type unit) and Q_m is the mixed-product underflow rate. Normally, a bimodal distribution is of no consequence, but if the first peak represents too large a fraction of the distribution, the product may become difficult to filter or dusty in appearance.

EXAMPLE 7.2.3-1

Using the previously derived theory, construct a hypothetical semilog population density plot of CSD from a crystallizer before and after the addition of a fines-removal system, considered as cases 1 and 2, respectively. For this example, in case 2, it is assumed that fines, in sizes 0 to L_F , are withdrawn with a flow rate $(R - 1)Q_o$, while product crystals, in the size range L_F to ∞ , are withdrawn at a rate Q_o , and where R is the ratio of product-to-fines drawdown times. Thus, the drawdown times will be

$$\begin{aligned} \tau_F &= V/RQ_o & \text{for } L < L_F \\ \tau_p &= V/Q_o & \text{for } L > L_F \end{aligned}$$

From previous theory it is known that crystal population in each size range will decay exponentially, inversely proportional to the product of growth rate times holding time. Thus, the population densities will be of the form

$$\begin{aligned} (n_F)_2 &= C_1 \exp(-L/G_2\tau_F) & \text{for } L < L_F \\ (n_p)_2 &= C_2 \exp(-L/G_2\tau_p) & \text{for } L > L_F \end{aligned} \quad (7.2-21)$$

where C_1 and C_2 are constants. Furthermore, $n_F = n_p$ when $L = L_F$, as the

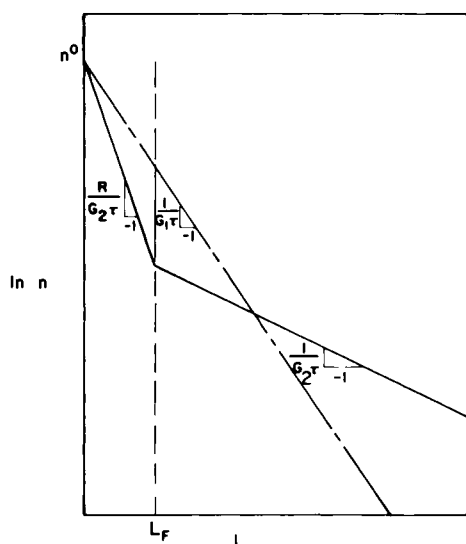


Fig. 7.2-3 Hypothetical population density plot (1) without (— — —) and (2) with (—) fines removal. [After M. A. Larson, and A. D. Randolph, *Chem. Eng. Progr. Symp. Ser.* (95) 65, 1 (1969).]

distribution is surely continuous. Thus, on the semilog plot (Fig. 7.2-3), a straight line can be drawn in the segment 0 to L_F with a negative slope R times that in the range (L_F, ∞) of the product crystals. The curve for the mixed-product case can be located as follows. The total mass in suspension M_T must be the same in both cases 1 and 2 (without and with fines dissolving) if a class II crystal system is assumed with recycling of dissolved fines. Thus, if both curves start out with the same density of nuclei $n_1^0 = n_2^0$, then curve 1 must have a slope intermediate between the slopes of the two sections of curve 2 in order for the integral of $L^3 n dL$ over the entire distribution to be equal in both cases. This locates curve 1 (qualitatively) in Fig. 7.2-3. As the drawdown time for case 1 is the same as τ_p in case 2, namely, $\tau = V/Q_o$, it must be concluded that the growth rates are different, and in fact that $G_2 > G_1$. Thus, the net effect of fines removal is to force the growth rate to a higher level, producing the same production with crystals of larger average size having less total surface area. ♦

In practice, an unchanged density of nuclei after implementation of fines dissolution would only occur if the nucleation rate increased in the same proportion as growth rate, that is, the nucleation sensitivity parameter i

had the value of unity. If the higher supersaturation produced with fines removal results in a greater than proportionate increase in nucleation rate ($i > 1$), then additional nuclei will be formed, and size improvement will be somewhat less than expected based on the previous analysis. An estimate of size improvement could be made from Eq. (7.2-19) (point fines trap) where the fraction β surviving the fines trap is given as

$$\beta = \exp(-Q_F L_F / GV) \quad (7.2-22)$$

CSD improvement with fines removal, including prediction of the bimodal weight distribution, could be obtained by solution of the equations of Section 7.1 with

$$C_w = R \quad \text{for } L < L_F$$

$$C_w = 1 \quad \text{for } L > L_F$$

$$C_p = 1 \quad \text{for all } L$$

together with actual physical parameters and kinetics of the particular system.

7.3 Classified Product Removal

Classified removal occurs when the mean retention probability of the particles varies over particle size ranges in which a significant fraction of the product mass is found. Removal of product-size crystals may be accelerated (decreased retention probability) or retarded (increased retention probability) relative to the mixed removal case, producing narrower or wider CSDs than the MSMPR distribution. Such product classification can occur inadvertently at the point of slurry removal in a mixed suspension, deliberately from a size-classified zone, or with ancillary process classification devices, such as wet screens, hydroclones, and eleutriators. An example of the first type is intermittent product removal from a vertical bootleg into which the larger crystals preferentially drift during the off portion of the cycle. Careful studies of solids removal from mixed slurries indicate that appreciable classification always occurs unless the slurry stream is removed isokinetically, that is, at the same vector velocity as the circulating magma at the point of removal.

Deliberate product classification in the form of accelerated removal of product-size material is often used to narrow the CSD and, mistakenly, to increase particle size of the product by not removing so many fines. A mixed-suspension crystallizer produces an inherently wide distribution of particle sizes, and it would seem that if all the crystals were left in the

magma until they were of some large product size, say L_p , then a large and narrow CSD could indeed be produced. This case, representing ideal classification, has been thoroughly studied in comparison with the MSMPR mode of operation [2]. An interesting result of this comparison of mixed and perfectly classified modes of removal is that under comparable operating conditions when the MSMPR dominant size is equal to the classified particle size L_p , the MSMPR distribution contains approximately 11 times as many crystals per pound of product as the single-size classified crystals. Another way to express this comparison is that the classified case can tolerate only one-eleventh the nucleation rate as the mixed case and still produce the same dominant size. For this reason, product classification is almost always accompanied by size reduction unless nucleation is independently controlled; thus, classification to control the form of CSD and fines removal to influence particle size are often implemented together. In the mixed withdrawal case, many small crystals are withdrawn in the product before they are of appreciable size, which automatically serves as an effective means of population control at the price of producing a wider CSD.

Product classification can be rigorously simulated by the CSD algorithm of Section 7.1 utilizing the $C_p(L)$ function defined as the ratio of actual solids removal at size L to perfectly mixed removal. The $C_p(L)$ function can be obtained from analysis of experimental solids concentration data in both suspension and withdrawal or as an idealized model of an external solids classifier. The latter is typically modeled simply as

$$\begin{aligned} C_w = C_p &= 1 & \text{for } L < L_p \\ C_w = C_p &> 1 & \text{for } L > L_p \end{aligned}$$

where L_p is the classification size at which significant deviation from mixed withdrawal begins. An idealized, yet realistic, model of a mixed-suspension, classified-product-removal crystallizer is given in the next example, in which product-size particles greater than size L_p are assumed to be removed at a rate z times those less than L_p in size. This model, representing a wet screen or hydroclone with a sharper cut point at size L_p and feed-to-under-size flow ratio of z , is idealized enough to permit analytic solution of the population balance, yet realistic enough to capture the qualitative effects of classification on CSD.

EXAMPLE 7.3-1 EFFECT OF CLASSIFICATION ON CSD

Construct a hypothetical semilog population density plot of CSD in a mixed-magma crystallizer before and after installation of a wet-screen classifying device, classifying at particle size L_p . Refer to operation with and without the wet screen as cases 2 and 1, respectively. Assume density of

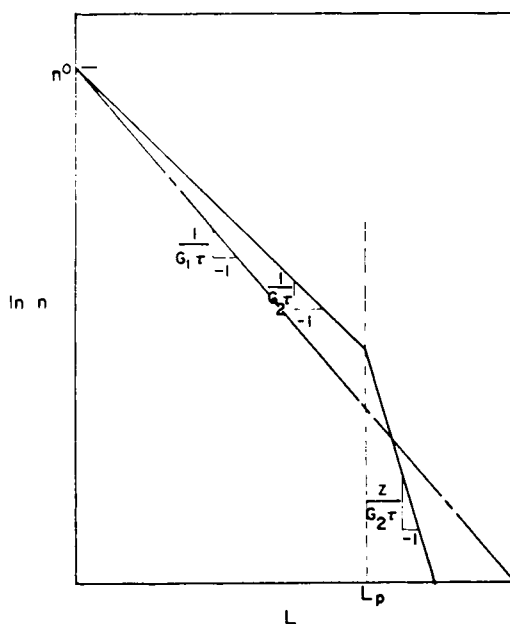


Fig. 7.3-1 Hypothetical population density plot (1) without (---) and (2) with (—) classified product removal. [After M. A. Larson and A. D. Randolph, *Chem. Eng. Progr. Symp. Ser.* 95(65), 1 (1969).]

nuclei remains constant. Physically, this would be true if the nucleation sensitivity parameter i is unity such that any changes in supersaturation brought about by classification result in proportionate changes in nucleation and growth rates and if nucleation is independent of the changes in solids concentration ($j = 0$). A sharp classification at size L_p is assumed such that the idealized undersize and oversize particle drawdown times can be defined as

$$\begin{aligned}\tau_u &= V/Q_o = \tau & \text{for } L < L_p \\ \tau_p &= V/zQ_o = \tau/z & \text{for } L > L_p\end{aligned}$$

Solving for population density in the magma gives

$$\begin{aligned}(n_u)_2 &= k_1 \exp(-L/G_2 \tau_u) & \text{for } L < L_p \\ (n_p)_2 &= k_2 \exp(-L/G_2 \tau_p) & \text{for } L > L_p\end{aligned} \quad (7.3-1)$$

where k_1 and k_2 are constants. Continuity requires that $n_u(L_p) = n_p(L_p)$, giving the two straight-line segments shown in Fig. 7.3-1 having negative slopes $1/G_2 \tau$ and $z/G_2 \tau$ below and above the classification size L_p . Population density for the MSMPR case is given by

$$n_1 = n^0 \exp(-L/G_1 \tau) \quad (7.3-2)$$

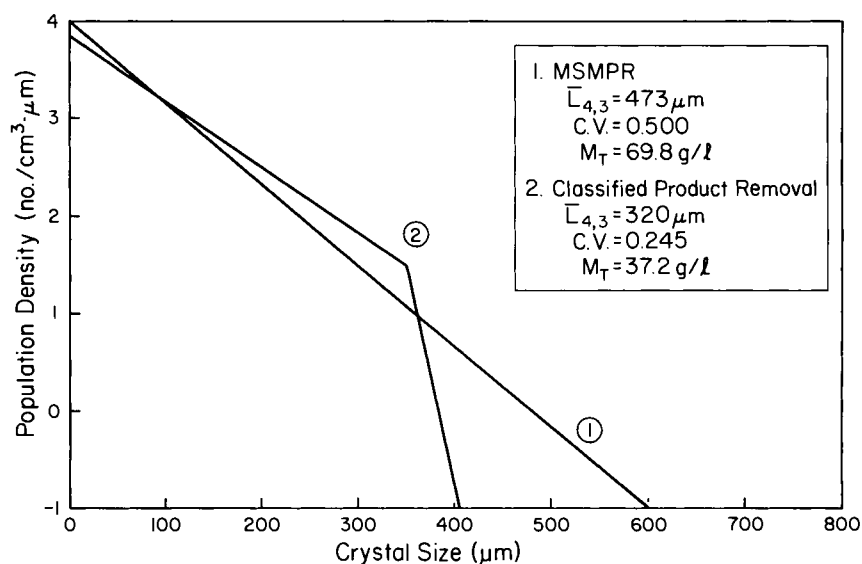


Fig. 7.3-2 Effect of product classification. (Kinetics representative of KCl system. See Appendix B.)

The location of the MSMPR line relative to the two segments of the classified removal distribution in Fig. 7.3-1 depends on the classification size L_p . The integral of $L^3 n dL$ over the entire distribution is not the same for both cases, but is less for the case of classification, as the slurry density has been drawn down by the preferential removal of oversize crystals. However, a finer distribution has been produced, having a greater specific surface area. Thus, total crystal area, the product of solids concentration times specific area, can either decrease or increase depending on the classification size. Typically, total crystal surface area will decrease. Thus, to produce the same production (class II system), the growth rate is forced to a higher level and $G_2 > G_1$. This locates the curves as shown in Fig. 7.3-1.

In the general case, nucleation will not increase in the same ratio as growth rate and the expected CSD with product classification can be calculated by the methods of Section 7.1 using empirical nucleation-growth rate kinetics. Analytic forms for CSD in suspension and in product for the above classification model using power-law nucleation-growth rate kinetics are given in a subsequent example.

Figure 7.3-2 shows a calculated semilog plot of crystals produced with or without product classification. The kinetics used are representative of the KCl-brine-NaCl system (brine saturated with NaCl). Values of the mean size $\bar{L}_{4,3}$ and coefficient of variation (c.v.) are shown for the two distribu-

tions in Fig. 7.3-2. Note that product classification narrows the distribution and produces product with a smaller average size. (See Appendix B for details of these calculations.)

An ideal crystallizer would permit the separation, at will, of residence-time distributions of solids versus liquor and solids as a function of size. Thus one could operate with arbitrary solids concentrations (by clear-liquor overflow), produce a narrow CSD with classified removal, and keep nucleation in balance with a fines-destruction system. Low driving forces (supersaturation) would be maintained by the heavy retained seed bed intermediate in size between fines and product, L_F and L_p . Such a crystallizer could be realistically modeled using the model developed in Section 7.1.

EXAMPLE 7.3-2 CLASSIFIED REMOVAL WITH FINES DESTRUCTION

Construct a hypothetical semilog population density plot of CSD from a crystallizer with clear liquor removal, fines-destruction system, and classified product removal. Use the same idealizations as in the previous examples.

Fines destruction will give a large drawdown rate for crystals below size L_F . As a result, a plot of the fines size distribution will have a slope R

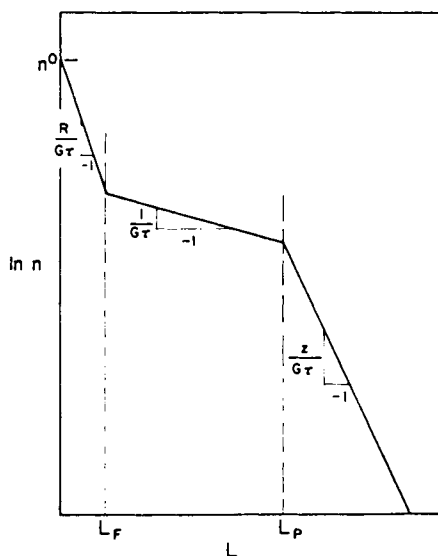


Fig. 7.3-3 Hypothetical population density plot with classified product removal and fines destruction. [After M. A. Larson and A. D. Randolph, *Chem. Eng. Progr. Symp. Ser.* **95**(65), (1969).]

times that of the crystal seed bed. This is shown by the first straight-line segment in Fig. 7.3-3. The second segment, representing the crystal seed bed, greater in size than fines but less than product crystals, decays with a negative slope of $1/G\tau$, where $\tau = V/Q_u$ and where Q_u , the underflow discharge rate, is determined by the amount of clear liquor overflow Q_o .

Accelerated product removal for sizes larger than L_p will give a draw-down in the third size range z times that of the seed-bed drawdown. This gives the final straight-line segment in Fig. 7.3-3, having a negative slope of $z/G\tau$.

Clear-liquor overflow Q_o separates the residence time of solids relative to liquor, thus affecting the total solids concentration but not the form of CSD. Solids concentration is determined by the absolute slopes in Fig. 7.3-3, hence by the absolute value of Q_u . Clear liquor overflow must be taken into account in writing mass balances, but not population balances. Only slurry streams need be considered in the latter. ♦

As in previous examples, actual values of solids concentration M_T and crystal growth rate G can be found by simultaneous solution of population and mass balances together with nucleation–growth rate kinetics. A more realistic analysis of complex residence-time crystallizers can be made if actual drawdown rates as a function of size as well as accurate nucleation–growth rate kinetics in the resulting region of supersaturation are known for the system. It should be obvious from these examples that much remains to be learned about actual classification mechanics as well as nucleation–growth rate kinetics.

EXAMPLE 7.3-3 PREDICTION OF WEIGHT-SIZE DISTRIBUTION

Solve the associated population and mass balances of the idealized crystallizer of Fig. 7.3-3 together with power-law kinetics to predict CSD (weight basis) in the backmixed crystallizer and in the classified product. Assume an ideal fines trap removing particles at a rate $Q_F = (R - 1)Q_u$ for $L < L_F$ and an ideal classifier removing product-size crystals at an accelerated rate zQ_u for $L > L_p$. The resultant population density plot was shown for this case in Fig. 7.3-3. Writing the distributions piecewise yields

$$\begin{aligned} n_1 &= n^0 \exp(-RL/G\tau) & \text{for } L & \text{ in } (0, L_F) \\ n_2 &= C_1 \exp(-L/G\tau) & \text{for } L & \text{ in } (L_F, L_p) \\ n_3 &= C_2 \exp(-zL/G\tau) & \text{for } L & \text{ in } (L_p, \infty) \end{aligned} \quad (7.3-3)$$

where $\tau = V/Q_u$. Continuity of the magma distribution requires that $n_1(L_F) = n_2(L_F)$ and $n_2(L_p) = n_3(L_p)$. (Note: Continuity of the product distribution is not required and does not hold with the discontinuous

changes in withdrawal rate of this example.) Making the dimensionless substitutions $x = L/G\tau$ and $y = n/n_0^0$ and evaluating the constants gives the dimensionless population distributions

$$\begin{aligned} y_1 &= \exp(-Rx) \\ y_2 &= \exp[-(R-1)x_1] \exp(-x) \\ y_3 &= \exp[-(R-1)x_1] \exp[(z-1)x_2] \exp(-zx) \end{aligned} \quad (7.3-4)$$

where $x_1 = L_F/G\tau$ and $x_2 = L_p/G\tau$.

From the definition of product weight distribution in suspension and product,

$$W(x) = \int_0^x x^3 y dx / \int_0^\infty x^3 y dx \quad (7.3-5)$$

$$W_P(x) = \int_0^x Q^P(x) x^3 y dx / \int_0^\infty Q^P(x) x^3 y dx \quad (7.3-6)$$

These integrals must be broken up into three parts for integration along the three segments of the distribution curve. Define the dimensionless arguments

$$\begin{aligned} p &= RL/G\tau, & x &= L/G\tau, & q &= zL/G\tau \\ p_2 &= RL_F/G\tau, & x_1 &= L_F/G\tau, & x_2 &= L_p/G\tau, & q_2 &= zL_p/G\tau \end{aligned}$$

Then, in terms of the dimensionless weight distribution function $w(x) = \frac{1}{6} \int_0^x p^3 e^{-p} dp$ (as tabulated in Appendix A), the cumulative weight distributions in suspension and product are given as

$$\begin{aligned} W(L) &= w(p)/R^4 D \\ W_P(L) &= w(p)/R^4 D_P \quad \text{for } L < L_F \end{aligned} \quad (7.3-7)$$

$$\begin{aligned} W(L) &= W(L_F) + \frac{\{\exp[-(R-1)x_1]\} [w(x) - w(x_1)]}{D} \\ W_P(L) &= W_P(L_F) + \frac{\{\exp[-(R-1)x_1]\} [w(x) + w(x_1)]}{D_P} \end{aligned}$$

for L in (L_F, L_p) (7.3-8)

$$\begin{aligned} W(L) &= W(L_p) + \frac{\{\exp[(z-1)x_2 - (R-1)x_1]\} [w(q) - w(q_2)]}{z^4 D} \\ W_P(L) &= W_P(L_p) + \frac{\{\exp[(z-1)x_2 - (R-1)x_1]\} [w(q) - w(q_2)]}{z^3 D_P} \end{aligned}$$

for L in (L_p, ∞) (7.3-9)

The dimensionless denominators D and D_p are given as

$$D = \frac{w(p_1)}{R^4} + \{\exp[-(R-1)x_1]\}[w(x_2) - w(x_1)] \\ + \frac{\{\exp[(z-1)x_2 - (R-1)x_1]\}[1 - w(q_2)]}{z^4} \quad (7.3-10)$$

$$D_p = \frac{w(p_1)}{R^4} + \{\exp[-(R-1)x_1]\}[w(x_2) - w(x_1)] \\ + \frac{\{\exp[(z-1)x_2 - (R-1)x_1]\}[1 - w(q_2)]}{z^3} \quad (7.3-11)$$

Equations (7.3-7)–(7.3-9) give the form of CSD for this complex process configuration; actual sizes must be determined by solving for the growth rate G that satisfies a mass balance for the process. Production rate is given in terms of the population distribution as

$$P = \rho k_v \int_0^\infty Q^p(L) n L^3 dL \quad (7.3-12)$$

Only one value of G will give an $n(L)$ that satisfies the above constraint. Writing out the above constraint in terms of the parameters of the system gives

$$P/\rho k_v = 6n_0^0 Q_u (G\tau)^4 \{ [w(p_1)/R^4] + \{\exp[-(R-1)x_1]\} \\ \times [w(x_2) - w(x_1)] + (1/z^3) \{\exp[-(R-1)x_1 + (z-1)x_2]\} \\ \times [1 - w(q_2)] \} \quad (7.3-13)$$

Inserting the power-law form of the density of nuclei $n^0 = k_N G^{i-1} M_T^j$

$$G^{i+3} = P/6\rho k_v k_N \tau^4 D_p(G) Q_u M_T^j \quad (7.3-14)$$

where $D_p(G)$ is a growth-rate-dependent term given by Eq. (8.4-11). Rearranging and substituting for M_T gives

$$G = [P/6Q_u D_p]^{(i-j)/(i+3)} (6D)^{-j/(i+3)} (k_N \rho k_v \tau^4)^{-1/(i+3)} \quad (7.3-15)$$

The above equation can be solved by standard trial-and-error methods for the correct value of G that satisfies this mass balance. The weight distribution equation can then be solved with this value of G to observe the effects of changes in dissolving and product classification on product weight-size distribution. Note that the retention time τ was based on underflow Q_u . Changes in clear liquor removal affect Q_u , hence G . Thus, the particle size, but not the basic form of CSD, is altered by clear liquor removal. ♦

The CSD equations of Example 7.3-3 can be used to predict actual weight distributions for the idealized fines-dissolving and product classification of Figs. 7.2-3 and 7.3-1. These models are idealized, yet realistic

enough to be useful in assessing the probable interaction of process configuration with given system kinetics to alter CSD. The five parameters defining possible process configurations are the fines-removal ratio R , product-removal ratio z , maximum fines-removal size L_F , product classification size L_p , and the ratio of clear liquor overflow to mixed underflow Q_o/Q_u . Fines removal and/or product classification is simulated when R and/or z are greater than unity for reasonable values of the parameters L_F and L_p . When $R = z = 1$, the equations coalesce to the growth-type MSMPR case.

7.4 Fines Dissolving in Batch Crystallizers

Selective fines segregation and dissolving is a widely practiced technology in continuous crystallization, which is used to increase the mean particle size of the product crystals. Surprisingly, this technology is not utilized in batch crystallization. In the operation of batch raw sucrose crystallizers, terms like “give the pan a drink” are used to describe the practice of adding water to control the graining of sucrose when too many fines are developing and/or the supersaturation is too high. However, this practice does not constitute selective removal and destruction of a prescribed size range of crystals. Jones *et al.* [3] first described the segregation and destruction of fines in a batch-operated crystallizer, using the inorganic K_2SO_4 –water system. Their study demonstrated the experimental feasibility of this technology to dramatically reduce the amount of fines in the final product CSD. They modeled their system with population balance-type models which were in agreement with experimental results. As in the continuous case, a knowledge of nucleation–growth rate kinetics is needed to predict the effect of fines dissolving on CSD. However, in the batch case, a well-defined growth rate–supersaturation model is vital for CSD prediction. After the initial nucleation event, CSD is determined mainly by subsequent growth of the existing crystals. Continuous crystallization, on the other hand, is production rate–driven, and the growth rate at steady state assumes that value necessary to conserve mass in the system. The effects of fines dissolving in class II continuous crystallizers can be modeled solely with a knowledge of the relative nucleation–growth rate sensitivity parameter i .

The effects of fines dissolving in constant-volume batch crystallizers can be predicted using a population-balance equation similar in form to that for CSD dynamics in continuous crystallizers. Thus

$$\frac{\partial n}{\partial t} + G \frac{\partial n}{\partial L} + \frac{Q(L)n}{V} \quad (7.4-1)$$

where $Q(L)$ is the selective removal rate of fines given as

$$Q(L) = \begin{cases} Q_F, & L < L_F \\ 0, & L > L_F \end{cases}$$

and where L_F is the maximum size of crystals removed in the fines classifier.

Associated nucleation, growth rate, and solute mass-balance equations must be solved simultaneously with the population balance of Eq. (7.4-1). Again, predictions from the above model will depend largely on the quality of the growth rate-supersaturation curve for the system studied.

Zipp [4] has reported a study of fines dissolving applied to a batch crystallizer using an organic system, pentaerythritol-water. Figure 7.4-1 shows initial and final cumulative number distributions in a batch pentaerythritol crystallizer, with and without fines dissolving. A dramatic decrease in fines is observed when operating with fines destruction.

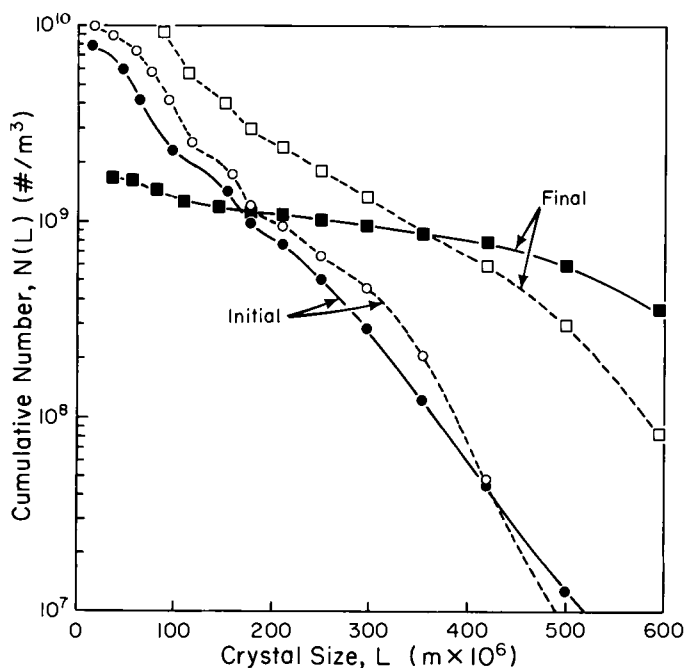


Fig. 7.4-1 Effect of fines dissolving on cumulative number distribution in a batch crystallizer [4]. Solid line: with fines destruction; dashed line: without fines destruction.

The use of fines destruction in batch crystallization can certainly produce a superior CSD, at least to reduce the amount of fines in the product crystals. The energy cost associated with fines destruction could be significantly reduced by exchange of energy between the outflowing fines stream and the returning dissolved fines. The economic benefits of such a process would be specific to a given system and would have to balance the increased energy cost of dissolving against better filtration and lower entrainment rates.

7.5 Summary

The CSD obtained from a crystallization system is determined not only by the relative kinetics of nucleation and growth, but also by the relative residence times of the various sizes of crystals. Various operation strategies have been shown to affect the size distribution. The effects of preferential removal of fines and their subsequent destruction as well as the effects of classified product removal were demonstrated.

In the design of crystallization systems, the requirements on the product CSD coupled with the fundamental kinetics of the system will determine the size-dependent residence-time distribution, which should be incorporated in the crystallizer design. The size-dependent RTD of particles will often override unfavorable crystal nucleation and growth kinetics, permitting production of a desirable CSD. The importance of particle RTD is shown by the gypsum CSD illustration in this chapter. A general CSD algorithm was developed that accounts for nonrepresentative crystal removal as a size-dependent function times the population density in the crystallizer magma. This modeling assumption has a profound affect in simplifying the resulting CSD equations.

All of the examples chosen in this chapter have been taken from the area of crystallization; similar effects of residence-time distribution are observed in other particulate processes. The techniques of this chapter are still valid, and the effects of residence-time distribution alter the form of a one-dimensional distribution in the same qualitative way, when the internal coordinate is linearly related to age in the environment, as in the case of particle size in crystallization. However, there is a large interaction between residence-time distribution and system kinetics; thus, specific results must be obtained through solution of the appropriate population and mass-balance equations.

Nomenclature

B^0	Nucleation rate, number/ volume time	n^0	Steady-state nuclei density, number/(volume size)
C	Concentration of solute, mass/volume	P	Production rate, mass/time
C_A, C_p, C_w	Dimensionless size-depen- dent flow ratios (com- pared to reference flow Q_B) in general CSD al- gorithm	p	Dimensionless fines size, RL/GT
$D(G), G_p(G)$	Dimensionless integrals of gamma function defined by Eqs. (7.3-10) and (7.3- 11)	Q_B	Reference flow in general CSD algorithm, volume/ time
G	Linear crystal growth rate, length/time	Q_i, Q_o, Q_u	Inlet, outlet (or overflow), and underflow streams, volume/time
G_0	Reference linear growth rate, length/time	q	Dimensionless crystal clas- sification size, zL/GT
g	Dimensionless growth rate, G/G_0	R	Fines removal ratio, Q_F/Q_B
k_N, i, j	Parameters in nucleation kinetics model, $B^0 =$ $k_N G^i M_T^j$	V	Magma volume, slurry or clear-liquor basis
L	Linear particle size, length	W	Cumulative mass fraction distribution
L_F, L_p	Fines product classification size, length	x	Dimensionless size, L/GT
M_T	Solids concentration in magma, mass/volume	y, y_i	Dimensionless population density, ng/n^0
n	Population density, num- ber/(volume size)	z	Product classification ratio, Q^P/Q_B
n_i, n_o, n_u	Population density of inlet, outlet (or overflow), and underflow streams, num- ber/(volume size)		
n^0	Nuclei density, number/ (volume size)		

GREEK SYMBOLS

β	Fraction of fines surviving fines dissolver
ρ	Crystal density, mass/ volume
T	Retention time, magma volume/flow rate

References

1. Randolph, A. D., Vaden, D. E., and Stewart, D. (1984). Improved crystal size distribution of gypsum from flue gas. In "Advances in Crystallization from Solutions" (G. Youngquist, ed.), Chem. Eng. Symp. Ser. **240** (80), 110.
2. Saeman, W. C. (1956). *AIChE J.* **2**, 107.
3. Jones, A. G., Chianese, A., and Mullin, J. W. (1984). Effect of fines destruction on batch cooling crystallization of potassium sulphate solutions. In "Industrial Crystallization 84" (S. J. Jancic and E. J. deJong, eds.), p. 191. Elsevier, Amsterdam.
4. Zipp, G. L. (1986). Selective fines destruction in batch crystallization. Unpublished M.S. thesis, Department of Chemical Engineering, University of Arizona, Tucson.

CSD DYNAMICS AND CONTROL

8.0 Introduction

Continuous crystallizers are in the main expected and designed to operate at constant conditions. Such steady-state operations are relatively easy to model when compared to batch systems, which, of course, exhibit conditions that vary in time and are consequently regarded as in the unsteady state. In the previous chapters we exploited this steady-state nature to develop relationships showing how the process conditions and kinetic rates affect the size distribution. In this chapter, we show how the unsteady-state number and mass balances arise and how they may be used in understanding both CSD transients and CSD stability.

CSD dynamics are comprised of both transients (the CSD responds to outside disturbances in feed rate and composition, temperature, slurry withdrawal rates, etc.) and in some cases instability (the CSD cycles through fairly regular long-term periods of coarse and fine material, even when disturbances from the outside have been virtually eliminated). In mathematical parlance, we are referring to CSD transients resulting from a nonhomogeneous forcing function or instability of the characteristic equation describing CSD.

The possibility of long-term CSD limit cycles developing in a crystallizer is due to the intrinsic process feedback of crystallizers discussed in Chapter 1 as shown in the information block diagram of an MSMR crystallizer

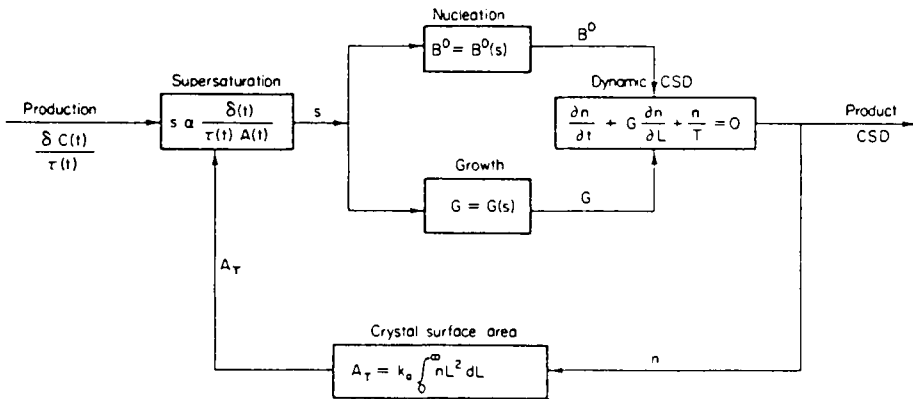


Fig. 8.0-1 Information block diagram of the MSMPR crystallizer showing internal CSD self-regulation feedback loop. Other feedback loops regulating secondary nucleation may exist.

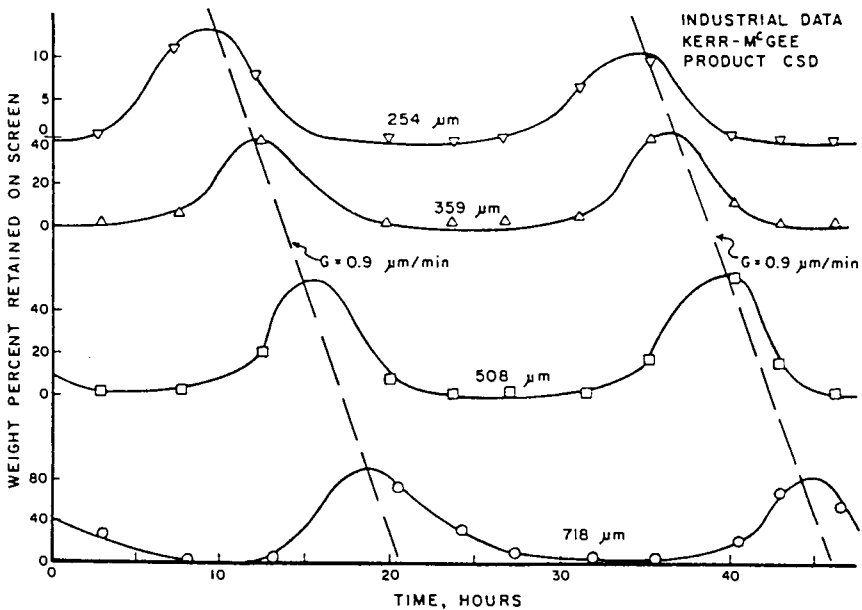


Fig. 8.0-2 CSD limit cycles in an industrial KCl crystallizer. Courtesy of Kerr-McGee Corporation, Trona, California. (After Randolph *et al.* [3].)

(Fig. 8.0-1). Figure 8.0-2 illustrates some of these long-term CSD limit cycles in an industrial crystallizer. The unsteady-state population and mass balances discussed in this chapter are applicable to the study of both CSD transients and stability, as well as being necessary for analytical CSD control studies.

The unsteady-state population balance has been presented with population density on a crystal-free liquor basis (e.g., Randolph and Larson [1] and co-workers) or on a total magma basis (e.g., Hulburt and Katz [2] and co-workers). In addition, the unsteady-state mass balance can assume two forms for class I (variable per pass yield) and class II (high yield) crystallizers. In the former case the solute concentration $C(t)$ must be retained as a dependent variable, while for class II systems a dynamic mass balance constraint on crystal growth rate is sufficient to close the set of equations. The following section will discuss crystallizer dynamics with equations developed for the above analytical formats. Simulations of CSD dynamics usually give only quantitative differences in any of these analytical frameworks.

8.1 Equations for CSD Dynamics

8.1.1 Unsteady-State Population Balance

8.1.1.A Population Density Based on Total Volume

Assume that the population density is based on total magma volume, that is, crystals plus clear liquor. We will make a population balance for the configuration shown in Figure 8.1-1. As the total magma volume and magma flow rates are assumed constant, the accumulation of population can be described solely by the term $\partial n / \partial t$. The unsteady-state population balance is given as

$$\frac{\partial n}{\partial t} + G \frac{\partial n}{\partial L} + h(L) \frac{n}{\tau} = 0 \quad (8.1-1)$$

where the function $h(L)$ describes the size-dependent removal rate compared to MSMPR operation and $\tau = V/Q_p$. (A value of $h = 1$ represents the MSMPR case with removal rate Q_p . See Chapter 7.)

8.1.1.B Population Density Based on Clear Liquor Volume

If the population density is based on solids-free liquor (a convention followed throughout this book), then the change in void fraction should be considered in the unsteady-state population balance. Thus

$$\frac{\partial}{\partial t}(\epsilon n) + G \frac{\partial n}{\partial L} + \frac{h(L)n}{\tau} = 0 \quad (8.1-2)$$

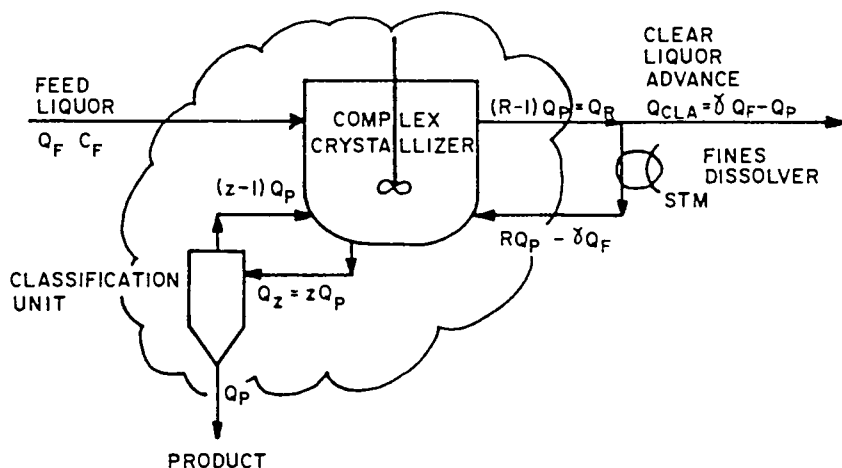


Fig. 8.1-1 Schematic of a crystallizer with a complex RTD. (After Beckman and Randolph [4].)

where ϵ is the clear-liquor fraction in the liquor/crystal magma. Equation (8.1-2) assumes total crystallizer volume remains constant. The change in void fraction with time, $\partial\epsilon/\partial t$, is often neglected in CSD dynamics studies resulting in an equation of the form of Eq. (8.1-1). Inclusion of the void fraction term has not yielded predictions of CSD dynamics having different qualitative features. Equation (8.1-3) below was derived and is exact for the class II MSMPR crystallizer. (Slurry density is invariant.) Thus

$$\frac{\partial n}{\partial t} + G \frac{\partial n}{\partial L} + \frac{n}{\tau} = 0 \quad (8.1-3)$$

where $\tau = V/Q_p$ and both V and Q_p can be on a clear-liquor or total-magma basis. Equation (8.1-3) is valid for all MSMPR crystallizers in the limit of "thin" slurries or high-yield systems. Errors might be made using Eq. (8.1-3) with the DDO configuration when large changes in the ratio Q_o/Q_u were being simulated. However, only slight differences are predicted in CSD dynamics, although intensive variables (e.g., M_T and the magnitude of n) will of course differ by the ratio of clear liquor to total suspension volumes. (See Fig. 8.2-6 for such a change in M_T for the DDO crystallizer after a large change in Q_o/Q_u .)

8.1.2 Unsteady-State Solute Mass Balance

8.1.2.A Population Density Based on Total Volume, Class I System

The single-component mass balance that must be solved together with the population balance of Eq. (8.1-1) should also be phrased in terms of

total crystallizer volume, solids plus clear liquor. Thus considering dynamics in both solute concentration $C(t)$ and solids void fraction ϵ , the solute balance becomes [4]

$$\epsilon \frac{dC}{dt} + (\rho - C) \frac{k_A G m_2}{2} = \left[\left(\frac{Q_F}{Q_P} \right) \frac{(C_F - \gamma C)}{\tau} \right] \times [(P_R/V)(1 - C/\rho)(R - \gamma Q_F/Q_P)/(R - 1)] \quad (8.1-4)$$

where $\gamma = (Q_P + Q_{CLA})/Q_F$ and m_2 is the second moment of the population density in the crystallizer. Equation (8.1-4) has $C(t)$ as a dependent variable and hence is in the general form suitable for class I calculations. The solute balance is linked to the population balance through the second moment of the population density, m_2 .

8.1.2.B Approximate Solute Balance, Liquid Phase

A solute mass balance can also be written on a clear-liquor basis, neglecting changes in void fraction. Thus

$$\frac{d(VC)}{dt} \doteq V \frac{dC}{dt} = Q_i C_i - Q_P C - \frac{G}{2} \rho k_A m_2 V \quad (8.1-5)$$

Equation (8.1-5) is an approximate solute balance that can be used for either class I or class II systems. For class II systems, $dC/dt = 0$ and Eq. (8.1-5) reduces to the growth-rate constraint of Eq. (1.3-1). Thus setting $dC/dt = 0$ gives

$$G = 2 \delta C / \rho k_A m_2 \tau \quad (8.1-6)$$

The rigorous mass balance, Eq. (8.1-4), can also be shown to reduce to a constraint on growth rate for high-yield MSMR systems. Thus P_R and $d\epsilon/dt$ are zero and Eq. (8.1-4) reduces to

$$G = \frac{(2/\rho - C) \delta C}{A \tau_F} = \frac{K \delta C}{A \tau_F} \quad (8.1-7)$$

where $\tau_F = V/Q_F$. (The term P_R is zero when no dissolved-fines recycle is included in the mass balance.)

Equations (8.1-6) and (8.1-7) are of the same form as Eq. (1.3-1). The physical interpretation is that in a high-yield system the growth rate is proportional to the concentration drop across the unit and inversely proportional to the average residence time of the crystals and their total surface area. These equations become a constraint on growth rate that can be used to simplify CSD dynamics calculations and that guarantees conservation of solute mass in the system. To summarize, Eq. (8.1-4) should be solved together with Eq. (8.1-1) (with n on a total magma basis), while Eq. (8.1-5) can be solved with Eq. (8.1-2) for class I or class II systems. The population

density can be on either a clear liquor or total magma basis. Equations (8.1-1) with (8.1-4) provide a rigorous analytical description of CSD dynamics. Forms of these equations are programmed in the CSD simulator presented in Appendix B. Equations (8.1-2) and (8.1-5), with $d\epsilon/dt = 0$, provide an approximate and somewhat simpler description of CSD dynamics. The basis for population density (clear liquor or slurry basis) does not affect CSD dynamics. In view of the uncertainties of knowing nucleation and growth-rate kinetics, all of the above analytical frameworks for calculating CSD dynamics may be considered equivalent.

8.2 CSD Transients

8.2.1 MSMPR Transients

The initial condition is whatever function describes the distribution at $t = 0$. If the system has been previously operating at steady state, then for the MSMPR crystallizer,

$$n(0, L) = n_0^0 \exp(-L/G_0\tau) \quad (8.2-1)$$

where the subscript indicates the condition during the steady-state operation.

Adding Eq. (8.2-1) to the equations in Section 8.1 provides a description of the transient behavior of the size distribution, and these equations may be solved numerically.

The solution of the above set is often difficult, and is impossible if the constants are not known, which is the case for most systems. However, by casting the system in dimensionless form, the effect of disturbances can be demonstrated. Letting the subscript zero denote initial steady-state values, we define

$$\begin{aligned} L/G_0\tau_0 &= x, & t/\tau_0 &= \theta, & G(t)/G_0 &= \rho(\theta) \\ \delta C(t)/C_0 &= \sigma(\theta), & Q_0/Q(t) &= \tau(\theta), & M_T(t)/M_{T_0} &= f_3(\theta) \\ A_T(t)/A_{T_0} &= f_2(\theta), & n(t, L)/n_0^0 &= y(\theta, x) \end{aligned} \quad (8.2-2)$$

Using these definitions with power-law nucleation kinetics, the set of Eqs. (8.1-3), (8.1-6), and (8.2-1) becomes

$$\frac{\partial y}{\partial \theta} + \rho \frac{\partial y}{\partial x} + \frac{y}{\tau} = 0 \quad (8.2-3)$$

$$\rho = \sigma/\tau f_2 \quad (8.2-4)$$

$$y^0 = \rho^{i-1} \quad (8.2-5)$$

$$y_0 = \exp(-x) \quad (8.2-6)$$

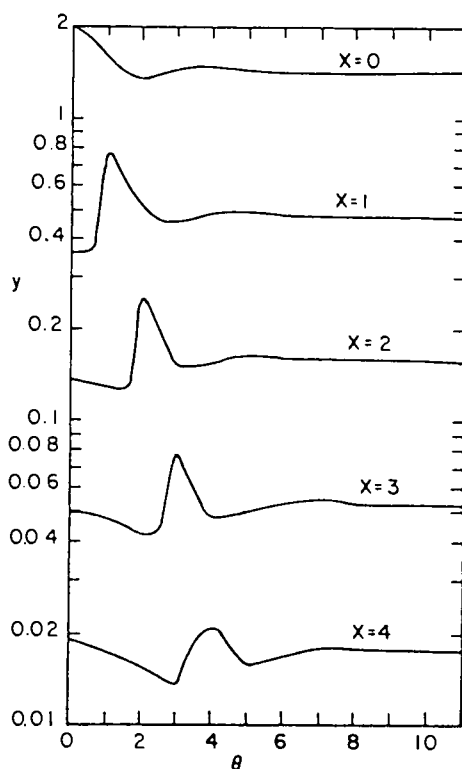


Fig. 8.2-1 Calculated dynamic response of class II MSMPR dimensionless population density to threefold increase in feed rate; $i = 4$. [After A. D. Randolph and M. A. Larson, *AIChE J.* **8**, 369 (1962)].

EXAMPLE 8.2-1-1

For a system where $i = 4$, find the time-varying behavior of the size distribution after a threefold increase in feed rate. Assume the system is initially at steady state at the lower feed rate.

A finite-difference scheme is used with $\sigma = 1$ and $\tau = \frac{1}{3}$. The results for various dimensionless sizes are shown in Fig. 8.2-1. Observe how the showers of nuclei formed at $\theta = 0^+$ grow down the size range as time passes.

Figure 8.2-2 shows the experimental transient CSD behavior of an ammonium sulfate cooling crystallizer. Note the same qualitative behavior. The fines transients die out quickly, indicating that the CSD is basically stable. The initial shower grows through the size range, perturbing the CSD at larger sizes over a long period of time. ♦

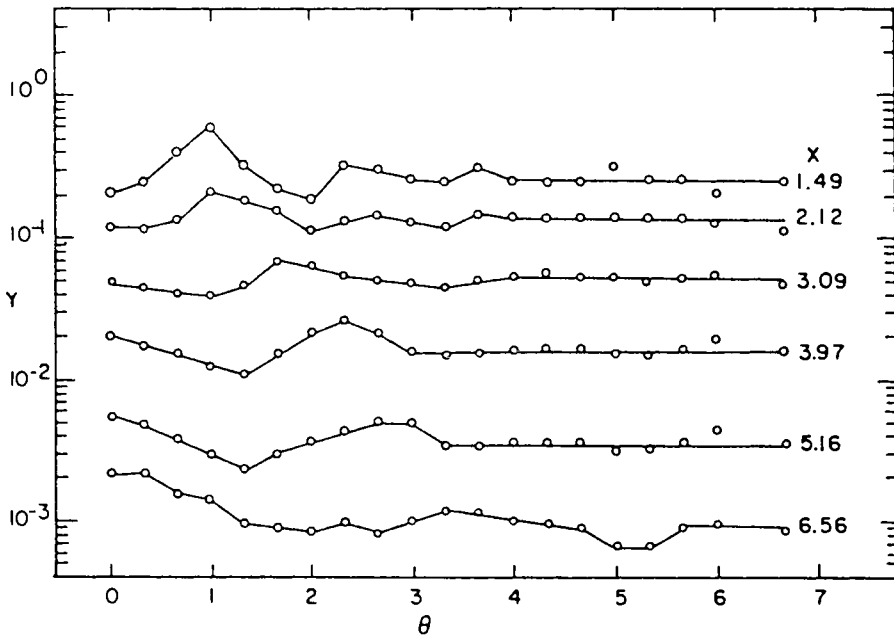


Fig. 8.2-2 Experimental dynamic response of population density to feed-rate increase for ammonium sulfate system. (After C. W. Chambliss, Ph.D. thesis, Iowa State University, Ames, Iowa, 1966, unpublished.)

8.2.2 Transient Moment Equations

The above set is difficult to solve numerically and becomes almost impossible if i is greater than 6 or 7. In addition, it is difficult to study the stability of the system working with the partial differential equation. To avoid these problems, it is only necessary to cast the set in terms of the moment equations.

Again define the j th moment of the dimensionless distribution as

$$\mu_j = \int_0^\infty y x^j dx, \quad j = 0, 1, 2, 3, 4 \quad (8.2-7)$$

As noted before, only the first four moments have physical significance, being related to the total number, length, area, and mass, respectively. It turns out that it is only necessary to work with these four moments to adequately define the system.

For simplicity, we define the normalized dimensionless moments as

$$f_j = \frac{\mu_j(\theta)}{\mu_j(0)} = \frac{\int_0^\infty y(\theta) x^j dx}{\int_0^\infty y_0 x^j dx} \quad (8.2-8)$$

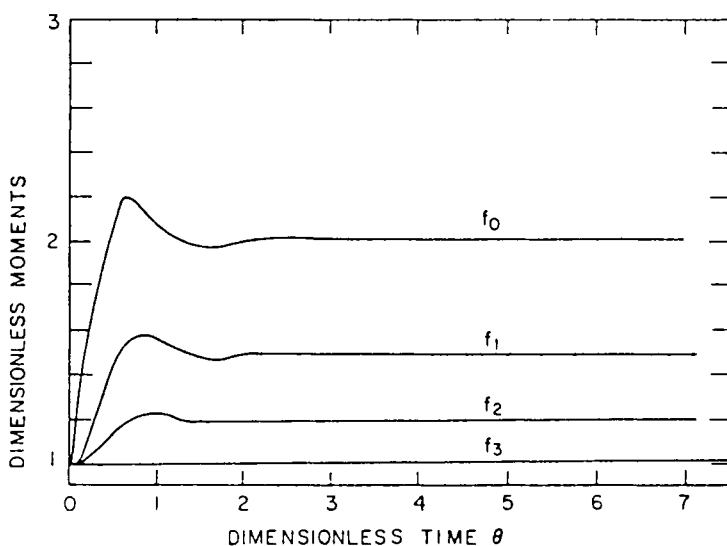


Fig. 8.2-3 Transient response of the CSD moments for a step change in holding time.

We note that the denominator of Eq. (8.2-8) for the first four moments is 1, 1, 2, and 6, respectively. Therefore,

$$f_j = \left(\int_0^\infty y(\theta) x^j dx \right) / j! \quad (8.2-9)$$

Multiplying Eq. (8.2-3) by dx and integrating gives¹

$$\int_0^\infty \frac{\partial y}{\partial \theta} dx + \rho \int_0^\infty y dx + \frac{1}{\tau} \int_0^\infty y dx = 0 \quad (8.2-10)$$

or

$$(d\mu_0/d\theta) - \rho y^0 + (\mu_0/\tau) = 0 \quad (8.2-11)$$

Using Eqs. (8.2-4) and (8.2-9) in Eq. (8.2-11) gives

$$df_0/d\theta + f_0/\tau = (\sigma/\tau f_2)^1 \quad (8.2-12)$$

Similarly, using the definition of normalized moments 1, 2, and 3, one obtains

$$df_1/d\theta + f_1/\tau = f_0\sigma/\tau f_2 \quad (8.2-13)$$

$$df_2/d\theta + f_2/\tau = f_1\sigma/\tau f_2 \quad (8.2-14)$$

$$df_3/d\theta + f_3/\tau = \sigma/\tau \quad (8.2-15)$$

¹Alternately, we could have simplified and made dimensionless substitutions in the macro-moment population balance.

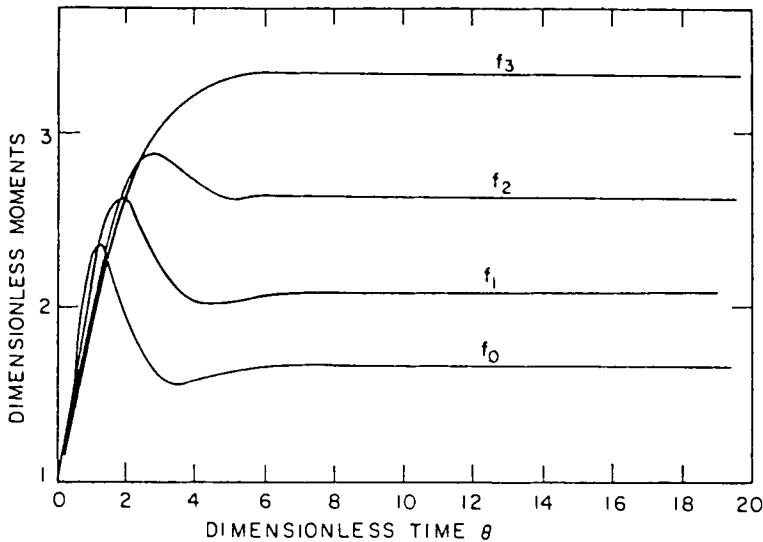


Fig. 8.2-4 Transient response of the CSD moments for a step change in rate of make.

The set of Eqs. (8.2-12)–(8.2-15) is a closed set of nonlinear ordinary differential equations with initial conditions of unity. In addition, the steady-state values of σ and τ are also unity. It is not possible to find an analytic solution to this set, but it is easily solved numerically.

For upsets in feed rate, τ becomes a function of time and the first three equations define the dynamics of the system. If the feed concentration is a variable, σ becomes time-varying and it is necessary to use all four equations to define the dynamics. Some typical responses to step changes in dimensionless residence time τ and production rate σ are shown in Figs. 8.2-3 and 8.2-4. Note that as residence time is shortened, more particles are formed, and more area is formed. This result is of course a function of the crystal nucleation–growth kinetics. Experimental moments are difficult to determine because it is not possible to enumerate all crystals to zero size.

These same moment equations will be used in a subsequent section to study the stability of CSD.

8.2.3 Transient Size Distribution by Method of Characteristics

A numerically simple and more accurate algorithm for solving CSD transients is given by program CRYSTAL.BALL listed in Appendix B. This program uses rigorous CSD dynamics, Eqs. (8.1-1) and (8.1-4), with magma-dependent power-law nucleation kinetics of the form $B^0 = k_N G^i M_T^j$.

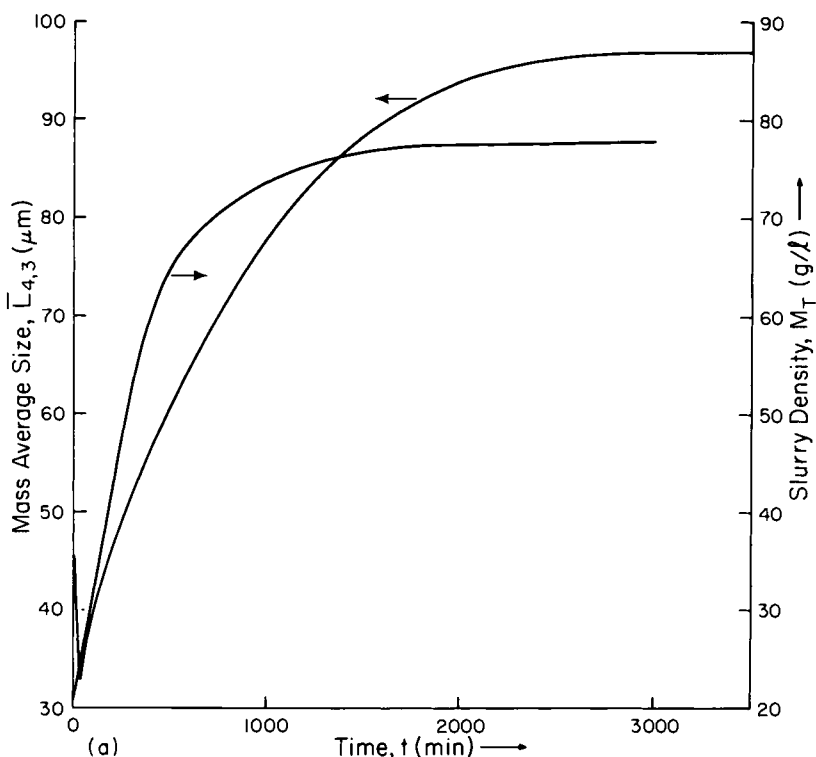


Fig. 8.2-5 Calculated CSD dynamics during transition from MSMPR to DDO operation. Kinetics representative of gypsum system. (a) Slurry density and mean particle size. (b) Growth rate and nuclei density.

The solution algorithm is based on the method of characteristics where each “packet” of particles is followed as it moves convectively along the size axis with the current growth velocity $G(t)$. See Appendix B for details of the calculation.

EXAMPLE 8.2-3-1 CALCULATED CSD TRANSIENTS FOR THE DOUBLE DRAW-OFF (DDO) CONFIGURATION

Table B-3 shows the calculated CSD from a DDO-configured crystallizer having nucleation–growth rate kinetics representative of the gypsum system, before and after a change in the overflow/underflow ratio Q_o/Q_u from 0 to 4, that is, before and after a change from MSMPR to DDO operation. Figures 8.2-5a and 8.2-5b show the calculated slurry density, mean size, growth rate, and nuclei density for this change. (See Appendix B for details of these calculations.)

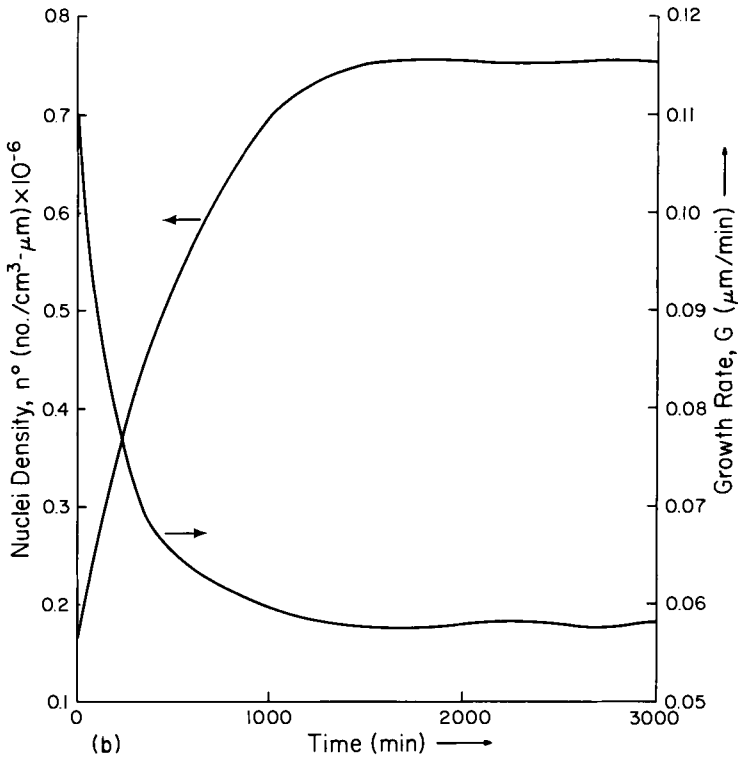


Fig. 8.2-5 Continued.

Figure 8.2-6 shows transients in calculated slurry density using Eq. (8.1-4), with or without the term for void fraction included in the mass balance. Although the curves are displaced, the transients are similar. The mean particle size was virtually unchanged whether or not the void fraction term was included, as shown in Table 8.2-1. These calculations indicate that use of the rigorous mass balance (inclusion of void fraction changes) has little effect on calculated CSD. ♦

8.3 Stability of CSD

The feedback loop shown in Fig. 8.0-1 acts as an effective means of self-regulation for the CSD produced in a continuous crystallizer. As with all feedback regulator controls, if the feedback is excessive, the system will overreact to changes and ultimately become unstable, that is, exhibit sustained oscillations independent of outside disturbances.

The stability of CSD can be analyzed at several levels of complication; however, the approach is essentially the same regardless of the level of

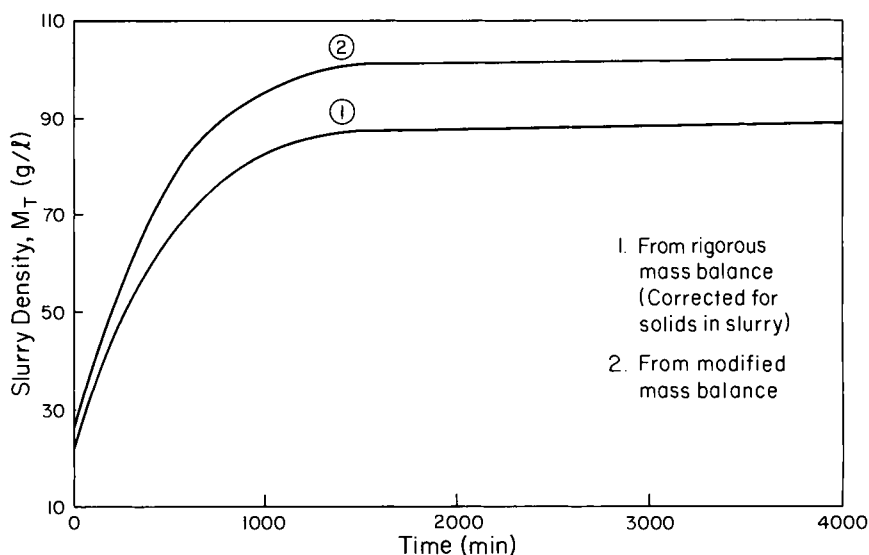


Fig. 8.2-6 Calculated dynamics of slurry density (1) with or (2) without inclusion of void fraction term.

Table 8.2-1

Calculated Gypsum Particle Size with the DDO Configuration

	Particle size (μm)	
	With void fraction changes	Ignoring void fraction changes
MSMPR	45	47
DDO	97	99

sophistication. Stability of CSD in an arbitrary mixed volume is defined by the transient macrodistributed population balance [see Eq. (3.5-10)]:

$$\frac{\partial n}{\partial t} + \frac{\partial}{\partial L}(Gn) + n \frac{d(\log V)}{dt} + B - D - \sum_k \frac{Q_k n_k}{V}$$

with auxiliary solute mass balance and system kinetics

$$V \frac{ds}{dt} = Q_i C_i - Q_o C - \rho k_a V \int_0^\infty \left(\frac{G}{2} \right) n L^2 dL \quad (8.3-1)$$

$$B^0 = B^0(s, n) \quad (8.3-2)$$

and

$$G = G(s) \quad (8.3-3)$$

Equation (8.3-2) recognizes that nucleation may be by secondary mechanisms and would therefore be a function of the distribution n . If the above set of equations admits of a steady, nonoscillating solution for any system disturbance of finite duration, the CSD in the mixed suspension V is stable. Note that such a definition considers nonlinear limit cycles of CSD as unstable operation. More particularly, if the roots of the characteristic equation of the linearized system equations all have negative real parts, the system is considered to be stable to small perturbations around a steady operating condition.

Numerous simplifications of Eqs. (3.5-10) and (8.3-1)–(8.3-3) are made before proceeding with a stability analysis. As discussed in Section 8.1, $dC/dt \cong 0$ for a class II system, and the instantaneous dynamic relationship of Eq. (8.1-6),

$$G = 2 \left(\frac{P}{Q_0} \right) / \left(\tau \rho k_a \int_0^\infty n L^2 dL \right)$$

may be substituted for Eqs. (8.3-1) and (8.3-3). There is only a quantitative difference in stability between class I systems operating with a reasonable crystal yield and class II systems; the latter type is certainly easier to analyze and is perhaps just as instructive, so only class II systems will be considered in the subsequent analysis. However, size-dependent crystal removal has a strong effect through the CSD equations, and even qualitative differences in CSD stability may occur for extremes in particle classification. Sherwin *et al.* [5], in their far-ranging and prescient study of CSD stability, first recognized the importance of particle classification of the larger sizes. Product classification is examined in Section 8.3-2. Such changes in removal rate as a function of size render nonconstant the size distribution equations' coefficient in the variable L and make a rigorous stability analysis difficult at best.

8.3.1 Stability of the MSMPR Crystallizer

The stability of CSD in a class II MSMPR system with a point fines trap is simple, yet instructive, and will be discussed in detail. A point fines trap is defined as a fines-removal system in which the excess particles are segregated and removed at a size vanishingly small compared to the resultant product crystal size.

The appropriate CSD moment equations, in dimensionless normalized form, may be written for this system as

$$\begin{aligned} df_0/d\theta + f_0 &= \rho y^0 \\ df_1/d\theta + f_1 &= \rho f_0 \\ df_2/d\theta + f_2 &= \rho f_1 \end{aligned} \tag{8.3-4}$$

with the growth rate constraint giving

$$\rho = 1/f_2 \quad (8.3-5)$$

and with generalized nucleation-growth rate kinetics

$$n_{\text{net}}^0 = \exp(-\lambda) n^0(G) \quad (8.3-6)$$

or in dimensionless form,

$$y^0 = \exp(\lambda_0 - \lambda) n^0/n_0^0 \quad (8.3-6')$$

where $\lambda = L_F Q_F / GV$ is the exponential decay ratio of the original nuclei, with Q_F and L_F the removal rate and maximum size of the fines, respectively. Decay ratios of 5–7 are not uncommon with excessive dissolving, indicating perhaps one out of a thousand original nuclei are left to grow as product.

These moment equations are linearized about their steady-state values by writing

$$f_j = 1 + \tilde{f}_j, \quad \rho = 1 + \tilde{\rho}, \quad y^0 = 1 + \tilde{y}^0 \quad (8.3-7)$$

where the tilde indicates a deviation from steady state.

This yields the linearized set

$$\begin{aligned} d\tilde{f}_0/d\theta + \tilde{f}_0 &= \tilde{\rho} + \tilde{y}^0 \\ d\tilde{f}_1/d\theta + \tilde{f}_1 &= \tilde{\rho} + \tilde{f}_0 \\ d\tilde{f}_2/d\theta + \tilde{f}_2 &= \tilde{\rho} + \tilde{f}_1 \end{aligned} \quad (8.3-8)$$

Equation (8.3-5) can be linearized with a Taylor expansion to give the first-order approximation

$$\tilde{\rho} = -\tilde{f}_2 \quad (8.3-9)$$

and similarly from Eq. (8.3-6')

$$\tilde{y}^0 = (dy^0/d\rho)|_{\rho=\rho_0, \lambda=\lambda_0} \quad (8.3-10)$$

Substituting Eqs. (8.3-9) and (8.3-10) in Eqs. (8.3-8) and Laplace-transforming with zero initial conditions gives

$$\begin{aligned} F_0(s+1) + \left[(dy^0/d\rho)|_{\rho_0, \lambda_0} + 1 \right] F_2 &= 0 \\ -F_0 + F_1(s+1) + F_2 &= 0 \\ -F_1 + F_2(s+2) &= 0 \end{aligned} \quad (8.3-11)$$

where s is the Laplace operator.

The characteristic equation for this set of transformed, linear, homogeneous differential equations is found to be

$$s^3 + 4s^2 + 6s + 4 + (dy^0/d\rho)|_{\rho_0, \lambda_0} = 0$$

Applying the Routh stability criterion to this characteristic equation gives the criterion for stability of CSD in terms of nucleation-growth rate kinetics as

$$(dy^0/d\rho)|_{\rho_0, \lambda_0} < 20 \quad (8.3-12)$$

Differentiating Eq. (8.3-6') gives the stability relationship in terms of the dissolving parameter λ_0 and nucleation kinetics. Thus,

$$[d(\log n^0)/d(\log G)]|_{n_0^0, G_0} < 20 - \lambda_0 \quad (8.3-13)$$

where the derivative is evaluated at the steady-state conditions. Recognizing that $B^0 = Gn^0$ yields an equivalent stability criterion in terms of nucleation rate. Thus,

$$[d(\log B^0)/d(\log G)]|_{B_0^0, G_0} < 21 - \lambda_0 \quad (8.3-14)$$

For an MSMR crystallizer with no dissolving, $\lambda_0 = 0$, and the well-known criterion

$$[d(\log B^0)/d(\log G)]|_{B_0^0, G_0} < 21 \quad (8.3-14')$$

results.

EXAMPLE 8.3-1

Discuss the stability criterion Eq. (8.3-14') in the context of power-law, Miers, and Volmer nucleation kinetic models.²

a. For a class II system, power-law nucleation kinetics can be written as $B^0 = k_N G^i$ and stability is guaranteed by

$$[d(\log B^0)/d(\log G)]|_{B_0^0, G_0} = i < 21 \quad (8.3-15)$$

Secondary nucleation mechanisms seldom result in power-law exponents i greater than three or four, and in regions where such secondary mechanisms are operative, the MSMR crystallizer is unconditionally stable.³ The value of 21 represents such an extreme kinetic order that the criterion can be thought of as a discontinuity in nucleation rate given by crossing the threshold of an operative nucleation mechanism. It is interesting to note that in the dozen or so MSMR kinetic studies that support the power-law form of kinetics, no CSD instability has been reported.

²See Chapter 5 for discussion of nucleation-growth rate kinetics models.

³Inclusion of the term M_T in the expression for secondary nucleation, that is, $B^0 = k_N G M_T^j$, does not explain cycling of CSD in an MSMR crystallizer and, in fact, predicts a somewhat more stable system.

b. Miers kinetics can be stated as

$$\begin{aligned} B^0 &= k_N (G - G_m)^i, & G > G_m \\ B^0 &= 0, & G < G_m \end{aligned} \quad (8.3-16)$$

for a class II system, where G_m is the value of growth rate at a metastable level of driving forces where nucleation begins. Applying the stability criterion to these kinetics yields

$$[d(\log B^0)/d(\log G)]|_{B^0, G_0} = [G_0/(G_0 - G_m)]i < 21 \quad (8.3-17)$$

It is obvious that as the point of operation G_0 decreases toward the metastable level G_m , the stability criterion is exceeded and an unstable CSD results. Such instability could be prevented by increasing the throughput of the system, thus raising the driving forces sufficiently above the metastable threshold. Miers-type kinetics could explain the cyclic behavior of CSD observed in some industrial crystallizers with long retention times.

c. Volmer kinetics can be stated for a class II system as

$$B^0 = k_1 \exp[-k_2/\log^2(1 + k_3 G)] \quad (8.3-18)$$

where it is assumed that growth rate is a linear function of supersaturation. Applying the stability criterion to Eq. (8.3-18) gives

$$\left. \frac{d(\log B^0)}{d(\log G)} \right|_{B^0, G_0} = \frac{2k_2 k_3 G_0}{(1 + k_3 G_0) \log^3(1 + k_3 G_0)} < 21 \quad (8.3-19)$$

Volmer kinetics are qualitatively the same as Miers kinetics for low driving forces. As the growth rate G_0 at the steady operating point approaches zero, the criterion is exceeded and CSD instability is predicted. As with Miers-type kinetics, this instability could be eliminated by forcing the throughput, thus raising the system driving forces. ♦

In all of the three cases discussed in Example 8.3-1, it should be remembered that the instabilities predicted were essentially at discontinuities of the nucleation function. *For the Miers and Volmer models, instability was predicted at the lower threshold of nucleation at low supersaturations.* In fact, if such discontinuities exist, they should be experimentally measurable and should appear as finite discontinuities in a $\log B^0$ versus $\log G$ plot (see Fig. 8.3-1).

Instability in industrial crystallizers, when it occurs, is usually associated with extremely long solids retention times, and/or solids classification, and/or excessive fines destruction. Thus, it is difficult, if not impossible, from the idealized analysis of the class II MSMR crystallizer to pinpoint the source of difficulty. A further difficulty in explaining CSD instability

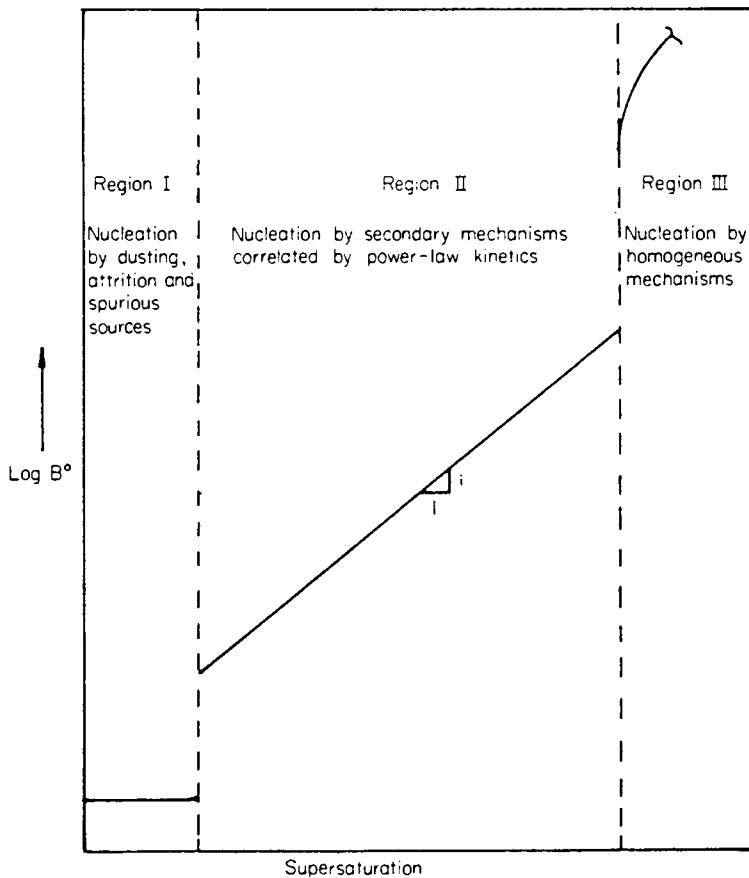


Fig. 8.3-1 Hypothetical nucleation-growth rate plot showing discontinuous regions causing CSD instability in an MSMPR crystallizer.

with the Miers and Volmer models is that instability is often observed with high rather than low driving forces when excessive fines dissolving forces the supersaturation to high levels. However, it is possible to explain this apparent anomaly. Secondary low-order mechanisms of nucleation predominate at supersaturations less than the threshold limits predicted by the Miers and Volmer models. The stability criterion can be exceeded when the suddenly appearing homogeneous nucleation predicted by the Miers and Volmer models, added to nucleation produced by secondary mechanisms, causes a discontinuity in total nucleation rate. The metastable limit would then be properly described as an upper level of supersaturation where a rapid increase in total nucleation occurred due to the beginning of homo-

neous nucleation, rather than a lower limit of supersaturation where all nucleation ceased. Conceivably, there exists a truly lower metastable limit below which even secondary nucleation ceases and crystal grain is only generated by breakage, dusting, and spurious sources. Such hypothetical upper and lower discontinuities in nucleation rate, shown in Fig. 8.3-1, could explain instability with both excessive fines removal and long retention times.

The contradictory effects of fines dissolution on CSD instability can be observed from the above discussion. Raising the supersaturation driving forces by fines destruction could, in principle, move the system away from a Miers-type lower metastable point, thus stabilizing the system. Alternatively, the driving forces could be forced toward an upper metastable threshold of homogeneous nucleation, thus causing instability. Much light could be shed on the problem of CSD instability if a bench-scale MSMPR unit could be operated as a CSD oscillator.

A further effect of fines destruction is that transient CSD response from system upsets is greatly improved due to accelerated removal of the excursions of nuclei. In long-holding-time crystallizers, it is somewhat difficult to distinguish CSD transients from CSD instability, thus making difficult an unambiguous judgement on whether fines removal is an asset or detriment to CSD dynamics in such a system. Figure 8.3-2 plots the

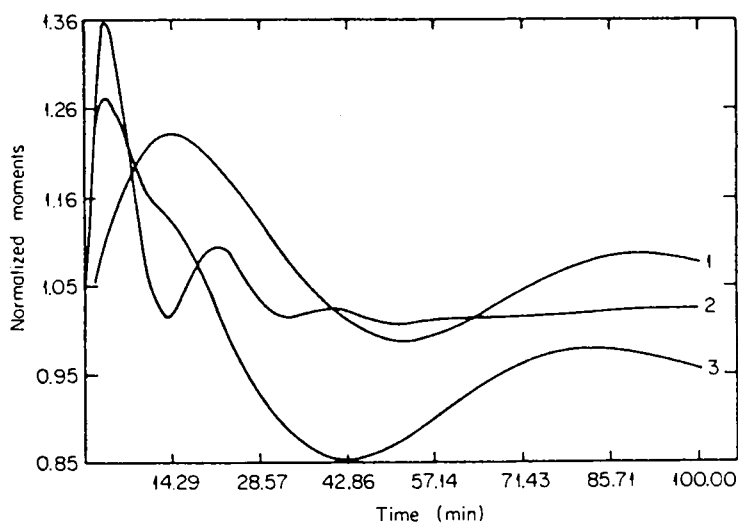


Fig. 8.3-2 Response of dimensionless total crystal population to step increase in production rate. (1) MSMPR, (2) fines removal — no recycle, (3) fines removal — solute recycle. (After H. E. Nuttall, Ph.D. thesis, University of Arizona, Tucson, Arizona, 1971, unpublished.)

dimensionless total crystal population (normalized zeroth moment) after a step change in production rate for a class II system operating with a mean retention time of 20 min and with nucleation sensitivity parameter $i = 5$. Curve 1 represents the MSMPR case, while curves 2 and 3 represent the same system with a distributed fines trap removing fines at a size representing a significant fraction ($\sim 20\%$) of the total production rate and with advance or dissolving and recycle of these fines, respectively. Curve 2 illustrates the excellent improvement in transient response that is expected with fines removal if the solute resources represented by fines removal are not recycled. Such performance could be obtained by recycling fines to crystallizer feed and maintaining constant feed composition and/or dissolving fines at a smaller size but higher withdrawal rate, in which case the fines would represent a negligible fraction of solute resources. Curve 3 illustrates that when an appreciable mass fraction of dissolved fines is recycled, negligible improvement in transient response to system upsets is obtained. It should be pointed out that the CSDs and hence zeroth moments are quite different in each of these three cases; thus, the above comments were based on response time and not absolute values of these dimensionless moments.

Classified product removal results in poorer transient response characteristics as well as lowering of the stability region. As described in the study by Sherwin *et al.*, idealized classification, represented by no particle removal

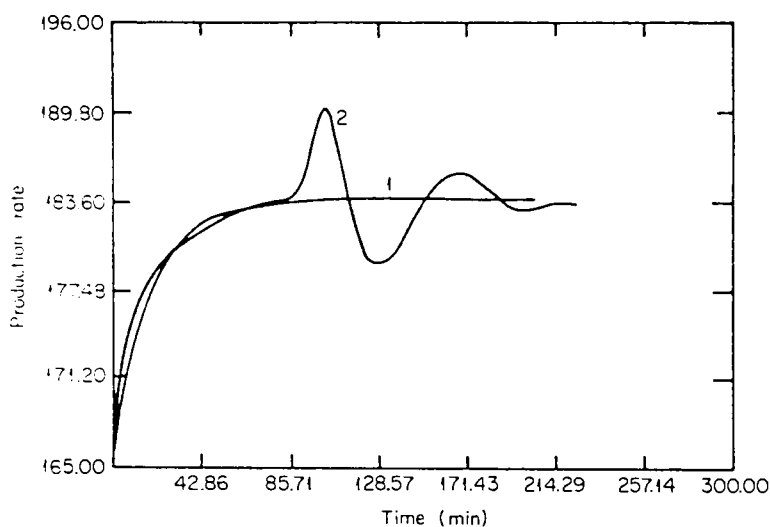


Fig. 8.3-3 Dynamic response of production rate after a 10% increase in solute resources with and without classified product removal. (1) MSMPR, (2) CPR. (After H. E. Nuttall, Ph.D. thesis, University of Arizona, Tucson, Arizona, 1971, unpublished.)

up to product size and immediate removal at that size, severely unstabilizes CSD [5]. More realistic classification models, in which mixed removal occurs up to product size with accelerated removal thereafter, result in a variable-coefficient dynamic population balance, which is examined in the next section. Figure 8.3-3 illustrates the detrimental effect of classified product removal on CSD transient response for the same system shown in Fig. 8.3-2. These curves plot the dynamic response of production rate after a 10% increase in solute resources. Curve 1 represents the MSMR case and curve 2 represents classified product removal.

8.3.2 Stability of the R - z Classified Product Crystallizer

A realistic crystallizer model that takes into account fines dissolving as well as intentional or inadvertent product classification is the so-called R - z model (see Chapter 7), wherein the fines and oversize are removed at R and z times the midsize range, respectively. Some industrial crystallizers with such a configuration have been reported to develop limit cycles of CSD. As the R - z crystallizer configuration encompasses most of the features of current mixed-magma continuous crystallizers, it is instructive to review a detailed stability analysis of this configuration. This stability study by Randolph *et al.* [6] only considered the stability limits, that is, the parameters defining the point of incipient instability, without simulation of the predicted CSD dynamics. Subsequent CSD simulators have verified these stability limits in all cases and have displayed some of the predicted CSD limit cycles. The stability analysis of the R - z crystallizer [6] starts with the dynamic population balance and class II growth-rate constraint. Thus

$$\frac{\partial n}{\partial t} + G \frac{\partial n}{\partial L} + \frac{h(L)n}{\tau} = 0 \quad (8.3-20)$$

and

$$G = \frac{P + (R - 1)Q\rho k_v \int_0^{L_F} nL^3 dL}{\rho VA/2} \quad (8.3-21)$$

where

$$h(L) = \begin{cases} R, & L < L_F \\ 1, & L \text{ in } (L_F, L_p) \\ z, & L > L_p \end{cases} \quad (8.3-22)$$

Note that the mass of dissolved recycled fines is included in the growth-rate constraint of Eq. (8.3-21). As more dissolved fines mass is recycled to the crystallizer, the growth rate is forced to higher levels. Conventional power-law nucleation kinetics are assumed. Thus

$$B^0 = k_N M_T^j G^i \quad (8.3-23)$$

These equations are made nondimensional and normalized by dividing by their steady-state values. These dimensionless transformations are given as

$$y = \frac{n}{n_0^0}, \quad y^0 = \frac{n^0}{n_0^0}, \quad \phi = \frac{G}{G_0}, \quad x = \frac{LQ}{VG_0}$$

$$\theta = \frac{tQ}{V}, \quad f_{j,k} = \frac{\int_0^{L_k} L^j n dL}{\int_0^{L_k} L^j n_0 dL}, \quad h = \frac{Q(L)}{Q}, \quad \bar{y} = y(x, 0)$$

In terms of dimensionless variables the set of dynamic CSD equations becomes

$$\frac{\partial y}{\partial \theta} + \phi \frac{\partial y}{\partial x} + hy = 0$$

$$\phi = \frac{1 + \beta f_{3,1}}{1 + \beta} \left(\frac{1}{f_2} \right) \quad (8.3-24)$$

$$y^0 = f_3 \phi^{i-1}$$

In the above, β is the ratio of fines mass dissolved to external production, given as

$$\beta = \frac{(R-1)}{6D_p} \int_0^{x_F} x^3 \bar{y} dx \quad (8.3-25)$$

where the function $D_p(G)$ is given as

$$D_p(G) = \frac{w(Rx_F)}{R^4} + \exp[-(R-1)x_F][w(x_p) - w(x_F)]$$

$$+ \frac{1}{z^3} \exp[(z-1)x_p - (R-1)x_F][1 - w(zx_p)]$$

with the dimensionless arguments x_F and x_p as above and where $w(p)$ is the dimensionless gamma distribution

$$\frac{1}{6} \int_0^p x^3 e^{-x} dx$$

tabulated in Appendix A. Equations (8.3-24) are nonlinear and are linearized by standard perturbation techniques, taking advantage of the unity value of all normalized steady-state variables to give the following linearized set in terms of small perturbations from steady state. Thus

$$\frac{\partial y}{\partial \theta} - \left(\frac{\beta}{1 + \beta} \right) h \bar{y} f_{3,1} + h \bar{y} f_2 + \frac{\partial y}{\partial x} + hy = 0 \quad (8.3-26)$$

with boundary condition

$$y^0 = jf_3 + \left(\frac{i-1}{1+\beta} \right) \beta f_{3,1} - (i-1)f_2 \quad (8.3-27)$$

Equation (8.3-26) represents the linearized dynamics of the class II crystallizer of arbitrary process configuration [given by the removal probability function $h(x)$] with magma-dependent nucleation kinetics and accounting for a fraction $\beta/(1+\beta)$ of total internal production rate recycled from a fines dissolver.

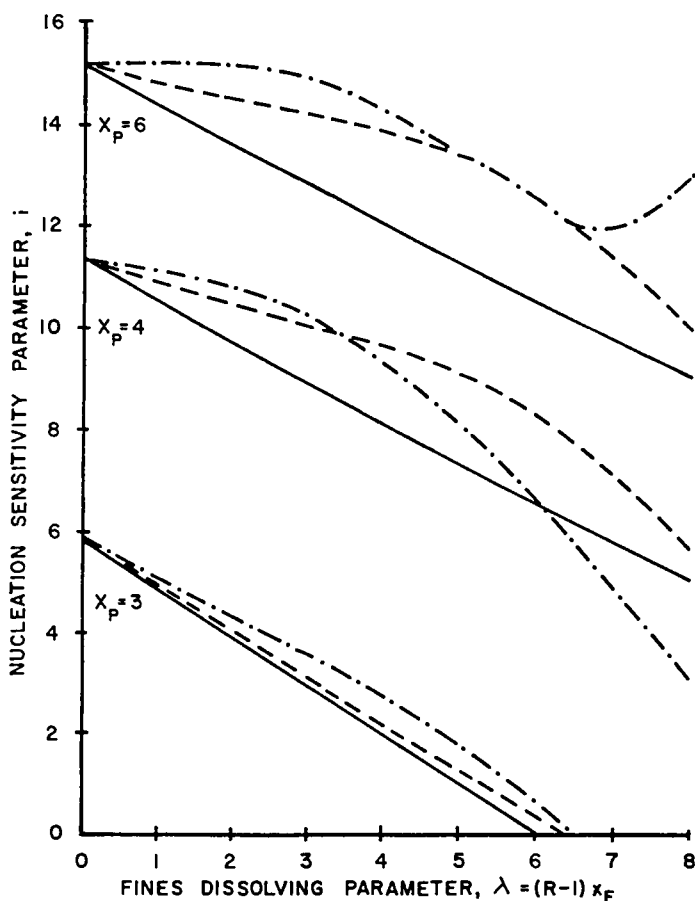


Fig. 8.3-4 Crystallizer stability for the R - z crystallizer with fines destruction and classified product removal (magma-dependent nucleation). Solid line: $x_F = 0.1$; dashed line: $x_F = 0.3$; dotted-dashed line: $x_F = 0.5$. $j = 1$, $z = 7$. (After Randolph *et al.* [6].)

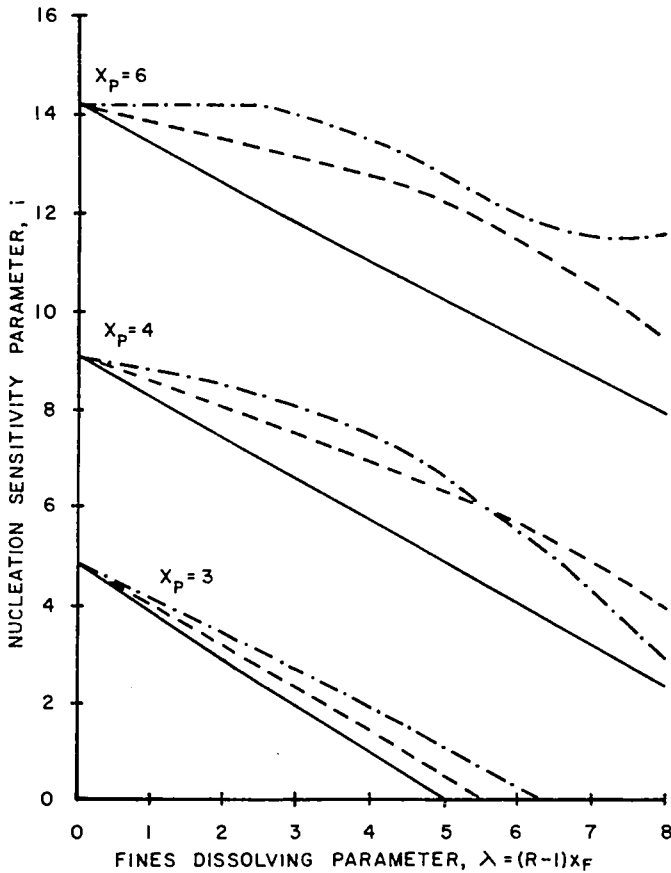


Fig. 8.3-5 Crystallize stability for the R - z crystallizer with fines distribution and classified product removal (magma-independent nucleation). Key is same as for Fig. 8.3-4; $j = 0$. (After Randolph *et al.* [6].)

The stability of this linearized set was determined in terms of relative nucleation/growth rate sensitivity i for reasonable ranges of the system parameters R , z , x_F , and x_p for the R - z fines removal/classified product crystallizer. The stability analysis follows closely the spectral technique of Lei *et al.* [7]. The product classification introduced in the R - z crystallizer model seriously destabilizes CSD, resulting in a much lower value of the nucleation-growth rate sensitivity parameter i at which instability would be predicted. Figures 8.3-4 and 8.3-5 display those low values of the parameter i for which CSD instability will be expected, with and without the influence of slurry density (i.e., $j = 1$ or 0). The stability limits in Fig. 8.3-4 and

8.3-5 are plotted versus the dimensionless dissolving parameter $\lambda = (R - 1)L_F/G\tau$ and are shown for product classification at various dimensionless sizes x_p .

Inspection of Figs. 8.3-4 and 8.3-5 shows that both product classification (at a low size ~ 3 times the characteristic size $G\tau$) and fines dissolving destabilize the CSD and could thus result in CSD limit cycles at the low values of nucleation sensitivity observed from MSMPR kinetics studies. This model of instability is referred to as "low-order cycling" to distinguish it from the higher-order (discontinuous) nucleation sensitivity values discussed in Section 8.3.1 for the MSMPR configuration.

A problem in unequivocally determining the mechanism of CSD cycling in an unstable crystallizer is that few well-documented experimental studies have been published that show this behavior. Randolph *et al.* [3] published

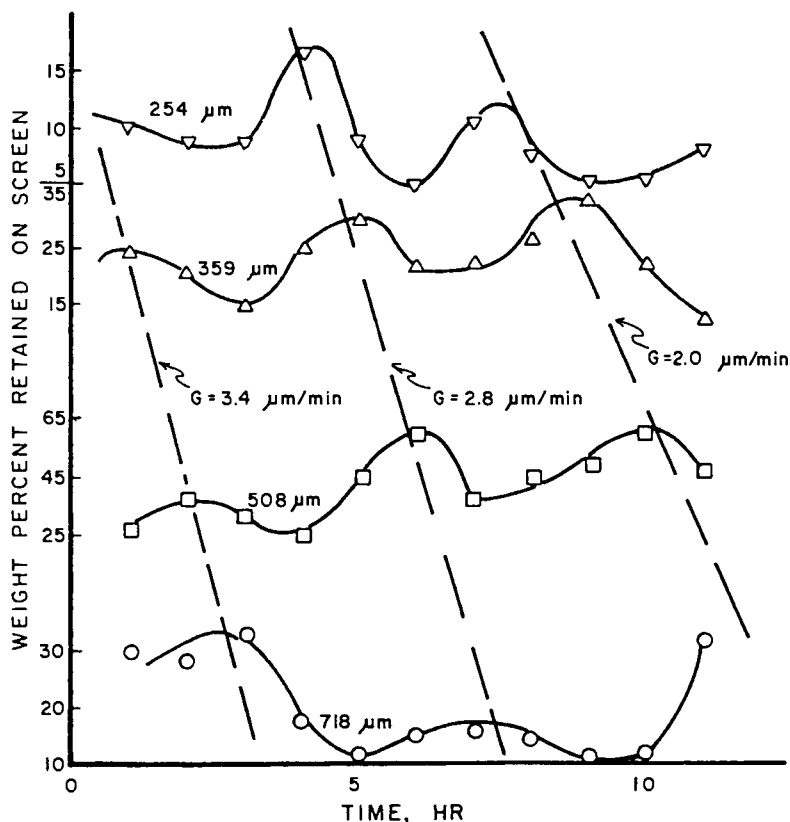


Fig. 8.3-6 CSD cycling in a bench-scale KCl crystallizer. $P = 8.5$ g/min; $Q_E = 150$ cm³/min; $Q_R = 2700$ cm³/min; feed tank temperature = 150°F. (From Randolph *et al.* [3].)

Table 8.3-1

Summary of Experimental and Predicted Stability for Crystallizer Runs

Run	Experimental run parameters used in computer simulation						Stability		Cycle period (min)		Time average growth rate ($\mu\text{m}/\text{min}$)	
	L_F (μm)	Q_F (l/min)	Q_R (l/min)	Q_p (l/min)	L_p^- (μm)	$(z-a)/(L_p^+ - L_p^-)$ (μm^{-1})	Exp.	Simulation	Exp.	Simulation	Exp.	Simulation
3/28/74	100	0.212	1.22	—	—	—	Stable	Stable	—	—	1.1	1.5
2/22/74	—	0.217	—	—	—	—	Stable	Stable	—	—	1.68	1.7
4/4/74	—	0.216	—	—	—	—	Stable	Stable	—	—	1.25	1.7
3/10/74	100	0.222	1.04	—	200	0.0038	Unstable	Unstable	400	510	—	1.9
7/15/76	150	0.400	3.00	—	—	—	Stable	Stable	—	—	4.5 ^a	4.8
6/29/76	90	0.285	2.70	0.150	300	0.0350	Unstable	Unstable	240	200	2.7 ^b	3.5
8/24/76	50	0.202	0.46	0.135	300	0.0320	Unstable	Unstable	390	270	1.3 ^b	2.1
8/31/76	60	0.250	1.36	0.130	450	0.0320	Unstable	Unstable	350	290	2.0 ^b	2.7

^aFrom fines trap analysis.

^bFrom sieve peak movement.

a study of a bench-scale KCl crystallizer having fines destruction and classified product removal that exhibited CSD cycling. The crystallizer was simulated using a dynamic version of the R - z crystallizer model [4]. Figure 8.3-6 shows experimental CSD limit cycles from this crystallizer when operated under unstable conditions.

Note that an estimate of the crystal growth rate as measured by the peak progression technique is $\sim 3 \mu\text{m}/\text{min}$, compared to the $1 \mu\text{m}/\text{min}$ value estimated for an industrial KCl crystallizer (Fig. 8.3-1). The cycle period is also shorter for the bench-scale unit. Table 8.3-1 shows experimental and simulated results from the bench-scale KCl study. Excellent agreement was obtained between experimental and calculated predictions of stability.

8.4 Feedback Control of CSD

Little work has been published on the problem of on-line feedback control of CSD. What little published work exists often is in the form of a theoretical control simulation assuming on-line CSD measuring technology that has not yet been developed. Nevertheless, these theoretical studies have sparked interest in the subject and have led to some experimental studies that have actually demonstrated the possibility of on-line CSD control.

8.4.1 Control of Nuclei

Gupta and Timm [8] theoretically studied feedback control of CSD using the set of dynamic moments of the MSMR crystallizer as response variables and using the zeroth moment (proportional to the total crystal number N_T) as the manipulated variable. (The zeroth moment would be largely dominated by the fines in the distribution, but how this variable was to be measured or manipulated in a practical sense was not disclosed.) Lie *et al.* [7] considered CSD control in a mixed-magma crystallizer using fines as a measured variable and throughput or fines removal as the manipulated variable. Beckman and Randolph [4] used a simulation of a complex RTD crystallizer (the R - z model) to show that estimation of nuclei density could be used to eliminate cycling and/or reduce transients of CSD. The fines removal rate Q_F was used as the manipulated variable in the simple proportional control law

$$(Q_F - \bar{Q}_F)/\bar{Q}_F = K_c(n^0 - \bar{n}^0)/\bar{n}^0 \quad (8.4-1)$$

where the overbar designates the steady state. A value of $K_c = 0.25$ stabilized an unstable R - z crystallizer, as also predicted by the theoretical stability study of Randolph *et al.* [6]. All of the above studies provoked interest in the possibility of instrumental feedback control of CSD, but the

field of experimental verification of control schemes lay fallow. This lack of experimental activity was mainly due to the fact that no reliable on-line control instrument was available to measure the state of the system (in the sense of on-line CSD measurements).

Randolph *et al.* [9] applied a light-scattering instrument to a well-conditioned fines stream (in the same 18-l bench-scale KCl crystallizer used by Beckman [3]) and showed that this partial measure of the state of the system gave on-line estimation of crystal nucleation and growth rates, suitable for control purposes. The possibility of controlling CSD using on-line supersaturation measurements was also studied (Rousseau and Howell [10]). Supersaturation measurements would have the advantage of a faster response time (before a concentration-induced burst of nuclei occurred) but would suffer from the facts that a supersaturation measurement would have to be developed for each crystal system controlled and that secondary nucleation does not depend only on supersaturation.

Randolph and Low [11] made the first attempt at experimental on-line CSD control by estimating nuclei density from light-scattering measurements in a fines-removal stream, manipulating either fines removal rate or the fraction of fines dissolved. Manipulation of fines removal rate gave poorer CSD control (when the system was challenged with a large burst of nuclei) than partial fines dissolving, possibly because the fines destruction stream was removed from the same fines-settling trap used for fines measurement. Thus changes in fines flow rate (the manipulated variable) upset fines measurement (the measured variable). A root-mean-square (rms) measurement of deviations in the screened product-sized crystals was used as a control performance index. Variations in product CSD were in general reduced using this on-line control scheme, but the experiments were not of a long enough duration for an unequivocal evaluation of controller efficacy. A patent was granted on this control scheme [12] based on the observation that at least about 3% of the fines mass had to be present in each fines-measurement "size window" in order for the estimate of nuclei density to be valid.

Randolph *et al.* [13] repeated these control experiments over a longer time period and demonstrated beyond doubt the efficacy of CSD control. Again the system was the same 18-l bench-scale KCl crystallizer, nuclei density was the inferred control variable, the fraction of a constant nuclei flow stream diverted to a total dissolver was the manipulated variable, a proportional control algorithm [Eq. (8.4-1)] was implemented, and the rms deviation of product crystals was used as a performance index (PI). The disturbance was again a sharp burst of nuclei at the beginning of the control period. Table 8.4-1 shows R_i values, the ratio of PIs for different screen sizes, without and with CSD control. Note that the average value of

Table 8.4-1

Ratio of Performance Indices (PI_2) with and without CSD Control^a

Size ($m \times 10^{-6}$) retained on	$R_i^b \frac{PI_2 \text{ without control}}{PI_2 \text{ control}}$
1000	1.6
841	2.7
707	5.9
595	3.4
500	3.4
< 500	3.2

^aAfter Randolph *et al.* (13).

^b $\bar{R} = \sum_i \Delta \bar{W}_i R_i = 3.45$.

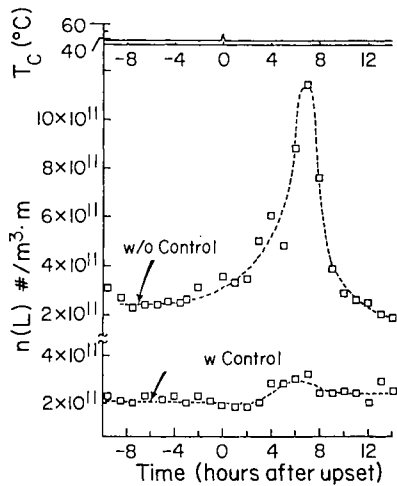


Fig. 8.4-1 Variation in population density in product crystals with and without nuclei density control. $\bar{L} = 458 \times 10^{-6}$ m. (After Randolph *et al.* [13].)

R , weighted by the mass fraction at that size, was 3.45. Thus on-line CSD control, by inferred control of nuclei density, reduced the rms fluctuations in product size by a factor of 3.5 for the particular upset of nucleation rate studied. Figure 8.4-1 shows the nuclei upset in the product after it has grown to an average size of $\sim 360 \mu\text{m}$. Note that this upset was virtually damped out in run 36 by application of nuclei density control. Figure 8.4-2 shows the nuclei pulse as a disturbance in product weight fraction at 460 and 650 μm . Note the large upset in weight fraction of product crystals, which only shows up 12 h after the upset in nucleation. Figure 8.4-3 shows

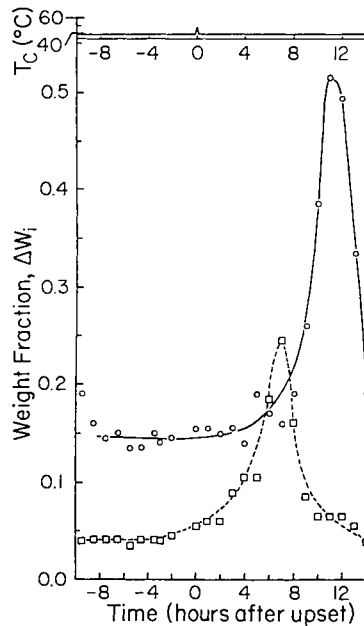


Fig. 8.4-2 Upsets in product weight fraction at sizes 460 (\square) and 650 (\circ) μm (without nuclei density control). (After Randolph *et al.* [13].)

the same upset in run 36 with CSD control. Note that nuclei density control has virtually eliminated product CSD upsets. This CSD control algorithm does not require any knowledge of the crystallizer process dynamics to implement. However, some means of fines segregation and destruction must be available. Many crystallizer upsets, such as concentration, temperature, and additives, first show up as disturbances in nucleation rate. Thus control of nuclei density should be effective as a generalized CSD control algorithm.

The two studies of nuclei density control cited above inferred n^0 by extrapolation of a conventional MSMPR semilog plot of fines population density [11] or by integrating the fines distribution to estimate nuclei density as $n^0 = KM_{TF}/(L_{4,3})_F^4$ [13]. These techniques represent derivative and integral methods of data regression, respectively. The latter technique smooths out much of the data noise and is preferred for control applications. An observation that was made using the integral technique was that the measured value of fines slurry density M_{TF} , rather than mean size $(L_{4,3})_F$, drove the n^0 estimate. Thus a simpler on-line fines slurry density instrument, rather than a particle size analyzer, may be sufficient for CSD control.

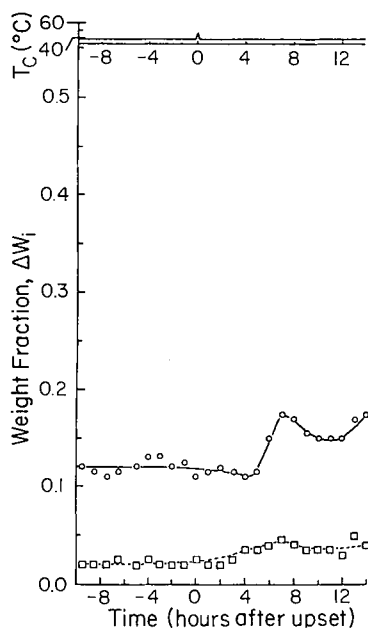


Fig. 8.4-3 Upsets in product weight fraction at sizes 460 (\square) and 650 (\circ) μm (with CSD control). (After Randolph *et al.* [13].)

8.4.2 CSD Control Using a State Space Formulation

Modern control theory often tries to cast the equations of the process to be controlled into a set of constant-coefficient linear ordinary differential equations, the so-called state space formulation, suitable for dynamic simulations and/or development of a control matrix with quantitative gains for the respective controller elements. Thus in compact vector/matrix notation the system equations are cast in the form

$$\dot{\mathbf{X}} = \mathbf{A}\mathbf{X} + \mathbf{B}\mathbf{U} \quad (8.4-2)$$

and

$$\mathbf{Y} = \mathbf{C}\mathbf{X} \quad (8.4-3)$$

where \mathbf{X} is the vector of internal variables describing the system, \mathbf{U} is a vector of input variables (some upsets, some manipulated), \mathbf{Y} is the vector of output variables (Y_i may or may not be equal to X_i), and where \mathbf{A} , \mathbf{B} , and \mathbf{C} are coefficient matrices in a linearized description of the process. Examples of state or output variables might be population densities in the crystallizer or discharge at different sizes L_i .

The control law in a state space formulation is then given as

$$\mathbf{U} = -\mathbf{K}\mathbf{Y} \quad (8.4-4)$$

where \mathbf{K} is the control matrix and specifies the gain for all of the manipulated variables in \mathbf{U} .

The crystal moments in MSMPR or batch crystallizers form a natural set of internal state variables \mathbf{X} , even though the moments must in general be calculated from the population density $n(L)$. The moments of complex RTD crystallizers (e.g., the R - z crystallizer) cannot be stated in a closed analytical form and thus are not useful as the state variables in a state space formulation of the control problem. This is unfortunate, as complex RTD crystallizers, rather than the simple MSMPR configuration, exhibit CSD limit cycles and a CSD that is sometimes difficult to control. Epstein and Sowul [14] used the linearized moment equations for the MSMPR crystallizer as state variables to easily construct a state space vector/matrix representation of CSD instability in this system.

Johnson *et al.* [15] used the moments of the MSMPR crystallizer as natural state variables in a state space control study of this crystallizer configuration. Temperature and slurry density (proportional to the third moment) were assumed to be measured with the rest of the moments estimated from the vector/matrix control equations. Numerical calculations showed excellent CSD responses to programmed setpoint changes and system upsets. Implementation of this state space control algorithm in an experimental study would require development of an exceptionally accurate slurry density instrument and would require the crystallizer to be well represented by the MSMPR model. Fortunately, well-designed MSMPR crystallizers seldom need a CSD controller; they are stable and self-correcting via their own internal feedbacks (e.g., the information feedback shown in Fig. 1.2-1).

The equations for a complex crystallizer (e.g., the R - z model) have been cast in state space vector-matrix form by Tsuruoka and Randolph [16]. The population balance equation, a one-dimensional hyperbolic wave equation, is put in the form of a set of ordinary differential equations with a slowly changing time-dependent coefficient matrix \mathbf{A} in the state space formulation. This state space formulation is illustrated in the following example.

EXAMPLE 8.4-2-1

Start with the dimensionless population density equations of the class II R - z crystallizer and transform the set to a state space vector-matrix formulation. (See Section 8.3.2 for a description of the class II R - z crystallizer.)

The starting point of the mathematical development is the following set of equations (Randolph *et al.* [6]), generally recognized to represent CSD

dynamics in crystallizers of complex configuration, such as with fines dissolving and classified product removal (the R - z crystallizer).

$$\frac{\partial u}{\partial \theta} + \phi \frac{\partial u}{\partial x} + hu = 0 \quad (8.4-5)$$

$$\phi = \frac{1 + \beta f_{3,1}}{1 + \beta} \left(\frac{1}{f_2} \right) \quad (8.4-6)$$

$$u_0 = f_3 \phi^{i-1} \quad (8.4-7)$$

where the variables have been rendered dimensionless and normalized by the following transformations:

Time	$\theta = \frac{t}{V/Q_p}$
Population density	$u = \frac{nG^0}{B^0}$
Growth rate	$\phi = \frac{G}{G^0}$
Particle size	$x = \frac{LQ_p}{VG}$
Removal rate	$h = \frac{Q(L)}{Q_p}$
Fraction mass dissolved	$\beta = \frac{(R-1)}{6D_p} \int_0^{x_F} x^3 \bar{u} dx$

where D_p is a dimensionless function of the third-order gamma distribution evaluated at the fines and product classification sizes [see Eq. (8.3-26)].

The normalized fractional moment is

$$f_{j,k} = \frac{\int_0^{L_k} L^j n dL}{\int_0^{L_k} L^j \bar{n} dL}$$

and where

$$h(L) = Q(L)/Q_p = \begin{cases} R, & x < x_F \\ 1, & x \text{ in } (x_F, x_p) \\ z, & x > x_p \end{cases}$$

which represents the size-dependent particle removal rate in the R - z crystallizer. Equation (8.4-5) is converted into a semidiscrete approximate formula using a fourth-order correct central difference. Thus,

$$\frac{du_i}{d\theta} + \phi \frac{u_{i-2} - 8u_{i-1} + 8u_{i+1} - u_{i+2}}{12\delta} + h_i u_i = 0 \quad (8.4-8)$$

$$A(\theta) = \frac{\phi}{12\delta} \begin{bmatrix} -22 + \frac{12h_0\delta}{\phi}, 36, & -18, & 4, & 0, & \dots & , & 0 \\ -4, & -6 + \frac{12h_1\delta}{\phi}, & 12, & -2, & 0, & \dots & , & 0 \\ 1, & -8, & \frac{12h_2\delta}{\phi}, & 8, & -1, & 0, & \dots & , & 0 \\ & & & & \vdots & & & & \\ 0, & \dots & , & 0, & 1, & -8, & \frac{12h_{i-1}\delta}{\phi}, & 8, & -1, & 0, & \dots & , & 0 \\ & & & & & \vdots & & & & & & & \\ 0, & \dots & & & & & 0, & 2, & -12, & 6 + \frac{12h_L-1\delta}{\phi}, & & 4 \\ 0, & \dots & & & & & & 0, & 4, & 18, & -36, & 22 + \frac{12h_L\delta}{\phi} \end{bmatrix}$$

Fig. 8.4-4 Matrix $A(\theta)$.

Two fictitious grid points are needed to approximate the boundary condition for Eq. (8.4-8). The sequential scheme of the numerical calculation is as follows. Suppose that all grid points, including fictitious points u_{-1} and u_{-2} , are known at time = 2. These known points give the next time-step points with a fourth-order correct approximation using four points. Nuclei density u_0 is independently calculated [from Eq. (8.4-7)] using all of the real points at time = 2 and replaced at time = 3. Then fictitious points are calculated using the new grid points at time = 3 and so forth.

Using a vector-matrix form, Eq. (8.4-5) becomes

$$\dot{\mathbf{u}}(\theta) = \mathbf{A}(\theta)\mathbf{u}(\theta) \quad (8.4-9)$$

where vector \mathbf{u} is

$$\mathbf{u} = (u_0, u_1, \dots, u_N)' \quad (8.4-10)$$

and A is shown in Fig. 8.4-4. The form of matrix A is pentadiagonal, as seen from Figure 8.4-4. Thus, matrix A is sparse, permitting rapid calculations, but can be of high order to cope with the parameter sensitivity of Eq. (8.4-5).

Equation (8.4-9) is of homogeneous state variable form, with a slowly changing time-variant matrix, and is useful as it stands for direct simulation of CSD dynamics and demonstration of system stability. To implement

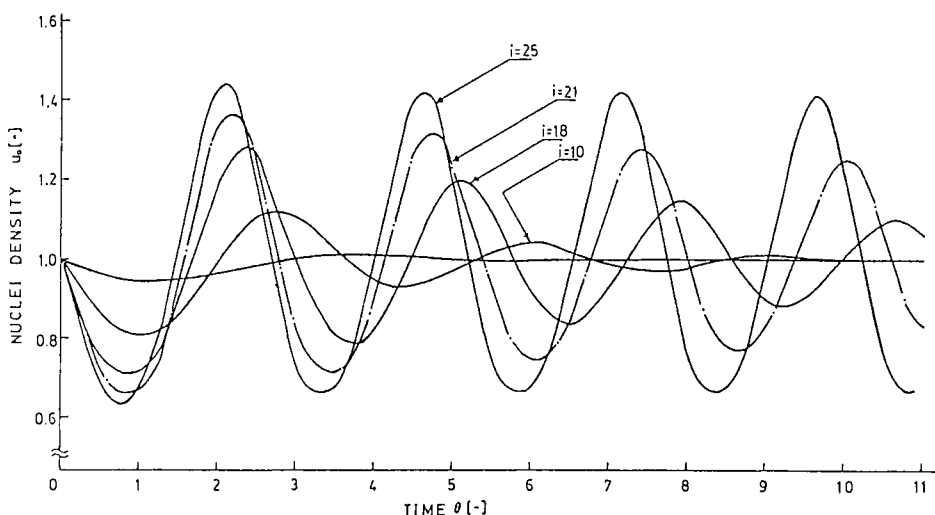


Fig. 8.4-5 Simulation results for an MSMPR crystallizer with various nuclei sensitivities.

numerical calculations, Eq. (8.4-9) can be arranged in a general form with an external input, represented as

$$\dot{\mathbf{u}}(\theta) = \mathbf{A}(\theta)\mathbf{u}(\theta) + \mathbf{B}\mathbf{r}(\theta) \quad (8.4-11)$$

where \mathbf{B} is the elementary matrix and $\mathbf{r}(\theta)$ represents external perturbations to the system. Equation (8.4-11) is converted to discrete form as

$$\mathbf{u}_{m+1} = \Phi_{m+1}\mathbf{u}_m + \int_0^{\theta_m} \Phi_m(\theta - a) \mathbf{B} \mathbf{r} m d\sigma \quad (8.4-12)$$

with

$$\Phi_m = \exp(\mathbf{A}_m \Delta\theta) \quad (8.4-13)$$

If the time increment $\Delta\theta$ is small enough and unique, Eqs. (8.4-12) and (8.4-13) can be rewritten as

$$\mathbf{u}_{m+1} = \Phi_{m+1}\mathbf{u}_m + \Delta\theta \frac{(\Phi_m \mathbf{B} \mathbf{r}_{m+1} - \Phi_m \mathbf{B} \mathbf{r}_m)}{2} \quad (8.4-14)$$

where

$$\Phi_m = \exp(\mathbf{A}_m \Delta\theta) \quad (8.4-15)$$

Simulations can be implemented using this algorithm as described below. Figure 8.4-5 shows simulation results for an MSMPR crystallizer with various nuclei sensitivity values i . The critical stability point for an MSMPR crystallizer is $i_c = 21$. These simulations, if carried out for longer times, show convergence for $i < 21$ and divergence for $i > 21$. Figure 8.4-6 shows

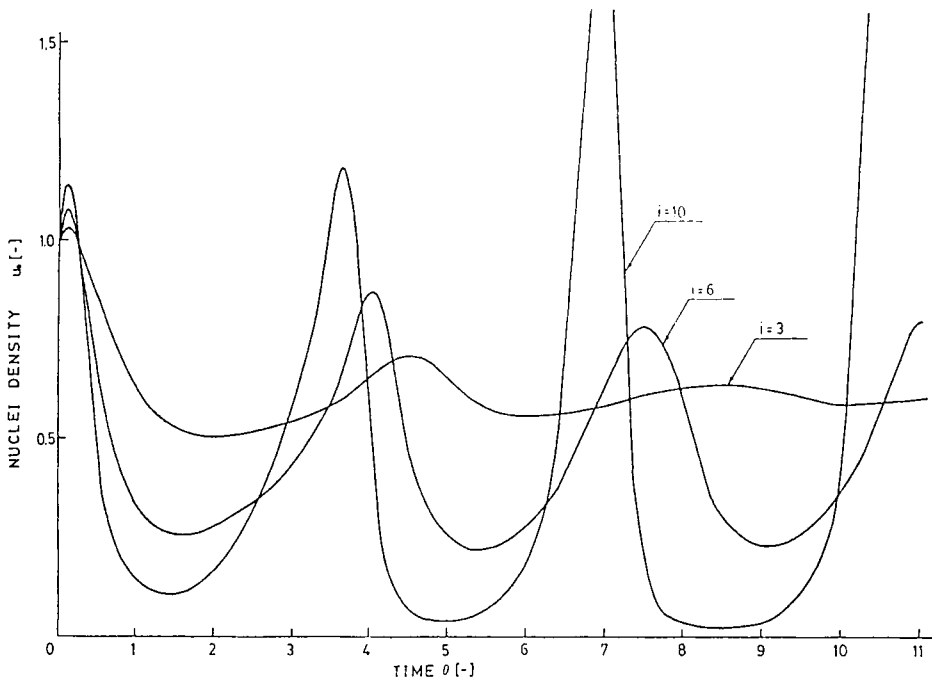


Fig. 8.4-6 Simulation results in nuclei density for an R - z crystallizer with various nuclei sensitivities, where $R = 8.5$, $z = 7$, $x_F = 0.2$, $x_p = 3$, and $j = 0$.

the simulation results for an R - z crystallizer with various nuclei sensitivity values. In this case, the critical point is $i_c = 3.8$ (Randolph *et al.* [6]). The dynamic CSD curves are consistent with this stability criterion. This simulation algorithm thus satisfies these criteria and can be assumed to numerically predict dynamic CSD in a continuous crystallizer.

8.5 Summary

Unsteady-state population and single-solute mass balances were presented, both on a clear-liquor or total-slurry basis and for class I (variable per pass yield) and class II (high yield) systems. It was demonstrated that a simplified mass balance, which ignores changes in liquor void fraction, gives calculated CSD dynamics only quantitatively different from dynamics calculated with the rigorous form of the solute balance.

CSD transients, experimental and calculated, were illustrated for MSMPR and R - z types of crystallizers. CSD stability limits were calculated for both

the MSMPR and R -z crystallizer types. Experimental evidence of CSD cycling in an R -z crystallizer was shown.

An experimental study of on-line CSD control was presented in which the manipulated variable was the fraction of fines flow reporting to a fines dissolver and the control variable was inferred nuclei density.

Finally, attempts at phrasing the CSD control problem in a state space formalism were discussed. A vector-matrix state space formulation of a complex crystallizer was derived. This formulation should prove useful for more realistic CSD control studies.

Nomenclature

A_T	Total specific crystal area, (length) ² /volume	m_{3r}	Third moment in fines trap
B^0	Birth rate at zero size, number/(volume time)	M_T	Slurry density in crystallizer, mass/volume
B-D	Net particle birth density distribution, number/(volume length time)	n^0	Nucleation density at zero size, number/(volume length)
C	Solute concentration, mass/volume	n	Population density function, number/(volume length)
C_F	Feed liquor solute concentration, mass/volume	P	Solids product rate, mass/time
C_0	Solute concentration initial condition, mass/volume	P_r	Solids destroyed in fines destruction system, mass/time
C_s	Saturated solute concentration, mass/volume	Q_{cla}	Slurry flow rate of clear liquor advance, volume/time
F	Ratio of feed rate to product rate, Q_F/Q_P	Q_f	Slurry based liquor feed rate, volume/time
f_j	Dimensionless moments	Q_p	Slurry based liquor feed rate, volume/time
G	Diameter growth rate, length/time	Q_r	Slurry based fines destruction rate, volume/time
$h(\xi)$	Withdrawal function	Q_z	Slurry based classifier feed rate, volume/time
i	Kinetic power of growth rate in nucleation birth function	R	Fines destruction ratio, $(Q_R + Q_P)/Q_P$
j	Kinetic power of solids concentration in nucleation birth function	t	Time
k_A	Area shape factor	V	Slurry or crystallizer volume, (length) ³
K_c	Proportional control constant	V_L	Clear liquor volume in crystallizer, (length) ³
k_g	Growth rate kinetic constant	$W(L)$	Cumulative weight fraction to size L
k_N	Nucleation rate kinetic constant	x	Dimensionless crystal size
k_v	Volumetric shape factor	x_F	$L_F/G\tau$
L	Particle size, length	x_p	$L_p/G\tau$
L_f	Upper limit of fines destruction, length	y	Dimensionless population density
L_p	Product classification size, length		
m_2	Second moment in crystallizer		

GREEK SYMBOLS

$\dot{\lambda}$	Fines dissolving parameter, $(R - 1)X_F$, dimensionless	σ	Dimensionless concentration
τ	V/Q_F , time	θ	Dimensionless time
ϵ	Void fraction	μ_j	j th moment of dimensionless distribution $y(x)$
ρ	Crystal density, mass/volume or dimensionless growth rate		

References

1. Randolph, A. D., and Larson, M. A. (1971). "Theory of Particulate Processes." Academic Press, New York.
2. Hulburt, H. M., and Katz, S. (1964). Some problems in particle technology: A statistics mechanical formulation. *Chem. Eng. Sci.* **19**, 555.
3. Randolph, A. D., Beckman, J. R., and Kraljevich, Z. I. (1977). Crystal size distribution dynamics in a classified crystallizer: Part I. Experimental and theoretical study of cycling in a potassium chloride crystallizer. *AIChE J.* **23**, 500.
4. Beckman, J. R., and Randolph, A. D. (1977). Crystal size distribution dynamics in a classified crystallizer: Part II. Simulated control of crystal size distribution. *AIChE J.* **23**, 510.
5. Sherwin, M. B., Shinnar, R., and Katz, S. (1969). Dynamic behavior of the well-stirred crystallizer with classified outlet. *Chem. Eng. Progr. Symp. Ser.* **95**(65), 75.
6. Randolph, A. D., Beer, G. L., and Keener, J. P. (1973). Stability of the class II classified product crystallizer with fines removal. *AIChE J.* **19**, 1140.
7. Lie, S. J., Shinnar, R., and Katz, S. (1971). The stability and dynamic behavior of a continuous crystallizer with fines trap. *AIChE J.* **17**, 1459.
8. Gupta, G., and Timm, D. C. (1971). Predictive/corrective control for continuous crystallization. *Chem. Eng. Progr. Symp. Ser.* **110**(67), 121.
9. Randolph, A. D., White, E. T., and Low, D. (1981). On-line measurement of fine-crystal response to crystallizer disturbances. *I&EC Proc. Des. Q.* **20**, 496.
10. Rousseau, R. W., and Howell, T. R. (1981). Evaluation of methods for control of CSD from continuous complex crystallizers. Presented at 90th Natl. AIChE Meeting, Reprint 48a, Houston, Texas, April.
11. Randolph, A. D. and Low, D. C. C. (1982). Some attempts at CSD control utilizing on-line measurement of nucleation rate. In "Industrial Crystallization 81" (J. Janeic and E. J. de Jong, eds.), p. 29. North Holland, Amsterdam.
12. Randolph, A. D. (1981). U.S. Patent 4,263,010. Control method and apparatus for crystallizer process control. April.
13. Randolph, A. D., Chen, L., and Tavana, A. (1987). Feedback control of CSD in a KCl crystallizer with fines dissolving. *AIChE J.* **33**, 583.
14. Epstein, M. A., and Sowul, L. (1980). Phase space analysis of limit-cycle development in CMSMPR crystallizers using three-dimensional computer graphics. *Chem. Eng. Progr. Symp. Ser.* **1983**(76), 6.
15. Johnson, J. L., Schork, F. J., and Myerson, A. S. (1985). Multivariable control of an MSMPR crystallizer. Paper 65b, presented at AIChE Annual Meeting, Chicago, Illinois, November.
16. Tsuruoka, S., and Randolph, A. D. (1987). State space representation of the dynamic crystallizer population balance: Application to CSD controller design. *Chem. Eng. Progr. Symp. Ser.* **253**(83), 104.

EXPERIMENTAL TECHNIQUES AND ANALYSIS OF RESULTS

Published crystallization kinetic data for use in the design of industrial crystallization systems are rare and of questionable applicability. Such data are not for the most part taken at process conditions existing in industrial crystallizers. The greatest difficulty with a large portion of published data is that the rates of nucleation and growth were measured separately under different conditions. Theoretical relationships based on homogeneous mechanisms are especially suspect because their mechanisms seldom obtain in industrial systems. Even published data developed by the techniques described in this chapter should only be used for first approximations because experimental results are very sensitive to minor errors in technique, as well as trace presence of impurities. Because of this, experimental data are not only often in error but have often been misinterpreted.

Until more is known about nucleation and growth-rate phenomena, it will be necessary to experimentally generate the necessary data for specific applications. In this chapter, we demonstrate how the analysis presented in the previous chapters can be used with the appropriate experimental procedures to develop kinetic expressions and to measure the effects of process conditions on the kinetics of crystallization in realistic crystallization environments approximating those in industrial practice. We discuss here how the continuous mixed-suspension, mixed-product-removal (MSMPR) crystallizer can be used to generate growth and nucleation data.

Such systems have the advantage that conditions similar to those in industrial-size units can be attained. The most important advantage is that the technique permits the measurement of both nucleation and growth rates simultaneously at identical levels of supersaturation, agitation, temperature, and suspension density. Moreover, these techniques permit the use (in fact, require the use) of plant liquors in experiments and the use of a variety of equipment sizes.

In addition, we discuss a number of specialized experimental techniques that are designed to develop a better understanding of the mechanisms associated with crystallization from solution. These include techniques to determine solution structure, the nature of secondary nucleation, and the nature of growth-rate dispersion. Various techniques for crystal size distribution measurement are also included.

9.1 Characteristics of Laboratory MSMPR Crystallizers

In order to meet the assumptions made in the previous analysis of MSMPR crystallizers using the population balance, the crystallization system must have certain well-defined characteristics. The characteristics listed below, as well as the physical realization of these characteristics discussed in the following section, apply just as well to production units as they do to experimental laboratory apparatus. The following requirements must be met:

(a) The crystallizer must be designed so that both the suspension and the mother liquor are well mixed—that is, the liquor composition and the crystal size distribution must be uniform throughout the volume of the vessel. This should be accomplished with a minimum power input by an agitator or circulating pump.

(b) Slurry discharge must be accomplished so that the discharge suspension density, size distribution, and liquid-phase composition are the same as they are in the crystallizer. There should be no size classification at the discharge point.

(c) The vessel must be small enough so that minimum feed material is required but large enough so that sampling does not result in appreciable disturbance to the system. Sieving is usually the method of choice to determine the product size distribution; therefore, the sample size must be large enough to provide an adequate supply of crystals for sieving.

(d) Other features are necessary if transient experiments are to be undertaken. These include effective control and regulation of rate of energy and rate of mass input or removal.

There are in general three types of crystallization processes classified by the way in which supersaturation is generated. *Evaporative* crystallizers are usually carried out under vacuum and depend on the evaporation of solvent to generate supersaturation, thus causing the deposition of solute as crystals. Systems exhibiting flat solubility curves, such as sodium chloride, are crystallized in this manner. *Cooling* crystallizers are those to which are fed concentrated preheated solutions. Cooling is accomplished in a variety of ways. The vessel can be surface cooled by vessel jacket or by circulating the solution through a heat exchanger. Preheated solution can be fed to a vacuum vessel with the supersaturation being generated by flash cooling as well as the effect of solvent loss. Or, a third-phase material can be sparged into the vessel, with its resultant evaporation providing the cooling effect. Systems exhibiting steep solubility curves are crystallized by such cooling techniques. *Precipitation* crystallizers are those in which supersaturation is generated by adding a third component in which the solute is insoluble or by carrying on a chemical reaction, the product of which is insoluble.

The MSMPR technique is applicable to all three types of crystallization. However, the last type is the most convenient to use for laboratory-scale experiments because crystallization can be carried out isothermally and at atmospheric pressure. Consequently, problems of heat transfer and pressure control are eliminated. Such precipitation systems are the most convenient for development of laboratory technique and analysis expertise, because fewer uncertainties are inherent in the experiments. In such systems one must be doubly sure that the system is well stirred so that the reaction (or precipitation) will not take place entirely in the immediate area of the inflow. Ultimately, however, one must use the type of crystallization for experiment that is required for the material at plant scale. Successful laboratory apparatus has been developed and used for all types of crystallization.

9.2 Equipment for Continuous Experiments

Laboratory MSMPR crystallizers from $\frac{1}{4}$ l in size upward to production size have been operated successfully when designed with concern for the factors mentioned above. The essential agitation required can be conveniently realized using a draft tube and an axial flow impeller (such as a marine propeller or pitched blade turbine) installed concentrically in the draft tube. Such an arrangement accomplishes the complete suspension and circulation of the dispersed solid phase with a minimum power input. While such a design eliminates the need of baffles, which would introduce increased nucleation because of impingement of crystals on the baffles, it is

helpful to put vertical vanes in the annular space to reduce the angular flow of the slurry. If the flow is down the draft tube and up the annular space, the cross section of the draft tube should be about equal to the cross section of the annulus. On the other hand, if the flow is directed up the draft tube, the draft-tube cross section should be smaller than the annulus cross section. This will reduce the velocity in the annulus and reduce the tendency for large crystals to segregate along the outer wall. The draft-tube design maintains uniform suspension with minimum high-energy crystal-crystal and crystal-apparatus contact, thus minimizing secondary nucleation.

Isokinetic withdrawal of the slurry is preferred; however, it is usually satisfactory if sampling or product-removal tubes are placed parallel to the circulation flow and withdrawal is made in the direction of flow. The withdrawal velocity must reasonably match the circulation velocity at the point of removal and be of such a magnitude that the settling effects due to density differences are minimized. If these criteria are followed, little classification at the outlet is encountered.

Laboratory crystallizers are usually operated with 15- to 60-min retention times; consequently, the average outflow rate is very low—too low to assure that no classification of the suspended solids occurs. It is therefore necessary to use intermittent product withdrawal so that high withdrawal velocities can be achieved. This is best done with a liquid-level control device, usually an electric contact device, and a time-delay relay. The relay activates a pump, which runs for a predetermined time. The relay operating time should be selected so that the pump removes no more than 10% of the vessel volume in a cycle. Care should also be taken so that the vessel fluid level is not lowered below the top of the draft tube. When the liquid level drops below the top of the draft tube, slurry circulation abruptly ceases. Figure 9.2-1 shows a typical apparatus used in precipitation crystallization, including agitator, draft tube, and withdrawal device. Sampling should be done with a separate withdrawal device, preferably a vacuum device, so that the sample does not pass through a pump. Care must be taken so that sampling meets the same isokinetic requirements as indicated for product withdrawal.

As mentioned before, mean residence times of 15–60 min are usual. Steady state is reached in 10–15 residence times. Normally a slurry sample of 500 ml is required to provide a suitable sample for sieve analysis. All of these factors suggests a crystallizer of about 10 l capacity. This would require a total feed supply of about 200 l for an experiment designed to measure the nucleation and growth rates of crystals. Smaller systems can be used, and if very small, the total contents of the crystallizer can constitute the sample after steady state is reached. Cooling systems have also been

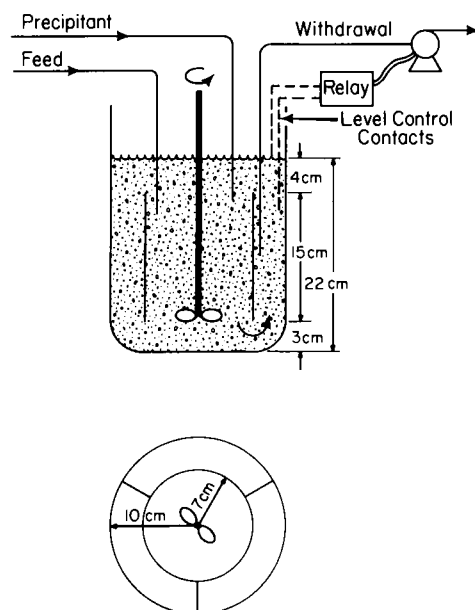


Fig. 9.2-1 Precipitation crystallizer with dimensions of that used in the Chemical Engineering Department, Iowa State University, Ames, Iowa.

designed that redissolve the product slurry and recycle this solution to the feed tank. If this is done, care must be taken that the feed concentration remains constant and free of foreign material.

EXAMPLE 9.2-1 PRECIPITATION CRYSTALLIZER

The crystallizer shown in Fig. 9.2-1 was used by the author [1] for a number of experiments designed to test the population-balance analysis and to determine the kinetics of nucleation and growth for a number of compounds in the presence of water and ethanol. The crystallizer had an approximate working volume of $5\frac{1}{2}$ l, and was made of Plexiglas with a Plexiglas draft tube fixed in place with three vertical vanes in the annular space. The approximate dimensions are given in the illustration. A Lightning V5 stirrer was used to provide agitation. Alcohol was fed through rotameters from constant-head sources, as was the feed solution. Peristaltic pumps, however, are more easily controlled and are more convenient to work with. The addition of ethanol created the supersaturated condition that resulted in crystallization. The two feed streams were fed directly into

the downflow draft tube so that complete dispersion was immediately achieved. This aspect of design is extremely important to precipitation crystallizers whether a chemical reaction takes place or not.

The product removal was accomplished by using a time delay with one electrode submerged in the solution and one electrode placed at the maximum desired liquid level. Product removal was achieved when the liquid surface came in contact with the electrode above the surface. This actuated a rotary pump that was operated through a time-delay relay. The delay relay operated the pump for the time required to remove 10% of the vessel contents and then reset. ♦

EXAMPLE 9.2-2 CYCLONITE CRYSTALLIZATION

The small bench-scale crystallization system used by Bransom *et al.* [2] in the crystallization of cyclonite is shown in Fig. 9.2-2. This experiment constituted the first reported use of the MSMPR crystallizer to obtain quantitative nucleation–growth rate kinetics. ♦

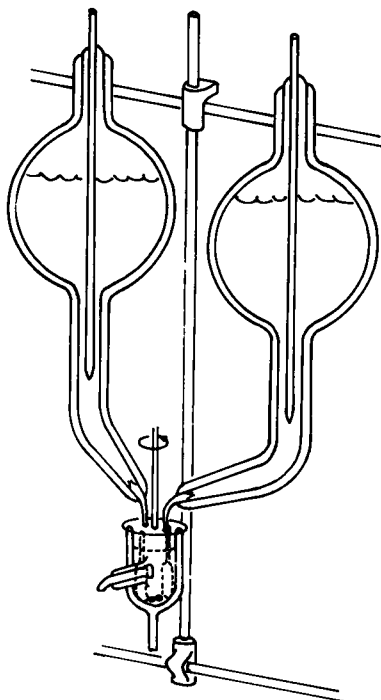


Fig. 9.2-2 Cyclonite crystallizer.

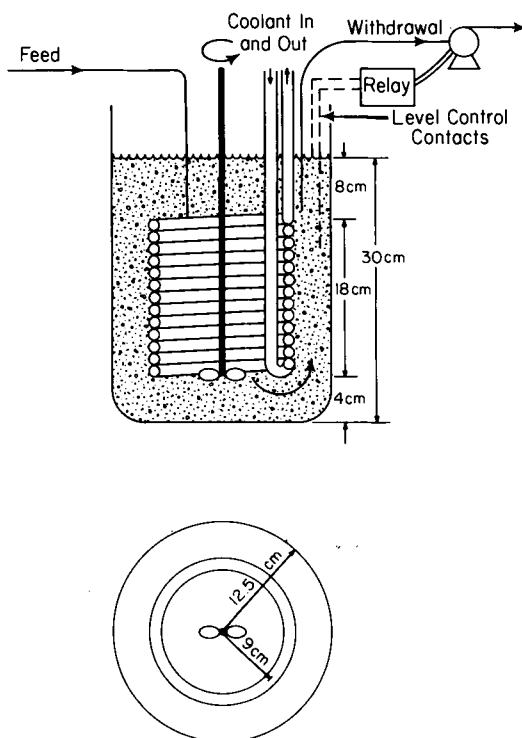


Fig. 9.2-3 Cooling crystallizer. (After Helt and Larson [4].)

EXAMPLE 9.2-3 COOLING CRYSTALLIZER

The cooling crystallizer shown in Fig. 9.2-3 is of the type used by Juzaszek and Larson [3] and Helt and Larson [4] to crystallize potassium nitrate. The crystallizer had a working volume of approximately 12 l and was made of Plexiglas. The cooling coil also served as a draft tube. The coolant used in the experiments referred to was ethylene glycol. The agitator was a Lightning V5 laboratory stirrer. Product removal was achieved as previously described in Example 9.2-1. The feed was contained in electrically heated drums, with the product returning to the drums for resolution. The feed was superheated by a line heat exchanger and passed through a line filter prior to entry into the crystallizer.

This apparatus was modified by Helt [4] as shown in Fig. 9.2-4. A withdrawal tube was placed in the side with a microscreen to withdraw supersaturated solution for introduction to a differential refractometer. The

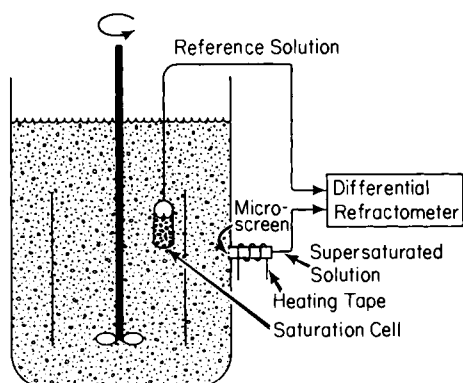


Fig. 9.2-4 Method for measuring supersaturation continuously using a differential refractometer.

solution was heated at the withdrawal point to avoid loss of supersaturation by crystallization. The reference stream was obtained from a submerged saturation cell that allowed the withdrawal of saturated solution.

Juzaszek and Larson further modified this system by placing a fines trap in the draft tube so that fines could be withdrawn, redissolved, and returned to the crystallizer. ♦

EXAMPLE 9.2-4 EVAPORATIVE CRYSTALLIZER

Laboratory-scale continuous-vacuum evaporative systems are much more difficult to design and operate. Figure 9.2-5 shows some of the additional features an evaporative crystallizer requires. Two receivers under vacuum

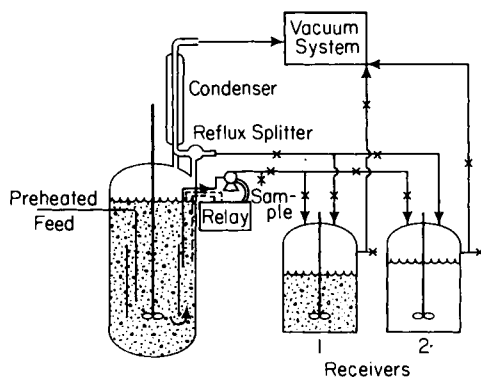


Fig. 9.2-5 Evaporative laboratory crystallizer.

are required, so that one can be emptied while the other is receiving the output from the crystallizer. The reflux condenser and reflux splitter are not directly needed for a strictly evaporative crystallizer. If the system requires a great deal of solvent to be removed, a heater is required and the reflux splitter is necessary to control the net rate of which solvent is removed. Sampling can only be done under vacuum. ♦

EXAMPLE 9.2-5

Figure 9.2-6 is the schematic flow diagram [5] for a combination cooling-precipitation crystallizer. Cooling and/or precipitation can be used in the apparatus to provide the driving forces for crystallization. The suspension holdup in this crystallizer is approximately 2 l, which approaches the lower limit on size for such systems. Reduction in scale was achieved by winding the cooling coil in a tight spiral to serve as a draft tube, as was shown in Fig. 9.2-3. Small amounts of product discharge (100 cm³) were removed for size analysis with the zone-sensing counter. Such units can be automated to operate several shifts (for example, overnight) without operator attention. It should be noted that the total run time to achieve steady-state CSD is a function of the retention time, not the size scale of the apparatus. ♦

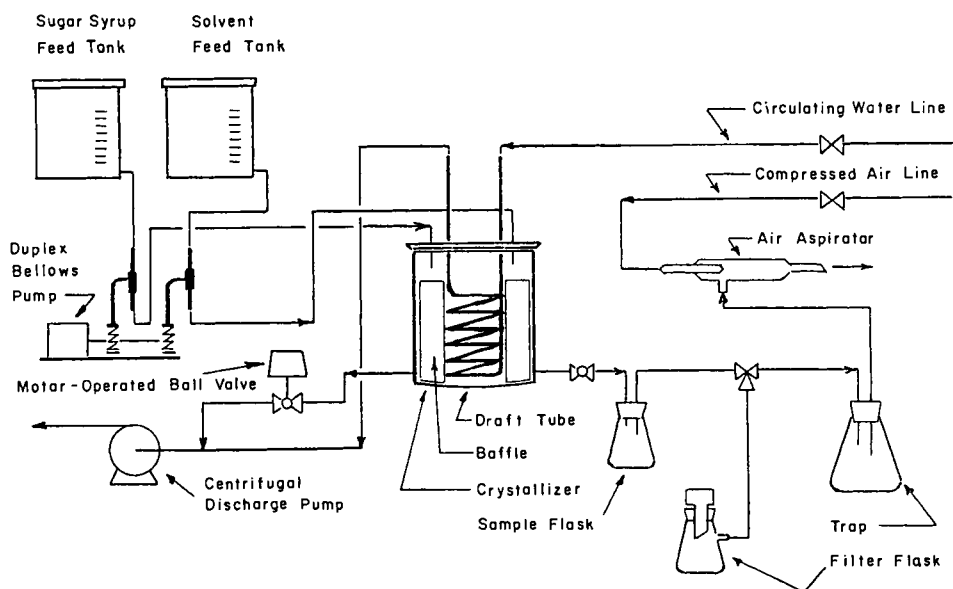


Fig. 9.2-6 Schematic flow diagram of a combination cooling-precipitation crystallizer.

EXAMPLE 9.2-6

A vexing problem in MSMPR crystallization studies is that nucleation depends on the distribution and amount of solids suspended in the slurry and one must run the unit 10–12 retention times in order for the suspension (especially at large particle sizes) to come to steady state. Furthermore, the suspension density is itself a dependent variable and cannot be manipulated independently. A partial solution to this problem is the cooling crystallizer mininucleator developed at the University of Arizona. See Fig. 9.2-7 for a photograph of this 1-l unit.

The essence of this unit is that the 1-l vessel itself operates with a relatively short residence time (~ 5 – 15 min), but it is seeded with a suspension of large product crystals representative of long residence time operation (~ 1 – 4 h). The large parent breeder crystals are totally retained in the suspension by a fine-mesh sieve on the exit stream, through which secondary nuclei pass to an in-line zone-sensing particle counter. Thus an exponential population density distribution of these fine crystals is formed and measured in “fast time” in the presence of the slowly changing “slow-time” distribution of parent seed. A saturated mother liquor is pumped in series circulation through a packed-bed solute saturator, in-line filters, the mininucleator crystallizer, and an in-line particle measuring device. The temperature drop between saturator and crystallizer is kept small, corresponding to the low supersaturation of the “slow-time” MSMPR that is being represented.

This 1-l mininucleator has proven useful to study the effects of agitator rpm, seed crystal density and size, and mother-liquor additives in cooling crystallizers. A second 240-ml mininucleator developed to study precipitation system will be described in Section 9.8-5. ♦

In addition to the basic vessel and the discharge technique, the apparatus must include appropriate feed tanks and metering and control devices, as well as in-line microfilters for filtering the feed. Care must be taken so that no crystallization takes place before the feed enters the crystallizer.

In the case of a precipitation system, two feed tanks and two feed streams are required. These streams should be introduced at the point of greatest agitation, namely, the draft tube, with downward flow in the draft tube. When transient runs are made that involve changes in the relative flow rates of the two streams, the effects of change in residence time must be accounted for.

Cooling crystallizers can be constructed of plastic, glass, or stainless steel and can be cooled by brines or suitable organic coolants. In any event, the surface area for cooling should be large, the temperature differences between the coolant and the mother liquor small, and the cooling surface

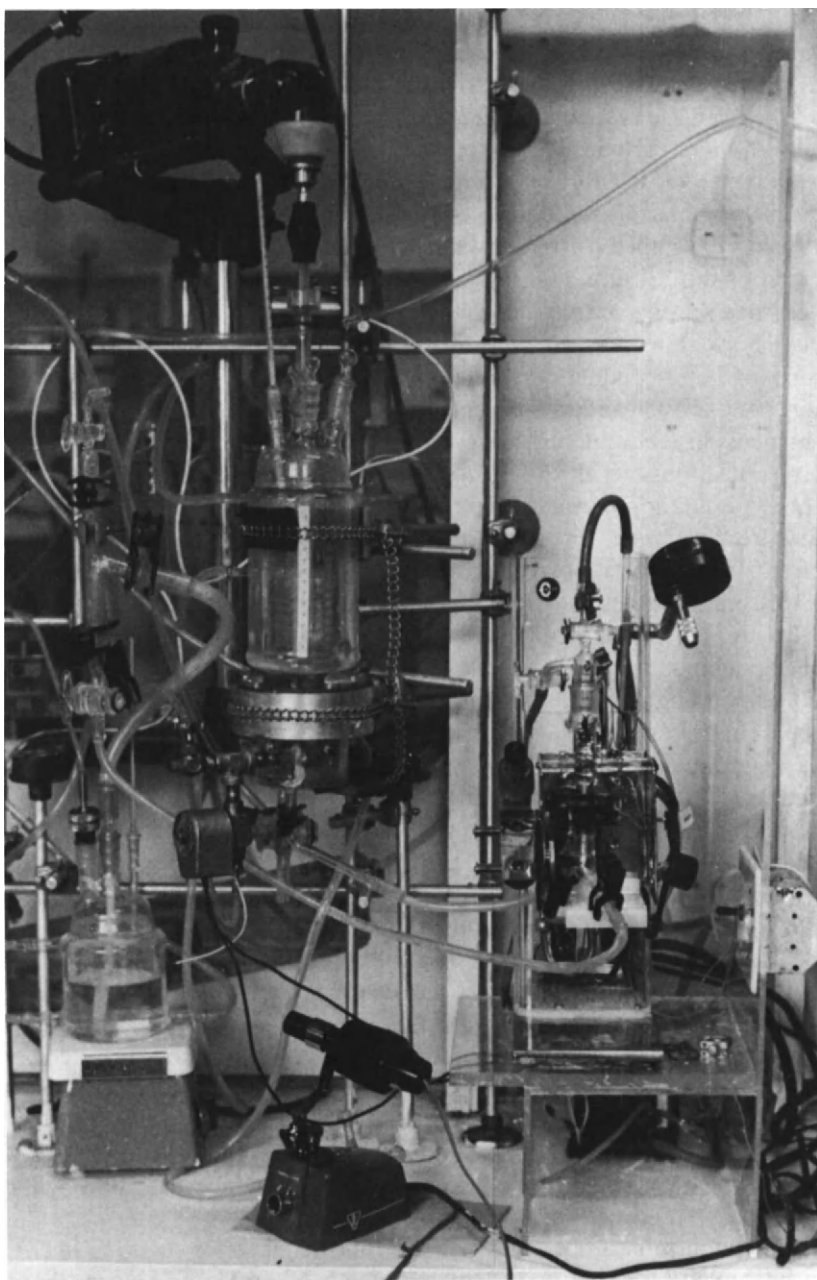


Fig. 9.2-7 One-liter cooling crystallization mininucleator (University of Arizona).

smooth and polished. All of these factors will help reduce crystal buildup on the surface of the draft tube or the vessel walls.

Transient experiments with cooling crystallizers are difficult to make because they generally require changes in flow rate. This requires commensurate changes in rate of heat transfer. Such requirements must be carefully addressed so that expected heat balances are achieved.

When cooling systems are used, crystallized material can be conserved by recycling the product to a redissolving tank and recycling it to the crystallizer. When this is done over long periods, care must be taken to ensure that evaporation does not take place, that no crystals remain undissolved, and that extraneous impurities (e.g., corrosion products) do not build up in the feed. However, product recycle to reconstitute the feed may often be advantageous or necessary for high value products.

Laboratory-size continuous evaporative crystallizers are much more difficult to operate because they are usually under vacuum. This causes difficulty in designing an acceptable product withdrawal system, as vacuum operation can cause vapor-lock.

9.3 Equipment for Batch Experiments

Experimental batch crystallizers require less associated equipment, and the desired heat or solvent removal can be achieved with simpler apparatus. A typical batch cooling crystallizer consists of a draft-tube-equipped vessel, with a cooling jacket and a tightly wound coil serving as the draft tube. Inlet and outlet fixtures and equipment are, of course, not necessary. Cooling surface area should be larger and provision should be made for programmed reduction in temperature. The crystallizer can be of any size from 100 ml upward in volume, depending on the crystal size expected and the sample treatment to be used. Ordinarily the total crystallizer contents can be used as the sample to be analyzed.

Evaporative systems ordinarily operate at a constant temperature and pressure. The apparatus shown in Fig. 9.3-1 was used by Baliga [6]. It was equipped with a reflux condenser and a controlled distillate splitter so that the net solvent removal rate could be controlled closely. It was thus not necessary to closely control the boilup rate. Provision was made for sampling during a run so that the CSD could be monitored as it changed in time. The CSD obtained was shown in Fig. 4.6-2. Care must be taken so that good mixing is maintained as the run progresses. The volume in the crystallizer decreases with time, while the suspension density increases.

Precipitation batch crystallizers should be classified as semibatch because they require continuous feeding as the batch run progresses. Evaporative

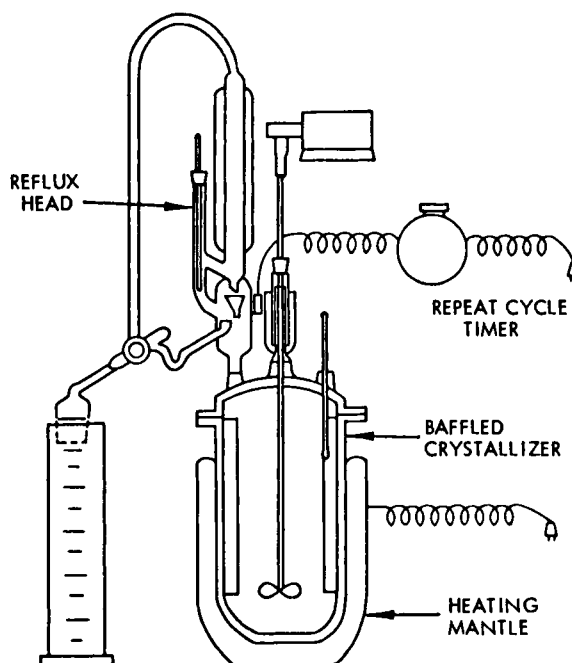


Fig. 9.3-1 Evaporative batch equipment. (After Baliga [6].)

systems can also be run in the semibatch mode. All of the CSD data analysis techniques previously discussed can be used with semibatch systems. In subsequent sections, we will describe special experiments that are necessarily done in a batch configuration.

9.4 Sampling Techniques and Sample Treatment

Even if all the experimental conditions required are met, the sampling and sample treatment procedure can affect the validity of the results. Poor sample handling technique is undoubtedly responsible for most “unexplainable” results. This is especially true if a sample is to be separated from its mother liquor and dried for sieve analysis or other methods of sizing.

A representative slurry sample must be removed rapidly and carefully so that crystals are not fractured and so that continued phase change is stopped or minimized. Because of the relatively low supersaturation expected in most back-mixed systems, continued crystallization after

withdrawal is not a problem if the temperature is maintained at the crystallizer temperature. The greatest difficulty lies in the separation of the crystals from the mother liquor. Care must be taken to assure that all crystals are removed from the mother liquor and, once "dewatered," that agglomeration does not occur.

Samples should be removed directly from the crystallizer using a vacuum bottle and a calibrated flask so that the exact volume of slurry can be determined. The slurry volume is needed so that the population density can be determined on a clear liquor or slurry volume basis. It is sometimes convenient to measure the filtrate volume immediately after separation of the crystalline solids. Only the filtrate volume and weight of dry crystals are needed in order to calculate slurry and population densities. The sample bottles should be the same temperature as the slurry from the crystallizer. The sample probes in the vessel should be placed similarly to that required for the continuous withdrawal. A micropore, Buchner-type vacuum filter works well for aqueous inorganic systems. The greatest difficulty lies in washing and drying the crystal sample. Usually a special technique must be developed for each application, but a good way to start is to add a suitable organic solvent, in which the crystals are not soluble, to the filtering funnel immediately after initial dewatering. The crystals should then be stirred and the solvent drawn off through the filter. After two or three such washes, the crystals will have little tendency to agglomerate. Suitable solvents are those that are partially miscible in water, such as acetone, light alcohol, light ketones, or light aldehydes. It is sometimes necessary to saturate the wash liquid with the solute.

The samples should be carefully removed from the filter, spread on a watch glass, and dried at a temperature well below the crystal decomposition temperature. Special care must be taken with hydrated crystals. Normally, such a procedure results in only light agglomeration, which can be broken up upon sieving. The authors have used this method extensively, with little agglomeration detectable under microscopic examination.

Such product crystal samples are normally sized by standard sieving techniques. Three-inch standard screens are useful because of sample size. Sizes below 100 μm are best examined by some other technique, such as a zone-sensing instrument. Typical instruments are Coulter countersTM or Particle DataTM counters. Laser light scattering, sedimentation, and photographic counting can also be used. Some of the latter are done *in situ*; thus, problems of sample removal and treatment are reduced but not eliminated.

The important concerns in sample treatment are that none of the distribution is lost and that no CSD alteration takes place because of the treatment.

9.5 Measurement of CSD

As pointed out in Chapter 2, the definition of size distribution depends entirely on the method used to determine CSD; therefore, when reporting the crystal size distribution, the method used for determining the size must be clearly stated. Each size-measuring method is based on a particular aspect of the particle. In the following paragraphs we discuss four common methods.

9.5.1 Sieving

Sieving is the most common method for sizing dry samples (although wet screening can be used) when size discrimination below 50 μm is not required. The method works well if the crystals are close to being equidimensional in habit. It is prone to considerable variability if the crystals are long needles, however. One normally regards the crystal size as the second largest diameter; however, it has been shown that data correlate well when the size is taken as the geometric mean of the single-crystal diameters. Standard sieving techniques should be used, bearing in mind that samples too large for the sieves used introduce considerable error. Sieves can be obtained with 2-in. diameters when only small samples are available. The distribution is obtained on a mass fraction basis and can be used as such or converted to cumulative weight percent. The mass fractions can be converted to number density by the following equation, previously discussed in Chapter 2:

$$n_i = (w_i) / (k_v(\Delta L) \bar{L}_i^3 \rho) \quad (9.5-1)$$

where w_i is the weight fraction on the i th sieve, ΔL is the difference in sieve size between screen i and $i + 1$, and \bar{L}_i is the arithmetic average crystal size with fraction.

If the data are taken from an MSMPR crystallizer, the cumulative mass distribution can be used in conjunction with the table in Appendix A to determine the growth rates and nucleation rates. For example, for an MSMPR crystallizer, $L_{50} = 3.67G$ where L_{50} is the median size. Using this information, G can be calculated, and by using the mass balance

$$M_T = 6k_v \rho n^0 (G\tau)^4$$

the nuclei number density n^0 can be calculated.

9.5.2 Zone Sensing

Zone-sensing methods (e.g., Coulter Counter®, Particle Data Elzone®) measure the electrical resistance of a conductive fluid through an orifice. The passage of a particle through the orifice causes a change in resistance,

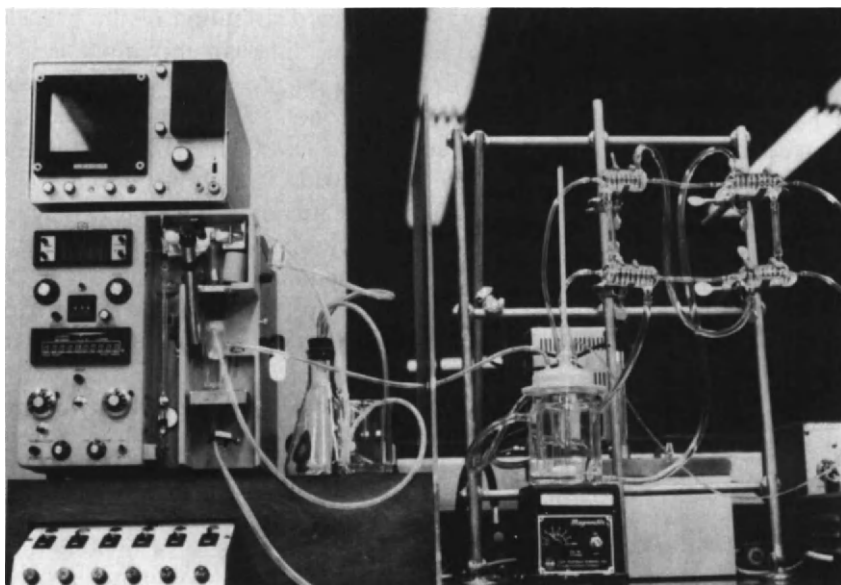


Fig. 9.5-1 Photo of particle data counter.

which gives rise to an electrical signal proportional to the particle volume. Such an instrument is shown in Fig. 9.5-1. The instrument measures particle volumes and reports data as the actual number of particles in a given size range, with size reported as the equivalent spherical diameter. These instruments can measure sizes from 0.5 to 1000 μm . However, the size range for a given sample is considerably narrower. Different size ranges require different orifice sizes selected to be no less than twice the size of the maximum crystal size in the sample.

Measurements are usually made by suspending the sample in a conductive fluid in which the sample is insoluble. Measurements have also been made *in situ* in crystallizing systems. The allowable suspension density is limited, however, and normally some method of removing large crystals is necessary. Particular applications will be discussed in Section 9.8.

9.5.3 Light Scattering

When a particle is illuminated by a beam of collimated light, scattering from this beam occurs. Such low-angle forward scattering of light is known as Fraunhofer scattering. We will not discuss the theory but only state that the pattern resulting from light scattering from a suspension of solid

particles can be interpreted to produce a size distribution of the particles present. Typical CSD ranges are 1–200 μm , although this range can be extended with proper instrument design. An intense collimated light beam can often be obtained more simply and economically using a laser light source, and most commercial instruments use laser light. High suspensions cannot be handled due to multiple scatter, that is, light scattering off of more than one particle surface. Multiple scatter is a function of particle number, and thus the allowable slurry density (above which multiple scatter invalidates the measurement) is a strong function of particle size.

Commercial and laboratory instruments are available. Typical instruments are the L & N MicrotracTM, the Celas GranulometerTM, and the MalvernTM Particle and Droplet Sizer. These instruments have been used to measure laboratory samples. Models also have been developed for continuous monitoring of crystal slurry flow streams.

9.5.4 Sedimentation

Sedimentation can also be used for size distribution determination, and standard procedures are available. The method is less discriminatory than those discussed above but can give accurate and reproducible results. The analysis of the data in a fluid medium requires consideration of the settling velocity of individual articles as well as measurement of the cumulative mass settled as a function of time.

9.6 Treatment and Interpretation of Data

Size distribution data are collected in various forms depending on the measurement instrument used. Data from screen-analysis and sedimentation-analysis techniques are usually reported as mass fraction in a given size range. Cumulative plots of these distributions can be made, and the table in Appendix A can be used to “smooth” the data to fit the MSMPR expected distribution form. Often, however, it is important that the character of the data be fully displayed before it is fitted to any standard form. This is best done by converting the mass distribution to a number distribution. This is the severest test of the data. From the mass fraction the number density is calculated by

$$n = \frac{\Delta w}{k_v \rho \bar{L}^3 (\Delta L)} \quad (9.6-1)$$

where Δw is the mass fraction in size range ΔL and \bar{L} is the arithmetic average size in the size range ΔL . The size range ΔL should be as small as feasible, depending on the crystal size and sample size. A semilog plot of n versus L will display any anomalies extant in the data and suggest where

sampling and data treatment errors may have occurred, as well as suggesting the existence of unusual process effects on kinetics.

Data from particle-counting devices are usually obtained as number distributions. These data need only to be converted to number density by dividing the number in a size range ΔL by the width of the size range.

Simple computer programs can be written for all of these suggested treatments, but if the data is to be fit arbitrarily to predetermined models it is essential that the validity of that fitting be checked visually or by some significant test.

Excessive populations of fines from MSMPR produced samples indicate either size-dependent growth, growth dispersion, or short fines retention time. It can also mean poor sampling or a poor sample treatment technique. All of the possibilities must be checked. A deficiency of fines probably means a poor sampling technique. A deficiency of large sizes suggests classified withdrawal or poor sampling. There may be other reasons for anomalies in CSD as well.

9.7 Experiments with Additives

The MSMPR experimental technique is very useful in screening additives that modify CSD. Dissolved additives, often in only parts per million, have a marked effect on the nucleation and growth rates and thus the size distribution. These effects also often change the crystal habit.

Laboratory MSMPR crystallizers can be operated at a fixed retention time and a fixed production rate but with various choices and concentrations of additives. Analysis of the CSD will give information about the additive effect on nucleation and growth. The effect on crystal yield can also be determined. This technique is a continuous process; thus it is difficult to determine the effect of additives on saturation concentration.

By chemical analysis of the crystalline product, the degree of additive incorporation in the crystal can also be determined.

Similar experiments can be designed to measure effect of temperature, mixing intensity, continuous seeding, ultrasonic excitation, agitator design, and suspension density on nucleation and growth rates.

9.8 Special Experimental Techniques

While MSMPR experiments and simple hatch experiments are helpful and necessary in any program to characterize the kinetics of a system, they often reveal phenomena that cannot be adequately understood by these techniques alone. Indeed, data obtained from MSMPR studies have indi-

cated phenomena previously unsuspected. The realization of the existence of these phenomena has given rise to new and unique experimental programs using other techniques. In this section we discuss a number of experimental approaches used by the authors to answer kinetic questions raised by MSMPR results and by observations of production size crystallizer behavior.

9.8.1 Point Nuclei Sources

Clontz and McCabe [7] developed a technique with which they could contact a single growing crystal with a metal or plastic rod in order to

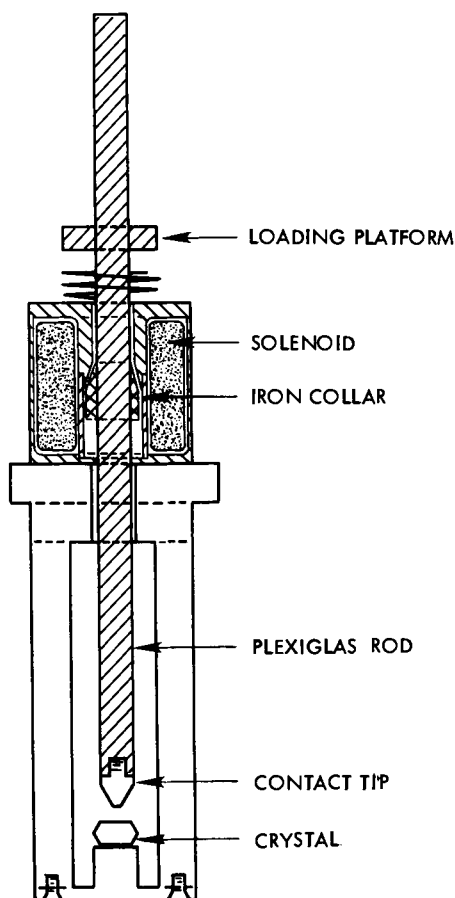


Fig. 9.8-1 Repetitive crystal contactor.

determine the degree to which nuclei were produced. This now classical experiment clearly revealed the mechanism of contact nucleation. Their apparatus used a single crystal contact and a subsequent waiting period for the resulting nuclei to grow to visible size. The experiment confirmed the importance of contact nucleation and its dependence on contact energy and supersaturation. Following Clontz and McCabe, Larson, Bauer, and Dallons [8] and Larson and Bendig [9] developed a continuous point-nuclei generation system, which had the advantage that the MSMPR crystal size-distribution model could be used to interpret the data.

When the site of nuclei formation can be clearly identified, such factors as supersaturation, contact area and energy, nature of the contact surface, and presence of impurities can be related to the actual number of nuclei produced per contact. Their viability as growing crystals can also be

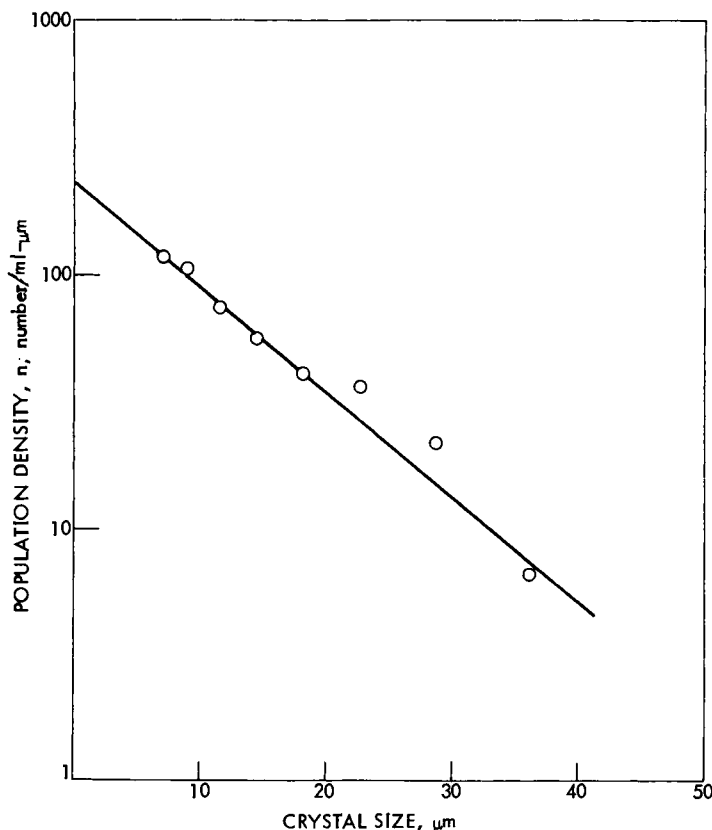


Fig. 9.8-2 CSD from point-source nucleator.

determined. Figure 9.8-1 shows a solenoid-activated crystal-contacting device [9], which, when placed in a well-mixed supersaturated solution, provides a point source of nuclei. The contactor is provided with a timer so that the crystal can be contacted at a specified frequency. The device can be equipped with contacting surfaces of various areas and hardness. The electromagnet raises and then drops the contactor, which can be loaded to provide various contact energies. The drop height and the frequency can be varied. When placed in a continuous-flow stirred vessel with conditions such that the solute resources are limited and the residence time is short, the device produces a concentration of small crystals sufficiently low in number that their CSD can be determined with a zone-sensing particle size-measuring instrument. Under such conditions, the supersaturation is unaffected by the presence of the growing crystals. In addition, there being

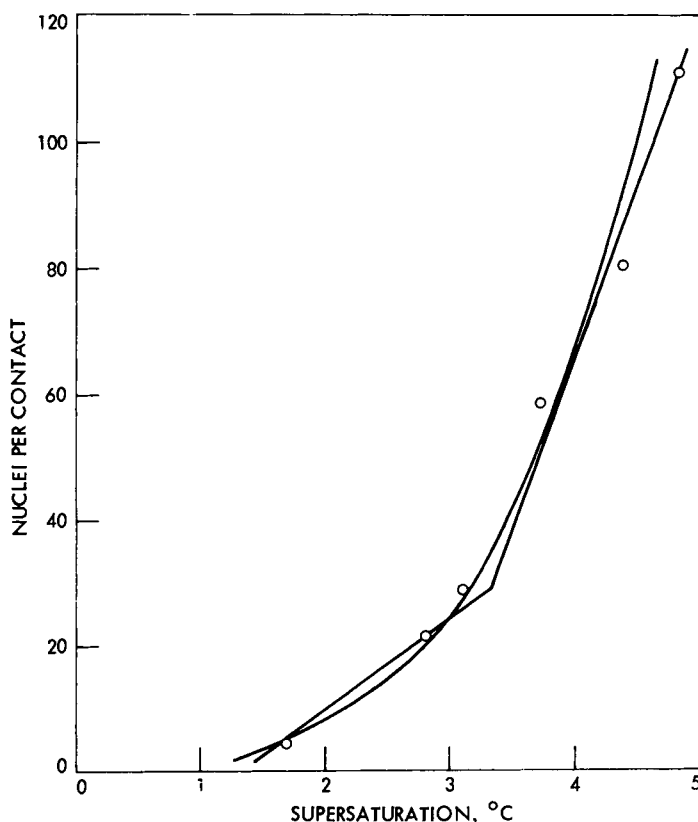


Fig. 9.8-3 Crystallization kinetics of $\text{MgSO}_4 \cdot 7\text{H}_2\text{O}$ from contact nucleation experiments. (After Larson and Bendig [9].)

only very small crystals in suspension, there are no second-generation nuclei formed. Thus the system is essentially an MSMPR crystallizer, with a point-nuclei source, a clearly defined supersaturation, and *in situ* CSD determination.

A plot of CSD extrapolated to zero, as shown in Fig. 9.8-2, gives the nuclei population density and thus the nucleation rate. With a knowledge of the contact frequency, the number of viable nuclei produced per contact can be determined.

Figure 9.8-3 shows the relationship of supersaturation, expressed as degrees undercooling with nuclei produced by contact for magnesium sulfate [9]. These data give the nucleation kinetics relationship $B^0 = k(s)^{2.7}$, where k reflects the contact energy and contact area. Larson and Bendig [9]

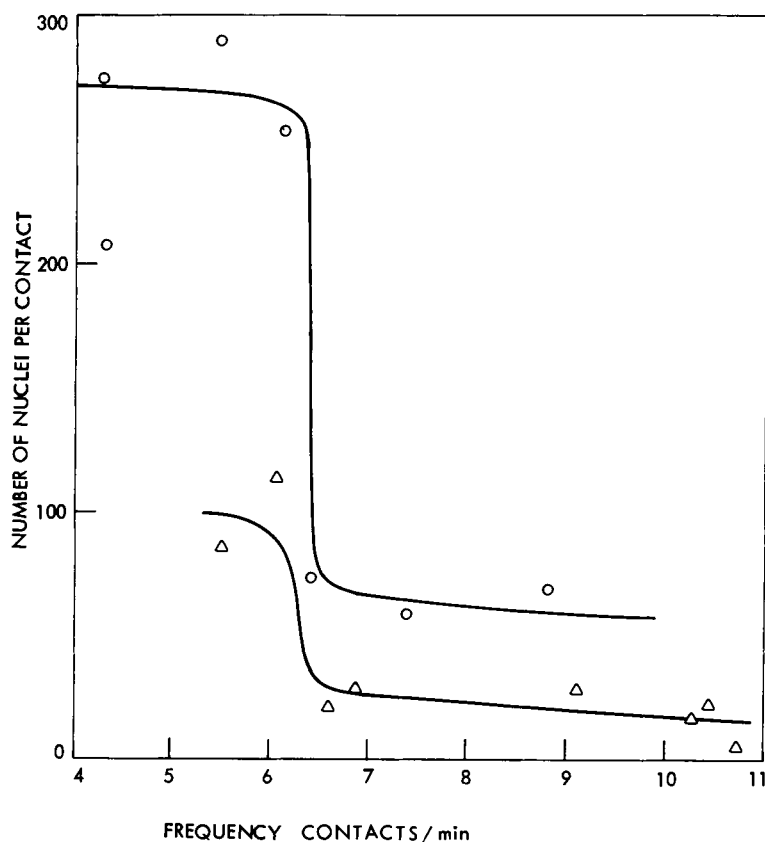


Fig. 9.8-4 Surface regeneration time. O, $\Delta T \sim 3.5^\circ\text{C}$, Δ , $\Delta T \sim 3.0^\circ\text{C}$. (After Larson and Bendig [9].)

found that the contact surface exhibited a regeneration time as shown in Fig. 9.8-4. At a contact frequency of approximately 6.5 contacts/min, the number of nuclei per contact dropped sharply. This evidence indicates that the contact nucleation mechanism is one of removal of solute queued up prior to incorporation in the lattice, rather than attrition of the crystal itself.

Work by Khambaty and Larson [10] using this apparatus showed the effect of Cr^{3+} on the growth and nucleation of MgSO_4 . As was shown in Fig. 5.5-1, both n_{eff} and G decrease as Cr^{3+} concentration increases. In addition, these experiments clearly indicate the presence of growth disper-

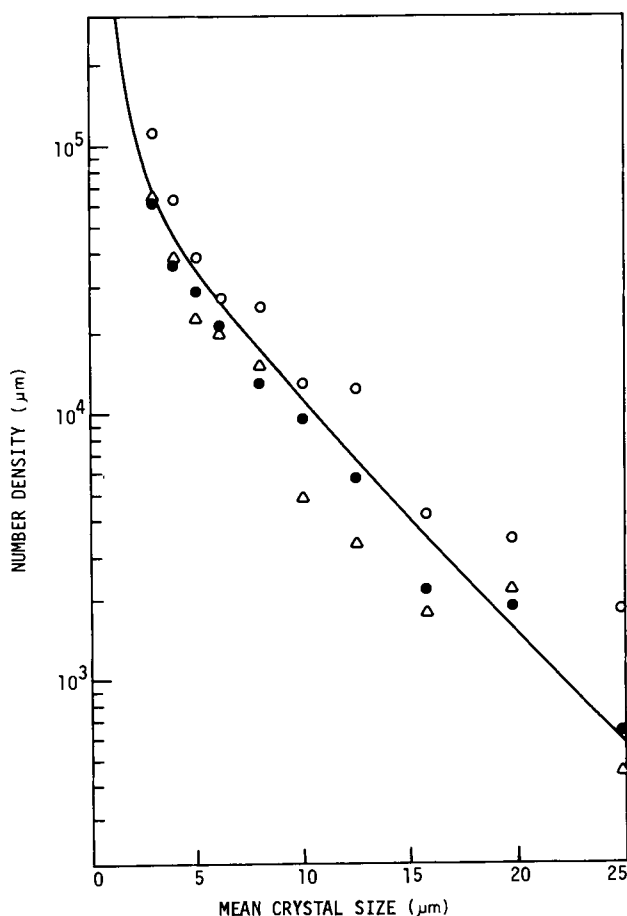


Fig. 9.8-5 CSD of potash alum $[\text{AlK}(\text{SO}_4)_2 \cdot 12\text{H}_2\text{O}]$ contact nuclei; $T = 30^\circ\text{C}$.

sion or size-dependent growth), as evidenced by the high population density at small sizes.

This system can also be used effectively in the batch mode as well. The growing crystal can be contacted once and the CSD of the generated nuclei determined immediately by use of a zone-sensing counter. This provides information about the CSD of the nuclei as well as how the CSD might change with variables such as contact-energy and supersaturation.

In Fig. 9.8-5 the CSD of potash alum nuclei [11] is shown as determined within 30 s of contact. Clearly a wide size range is produced, and this

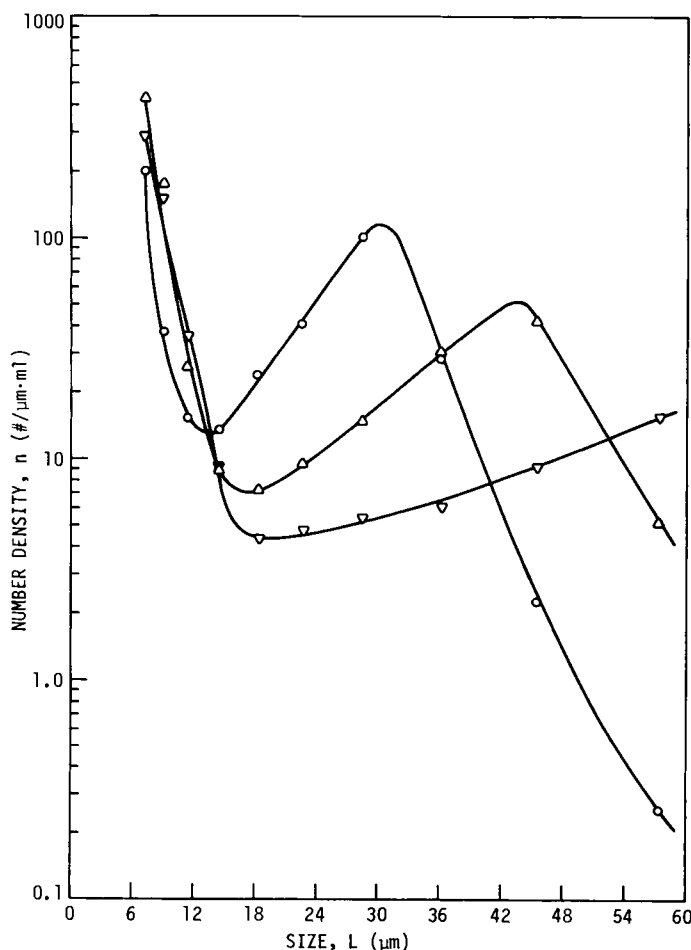


Fig. 9.8-6 Growth of KNO_3 nuclei. ○, 30 sec; Δ, 67 sec; ▽, 100 sec; $\Delta T = 0.40^\circ\text{C}$. (After Purves and Larson [12].)

number and distribution is highly dependent on supersaturation. Figure 9.8-6 shows the results obtained by Purves and Larson [12] by letting KNO_3 contact nuclei grow. These CSD are typical batch crystallization CSD, showing a large number of crystals not growing at any appreciable rate and a smaller number growing at a fairly uniform rate. The latter is indicated by the parallel distribution lines obtained as time progressed.

We present here only a few of the results obtained using this experimental technique. They show, however, that this technique can reveal important information about the mechanism of nucleation and growth and the effect of operating conditions on the kinetics. This technique cannot, however, give information about individual crystals. The following discussion suggests some techniques that can be used to study individual crystals.

9.8.2 *Photographic Nucleation Studies*

It is often useful to determine the growth characteristics of individual crystals or nuclei produced and growing under particular conditions. The technique described in Section 9.8.1 only provides information on the collective behavior of large populations of crystals.

A useful technique for such studies utilizes the nucleation and growth cell developed by Gerside and Larson [13], as shown in Fig. 9.8-7. This cell has a chamber for crystal nucleation and growth and a chamber for circulation of temperature-controlled water. The chambers are separated by glass so that crystals can be back-lighted and photographed through an optical microscope. Thus the number and size of the growing nuclei can be observed and both nucleation and growth rates can be calculated. Video pictures can also be obtained and portrayed in a CST. The cell shown is a batch cell, but flow cells can also be used when it is desired to conduct growth studies of long duration.

In operation, a single crystal is allowed to grow for a short period of time, and then is contacted or subjected to a sliding contact by drawing it along a glass surface, as shown. The resulting nucleation is photographed or videotaped. In a flow cell the growth rates of the individual crystals can be monitored by taking sequential photographs. From the photographs, the number and size can be determined and two-dimensional growth rates determined. Figure 9.8-8 shows a photograph taken of crystals of NaNO_3 produced by a sliding contact of a growing crystal. Photos were taken 2 min apart and showed that different crystals grow at different rates. Figure 9.8-9 shows individual citric acid crystal sizes as a function of time, as determined by Berglund and Larson [14]. These are similar to those presented in Chapter 4. Note that they have a variety of growth rates, but they each grow at a constant rate.

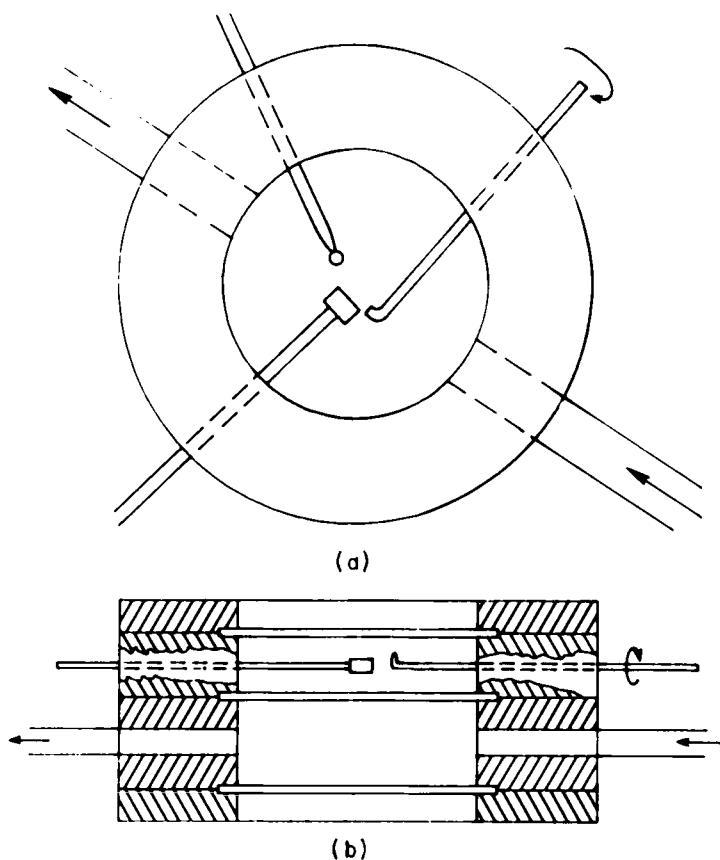


Fig. 9.8-7 Photographic nucleation and growth cell. (a) Top view, (b) side view.

This technique has been used to determine the presence of growth dispersion in a variety of materials, as well as the extent to which contact nucleation is important at various supersaturation levels. It can also be used to determine the effects of impurities and additives, not only on nucleation but on growth dispersion as well.

9.8.3 Scanning Potential Crystal Modifiers

Chemical compounds can often be found that modify growth rates, inhibit nucleation, or promote single-faceted crystal growth. Modifiers that inhibit either growth or nucleation are often effective at the low ppm concentration level. This observation, together with the surface-active nature of many of these compounds, has led to the speculation that inhibition

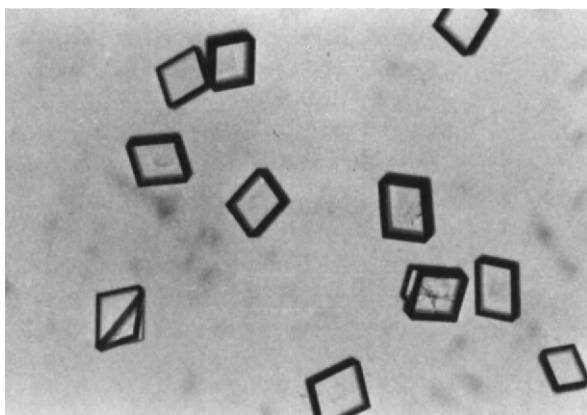


Fig. 9.8-8 Photo of NaNO₃ nuclei after a 2 min growth period.

occurs by attachment of the modifiers on the crystal surface, with the resultant blockage of crystal growth sites (e.g., Van Rosmalen [15]).

Inhibition may also occur due to complexing or ion pairing in solution. This would lower the ion activity (supersaturation) in solution and result in a decrease in crystal growth and/or nucleation rates. Additives that inhibit growth or nucleation by a complexing mechanism must typically be added in higher concentrations, approaching solute concentration. Such additives are not really inhibitors *per se*, but merely act by lowering the level of supersaturation.

Regardless of the mechanism, the search for active crystal modifiers is tedious, and rapid scanning techniques are of value. If the given crystal modifier extends the metastable supersaturation limit (by inhibiting the formation or growth of crystal embryos), then such an additive can be scanned and quantitatively ranked using an apparatus similar to the mininucleator in conjunction with the up-down-up statistical test developed for explosives sensitivity testing by Dixon and Mood [16]. In this test a stimulus is applied to the system and a "go" or "no go" response to the stimulus is observed. If the result is "no go," the stimulus is incremented by one equally spaced level (arithmetic or logarithmic). The level of stimulus is incremented in this manner until a "go" event is observed, after which the level of stimulus is decremented. The rule is that after each "no go" event the stimulus is incremented; after each "go" event the level is decremented.

The up-down-up method was used by Kelly [17] to rank crystal modifiers as to their ability to inhibit precipitation of $\text{CaSO}_3 \cdot \frac{1}{2}\text{H}_2\text{O}$ in simulated stack-gas scrubber liquors. The stimulus was the concentration of

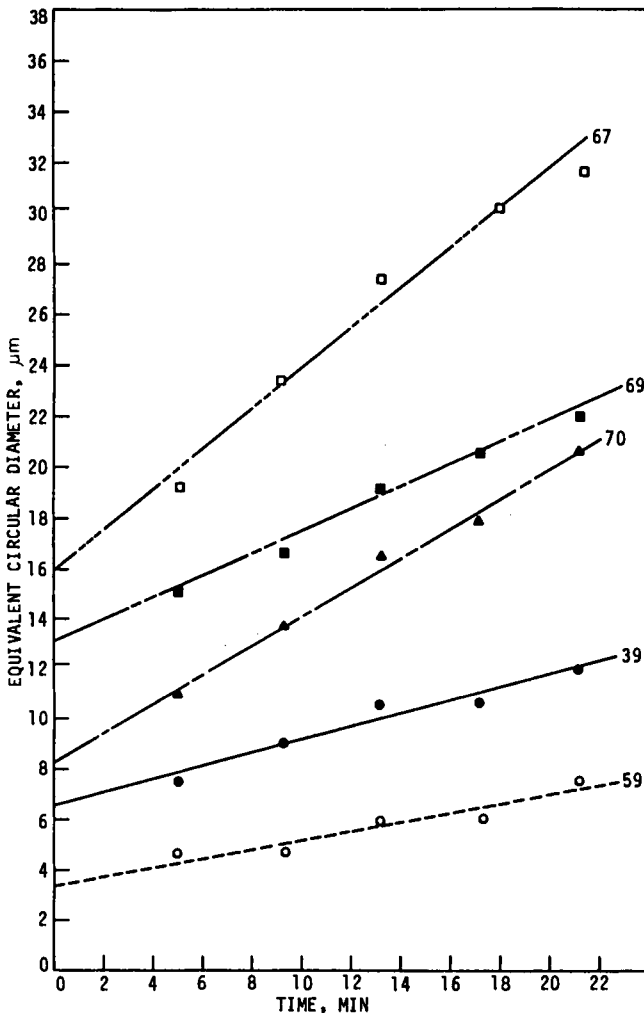


Fig. 9.8-9 Growth rate of citric acid crystals. $T = 30^{\circ}\text{C}$; $\Delta T = 1^{\circ}\text{C}$. (After Berglund and Larson [14].)

SO_3^{2-} in the feed liquor (the limiting ion, added at time zero). The response was the observation of any newly formed particles with the zone-sensing particle counter ($5\ \mu\text{m}$ detection limit) after a waiting time of exactly 15 min. An NG was entered for no observable nucleation, while G was recorded when particles were observed. The pattern of NGs and Gs is entered on a grid showing the level of stimulus, as illustrated in Fig. 9.8-10, and fit to a normal (equal spaced stimuli) or log-normal (equal spaced log

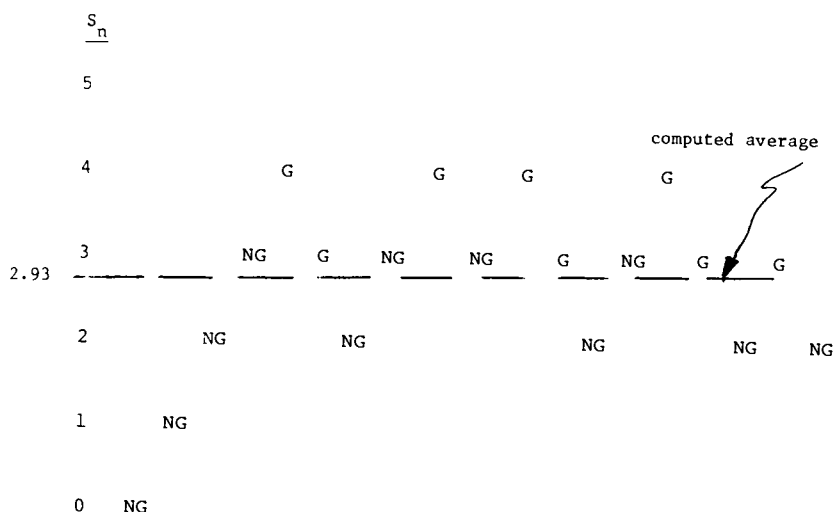


Fig. 9.8-10 Hypothetical pattern of Go-No Go events, illustrating the up-down-up metastability test.

stimuli) distribution. The 50% go/no go level of stimulus, calculated as

$$\bar{S}_{50} = C/N$$

is an average or log average, depending on whether or not increments were arithmetically or geometrically spaced. The values C or N are calculated as

$$C = \sum_{n=2}^{N+1} S_n \quad (\text{or} \quad \log S_n)$$

where n is the run number ($n = 1$ is defined as the first run in which an opposite response is obtained from the immediately preceding run), and N is the total number of runs after run $n = 1$. For the NG-G pattern shown in Fig. 9.8-10,

$$N = 15 - 1 = 14 \quad C = \sum_{n=2}^{15} S_n = 41$$

and

$$\bar{S}_{50} = \frac{41}{14} = 2.93$$

If logarithmic increments of stimulus were used, then $\log \bar{S}_{50}$ is calculated and the actual stimulus is $\exp(\bar{S}_{50})$.

In the tests of Kelly, only NMTP [nitrilotris(methylene)triphosphonic acid] and citric acid were found to be effective in extending the metastable supersaturation limit of calcium sulfite, giving metastable limits of 921% and 294%, respectively.

It is important to distinguish between the terms nucleation and nucleation rate. When NMTP was added to a 9-l continuous MSMPR crystallizer, *nucleation rate* increased. However, *nucleation* was dramatically inhibited in the metastability tests. This observation suggests NMTP acts to block growth rather than nucleation. The MSMPR crystallizer is a concentration-driven process; if growth is inhibited, concentration builds until nucleation (with low growth rate) overwhelms the system. The result is that finer particles are produced using a supposed nucleation "inhibitor."

9.8.4 Solution-Structure Studies

When an experimental program is initiated to characterize crystallization kinetics, the study normally is focused on the nature and behavior of the solid phase. A study of the nature of the supersaturated solution is often neglected, but in most instances it is essential that as much as possible be known about the state of the solute in solution. Many studies have been unproductive, however. As a solution passes into the supersaturated state, changes in properties such as electrical conductivity, refractive index, or viscosity reveal very little about the changing structure of the solution. It is important to know, however, the degree to which there is solute structuring or clustering prior to phase change, as well as the character of the structuring that occurs. It must be presumed also that the presence of additives or impurities affects the degree to which the structuring occurs and the equilibrium saturation concentration of the system. Two experimental techniques have been useful in providing information about solution structuring or solute clustering. The principles were discussed in Chapter 5. The techniques are (1) spectroscopic analysis of supersaturated solution and of solution regions close to the growing crystal surface, and (2) the analysis of concentration gradients formed in supersaturated (but nonnucleated) solutions as a result of gravitational or centrifugal force field.

Both X-ray and Raman laser spectroscopic studies have been conducted on concentrated and supersaturated solutions. Here we discuss only the use of Raman spectroscopy, which the authors have used to characterize structuring in concentrated and supersaturated solutions of alkali nitrates. Raman spectroscopy has the advantage that aqueous solution of nitrates, phosphates, and chlorates produces spectra that can be interpreted with confidence and that show how solute clustering is related to concentration. Examinations of single-phase systems have shown that a variety of ions and molecular associations can occur and that these increase as concentration increases. Figure 9.8-11 shows the Raman spectra of a 4M solution of sodium nitrate [18]. The composite band is the experimental spectral band, and the component bands result from the deconvolution of the experimental band. In this instance the four species giving rise to the experimental

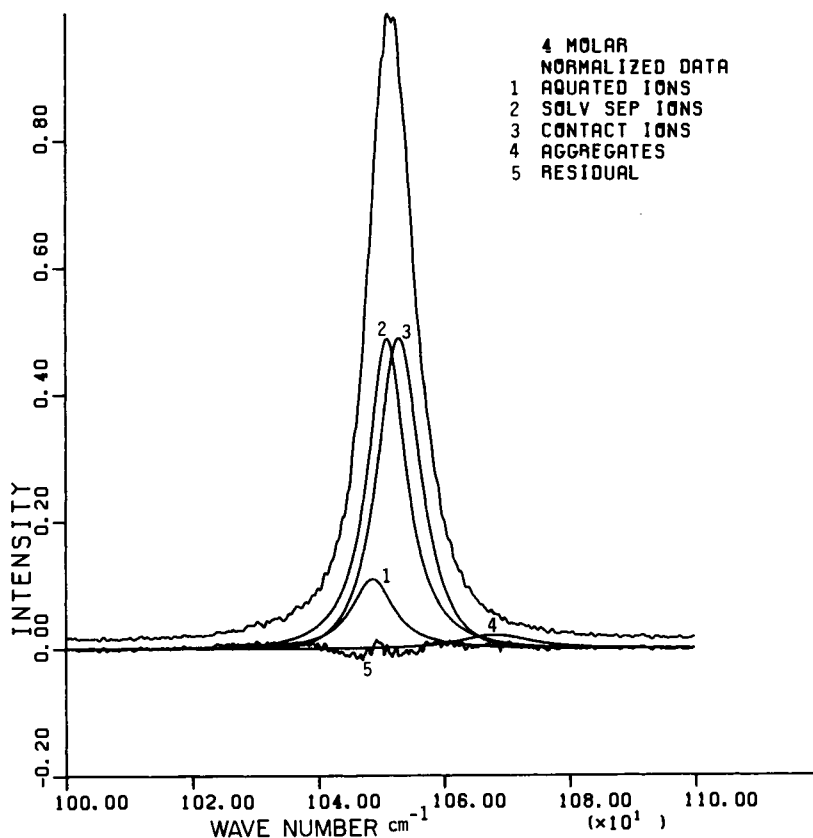


Fig. 9.8-11 Raman spectra of NaNO₂ solution. (After Hussmann et al. [18].)

band are aquated ions, solvent-separated ion pairs, ion pairs, and clusters. The area under each component band is a measure of the relative portion of the solute existing in a particular state of association. *In situ* studies of regions near the surface of growing crystals can also be done. Unfortunately, present technology permits examination no closer than about $5\mu\text{m}$ from the surface. Detailed analyses procedures and results are reported by Hussman, Berglund, and Larson [18].

A simple but revealing experiment can be developed, capitalizing on the fact that supersaturated solutions generate concentration gradients in gravitational fields [19]. A simple jacketed glass column about 20 mm in diameter and about 40 cm in height is all that is required. This column should be jacketed to assure an absolutely uniform temperature. As shown in Fig. 9.8-12, it is equipped with three or four sampling ports, preferably

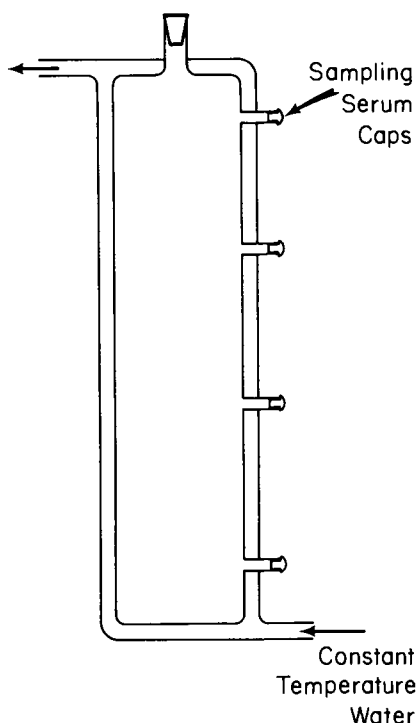


Fig. 9.8-12 Concentration-gradient apparatus.

serum caps for sampling with a syringe and needle. A solution is placed in the column, heated to remove all crystals, and then cooled to the required supersaturation.

Concentration gradients normally appear within 24 h. If no nucleation has taken place, the column is sampled at all sample ports, the temperature of each sample immediately raised to prohibit nucleation, and then density measured. An Anton Parr frequency-density measuring instrument has been used with success. One would expect density differences of order 10^{-3} to 10^{-4} g/cm³. The size of clusters can then be estimated by

$$\ln(C_T/C_B) = y[(M - \rho\nu)/RT]gH$$

where C_T and C_B are the concentrations exceeding saturation at the top and bottom, respectively, M is the solute molecular weight, ρ is solution density, ν is the cluster molecular volume, H is the column height, and y is the number of molecules in a cluster.

One would not expect to obtain usable results for sparingly soluble material, but the technique has worked well with materials such as NaNO₃, sucrose, and citric acid.

9.8.5 Mininucleator Studies

The MSMPR crystallizer apparatus can be miniaturized and automated for use in the routine testing of additives, process conditions, or new mother liquors, provided the particles are formed or segregated into a small enough size range for operation of an *in situ* zone-sensing counter probe. In this case the probe from the particle counter sits directly in the suspension or is



Fig. 9.8-13 Precipitation mininucleator apparatus, $v = 240$ ml (Chemical Engineering Department, University of Arizona).

close-coupled in a sampling cell with a circulating flow of solution from the crystallizer. Typically counter orifice diameters of $\sim 300 \mu\text{m}$ are used, permitting direct in-line counting of particles up to $120 \mu\text{m}$. Thus the entire distribution of particles should be below this size to prevent frequent plugging of the counter orifice.

A particular unit assembled at the University of Arizona, referred to as a precipitation mininucleator, is shown in Fig. 9.8-13. The crystallizer is a stirred beaker of $\sim 240 \text{ ml}$ capacity mounted directly below the counting probe of a PDI Elzone[®] zone-sensing particle counter. During the counting cycle, particles are drawn through the orifice directly from the suspension with little chance for sample error.

Liquid level is maintained by an aspirator system, which still permits a close approach to the ideal of mixed product removal. Note that the aspirator tube takes suction of an air-liquid mixture at the surface of the liquid-level bowl, while a continuous stream of liquid enters the bottom of the product dip-tube, thus preserving the constraint of mixed-product removal, even at low throughput rates. A schematic of the mininucleator is shown in Fig. 9.8-14 that shows the liquid-level aspirator and the counting probe.

The Elzone[®] instrument is programmed to process raw population-size counts and fit them to the exponential distribution, thus obtaining estimates for nucleation rate B^0 and growth rate G . Cumulative, rather than density, number-size plots are used for this data fitting operation. The cumulative greater-than-size L function is given in terms of the population density as

$$N_{(+)}(L) \equiv \int_L^{\infty} n dL \quad (9.8.5-1)$$

However, population density for the MSMR crystallizer is given as $n(L) = (B^0/G) \exp(-L/G)$. Using this form of the population density and integrating Eq. (9.8.5-1) gives

$$N_{(+)}(L) = B^0 \tau \exp(-L/G\tau) \quad (9.8.5-2)$$

Thus the cumulative greater-than-size- L population distribution is also an exponential function and on a semilog plot has the same slope as the population density, namely $-1/G\tau$. However, the intercept is $\log(B^0\tau)$ rather than $\log(B^0/G)$. An advantage to this method of data treatment is that the data points are automatically smoothed in the calculation of the cumulative distribution. A disadvantage is that only distributions of essentially exponential form over the entire size range can be processed. The technique would fail if significant particle classification occurred at the larger sizes. Figure 9.8-15 is a typical data output from the mininucleator used to precipitate calcium sulfite from simulated stackgas scrubber mother

Dimensions:

diameter = 5.7 cm

height = 13.0 cm

volume = 240 ml

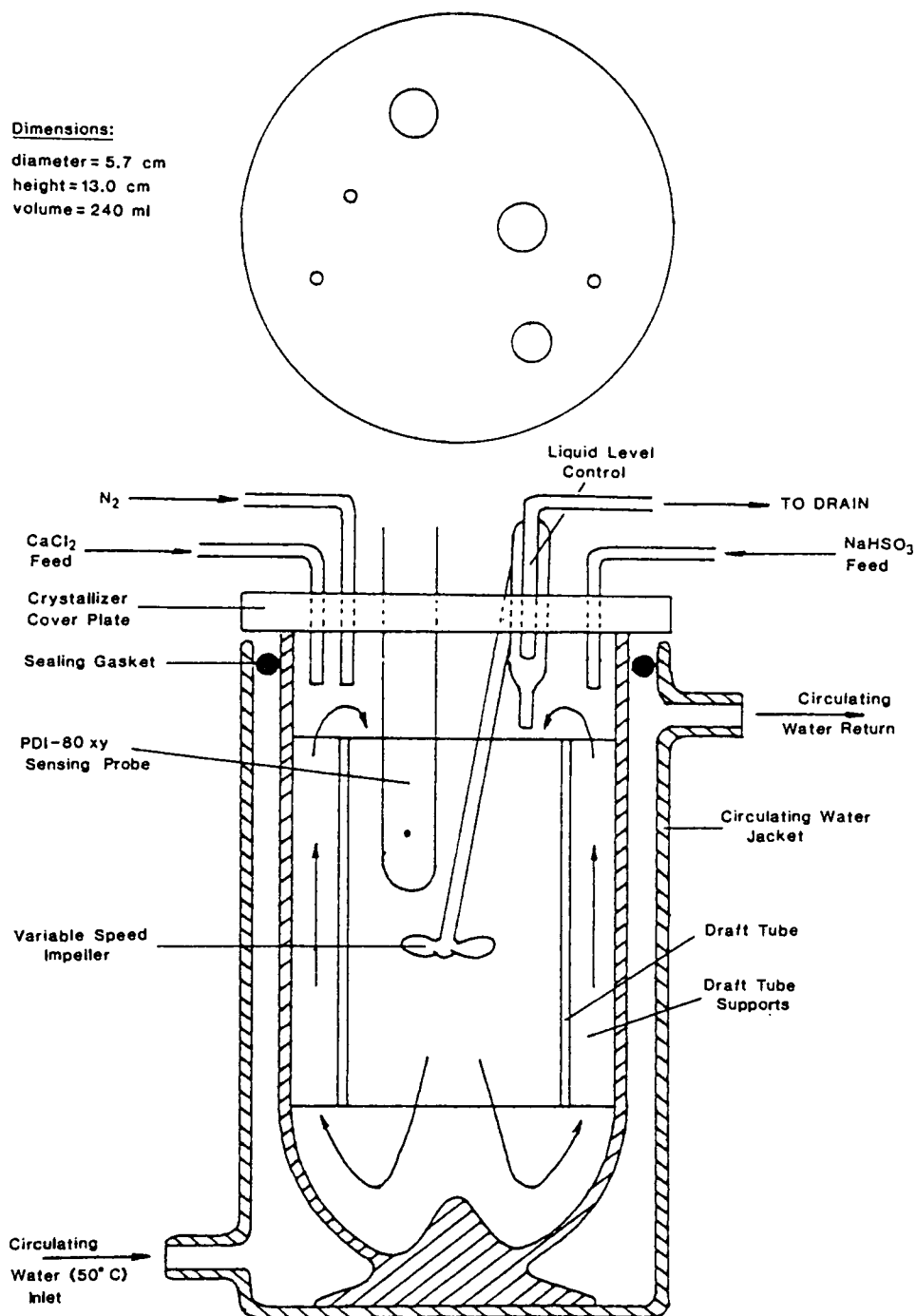


Fig. 9.8-14 Schematic of 240-ml precipitation mininucleator vessel with internals (University of Arizona).

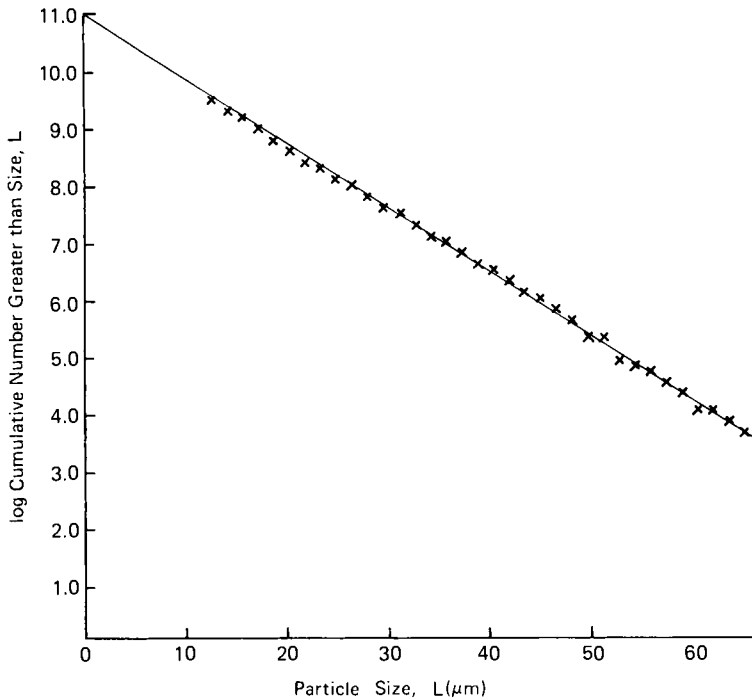


Fig. 9.8-15 Typical precipitation mininucleator data correlation plot of $N(L)$ versus L ; $\text{CaSO}_3 \cdot \frac{1}{2}\text{H}_2\text{O}$ system (University of Arizona).

liquors. Note the least-squares correlation line passing through the data points. The algorithm for correlation coefficient was erroneously programmed, and this value is not shown.

The following is a list of typical conditions/constraints/systems/advantages/limitations of this miniaturized variation of the MSMPR technique.

Used for study of precipitation systems with two separate liquid feeds.

Used successfully for precipitation systems such as calcium sulfite and calcium oxalate.

Typical retention times of 10–20 min, that is, combined flow of ~ 10 –25 ml/min.

Problems develop with coincident counting errors when particle counts are $> \sim 20,000$ particles/ml.

Slurry densities should be $< \sim 1000$ mg/l.

Orifice tube can be kept free of fouling by introduction of an air (or N_2) barrier in a concentric shielding tube surrounding orifice during periods when counts are not being made.

Large parent seed crystals cannot be maintained to induce secondary nucleation; the apparatus is suited for precipitation systems, producing small particles by primary nucleation mechanisms.

Wall fouling is a problem at the high supersaturation necessary for primary nucleation.

9.8.6 “Mode Progression” Growth Rate Technique

The mininucleator apparatus described in Section 9.8.5 is ideal for scanning the effect of growth-rate modifiers using a technique that obviates much of the time-consuming methodology of the MSMPR crystallizer. The mode progression technique is suitable for such rapid scanning of additives if the following conditions hold.

1. A supersaturated but metastable liquor can be charged to the mininucleator.
2. A fine inoculum of seed crystals can be added, typically in the size range 0–10 μm .

The size of the seed crystals is then followed in time by *in situ* particle measurement using the zone-sensing particle counter. The amount of solute precipitation on the added seed should be small compared with the solute in solution as supersaturation. Thus the crystallizer acts as a differential reactor, and growth rates can be measured at essentially constant supersaturation. Some trial and error is required to determine the amount and preparation of seed crystals in order to have enough seeds to measure with the particle counter while not having so many that supersaturation is depleted and the differential reactor assumption is invalidated.

The seeds (in a reaction-driven precipitation system) are prepared by homogeneous nucleation resulting from rapid mixing of two concentrated reagent streams. Typically a drop or two of such a homogeneously nucleated solution is enough to inoculate the solution in the mininucleator. Addition of these fine seeds represents $t = 0$, and the mode (or mean) of the seed distribution is followed in time with the particle counter, perhaps on a 5-min counting period. The mode of the distribution can easily be determined by inspection of the count total in each size range of the counter.

Processing of the data to obtain growth rates is simply done by plotting the mode (or mean) size versus sample time. The slope of this line is by definition the growth rate of the mode size in the distribution. Figure 9.8-16 shows data obtained for the calcium oxalate system using this technique.

Measured growth rates vary with both the initial supersaturation charged to the vessel and the growth modifiers added to the solution. The technique

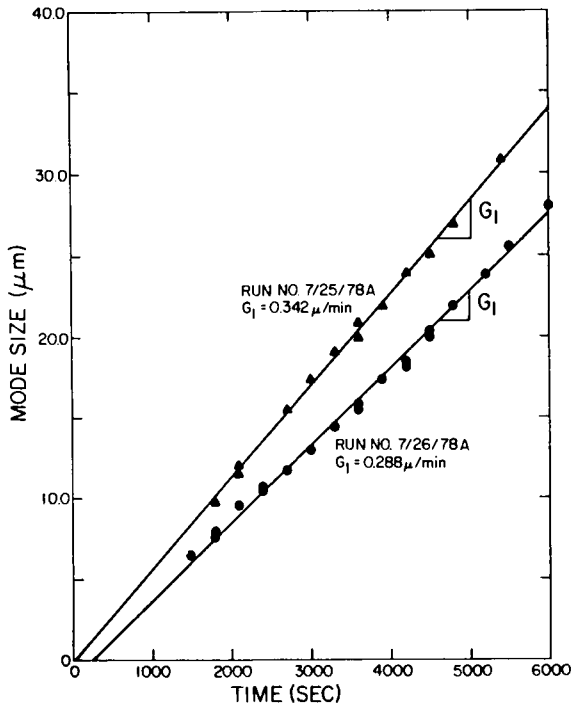


Fig. 9.8-16 Measurement of calcium oxalate growth rate in synthetic urines using the mode progression technique. [After Randolph and Drach, *J. Crystal Growth*, **53**: 195 (1981).]

is thus useful for measuring G versus s kinetics that would be used with secondary nucleation kinetics to model CSD and yield in continuous crystallizers, as well as for rapidly scanning the effects of suspected growth modifiers.

The technique fails under conditions in which copious showers of nuclei are formed upon addition of the nuclei inoculum or when large crystals are formed or added, thus plugging the counting orifice. A similar technique was published by White and Write [20] on the sucrose–water system. In this study, conventional sieves were used to monitor particle size, and large seed crystals were added to initiate the run. *In situ* particle sizing was not feasible.

The mode progression technique is ideally suited for precipitation systems that nucleate by homogeneous mechanisms at high supersaturation but retain a significant metastability at moderate supersaturation and do not readily generate secondary nuclei.

9.9 Summary

In this chapter we have described a number of experimental techniques using the MSMRP concept. Kinetic data can be obtained easily and with confidence if the indicated sampling precautions are taken. This discussion is only a sampling of the methods that can be utilized.

We also discussed a number of very specialized techniques to obtain specific information. Again, we have not been exhaustive. The material presented should suggest additional techniques and apparatus design that can be used to advantage.

References

1. Murray, D. C., and Larson, M. A. (1965). *AIChE J.* **11**, 728.
2. Branson, S. H., Dunning, W. J., and Millard, B. (1949). *Discuss. Faraday Soc.* **5**, 83.
3. Juzaszek, P., and Larson, M. A. (1977). *AIChE J.* **23**(4), 460.
4. Helt, J. E., and Larson, M. A. (1977). *AIChE J.* **23**(6), 822.
5. Crawford, R., and Randolph, A. D. (1970). Univ. of Arizona, Tucson, Arizona, unpublished master's thesis.
6. Baliga, J. B. (1970). Crystal nucleation and growth kinetics in batch evaporative crystallization. Ph.D. thesis, Iowa State University, Ames, Iowa, unpublished.
7. Clontz, N. A., and McCabe, W. L. (1971). *Chem. Eng. Progr. Symp. Ser.* **110**(67), 6.
8. Bauer, L. G., Larson, M. A., and Dallons, V. J. (1974). *Chem. Eng. Sci.* **29**, 1253.
9. Larson, M. A., and Bendig, L. L. (1976). *AIChE Symp. Ser.* **153**(72), 21.
10. Khambaty, S., and Larson, M. A. (1978). *I & EC Fund.* **17**, 160.
11. Garside, J., Rusli, I. T., and Larson, M. A. (1979). *AIChE J.* **25**(1), 57.
12. Purves, W. T., and Larson, M. A. (1980). *Int. Chem. Eng. Symp. Ser.* **59**, 7:5/1.
13. Garside, J., and Larson, M. A. (1978). *J. Cryst. Growth* **43**, 694.
14. Berglund, K. A., and Larson, M. A. (1982). *AIChE Symp. Ser.* **215**(78), 9.
15. Van Rosmalen, G. M. (1981). *Scale Prevention*, Delf University Press, The Netherlands.
16. Dixon, W. J., and Mood, A. M. (1948). *J. Am. Stat. Assoc.* **43**, 109.
17. Kelly, B. J. (1983). Study of $\text{CaSO}_3 \cdot \frac{1}{2}\text{H}_2\text{O}$ nucleation on growth rates in simulated flue-gas desulfurization liquor. Unpublished master's theses, University of Arizona, Tucson, Arizona.
18. Hussmann, G. A., Berglund, K. A., and Larson, M. A. (1984). Characterization of solution structure near the surface of a growth crystal by Raman spectroscopy. *Proc. 9th Symp. Ind. Crystallization*, The Hague, September 25.
19. Larson, M. A., and Garside, J. (1986). *Chem. Eng. Sci.* **41**(5), 1285.
20. White, E. T., and Wright, P. G. (1971). Magnitude of size dispersion effects in stirred crystallizers. *Chem. Eng. Prog. Ser.* **110**(67), 81.

APPLICATION TO OTHER SYSTEMS

We have seen in previous chapters how the population balance can be used to analyze size distributions of crystals obtained from processes where crystal nucleation and growth are occurring simultaneously. The numbers (population) balance is of considerable utility in analysis of other systems composed of countable entities. There are many examples in the process industries where discrete entities are created, destroyed, or changed in some way as a result of processing. Many biochemical processes have characteristics that lend themselves to analysis via the population balance. Even plant, animal, or human populations can be represented in time, place, and state space in the same manner as are crystal-size distributions.

In this chapter, we review some of the literature already available that shows how the numbers balance has been of use in predicting particle-size distributions in grinding processes and in characterizing polymerization processes, microbial processes, age distributions, dispersed-phase liquid systems, agglomeration, and demographic population distributions.

10.1 Comminution

There are several books and reviews for the design and modeling of comminution mills (e.g. [1], [2], [3]). The person that is deeply involved in the design and modeling of such grinding processes would most likely have these and other references at hand. It is not our purpose to review the

comminution literature nor to present a new study on the modeling of grinding mills as a particulate process. Rather, our purpose here is to set forth some of the conventional ways that particle-size distribution (PSD) has been modeled in comminution processes vis-à-vis the approach that has been taken in this book for crystallization processes. In particular, attention will be paid to formulation and estimation of the birth and death functions and to the interaction of breakage kinetics with the process RTD.

The population balance approach has been productive in modeling both crystallization and comminution processes, and there are areas where these processes truly overlap, such as modeling CSD in a crystallizer where significant particle breakage occurs. Another example might be modeling the PSD of the crystalline pieces when a shock-wave lithotripter is used to break up a kidney stone so it can be removed by natural urine voiding, rather than surgically. The PSD of the resulting kidney stone pieces is certainly important in determining their ease of passage and quite likely important in determining whether or not they might form the nidus of a new stone. Is this a crystallization, a comminution, or an agglomeration problem? Obviously there are components of each.

10.1.1 Formulation of Particle Birth and Death Functions.

Comminution researchers have conventionally referred to the birth and death functions discussed in this book as the breakage function $B(x, L)$ and the selection-for-breakage function $S(L)$. The $S(L)$ function is literally the rate constant describing the breakage of particles of size L in a grinding mill when treated as a first order rate process. The breakage function $B(x, L)$ represents the cumulative weight fraction of particles falling below size x when particles of size L are broken. If breakage is assumed proportional to the mass of particles existing at size L , then the equivalence of the comminution breakage function and the crystallization birth function $B_c(v)$ (expressed on a number rate versus particle volume basis) would be

$$S(L) \frac{\partial B(x, L)}{\partial x} m(L) dL dx = \rho v B_c(v) dv \quad (10.1-1)$$

where $S(L)$ in time^{-1} is the rate constant for breakage (or selection-for-breakage function), $m(L) dL$ is the mass of particles in the grinding mill at size L , and v is the volume of a particle of size x . It can easily be seen that both terms in Eq. (10.1-1) have the units of mass/time. The $S(L)$ function of comminution is directly related to the crystallization death function as

$$m(L) dL S(L) = \rho v D_c(v) dv \quad (10.1-2)$$

Note that the death function is expressed as a density function and thus

must be multiplied by dv . The term $S(L)$ is obtained directly as a rate constant from the exponential decay of particle mass at size L in a grinding mill and thus has the units of time^{-1} . Austin *et al*, [1, Chapter 9] give an excellent description of the S and B grinding functions and how they can be obtained from batch grinding data. Very simply, the mill is loaded with a particle charge of uniform size L (all within one $\sqrt{2}$ screen-size increment). The mill is stopped, and mass at the original screen size plotted on a semilog plot versus time. If the grinding process is first-order, this plot is a straight line and the slope is the rate constant $S(L)$. The $B(x, L)$ breakage function is obtained by grinding for shorter times and measuring the cumulative fraction of the broken particles below size x . Relatively longer grinding times can be used to determine $S(L)$, as continued breakage of the fragments does not affect the amount broken from the original size L . Continued breaking of the smaller pieces does, however, affect the $B(x, L)$ function.

10.1.2 Correlation of $S(L)$ and $B(x, L)$ Functions

Correlation of the grinding-mill S and B functions is a subject far too complex to discuss at this point. However, some simple power-law and similarity correlations have been proposed that often fit grinding data. These correlations are used in the next section to fit some continuous-mill grinding data to illustrate the interaction of size-dependent RTD with breakage kinetics in a continuous mill. A simple power-law correlation of the $S(L)$ function is given as

$$S(L) = aL^\alpha \quad (10.1-3)$$

Under normal grinding conditions the $S(L)$ function is a constant for each size L (i.e., the breakage process is truly first-order) and usually follows the above power-law form with respect to L . The breakage function $B(x, L)$ can often be expressed with the Herbst–Fuerstenau parameterization given as

$$B(x, L) = (L/x)^\alpha \quad (10.1-4)$$

Thus the breakage from larger to smaller sizes is independent of the two sizes and is only a function of their ratio. Equations (10.1-3) and (10.1-4) contain a minimum of parameters if the value of α is the same for the $S(L)$ and $B(x, L)$ functions. A more generalized form of the breakage function is given as

$$B(x, L) = (L/x)^n \quad (10.1-5)$$

where $n \neq \alpha$ is an independent parameter.

10.1.3 Effect of RTD on PSD in a Comminution Process

Analogously to CSD in a crystallization process, the PSD in a grinding circuit is described by the complex interaction between breakage kinetics and size-dependent residence times in the mill. The following example illustrates that in an open-circuit grinding mill the PSD is somewhat affected by the mill RTD, while in a closed-circuit grinding mill the PSD is hardly affected. The amount of recycle of unground particles is of course grossly effected by the grinding kinetics and residence time. Changes in recycle load may change PSD.

EXAMPLE 10.1-3 [4]

Show that PSD is affected by the assumed mill RTD in open-circuit but not in closed-circuit operation. The four simulated mill configurations are shown in Fig. 10.1-1 as one or two mixed stages with or without closed-circuit recycle through a hydroclone with a size classification $C(X)$. The $S(L)$

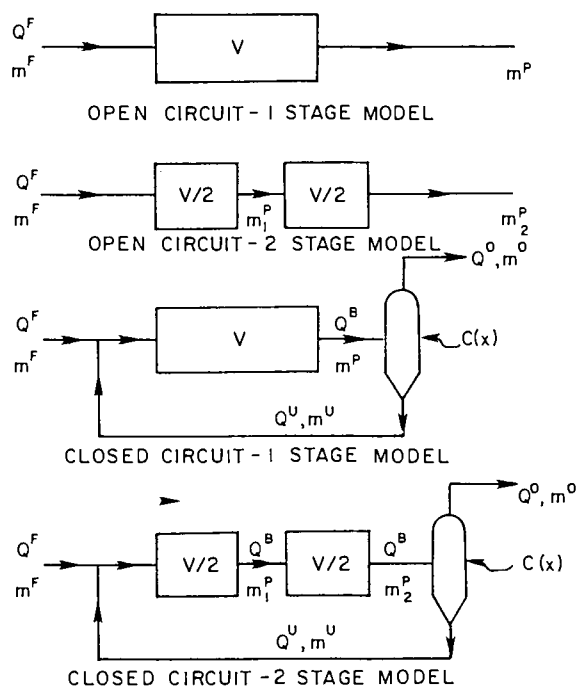


Fig. 10.1-1 Four mill configurations studied in PSD simulation. (1) Classifier overflow—1 and 2 stage models, (2) open circuits product—2 stage model, (3) open circuit product—1 stage model, (4) feed to grinding unit. (After Randolph and Ranjan [4].)

and $B(x, L)$ functions were determined by data fitting on an operating mill of the ANAMAX Mining Company (Tucson, Arizona) and are given as

$$S(L) = 0.063L^{0.719} \quad (10.1-6)$$

and

$$B(x, L) = (L/x)^{0.26} \quad (10.1-7)$$

The PSD was calculated for these four configurations by a simple mass balance using the empirical breakage kinetics of Eq. (10.1-6) and (10.1-7). Thus, as an example, the one-stage open-circuit mass density function was

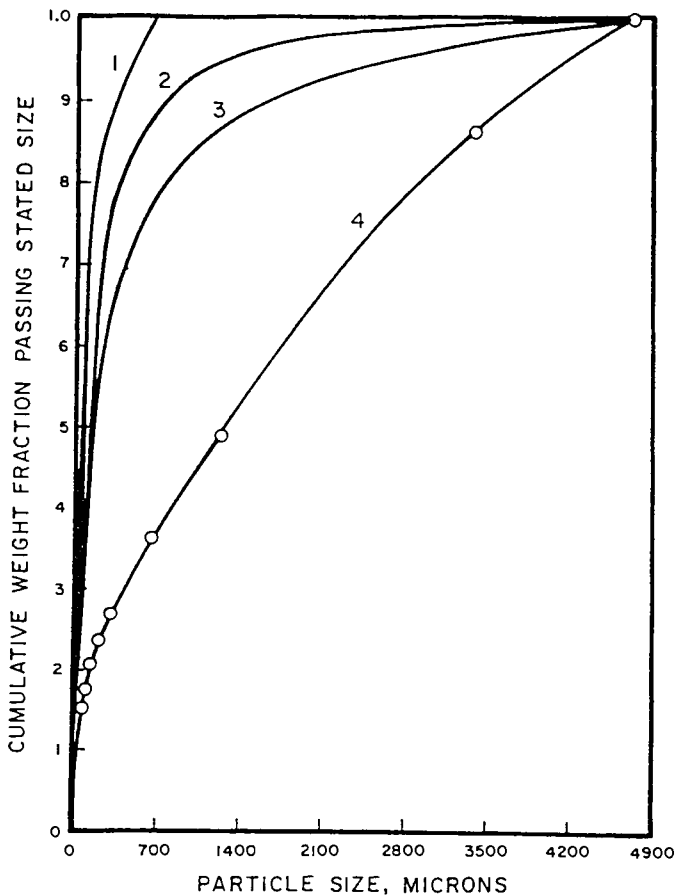


Fig. 10.1-2 Predictions of PSD for open- and closed-circuit mill configurations. (After Randolph and Ranjan [4].)

calculated as

$$M^P(X) = \frac{M^F(x) + \tau \int_x^\infty S(L) (\partial B / \partial x) M^P(L) dL}{1 + \tau S(x)} \quad (10.1-8)$$

Similar, but more complicated, equations can be derived for the closed-circuit and two-stage configurations. Closed-circuit configurations would of course involve the hydroclone classification function $C(x)$ in the modeling equation. Figure 10.1-2 plots the feed, open-circuit discharge, and closed-circuit classifier overflow PSDs. While there were some differences in PSD with an assumed mill RTD of one or two back-mixed stages in open-circuit operation (see curves 2 and 3 in Fig. 10.1-2), this difference totally disappeared for closed-circuit operation. In effect, the particles in closed-circuit operation recycle in the mill until ground. ♦

10.2 Microbial Populations

The birth, growth, and death rates of microorganisms in biochemical processes can be modeled with the aid of the population balance. The work of Tsuchiya *et al.* [5] forms the basis for the analysis of such systems and will be summarized here. We will show how the treatment relates to the general population balance developed in Chapter 3.

This system is somewhat more complex than a crystallization system in that cell death must be accounted for and birth occurs at a measurable mass. We assume that new entity formation (birth) results from the division of cells into two parts of substantially equal mass.

We consider a well-mixed fermentor in which resides a growing culture of microorganisms. We chose to characterize the cell by mass rather than by radial dimension. Thus, the population density is defined as

$$n = \lim_{\Delta m \rightarrow 0} (\Delta N / \Delta m) \quad (10.2-1)$$

Let the cell growth rate be represented by G , where

$$G = G(m, C) \quad (10.2-2)$$

and G has the dimensions of mass per unit time. Alternatively, the age of the cell might be used for characterization, but Koch and Schawchter [6] have shown that mass is a better predictor of division (hence birth) than is age. Using these definitions, Eq. (3.5-10) becomes

$$(\partial n / \partial t) + [\partial (Gn) / \partial m] + D - B = (Q/V)(n_i - n) \quad (10.2-3)$$

where D and B are death and birth functions relating these rates to the cell mass m .

Birth occurs by division of large cells and the rate is formulated as follows. The fraction Γ of cells of mass m that divide in time dt is given by

$$\Gamma = D_f(m, C) dm/n(m)$$

where C is the concentration of the nutrient required for growth, and $P(\xi, m) dm$ is the probability that an original cell of mass ξ undergoing fission will result in a daughter cell of size m . For every fission, two cells result. Thus, the rate at which new daughter cells are obtained, the birth function, is given as

$$B(m) dm = 2 \int_m^\infty P(\xi, m) D_f(\xi) d\xi dm \quad (10.2-4)$$

Death occurs in two ways: as a result of fission, and as true biological death. The rate of the former is simply

$$d_f dm = \Gamma(m, t) n(m, t)$$

For the latter, we define $T(m, C) dt$ as the fraction of cells of mass m that die in the time period dt . The total death-rate function is then

$$D = \Gamma(m, t) n(m, t) + T(m, t) n(m, t) \quad (10.2-5)$$

Substituting into the original number balance gives

$$\frac{\partial n}{\partial t} + \frac{\partial(Gn)}{\partial m} + \left(\Gamma + T + \frac{Q}{V} \right) n = 2 \int_m^\infty n(\xi) \Gamma(\xi) P(m, \xi) d\xi \quad (10.2-6)$$

This equation accounts only for living cells. To completely describe the total population including biologically dead cells, another equation is required. Let n' represent the number density of dead cells. A number balance assuming no introduction of dead cells is

$$\partial n' / \partial t = B' - (Q/V) n' \quad (10.2-7)$$

Dead cells do not grow, nor do they die. The "birth function" B' is the biological death function of Eq. (10.2-6); hence, the population of dead cells is given dynamically as

$$\frac{\partial n'}{\partial t} = \int_0^\infty T(m, t) n(m, t) dm - \frac{Q}{V} n' \quad (10.2-8)$$

10.3 Emulsion Polymerization

The population balance is applicable for the analysis of polymerization processes both at the particulate level and the molecular level. There are four types of polymerization that can be considered: bulk, solution, suspension, and emulsion. Of these, the one most similar to crystallization for

analysis purposes is emulsion polymerization considered at the polymer particle level. Polymerization has been treated at the molecular level considering a population balance of molecules of different chain lengths (Zeman and Amundson [7]).

A direct application of the general macroscopic population balance was described by Thompson and Stevens [8]. They modeled processes similar to the emulsion polymerization processes that produce styrene beads. The result is a characterization of the polymer bead size distribution. The development that follows was taken from their work.

In this treatment size is characterized by particle volume rather than diameter; therefore number density is

$$n_m = dN_m/dv$$

when m is a measure of the number of free radicals in a growing particle. The population balance is written for each class of particles having m free radicals ($m = 1, 2, \dots, \infty$). Thus for the total MSMPR system, m population balance equations are required giving distributions, the sum of which gives the distribution for the system. From the macroscopic number balance in Chapter 3 we write for the class m

$$\frac{\partial n_m}{\partial t} + \frac{\partial}{\partial v}(n_m R_{vm}) = \frac{n_{mi} - n_m}{\tau} + r_{nm} \quad (10.3-1)$$

where R_{vm} is the volumetric growth rate of a particle and r_{nm} is the net rate of formation of an m -type particle, and n_{mi} is the number density of m -type particles in the inflow stream.

Following Gardon [9], the particle growth rate is related to m by

$$R_{vm} = Km \quad (10.3-2)$$

where R_{vm} is proportional to the number of growing chains present; K , however can be slightly size-dependent. In this treatment it will be assumed constant.

For r_{nm} the Smith-Ewart [10] recursion relationship is modified to allow radical capture to be proportional to surface area of the particle. Thus

$$r_{nm} = \frac{\alpha}{v} [(m+2)(m+1)n_{m+2} - m(m-1)n_m] + \frac{\beta}{v^{2/3}}(n_{m-1} - n_m) + \frac{\gamma}{v^{1/3}} [(m+1)n_{m+1} - mn_m] \quad (10.3-3)$$

$$\alpha = \frac{k_t}{N_A} \quad \beta = \frac{(4\pi)^{1/3}(3)^{2/3}\rho_A}{s} \quad \gamma = (4\pi)^{1/3}(3)^{2/3}k_0$$

Here k_t is the termination rate constant and k_0 is the desorption rate constant; ρ_0 is rate of feed radical production; and N_A is Avogadro's

number. Using these expressions for the rate quantities give

$$\begin{aligned} \frac{\partial n_m}{\partial t} + K \frac{\partial}{\partial v} (mn_m) &= \frac{n_{m_i} - n_m}{\tau} \\ &+ \frac{\alpha}{v} [(m+2)(m+1)n_{m+2} - m(m-1)n_m] \\ &+ \beta v^{1/3} (n_{m-1} - n_m) + \frac{\gamma}{v^{1/3}} [(m+1)n_{m+1} - mn_m] \end{aligned} \quad (10.3-4)$$

Negatively subscripted quantities are taken as zero. Assuming steady state and substituting the dimensionless groups

$$y_m = \frac{n_m}{n_{T0}}, \quad \zeta = \frac{v}{v_0}, \quad \text{and} \quad \theta = \frac{v_0 t}{K}$$

gives

$$\begin{aligned} \frac{d}{d\zeta} (my_m) &= -A_5 y_m + \frac{A_7}{\zeta} [(m+2)(m+1)y_{m+2} - m(m-1)y_m] \\ &+ A_4 \zeta^{2/3} \left\{ y_{m-1} - y_m \frac{A_6}{\zeta^{1/3}} [(m+1)y_{m+1} - my_m] \right\} \end{aligned} \quad (10.3-5)$$

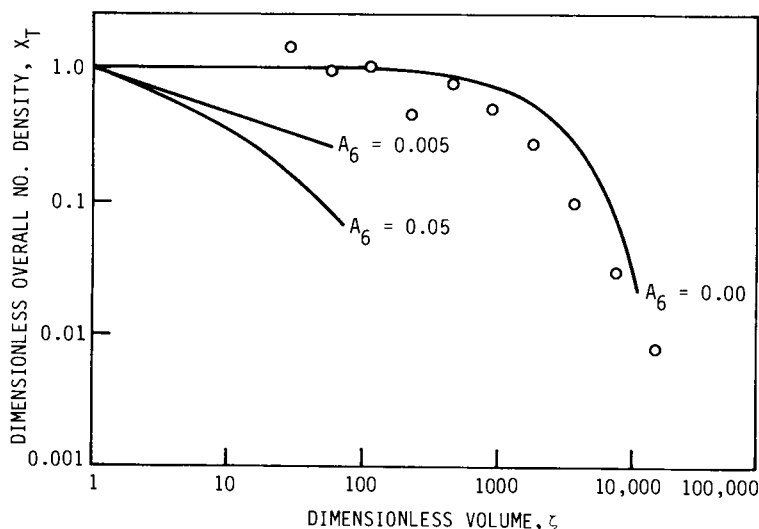


Fig. 10.3-1 Population-balance model prediction. $A_4 = 5.644 \times 10^{-11}$, $A_5 = 3.299 \times 10^{-4}$, $A_7 = 1.1005 \times 10^2$. Data from Stevens and Funderburk [11].

where n_{T_0} is the number density of zero-size polymer particles and v_0 is the micellar volume.

The four constants A_4 , A_5 , A_6 , and A_7 represent the ratios of the four mechanisms (radical capture, bulk flow, radical desorption, and radical termination) to the growth constant K . The necessary initial condition on y assumes that for $y_m^0 = 0$, $m \neq 1$. The boundary condition is explained by Thompson and Stevens and is taken as

$$x_1^0 = \frac{1 + A_3}{1 + A_1 + 2A_3} \quad (10.3-6)$$

The set of n equations was solved testing parameters developed by Stevens and Funderbuck [11] for styrene polymerization. The results are plotted in Fig. 10.3-1 along with the Stevens and Funderbuck [11] data. Taking $A_6 = 0$ gives results that approximate the data.

10.4 Dispersed-Phase Mixing

In fluid-fluid contacting operations, one fluid is dispersed in a continuous phase in the form of droplets or bubbles. It is of interest to characterize the properties of these droplets in order to relate these properties to the rate of mass transfer or chemical reaction that may occur in a process. The droplets may be of different size and of different solute concentration. The distribution of these drops in the property state space and all of the drop properties can be represented by using the basic macroscopic population balance of Eq. 3.5-10):

$$\frac{\partial n}{\partial t} + \nabla \cdot \mathbf{v}_i n + n \frac{d(\log V)}{dt} = B - D - \sum \frac{Q_k n_k}{V}$$

Curl [12] discussed a continuous-flow, dispersed-phase reactor of constant volume where a reaction of arbitrary order takes place by a reactant that is in the dispersed phase. The reactor was assumed to be macroscopically well mixed—that is, the distribution of the dispersed phase was “uniform” throughout the vessel. The droplet distribution was characterized by the reactant concentration in each droplet, and the droplet size was assumed to be uniform throughout the reactor. Taking $n = n(C, t)$ and regarding n as the number frequency rather than the population density (i.e., at steady state, $\int_0^\infty n dC = 1$), Eq. (3.5-10) becomes

$$\frac{\partial n}{\partial t} - k \frac{\partial(C^n n)}{\partial C} = B - D + \frac{n_0}{\tau} - \frac{n}{\tau} \quad (10.4-1)$$

Here, the second term represents the rate of change of concentration in the droplets of the distribution due to chemical reaction of order s . The terms n_0/τ and n/τ represent the inflow and outflow of droplets, respectively. The quantity k is the reaction rate constant and $\tau = VQ_1/QQ_2$, where Q_1 is the fraction of dispersed phase in the inflow and Q_2 is the fraction in the outflow. Presumably, these two quantities are nearly equal. Because the reactor volume remains constant, the third term of Eq. (3.4-10) does not appear.

Curl considered a coalescence and dispersion model based on the assumption that only binary collisions occurred and the resulting coalesced droplets immediately redispersed into two droplets of equal size. Letting C_1 and C_2 represent the concentrations of two colliding droplets, respectively, the two droplets resulting from the redispersion will have a reactant concentration $(C_1 + C_2)/2$. This collision and dispersion model results in expressions for B and D as follows:

$$D = (2u/U)n \quad (10.4-2)$$

$$B = \frac{Au}{U} \int_0^C n(C - \alpha)n(C + \alpha) d\alpha \quad (10.4-3)$$

The quantity u is the collision rate and U is the total number of droplets in the dispersion; α is a dummy variable.

Substituting into Eq. (3.5-10) gives for the population balance

$$\frac{\partial n}{\partial t} - k \frac{\partial (C^s n)}{\partial C} + \frac{n}{\tau} = \frac{n_0}{\tau} + \frac{2u}{U} \left[2 \int_0^C n(C - \alpha)n(C + \alpha) d\alpha - n \right] \quad (10.4-4)$$

The above equation has no known analytic solution. However, it can be solved numerically for zeroth-, first-, second-, and perhaps higher-order reactions for assumed values of $2u/U$.

Again the moments of the distribution have significance. For example, the first moment is the average droplet concentration in the suspension:

$$m_1 = \int_0^\infty Cn dC \quad (10.4-5)$$

EXAMPLE 10.4-1

Assume a continuous, back-mixed, dispersed system in which reactant A of concentration C in the dispersed phase undergoes a first-order reaction. At steady state and when no collisions occur, u is zero and Eq. (10.4-4) becomes

$$k [d(Cn)/dC] - (n/\tau) = -n_0/\tau \quad (10.4-6)$$

Let $n_0 = -\delta(C - C_0)$; then

$$k [d(Cn)/dC] - (n/\tau) = (1/\tau) \delta(C - C_0) \quad (10.4-7)$$

Integrating using the integrating factor $\exp(k\tau - 1)/k\tau$ gives

$$n = (1/k\tau C)(C/C_0)^{1/k\tau} \quad (10.4-8)$$

The above concentration C is

$$m_1 = \bar{C} = \int_0^C \left(\frac{1}{k\tau} \right) \left(\frac{C}{C_0} \right)^{1/k\tau} dC \quad (10.4-9)$$

$$\bar{C} = C_0/(1 + k\tau) \quad (10.4-10)$$

We note this is the same result as is obtained from a perfectly mixed system. ♦

EXAMPLE 10.4-2

Repeat Example 10.4-1 assuming a second-order reaction. Here, Eq. (10.4-4) becomes

$$k [d(C^2n)/dC] - (n/\tau) = (1/\tau) \delta(C - C_0) \quad (10.4-11)$$

Equation (10.4-11) can be solved using the integration $C^2 \exp(1/k\tau C)$ to get

$$n = \frac{1}{C^2 k \tau} \exp \left[\frac{1}{k \tau} \left(\frac{1}{C_0} - \frac{1}{C} \right) \right] \quad (10.4-12)$$

Clearly, it is possible to use other collision and coalescence models as well as other state properties for studying dispersed systems. The difficulty arises in obtaining realistic parameters for representing the collision frequency and dispersion frequency.

10.5 Residence-Time Distributions

The concept of residence-time distributions in flow-processing vessels as summarized by Danckwerts [13], Wolff and Resnick [14], and others is related to the population distribution we discuss in this volume. We consider first a well-stirred flow reactor with a feed and discharge consisting of a single phase. The "discrete entity" is regarded as an arbitrarily small element of the liquid phase, that we shall imagine retains its integrity during its journey through the vessel. Because the vessel is perfectly mixed, we do not concern ourselves with the spatial position of these particles. We

characterize the particle only by its state, namely, its age—that is, the time it has been in the vessel.

The population density function now becomes a function of time and a function of the age of the element. We distinguish between “age” and time because the age distribution can in general vary in time. This gives

$$n = n(t, \theta)$$

where θ is the age in the environment of the element and n is now thought of as a density fraction of entities in the range $\theta + d\theta$ such that the number of elements with current residence θ in the environment is given as $N_T n d\theta$, where N_T is the total number of elements in the system.

For the case of a single-stage, perfectly mixed vessel, Eq. (3.5-10) becomes

$$(\partial n / \partial t) + (\partial n / \partial \theta) + (n / \tau) = NQ \delta(\theta) / V \quad (10.5-1)$$

There are no birth or death terms, and all input elements enter at age zero; thus, the input term becomes $(N/F)Q \delta(0)$, where N can be thought of as the concentration of elements per unit volume of inflow, Q is the inflow rate, V is the volume of the vessel, and $\delta(0)$ is the unit impulse. We note that age is gained in a one-to-one correspondence with the passing of time, so the “growth term” coefficient is unity.

If we specify an initial condition on the distribution, namely, $n(0, \theta)$, then Eq. (10.5-1) can be solved to give

$$n(t, a) = \exp(-t/\tau) n(\theta - t, 0) + (N/\tau) \exp(-\theta/\tau) [U(\theta) - U(\theta - t)] \quad (10.5-2)$$

where $U(\theta)$ is the unit function such that

$$U(\theta) = \begin{cases} 0, & \theta < 0 \\ 1, & \theta > 0 \end{cases} \quad (10.5-3)$$

For a well-mixed vessel at steady state, Eq. (10.5-3) reduces to

$$n = (N/\tau) \exp(-\theta/\tau) \quad (10.5-4)$$

the classic residence-time distribution function for a well-mixed vessel.

The zeroth moment,

$$m_0 = \int_0^\infty n(\theta) d\theta = N [1 - \exp(-\theta/\tau)] \Big|_{\theta=0}^{\theta=\infty} = N_T \quad (10.5-5)$$

gives the total number of elements of all ages in the system. The first moment divided by the zeroth moment gives the average age of all elements, namely, the mean residence time τ :

$$\frac{m_1}{m_0} = \frac{\int_0^\infty (N/\tau) \theta \exp(-\theta/\tau) d\theta}{\int_0^\infty (N/\tau) \exp(-\theta/\tau) d\theta} = \frac{N\tau}{N} = \tau \quad (10.5-6)$$

For distributed flows, one must start with Eq. (3.4-6), which accounts for spatial variation of the distribution.

10.6 Particle Agglomeration

The details of the analysis of particle agglomeration processes, such as those used in the mixed fertilizer industry, are quite different from those we have previously considered. The objective of such processes is to build larger particles by "sticking together" two or more smaller particles. The particles that come together are all of measureable size; therefore, the growth of an agglomerate takes place in finite steps. Except in cases where precipitation takes place on the surface of the agglomerate, continuous growth does not occur and the corresponding term is absent from the model. The size-distribution change is wholly a fraction of particle birth and death, and particle inflow to and outflow from the system.

Hulburt and Katz [15] considered the case of a plugflow agglomerator where the size distribution must be considered a function of axial position as well as time. Hence, we define the number density as a function of axial position x , mass m , and time t :

$$n = n(x, m, t) \quad (10.6-1)$$

It is assumed here that the distribution does not vary in the radial direction.

In order to model this situation, it is necessary to start with Eq. (3.4-6), the micropopulation balance, because the number density is a function of position as well as state and time. The balance becomes

$$(\partial n / \partial t) + u_x (\partial n / \partial x) = h(x, m, t) \quad (10.6-2)$$

Here, h represents the net rate of formation at size m , that is,

$$h(x, m, t) = B - D \quad (10.6-3)$$

Note that no growth term appears. The second term is the flow velocity u_x multiplied by the rate of change of number density with position. It represents the changes in size distribution with position along the axis of the agglomerator.

Hulburt and Katz proposed a mechanistic model for birth and death as follows. Particle nucleation under the influence of the chemical environment is ignored. Only particle birth due to collisional agglomeration is considered. At some time t and position x , we let the rate of agglomeration of particles of mass m_1 and m_2 be proportional to the product of the number densities $n(x, m_1, t)$ and $n(x, m_2, t)$. The proportionality factor for collision $a(x, t)$ depends only on the environment and not on the

particle size or shape. Thus, particles of mass m will be formed at the rate

$$B(m) = \frac{1}{2} a(x, t) \int_0^\infty n(x, m - \xi, t) n(x, \xi, t) d\xi \quad (10.6-4)$$

where ξ is the mass of one of the colliding particles and $m - \xi$ is the mass of the other. The factor $\frac{1}{2}$ ensures that collisions are not counted twice. Particles of mass m will be lost by agglomeration at the rate

$$D(m) = a(x, t) n(x, m, t) \int_0^\infty n(x, \xi, t) d\xi \quad (10.6-5)$$

Incorporating these two functions in the population balance gives

$$\frac{\partial n}{\partial t} + u_x \frac{\partial n}{\partial x} = a \left[\frac{1}{2} \int_0^\infty n(x, m - \xi, t) n(x, \xi, t) d\xi - n(x, m, t) \int_0^\infty n(x, \xi, t) d\xi \right] \quad (10.6-6)$$

The flow velocity u_x must be obtained from a momentum balance on the system, and the factor $a(x, t)$ reflects the chemical and thermal environment and is related to the external material and energy balances.

The moments of the distribution are defined as

$$m_j = \int_0^\infty p^j n(x, p, t) dp \quad (10.6-7)$$

where p is a dummy of integration. This moment transformation can be used to reduce Eq. (10.4-6) to

$$(\partial m_0 / \partial t) + u_x (\partial m_0 / \partial x) = (-1/2) a m_0^2 \quad (10.6-8)$$

for $j = 0$.

The solution to Eq. (10.6-8) gives the time and space variance of the total number of agglomerates, that is, the total number of particles per unit volume as a function of axial dimension x at some point in time.

10.7 Protein Precipitation

In the precipitation of biological products (e.g. soy protein), the particle-size distribution plays an important role in determining product purity and in the efficiency of the subsequent solid-liquid separation step. Particle growth is predominantly by aggregation of very small primary precipitant particles with larger aggregates. Stirring the suspension, however, results in substantial particle-size reduction because of fluid shear forces. In studying such processes it is of interest to relate the particle-size distribution to

process conditions. The conditions that affect particle size to the greatest extent are suspension density and the intensity of the shearing action induced by agitation.

An example of such a process is the precipitation of soy-protein particles from solution at the isoelectric point. Protein extract and sulfuric acid are fed continuously to a continuous stirred tank reactor. At the isoelectric point protein precipitates and subsequently aggregates into larger particles. Glatz, Hoare and Landa-Vertiz [16] modeled the particle-size distribution obtained from this process using the population balance written for a well-mixed continuously fed vessel. The model was based on the following assumptions about the mechanism of particle formation and growth.

1. Protein precipitates quickly. That is, it is assumed to be totally insoluble.
2. Aggregate growth occurs by collision of submicrometer primary particles with aggregates and no appreciable aggregate-aggregate bonding occurs.
3. The *effectiveness* of those collisions that result in aggregate growth is independent of the size of the aggregates.
4. Aggregates break up into smaller aggregates due to shearing action induced by agitation. Daughter aggregates are assumed to be equal in volume. Larger aggregates break up into larger numbers of pieces. Breakup susceptibility increases with size.

The steady/state aggregate population balance from Chapter 3 is

$$\frac{d(Gn)}{dL} + \frac{n}{\tau} + D - B = 0 \quad (10.7-1)$$

where G , D , and B are functions of size L .

From assumptions 1, 2, and 3 above, the growth rates of aggregates by collisions with primary particles is given by

$$G(L) = K_0 L \quad (10.7-2)$$

where K_0 incorporates the collision effectiveness.

From assumption 4,

$$D(L) = kL^\beta n(L) \quad (10.7-3)$$

where k is related to shear rate, and β accounts for the assumption that large aggregates have a greater probability of breakup.

Also from assumption 4 and accounting for the facts that birth comes only from breakup and mass must be conserved,

$$B(L) = (f) D(f^{1/3} L) \quad (10.7-4)$$

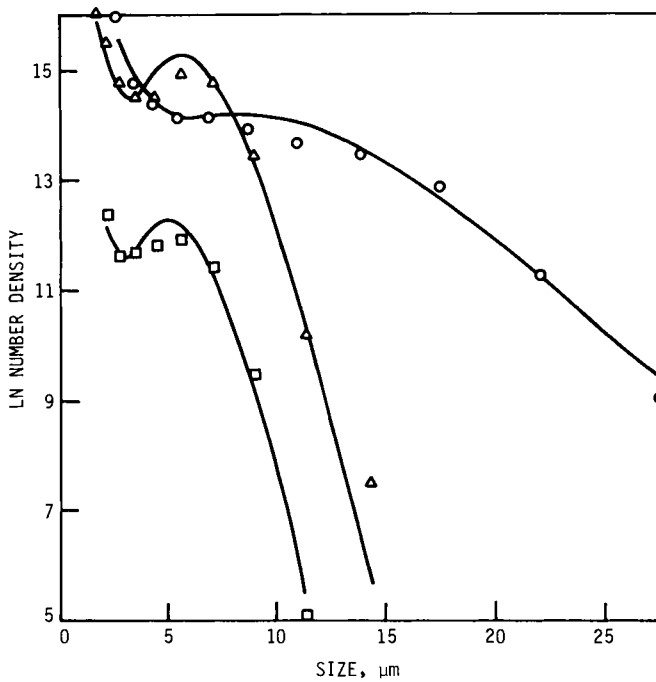


Fig. 10.7-1 PSD of protein aggregate in a continuous stirred tank reactor: comparison of model with experimental data. (From Glatz *et al.* [16].) □, 0.15 kg/m³; Δ, 3.00 kg/m³; ○, 25.00 kg/m³.

where f is a measure of the number of particles resulting from the breakage of a single particle.

Substituting Eqs. (10.7-2), (10.7-3), and (10.7-4) into Eq. (10.7-1) gives

$$\frac{dn}{dL} = \frac{k}{K_0} L^{\beta-1} [f^{\beta/3+1} n (f^{1/3} L) - n] - \frac{n}{L} \left(1 + \frac{1}{\tau K_0} \right) \quad (10.7-5)$$

Glatz *et al.* found that $f = 2$ and $\beta = 2.3$ were reasonable values for these parameters. Using these parameters, Eq. (10.7-5) was solved numerically until values of k and K_0 were found that gave results that agreed with the data. In order to solve Eq. (10.7-5) it was necessary to set the boundary conditions, namely, the number density of the maximum size. The model fit experimental data quite well, as shown in Fig. 10.7-1. The experimental data points were obtained at three different suspension densities but at the same stirring speed.

The model predicts and the data show that higher suspension densities produce larger aggregates. The authors also showed that the model represented the effect of stirring speed equally well, showing that higher agitator

speeds resulted in smaller particles. The constant k varied by less than a factor of 2 over the suspension density ranges studied.

10.8 Inorganic Precipitation with Agglomeration

In many precipitation processes where the precipitant is a sparingly soluble salt, particle size is determined mainly by agglomeration of the very small primary crystallites with little or no particle fracture from shearing forces or impact as a result of stirring. Success in modeling the size distribution of these materials can be achieved with a simplified model that eliminates the need for birth and death terms, terms that greatly increase the complexity of solution. The basic assumption is that little error is introduced by representing the agglomeration mechanism as continuous growth in the same sense as crystal growth.

The example discussed here follows the work of Hoyt [17]. In this work he analyzed the effect of process conditions on the size distribution of ammonium polyuranate particles produced in a continuous (MSMPR) precipitator. The nature of the size distribution and the structure of the precipitated particles are important in the subsequent processing of the material, which is ultimately used as nuclear reactor fuel.

It is assumed that three types of particles can be distinguished, namely, (1) crystallites of primary particles, (2) clusters that are made of aggregated crystallites, and (3) agglomerates that mainly arise from the agglomeration of clusters. Each class of particles is modeled separately, with the sum of the three distributions representing the PSD of the suspension.

The crystallites are produced by nucleation and growth at a rate G_x . They are removed continuously in the product flow stream, but they also disappear by forming clusters and by aggregating with agglomerates. The last two phenomena are represented by removal terms $k'_x n_x$ and $k''_x n_x$, respectively, when the constant are measures of the clustering and agglomeration rates. Thus for the crystallites in an MSMPR precipitator,

$$\frac{\partial n_x}{\partial t} + \frac{\partial (G_x n_x)}{\partial L} + \left(\frac{1}{\tau} + k'_x + k''_x \right) n_x = 0 \quad (10.8-1)$$

Assuming McCabe's ΔL law and solving for a steady-state size distribution gives

$$n_x = n_x^0 \exp(-L/G_{e,x}\tau) \quad (10.8-2)$$

The term $G_{e,x}$ is the *effective* crystallite growth rate and is given as

$$\frac{G_x}{1 + \tau(k'_x + k''_x)} \quad (10.8-3)$$

Clusters grow by a pseudo-growth rate G_e , which is proportional to

$$k'_x \sqrt[3]{L_k}$$

when L_x is the mean size of the crystallites. Clusters disappear by flow from the crystallizer and by agglomeration to form agglomerates. The agglomeration rate constant is k_c ; thus for clusters,

$$\frac{\partial n_c}{\partial t} + (G_c + G_x) \frac{\partial n_c}{\partial L} + \left(\frac{1}{\tau} + k_0 \right) n_c = 0 \quad (10.8-4)$$

The term G_x is included because presumably the clusters would grow by the primary growth mechanism as well. For steady state the solution is

$$n_c = n_c^0 \exp(-L/G_{e,c}\tau) \quad (10.8-5)$$

where $G_{e,c}$, the effective cluster growth rate, is

$$G_{e,c} = \frac{G_c + G_x}{1 + \tau k_c} \quad (10.8-6)$$

Similarly, for agglomerate growth, G_a is taken as the growth due to agglomerate growth and G'_a is growth due to incorporation of crystallites. The population balance is

$$\frac{\partial n_a}{\partial t} + (G_a + G'_a + G_x) \frac{\partial n_a}{\partial L} + \frac{1}{\tau} n_a = 0 \quad (10.8-7)$$

at steady state

$$n_a = n_a^0 \exp(-L/G_{e,a}g\tau) \quad (10.8-8)$$

$$G_{e,a} = G_a + G'_a + G_x$$

The size distribution of the composite is therefore

$$n_T = n_x^0 \exp(-L/G_{e,x}\tau) + n_c^0 \exp(-L/G_{e,c}\tau) + n_a \exp(-L/G_{e,a}\tau) \quad (10.8-9)$$

The term n_x^0 is the true crystallite nuclei population density and $n_x^0 G_x$ is the nucleation rate; n_a^0 and n_c^0 are pseudo-agglomerate and cluster number densities at zero size. They are fictitious but can be used to characterize cluster and agglomerate formation.

Because these three classes of particles exist in distinguishably different size ranges, an analysis of the composite size distribution provides a method for determining the rates of clustering and agglomeration. In the example cited (Hoyt [17]), the sizes of the crystallites of ammonium polyuranate are too small to be detected with a particle counter. However, the data as shown in Fig. 10.8-1 clearly show the regions where clusters dominate and

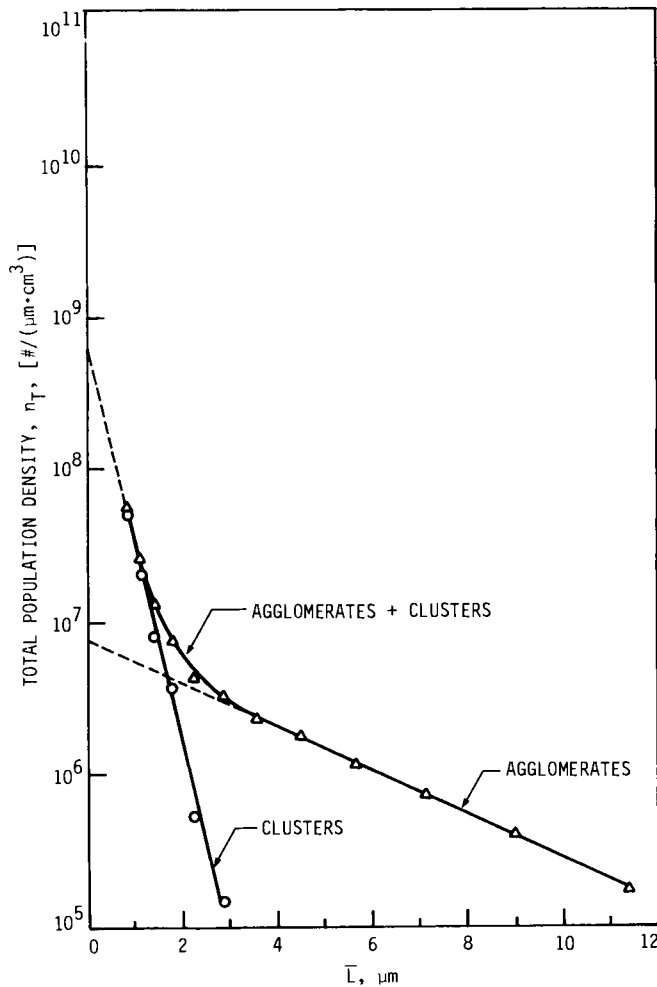


Fig. 10.8-1 CSD of ammonium polyuranate showing clusters and agglomerates. (Data from Hoyt [17].) NH_3 : Uranium mole ratio = 2.20; pH = 7.10; τ = 13 min; T = 25°C.

where agglomerates dominate. A measure of the growth rates $G_{e,c}$ and $G_{e,a}$ can be obtained from the slopes of the two sections of the plot, and the intercept of these two sections gives a measure of the clustering and agglomeration rates.

This type of analysis is useful in any system where two or more classes of particles are formed simultaneously.

10.9 Modeling Agglomeration / Aggregation

ASTM Designation E-20-85 defines an agglomerate as “a mass formed by the cementation of individual particles, probably by chemical forces,” while an aggregate is “a mass formed of mixtures of particulate and agglomerate particles having a binding force intermediate between agglomerates and flocculates” [18]. Clearly this definition indicates that agglomerates are the stronger of the two types of particles and would be least likely to rupture after forming. When two or more crystal particles are brought together in an agitated solution—say, by fluid shear or local velocity fluctuations—their natural attraction (due to van der Waals forces summed over all molecules in both particles) first brings them together as aggregates. In a supersaturated solution, crystal–crystal bonds form and the particles are eventually cemented firmly together as agglomerates. Such an aggregation/agglomeration mechanism is a likely first step in the formation of a kidney stone.

Figure 10.9-1 shows a two-stage crystallizer/aggregator that was used to study the kinetics of calcium oxalate (CaOx) aggregation in a urine-like mother liquor [19]. (In the spirit of ASTM E-20-85, the particles are referred to as aggregates, rather than agglomerates, as a particle rupture term was needed to model the aggregated distribution.)

The first stage in the apparatus shown in Fig. 10.9-1 was an intensely agitated MSMPR crystallizer, which discharged directly to an in-line zone-sensing particle counter or to an annular vessel having a rotating inner cylinder, thus causing rotational vortex flow in the annulus. The annular

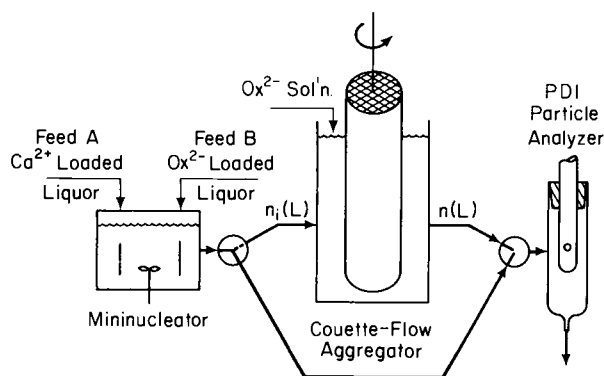


Fig. 10.9-1 Schematic of mininucleator/aggregator apparatus. (After Hartel *et al.* [19].)

and MSMPR volumes were approximately equal. With the flows used, a retention time of 8–10 min in each vessel was obtained. The degree of aggregation obtained (as a function of CaO_x concentration and inner cylinder rotation speed) was measured in-line with the particle counter, with or without passing the stream through the aggregator. Negligible aggregation occurred in the MSMPR vessel as evidenced by the excellent fit of these data to the MSMPR exponential distribution.

EXAMPLE 10.9-1

Fit the CSD data from the two-stage crystallizer/aggregator to the continuous-flow steady state aggregation model of Eq. (3.7.1-10) to obtain aggregation (agglomeration) aggregate rupture rate constants [20].

Equation (3.7.1-10) assumes the aggregator is back-mixed, although the annulus was typically in the flow regime of Taylor vortex flow. The back-mixed assumption permitted solution of the aggregation equations

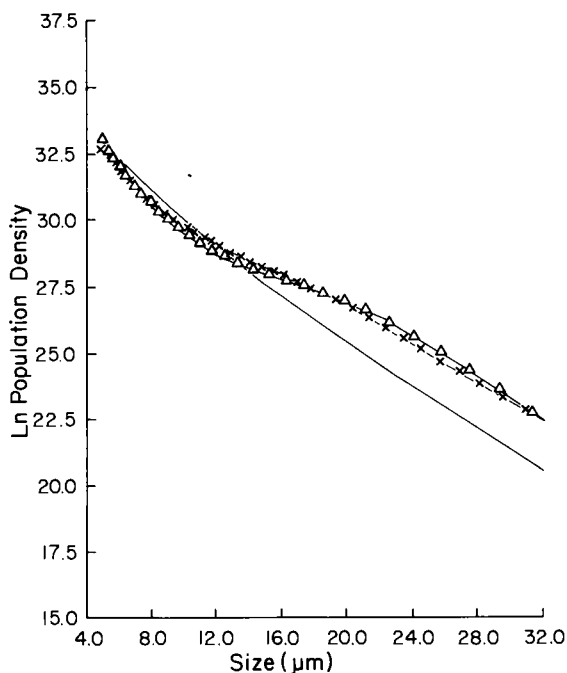


Fig. 10.9-2 Comparison of predicted model distribution with aggregator distribution at 250 RPM spindle rotation. $C_A = 300$, $K_D = 1,000,000$. Δ , Model; \times , aggregator; —, crystallizer. Data for experiment 3/24B with population density expressed in volume coordinates (number per cubic centimeter per cubic centimeter). (After Hartel and Randolph [20].)

with an existing computer program, Program AEROSOL [21]. The population balance for the aggregator, written in number density versus particle volume coordinates [see Eq. (3.7.1-10)], is given as

$$\frac{d(G_v n)}{dv} + \frac{Q}{V}(n - n_i) = (B - D)_A + (B - D)_R + B^0 \quad (10.9-1)$$

where

$$(B - D)_A = \frac{1}{2} \int_0^v C_A(v, v-u) n(u) n(v-u) du - n(v) \int_0^\infty C_A(v, u) n(u) du \quad (10.9-2)$$

represents the aggregation model (taken analogously to aerosol coagulation) and the aggregate rupture terms were given by the two-body, equal-volume breakage model as

$$(B - D)_R = K_D [2(2v)^a n(2v)] - v^a n(v) \quad (10.9-3)$$

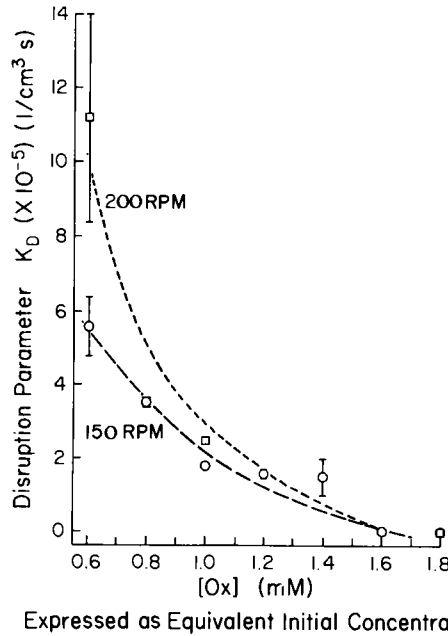


Fig. 10.9-3 Variation of disruption parameter K_p with oxalate concentration in the aggregator. (After Hartel and Randolph [20].)

Equations (10.9-1)–(10.9-3) only have three adjustable constants, C_A , K_D , and B^0 . In fitting the data from the aggregator to the above model, all data were converted from population-size density to population-volume density. The MSMPR growth rate was used in the aggregator equation. (This assumption had a negligible effect on the data fit, as the aggregation and rupture terms dominate the equation.)

Figure 10.9-2 shows the model fit to experimental data with conditions when both aggregation and rupture was important in shaping the distribution. Figure 10.9-3 shows the dramatic effect of increased CaO_x concentration in reducing the disruption coefficient K_D . High levels of supersaturation rapidly convert the aggregates into agglomerates by crystal growth at the particle contacts.

10.10 Bubble-Size Distribution in Aeration Processes

In the aeration of lakes, ponds, or unagitated tanks, it is of interest to determine the rate of mass transfer from the bubbles as they rise to the surface. The rate depends on the surface area, and thus the size distribution of the bubbles, for transfer. As the bubbles rise, the number and size change because of mass transfer and change in pressure and temperature because of coalescence or dispersion. Here we consider a method of modeling this distribution so that the distribution can be characterized as a function of height above a sparger. An example calculation (Martin [22]) is made demonstrating the model for the aeration of a stagnant lake with pure oxygen.

Valentes *et al.* [23] have shown that bubbles from a sparger tend to have a log-normal volume-based distribution. Their model converted to a diameter-based distribution is

$$n_0(D) = \frac{3}{\sqrt{2\pi}} \left(\frac{K}{L\sigma} \right) \exp \left[-\frac{(L^3/\bar{L}^3 - \sigma^2/2)}{2\sigma^2} \right] \quad (10.10-1)$$

Using this initial distribution, we show how the distribution changes as the bubbles rise to the surface.

The starting point will be the microdistributed population balance developed in Chapter 3:

$$\frac{\partial n}{\partial t} + \nabla \cdot U_s n + \nabla \cdot U_i n = B - D_p \quad (10.10-2)$$

Assuming steady state, considering the motion of the bubbles to be only in the vertical direction, and characterizing the bubbles by their diameter only results in the first term becoming zero, the second term reducing to the

vertical velocity vector, and the third term reducing to the bubble-growth velocity vector. Thus,

$$\frac{\partial(U_x n)}{\partial X} + \frac{\partial(Gn)}{\partial L} = B - D_p \quad (10.10-3)$$

The growth rate G , although a function of time, can be expressed as a function of vertical position X :

$$G = \frac{dL}{dt} = \frac{dL}{dX} \frac{dX}{dt} = \frac{dL}{dX} U_x \quad (10.10-4)$$

The size L is a function of temperature, pressure, and mass transfer. Thus,

$$\frac{dL}{dX} = \left(\frac{\partial L}{\partial p} \right)_{T,m} \frac{dP}{dX} + \left(\frac{\partial L}{\partial T} \right)_{P,m} \frac{dT}{dX} + \left(\frac{\partial L}{\partial m} \right)_{T,P} \frac{dm}{dX} \quad (10.10-5)$$

Let the pressure P at height X be expressed by

$$P = P^0 + H - X \quad (10.10-6)$$

and an assumed linear temperature gradient be represented by

$$T = T^0 + (H - X)\alpha \quad (10.10-7)$$

Using the above, assuming the ideal gas law applies, and representing the bubbles as spheres gives

$$\frac{dP}{dX} = -1 \quad (10.10-8)$$

$$\frac{dT}{dX} = -\alpha \quad (10.10-9)$$

$$\left(\frac{\partial L}{\partial P} \right)_{T,m} = -\frac{L}{3P} = -\frac{\frac{1}{3}L}{P^0 + H - X} \quad (10.10-10)$$

$$\left(\frac{\partial L}{\partial T} \right)_{m,P} = \frac{\frac{1}{3}L}{T} = \frac{\frac{1}{3}L}{[T^0 + (H - X)\alpha]} \quad (10.10-11)$$

Mass transfer is accounted for by letting

$$\frac{dm}{dX} = \frac{dm}{dt} \frac{dt}{dX} = \frac{dm}{dt} \left(\frac{1}{U_x} \right) \quad (10.10-12)$$

Because we consider only pure oxygen bubbles, only mass transfer through the liquid film need be considered. Thus,

$$\frac{dm}{dt} = A_D k_L (C_L - C^*) \quad (10.10-13)$$

Assuming spherical bubbles,

$$\frac{dm}{dX} = \frac{\pi D^2 k_L (C_L - C^*)}{U_x} \quad (10.10-14)$$

In the same manner as shown for Eq. (10.10-10) and (10.10-11),

$$\frac{\partial L}{\partial m} = \frac{1}{3} \left(\frac{L}{m} \right) = \left(\frac{2}{\pi} \right) \frac{R_g T}{PL^2} = \left(\frac{3}{\pi} \right) \frac{R_g [T^0 + (H - X)\alpha]}{L^2 (P^0 + H - X)} \quad (10.10-15)$$

Assuming the bubbles are always at their terminal velocity U and further that the temperature parameter $\alpha = 0$, the above equations when substituted into Eq. (10.10-3) give

$$\begin{aligned} \frac{\partial n}{\partial X} + \frac{\frac{1}{3}L + [2k_L(C_L - C^*)R_g T]/U_x}{P^0 + H - X} \left(\frac{n}{D} \right) \\ = - \left(\frac{1}{P^0 + H - X} \right) \left[\frac{1}{3} + \frac{1}{3} \left(\frac{L}{U} \right) \frac{dU}{dL} \right] n + \frac{G - D_p}{U_x} \end{aligned} \quad (10.10-16)$$

The final term in Eq. (10.10-16) accounts for coalescence and dispersion. If bubbles are smaller than 1.5 cm, breakup is negligible and can be neglected. When coalescence occurs, birth B has a value, as well as the death function D_p . This phenomenon can be represented by the equation of Hidy and Brock [24], which written in continuous variables and size rather than volume-based gives

$$\begin{aligned} (G - D_p) = \frac{\partial n(L, t)}{\tau} = \frac{2}{\pi} \int_0^{L/\sqrt{3}} \frac{b(y, z)n(y, t)n(z, t)}{y^2} dz \\ - \frac{n(L, t)}{L^2} \int_0^\infty b(L, z)n(z, t) dz \end{aligned} \quad (10.10-17)$$

Because volume must be conserved when coalescence occurs, y is related to z as follows:

$$y = (L^3 - z^3)^{1/3} \quad (10.10-18)$$

The collision parameter b must be chosen according to an assumed mechanism for collision. For a very clean system or a system of relatively large bubbles, interfacial mobility will be high. In this instance inertial forces will dominate, and the approximate collision parameter can be obtained from a potential flow function. For this case the equation of Hidy and Block [24], written in terms of the diameter D , is appropriate:

$$b(y, z) = \frac{\pi}{4} [L(y) + L(z)]^2 \left\{ 1 - \frac{L(z)^3}{[L(y) + L(z)]^3} \right\} [U(z) - U(y)]$$

There are a number of ways to determine the mass-transfer coefficient k_L . One possibility is the use of the correlation derived by Murkerjee (1973)

for rising bubbles:

$$k_L = \frac{2D}{D} + 2 \frac{U_x}{\pi L} \quad (10.10-20)$$

The diffusion coefficient can be related to temperature if the coefficient at some pressure T^0 is known,

$$\mathcal{D}_T = \mathcal{D}_T \frac{T}{T^0} \quad (10.10-21)$$

The above set of equations describe the system and can be solved by a combination of the method of characteristics as explained by Courant and Hilbert [25] and a numerical integration. In this method the partial differential equation is changed to a system of ordinary differential equations.

10.11 Demographic Analysis

The dynamics of human population change have always been a topic of interest and wonder. The current population pressures in our cities, in many countries, and in the world in general have caused a good deal more interest in the growth and decline of human populations. Not since the gloomy predictions of Malthus has the concern for this problem been as great.

The model used consistently throughout this volume can serve as an analytical framework for demographers in their study of the response of populations to various stimuli. Of course, as with many population-balance-based studies, the critical factor in the validity and usefulness of such models is the proper formulation and verification of empirical population kinetics.

As an example, let us consider a geographic identity (city or country) whose population may be considered a continuum. That is, if we characterize a person by his/her age θ , we consider the age distribution of any large segment of the population as a continuous function. Consider the density function $n(t, \theta) d\theta$ to be the population having an age in the interval θ to $\theta + d\theta$ at time t . Further, define $N_i(t, \theta)$ as the number of people of age θ entering the system by immigration and $N_o(t, \theta)$ the number rate of people of age θ leaving by emigration. Neglecting spatial variations of population within the geographic unit under consideration, Eq. (3.5-10) becomes

$$\frac{\partial n}{\partial t} + v_\theta \frac{\partial n}{\partial \theta} + v_p \frac{\partial n}{\partial p} + D(n, \theta, p) - \delta(\theta - 0) B^0 = N_i(t, \theta, p) - N_o(t, \theta, p) \quad (10.11-1)$$

where B^0 is the births at age zero resulting from the current age distribu-

tion of the population and where the convective velocity along the age axis v_θ is identically equal to unity, that is, $d\theta/dt = 1$. The variable p represents any second orthogonal phase space coordinate. Birth is related to the age distribution of the population and is heavily weighted toward the distribution of ages between, say, 16 and 45. The death function is, of course, related to the whole distribution but is heavily dependent on the age distribution at the older end of the distribution. In either case, functions for these two terms could be obtained accurately from insurance-company birth and mortality tables. If a more detailed analysis of the population dynamics is desired, it is clear that two population-age distributions could be computed, one for each sex, forming a coupled set (no pun intended) of equations describing the entire system.

Immigration represents an outside arbitrary disturbance to the system, although the rate N_i might be expected to couple weakly with the current state of the population n . Given a specified immigration function $N_i(t, \theta)$, the dynamic effects on population distribution can easily be determined. Certainly, emigration would be age-dependent. Thus, output from the population unit under consideration might be represented by an age-dependent mean retention probability as $N_o = n(t, \theta)/\tau(\theta)$. Such a formulation is analogous to the crystallization problem of classified withdrawal. By arbitrarily specifying the mean retention probability $\tau(\theta)$, effects of various types of emigration can be determined.

We note that the moments over the age distribution have significance as in the case of other distributions. Thus, total population $N_T(t)$ is given as

$$N_T(t) = \int_0^\infty n d\theta = m_0 \quad (10.11-2)$$

and

$$\bar{\theta} = \int_0^\infty \theta n d\theta / \int_0^\infty n d\theta = m_1/m_0 \quad (10.11-3)$$

where $\bar{\theta}$ is the average age of the population.

The above analysis could be applied to countries, continents, or any geographic, economic, or ethnic group. By returning to the distributed forms of the population balance given in Chapter 3, one can develop a geographic representation as well. This general representation permits modeling of population-geographic as well as population-age distributions if the appropriate spatial and age dependence of the birth and death rates is known.

Other population phase plane coordinates besides age can be defined, such as a coordinate p describing the material wealth of a population segment. The term $n(t, p) dp$ would then represent the number of people in

a geographic unit at a given time having wealth in the range p to $p + dp$. Population dynamics in this case could reasonably be influenced by many factors, such as continuous net earnings [given by wealth-dependent "growth" rate $v_p = v_p(p)$], transfer between population groups [given by "birth" and "death" terms $B(p)$ and $D(p)$], and wealth-dependent input and output rates [given by input-output terms $N_i = N_i(t, p)$ and $N_o = n(t, p)/\tau(p)$]. Realistically, wealth in population kinetics depends heavily on population age; the dynamic multivariate age and wealth density distribution function $n(t, \theta, p)$ can be described by these techniques given correct information on population kinetics. All total and average properties of interest can be readily calculated from the population density function.

Such dynamic population models would demand the full formalism of the distribution theory presented in this book.

EXAMPLE 10.11-1

Use the macropopulation balance to set up equations describing the steady-state population-age distribution and total population of a closed society. Calculate the fraction of original births that are still living at age 70. Assume that population dynamics for this society can be represented statistically by the following equations:

$$\begin{aligned} B^0 &= \int_0^\infty B^0(\theta) d\theta = k \int_0^\infty \left[\frac{n(\theta)}{n^0} \right] \rho(\theta) d\theta \\ &= k \int_0^\infty f(\theta) \rho(\theta) d\theta \quad \text{births/year} \end{aligned} \quad (10.11-4)$$

where $B^0(\theta) d\theta$ is the number of births from the adult population of age θ to $\theta + d\theta$, $n(\theta) d\theta$ is the population in age group θ to $\theta + d\theta$, $f(\theta)$ is the fraction of original population left alive at age group θ , $\rho(\theta)$ is a weighting function of age group θ , and k is an overall fertility "inclination" factor, which involves the amount of resources available for population growth. Assume that the weighting factor can be expressed as a log-normal distribution around a median female fecund age of 25 years. Thus,

$$\frac{B^0(\theta)}{kf(\theta)} = \rho(\theta) = \frac{1}{(2\pi)^{1/2} \log \sigma'} \exp \left[-\frac{\log^2(\theta/25)}{2 \log^2 \sigma'} \right] \quad (10.11-5)$$

Approximately $\frac{1}{2}\%$ of each age group dies each year until age 40, when the death frequency increases markedly. These death statistics may be represented by a death function given as proportional to the population density times a polynomial weighting factor. Thus,

$$D(\theta) = 0.005 [1 + 2(\theta/40)^4] n(\theta) \quad \text{deaths/year} \quad (10.11-6)$$

in age group θ . Immigration and emigration from the society can be neglected.

The macropopulation balance of Eq. (10.11-1) simplifies in this case to

$$v_\theta \, dn/d\theta = -D(\theta) \quad (10.12-7)$$

where $v_\theta = d\theta/dt = 1$. The boundary condition for this equation is

$$n^0 = n(0) = \frac{B^0}{v_\theta} = \frac{k}{(2\pi)^{1/2} \log \sigma'} \int_0^\infty f(p) \exp \left[\frac{-\log^2(p/25)}{2 \log^2 \sigma'} \right] dp \quad (10.11-8)$$

where p is a dummy of integration. Solving Eq. (10.11-7) for population density gives

$$dn/n = -0.005 \left[1 + 2(\theta/40)^4 \right] d\theta \quad (10.11-9)$$

Integrating from $n = n^0$ and $\theta = 0$ gives

$$f(\theta) = n/n^0 = \exp \left\{ -0.005 \left[\theta + 2\theta^5/(5)(40)^4 \right] \right\} \quad (10.11-10)$$

Equations (10.11-8) and (10.11-10) are then solved for the population density $n(\theta)$. Thus

$$\begin{aligned} n(\theta) = & \frac{k}{(2\pi)^{1/2} \log \sigma'} \int_0^\infty \exp \left\{ -0.005 \left[\frac{p + 2p^5}{(5)(40)^4} \right] - \frac{\log^2(p/25)}{2 \log^2 \sigma'} \right\} dp \\ & \times \exp \left\{ -0.005 \left[\frac{\theta + 2\theta^5}{(5)(40)^4} \right] \right\} \end{aligned} \quad (10.11-11)$$

The total population in the society is given as

$$N_T = \int_0^\infty n(\theta) \, d\theta = n^0 \int_0^\infty \exp \left\{ -0.005 \left[\frac{\theta + 2\theta^5}{(5)(40)^4} \right] \right\} d\theta \quad (10.11-12)$$

The fraction of original births still alive at age 70 is

$$f(70) = \exp \left\{ -0.005 \left[70 + (2)(70)^5/(5)(40)^4 \right] \right\} = 0.19 \quad (10.11-13)$$

Thus, 19% of the population is predicted to live to at least 70 years. ♦

The above example, although perhaps trivial, illustrates the use of this formalism to study population problems. It should be noted that the function $1000D(\theta)/n(\theta)$ represents the deaths per thousand in any population group of age θ and can be determined directly from actuarial statistics. A polynomial expression, as illustrated above, should prove a fruitful way to correlate these data. The function $1000B^0(\theta)/f(\theta)B^0$ represents the births per thousand from each population group of age θ . The birth

weighting function $\rho(\theta)$ could be assembled directly from actuarial statistics, in this example, by plotting $B^0(\theta)/n(\theta)$ versus θ on log-normal probability paper. Both $B^0(\theta)$ and $D(\theta)$ can be expressed as functions of time by extrapolating actuarial statistics, thus enabling prediction of dynamic population distributions.

In the previous example, the level of population was established with the parameter k . The death function and birth weighting terms merely shaped the form of the age distribution and apportioned the total births, respectively. A difficult problem in demographic analysis is in establishing and predicting the total birth rate (established in this case by the parameter k) as a function of both population resources available and current levels of population.

EXAMPLE 10.11-2

The closed society of Example 10.11-1 is suddenly threatened from without, causing the birth factor k to increase by 10% and the log-normal birth weighting function to widen from a σ' of 1.2 to 1.25. Write the equations describing the dynamic population-age distribution and show their interrelationship in an information flow diagram. Write an equation showing the increase as a function of time in the 5- to 18-year-olds resulting from this change.

The steady-state starting population distribution $n_0(\theta)$ is obtained by solution of the steady-state equations in the previous example with $\sigma' = 1.2$ and the original population constant k_0 .

Dynamic population distribution is then described by the following set of equations:

$$\frac{\partial n}{\partial t} + \frac{\partial n}{\partial \theta} = -0.005 \left[1 + 2 \left(\frac{\theta}{40} \right)^4 \right] \quad (10.11-14)$$

$$n(0, \theta) = n_0(\theta) \quad (10.11-15)$$

$$n(t, 0) = \frac{(k_0)(1.1)}{(2\pi)^{1/2}(1.25)} \int_0^\infty f(p) \exp \left[\frac{-\log^2(p/25)}{(2)(1.25)^2} \right] dp \quad (10.11-16)$$

The percentage increase in school-age children in the 5- to 18-year age group is then given as

$$\text{Percent increase} = 100 \int_5^{18} \left[\frac{n}{n_0} - 1 \right] d\theta \quad (10.11-17)$$

Of course, no increase in school-age population would appear in Eq. (10.11-17) until 5 years after the initial birth-rate upset.

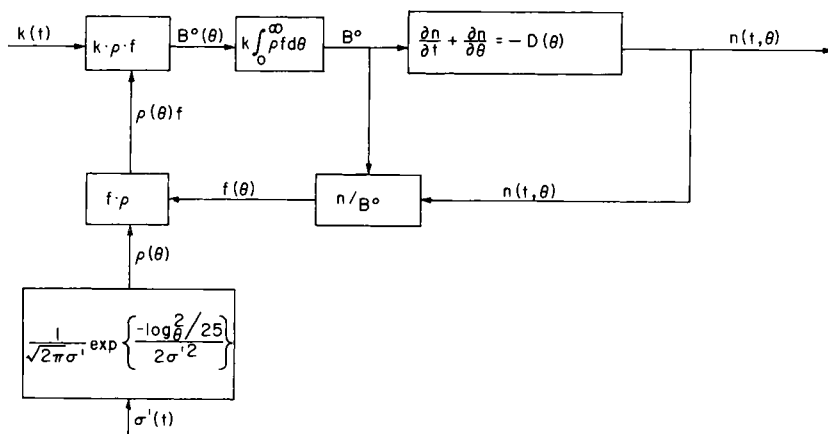


Fig. 10.11-1 Information flow diagram showing adjustments in population-age distribution resulting from changes in population parameters.

An information-flow diagram for this population problem is shown in Fig. 10.11-1. ♦

10.12 Summary

We have given here brief examples of several population distributions where the analyses used in crystallization could be of use. The treatments have necessarily been brief, and for those taken from other authors, we refer the reader to the original work. The examples chosen are not exhaustive, and many others are surely subject to this analysis. We hasten to add that we claim no particular expertise in the fields of polymerization, microbiology, or demography. The birth and death models given in this chapter are not claimed to be representative of any great amount of accumulated data and should therefore be regarded as examples to illustrate a possible application of the population balance.

The analyses and developments in Chapters 2 and 3 are directly applicable to all of these examples. This general population balance should now be studied in the context of the example of interest. The complete analyses of crystallization in Chapters 4 and 6-9 should provide many analogies to the examples listed in these chapters as well as other distribution examples. With these techniques as a starting point, much can be done to improve understanding of the dynamics of population distributions.

References

1. Austin, G. L., Klimpel, R. R., and Ludie, T. T. (1984). "Process Engineering of Sip Reduction: Ball Milling." Amer. Inst. of Mining, Metals and Petroleum Engineering, Inc., New York.
2. Lynch, A. J. (1982). "Mineral Crushing and Grinding Circuits," Elsevier Press, Amsterdam.
3. Herbst, J. A. (1979). Rate processes in multiparticle metallurgical systems. In "Rate Processes of Extractive Metallurgy" (H. Y. Sohn and M. E. Wadsworth, eds.). Plenum Press, New York.
4. Randolph, A. D., and Ranjan, R. (1977). Effect of a material-flow model in prediction of particle-size distributions in open- and closed-circuit mills, *Int. J. Mineral Processing* **4**, 99.
5. Tsuchiya, A. C., Fredrickson, A. G., and Aris, R. (1966). *Adv. Chem. Eng.* **6**, 192.
6. Koch, A. L., and Schawchter, M. (1962). *J. Gen. Microbiol.* **29**, 435.
7. Zeman, R. J., and Amundson, N. R. (1965). *Chem. Eng. Sci.* **20**, 331.
8. Thompson, R. W., and Stevens, J. D. (1965). *Chem. Eng. Sci.* **22**, 311.
9. Gardon, J. L. (1968). *J. Polymer Sci.* **6**, 623.
10. Smith, W. V., and Ewart, E. H. (1948). *J. Chem. Phys.* **16**, 592.
11. Stevens, J. D., and Funderburk, J. O. *I & EC Proc. Des. Dev.* **11**, 360.
12. Curl, R. L. (1963). *AIChE J.* **9**, 175.
13. Danckwerts, P. (1953). *Chem. Eng. Sci.* **2**, 1.
14. Wolff, D., and Resnick, W. (1963). *Ind. Eng. Chem. Fundam.* **2**, 287.
15. Hulburt, H. M., and Katz, S. (1964). *Chem. Eng. Sci.* **19**, 555.
16. Glatz, C. E., Hoare, M., and Landa-Vertiz, J. (1967). *AIChE J.* **32**, 1196.
17. Hoyt, R. C. (1978). Precipitation kinetics of a continuous precipitator with application to precipitation of ammonium polyuranate. Ph.D. dissertation, Iowa State University Library, Ames, Iowa.
18. ASTM Designation E-20-85, Vol. 14.02, p. 19.
19. Hartel, R. W., Gotting, B. E., Randolph, A. D., and Drack, G. W. (1986). Mechanisms and kinetic modeling of calcium oxalate crystal aggregation in a urine-like liquor: Part I, Mechanisms. *AIChE J.* **32**, 1176.
20. Hartel, R. W., and Randolph, A. D. (1986). Mechanisms and kinetic modelling of calcium oxalate crystal aggregation in a urine-like liquor: Part II, Kinetic modelling. *AIChE J.* **32**, 1136.
21. Gebbard, F. (1981). "AEROSL User's Manual," Sandia Natural Laboratory, NUREG/CR-137, SAND80-0403, R7 (Mar.).
22. Martin, G. C. (1976). Bubble size distribution in aeration processes. Unpublished M.S. thesis, Iowa State University Library, Ames, Iowa.
23. Valentes, K. J., Bilous, O., and Amundson, N. R. (1966). *I & EC Fundam.* **5**, 271.
24. Hidy, G. M., and Brock, J. R. (1970). "International Reviews in Aerosol Physics and Chemistry," Vol. 1. Pergamon Press, Oxford.
25. Courant, R., and Hilbert, D. (1955). "Methods of Mathematical Physics," Vol. 2. Interscience, New York.

DIMENSIONLESS WEIGHT-FRACTION FUNCTION

A characteristic CSD function that appears in many of the cumulative weight-size distribution equations is the gamma-type function

$$w(x) = \frac{1}{6} \int_0^x \exp(-p) p^3 dp$$

This function naturally arises when the population density is of at least piecewise exponential form. Thus, consider the population density in a size range L in (a, b) to be given exponentially as

$$n = c_1 \exp(-c_2 L)$$

where a , b , c_1 , and c_2 are constants. The weight fraction occurring in this size range is then given as

$$W(a, b) = \rho k_v \int_a^b \frac{n L^3}{M_T} dL$$

or

$$W(a, b) = K \int_a^b \exp(-c_2 L) L^3 dL$$

Making the dimensionless substitution $p = c_2 L$ gives

$$W(a, b) = K' \int_{a'}^{b'} \exp(-p) p^3 dp$$

where a' and b' are the dimensionless sizes

$$a' = c_2 a, \quad b' = c_2 b$$

Finally, in terms of the dimensionless weight distribution function,

$$W(a, b) = 6K'[w(b') - w(a')]$$

Thus, the dimensionless $w(x)$ function appears in any calculations of weight-size distribution when the population density is given in terms of exponentials.

The dimensionless $w(x)$ function is given in Table A-1 over the interval x in $(0, 10)$ in increments of 0.1. The function can be easily integrated and can alternately be carried in analytic form as a computational subroutine in CSD algorithms. Thus,

$$w(x) \equiv \frac{1}{6} \int_0^x \exp(-p) p^3 dp = 1 - \exp(-x) \left(1 + x + \frac{1}{2} x^2 + \frac{1}{6} x^3 \right)$$

Figure A-1 is a plot of cumulative weight-size CSD from an MSMPR crystallizer producing Glauber's salt ($\text{Na}_2\text{SO}_4 \cdot 10\text{H}_2\text{O}$). The axis is scaled as the theoretical MSMPR distribution, the third-order gamma function. This third-order gamma plot is a convenient way of testing to see if crystallizer data fit the expected MSMPR form without going through the difficulty of converting to population density. The error bars were calculated from the maximum expected error in each size. The data points are actual weight averages for two screenings.

Table A-1*Dimensionless Weight Fraction $W(X)$ versus Dimensionless Size X*

$w(x)$	x	$w(x)$	x	$w(x)$	x	$w(x)$	x
0.000	0.01	0.002	0.51	0.020	1.01	0.067	1.51
0.000	0.02	0.002	0.52	0.020	1.02	0.068	1.52
0.000	0.03	0.002	0.53	0.021	1.03	0.070	1.53
0.000	0.04	0.002	0.54	0.022	1.04	0.071	1.54
0.000	0.05	0.003	0.55	0.022	1.05	0.072	1.55
0.000	0.06	0.003	0.56	0.023	1.06	0.073	1.56
0.000	0.07	0.003	0.57	0.024	1.07	0.075	1.57
0.000	0.08	0.003	0.58	0.024	1.08	0.076	1.58
0.000	0.09	0.003	0.59	0.025	1.09	0.077	1.59
0.000	0.10	0.003	0.60	0.026	1.10	0.079	1.60
0.000	0.11	0.004	0.61	0.027	1.11	0.080	1.61
0.000	0.12	0.004	0.62	0.027	1.12	0.082	1.62
0.000	0.13	0.004	0.63	0.028	1.13	0.083	1.63
0.000	0.14	0.004	0.64	0.029	1.14	0.084	1.64
0.000	0.15	0.005	0.65	0.030	1.15	0.086	1.65
0.000	0.16	0.005	0.66	0.030	1.16	0.087	1.66
0.000	0.17	0.005	0.67	0.031	1.17	0.089	1.67
0.000	0.18	0.005	0.68	0.032	1.18	0.090	1.68
0.000	0.19	0.006	0.69	0.033	1.19	0.092	1.69
0.000	0.20	0.006	0.70	0.034	1.20	0.093	1.70
0.000	0.21	0.006	0.71	0.035	1.21	0.095	1.71
0.000	0.22	0.006	0.72	0.036	1.22	0.096	1.72
0.000	0.23	0.007	0.73	0.036	1.23	0.098	1.73
0.000	0.24	0.007	0.74	0.037	1.24	0.099	1.74
0.000	0.25	0.007	0.75	0.038	1.25	0.101	1.75
0.000	0.26	0.008	0.76	0.039	1.26	0.102	1.76
0.000	0.27	0.008	0.77	0.040	1.27	0.104	1.77
0.000	0.28	0.008	0.78	0.041	1.28	0.106	1.78
0.000	0.29	0.009	0.79	0.042	1.29	0.107	1.79
0.000	0.30	0.009	0.80	0.043	1.30	0.109	1.80
0.000	0.31	0.010	0.81	0.044	1.31	0.110	1.81
0.000	0.32	0.010	0.82	0.045	1.32	0.112	1.82
0.000	0.33	0.010	0.83	0.046	1.33	0.114	1.83
0.000	0.34	0.011	0.84	0.047	1.34	0.115	1.84
0.000	0.35	0.011	0.85	0.048	1.35	0.117	1.85
0.001	0.36	0.012	0.86	0.049	1.36	0.119	1.86
0.001	0.37	0.012	0.87	0.050	1.37	0.120	1.87
0.001	0.38	0.013	0.88	0.052	1.38	0.122	1.88
0.001	0.39	0.013	0.89	0.053	1.39	0.124	1.89
0.001	0.40	0.014	0.90	0.054	1.40	0.125	1.90
0.001	0.41	0.014	0.91	0.055	1.41	0.127	1.91
0.001	0.42	0.015	0.92	0.056	1.42	0.129	1.92
0.001	0.43	0.015	0.93	0.057	1.43	0.131	1.93
0.001	0.44	0.016	0.94	0.058	1.44	0.132	1.94
0.001	0.45	0.016	0.95	0.060	1.45	0.134	1.95
0.001	0.46	0.017	0.96	0.061	1.46	0.136	1.96
0.001	0.47	0.017	0.97	0.062	1.47	0.138	1.97
0.002	0.48	0.018	0.98	0.063	1.48	0.139	1.98
0.002	0.49	0.018	0.99	0.064	1.49	0.141	1.99
0.002	0.50	0.019	1.00	0.066	1.50	0.143	2.00

Table A-1. *Continued*

$w(x)$	x	$w(x)$	x	$w(x)$	x	$w(x)$	x
0.145	2.01	0.245	2.51	0.355	3.01	0.466	3.51
0.147	2.02	0.247	2.52	0.357	3.02	0.468	3.52
0.148	2.03	0.249	2.53	0.360	3.03	0.470	3.53
0.150	2.04	0.251	2.54	0.362	3.04	0.472	3.54
0.152	2.05	0.253	2.55	0.364	3.05	0.474	3.55
0.154	2.06	0.255	2.56	0.366	3.06	0.476	3.56
0.156	2.07	0.258	2.57	0.369	3.07	0.478	3.57
0.158	2.08	0.260	2.58	0.371	3.08	0.481	3.58
0.160	2.09	0.262	2.59	0.373	3.09	0.483	3.59
0.161	2.10	0.264	2.60	0.375	3.10	0.485	3.60
0.163	2.11	0.266	2.61	0.377	3.11	0.487	3.61
0.165	2.12	0.268	2.62	0.380	3.12	0.489	3.62
0.167	2.13	0.271	2.63	0.382	3.13	0.491	3.63
0.169	2.14	0.273	2.64	0.384	3.14	0.493	3.64
0.171	2.15	0.275	2.65	0.386	3.15	0.495	3.65
0.173	2.16	0.277	2.66	0.389	3.16	0.498	3.66
0.175	2.17	0.279	2.67	0.391	3.17	0.500	3.67
0.177	2.18	0.282	2.68	0.393	3.18	0.502	3.68
0.179	2.19	0.284	2.69	0.395	3.19	0.504	3.69
0.181	2.20	0.286	2.70	0.398	3.20	0.506	3.70
0.183	2.21	0.288	2.71	0.400	3.21	0.508	3.71
0.185	2.22	0.290	2.72	0.402	3.22	0.510	3.72
0.187	2.23	0.293	2.73	0.404	3.23	0.512	3.73
0.189	2.24	0.295	2.74	0.406	3.24	0.514	3.74
0.191	2.25	0.297	2.75	0.409	3.25	0.516	3.75
0.193	2.26	0.299	2.76	0.411	3.26	0.518	3.76
0.195	2.27	0.301	2.77	0.413	3.27	0.520	3.77
0.197	2.28	0.304	2.78	0.415	3.28	0.522	3.78
0.199	2.29	0.306	2.79	0.418	3.29	0.525	3.79
0.201	2.30	0.308	2.80	0.420	3.30	0.527	3.80
0.203	2.31	0.310	2.81	0.422	3.31	0.529	3.81
0.205	2.32	0.313	2.82	0.424	3.32	0.531	3.82
0.207	2.33	0.315	2.83	0.426	3.33	0.533	3.83
0.209	2.34	0.317	2.84	0.429	3.34	0.535	3.84
0.211	2.35	0.319	2.85	0.431	3.35	0.537	3.85
0.213	2.36	0.321	2.86	0.433	3.36	0.539	3.86
0.215	2.37	0.324	2.87	0.435	3.37	0.541	3.87
0.217	2.38	0.326	2.88	0.437	3.38	0.543	3.88
0.219	2.39	0.328	2.89	0.440	3.39	0.545	3.89
0.221	2.40	0.330	2.90	0.442	3.40	0.547	3.90
0.223	2.41	0.333	2.91	0.444	3.41	0.549	3.91
0.226	2.42	0.335	2.92	0.446	3.42	0.551	3.92
0.228	2.43	0.337	2.93	0.448	3.43	0.553	3.93
0.230	2.44	0.339	2.94	0.450	3.44	0.555	3.94
0.232	2.45	0.342	2.95	0.453	3.45	0.557	3.95
0.234	2.46	0.344	2.96	0.455	3.46	0.559	3.96
0.236	2.47	0.346	2.97	0.457	3.47	0.561	3.97
0.238	2.48	0.348	2.98	0.459	3.48	0.563	3.98
0.240	2.49	0.351	2.99	0.461	3.49	0.565	3.99
0.242	2.50	0.353	3.00	0.463	3.50	0.567	4.00

Table A-1. *Continued*

$w(x)$	x	$w(x)$	x	$w(x)$	x	$w(x)$	x
0.569	4.01	0.659	4.51	0.736	5.01	0.799	5.51
0.570	4.02	0.661	4.52	0.738	5.02	0.801	5.52
0.572	4.03	0.663	4.53	0.739	5.03	0.802	5.53
0.574	4.04	0.664	4.54	0.741	5.04	0.803	5.54
0.576	4.05	0.666	4.55	0.742	5.05	0.804	5.55
0.578	4.06	0.668	4.56	0.743	5.06	0.805	5.56
0.580	4.07	0.669	4.57	0.745	5.07	0.806	5.57
0.582	4.08	0.671	4.58	0.746	5.08	0.807	5.58
0.584	4.09	0.673	4.59	0.747	5.09	0.808	5.59
0.586	4.10	0.674	4.60	0.749	5.10	0.809	5.60
0.588	4.11	0.676	4.61	0.750	5.11	0.811	5.61
0.590	4.12	0.678	4.62	0.751	5.12	0.812	5.62
0.592	4.13	0.679	4.63	0.753	5.13	0.813	5.63
0.593	4.14	0.681	4.64	0.754	5.14	0.814	5.64
0.595	4.15	0.682	4.65	0.755	5.15	0.815	5.65
0.597	4.16	0.684	4.66	0.758	5.16	0.816	5.66
0.599	4.17	0.686	4.67	0.758	5.17	0.817	5.67
0.601	4.18	0.687	4.68	0.759	5.18	0.818	5.68
0.603	4.19	0.689	4.69	0.761	5.19	0.819	5.69
0.605	4.20	0.690	4.70	0.762	5.20	0.820	5.70
0.607	4.21	0.692	4.71	0.763	5.21	0.821	5.71
0.608	4.22	0.694	4.72	0.765	5.22	0.822	5.72
0.610	4.23	0.695	4.73	0.766	5.23	0.823	5.73
0.612	4.24	0.697	4.74	0.767	5.24	0.824	5.74
0.614	4.25	0.698	4.75	0.768	5.25	0.825	5.75
0.616	4.26	0.700	4.76	0.770	5.26	0.826	5.76
0.617	4.27	0.701	4.77	0.771	5.27	0.827	5.77
0.619	4.28	0.703	4.78	0.772	5.28	0.828	5.78
0.621	4.29	0.704	4.79	0.773	5.29	0.829	5.79
0.623	4.30	0.706	4.80	0.775	5.30	0.830	5.80
0.625	4.31	0.707	4.81	0.776	5.31	0.831	5.81
0.626	4.32	0.709	4.82	0.777	5.32	0.832	5.82
0.628	4.33	0.710	4.83	0.778	5.33	0.833	5.83
0.630	4.34	0.712	4.84	0.780	5.34	0.834	5.84
0.632	4.35	0.713	4.85	0.781	5.35	0.835	5.85
0.634	4.36	0.715	4.86	0.782	5.36	0.836	5.86
0.635	4.37	0.716	4.87	0.783	5.37	0.837	5.87
0.637	4.38	0.718	4.88	0.784	5.38	0.838	5.88
0.639	4.39	0.719	4.89	0.786	5.39	0.839	5.89
0.641	4.40	0.721	4.90	0.787	5.40	0.840	5.90
0.642	4.41	0.722	4.91	0.788	5.41	0.841	5.91
0.644	4.42	0.724	4.92	0.789	5.42	0.842	5.92
0.646	4.43	0.725	4.93	0.790	5.43	0.842	5.93
0.648	4.44	0.727	4.94	0.791	5.44	0.843	5.94
0.649	4.45	0.728	4.95	0.793	5.45	0.844	5.95
0.651	4.46	0.729	4.96	0.794	5.46	0.845	5.96
0.653	4.47	0.731	4.97	0.795	5.47	0.846	5.97
0.654	4.48	0.732	4.98	0.796	5.48	0.847	5.98
0.656	4.49	0.734	4.99	0.797	5.49	0.848	5.99
0.658	4.50	0.735	5.00	0.798	5.50	0.849	6.00

Table A-1. *Continued*

$w(x)$	x	$w(x)$	x	$w(x)$	x	$w(x)$	x
0.850	6.01	0.889	6.51	0.919	7.01	0.941	7.51
0.851	6.02	0.890	6.52	0.919	7.02	0.942	7.52
0.852	6.03	0.890	6.53	0.920	7.03	0.942	7.53
0.852	6.04	0.891	6.54	0.920	7.04	0.942	7.54
0.853	6.05	0.892	6.55	0.921	7.05	0.943	7.55
0.854	6.06	0.892	6.56	0.921	7.06	0.943	7.56
0.855	6.07	0.893	6.57	0.922	7.07	0.944	7.57
0.856	6.08	0.894	6.58	0.922	7.08	0.944	7.58
0.857	6.09	0.894	6.59	0.923	7.09	0.944	7.59
0.858	6.10	0.895	6.60	0.923	7.10	0.945	7.60
0.858	6.11	0.896	6.61	0.924	7.11	0.945	7.61
0.859	6.12	0.896	6.62	0.924	7.12	0.945	7.62
0.860	6.13	0.897	6.63	0.925	7.13	0.946	7.63
0.861	6.14	0.897	6.64	0.925	7.14	0.946	7.64
0.862	6.15	0.898	6.65	0.926	7.15	0.946	7.65
0.863	6.16	0.899	6.66	0.926	7.16	0.947	7.66
0.863	6.17	0.899	6.67	0.927	7.17	0.947	7.67
0.864	6.18	0.900	6.68	0.927	7.18	0.948	7.68
0.865	6.19	0.901	6.69	0.928	7.19	0.948	7.69
0.866	6.20	0.901	6.70	0.928	7.20	0.948	7.70
0.867	6.21	0.902	6.71	0.929	7.21	0.949	7.71
0.867	6.22	0.902	6.72	0.929	7.22	0.949	7.72
0.868	6.23	0.903	6.73	0.930	7.23	0.949	7.73
0.869	6.24	0.904	6.74	0.930	7.24	0.950	7.74
0.870	6.25	0.904	6.75	0.930	7.25	0.950	7.75
0.871	6.26	0.905	6.76	0.931	7.26	0.950	7.76
0.871	6.27	0.905	6.77	0.931	7.27	0.951	7.77
0.872	6.28	0.906	6.78	0.932	7.28	0.951	7.78
0.873	6.29	0.907	6.79	0.932	7.29	0.951	7.79
0.874	6.30	0.907	6.80	0.933	7.30	0.952	7.80
0.874	6.31	0.908	6.81	0.933	7.31	0.952	7.81
0.875	6.32	0.908	6.82	0.934	7.32	0.952	7.82
0.876	6.33	0.909	6.83	0.934	7.33	0.953	7.83
0.877	6.34	0.910	6.84	0.934	7.34	0.953	7.84
0.877	6.35	0.910	6.85	0.935	7.35	0.953	7.85
0.878	6.36	0.911	6.86	0.935	7.36	0.953	7.86
0.879	6.37	0.911	6.87	0.936	7.37	0.954	7.87
0.880	6.38	0.912	6.88	0.936	7.38	0.954	7.88
0.880	6.39	0.912	6.89	0.936	7.39	0.954	7.89
0.881	6.40	0.913	6.90	0.937	7.40	0.955	7.90
0.882	6.41	0.913	6.91	0.937	7.41	0.955	7.91
0.883	6.42	0.914	6.92	0.938	7.42	0.955	7.92
0.883	6.43	0.915	6.93	0.938	7.43	0.956	7.93
0.884	6.44	0.915	6.94	0.939	7.44	0.956	7.94
0.885	6.45	0.916	6.95	0.939	7.45	0.956	7.95
0.885	6.46	0.916	6.96	0.939	7.46	0.957	7.96
0.886	6.47	0.917	6.97	0.940	7.47	0.957	7.97
0.887	6.48	0.917	6.98	0.940	7.48	0.957	7.98
0.888	6.49	0.918	6.99	0.941	7.49	0.957	7.99
0.888	6.50	0.918	7.00	0.941	7.50	0.958	8.00

Table A-1. *Continued*

$w(x)$	x	$w(x)$	x	$w(x)$	x	$w(x)$	x
0.958	8.01	0.970	8.51	0.979	9.01	0.985	9.51
0.958	8.02	0.970	8.52	0.979	9.02	0.985	9.52
0.959	8.03	0.971	8.53	0.979	9.03	0.986	9.53
0.959	8.04	0.971	8.54	0.979	9.04	0.986	9.54
0.959	8.05	0.971	8.55	0.980	9.05	0.986	9.55
0.959	8.06	0.971	8.56	0.980	9.06	0.986	9.56
0.960	8.07	0.971	8.57	0.980	9.07	0.986	9.57
0.960	8.08	0.972	8.58	0.980	9.08	0.986	9.58
0.960	8.09	0.972	8.59	0.980	9.09	0.986	9.59
0.960	8.10	0.972	8.60	0.980	9.10	0.986	9.60
0.961	8.11	0.972	8.61	0.980	9.11	0.986	9.61
0.961	8.12	0.972	8.62	0.981	9.12	0.986	9.62
0.961	8.13	0.973	8.63	0.981	9.13	0.987	9.63
0.962	8.14	0.973	8.64	0.981	9.14	0.987	9.64
0.962	8.15	0.973	8.65	0.981	9.15	0.987	9.65
0.962	8.16	0.973	8.66	0.981	9.16	0.987	9.66
0.962	8.17	0.973	8.67	0.981	9.17	0.987	9.67
0.963	8.18	0.973	8.68	0.981	9.18	0.987	9.68
0.963	8.19	0.974	8.69	0.982	9.19	0.987	9.69
0.963	8.20	0.974	8.70	0.982	9.20	0.987	9.70
0.963	8.21	0.974	8.71	0.982	9.21	0.987	9.71
0.964	8.22	0.974	8.72	0.982	9.22	0.987	9.72
0.964	8.23	0.974	8.73	0.982	9.23	0.987	9.73
0.964	8.24	0.975	8.74	0.982	9.24	0.988	9.74
0.964	8.25	0.975	8.75	0.982	9.25	0.988	9.75
0.965	8.26	0.975	8.76	0.982	9.26	0.988	9.76
0.965	8.27	0.975	8.77	0.983	9.27	0.988	9.77
0.965	8.28	0.975	8.78	0.983	9.28	0.988	9.78
0.965	8.29	0.975	8.79	0.983	9.29	0.988	9.79
0.966	8.30	0.976	8.80	0.983	9.30	0.988	9.80
0.966	8.31	0.976	8.81	0.983	9.31	0.988	9.81
0.966	8.32	0.976	8.82	0.983	9.32	0.988	9.82
0.966	8.33	0.976	8.83	0.983	9.33	0.988	9.83
0.966	8.34	0.976	8.84	0.983	9.34	0.988	9.84
0.967	8.35	0.976	8.85	0.984	9.35	0.989	9.85
0.967	8.36	0.977	8.86	0.984	9.36	0.989	9.86
0.967	8.37	0.977	8.87	0.984	9.37	0.989	9.87
0.967	8.38	0.977	8.88	0.984	9.38	0.989	9.88
0.968	8.39	0.977	8.89	0.984	9.39	0.989	9.89
0.968	8.40	0.977	8.90	0.984	9.40	0.989	9.90
0.968	8.41	0.977	8.91	0.984	9.41	0.989	9.91
0.968	8.42	0.978	8.92	0.984	9.42	0.989	9.92
0.968	8.43	0.978	8.93	0.984	9.43	0.989	9.93
0.969	8.44	0.978	8.94	0.985	9.44	0.989	9.94
0.969	8.45	0.978	8.95	0.985	9.45	0.989	9.95
0.969	8.46	0.978	8.96	0.985	9.46	0.989	9.96
0.969	8.47	0.978	8.97	0.985	9.47	0.989	9.97
0.970	8.48	0.979	8.98	0.985	9.48	0.990	9.98
0.970	8.49	0.979	8.99	0.985	9.49	0.990	9.99
0.970	8.50	0.979	9.00	0.985	9.50		

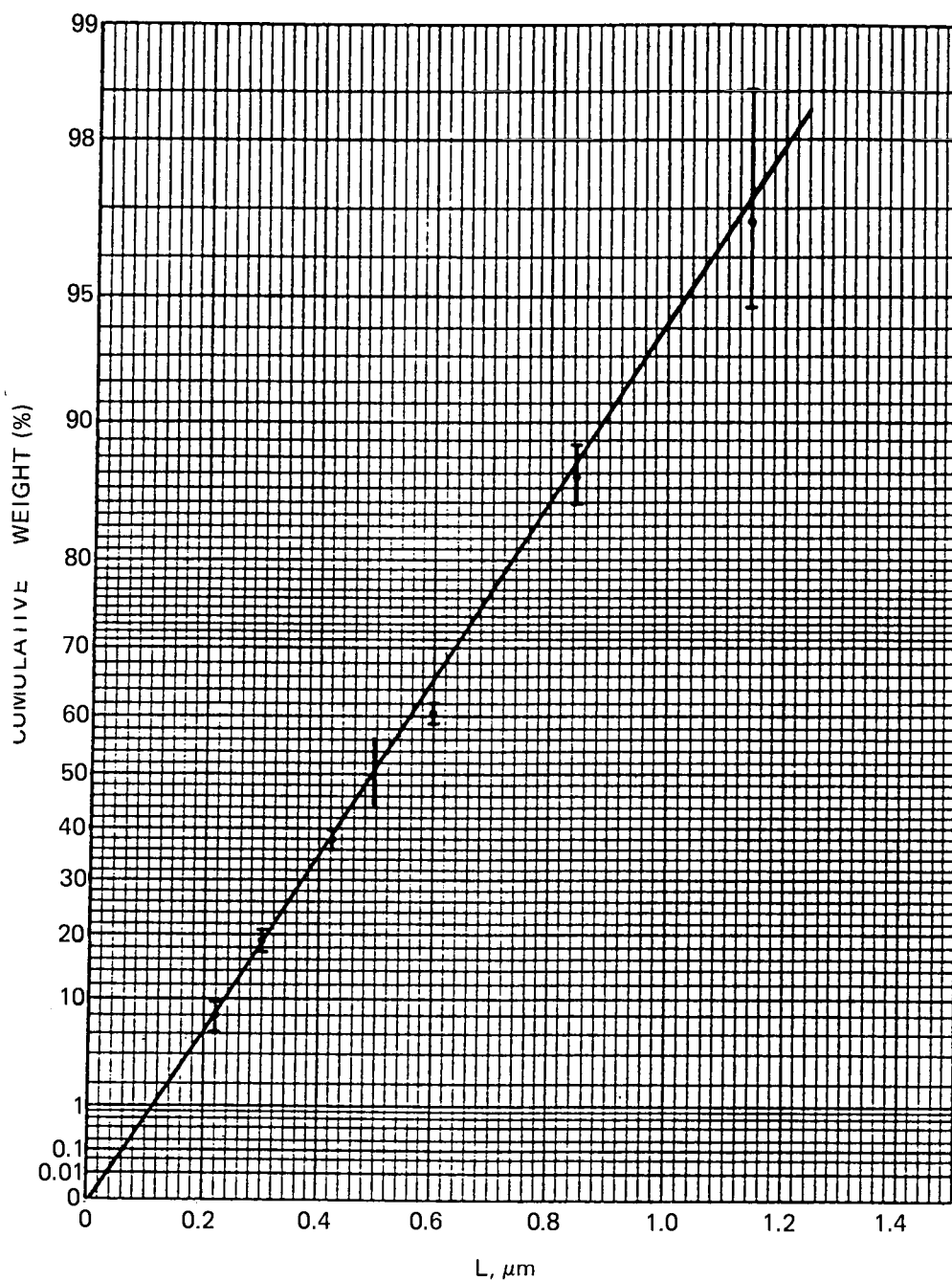


Fig. A-1 Cumulative mass plot on third-order gamma paper. A straight line should result if the MSMPR assumptions apply. Data for Na_2SO_4 produced in MSMPR crystallizer. [After E. T. White and A. D. Randolph, *AIChE J.* 33, 86 (1987).]

CRYSTAL.BALL PROGRAM

A complete listing of a program (Program CRYSTAL.BALL) to calculate CSD dynamics in a crystallizer of complex configuration is given below. The crystallizer's configuration is as shown in Fig. B-1. This program, with appropriate data input, permits simulation of CSD dynamics with fines and classified product removal (the so-called *R-z* crystallizer model) as well as arbitrary separation of liquid/solids residence times. The program can be run interactively.

Table B-1 lists the variables for this program together with representative values for simulation of high-yield KCl and variable-yield gypsum crystallizers. The equations that are programmed in the CRYSTAL.BALL simulator follow directly from the macrodistributed population balance, $\partial n / \partial t + G \partial n / \partial L + h(L)n / \tau = 0$, written on a total magma volume basis as three ODEs along a particle characteristic [Eq. (3.4-12)]. These equations along a characteristic *s* are summarized as follows:

$$ds = dt \quad \text{or} \quad \Delta s = \Delta t \quad (\text{B-1})$$

$$dL = G ds \quad \text{or} \quad \Delta L = G(t) \Delta t \quad (\text{B-2})$$

with population decaying exponentially along the characteristic as

$$dn/ds = -h(L)n/\tau \quad (\text{B-3})$$

An associated mass balance must be solved with Eqs. (B-1)–(B-3). The rigorous form of the mass balance, expressed on a total slurry basis [see Eq. (8.1-4)], is programmed in CRYSTAL.BALL. The void fraction ϵ , which

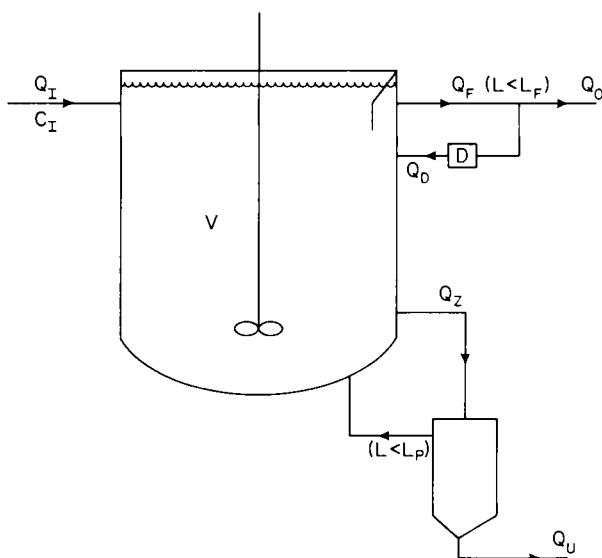


Fig. B-1 Schematic flow diagram of generalized crystallizer configuration simulated by program CRYSTAL.BALL.

occurs in Eq. (8.1-4), is calculated from the suspension slurry density as the calculation proceeds. CSD dynamics are little affected whether the rigorous form of the mass balance [Eq. (8.1-4)] or the approximate form [Eq. (8.1-5)] is used. The nucleation-growth rate kinetics used in CRYSTAL.BALL are of a general power-law form (see Table B-1).

The discretized equations as they are used in CRYSTAL.BALL are given by population densities n'_i moving along sizes L'_i where superscript t represents time and subscript i represents the i th packet of particles (increasing in size as i increases) moving convectively along a particle characteristic.

The length of each time step, Δt , is adjusted according to the equation

$$\Delta t' = \Delta L / G' \quad (\text{B-4})$$

The distance traveled by the packets, ΔL , during any time interval remains unchanged.

As the particles are moved along size space by Eq. (B-4), their population is adjusted as

$$n'_i = n'_{i-1} \exp(-\Delta t h'_{i-1} / \tau) \quad (\text{B-5})$$

The steady-state form of Eq. (B-5) is

$$n_i^0 = n_{i-1}^0 \exp[(-\Delta t) h_{i-1}^0 / \tau] \quad (\text{B-6})$$

Table B-1

Variables Used in CRYSTAL BALL CSD Simulator with Units and Representative Values for High-Yield (KCl) and Low-Yield (Gypsum) Systems

Symbol	Description	Units	Gypsum	KCl
Q_1	Feed flow rate	cm^3/min	100	100
Q_F	Fines removal rate (solids plus liquor)	cm^3/min	80	500
Q_o	Overflow rate (solids plus liquor)	cm^3/min	80	50
Q_u	Underflow rate (solids plus liquor)	cm^3/min	20	50
Q_z	Flow rate to classifier (solids plus liquor)	cm^3/min	100	350
C_1	Concentration in feed	g/cm^3	0.025	0.300
C_s	Saturation concentration	g/cm^3	0.0024	0.186
VOL	Volume of crystallizer	ml	10,000	10,000
L_F	Overflow cut size	μm	20	75
L_p	Cut size for classifier	μm	100	350
L_{\max}	Estimated largest crystal size	μm	500	4000
DELL	Distance between adjacent characteristics	μm	2	10
I	Kinetic parameters of nucleation equation $B^0 = k_N M_T^l G^i$	—	1.47	2.77
J		—	1.28	0.91
K_N		Units of K_N must map M_T (g/l) into B^0	9800	0.88
K_g	$G = K_g (C - C_s)^\alpha$	$\text{G} (\mu\text{m}/\text{min})$ $(\text{number}/\text{cm}^3 \text{ min})$	494,000	1,850
α	Exponent of above equation	—	2.23	1.0
K_A	Area shape factor	—	3.142	3.142
K_v	Volume shape factor	—	0.523	0.523
ρ	Density of crystals	g/cm^3	2.32	2.0
CLASS	Low yield = 1 High yield = 2	—	1	2
I_{VALUE}	Variable to be perturbed: Value Variable	—	—	—
	1 Q_1 and Q_F			
	2 Q_u and Q_1			
	3 Q_F and Q_D			
	4 Q_u and Q_F			
	5 Q_z and Q_R			
	6 K_N			
	7 C_1			
	8 C_s			
	9 VOL			
FACTOR	Factor by which variable to be perturbed is upset	—	—	—
DYSTEPS	Number of dynamic steps during upset	—	—	—

Define a population factor PF_i^t as

$$PF_i^t = n_i^t / n_i^0 \quad (\text{B-7})$$

Then Eqs. (B-4)–(B-6) can be combined to give

$$PF_i^t = PF_{i-1}^{t-1} \exp \left\{ \Delta L \left[\left(\frac{h}{G\tau} \right)_{i-1}^{t-1} - \left(\frac{h}{G\tau} \right)_{i-1}^0 \right] \right\} \cdots$$

$$(i = 1, \infty) \quad (\text{B-8})$$

The exponential term on the RHS is defined as the convective factor CF_{i-1}^{t-1} . With this definition,

$$PF_i^t = PF_{i-1}^{t-1} CF_{i-1}^{t-1} \cdots \quad (i = 1, \infty) \quad (\text{B-9})$$

At the boundary ($i = 0$), PF is given as

$$PF_0^t = BF^t = n_0^t / n_0^0 \quad (\text{B-10})$$

where BF^t is the boundary factor. Population density is then simply given as

$$n_i^t = n_i^0 PF_i^t \quad (\text{B-11})$$

with Eq. (B-10) used at the size boundary (nuclei). At each time step the program computes a convective factor corresponding to each classification range, and a boundary factor. The computational efficiency of this scheme is seen from the fact that the R - z model requires just four new terms for each time step. The moments of the crystallizer population distribution are then calculated as:

$$m_j^t = \sum_{i=1}^{I_{\text{total}}} W_{T_i}^t PF_i^t$$

where W_{T_i} , the steady-state contribution of a size window, is given by

$$W_{T_i}^t = [(n_i^0 + n_{i-1}^0)/2][L_i + L_{i-1}]/2 \Delta L \quad (\text{B-12})$$

The moments in the crystal product are calculated as

$$m_j^t = \sum_{i=1}^{I_{\text{total}}} h_i^t W_{T_i}^t PF_i^t \quad (\text{B-13})$$

These moments are used in calculating average sizes in the crystallizer and product as well as adjusting the growth rate G^t .

Table B-2 details the algorithm that is used to converge the steady-state and dynamic solutions. The algorithm consists essentially of guessing a value of the growth rate G , calculating concentration from an inversion of the growth rate–concentration kinetic statement, calculating the distribu-

Table B-2

Dynamic Solution Algorithm used in CRYSTAL.BALL CSD Simulator

Step	Purpose	Function
1.	Guess growth rate G	G is set internally
2.	Calculate concentration	$C = C_s + (G/k_g)^{1/\alpha}$
3.	Calculate population density $n(t)$	Dynamic Eqs. (B-8)–(B-9)
4.	Calculate nuclei density	$n(0) = k_N G^{i-1} M_T^j$
5.	Calculate moments	$m_j = \sum L^j n(L) dL$
6.	Calculate growth rate G	Solute balance
7.	Compare steps 1 and 6	Error = G (step 1) – G (step 7)
8.	Error tolerance	Error \leq tolerance
9.	Decision	Return to step 1 if 8 false

tion $n(L)$ from the assumed growth rate and population density, calculating the moments of the distribution to use in a mass balance, and then updating the values of growth rate, nuclei density, and concentration. The process is repeated until convergence is achieved.

The program does not have a separate algorithm for arriving at the steady-state solution. Instead, it uses the dynamic algorithm to stimulate hypothetical dynamics from an arbitrary initial state (guessed values of growth and nucleation rate) to the desired initial steady state. Besides being more compact, this method virtually ensures convergence.

The program assumes that neither intrinsic size-dependent growth rate nor size dispersion occurs, so the converged value of $G(t)$ is applicable to all size increments. Note again that the convective factor CF' is only a function of the classification function h_i' . This simplification would not be possible if growth rate were size-dependent.

Program CRYSTAL.BALL is written in standard FORTRAN 77 version 4.5. The program compiles and runs on a VAX 8600 computer with the VMS operating system. Run times on the VAX 8600 are typically of the order of 15 s for a CSD dynamics calculation covering 30–50 h of process time. Such long process response times are typical of crystallizers with the double draw-off configuration. Program CRYSTAL.BALL was developed as part of the master of science thesis of R. Sharnez (1).

Table B-3 shows representative data input and calculated CSDs for the gypsum system after manipulation of the DDO ratio (Q_o/Q_u) from 0 to 4 (a DDO ratio of zero represents MSMPR operation). The steady-state CSD [as population density $n(L)$] is shown before and after the upset, with representative crystallization parameters shown as a function of time during the period of transient CSD. Table B-4 shows similar calculations for a KCl

Table B-3*Effect of DDO Ratio on Calculated Gypsum CSD*

Effects of fines overflow on CSD (kinetics of gypsum)					
QI =	100.	QU =	100.	QF =	0.
QZ =	100.	CI =	0.025	CS =	0.002
VOL =	10,000.	I =	1.480	J =	1.270
KN =	9800.000	KG =	494,000.00	ALPHA =	2.230
CLASS =	1.	KA =	3.14	KV =	0.52
RHO =	2.30	LF =	30.	LP =	600.
LMAX =	600.	DELL =	1.	DUMMY =	1.
VARB =	4	FACT =	0.20	DYST =	20,000

Steady-state values before upset

Nucleation rate (number/cm ³ min)	= 0.195E + 05
Growth rate (μm/min)	= 0.115
Supersaturation (g/l)	= 0.106E + 01
Avg. crystal size in crystallizer (μm)	= 45
Avg. crystal size in prod. (μm)	= 45
c.v. In product (wt. basis)	= 0.500

Initial population distribution

Size (μm)	Population density (number/cm ³ μm)	
	Crystallizer	Product
0.0	0.169E + 06	0.169E + 06
30.0	0.125E + 05	0.125E + 05
60.0	0.917E + 03	0.917E + 03
90.0	0.675E + 02	0.675E + 02
120.0	0.497E + 01	0.497E + 01
150.0	0.366E + 00	0.366E + 00
180.0	0.269E - 01	0.269E - 01
210.0	0.198E - 02	0.198E - 02
240.0	0.146E - 03	0.146E - 03
270.0	0.107E - 04	0.107E - 04
300.0	0.789E - 06	0.789E - 06
330.0	0.581E - 07	0.581E - 07
360.0	0.428E - 08	0.428E - 08
390.0	0.315E - 09	0.315E - 09
420.0	0.232E - 10	0.232E - 10
450.0	0.170E - 11	0.170E - 11
480.0	0.125E - 12	0.125E - 12
510.0	0.923E - 14	0.923E - 14
540.0	0.679E - 15	0.679E - 15
570.0	0.500E - 16	0.500E - 16

Table B-3. Continued

T (min)	n_0 (number/cm ³ μm)	G ($\mu\text{m}/\text{min}$)	$L_{4,3}$ (μm)	M_T (g/l)	Prod. (g/min)	Q_o/Q_u
0.	0.169E + 06	0.11	45	21.4	2.1	1.0
9.	0.175E + 06	0.11	33	21.9	0.7	4.0
18.	0.184E + 06	0.11	34	23.1	0.9	4.0
37.	0.201E + 06	0.10	35	25.4	0.9	4.0
57.	0.219E + 06	0.10	37	27.7	1.0	4.0
78.	0.237E + 06	0.09	38	30.1	1.0	4.0
100.	0.257E + 06	0.09	40	32.6	1.0	4.0
123.	0.277E + 06	0.09	41	35.2	1.1	4.0
147.	0.297E + 06	0.08	43	37.7	1.1	4.0
172.	0.318E + 06	0.08	45	40.3	1.1	4.0
198.	0.338E + 06	0.08	46	42.9	1.2	4.0
225.	0.359E + 06	0.07	48	45.4	1.2	4.0
252.	0.379E + 06	0.07	49	48.0	1.2	4.0
280.	0.398E + 06	0.07	51	50.5	1.3	4.0
309.	0.419E + 06	0.07	52	53.0	1.4	4.0
354.	0.448E + 06	0.07	55	56.5	1.4	4.0
400.	0.477E + 06	0.07	57	59.9	1.5	4.0
447.	0.504E + 06	0.06	58	63.0	1.5	4.0
494.	0.531E + 06	0.06	60	66.0	1.6	4.0
559.	0.563E + 06	0.06	63	69.5	1.7	4.0
640.	0.598E + 06	0.06	66	73.4	1.8	4.0
740.	0.634E + 06	0.06	69	77.1	1.8	4.0
856.	0.671E + 06	0.06	73	80.5	1.9	4.0
1006.	0.705E + 06	0.06	77	83.7	2.0	4.0
1172.	0.726E + 06	0.06	81	85.8	2.1	4.0
1337.	0.744E + 06	0.06	85	86.9	2.1	4.0
1501.	0.750E + 06	0.06	88	87.5	2.1	4.0
1665.	0.749E + 06	0.06	90	87.7	2.2	4.0
1829.	0.749E + 06	0.06	92	87.6	2.2	4.0
1993.	0.751E + 06	0.06	94	87.5	2.2	4.0
2158.	0.747E + 06	0.06	95	87.5	2.2	4.0
2323.	0.745E + 06	0.06	95	87.5	2.2	4.0
2488.	0.746E + 06	0.06	96	87.5	2.2	4.0
2654.	0.749E + 06	0.06	96	87.7	2.2	4.0
2819.	0.747E + 06	0.06	97	87.7	2.2	4.0
2985.	0.747E + 06	0.06	97	87.8	2.2	4.0
3151.	0.748E + 06	0.06	97	87.8	2.2	4.0

Steady-state values after upset

Nucleation rate (number/cm³ min) = 0.454E + 05Growth rate ($\mu\text{m}/\text{min}$) = 0.061

Supersaturation (g/l) = 0.788E00

Avg. crystal size in crystallizer (μm) = 116Avg. crystal size in prod. (μm) = 97

c.v. In product (wt. basis) = 0.701

Table B-3. *Continued*

Size (μm)	Final population distribution	
	Population density (number/cm ³ μm)	
	Crystallizer	Product
0.0	0.748E + 06	0.748E + 06
30.0	0.517E + 04	0.517E + 04
60.0	0.193E + 04	0.386E + 03
90.0	0.713E + 03	0.143E + 03
120.0	0.261E + 03	0.522E + 02
150.0	0.972E + 02	0.194E + 02
180.0	0.366E + 02	0.732E + 01
210.0	0.139E + 02	0.279E + 01
240.0	0.488E + 01	0.975E + 00
270.0	0.139E + 01	0.278E + 00
300.0	0.465E + 00	0.931E - 01
330.0	0.549E + 00	0.110E + 00
360.0	0.119E + 00	0.238E - 01
390.0	0.876E - 02	0.175E - 02
420.0	0.644E - 03	0.129E - 03
450.0	0.474E - 04	0.948E - 05
480.0	0.349E - 05	0.698E - 06
510.0	0.257E - 06	0.514E - 07
540.0	0.189E - 07	0.378E - 08
570.0	0.139E - 08	0.278E - 09

Table B-4

Effect of Product Classification on Calculated KCl CSD

QI =	100.	QU =	100.	QF =	0.
QZ =	100.	CI =	0.250	CS =	0.186
VOL =	10,000.	I =	2.770	J =	0.910
KN =	0.880	KG =	1850.00	ALPHA =	1.000
CLASS =	2.	KA =	3.14	KV =	0.52
RHO =	2.00	LF =	0.	LP =	350.
LMAX =	2000.	DELL =	10.	DUMMY =	10.
VARB =	5	FACT =	7.00	DYST =	10,000

Steady-state values before upset

Nucleation rate (number/cm³ min) = 0.670E + 02
 Growth rate ($\mu\text{m}/\text{min}$) = 1.184
 Supersaturation (g/l) = 0.640E00
 Avg. crystal size in crystallizer (μm) = 473
 Avg. crystal size in prod. (μm) = 473
 c.v. In product (wt. basis) = 0.500

Table B-4 *Continued*

Initial population distribution						
Size (μm)	Population density (number/cm ³ μm)					
	Crystallizer		Product			
0.0	0.566E + 02		0.566E + 02			
100.0	0.243E + 02		0.243E + 02			
200.0	0.104E + 02		0.104E + 02			
300.0	0.449E + 01		0.449E + 01			
400.0	0.193E + 01		0.193E + 01			
500.0	0.829E + 00		0.829E + 00			
600.0	0.356E + 00		0.356E + 00			
700.0	0.153E + 00		0.153E + 00			
800.0	0.658E - 01		0.658E - 01			
900.0	0.283E - 01		0.283E - 01			
1000.0	0.121E - 01		0.121E - 01			
1100.0	0.522E - 02		0.522E - 02			
1200.0	0.224E - 02		0.224E - 02			
1300.0	0.964E - 03		0.964E - 03			
1400.0	0.414E - 03		0.414E - 03			
1500.0	0.178E - 03		0.178E - 03			
1600.0	0.765E - 04		0.765E - 04			
1700.0	0.329E - 04		0.329E - 04			
1800.0	0.141E - 04		0.141E - 04			
1900.0	0.607E - 05		0.607E - 05			

T (min)	n_0 (number/cm ³ μm)	G ($\mu\text{m}/\text{min}$)	$L_{4,3}$ (μm)	M_T (g/l)	Prod. (g/min)	Q_z/Q_u
0.	0.566E + 02	1.18	473	69.9	7.0	1.0
8.	0.563E + 02	1.26	553	61.4	30.3	7.0
46.	0.526E + 02	1.64	394	34.1	7.6	7.0
64.	0.493E + 02	1.58	342	34.2	6.5	7.0
91.	0.466E + 02	1.50	317	35.8	6.3	7.0
160.	0.459E + 02	1.42	312	39.0	6.7	7.0
223.	0.484E + 02	1.46	321	39.0	7.2	7.0
289.	0.500E + 02	1.55	326	36.3	7.3	7.0
354.	0.482E + 02	1.51	318	36.3	6.7	7.0
421.	0.475E + 02	1.47	317	37.7	6.8	7.0
489.	0.484E + 02	1.49	320	37.8	7.1	7.0
555.	0.488E + 02	1.51	322	37.0	7.1	7.0
622.	0.483E + 02	1.50	320	36.9	6.9	7.0
689.	0.481E + 02	1.49	319	37.4	6.9	7.0
756.	0.483E + 02	1.49	320	37.4	7.0	7.0
822.	0.485E + 02	1.50	320	37.2	7.0	7.0
889.	0.483E + 02	1.50	320	37.1	7.0	7.0
956.	0.483E + 02	1.49	320	37.3	6.9	7.0
1023.	0.483E + 02	1.50	320	37.3	7.0	7.0
1090.	0.484E + 02	1.50	320	37.2	7.0	7.0
1156.	0.483E + 02	1.50	320	37.2	7.0	7.0
1223.	0.483E + 02	1.50	320	37.2	7.0	7.0
1290.	0.483E + 02	1.50	320	37.3	7.0	7.0

Table B-4. Continued

Steady-state values after upset

Nucleation rate (number/cm ³ min)	= 0.724E + 02
Growth rate (μm/min)	= 1.497
Supersaturation (g/l)	= 0.809E00
Avg. crystal size in crystallizer (μm)	= 271
Avg. crystal size in prod. (μm)	= 320
c.v. In product (wt. basis)	= 0.245

Size (μm)	Final population distribution	
	Population density (number/cm ³ μm)	
	Crystallizer	Product
0.0	0.483E + 02	0.483E + 02
100.0	0.248E + 02	0.248E + 02
200.0	0.127E + 02	0.127E + 02
300.0	0.651E + 01	0.651E + 01
400.0	0.450E + 00	0.315E + 01
500.0	0.419E - 02	0.293E - 01
600.0	0.390E - 04	0.273E - 03
700.0	0.364E - 06	0.254E - 05
800.0	0.339E - 08	0.237E - 07
900.0	0.316E - 10	0.221E - 09
1000.0	0.294E - 12	0.206E - 11
1100.0	0.273E - 14	0.191E - 13
1200.0	0.254E - 16	0.178E - 15
1300.0	0.238E - 18	0.166E - 17
1400.0	0.221E - 20	0.155E - 19
1500.0	0.205E - 22	0.144E - 21
1600.0	0.191E - 24	0.134E - 23
1700.0	0.179E - 26	0.125E - 25
1800.0	0.168E - 28	0.117E - 27
1900.0	0.154E - 30	0.108E - 29

system where the classification ratio (Q_z/Q_u) is stepped from 1 to 7, thus narrowing the distribution. Note that classification reduced the coefficient of variation of the product from 0.5 to 0.25. Mean particle size was also reduced from 473 μm to 320 μm.

Organizations desiring to use Program Crystal.Ball should write to the Department of Chemical Engineering, University of Arizona, Tucson, Arizona 85721, to purchase a diskette containing the program.

```

C      CRYSTAL.BALL
C      WRITTEN BY RIZWAN SHARNEZ
C      COPYRIGHT, UNIVERSITY OF ARIZONA 1987

COMMON/A1/QI,QU,QF,QZ,CI,CS,VOL,TAU,R,RSS,Z,ZSS,F
COMMON/A2/KN,KG,I,J,ALPHA,KV,KA,RHO,CLASS,DUMMY,FLAG,LAP
COMMON/A3/LF,LP,LMAX,DELL,DELT,STEPS,NUMBER
COMMON/A4/M2,M3,M4,MT,MTU,PROD
COMMON/A5/CFSS,KNSS,NOSS,TAUSS,QISS,QUSS,QFSS,QZSS,CSSS,VOLSS
COMMON/A6/GN,GG,C1,CO,M21,M20,M31,M30,M41,M40,M3F,M3P,M4P,M5P
COMMON/A7/FACTOR,DYSTEPS,VARIABL
COMMON/A8/SIZE(2500),POP(2500),WT(2500,5),H(2500)
COMMON/A10/FAC1(2500),FLAG1

REAL KN,KG,I,J,KV,KA,M2,M3,M4,MT,M20,M21,M30,M31,M41
1      ,NOSS,KNSS

OPEN(UNIT=5,FILE='CRYSTAL.DAT',STATUS='OLD')
OPEN(UNIT=6,FILE='CRYSTAL.OUT',STATUS='NEW')

DO LAP = 1,10

CALL INTERFACE

CALL SETUP

CALL EXECUTE

END DO

STOP
END

SUBROUTINE INTERFACE

COMMON/A1/QI,QU,QF,QZ,CI,CS,VOL,TAU,R,RSS,Z,ZSS,F
COMMON/A2/KN,KG,I,J,ALPHA,KV,KA,RHO,CLASS,DUMMY,FLAG,LAP
COMMON/A3/LF,LP,LMAX,DELL,DELT,STEPS,NUMBER
COMMON/A4/M2,M3,M4,MT,MTU,PROD
COMMON/A7/FACTOR,DYSTEPS,VARIABL

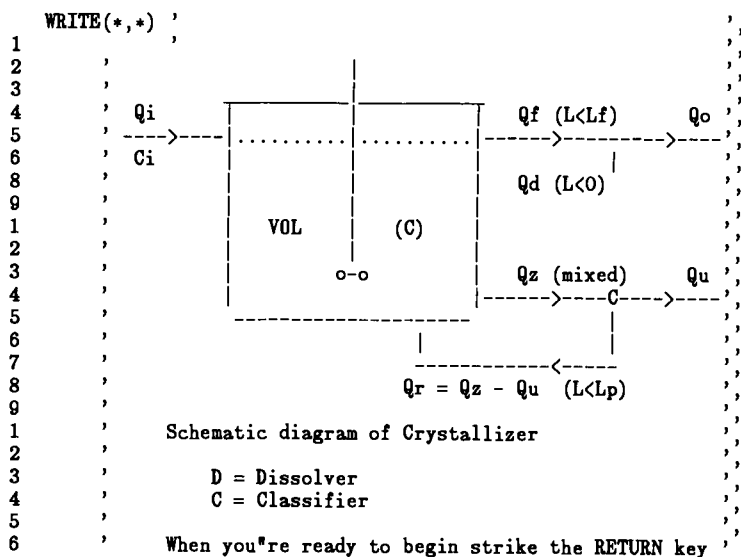
INTEGER VARIABL,DYSTEPS
REAL LF,LP,KN,KG,I,J,KV,KA,M2,M3,M4,MT,KNSS,LMAX
CHARACTER TITLE*100,OPTION*6,START*6,CHECK*10

IF(LAP.GT.1) RETURN

WRITE(*,*) '      * * * * WELCOME TO CRYSTAL.BALL * * * *',
1      ,
2      ,
3      ,      DO YOU WISH TO RUN CRYSTAL.BALL
4      ,      INTERACTIVELY?
5      ,
6      ,      Enter Y/N

READ(*,1) OPTION
1      FORMAT(A6)
IF(OPTION.EQ.'N'.OR.OPTION.EQ.'n') GO TO 100

```



```

2  READ(*,2) START
   FORMAT(A6)

   WRITE(*,*) 'You may now begin entering the data
1  ,
2  , Remember: All entries must have a decimal point
3  ,
4  , Enter a title if you wish to; it will be echoed
5  , along with the other data in your Output File :
6  , CRYSTAL.OUT. Then strike RETURN
7  ,

   READ(*,50) TITLE
50  FORMAT(A60)

   WRITE(*,*) 'Enter Qi; Feed flow rate (cm3/min)
   READ(*,*) QI
   WRITE(*,*) 'Enter Qu; Underflow rate (cm3/min) '
   READ(*,*) QU
   WRITE(*,*) 'Enter Qf; Overflow rate (cm3/min) '
   READ(*,*) QF
   WRITE(*,*) 'Enter Qz; Flow rate to classifier (cm3/min) '
   READ(*,*) QZ
   WRITE(*,*) 'Enter Ci; Concentration in feed (g/cc) '
   READ(*,*) CI
   WRITE(*,*) 'Enter Cs; Saturation concentration (g/cc) '
   READ(*,*) CS
   WRITE(*,*) 'Enter VOL; Volume of crystallizer (cc) '
   READ(*,*) VOL
   WRITE(*,*) 'Enter Lf; Overflow cut size (microns) '
   READ(*,*) LF
   WRITE(*,*) 'Enter Lp; Cut size for classifier (microns) '
   READ(*,*) LP
   WRITE(*,*) 'Enter Lmax; Estimated largest crystal size(microns)'
   READ(*,*) LMAX

```

```

WRITE(*,*) 'Enter DELL; distance between adjacent characteristics',
1      '(microns). If unsure enter 5.0'
  READ(*,*) DELL
  WRITE(*,*) 'The next three variables are parameters of the',
    'equation :',
2      '          o   j   i',
3      '          B = k M G',
4      '          N   T',
5      'Enter i'
  READ(*,*) I
  WRITE(*,*) 'Enter j'
  READ(*,*) J
  WRITE(*,*) 'Enter kN; Units of kN must map G (microns/min)',
1      'and MT (g/L) into BO (#/cc min)'
  READ(*,*) KN
  WRITE(*,*) 'The next two variables are parameters of the',
2      'equation :',
3      '          G = K (C - C )^a',
4      '          g       s',
5      'Enter Kg; (micron cc/min g)'
  READ(*,*) KG
  WRITE(*,*) 'Enter a'
  READ(*,*) ALPHA
  WRITE(*,*) 'Enter Ka; Area shape factor'
  READ(*,*) KA
  WRITE(*,*) 'Enter Kv; Volume shape factor'
  READ(*,*) KV
  WRITE(*,*) 'Enter rho; Density of crystals (g/cc)'
  READ(*,*) RHO
  WRITE(*,*) 'Enter CLASS; Low yield = 1 (Gypsum)',
2      'High yield = 2 (KCl)',
3      'If solution does not converge, or program',
4      'terminates prematurely, retry with other value'
  READ(*,*) CLASS
  WRITE(*,*) 'Enter VARIABLE; enter your variable number',
1      'from the following list :',
2      'Variable      Value',
3      'Qi & Qf        1',
4      'Qu & Qi        2',
5      'Qf & Qd        3',
6      'Qu & Qf        4',
7      'Qz & Qr        5',
8      'Kn            6',
9      'Ci            7',
1     'Cs            8',
2     'VOL           9',
3     'Enter a number between 1 and 9 depending on',
4     'which variable (or pairs of variables) you',
5     'wish to upset. In case of pairs, the',
6     'variable that appears first is perturbed;',
7     'the other variable is then adjusted in',
8     'accordance with mass balance.'
  READ(*,*) VARIABLE
  WRITE(*,*) 'Enter FACTOR; This is the factor by which the',

```

```

1      'perterbed variable is upset'
      READ(*,*) FACTOR
      WRITE(*,*) 'Enter DYSTEPS; Number of time steps in upset',
1      'If upset is a step change, enter 10000.'
      READ(*,*) DYSTEPS

      GO TO 200

100    CONTINUE

      READ(5,*) TITLE
      READ(5,*) QI,QU,QF,QZ,CI,CS,VOL
      READ(5,*) I,J,KN,KG,ALPHA,CLASS
      READ(5,*) KA,KV,RHO
      READ(5,*) LF,LP,LMAX,DELL,DUMMY
      READ(5,*) VARIABL,FACTOR,DYSTEPS

200    WRITE(*,10) TITLE
      WRITE(6,10) TITLE
10     FORMAT(/70(' ')/5X,A60//70(' ')/)

      WRITE(*,15) QI,QU,QF,QZ,CI,CS,VOL,I,J,KN,KG,ALPHA,CLASS,KA,KV
1      ,RHO,LF,LP,LMAX,DELL,DUMMY,VARIABL,FACTOR,DYSTEPS

      WRITE(6,15) QI,QU,QF,QZ,CI,CS,VOL,I,J,KN,KG,ALPHA,CLASS,KA,KV
1      ,RHO,LF,LP,LMAX,DELL,DUMMY,VARIABL,FACTOR,DYSTEPS

15     FORMAT(5X,' QI = ',F10.0,5X,' QU = ',F10.0,5X,' QF = ',F10.0/
1         5X,' QZ = ',F10.0,5X,' CI = ',F10.3,5X,' CS = ',F10.3/
2         5X,' VOL = ',F10.0,5X,' I = ',F10.3,5X,' J = ',F10.3/
3         5X,' KN = ',F10.3,5X,' KG = ',F10.2,2X,' ALPHA = ',F10.3/
4         2X,' CLASS = ',F10.0,5X,' KA = ',F10.2,5X,' KV = ',F10.2/
5         5X,' RHO = ',F10.2,5X,' LF = ',F10.0,5X,' LP = ',F10.0/
6         4X,' LMAX = ',F10.0,4X,' DELL = ',F10.0,3X,' DUMMY = ',F10.0/
7         4X,' VARB = ',I10, 4X,' FACT = ',F10.2,4X,' DYST = ',I10)

      IF(CLASS.GE.2) CLASS = CLASS + 6

      WRITE(6,20)
      WRITE(*,20)
20     FORMAT(/70(' ')/)

      WRITE(*,*) 'Check the echoed data; if it's alright,
1 strike the RETURN key '
      READ(*,40) CHECK
40     FORMAT(A10)

      RETURN
      END

SUBROUTINE SETUP

COMMON/A1/QI,QU,QF,QZ,CI,CS,VOL,TAU,R,RSS,Z,ZSS,F
COMMON/A2/KN,KG,I,J,ALPHA,KV,KA,RHO,CLASS,DUMMY,FLAG,LAP
COMMON/A3/LF,LP,LMAX,DELL,DELT,STEPS,NUMBER
COMMON/A4/M2,M3,M4,MT,MTU,PROD
COMMON/A5/CISS,KNSS,NOSS,TAUSS,QISS,QUSS,QFSS,QZSS,CSSS,VOLSS
COMMON/A6/GN,GG,C1,CO,M21,M20,M31,M30,M41,M40,M3F,M3P,M4P,M5P

```

332 / APPENDIX B CRYSTAL.BALL PROGRAM

```
COMMON/AB/SIZE(2500),POP(2500),WT(2500,5),H(2500)
```

```
INTEGER COUNT,DELTAL
```

```
REAL LF,LP,KN,KG,I,J,KV,KA,M2,M3,M3F,MTF,M4,MT,NOSS,KNSS,MTMB
```

```
REAL LMAX,M5,M3P,M4P,M5P
```

```
FLAG = 0
```

```
SIZE(1)=0.0
```

```
IF (LF.GT.0) THEN
```

```
  DIVLF=LF/DELL
```

```
  DIVLF=FLOAT(INT(DIVLF) + 1)
```

```
  DELL=LF/DIVLF
```

```
  IF (DELL.LT.1) DELL=1.0
```

```
ENDIF
```

```
NUMBER=LMAX/DELL
```

```
TAU=VOL/QU
```

```
QISS=QI
```

```
IF (QU.EQ.0) QU=0.01
```

```
QUSS=QU
```

```
IF (QF.EQ.0) QF=0.01
```

```
QFSS=QF
```

```
IF (QZ.EQ.0) QZ=QU
```

```
QZSS=QZ
```

```
CISS=CI
```

```
CSSS=CS
```

```
KNSS=KN
```

```
TAUSS=TAU
```

```
VOLSS=VOL
```

```
R=QF/QU + 1.
```

```
RSS=R
```

```
Z=QZ/QU
```

```
IF (Z.LE.1) Z=1.
```

```
ZSS=Z
```

```
F=QI/QU
```

```
IF ((F - 1.).EQ.0) F = F + 0.001
```

```
IF ((R - 1.).EQ.0) R = R + 0.001
```

```
IF ((F - R).EQ.0) F = R + 0.001
```

```
DO K=2,NUMBER
```

```
  II=K-1
```

```
  SIZE(K)=SIZE(II)+DELL
```

```
END DO
```

```
DO K=1,NUMBER
```

```
  IF (SIZE(K).LE.LF) THEN
```

```
    H(K) = R
```

```
  ELSE
```

```
    IF (SIZE(K).LE.LP) THEN
```

```
      H(K) = 1.
```

```
    ELSE
```

```
      H(K) = Z
```

```
    ENDIF
```

```
  ENDIF
```



```

END DO

GFACT = CLASS + LAP - 1
GG = 0.0125 * GFACT ** 2
MT = 0.0125 * GFACT ** 2
M2 = 0.
M3 = 0.
M3F = 0.
M4 = 0.
M5 = 0.
POPLF = 0.
POPLP = 0.

GN=KN*GG**(I-1.)*(MT*1000.)**J
POP(1)=GN

DO K=2,NUMBER

    II = K-1

    IF (SIZE(K).LE.LF) THEN
        POP(K)=GN*EXP(-RSS*SIZE(K)/GG/TAU)
    ELSE

        IF(SIZE(K).LE.LP) THEN
            IF(POPLF.EQ.O) POPLF = GN*EXP(-RSS*LF/GG/TAU)
            POP(K)=POPLF*EXP(-(SIZE(K)-LF)/GG/TAU)
        ELSE

            IF(POPLP.EQ.O) POPLP = POPLF*EXP(-(LP-LF)/GG/TAU)
            POP(K)=POPLP*EXP(-ZSS*(SIZE(K)-LP)/GG/TAU)
        ENDIF
    ENDIF

    WT(K,2)=(POP(K)+POP(II))/2.0*DELL*
1      ((SIZE(K)+SIZE(II))/2.0)**2

    WT(K,3)=(POP(K)+POP(II))/2.0*DELL*
1      ((SIZE(K)+SIZE(II))/2.0)**3

    WT(K,4)=(POP(K)+POP(II))/2.0*DELL*
1      ((SIZE(K)+SIZE(II))/2.0)**4

    WT(K,5)=(POP(K)+POP(II))/2.0*DELL*
1      ((SIZE(K)+SIZE(II))/2.0)**5

    M2 = M2 + WT(K,2)
    M3 = M3 + WT(K,3)
    IF (SIZE(K).LE.(LF+0.1)) M3F = M3F + WT(K,3)
    M4 = M4 + WT(K,4)
    M5 = M5 + WT(K,5)

END DO

CO=(GG/KG)**(1./ALPHA) + CS
AT=KA*M2*1.E-8
MTF=RH0*KV*M3F*1.E-12
MT=RH0*KV*M3*1.E-12

```

```
RETURN
END
```

SUBROUTINE PERTURB

```
COMMON/A1/QI,QU,QF,QZ,CI,CS,VOL,TAU,R,RSS,Z,ZSS,F
COMMON/A2/KN,KG,I,J,ALPHA,KV,KA,RHO,CLASS,DUMMY,FLAG,LAP
COMMON/A3/LF,LP,LMAX,DELL,DELT,STEPS,NUMBER
COMMON/A5/CISS,KNSS,NOSS,TAUSS,QISS,QUSS,QFSS,QZSS,CSSS,VOLSS
COMMON/A7/FACTOR,DYSTEPS,VARIABLE
COMMON/A8/SIZE(2500),POP(2500),WT(2500,5),H(2500)
```

```
INTEGER COUNT,VARIABLE,DYSTEPS
REAL LF,LP,KN,KG,I,J,KV,KA,M2,M3,M4,MT,KNSS,LMAX
```

```
GO TO (10,20,30,40,50,60,70,80,90) VARIABLE
```

```
10  QI = QISS * FACTOR
    QF = QFSS + (QI - QISS)
    IF(QF.LE.0) QF = 0.01
    F = QI/QU
    R = QF/QU + 1.
    GO TO 1000
```

```
20  QU = QU * FACTOR
    QI = QISS * (QU - QUSS)
    TAU = VOL/QU
    F = QI/QU
    R = QF/QU + 1.
    GO TO 1000
```

```
30  QF = QFSS * FACTOR
    R = QF/QU + 1.
    GO TO 1000
```

```
40  QU = QUSS * FACTOR
    QF = QFSS - (QU - QUSS)
    IF(QF.LE.0) QF = 0.01
    TAU = VOL/QU
    F = QI/QU
    R = QF/QU + 1.
    GO TO 1000
```

```
50  QZ = QZSS * FACTOR
    Z = QZ/QU
    GO TO 1000
```

```
60  KN = KNSS * FACTOR
    RETURN
```

```
70  CI = CISS * FACTOR
    RETURN
```

```
80  CS = CSSS * FACTOR
    RETURN
```

```
90  VOL = VOLSS * FACTOR
    TAU = VOL/QU
```

```

RETURN

1000  IF((F - 1.).EQ.0) F = F + 0.001
      IF((R - 1.).EQ.0) R = R + 0.001
      IF((F - R).EQ.0) F = R + 0.001

      DO K=1,NUMBER

          IF(SIZE(K).LE.LF) THEN
              H(K) = R
          ELSE
              IF(SIZE(K).LE.LP) THEN
                  H(K) = 1.
              ELSE
                  H(K) = Z
              ENDIF
          ENDIF

      END DO

RETURN
END

SUBROUTINE EXECUTE

COMMON/A1/QI,QU,QF,QZ,CI,CS,VOL,TAU,R,RSS,Z,ZSS,F
COMMON/A2/KN,KG,I,J,ALPHA,KV,KA,RHO,CLASS,DUMMY,FLAG,LAP
COMMON/A3/LF,LP,LMAX,DELL,DELT,STEPS,NUMBER
COMMON/A4/M2,M3,M4,MT,MTU,PROD
COMMON/A5/CISS,KNSS,NOSS,TAUSS,QISS,QUSS,QFSS,QZSS,CSSS,VOLSS
COMMON/A6/GN,GG,C1,CO,M21,M20,M31,M30,M41,M40,M3F,M3P,M4P,M5P
COMMON/A7/FACTOR,DYSTEPS,VARIABLE
COMMON/A8/SIZE(2500),POP(2500),WT(2500,5),H(2500)
COMMON/A10/FAC1(2500),FLAG1

CHARACTER STATUS1*10,STATUS2*10,ANSWER*10,PAUSE*10
INTEGER COUNT,STEPS,VARIABLE,DYSTEPS
REAL LF,LP,KN,KG,I,J,KV,KA,M2,M3,M4,MT,M20,M21,M30,M31,M40,M41
REAL NOSS,KNSS,M3P,M4P,M5P,NEWG,MTU
DIMENSION POPPR(2500)

8000  T = 0.
      STEPS = 1
      OLDG = GG
      ANSWER = 'NO'

      IF(FLAG1.EQ.0) THEN
          WRITE(*,*) ' THE TABLE THAT FOLLOWS LISTS CALCULATIONS',
1          ' FOR CONVERGING TO AN INITIAL CONDITION',
2          ' STEADY STATE; IT IS NOT PART OF THE RESULTS',
3          '
          ELSE
              WRITE(*,*) ' THE STEADY STATE SOLUTION HAS CONVERGED.',
1          ' WHAT FOLLOWS IS THE DYNAMIC SOLUTION',
2          '
          ENDIF

      WRITE(*,*) ' Strike RETURN when ready

```

```

      READ(*,90)  PAUSE
90      FORMAT(A5)

7000    CONTINUE

      CALL CONVERGE

      IF(FLAG.EQ.1) RETURN
      STEPS = STEPS + 1
      IF(FLAG1.EQ.0.AND.DELT.GT.250) DELT = 10.
      T = T + DELT
      M20 = M21
      DELMT = (M31 - M30) * RHO * KV * 1.E-12
      M30 = M31
      M3F0 = M3F1
      M40 = M41
      DELC = C1 - CO
      CO = C1
      NEWG = GN
      COUNT = COUNT + 1
      GCHANGE = ABS(NEWG - OLDG) / OLDG

      IF(GCHANGE.GT.0.05.OR.COUNT.GE.10) THEN

      SD = MT*1000.
      LBARP = M4P/M3P
      PROD = (QI * (CI - C1) - ((DELMT + (1. - MT / RHO) * DELC)
1 / DELT * VOL)) / (1. - C1 / RHO)

      WRITE(*,100) T,GN,GG,LBARP,SD,PROD
      IF(FLAG1.EQ.1) WRITE(6,100) T,GN,GG,LBARP,SD,PROD

      OLDG = GN
      COUNT = 0

      ENDIF

100    FORMAT(6X,F6.0,2X,E9.3,F7.2,I9,2F12.1)

      IF(FLAG1.EQ.1.AND.STEPS.EQ.DYSTEPS) THEN
      FACTOR = 1.0
      CALL PERTURB
      ENDIF

      TCHECK = TCHECK + DELT
      IF(TCHECK.GT.1000) THEN
      TCHECK = 0.

      IF(FLAG1.EQ.0) THEN
      WRITE(*,*) '
1          ' IF CALCULATIONS HAVE REACHED A STEADY STATE',
2          ' FOR AT LEAST TWO CONSECUTIVES LAPS',
3          ' ENTER : YES ; IF NOT, ENTER : NO',
4          ' ( STRIKE RETURN TO CONTINUE )'
      ELSE
      WRITE(*,*) '
1          ' IF CALCULATIONS HAVE REACHED A STEADY STATE',
2          ' OR YOU WISH TO DISCONTINUE',
3          ' ENTER : YES ; IF NOT, ENTER : NO',

```

```

4      ' ( STRIKE RETURN TO CONTINUE ) '
      ENDIF

      READ(*,110) ANSWER
110    FORMAT(A10)
      ENDIF

      IF(ANSWER.EQ.'NO'.OR.ANSWER.EQ.'no') GO TO 7000

      DO K=1,NUMBER

          II = K - 1

          IF(FLAG1.EQ.0) THEN

              IF (SIZE(K).LE.LF) THEN
                  POP(K)=GN*EXP(-RSS*SIZE(K)/GG/TAU)
              ELSE

                  IF (SIZE(K).LE.LP) THEN
                      IF(POPLF.EQ.0) POPLF = GN*EXP(-RSS*LF/GG/TAU)
                      POP(K)=POPLF*EXP(-(SIZE(K)-LF)/GG/TAU)
                  ELSE

                      IF(POPLP.EQ.0) POPLP = POPLF*EXP(-(LP-LF)/GG/TAU)
                      POP(K)=POPLP*EXP(-ZSS*(SIZE(K)-LP)/GG/TAU)
                  ENDIF
              ENDIF

              WT(K,2)=(POP(K)+POP(II))/2.0*DELL*
              ((SIZE(K)+SIZE(II))/2.0)**2
1          WT(K,3)=(POP(K)+POP(II))/2.0*DELL*
              ((SIZE(K)+SIZE(II))/2.0)**3
1          WT(K,4)=(POP(K)+POP(II))/2.0*DELL*
              ((SIZE(K)+SIZE(II))/2.0)**4
1          WT(K,5)=(POP(K)+POP(II))/2.0*DELL*
              ((SIZE(K)+SIZE(II))/2.0)**5

              ELSE

                  POP(K) = POP(K) * FAC1(K)

              ENDIF

          END DO

      DO K = 1,NUMBER

          IF (SIZE(K).LE.LF) THEN
              POPPR(K) = POP(K)
          ELSE
              IF (SIZE(K).LE.LP) THEN
                  POPPR(K) = POP(K) / R
              ELSE
                  POPPR(K) = POP(K) * Z / R
              ENDIF
          ENDIF
      
```

```

ENDIF

END DO

IF(FLAG1.EQ.0) THEN
  STATUS1 = 'INITIAL'
  STATUS2 = 'BEFORE'
ELSE
  STATUS1 = 'FINAL'
  STATUS2 = 'AFTER'
ENDIF

BO = GN * GG
LBARX = M4/M3
SUPER = (C1 - CS) * 1000.
CV = SQRT( M3P * M5P / ( M4P**2 ) -1. )

IF(STATUS1.EQ.'FINAL') WRITE(6,9000)

WRITE(6,15) STATUS2
15  FORMAT('          STEADY STATE VALUES ',A6,' UPSET'/'
1      '
      _____')
25  WRITE(6,25) BO,GG,SUPER,LBARY,LBAP,CV
      FORMAT('          NUCLEATION RATE (# / cc. min)      = ',E8.3/
1      '          GROWTH RATE (mic. / min)                = ',F5.3/
2      '          SUPERSATURATION (g / L)                 = ',E8.3/
3      '          AVG. CRYSTAL SIZE IN X*ZER (mic.)        = ',I5/
4      '          AVG. CRYSTAL SIZE IN PROD. (mic.)        = ',I5/
5      '          C. V. IN PRODUCT (wt. basis)            = ',F5.3/)

75  WRITE(6,75) STATUS1
      FORMAT(/70(' '))//
1      '          ',A8,'POPULATION DISTRIBUTION  '
      WRITE(6,*) '
      _____',
1      '          POPULATION DENSITY',
2      '          SIZE',
3      '          (#/cc. micron)',
4      '          (microns)',
5      '          CRYSTALLIZER      PRODUCT',
6      '          _____',
7      '          |          |          |',
8      '          |          |          |'

DELTAL = NUMBER/20
DO K=1,NUMBER,DELTAL

      WRITE(6,5000) SIZE(K),POP(K),POPPR(K)

END DO

5000  FORMAT('          ',F8.1,'          |          ',E10.3,'          |          ',E10.3)
      WRITE(6,*) '
1      '
      _____

IF(STATUS1.EQ.'INITIAL') THEN

  FLAG1 = 1

```

```

        WRITE(6,6000)
6000  FORMAT(/4X,70(' ')/)
1      MT = 0.
        PROD = 0.
        SD = MT * 1000.
        PROD = (QI * (CI - C1) - ((DELMT + (1. - MT / RHO) * DELC)
1      / DELT * VOL)) / (1. - C1 / RHO)
        WRITE(*,100) T,GN,GG,LBARP,SD,PROD
        WRITE(6,100) T,GN,GG,LBARP,SD,PROD
        CALL PERTURB
        GO TO 8000

    ELSE

        WRITE(6,9000)
9000  FORMAT(/70(' ')/)
        ENDIF

        WRITE(*,200)
200  FORMAT(/70(' ')/5X,'Your Data has been processed; for an ',
1      'output enter : TYPE CRYSTAL.OUT')
        LAP = 10
        RETURN
        END

SUBROUTINE CONVERGE

COMMON/A1/QI,QU,QF,QZ,CI,CS,VOL,TAU,R,RSS,Z,ZSS,F
COMMON/A2/KN,KG,I,J,ALPHA,KV,KA,RHO,CLASS,DUMMY,FLAG,LAP
COMMON/A3/LF,LP,LMAX,DELL,DELT,STEPS,NUMBER
COMMON/A4/M2,M3,M4,MT,MTU,PROD
COMMON/A5/CISS,KNSS,NOSS,TAUSS,QISS,QUSS,QFSS,QZSS,CSSS,VOLSS
COMMON/A6/GN,GG,C1,CO,M21,M20,M31,M30,M41,M40,M3F,M3P,M4P,M5P
COMMON/A8/SIZE(2500),POP(2500),WT(2500,5),H(2500)
COMMON/A10/FAC1(2500),FLAG1

CHARACTER NEXT*6
INTEGER COUNT,STEPS,DYSTEPS
REAL LF,LP,KN,KG,I,J,KV,KA,M2,M3,M4,MT,M20,M21,M30,M31,M40,M41
1 ,NOSS,KNSS,M3FO,M3F1,M3F,MTF,M3P,M4P,M5P,MTU,M3U

DIMENSION FACO(2500),BFO(2500),BF1(2500)

IF (STEPS.EQ.1) THEN

    GSS = GG
    NOSS = GN
    M20 = M2
    M30 = M3
    M3FO = M3F
    M40 = M4
    G1 = GG

    DO 500 K = 1,NUMBER

        FACO(K) = 1.0
        FAC1(K) = 1.0

```

```

500    CONTINUE

      ENDIF

      GINC = 0.01
      GO = G1
      COUNT = 0
      OLDSIGN = 0

      DO 1500 K = 1,NUMBER

          FACO(K) = FAC1(K)

1500    CONTINUE
1000    CONTINUE

      G1 = (2. * GG) - GO
      DELT = DELL/GG

      PFR = EXP(DELL * ( (RSS/(GSS*TAUSS)) - (R/(GG*TAU)) ))
      PF1 = EXP(DELL * ( (1./(GSS*TAUSS)) - (1./(GG*TAU)) ))
      PFZ = EXP(DELL * ( (ZSS/(GSS*TAUSS)) - (Z/(GG*TAU)) ))

      FAC1(1) = GN/NOSS

      M21=0.
      M31=0.
      M3F1=0.
      M41=0.
      M3P=0.
      M4P=0.
      M5P=0.
      M3U=0.

      DO K=2,NUMBER

          II = K - 1
          IF (SIZE(K).LE.LF) THEN
              FAC1(K) = FACO(II) * PFR
          ELSE
              IF (SIZE(K).LE.LP) THEN
                  FAC1(K) = FACO(II) * PF1
              ELSE
                  FAC1(K) = FACO(II) * PFZ
              ENDIF
          ENDIF

          FAC = (FAC1(II) + FAC1(K))/2.

          M21 = M21 + WT(K,2) * FAC
          M31 = M31 + WT(K,3) * FAC

          IF (SIZE(K).LT.(LF+0.1)) M3F1 = M3F1 + WT(K,3) * FAC

          M41 = M41 + WT(K,4) * FAC
          M3P = M3P + WT(K,3) * H(K) * FAC
          M4P = M4P + WT(K,4) * H(K) * FAC
          M5P = M5P + WT(K,5) * H(K) * FAC

```



```

      IF (SIZE(K).LT.LP) THEN
      M3U = M3U + WT(K,3) * FAC
      ELSE
      M3U = M3U + WT(K,3) * H(K) * FAC
      ENDIF

END DO

IF(G1.LE.0) G1 = 1.E-4
IF(GG.LE.0.OR.COUNT.GT.1500) THEN

  IF(LAP.LT.10) THEN
    WRITE(*,*) ' SOLUTION DID NOT CONVERGE; INITIATING NEW LAP',
1      ' strike RETURN when ready'
    READ(*,150) NEXT
150  FORMAT(A6)
    ELSE
    WRITE(*,*) ' SOLUTION DID NOT CONVERGE AFTER TEN LAPS;',
1      ' CHECK VALIDITY OF DATA AND TRY AGAIN',
2      ' WITH A DIFFERENT VALUE OF "CLASS".',
3      ' ELSE CHANGE GG = 0.0125 AND MT = 0.0125',
4      ' IN SUBROUTINE SETUP TO A DIFFERENT VALUE'
    STOP
    ENDIF

  FLAG = 1
  RETURN
  ENDIF

  C1 = (G1/KG)**(1./ALPHA) + CS
  CAVG = (GG/KG)**(1./ALPHA) + CS
  M2 = (M21 + M20)/2.
  M3 = (M31 + M30)/2.
  M3F = (M3F1 + M3F0)/2.
  M4 = (M41 + M40)/2.

  AT = M2 * KA * 1.E-8
  MT = M3 * RHO * KV * 1.E-12
  MTU = M3U * RHO * KV * 1.E-12
  MTF = M3F * RHO * KV * 1.E-12
  DELC = C1 - CO
  CORRTNF = (1. - M3F * KV * 1.E-12)
  CORRTN = (1. - M3U * KV * 1.E-12)
  GN = KN*GG**(I-1.)*(MT*1000.)**J

  GCAL=2.E4*(F/TAU*(CI-((F-1.)*CORRTNF+CORRTN)/F*CAVG)-CORRTN*DELC
1  /DELT - CAVG*(MTU+MTF*(F-1.))/RHO/TAU - MTF*(F-1.)/TAU*(F-R)/
2  (R-1.))/ ( AT * ( RHO - CAVG))

  ERROR=GCAL - GG
  GG=GCAL
  COUNT = COUNT + 1

  IF(COUNT.GT.100) THEN
    SIGN = ERROR/ABS(ERROR)
    CHECK = SIGN + OLDSIGN
    IF(CHECK.EQ.0) GINC = GINC * 0.25
    OLDSIGN = SIGN

```

```

      IF (GCAL.LT.GG) GG = GG - GINC
      IF (GCAL.GT.GG) GG = GG + GINC

      ENDIF

      IF (ABS(ERROR).LT.0.0005) THEN
      RETURN
      ELSE
      GO TO 1000
      ENDIF

      END

```

Reference

1. Sharenz, R. (1987). Dynamic simulation and control of crystal size distribution in a complex crystallizer. M.S. Thesis, University of Arizona, Tucson.

SAMPLE PROBLEMS

Chapter 2

- 2.1 Given the normal distribution function

$$f(L) = [1/\sigma(2\pi)^{1/2}] \exp[-(L - \bar{L})^2/2\sigma^2]$$

prove that the parameter σ satisfies the definition

$$\sigma^2 = \int_{-\infty}^{\infty} (L - \bar{L})^2 f(L) dL$$

and that the parameter \bar{L} satisfies the definition of mean size

$$\bar{L} = \int_{-\infty}^{\infty} L f(L) dL$$

- 2.2 Show that the normal and log-normal distributions are normalized over their respective axes, that is,

$$\int_{-\infty}^{\infty} f(L) dL = 1$$

and

$$\int_{L=0}^{L=\infty} f(\log L) d(\log L) = 1$$

- 2.3 Show that the truncated log-normal distribution of Eq. (2.2-7) is normalized over the axis $\log[(L - L_1)/(L_2 - L)]$ in the interval L in (L_1, L_2) .

- 2.4 A gamma distribution of the form in Example 2.2-1 represents the distributive weight-size distribution of crystals from a steady-state mixed suspension crystallizer. If the mode size b is $300\ \mu\text{m}$, find the average size \bar{L} and the median size \bar{L}_{50} of the distribution.
- 2.5 Calculate the skewness and kurtosis of the gamma-type CSD described in Problem 2.4.
- 2.6 Calculate the parameters (\bar{L}, σ) , (\bar{L}, σ') , and (a, b) and plot the normal, log-normal, and gamma distributions for an experimental particle weight-size distribution that has a mode of $500\ \mu\text{m}$ and has 90% of its mass less than $800\ \mu\text{m}$. Calculate the coefficient of variation predicted by each of these three distributions. Calculate the size below which 99% of the distribution is predicted to occur using these three distributions.
- 2.7 A gamma population distribution having a c.v. of 35.3% has a median size \bar{L}_{50} of $600\ \mu\text{m}$. Calculate the area-weighted mean size $\bar{L}_{3,2}$.
- 2.8 A particle weight distribution has a median size of $400\ \mu\text{m}$ and a c.v. (working definition) of 0.35. Find the parameters in the normal, log-normal, gamma, and Rosin-Rammler distributions that have the same medians and c.v. values. What are the mean sizes predicted by these four distributions?
- 2.9 An experimental Glauber's salt weight size distribution is given below:

Sieve Analysis for Glauber's Salt Crystallization, 11-l Crystallizer
 $(\tau = 90\ \text{min}, \rho k_v = 810\ \text{kg/m}^3, M_T = 300\ \text{kg/m}^3)$

Sieve aperture (mm)	Mean size (mm)	Percent mass on sieve	Cumulative percent mass	Specific pop. density ($\times 10^9/\text{mm-m}^3$)	Specific cumulative number ($\times 10^9/\text{m}^3$)
	1.414	3.4		0.024	
1.189	1.000	10.0	96.6	0.29	0.012
0.841	0.707	26.6	86.6	3.1	0.112
0.595	0.500	22.7	60.0	10.4	0.86
0.420	0.354	18.7	37.3	34	2.68

Sieve aperture (mm)	Mean size (mm)	Percent mass on sieve	Cumulative percent mass	Specific pop. density ($\times 10^9/\text{mm-m}^3$)	Specific cumulative number ($\times 10^9/\text{m}^3$)
0.297			18.6		6.9
	0.250	10.8		79	
0.210			7.8		13.8
	0.177	7.8		229	
0.149			0.0		27.9

Find the parameters in the normal, log-normal, gamma, and Rosin-Rammler distributions having the same median size and c.v. (use working definition). Plot the experimental distribution on normal, log-normal, and Rosin-Rammler graphs, respectively. Show both calculated and experimental distributions.

- 2.10 An MSMPR crystal population distribution has a mean size $L_{10} = 60 \mu\text{m}$. Find the parameters in the normal, log-normal, and Rosin-Rammler distributions that have the same mean size (weight basis) as the MSMPR distribution. Are these normal, log-normal, and Rosin-Rammler distributions unique?
- 2.11 Derive the formula for the c.v., on a weight basis, in terms of moments of an unnormalized population distribution.

Chapter 3

- 3.1 Show that the dynamic one-dimensional population balance given as

$$\frac{\partial n}{\partial t} + \frac{\partial}{\partial L}(Gn) + \frac{n}{\tau} = 0$$

satisfies the general hyperbolic form

$$A \frac{\partial^2 n}{\partial t^2} + 2B \frac{\partial^2 n}{\partial L \partial t} + C \frac{\partial^2 n}{\partial L^2} = F\left(t, L, n, \frac{\partial n}{\partial t}, \frac{\partial n}{\partial L}\right)$$

where $B^2 - AC > 0$.

- 3.2 Simplify the macroscopic population balance for two equal-volume, mixed-suspension cooling crystallizers operating in series. Assume

different but constant conditions in each vessel, that is, $G_1\tau \neq G_2\tau$. Laplace-transform to obtain a single second-order transform describing population density in the second vessel in terms of G_1 , G_2 , n_1^0 , and n_2^0 .

- 3.3 Solve Problem 3.2 for $n_2(L)$ in terms of G_1 , G_2 , n_1^0 , and n_2^0 . What simplification in this form of CSD results when $G_1 = G_2$ and $n_2^0 = 0$? Express this simplified form as a dimensionless equation $y = y(x)$, where $y_2 = n_2/n_1^0$ and $x = L/G\tau$. Plot this dimensionless distribution and identify it with one of the distributions discussed in Chapter 2.
- 3.4 Write the macromoment population balance for a steady-state, mixed-suspension crystallizer to obtain an algebraic recursion relationship for the $(j-1)$ th and j th moments. Show that the exponential distribution $n = n^0 \exp(-L/G\tau)$ generates moments that satisfy this recursion relation.
- 3.5 Recognizing that the Laguerre polynomial is orthogonal on the interval $(0, \infty)$ with respect to the gamma-distribution weighting function, develop an orthogonal expansion of an arbitrary distribution $f(L)$ in terms of its Laguerre polynomial expansion without trying to constrain the first three moments to agree with the moments of $f(L)$. The coefficients in this expansion will again be a function of the moments $\{m_j\}$. Test the expansion by recovering the log-normal distribution described in Example 3.8-1.

Chapter 4

- 4.1 Calculate the coefficient of variation of the population, length, area, and mass distributions of the ideal MSMPR crystal-size distribution.
- 4.2 An experimental CSD from a MSMPR crystallizer has a mass-averaged size $\bar{L}_{4,3}$ of 500 μm . The crystallizer operates with a suspension holdup of 800 gal and has a slurry discharge rate of 10 gal/min. Calculate the linear crystal growth rate in $\mu\text{m}/\text{min}$. If the suspension density is 0.15 g crystals/ cm^3 of slurry and the product of the shape factor and the crystal density is 2.5 g/ cm^3 , calculate density of nuclei and nucleation rate, number/ $\text{cm}^3 \mu\text{m}$, and number/ $\text{cm}^3 \mu\text{m}$, respectively.

[Ans. $G = 1.56 \mu\text{m}/\text{min}$, $n^0 = 41 \text{ nuclei}/\text{cm}^3 \mu\text{m}$, $B^0 = 64 \text{ nuclei}/\text{cm}^3 \text{ min}$.]
- 4.3 A crystal product obtained from an MSMPR crystallizer has an average size $\bar{L}_{1,0}$ of 600 μm . The crystals are cubic in habit and have a specific gravity of 2.00. The suspension density is 200 g/l of crystal-

lizer volume. The crystallizer has a working volume of 1000 gal and the slurry discharge rate is 10 gal/min. Calculate the crystal growth rate G ($\mu\text{m}/\text{min}$) and the nucleation rate B^0 (number/l min).

[Ans. $G = 6 \mu\text{m}/\text{min}$.]

- 4.4 When the crystallizer described in Problem 4.3 was operated with a concentration change δC of 100 g/l and a residence time of 200 min, the dominant particle size was 700 μm . When the residence time was changed to 50 min, the dominant particle size was 300 μm . Calculate and compare the growth and nucleation rates for each case. Comment on the character of the kinetics of nucleation and growth as they relate to supersaturation. Qualitatively discuss these relationships in the context of the feedback relationship shown in Fig. 4.5-1.

[Ans. $G_1 = 1.17 \mu\text{m}/\text{min}$, $B_1^0 = 3.27 \times 10^3$ nuclei/l min, $G_2 = 2.00 \mu\text{m}/\text{min}$, $B_2^0 = 1.67 \times 10^5$ nuclei/l min.]

- 4.5 A crystal system with a size-dependent growth rate of the form $G = G_0(1 + aL)$ is being produced in an MSMPR crystallizer. Using the steady-state equation for the third moment, show that $a < 0.333/G_0\tau$ is a necessary restriction to achieve a stable CSD having a finite third moment.
- 4.6 Droplet breakup in a dispersed-phase liquid-liquid system is given by $D(L) = kn(L)L^4$. Each drop breaks into three new liquid droplets of mass $\frac{1}{2}$, $\frac{1}{4}$, and $\frac{1}{4}$ of the original mass, respectively. Phrase a consistent birth function for this system $B(L)$ (neglecting coalescence) that conserves total droplet mass.
- 4.7 (a) The following nucleation-growth kinetics apply for a crystallization system: $B^0 = kG$. Show that at the same rate of make in an MSMPR crystallizer, a change in holding time alone will not change the size distribution.
- (b) Show the effect of a fourfold change of holding time on a system that exhibits fourth-order kinetics ($i = 4$). Compare with the effect of a fourfold change in holding time on a system that exhibits negative-order kinetics (e.g., $i = -2$).
- 4.8 Show that the two kinetic models proposed below give the same result when comparing size distributions obtained at two different rates of make. Take the holding time in the two cases to be equal.

$$B^0 = kM_T^i G^i$$

$$B^0 = kA_T^i G^i$$

It is clear from this example that the simple MSMR crystallizer cannot be used to determine the exact mechanism of secondary nucleation.

Chapter 7

- 7.1 Fines dissolution is initiated in a class II system having secondary nucleation kinetics of the form

$$B^0 = k_N G^4 M_T^{0.5}$$

Fines are removed at a size L_F small compared to product size at a rate Q_F such that the dissolution parameter λ is

$$\lambda = Q_F L_F / GV = 4.3$$

Estimate the maximum expected size improvement measured as ratio of dominant size in product after and before initiation of fines dissolution.

- 7.2 Calculate the zeroth, first, and second moments of the weight distributions for the R - z CSD model with fines removal only (i.e., with $z = 1$) as a function of the dissolution parameter R and size of dissolution $x_1 = L_F / G\tau$. Calculate the c.v. of the distribution as a function of x_1 and R . (Note: Product and crystallizer distributions are identical.)
- 7.3 Repeat Problem 7.2 with product classification but no dissolution (i.e., $R = 1$) as a function of the classification parameter z and classification size $x_2 = L_p / G\tau$. Calculate the c.v. of the product and crystallizer distributions as a function of z and x_2 .
- 7.4 Show that fines dissolution is less effective as the order of nucleation increases. Explain the result qualitatively.
- 7.5 Solve the equation for size distribution from a batch evaporative system when the heat load is held constant. Assume growth rate is not a function of size and that nucleation rate is not a function of suspension density. Assume a single-size size distribution for an initial condition.
- 7.6 A 10-l MSMR laboratory crystallizer with kinetics and properties similar to those of KCl in Appendix B operates with an exit magma flow of 200 cm³/min and slurry density (clear liquor basis) of 0.1 g/cm³. Predict the mean mass-weighted particle size in the distribution. Estimate the crystal growth rate.

- 7.7 A fines dissolver is to be installed on the crystallizer of 7.6, removing crystals at sizes less than $100\text{ }\mu\text{m}$. What fines-dissolver flow rate would be required to make an average particle size of $500\text{ }\mu\text{m}$?
- 7.8 The crystallizer of Problem 7.6 has a product classification at size $L_P = 400\text{ }\mu\text{m}$ with a classification ratio $\beta = 3.0$. Calculate the expected mean size and coefficient of variation (weight basis).
- 7.9 Show that for a crystallizer with a fines dissolver for sizes $L < L_F$, and with a dissolver flow rate R times the under flow rate, the fraction of nuclei left undissolved is $\beta = \exp[-RL_F/G\tau]$. [Hint: Construct a semilog population plot for the distributions with and without fines dissolving and apply continuity $aL = L_F$].
- 7.10 A class II R - z crystallizer has parameters as follows:

$$\begin{array}{ll} R = 6 & L_F = 75\text{ }\mu\text{m} \\ z = 3 & L_P = 600\text{ }\mu\text{m} \\ i = 1.5 & P = 59/\text{min} \\ j = 1 & \tau = 100\text{ min} \\ \rho k_v = 2.0\text{ g/cm}^3 & Q_m = 100\text{ cm}^3/\text{min} \\ k_N = 10^4 \text{ (maps } G^{1.5}M_T \text{ into number/cm}^3 \text{ min)} & \end{array}$$

Find the value of growth rate in $\mu\text{m}/\text{min}$ that satisfies a mass balance for this system.

- 7.11 A bench scale class II R - z crystallizer with a total dissolver can be described by the following physical parameters:

$$\begin{array}{l} Q_i = Q_u = 100\text{ cm}^3/\text{min} \text{ (cooling crystallizer)} \\ R = Q_F/Q_u = 6 \\ Z = Q_p/Q_u = 3 \\ \rho = 2.0\text{ g/cm}^3 \\ \tau = 12\text{ g/min} \\ L_F = 75\text{ }\mu\text{m} \\ L_P = 600\text{ }\mu\text{m} \end{array}$$

Assume the crystals are approximately spherical in shape. Assume power-law kinetics given as $B^0 = 10G^{1.5}M_T$ where $B^0 = \text{number/cm}^3 \text{ min}$, $G = \mu\text{m}/\text{min}$, and $M_T = \text{g/cm}^3$. Calculate the expected crystal growth rate and mass-weighted size in the crystallizer and product.

$$[\text{Ans. } G = 1.45\text{ }\mu\text{m}/\text{min}, L_{4,3\text{ cryst}} = 420\text{ }\mu\text{m}, L_{4,3\text{ product}} = 453\text{ }\mu\text{m}.]$$

Chapter 8

- 8.1 Write out the transient moment equations for a class I system in a MSMPR cooling crystallizer of volume V . Close the set by adding appropriate side and initial conditions. Assume system kinetics are given by

$$G = k_g (C - C_s) \quad \mu\text{m}/\text{min}$$

$$B^0 = k_N (C - C_s)^i \quad \text{number}/\text{min volume slurry}$$

and the system is fed with flow rate Q and concentration C_i . What is the highest moment that has to be calculated to close the set? [Note: Nucleation kinetics are given on a slurry basis. Thus, the moments can be written on a slurry basis and the $d(\log V)/dt$ term dropped.]

- 8.2 Write out the transient moment equations for a class II system in a MSMPR cooling crystallizer of constant volume V . Assume system kinetics of the form

$$B^0 = k_N G^i \quad \text{number}/\text{min volume slurry}$$

with growth-rate constraint

$$G = (K \delta C) / \left(\tau \int_0^\infty n L^2 dL \right)$$

where K is a constant, $\delta C = (Q_i/Q_o)C_i - C_s$, and $\tau = V/Q_o$. What is the highest moment that is necessary to close the set? Assuming that the solute resources δC are dynamically varied, what is the highest moment that must be included to calculate transient production rate from the dynamic moments? Write an alternate differential equation to calculate transient production rate directly. This equation would serve as a check on the moment equations.

- 8.3 Assume the class II system of Problem 5.2 with secondary nucleation kinetics given as

$$B^0 = k_N G^i m_1^j$$

and all system inputs invariant in time.

- (a) Make the set of moment equations dimensionless with the transformation

$$\theta = t/\tau, \quad y_j = m_j(\theta)/(m_j)_0, \quad \rho = G/G_0$$

utilizing the steady-state recursion relationship

$$(m_j)_0 = j G_0 \tau (m_{j-1})_0$$

- (b) Linearize this set of dimensionless moment equations about the steady-state operating conditions $(y_j)_0 = \rho_0 = 1$.
- (c) Transform and write the characteristic equation of this linearized transformed set.

$$[Ans. \quad s^3 + 4s^2 + (6 - j)s + (3 + i - 2j) = 0.]$$

- (d) Apply the Routh stability criterion to this characteristic equation to obtain a CSD stability criterion in terms of the parameters i and j .

$$[Ans. \quad i + 2j < 21.]$$

- 8.4 Repeat Problem 5.3 with secondary nucleation kinetics of the form

$$B^0 = k_N G^i m_4^j$$

Compare stability criteria in this and the previous problem with the criterion ($j = 0$) given in Chapter 5, namely, $i < 21$. Which kinetic expression gives the most limited stability region?

$$[Ans. \quad 5.4(c) \quad s^4 + 5s^3 + 10s^2 + (9 + i)s + (3 + i + j) = 0.]$$

$$Ans. \quad 5.4(d) \quad i^2 - 7i + 25j < 294.]$$

- 8.5 If the fines dissolver of Problem 7.6 were combined with the classifier of problem 7.7, estimate the critical nucleation/growth rate sensitivity i_c at which cycling would begin. Assume crystallizer flow conditions of Problem 7.5.
- 8.6 A 10-l laboratory R - z crystallizer has a fines flow rate of $600 \text{ cm}^3/\text{min}$, a product rate of $100 \text{ cm}^3/\text{min}$, a fines size $L_F = 0.75 \text{ } \mu\text{m}$, a product classification size $L_P = 600 \text{ } \mu\text{m}$, and a classification ratio of 7.0. The slurry density nucleation exponent is $j = 0$. If a value of $G = 2 \text{ } \mu\text{m}/\text{min}$ satisfies the mass balance, at what value of i_c will the CSD go unstable?
- 8.7 If the classification size in Problem 8.6 is lowered to $400 \text{ } \mu\text{m}$, how will the stability limit change?

SELECTED BIBLIOGRAPHY

I Books

- Buckley, H. E. (1951). "Crystal Growth." Wiley, New York.
- Gibbs, J. W. (1948). "Collected Works, Volume I, Thermodynamics." Yale University Press, New Haven, Connecticut.
- Mullin, J. W. (1972). "Crystallization," 2nd ed. Butterworth, London.
- Nielsen, A. E. (1964). "Kinetics of Precipitation." Macmillan, New York.
- O'Hara, M., and Reid, R. C. (1973). "Modeling Crystal Growth Rates from Solution." Prentice-Hall, Englewood Cliffs, New Jersey.
- Petrov, T. G., Treivus, E. B., and Kasatkin, A. P. (1969). "Growing Crystals from Solution." Consultants Bureau, New York.
- Strickland-Constable, R. F. (1968). "Kinetics and Mechanisms of Crystallization." Academic Press, New York.

II Population Balances

- Hulburt, H. M., and Katz, S. (1964). *Chem. Eng. Sci.* **19**, 555.
- Randolph, A. D. (1964). *Can. J. Chem. Eng.* **42**, 280.
- Randolph, A. D. (1979). *Ind. Crystallization* **78**, 295-308.

III Crystal-Size Distribution

- Abegg, C. F. (1966). Analysis of crystal size distribution when growth rate is size dependent. Ph.D. thesis, Iowa State University of Science and Technology, Ames, Iowa, unpublished.
- Abegg, C. F., and Balakrishnan, N. S. (1971). A mathematical model of real crystallizers based on cascade of perfectly mixed crystallizers. *Chem. Eng. Progr. Ser.* **110**(67), 88.

- Abegg, C. F., Stevens, J. D., and Larson, M. A. (1968). *AIChE J.* **14**, 118.
- Baliga, J. B. (1970). Crystal nucleation and growth kinetics in batch evaporative crystallization. Thesis, Iowa State University of Science and Technology, Ames, Iowa, unpublished.
- Becker, G. W. (1970). Intrinsic classified withdrawal in continuous well mixed crystallization. Ph.D. thesis, Iowa State University of Science and Technology, Ames, Iowa, unpublished.
- Becker, G. W., Jr., and Larson, M. A. (1969). *Chem. Eng. Progr. Symp. Ser.* **95**(65), 14.
- Bennett, R. C. (1969). *Chem. Eng. Progr. Symp. Ser.* **95**(64), 34.
- Bransom, S. H. (1960). *Br. Chem. Eng.* **5**, 838.
- Canning, T. F., and Randolph, A. D. (1967). *AIChE J.* **13**, 5.
- Canning, T. F. (1970). *Chem. Eng. Progr.* **66**, 80.
- Estrin, J. W., Sauter, A., and Karshina, G. W. (1969). *AIChE J.* **15**, 289.
- Garside, J., and Jancic, S. J. (1978). *Chem. Eng. Sci.* **33**, 12.
- Garside, J., Rusli, I. T., and Larson, M. A. (1979). *AIChE J.* **25**, 1.
- Han, C. D., and Shinnar, R. (1968). *AIChE J.* **14**, 612.
- Hulburt, H. M., and Stefango, D. G. (1969). *Chem. Eng. Progr. Symp. Ser.* **95**(65), 50.
- Janse, A. H., and de Jong, E. J. (1979). *Ind. Crystallization* **78**, 135. North Holland, Amsterdam.
- Janse, A. H., and de Jong, E. J. (1976). *Ind. Crystallization* **145**, Plenum, New York.
- Larson, M. A., and Randolph, A. D. (1969). *Chem. Eng. Progr. Symp. Ser.* **95**(65), 1.
- Larson, M. A., and Wolff, P. R. (1971). Crystal-size distributions from multi-stage crystallizers. *Chem. Eng. Progr. Symp. Ser.* **110**(67), 97.
- Lee, H. H. (1978). *AIChE J.* **24**, 3.
- Lie, S. J., Shinnar, R., and Katz, S. (1971). Feedback control of a continuous crystallizer with and without fines trap. *Chem. Eng. Progr. Symp. Ser.* **110**(67), 129.
- Liu, Y., and Botsaris, G. D. (1973). *AIChE J.* **19**, 3.
- Mullin, J. W., and Nyvlt, J. (1970). *Chem. Eng. Sci.* **25**, 131.
- Nan't Land, C. M., and Wienk, B. G. (1975). *Ind. Crystallization* **51**. Plenum Press, New York.
- Nauman, E. B. (1971). Selective fines destruction in recycle crystallizers. *Chem. Eng. Progr. Ser.* **110**(67), 116.
- Nauman, E. B., and Szabo, T. T. (1971). Non-selective fines destruction in recycle crystallizers. *Chem. Eng. Progr. Symp. Ser.* **110**(67), 108.
- O'Dell, F. P., and Rousseau, R. W. (1978). *AIChE J.* **24**, 738-741.
- Randolph, A. D. (1965). *AIChE J.* **11**, 424.
- Randolph, A. D. (1969). *Ind. Eng. Chem. Fundam.* **8**, 58.
- Randolph, A. D. (1970). *Chem. Eng.* **27**, 80.
- Randolph, A. D. (1962). Size distribution dynamics in a mixed suspension. Ph.D. thesis, Iowa State University of Science and Technology, Ames, Iowa, unpublished.
- Randolph, A. D., Deepak C., and Iskander, M. (1968). *AIChE J.* **14**, 827.
- Randolph, A. D., and Larson, M. A. (1962). *AIChE J.* **8**, 639.
- Randolph, A. D., and Larson, M. A. (1965). *Chem. Eng. Progr. Symp. Ser.* **55**(61), 147.
- Saeman, W. C. (1956). *AIChE J.* **2**, 107.
- Sherwin, M. B., Shinnar, R., and Katz, S. (1967). *AIChE J.* **13**, 1141.
- Sherwin, M., Shinnar, R., and Katz, S. (1969). *Chem. Eng. Progr. Symp. Ser.* **95**(65), 75.
- Stone, P. D. (1967). An experimental study of crystal-size distribution in a continuous, backmixed, gas-phase reactor. M.S. thesis, University of Florida, Gainesville, Florida, unpublished.
- Stone, P. D., and Randolph, A. D. (1969). *Chem. Eng. Progr. Symp. Ser.* **95**(65), 24.
- White, E. T., and Wright, P. G. (1971). Magnitude of size dispersion effects in stirred crystallizers. *Chem. Eng. Progr. Ser.* **110**(67), 81.
- Wolff, P. R. (1965). Suspension density transients in a mixed suspension crystallizer, M.S. thesis, Iowa State University of Science and Technology, Ames, Iowa, unpublished.

IV Dynamics and Stability of Crystallizers

- Gupta, G., and Timm, D. C. (1971). Predictive/corrective control for continuous crystallization. *Chem. Eng. Progr. Symp. Ser.* **110**(67), 121.
- Han, C. D. (1967). *Chem. Eng. Sci.* **22**, 611.
- Han, C. D. (1968). *Chem. Eng. Sci.* **23**, 321.
- Han, C. D. (1969). *Ind. Eng. Chem. Proc. Des. Develop.* **8**, 150.
- Han, C. D., and Shinnar, R. (1968). *AIChE J.* **14**, 612.
- Hulburt, H. M., and Stefango, D. G. (1969). *Chem. Eng. Progr. Symp. Ser.* **95**(65), 50.
- Lie, S. J., Shinnar, R., and Katz, S. (1971). The stability and dynamics behavior of a continuous crystallizer with fines trap. *Chem. Eng. Progr. Symp. Ser.* **110**(67).
- Mullin, J. W., and Nyvlt, J. (1970). *Chem. Eng. Sci.* **25**, 131.
- Randolph, A. D. (1962). Size distribution dynamics in a mixed suspension. Ph.D. thesis, Iowa State University of Science and Technology, Ames, Iowa, unpublished.
- Randolph, A. D., and Larson, M. A. (1965). *Chem. Eng. Progr. Symp. Ser.* **55**(61), 147.
- Sherwin, M. B., Shinnar, R., and Katz, S. (1967). *AIChE J.* **13**, 1141.
- Sherwin, M., Shinnar, R., and Katz, S. (1969). *Chem. Eng. Progr. Symp. Ser.* **95**(65), 75.

V Nucleation–Growth Rate Kinetics

- Amin, A. B. (1966). Calcium sulfate crystallization in phosphoric acid. Ph.D. thesis, Iowa State University of Science and Technology, Ames, Iowa, unpublished.
- Amin, A. B., and Larson, M. A. (1968). *Ind. Eng. Chem. Process Develop.* **7**, 133.
- Bauer, L. G., Larson, M. A., and Dallons, V. J. (1974). *Chem. Eng. Sci.* **29**, 1253.
- Bauer, L. G., Rousseau, R. W., and McCabe, W. L. (1974). *AIChE J.* **20**, 653.
- Bennema, P. (1976). *Ind. Crystallization* **91**. Plenum Press, New York.
- Bennett, R. C. (1962). *Chem. Eng. Progr.* **58**, 76.
- Bennett, R. C., and Van Buren, M. (1969). *Chem. Eng. Progr. Symp. Ser.* **65**, 44.
- Berglund, K. A., and Larson, M. A. (1984). *AIChE J.* **30**, 280.
- Boistelle, R. (1976). *Ind. Crystallization* **203**. Plenum Press, New York.
- Botsaris, G. D. (1976). *Ind. Crystallization* **3**. Plenum Press, New York.
- Botsaris, G. D., and Denk, E. G. (1970). *Ind. Eng. Chem. Fundam.* **9**, 276.
- Botsaris, G. D., Denk, E. G., and Chua, J. O. (1972). *AIChE J. Symp. Ser.* **68**, 21.
- Botsaris, G. D., and Liu, Y. A. (1970). Impurity effects in continuous flow mixed suspension crystallizers. 63rd Annu. Meeting AIChE, Chicago, Illinois, December, Preprint 18c.
- Botsaris, G. D., Mason, E. A., and Reid, R. C. (1966). *J. Chem. Phys.* **45**, 1893.
- Botsaris, G. D., and Sutwala, G. (1976). *AIChE Symp. Ser.* **72**, 7.
- Bransom, S. H., Dunning, W. J., and Millard, B. (1949). *Discuss. Faraday Soc.* **5**, 83.
- Bujac, P. D. B. (1976). *Ind. Crystallization* **23**. Plenum Press, New York.
- Bunn, C. W., and Emmet, H. (1949). *Disc. Faraday Soc.* No. 5, p. 119.
- Burton, W. K., Cabrera, N., and Frank, F. C. (1951). *Phil. Trans. R. Soc. London Ser. A* **243**, 299.
- Cabrera, N., and Vermilyea, D. A. (1958). "Growth and Perfection of Crystals." Wiley, New York, p. 393.
- Cayey, N. W., and Estrin, J. (1967). *Ind. Eng. Chem. Fundam.* **6**, 13.
- Chambliss, C. W. (1966). Nucleation and growth kinetics in a cooling crystallizer. Thesis, Iowa State University of Science and Technology, Ames, Iowa, unpublished.
- Cise, M. D., and Randolph, A. D. (1972). *AIChE Symp. Ser.* **68**, 42.
- Clontz, N. A., and McCabe, W. L. (1971). *AIChE Symp. Ser.* **67**, 6.

- Crawford, R. (1970). The continuous nucleation of sucrose. M.S. thesis, University of Arizona, Tucson, Arizona, unpublished.
- Davey, R. J. (1976). *J. Crystal Growth* **34**, 109.
- Davey, R. J. (1979). *Ind. Crystallization* **78**, 169. North Holland, Amsterdam.
- Davey, R. J., and Mullin, J. W. (1974). *J. Crystal Growth* **26**, 45.
- Denk, E. G., and Botsaris, G. D. (1972). *J. Crystal Growth* **13/14**, 493.
- Denk, E. G., and Botsaris, G. D. (1972). *J. Crystal Growth* **15**, 57.
- Desai, R. M., Rachow, J. W., and Timm, D. C. (1974). *AIChE J.* **20**, 43.
- Dunning, W. J. (1969). In "Nucleation." A. C. Zettlemeyer, ed. Marcel Dekker, New York, pp. 1-67.
- Estrin, J. (1976). *Secondary Nucleation* **2**, 1.
- Estrin, J., and Youngquist, G. R. (1976). *Ind. Crystallization* **61**. Plenum Press, New York.
- Evans, T. W., Margolis, G., and Sarofim, A. F. (1974). *AIChE J.* **20**, 950.
- Frank, F. C. (1949). *Disc. Faraday Soc.* No. 5, p. 48.
- Frank, F. C. (1958). "Growth and Perfection of Crystals." Wiley, New York, p. 411.
- Garabedian, H., and Strickland-Constable, R. F. (1972). *J. Crystal Growth* **12**, 53.
- Garabedian, H., and Strickland-Constable, R. F. (1972). *J. Crystal Growth* **13/14**, 506.
- Garside, J. (1979). *Ind. Crystallization* **78**, 143. North Holland, Amsterdam.
- Garside, J., and Davey, R. J. (1979). 2nd annual AIChE meeting, San Francisco, November.
- Garside, J., and Jancic, S. J. (1976). *AIChE J.* **22**, 887.
- Garside, J., and Jancic, S. J. (1979). *AIChE J.* **25**, 948.
- Garside, J., and Larson, M. A. (1978). *J. Crystal Growth* **43**, 694.
- Garside, J., and Mullin, J. W. (1966). *Chem. Ind. (London)* **48**, 2007.
- Garside, J., Phillips, V. R., and Shah, M. B. (1976). *Ind. Eng. Chem. Fundam.* **15**, 230.
- Genck, W. J. (1970). Temperature effects on growth and nucleation rates in mixed suspension crystallization. Ph.D. thesis, Iowa State University of Science and Technology, Ames, Iowa, unpublished.
- Genck, W. J., and Larson, M. A. (1972). *Chem. Eng. Progr. Symp. Crystallization from Solution Nucleation Phenomena*, **68**(121), 42.
- Helt, J. E. (1976). Effects of supersaturation and temperature on nucleation and crystal growth in a MSMR crystallizer. Ph.D thesis, Iowa State University, Ames, Iowa.
- Helt, J. E., and Larson, M. A. (1977). *AIChE J.* **23**, 822.
- Hunt, S. L. (1979). Contact nucleation in the presence of chromium ion. M.S. thesis, Iowa State University, Ames, Iowa.
- Hussman, G. A., Larson, M. A., and Berglund, K. A. (1984). *Ind. Crystallization* **84**, 21. Elsevier, Amsterdam.
- Johnson, R. T., Factors affecting contact nucleation and growth rates for crystals in super-saturated aqueous solution. Ph.D thesis, North Carolina State University, Raleigh, North Carolina.
- Johnson, R. T., Rousseau, R. W., and McCabe, W. L. (1972). *AIChE Symp. Ser.* **68**, 31.
- Kane, S. G., and Evans, T. W. (1974). *AIChE J.* **20**, 855.
- Khambaty, S., and Larson, M. A. (1978). *Ind. Eng. Chem. Fundam.* **17**, 160.
- Lal, D. P., Mason, R. F. A., and Strickland-Constable, R. F. (1969). *J. Crystal Growth* **5**, 1.
- Larson, M. A. (1967). *Chem. Eng. Progr. Symp. Ser.* **70**(63), 58.
- Larson, M. A., and Bendig, L. L. (1972). *AIChE Symp. Ser.* **72**, 153.
- Larson, M. A., and Garside, J. (1986). *Chem. Eng. Sci.* **41**, 1285.
- Larson, M. A., and Garside, J. (1986). *J. Crystal Growth* **76**, 88.
- Larson, M. A., and Mullin, J. W. (1973). *J. Crystal Growth* **20**, 3.
- Larson, M. A., Timm, D. C., and Wolff, P. R. (1968). *AIChE J.* **14**, 448.
- Larson, M. A., White, E. T., Ramanarayanan, K. A. and Berglund, K. A. (1985). *AIChE J.* **30**, 90.

- Liu, C. Y., Tsuei, H. S., and Youngquist, G. R. (1971). Crystal growth from solution. *Chem. Eng. Progr. Symp. Ser.* **110**(67), 43.
- Mason, R., and Strickland-Constable, R. F. (1966). *Trans. Faraday Soc.* **62**, 158.
- McCabe, W. J., and Stevens, R. P. (1951). *Chem. Eng. Progr.* **45**, 168.
- Melia, T. P., and Moffitt, W. P. (1964). *Ind. Eng. Chem. Fundam.* **3**, 4.
- Melia, T. P., and Moffitt, W. P. (1964). *J. Colloid Sci.* **119**, 5.
- Miers, H. A. (1911). *J. Oxford Jr. Sci. Club*, June, p. 3.
- Miers, H. A., and Issac, F. (1906). *J. Chem. Soc.* **89**.
- Miller, P., and Saeman, W. C. (1947). *Chem. Eng. Progr.* **43**, 667.
- Misra, C., and White, E. T., (1971). Kinetics of crystallization of aluminum trihydroxide from seeded caustic solution. *Chem. Eng. Progr. Symp. Ser.* **110**(67), 53.
- Mullin, J. W., and Jancic, S. J. (1979). *Trans. Inst. Chem. Eng.* **57**, 188.
- Mullin, J. W., and Leci, C. L. (1972). *Chem. Eng. Progr. Symp. Crystallization from Solution Nucleation Phenomena*, **68**(121), 8.
- Mullin, J. W., and Amatavivadhana, A. (1967). *J. Appl. Chem.* **17**, 151.
- Mullin, J. W., and Gaska, C. (1969). *Can. J. Chem. Eng.* **45**, 483.
- Mullin, J. W., and Lui, C. L. (1969). *J. Crystal Growth* **5**, 75.
- Murray, D.C. (1964). Size distribution dynamics in continuous crystallization. Thesis, Iowa State University of Science and Technology, Ames, Iowa, unpublished.
- Murray, D. C., and Larson, M. A. (1965). *AIChE J.* **11**, 728.
- Nancollas, G. H., and Purdie, N. (1964). *Q. Rev. Chem. Soc.* **18**, 1.
- Ness, J. N., and White, E. T. (1976). *AIChE Symp. Ser.* **72**, 153.
- Powers, H. E. C. (1963). *Ind. Chem.* **39**, 7.
- Purves, W. T. (1979). Contact nucleation of potassium nitrate. M.S. thesis, Iowa State University, Ames, Iowa.
- Rajagopol, K. (1968). An experimental study of crystal nucleation growth rate kinetics for the potassium sulphate system. M.S. thesis, University of Florida, Gainesville, Florida, unpublished.
- Ramanarayanan, K., Berglund, K. A., and Larson, M. A. (1985). *Chem. Eng. Sci.* **40**, 1604.
- Randolph, A. D. (1971). Comments on recent advances in the analysis of crystallization processes. *Chem. Eng. Progr. Symp. Ser.* **110**(67), 1.
- Randolph, A. D., and Cise, M. D. (1972). *AIChE J.* **118**, 4.
- Randolph, A. D., and Rajagopol, K. (1970). *Ind. Eng. Chem. Fundam.* **9**, 165.
- Randolph, A. D., and Sikdar, S. K. (1974). *AIChE J.* **20**, 2.
- Randolph, A. D., and Sikdar, S. K. (1976). *Ind. Eng. Chem. Fundam.* **15**, 1.
- Robinson, J. N., and Roberts, J. E. (1957). *Can. J. Chem. Eng.* **35**, 105.
- Rosen, H. N. (1974). *AIChE J.* **20**, 2.
- Rosen, H. N., and Hulburt, H. M. (1971). Continuous vacuum crystallization of potassium sulfate. *Chem. Eng. Progr. Symp. Ser.* **67**, 18.
- Rosen, H. N. and Hulburt, H. M. (1971). Growth rate of potassium sulfate in a fluidized bed crystallizer. *Chem. Eng. Progr. Symp. Ser.* **110**(67), 27.
- Rosseau, T. W., Craig, S., and McCabe, W. L. (1979). *Ind. Crystallization* **78**, 19. North Holland, Amsterdam.
- Rousseau, R. W., Li, K. K., and McCabe, W. L. (1976). *AIChE Symp. Ser.* **153**, 72.
- Rousseau, R. W., McCabe, W. L., and Tai, C. Y. (1975). *AIChE J.* **21**, 1017.
- Rusli, I. T. (1978). Origin, size distribution and growth of small crystals in contact nucleation. M.S. thesis, Iowa State University, Ames, Iowa.
- Rusli, I. T., Larson, M. A., and Garside, J. (1979). *AIChE J.* **25**, 57.
- Sears, G. W. (1958). *J. Chem. Phys.* **29**, 1045.
- Shor, M. (1970). Effects of surfactants and inorganic additives on kinetics in mixed suspension crystallization. Ph.D. thesis, Iowa State University of Science and Technology, Ames, Iowa, unpublished.

- Shor, S. M. and Larson, M. A. (1971). Effects of additives on crystallization kinetics. *Chem. Eng. Progr. Symp. Ser.* **110**(67), 32.
- Sikdar, S. K., and Randolph, A. D. (1976). *AIChE J.* **22**, 110.
- Strickland-Constable, R. F. (1972). *AIChE Symp. Ser.* **68**, 1.
- Strickland-Constable, R. F. (1976). *Ind. Crystallization* **33**. Plenum Press, New York.
- Sung, C. Y., Estrin, J., and Youngquist, G. R. (1973). *AIChE J.* **19**, 957.
- Tai, C. Y., McCabe, W. L., and Rousseau, R. W. (1975). *AIChE J.* **21**, 351.
- Timm, D. C. (1965). Crystal size distribution dynamics. M.S. thesis, Iowa State University of Science and Technology, Ames, Iowa, unpublished.
- Timm, D. C. (1967). Effect of residence time and suspension density on crystal size distributions in continuous crystallization. Ph.D. thesis, Iowa State University of Science and Technology, Ames, Iowa, unpublished.
- Timm, D. C., and Cooper, T. R. (1971). Steady state crystallization kinetics as a function of supersaturation. *AIChE J.* **17**, 285.
- Timm, D. C., and Larson, M. A. (1968). *AIChE J.* **14**, 452.
- Ting, H. H., and McCabe, W. L. (1934). *Ind. Eng. Chem.* **26**, 1201.
- White, E. T., Bendig, L. L., and Larson, M. A. (1976). *AIChE Symp. Ser.* **72**, 41.
- Youngquist, G. R., and Randolph, A. D. (1972). *AIChE J.* **18**, 421.

VI Grinding References

A. Probabilistic Breakage and Selection Matrix Models

- Broadbent, S. R., and Callcott, T. G. (1956). *J. Inst. Fuel* **29**, 258.
- Epstein, B. (1948). *Ind. Eng. Chem.* **40**, 2289.
- Klimpel, R. R., and Austin, L. G. (1970). *Ind. Eng. Chem. Fundam.* **9**, 230.

B. Kinetic Grinding Models

- Freeh, E. J., Horst, W. E., and Kellner, R. C. (1967). *Trans. AIME* **238**, 167.
- Herbst, J. A., and Fuerstenau, D. W. (1968). *Trans. AIME* **241**, 538.
- Horsts, W. E. (1967). Mathematical description of a comminution process. Ph.D. thesis, University of Arizona, Tucson, Arizona, unpublished.
- Roberts, E. J. (1950). *Trans. AIME* **187**, 1267.

C. Population-Balance-Derived Grinding Model

- Durando, A. (1970). A mathematical study of particle-size distributions produced in a continuous grinding circuit. M.S. thesis, University of Arizona, Tucson, Arizona, unpublished.
- Randolph, A. D., and Durando, A. K. (1971). Population-balance models for predicting grinding mill performance. AIME Centennial Annu. Meeting, New York, March, Preprint 71-B-78.

AUTHOR INDEX

Numbers in parentheses are reference numbers and indicate that an author's work is referred to, although the name is not cited in the text. Italic numbers show the page on which the complete reference is listed.

A

Abegg, C. F., 99, 100, 108, 352
 Allen, A. T., 110, 133
 Amatavivadhana, A., 356
 Amin, A. B., 354
 Amundson, N. R., 284, 300, 309
 Aris, R., 282(5), 309
 Austin, L. G., 277(1), 279, 309, 357

B

Balakreshnan, N. S., 352
 Baliga, J. B., 96, 97(1), 98, 108, 249, 250, 276, 353
 Bauer, L. G., 257, 276, 354
 Becker, G. W., 353
 Beckman, J. R., 161(4), 162(4), 163(4), 173, 201(3), 203, 224(3), 226(4), 227, 237
 Beer, G. L., 220(6), 222(6), 223(6), 226(6), 231(6), 235(6), 237
 Bendig, L. L., 124, 125, 134, 257, 258(9), 259, 276, 355, 357
 Bennema, P., 74(7), 79, 354
 Bennett, R. C., 82, 108, 124, 134, 353, 354
 Berglund, K. A., 101(3), 108, 111(4), 121, 124, 125, 133, 262, 265, 267(18), 268, 276, 354, 355, 356
 Bilous, O., 300, 309
 Boistelle, R., 354

Botsaris, G. D., 353, 354, 355
 Branson, S. H., 243, 276, 353, 354
 Broadbent, S. R., 357
 Brock, J. R., 302, 309
 Buckley, H. E., 352
 Bujac, P. D. B., 354
 Bunn, C. W., 354
 Burton, W. K., 120, 133, 354

C

Cabrera, N., 120, 133, 354
 Callcott, T. G., 357
 Callis, C. F., 11, 17, 18, 41(1), 49
 Canning, T. F., 353
 Cayey, N. W., 354
 Chambliss, C. W., 207, 354
 Chang, Y. C., 112, 133
 Chen, L., 227(13), 228(13), 229(13), 230(13), 237
 Chianese, A., 169(10), 173, 196(3), 199
 Chua, J. O., 354
 Cise, M. D., 354, 356
 Clontz, N. A., 118, 123, 133, 256, 257, 276, 355
 Cooper, T. R., 357
 Courant, R., 303, 309
 Craig, S., 356
 Crawford, R., 246(5), 276, 355
 Curl, R. L., 286, 309

D

- Dallons, V. J., 257, 276, 354
 Danckwerts, P., 288, 309
 Davey, R. J., 122, 128, 129, 133, 134, 355
 Deepak, C., 353
 de Jong, E. J., 104, 108, 128, 134, 164, 173, 353
 Denk, E. G., 354, 355
 Desai, R. M., 355
 Dixon, T. K., 264, 276
 Drack, J., 275, 297(19), 309
 Drake, R. L., 70, 79
 Dunning, W. J., 243(2), 276, 354, 355
 Durando, A., 357

E

- Emmet, H., 354
 Enkevort, W. J. P., 74(7), 79
 Epstein, B., 357
 Epstein, M. A., 231, 237
 Estrin, J. W., 123, 134, 353, 354, 355, 357
 Evans, T. W., 355
 Ewart, E. H., 284, 297(19), 309

F

- Fiedelman, H., 124, 134
 Fisher, J. C., 116(9), 133
 Frank, F. C., 120, 133, 354, 355
 Fredrickson, A. G., 282(5), 309
 Freeh, E. J., 357
 Friedlander, S. K., 70, 79
 Fuerstenau, D. W., 357
 Funderburk, J. O., 285, 286, 309

G

- Garabedian, H., 355
 Gardon, J. L., 284, 309
 Garside, J., 110, 114, 118, 119, 122, 124, 127, 128, 133, 134, 158, 167, 168, 173, 261(11), 262, 268(19), 276, 353, 355, 356, 357
 Gaska, C., 356
 Gebbard, F., 299, 309

Genk, W. J., 355

- Gibbs, J. W., 112, 114, 133, 352
 Glatz, C. E., 292, 293, 309
 Gotting, B. E., 297(19), 309
 Gupta, G., 226, 237, 354

H

- Han, C. D., 353, 354
 Hartel, R. W., 297, 298, 299, 309
 Hartman, P., 10, 11, 17, 18
 Helt, J. E., 244, 276, 355
 Herbst, J. A., 277(1), 309, 357
 Hidy, G. M., 302, 309
 Hilbert, D., 303, 309
 Hoare, M., 292, 293(16), 309
 Horsts, W. E., 357
 Howell, T. R., 227, 237
 Hoyt, R. C., 294, 295, 296, 309
 Hulburt, H. M., 63, 67(3), 79, 202, 237, 290, 309, 352, 353, 354, 356
 Human, H. J., 74(7), 79
 Hunt, S. L., 355
 Hussmann, G. A., 111, 133, 267(18), 268, 276, 355

I

- Irani, R. R., 11, 17, 18, 41(1), 49
 Iskander, M., 353
 Issac, F., 116(11), 133, 356

J

- Jancic, S. J., 353, 355, 356
 Janse, A. H., 104, 108, 128, 134, 164, 173, 353
 Johnson, J. L., 231, 237
 Johnson, R. T., 355
 Jones, A. G., 169, 173, 196, 199
 Juzaszek, P., 156, 157, 173, 244, 245, 276

K

- Kane, S. G., 355
 Karshina, G. W., 353

Kasatkin, A. P., 352
 Katz, S., 63, 67(3), 79, 202, 213(5), 219(5),
 220(5), 223(7), 226(7), 237, 290, 309,
 352, 353, 354
 Keener, J. P., 220(6), 222(6), 223(6), 226(6),
 231(6), 235(6), 237
 Kellner, R. C., 357
 Kelly, E. G., 22, 49, 264, 266, 276
 Khambaty, S., 120, 131, 134, 260, 276, 355
 Klimpel, R. R., 277(1), 279(1), 309, 357
 Koch, A. L., 282, 309
 Kraljevich, Z. I., 161(4), 162(4), 163(5), 173,
 201(3), 224(3), 227(3), 237

L

Lal, D. P., 355
 Landa-Vertiz, J., 292, 293(16), 309
 Larson, M. A., 99(2), 100(2), 101(3), 103(5),
 104, 105, 106, 108, 110, 111(4), 111(5),
 114, 118, 121, 124, 125, 127, 130, 131,
 133, 134, 141, 143, 144, 151, 156, 157,
 158, 164, 167, 168, 173, 187, 190, 192,
 202, 206, 237, 242(1), 244, 245, 257,
 258(9), 259, 260, 261, 262, 265, 267(18),
 268, 276, 353, 354, 355, 356, 357
 Leci, C. L., 110, 133, 356
 Lee, H. H., 353
 Levich, V. G., 70(6), 79
 Li, K. K., 356
 Lie, S. J., 223, 226, 237, 353, 354
 Liu, C. Y., 356
 Liu, Y. A., 353, 354
 Low, D. C. C., 227, 229(11), 237
 Ludie, T. T., 277(1), 279(1), 309
 Lui, C. L., 356
 Lynch, A. J., 277(1), 309

M

McCabe, W. L., 118, 123, 133, 256, 257, 276,
 354, 355, 356, 357
 McDonald, M. P., 110(2), 133
 McMahon, P., 111, 133
 Margolis, G., 355
 Martin, G. C., 300, 309
 Mason, E. A., 354
 Mason, R. E. A., 355, 356

Melia, T. P., 356
 Merzluna, K. A., 111(5), 133
 Miers, H. A., 116(11), 133, 356
 Millard, B., 243(2), 276, 354
 Miller, P., 356
 Misra, C., 356
 Moffitt, W. P., 356
 Mood, A. M., 264, 276
 Mullin, J. W., 110, 118, 129, 133, 134, 167,
 169, 173, 196(3), 199, 352, 353, 354,
 355, 356
 Murray, D. C., 242(1), 276, 356
 Myerson, A. S., 112, 133, 231, 237

N

Nancollas, G. H., 356
 Nan't Land, C. M., 353
 Nauman, E. B., 353
 Ness, J. N., 356
 Nichol, N. W., 110(2), 133
 Nielsen, A. E., 116, 133, 352
 Nuttall, H. E., 218, 219
 Nyvlt, J., 167, 173, 353, 354

O

O'Dell, F. P., 353
 O'Hara, M., 119, 133, 352

P

Petrov, T. G., 352
 Phillips, V. R., 355
 Powers, H. E. C., 123, 134, 356
 Purdie, N., 356
 Purves, W. T., 127, 134, 261, 262, 276, 356

R

Rachow, J. W., 355
 Rajagapol, K., 356
 Ramanarayanan, K. A., 103(5), 104(5), 105(5),
 106(5), 108, 164(6), 173, 356

Randolph, A. D., 67(2), 74(8), 79, 101(4),
103, 108, 124, 134, 161, 162, 163, 173,
182, 183(1), 184, 187, 190, 192, 199,
201, 202, 203, 206, 220, 222, 223, 224,
226, 227, 228, 229, 230, 231, 235, 237,
246(5), 275, 276, 280, 281, 298, 299,
309, 352, 353, 354, 356, 357
Ranjan, R., 280, 281, 309
Reid, R. C., 119, 133, 352, 354
Reiddick, A. J., 122, 128, 133
Resnick, W., 288, 309
Risitic, R. F., 128, 134
Rivera, T., 67(2), 79
Roberts, E. J., 357
Roberts, J. E., 356
Robinson, J. N., 356
Rosen, H. N., 356
Rousseau, R. W., 227, 237, 353, 354, 355,
356, 357
Rusli, I. T., 118, 124, 127, 128, 133, 261(11),
276, 353, 357

S

Saeman, W. C., 189(2), 199, 353, 356
Sarojim, A. F., 355
Sauter, A., 353
Schawchter, M., 282, 309
Schork, F. J., 231, 237
Sears, G. W., 357
Shah, M. B., 355
Sherwin, M. B., 213, 219, 220(5), 237, 353,
354
Shinnar, R., 213(5), 219(5), 220(5), 223(7),
226(7), 237, 354
Shor, S. M., 131, 134, 357
Sikdar, S. K., 356, 357
Smith, W. V., 284, 309
Sowul, L., 231, 237
Spottiswood, D. J., 22, 49
Stefango, D. G., 353, 354
Stevens, J. D., 99(2), 100(2), 108, 284, 285,
286, 309, 353
Stevens, R. P., 356
Stewart, D., 182(1), 183(1), 184(1), 199
Stone, P. D., 353
Strickland-Constable, R. F., 122, 123, 134,
352, 355, 356, 357
Sung, C. Y., 123, 134, 357
Sutwala, G., 354

Swift, D. L., 70, 79
Szabo, T. T., 353

T

Tai, C. Y., 356, 357
Tavana, A., 227(13), 228(13), 229(13), 230(13),
237
Thompson, R. W., 284, 309
Timm, D. C., 141(11), 143(11), 173, 226, 237,
353, 355, 356, 357
Ting, H. H., 357
Tolman, R. C., 114, 133
Toschev, S., 11, 17(2), 18
Trevius, E. B., 352
Tsuchiya, A. C., 282, 309
Tsuei, H. S., 356
Tsuroka, S., 231, 237
Turnball, D., 116(9), 133

V

Vaden, D. E., 182(1), 183(1), 184(1), 199
Valentes, K. J., 300, 309
Van Buren, M., 82, 108, 354
Van Rosmalen, G. M., 264, 276
Vermilyea, D. A., 354

W

Webster, G., 122, 128, 133
White, E. T., 74(8), 79, 101(4), 103, 108,
164(6), 173, 227(9), 237, 275, 276,
353, 356, 357
Wienk, B. G., 353
Wolff, D., 288, 309
Wolff, P. R., 141(11), 143(11), 144, 151, 173,
353, 356
Wood, R. M., 110(2), 133
Wright, P. G., 275, 276, 353

Y

Youngquist, G. R., 123, 124, 134, 355, 356,
357

Z

Zeman, R. J., 284, 309
Zipp, G. L., 197, 199

SUBJECT INDEX

A

- Aeration process, bubble-size distribution, 300–303
- Agglomerate, definition, 17, 297
- Agglomeration, model, 297–300
- Aggregate, definition, 17, 297
- Aggregation, model, 297–300
- Ammonium sulfate crystallizer, crystal-size distribution dynamics 206–207
- Anton Parr frequency, density measuring instrument, 269

B

- Batch crystallization, growth dispersion effects on crystal-size distribution, 166–171
- Batch crystallization system
 - constraints, 94–99
 - definitions, 94–99
- Batch crystallizer, 94–106
 - finest dissolution in, 196–198
- Biochemical processes
 - birth rate, 282–283
 - death rate, 282–283
 - growth rate, 282–283
 - population balance and, 282–283
- Birth function, $63n$, 69, 278, 282–283
- Birth rate, biochemical processes, 282–283
- Breakage function, 278–279

C

- Calcium oxalate
 - crystal growth rate, 274–275

- kinetics, 297–300
- Calcium sulfate, crystal modifiers effect on, 264–266
- Classified product removal, 159–161, 179, 188–196
 - Crystal-size distribution transients, 219–220
 - with fines destruction, 192–193
- Closed grinding circuit, 60–62
 - birth function, 60–61
 - death function, 60–61
 - transients, 60–62
 - See also* Grinding mills
- Coefficient of variation, 37–38, 88, 90, 152
- Comminution process, 7, 9, 277–282
 - breakage kinetics, 280
 - particle-size distribution, 278, 280–282
 - population balance and, 278–282
 - residence-time distribution, 280–282
- Conglomerate, definition, 17
- Contact nucleation, 123–126
- Continuously fed crystallizer, 80–94
 - constraints, 83
 - definition, 80–83
- Cooling crystallizer, 168–170
- Cooling-precipitator crystallizer, 246
- Crystal agglomeration, 251
- Crystal formation, nucleation and, 112, 115–116
- Crystal growth
 - crystal modifiers, 263–267
 - diffusion, 117–122
 - dislocation controlled, 128–129
 - dispersion, 101, 122, 164–166
 - function, 166
 - effects of impurities and additives, 129–130

- Crystal growth (*cont.*)
 - integration, 117–122
 - model
 - Burton-Casberra-Frank, 120–121
 - continuous growth, 119
 - size-dependent, 99–100
 - surface-nucleation growth, 119–120
 - nucleation, 112
 - particle phase space, 52–53*n*,
 - photographic nucleation studies, 262–263
 - rate constraint, 5
 - screw dislocation, 120
 - size dependence, 164
- Crystal growth mechanisms, 117–122
- Crystal habit, 9–11, 17
- Crystal morphology, 9–11, 17
- Crystal population density, calculation of, 15–16
- Crystallization, from solution, 109
- Crystallization kinetics, 109–132
 - crystal growth mechanisms, 117–122
 - effects of impurities and additives, 129–132
 - experimental results, and analyses, 238–276
 - mininucleator studies, 270–274
 - primary nucleation, 111–117
 - sample treatment, 250–251
 - sampling techniques, 250–251
 - secondary nucleation, 122–129
 - solute clustering, 267–269
 - supersaturation, 110–111
- Crystallization process, 3
 - feedback interactions, 3
 - scale up of, 5
 - supersaturation and, 240
- Crystallizer
 - batch, 94–106, 249–250
 - cascade system, 144–152
 - combination cooling-precipitator, 246
 - continuously fed, 80–94
 - cooling, 240, 244–245
 - cooling crystallizer mininucleator, 168–170, 247–249
 - draft-tube baffle, 81–82, 152–154
 - draft-tube, 160–161
 - evaporation, 240, 245–246
 - evaporative batch, 167–171, 249–250
 - finest-dissolution, 154–157
 - growth-type, 180–182
 - mixed magma, 175–178
 - mixed-suspension, mixed-product removal
 - versus fines dissolution, 80–94, 154–157
 - potassium chloride, 201, 224, 226–227
 - precipitation, 240
 - precipitation batch, 249–250
 - residence-time distribution, 231
 - R*–*z*, 220–226
 - single-stage, 144–147
 - two-stage, 150–152
 - two-stage aggregator, 297–300
 - vessel fouling in, 4–5
- Crystallizer cascades, 144–152
- Crystallizer operation, problems, 2–4
- Crystal-size distribution
 - alteration of, 152, 174
 - analytic formulation, 13–17
 - batch crystallization, 96–99
 - classification effect on, 159–161, 188–196
 - crystal growth rate and, 5
 - crystallizer cascades and, 144–152
 - crystallizer interaction with, 4–7
 - data analysis, 254–255
 - dimensionless variables, 145–146
 - evaporation versus nucleation batch systems, 170–171
 - experiments with additives, 255
 - feedback control, 226–235
 - finest dissolution effect, 196–198
 - growth dispersion effect, 166–167
 - ineffective volume effects, 157–159
 - mixing effects, 157–159
 - model
 - growth dispersion, 101
 - intrinsic growth dispersion, 103–106
 - random growth dispersion diffusivity, 101–102
 - reaction engineering, 175–179
 - size-dependent growth, 99
 - nonisokinetic withdrawal, 159–163
 - point-source nucleator, 256–262
 - poorly mixed dispersed phase, 159
 - process reaction engineering of, 174–198
 - properties, 2–4
 - supersaturation and, 2–4, 136–140
 - suspended solids and, 140–141
 - withdrawal effects, 159–163
- Crystal-size distribution algorithm
 - product classification, 189

Crystal-size distribution feedback control, 226–235
 with state space formulation, 230–235
 Crystal-size distribution dynamics, 200–226
 instability, 200
 simulation, 318–342
 transients, 200
 unsteady state, 202–205
 Crystal-size distribution general algorithm, 175–180
 classified product removal, 179
 fines removal, 179
 size-dependent growth rate, 178
 staging, 178
 Crystal-size distribution limit cycles, 200, 202, 220, 224, 226
 Crystal-size distribution measurement, 252–254
 light scattering, 253–254
 sedimentation, 254
 sieving, 252
 zone sensing, 252–253
 Crystal-size distribution self-regulation
 feedback loop, 201
 Crystal-size distribution stability, 211–226
 classified product removal, 219–220
 mixed-suspension, mixed-product-removal
 crystallizer class II system, 213–220
 unsteady-state mass balance, 200
 unsteady-state number balance, 200
 Crystal-size distribution transients, 205–211
 algorithm CRYSTAL.BALL, 209–210, 328–342
 classified product removal and, 219–220
 double draw-off crystallizer, 210–211
 dynamics, 200
 unsteady-state mass balance, 200
 unsteady-state number balance, 200
 Crystal-size responses, 135–172
 for batch crystallizers, 135, 166–171
 for continuous crystallizers, 135–166
 CSD, *see* Crystal-size distribution
 Cyclonite, crystallization, 243

D

DDO, *see* Double draw-off crystallizer
 Death function, 63*n*, 69, 278, 282–283

Death rates, biochemical processes, 282–283
 Demographic analysis
 immigration, 304
 population balance and, 303–308
 Density-distribution function,
 coefficient of variation, 31
 definition, 14–15
 mean, 31
 Diffusion, crystal growth and, 117–122
 Dimensionless distribution, *j*th moment, 207
 Dimensionless weight-fraction function, 310–317
 Dislocation-controlled growth, 128–129
 Dispersed-phase mixing, population balance and, 286–288
 Distribution, *see* Crystal-size distribution;
 Particle distribution; Particle-size distribution;
 Residence-time distribution
 Distribution function, 20–22
 data plotting, 27–31
 dimensionless, 87
 empirical representation, 23–27
 gamma, 25
 Gaudin–Melloy, 26–27
 log-normal, 24–25
 normal, 23–24
 one-dimensional, 23–25
 parameter estimation, 27–31
 physical representation, 37
 Rosin–Rammler, 26
 Double draw-off crystallizer, 182–184
 modeling equations, 183
 population density versus average size, 184
 Draft-tube baffle crystallizer, 81–82, 152–154
 Draft-tube crystallizer, 160–161 particle-size distribution, 82–83

E

Emulsion polymerization, population balance and, 283–286
 Evaporative batch crystallizer, 167–171, 249–250
 Evaporative crystallizer, 240, 245–246
 Exponential distribution, 88–92
 External coordinate region, population balance over, 56–62

F

- Faceted crystals, 18
- Feedback interaction, in crystallization processes, 3
- Fines destruction, 152–157, 227
 - classified product removal, 192–193
 - growth rate and, 185
 - larger particle sizes, 185–188
 - solute recycling with, 183–188
- Fines dissolution, 196–198, 227
 - crystal-size distribution and, 171
 - crystal-size distribution instability and, 218
- Fines removal, 227
 - increased crystal size, 170
 - maximum size improvement with, 185
 - narrow size distribution, 170

G

- Gamma distribution
 - coefficient of variation, 38
 - j th moment defined, 34–35
 - mean, 38
 - moments, 34–35
 - plotting, 29
- Gamma function
 - distribution, 25
 - inverse, 164–165
- Gaudin–Melloy distribution
 - coefficient of variation, 40
 - j th moment definition, 36
 - mean, 40
 - moments, 36
 - plotting, 29–31
- Gaudin–Melloy distribution function, 26
- Gibbs–Thompson effect, 158
- Gibbs–Thompson equation, 113
- Grinding mills, 277–282
 - data correlation, 279
 - particle-size distribution, 280
 - See also* Closed grinding circuits
- Growth. *See* Crystal growth; Particle growth
- Growth dispersion, 126–129
- Growth function, 282
- Growth rate, random fluctuations in, 73–76
- Growth-rate distribution, 104–106
- Growth-type crystallizer, 180–182

I

- Immigration, population balance and, 304
- Integration, crystal growth and, 117–122

J

- j th moment
 - definition, 32–36
 - of dimensionless distribution, 207
 - of distribution, 63

L

- Log-normal distribution
 - coefficient of variation, 38
 - j th moment defined, 33–34
 - mean, 38
 - moments, 33–34
 - plotting, 28
- Log-normal distribution function, 24–25

M

- McCabe ΔL law, 14, 55, 59, 84, 178, 294
- Macromoment equations, 65–67
- Macromoment population balance, 77–78
- Macroscopic population balance, 56–62
- Magnesium sulfate, crystal-size distribution, 258–260
- Mass-averaged size distribution, 88
- Mass balance
 - batch crystallizer, 95
 - effect on crystal-size distribution, 211
 - mixed-suspension, mixed-product-removal crystallizer, 92–94
 - unsteady state, 202
- Mass density, particle-size formulation, 72–73
- Mass distribution
 - cumulative function, 147
 - differential function, 147
 - two-stage system, 147–149
- Method of characteristics, for transient size distribution, 209–211
- Micromoment population balance, 77–78
- Miers nucleation growth rate kinetics model, 215–218
- Miller indices, 10, 17

Mininucleator crystallizer, 270–274
 mode progression growth rate technique, 274–275
 particle counter and, 274
 particle counting, 271
 supersaturation in, 274
 Mixed magma crystallizer, 189–192
 Mixed-suspension, mixed-product-removal crystallizer, 80–94, 231
 class I, 93, 213
 class II, 93, 203, 206, 213, 215, 219, 231
 classified product removal, 191
 crystal-size distribution, 83
 crystal-size distribution dynamics, 202–205
 crystal-size distribution stability, 213
 crystal-size distribution transients, 205–207
 design features, 239–240
 dimensionless distribution function, 87
 equipment, 240–249
 experimental techniques, 255–275
 exponential distribution, 88–92
 fines removal system, 213
 mass balance, 92–94
 mininucleator, 270–274
 nucleation growth-rate kinetics, 86–87, 243
 number, length, area, and mass distribution functions, 89–91
 physical features of, 240–242
 population balance, 75–76
 simulation results, 234
 steady state, 205
 supersaturation, 136–140
 suspension density versus crystal-size distribution, 140–141
 Moment equations, 63–65
 macro-moment, 65–67
 Moments, recovery of particle-size distribution function, 67–68
 Moment transformation, of population balance, 62–67
 MSMR crystallizer. *See* Mixed-suspension, mixed-product-removal crystallizer
 Multicrystals, definition, 17–18
 Murkerjee correlation, 302–303

N

Normal distribution
 coefficient of variation, 37–38

*j*th moment definition, 32–33
 mean, 37–38
 moments, 32–33
 plotting, 28
 variance and mean, 23
 Nucleation
 crystal formation, 111–117
 effects of impurities and additives, 129–132
 nucleation rate versus, 267
 primary, 111–117
 secondary, 111–112, 115–117, 122–129
 Nucleation growth-rate kinetics
 crystal-size distribution instability, 216
 growth-type crystallizer, 180–182
 mixed-suspension, mixed-product-removal crystallizer, 86–87, 243
 model
 Miers, 215–218
 Volmer, 215–217
 Nucleation kinetics, power law, 205
 Nucleation rate, kinetic expression for, 86
 Nuclei, control of, 226–229
 Number flux, equation for, 74

O

One-dimensional distribution function, 23

P

Particle
 birth function, 278
 breakage function, 278–279
 death function, 278
 definition, 18
 selection-for-breakage function, 278–279
 Particle agglomeration, 71–72
 inorganic precipitation and, 294–296
 population balance and, 290–291
 Particle coalescence, 69–70
 Particle distribution, 12–17
 birth function, 53
 coordinate axes, 20–21
 coefficient of variation, 36–39
 death function, 53
 empirical characterization, 21–27
 mean size, 36

- Particle distribution (*cont.*)
 - particle concentration, 19
 - particle size, 19
 - predictive multidimensional theory, 50, 54
 - truncation, 40–41
- Particle distribution shape
 - kurtosis, 41–42
 - skewness, 41–42
- Particle morphology, 7–11
 - definition, 18
- Particle-number distribution, significance of
 - model, 85–87
- Particle-number continuity equation, 53–56
- Particle phase space, 21, 51–53
- Particle phase-space velocity, 52
- Particle size
 - definition, 11
 - measurement, 11–13
 - secondary nucleation kinetics, 184–188
- Particle-size distribution, 1–18
 - comminution process, 278
 - effect on residence-time distribution, 280–282
 - grinding circuits and, 60–61
 - grinding mills and, 280–282
 - properties, 2–4
 - two-stage system, 147–152
 - three-stage system, 147–152
- Particle-size formulation, mass density and, 72–73
- Particulate process,
 - descriptive model, 16
 - predictive model, 16
- Point fines dissolver, 185
- Population balance
 - alternate coordinate systems, 68–73
 - application to other systems, 277–308
 - batch system, 94
 - equation for, 53
 - macrodistributed, 74–75, 77
 - macromoment, 78
 - macro-moment equation, 65–67
 - macroscopic, 58–60
 - over macroscopic external coordinate region, 56–62
 - microdistributed, 74, 77
 - micromoment, 77
 - in mixed-suspension, mixed-product-removal crystallizer, 75–76, 84–85
 - moment transformation of, 62–68
 - number-volume coordinates system, 71
 - residence-time distribution, 288–290
 - solute mass balance, 204
 - transient macrodistributed, 212
 - unsteady state, 202–203
- Population counter
 - Coulter®, 13
 - Particle Data Elzone®, 13, 251–252, 271
- Population density
 - classified product removal, 192–193
 - clear liquid volume basis, 202–203
 - finest removal, 192–193
 - particle volume formulation, 69–73
 - solids free or total volume, 58*n*
 - total magma volume basis, 202
- Population density distribution function
 - particle size, 46
 - suspension properties, 42–47
- Population flux, 51–53, 74
- Population model
 - dynamic, 303–308
 - macropopulation balance, 305–306
- Potash alum, crystal-size distribution, 260–262
- Potassium chloride crystallizer, 201, 224, 226–227
 - crystal-size distribution limit cycles, 224
- Potassium nitrate
 - crystallization, 244–245
 - crystal-size distribution, 262
- Potassium sulfate, crystal-size distribution, 169–170
- Power law kinetics model, 215
- Power law model, 151
- Power law nucleation kinetics, 209
- Product classification, effect on crystal-size distribution, 159–161
- Product removal, effect on crystal-size distribution, 161
- Protein precipitation, population balance and, 291–294

R

- Raman spectroscopy, solute structuring characterization, 267–268
- Reaction engineering of crystal-size distribution, 174–198
- Residence-time distribution, 174, 198

population balance and, 288–290
 crystallizer, 231
 Rosin–Rammler distribution
 coefficient of variation, 38–39
 j th moment defined, 35
 mean, 38
 moments, 35
 Rosin–Rammler distribution function, 26
 Routh stability criterion, 215
 RTD, *see* Residence-time distribution
 R–z crystallizer, 220–226, 231
 class II, 231–233
 crystal-size distribution instability in,
 223–224
 fines dissolution, 220–226
 product classification, 220–224
 simulation results, 235
 stability, 220–226
 stability analysis, 220–226

S

Secondary nucleation, 112–113, 115–117,
 112–129
 particle formation, 115–116
 relation to suspension density, 142–143
 Secondary nucleation kinetics, particle size,
 184–188
 Secondary nucleation mechanisms
 attrition, 122–123
 contact, 123. *See also* Contact nucleation
 fluid shear, 123
 fracture, 122
 initial breeding, 122
 needle breeding, 123
 Secondary nuclei
 growth, 126
 sources, 122–123
 Selection-for-breakage function, 278–279
 Slurry velocity, random fluctuations, 73–76
 Smith–Ewart recursion relationship, 284
 Sodium chloride, size distribution, 7
 Sodium nitrate
 crystal growth rate, 262, 264
 Raman spectra, 267–268
 Solid state, particulate properties, 1–2
 Solute clusters, 110–111, 114, 117, 119
 Solute mass, conservation, 204
 Solute mass balance

 clear liquid volume basis, 204
 unsteady state, 203–205
 Stability criterion, 215
 power law, 215
 State space formulation, control law, 230–235
 Sugar, size distribution, 7
 Supersaturation, 110–111
 contact nucleation, 123–126
 crystal size, 137
 crystal-size distribution, 2–4, 136–140, 167
 definition, 109
 growth as function of, 93
 nucleation, 93, 109–110, 167, 227
 power law function of, 116
 solute clustering, 267–269

T

Table salt. *See* Sodium chloride
 Taylor vortex flow, 298
 Transient moment equations, 297–209
 Twinned crystals, definition, 18

U

Unsteady state
 crystal-size distribution dynamics, 202–205
 crystal-size distribution transients, 202
 mass balance, 202
 population balance, 202–203
 solute mass balance, 203–205

V

Van der Waals forces, 17, 297
 Void fraction, 211
 change in, 202–204
 Volmer nucleation growth rate kinetics model,
 215–217

W

Weight density distribution function, 44
 Weight-fraction function, 44
 dimensionless, 310–317
 Weight-size distribution, prediction of,
 193–196